



Impact and Feasibility Study of Solutions for Doubling Heavy Vehicles

Contract # DTRT12GUTC12 with USDOT Office of the Assistant Secretary for Research and Technology (OST-R)

Final Report

February 2015

Principal Investigator: Nasim Uddin, Ph.D.



National Center for Transportation Systems Productivity and Management

O. Lamar Allen Sustainable Education Building
788 Atlantic Drive, Atlanta, GA 30332-0355

P: 404-894-2236 F: 404-894-2278
nctspm@ce.gatech.edu nctspm.gatech.edu



DISCLAIMER

The contents of this report reflect the views of the authors, who are responsible for the facts and the accuracy of the information presented herein. This document is disseminated under the sponsorship of the U.S. Department of Transportation's University Transportation Centers Program, in the interest of information exchange. The U.S. Government assumes no liability for the contents or use thereof.

Materials Research Report
Draft Final Report

February 2015

UAB Project
Contract No.

IMPACT AND FEASIBILITY STUDY OF SOLUTIONS FOR DOUBLING HEAVY VEHICLES

Principal Investigator (PI): Nasim Uddin, PhD, P.E., F. ASCE ^a

Co-PI: Ton-Lo Wang, PhD, P.E. ^b
Necati Catbas PhD, P.E ^c

^a University of Alabama Birmingham (UAB),

^b Florida International University (FIU),

^c University of Central Florida (UCF)



DISCLAIMER

The opinions, findings, and conclusions expressed in this publication are those of the authors and not necessarily those of the State of Florida Department of Transportation.

SI CONVERSION FACTORS

SYMBOL	WHEN YOU KNOW	MULTIPLY BY	TO FIND	SYMBOL
LENGTH				
in	inches	25.4	millimeters	mm
ft	feet	0.305	meters	m
yd	yards	0.914	meters	m

SYMBOL	WHEN YOU KNOW	MULTIPLY BY	TO FIND	SYMBOL
AREA				
in²	square inches	645.2	square millimeters	mm ²
ft²	square feet	0.093	square meters	m ²
yd²	square yard	0.836	square meters	m ²

SYMBOL	WHEN YOU KNOW	MULTIPLY BY	TO FIND	SYMBOL
VOLUME				
ft³	cubic feet	0.028	cubic meters	m ³
yd³	cubic yards	0.765	cubic meters	m ³
NOTE: volumes greater than 1000 L shall be shown in m ³				

SYMBOL	WHEN YOU KNOW	MULTIPLY BY	TO FIND	SYMBOL
MASS				
oz	ounces	28.35	grams	g
lb	pounds	0.454	kilograms	kg

SYMBOL	WHEN YOU KNOW	MULTIPLY BY	TO FIND	SYMBOL
FORCE and PRESSURE or STRESS				
lbf	pound force	4.45	newton	N
lbf/in²	pound force per square inch	6.89	kilopascals	kPa

1. Report No.:	2. Government Accession No.:		3. Recipient's Catalog No.:
4. Title and Subtitle: Impact and Feasibility Study of Solutions for Doubling Heavy Vehicles		5. Report Date: February 2015	
		6. Performing Organization Code:	
7. Author(s): Nasim Uddin, Ton-Lo Wang, Necati Catbas, and Adel Elfayoumy		8. Performing Organ. Report No.:	
9. Performing Organization Name and Address: - University of Alabama – Birmingham (UAB), - Florida International University (FIU), - University of Central Florida (UCF)		10. Work Unit No.:	
		11. Contract or Grant No.:	
12. Sponsoring Agency Name and Address: Federal Highway Administration University Transportation Center		13. Type of Report and Period Covered: 14. Sponsoring Agency Code:	
15. Supplementary Notes: N/A			
16. Abstract: This research aims to study the effect of increasing the weight of trucks and/or the number of heavy vehicles on bridges. In this study, the weigh-in-motion (WIM) and bridge WIM (BWIM) recorded data were used to identify the main characteristics of the representative heavy vehicle and the site-specific fatigue truck. These representative trucks along with the AASHTO design truck were used to characterize the steel and prestressed concrete bridge population sensitive to flexure using CSiBridge and AASHTOWare Bridge Rating programs. Also, the effects of different types of vehicles on the dynamic response of bridges were studied. The remaining service life along with fatigue assessment was calculated under different possible scenarios to meet the increase in freight demand on steel bridges with RC deck. Furthermore, bridge load rating and reliability was calculated for prestressed concrete girder bridges with AASHTO girder type versus those of Florida I-beam girder. Finally, the cost increase due to different loading scenarios was calculated for different possible remedy actions. This cost impact was used to calculate the bridge's cost over the span of planning period (PP) of interest.			
17. Key Words: Increasing heavy vehicle load, representative vehicle, characteristic bridge, bridge remaining life, and cost impact		18. Distribution Statement:	
19. Security Classification (of this report): Unclassified	20. Security Classification (of this page): Unclassified	21. Number of Pages: 522	22. Price:

Form DOT F 1700.7 (8-72)

DISCLAIMER

The opinions, findings, and conclusions expressed in this publication are those of the authors and not necessarily those of the State of Florida Department of Transportation or any other state or federal agency.

ABSTRACT

The use of heavy vehicles is the backbone of freight shipment and the corner stone of economic success in the United States. National projections predict that freight shipments will double in the next ten years. This increase in freight demand must be accommodated by increasing the number of trucks, increasing the weight of trucks, or both. It is quite obvious that increasing the number of heavy vehicles or the weight of heavy vehicles will inversely affect the bridge lifespan. Thus, congestion problem due to increased number of heavy vehicles must be addressed. Moreover, additional repetitive loading may cause fatigue cracking in these bridge superstructures and limit their service lives.

The useful life of highway bridge superstructures is directly affected by trucks' configurations (e.g. gross vehicle weight, axle weight, and axle spacing), as well as the damages that occur in the bridge deck and in the main superstructure elements. Also, the damage magnitude depends on the construction material and the structure's components. Additionally, to maintain the bridge functionality, accelerated maintenance actions increases the associated bridge costs.

In this study, the weigh-in-motion (WIM) and bridge WIM (BWIM) recorded data were used to identify the main characteristics that widely affect the bridge's lifespan and cause serious fatigue stress problems due to the most prevalent trucks passing over the bridge. These characteristics include the configurations of the representative heavy vehicle, gross vehicle weight (GVW), axle weight (AW), axle spacing, and the characteristics of the bridge population sensitive to load effect and fatigue.

Characteristics of typical trucks were synthesized and processed from acquired data. The total numbers of trucks with different axle configurations were recorded monthly during a certain period. Histograms of the percentage distribution of truck traffic classified by the number of axles in both directions were developed. The results showed that the most prevalent trucks were two-axle and five-axle. The gross vehicle weight data of these trucks was processed by a MATLAB program to predict the Generalized Extreme Value (GEV) of the GVW over a 1000 year return-period using the Extreme Value Theory (EVT). Accordingly, different axle weights were calculated. In the same way, the observed axle weights data were processed to estimate the extreme axle weights and, as well, the corresponding GVW.

Characterizing the bridge population sensitive to load effect and fatigue was done based on a static and dynamic analysis of the estimated characterized truck, proposed 97-kip truck, and the current rating 80-kip truck, as well as the most frequent GVW. According to the recorded WIM data of two- and five-axle trucks, histograms were built to detect the most frequent GVW. Steel and concrete girder bridges of different spans were modeled by two field-verified different computer programs, a commercial program (CSiBridge) and AASHTOWare program (Virtis), in addition to a limited case using LS-DYNA. The results provided the most critical sections and rating factors of girders in different bridges' span lengths under selective heavy truck presence.

Increased freight demand may adversely affect the bridge's life-span. There were two different scenarios that may be applied when a current traffic situation changes. These

scenarios either change the traffic (doubling the number of heavy vehicles) or change the traffic load (increase the heavy vehicle weight limit). Bridge analysis for the bridge's remaining life was done for both these scenarios. The synthesized recorded WIM data, along with the results of different specialized softwares (CSiBridge and Virtis), were used to calculate the total lifespan of steel bridges (steel component and concrete deck) following the AASHTO fatigue calculation procedures. The data compared the effect of heavier trucks to the effect of doubling the number of heavy vehicles under the present limits of the bridge's service life. The total number of maintenance periods was directly affected by the estimated service life of the bridge.

Also, the effects of different types of vehicles on the dynamic response of bridges were studied. Dynamic model and equations of motion, describing the dynamic model of eleven different types of truck were developed. The list of trucks includes the current widely used trucks such as Type 3S2 (FDOT Truck) in addition to some Longer Combination Vehicles (LCV) that can carry much heavier loads but are not being used as often as the older truck types.

In addition to that, a comparative analysis of two bridges that are separately modeled utilizing the two most commonly used prestressed concrete girders in Florida was studied. The two bridges in question have exactly the same geometric and quantitative specifications in terms of the traffic lanes, spans and height, but only one difference that is girder being of different type for two models; namely AASHTO Type III (American Association of State Highway and Transportation Officials) and Florida I-Beam 45. The two bridges are

subjected to three different loadings. The loadings considered in scope of this study are HL-93, Florida legal and long combination vehicle loads. The evaluations based on the response of the bridges are made and given in terms of load rating factor and reliability index. Finite Element Modeling approach is followed as a solution method of each comparison case. For this purpose, physical FE models are employed and solved under predefined loading and strength losses. Briefly, the results indicate that Florida I-Beam tends to have a higher load carrying capacity, lateral stiffness, cost efficiency, load rating factor and a better reliability in element level when compared to AASHTO Type girders.

The bridge cost and the whole life cost is directly impacted upon by the changing of the current traffic situation. Increasing the number and/or weight of heavy vehicles impacts cost. These costs are calculated using an NCHRP project program. Cost impact associated with different possible remedy actions was calculated. This cost impact was used to calculate the bridge's cost over the span of planning period (PP) of interest.

Finally, as the research covers various aspects (static and dynamic analysis), starting with the vehicle characterization thru characterizing bridge population, and ending with the investigation of the effect of increasing traffic and/or traffic loads on bridges' lifespan and the associated cost impact during a planning period of interest; it may be considered as a decision-making tool for departments of transportation (DOTs). These

tools included a BMS, with the PP cost, for the current and future traffic situations, along with different remedy actions and cost impacts.

Keywords: Increasing heavy vehicle load, characteristic vehicle, characteristic bridge, bridge management, bridge remaining life, and cost impact

TABLE OF CONTENTS

DISCLAIMER	II
SI CONVERSION FACTORS	III
DISCLAIMER	V
ABSTRACT.....	VI
TABLE OF CONTENTS.....	XI
LIST OF TABLES	XVII
LIST OF FIGURES	XXIII
1. INTRODUCTION	1
1.1 PROBLEM STATEMENT	4
1.2 RESEARCH OBJECTIVES	5
1.3 RESEARCH APPROACH	5
2. DETERMINATION OF THE CHARACTERISTIC TRUCK BY WIM DATA .	8
2.1 INTRODUCTION	8
2.1.1 <i>Data Collection and Analysis</i>	9
2.1.2 <i>Detection of Characteristic Heavy Vehicle - Approach</i>	13
2.1.3 <i>Typical Truck Characteristics</i>	17
2.1.4 <i>Prediction of the Representative Heavy Vehicle</i>	22
2.1.5 <i>Prediction of Representative Fatigue Truck</i>	29
3. CHARACTERISTIC BRIDGE TRAFFIC LOAD EFFECTS	35
3.1 INTRODUCTION	35
3.2 CHARACTERISTIC BRIDGE LOAD APPROACH	35
3.3 VEHICULAR LOADS	36
3.3.1 <i>HL-93 Truck Load</i>	36

3.3.2	<i>Proposed 97-kip Truck</i>	38
3.3.3	<i>170 kip truck</i>	39
3.3.4	<i>85 kip truck</i>	39
3.4	BRIDGES CONFIGURATIONS	39
3.5	STEEL TYPE BRIDGE	45
3.5.1	<i>Results and Discussion</i>	50
3.6	PRESTRESSED GIRDER TYPE BRIDGE	61
3.6.1	<i>Results and Discussion</i>	68
3.7	BRIDGE-VEHICLE INTERACTION AND NUMERICAL METHODS.....	76
4.	DYNAMIC CHARACTERISTICS OF DIFFERENT GROUP OF TRUCKS ...	91
4.1	INTRODUCTION	91
4.2	DERIVATION OF EQUATIONS OF MOTION FOR “H20-44 TRUCK”.....	94
4.3	DERIVATION OF EQUATIONS OF MOTION FOR “H20-44 TRUCK”	96
4.4	DERIVATION OF EQUATIONS OF MOTION FOR “HS20-44 TRUCK”	101
4.5	DERIVATION OF EQUATIONS OF MOTION FOR “TYPE 3 TRUCK”	109
4.6	DERIVATION OF EQUATIONS OF MOTION FOR “TYPE 3S2 TRUCK (FDOT TRUCK)”	113
4.7	DERIVATION OF EQUATIONS OF MOTION FOR “TYPE 3S3 TRUCK”	123
4.8	DERIVATION OF EQUATIONS OF MOTION FOR “TYPE 3S1 TRUCK”	134
4.9	DERIVATION OF EQUATIONS OF MOTION FOR “TYPE 2S2 TRUCK”	142
4.10	DERIVATION OF EQUATIONS OF MOTION FOR “SU4 TRUCK”	152
4.11	DERIVATION OF EQUATIONS OF MOTION FOR “9 AXLE TURNPIKE DOUBLE” 157	
4.12	DERIVATION OF EQUATIONS OF MOTION FOR “7-AXLE ROCKY MOUNTAIN DOUBLE”	171
4.13	DERIVATION OF EQUATIONS OF MOTION FOR “8 AXLE B-TRAIN DOUBLE”	183
4.14	ROAD SURFACE ROUGHNESS	195
5.	DYNAMIC AMPLIFICATION FACTOR ANALYSIS	200
5.1	TIRE TRUCK FORCES ON THE ROAD	200
5.2	TIRE TRUCK FORCES ON THE BRIDGE	206
6.	LEGAL AND LONGER COMBINATION VEHICLES IN FLORIDA STATE 269	
6.1	GENERAL OVERVIEW	269
6.2	FLORIDA LEGAL LOAD TRUCKS.....	270

6.3	LONGER COMBINATION VEHICLES (LCV)	271
7.	BRIDGE ANALYSIS – PRESTRESSED BRIDGES	275
7.1	INTRODUCTION	275
7.2	FINITE ELEMENT MODEL	280
7.2.1	<i>Overview of the Full Finite Element Model</i>	280
7.2.2	<i>Modeling of the Link Elements</i>	284
7.2.3	<i>Modeling of the Tendons</i>	285
7.3	HISTORY AND DEVELOPMENT OF PRESTRESSED CONCRETE	287
7.4	INITIAL PRESTRESS LOSSES.....	289
7.4.1	<i>Elastic Shortening of the Concrete</i>	289
7.5	TIME DEPENDENT PRESTRESS LOSSES	291
7.5.1	<i>Relaxation of the Strands</i>	291
7.5.2	<i>Creep Loss</i>	292
7.5.3	<i>Shrinkage Loss</i>	293
8.	LOAD RATING AND RELIABILITY	296
8.1	LOAD RATING FACTOR (LRF)	296
8.2	RELIABILITY INDEX (RI)	315
8.3	RESULTS AND DISCUSSION.....	323
9.	THE EFFECT OF INCREASING HEAVY VEHICLE LOADS ON A BRIDGE LIFESPAN	339
9.1	INTRODUCTION	339
9.2	LITERATURE REVIEW	346
9.2.1	<i>Fatigue Resistance Characterization [43]</i>	346
9.2.2	<i>Elastic Fracture Mechanics approach</i>	348
9.2.3	<i>Steel Bridge Fatigue</i>	349
9.2.4	<i>Steel Bridges Fatigue Life Estimation Approach</i>	350
9.2.5	<i>Fatigue Serviceability Index [45]</i>	364

9.2.6	<i>Reinforced Concrete (RC) Deck Fatigue</i>	366
9.2.7	<i>Reinforced Concrete Deck Fatigue Life Estimation Approach</i>	367
9.3	NEGATIVE REMAINING LIFE	370
9.4	FATIGUE EVALUATION PROCEDURE [49]	371
9.4.1	<i>Fatigue Truck</i>	371
9.4.2	<i>Bending Moment</i>	372
9.4.3	<i>Stress Range</i>	372
9.4.4	<i>Detail Category Constant</i>	372
9.5	STEEL BRIDGES REMAINING LIFE (Y_R) - CASE STUDY	372
9.5.1	<i>Current Traffic Conditions (CT)</i>	374
9.5.2	<i>Double Traffic Volume Scenario (DTV)</i>	388
9.5.3	<i>Double Traffic Load Scenario (DTL)</i>	399
9.6	RC DECK SLAB REMAINING LIFE (Y_R) – CASE STUDY.....	411
9.6.1	<i>Current Traffic Conditions (CT)</i>	411
9.6.2	<i>Double Traffic Volume Scenario (DTV)</i>	414
9.6.3	<i>Double Traffic Load Scenario (DTL)</i>	415
9.7	DIFFERENT LOADING SCENARIOS	418
9.7.1	<i>Steel Bridge Fatigue Assessment</i>	420
9.7.2	<i>Reinforced Concrete Deck Fatigue Assessment</i>	424
9.8	SUMMARY.....	427
9.9	STEEL GIRDERS.....	428
9.10	RC DECK	428
10.	COST IMPACT OF INCREASING HEAVY VEHICLE LOADS ON BRIDGES	429
10.1	INTRODUCTION	429
10.2	LITERATURE REVIEW	429
10.2.1	<i>Life-Cycle Cost Analysis (LCCA)</i>	429

10.2.2	<i>Identification of Maintenance Alternatives.....</i>	430
10.2.3	<i>Agency Costs.....</i>	431
10.2.4	<i>User Costs.....</i>	431
10.3	TRUCK WEIGHT EFFECT ON BRIDGE NETWORK COSTS.....	431
10.3.1	<i>Deficiency Due to Overstress for Existing Bridges</i>	432
10.3.2	<i>Deficiency Due to Overstress for New Bridges</i>	433
10.4	COST IMPACT ESTIMATING METHODOLOGIES OF BRIDGE NETWORKS.....	433
10.4.1	<i>Fatigue of Existing Steel Bridges (Cat. 1)</i>	433
10.4.2	<i>Fatigue of Reinforced Concrete Decks (Cat. 2).....</i>	435
10.4.3	<i>Deficiency Due to Overstress for Existing Bridges (Cat. 3).....</i>	436
10.4.4	<i>Deficiency Due to Overstress for New Bridges (Cat. 4).....</i>	438
10.5	COST IMPACT ESTIMATING APPROACH	439
10.5.1	<i>Carris Program Manual [53]</i>	440
10.6	BRIDGES WHOLE LIFE CYCLE COST AND BRIDGE MANAGEMENT	444
10.7	TRUCK WEIGHT LIMIT CHANGE COST IMPACT – CASE STUDY	447
10.7.1	<i>General Factors and Parameters</i>	449
10.7.2	<i>Typical Truck Characteristics.....</i>	449
10.7.3	<i>Sampling and Stratifying.....</i>	452
10.7.4	<i>Current Traffic Conditions – Base Case (BC).....</i>	453
10.7.5	<i>Double Traffic Load (DTL) – Alternative Scenario (AS1).....</i>	455
10.7.6	<i>Double Traffic Volume (DTV) – Alternative Scenario (AS2)</i>	458
	<i>Proposed 97-kip Truck - Alternative scenario (AS3).....</i>	466
10.8	SUMMARY.....	471
	CONCLUSION.....	476
10.9	SUMMARY OF RESULTS	476

REFERENCES	484
------------------	-----

LIST OF TABLES

Table 2-1: Commonly used sensors for permanent WIM sites [5].....	12
Table 2-2: No. of axles and trucks at site 915 (South bound).....	19
Table 2-3: No. of axles and trucks at site 915 (North bound).....	20
Table 2-4 :No. of trucks in northbound classified by GVW	31
Table 2-5: No. of trucks in northbound classified by GVW	32
Table 3-1: Steel bridges' configurations.....	45
Table 3-2: Steel girders moment and shear capacity	47
Table 3-3: CsiBridge Program – Bending moment induced in exterior and interior girders	51
Table 3-4: AASHTOWare Bridge rating program (Virtis) – Bending moment induced in exterior and interior girders	52
Table 3-5: Prestressed concrete bridge girders' configuration	63
Table 3-6: Dimensions of AASHTO I-Girder (inches)	63
Table 3-7: Properties of AASHTO I-Girder	64
Table 3-8: CsiBridge Program – Bending moment induced in exterior and interior girders	66
Table 3-9: AASHTOWare Bridge rating program (Virtis) – Bending moment induced in exterior and interior girders	67
Table 3-10: Bridge Models Frequencies.....	80
Table 4-1: Axle Weights and Gross Vehicle Weight of Trucks	95
Table 4-2: Degrees of Freedom of H20-44 Truck	98
Table 4-3: Relative Displacements at Spring Locations of H20-44 Truck.....	98
Table 4-4	102

Table 4-5: Relative Displacements at Spring Locations of HS20-44 Truck	104
Table 4-6: Degrees of Freedom of Type 3 Truck	109
Table 4-7: Relative Displacements at Spring Locations of Type 3 Truck.....	112
Table 4-8: Degrees of Freedom of Type 3S2 Truck	115
Table 4-9: Relative Displacements at Spring Locations of Type 3S2 Truck	117
Table 4-10: Degrees of Freedom of Type 3S3 Truck	125
Table 4-11: Relative Displacements at Spring Locations of Type 3S3 Truck	126
Table 4-12: Degrees of Freedom of Type 3S1 Truck	135
Table 4-13: Relative Displacements at Spring Locations of Type 3S1 Truck	137
Table 4-14: Degrees of Freedom of Type 2S2 Truck	142
Table 4-15: Relative Displacements at Spring Locations of Type 2S2 Truck	145
Table 4-16: Degrees of Freedom of SU4 Truck	152
Table 4-17: Relative Displacements at Spring Locations of SU4 Truck.....	154
Table 4-18: Degrees of Freedom of 9 Axle Turnpike Double.....	159
Table 4-19: Relative Displacements at Spring Locations of 9 Axle Turnpike Double	160
Table 4-20: Degrees of Freedom of 7-Axle Rocky Mountain Double	172
Table 4-21: Relative Displacements at Spring Locations of 7-Axle Rocky Mountain Double.....	173
Table 4-22: Degrees of Freedom of 8 Axle B-Train Double.....	184
Table 4-23: Relative Displacements at Spring Locations of 8 Axle Turnpike Double	185
Table 5-1: Tire Impact Factors of H-20 Truck	200
Table 5-2: Suspension Impact Factors of H-20 Truck.....	201
Table 5-3: Tire Impact Factors for All Trucks [35 mph Speed]	203

Table 5-4: Tire Impact Factors for All Trucks [25 mph Speed]	204
Table 5-5: Dynamic Amplification Factor for Prestressed Concrete Bridges (“Good” Surface)	221
Table 5-6: Dynamic Amplification Factor for Steel Bridges (“Good” Surface)	222
Table 5-7: Different Truck Categories.....	223
Table 5-8: Dynamic Amplification Factor for Prestressed Concrete Bridges (“Very Good” Surface)	251
Table 5-9: Dynamic Amplification Factor for Steel Bridges (“Very Good” Surface)	
.....	252
Table 7-1: Parameters and Assumptions.....	281
Table 7-2: Section Properties.....	282
Table 7-3: Finite Element Model Information.....	283
Table 7-4 :Initial and Time dependent Loss Calculation Results	295
Table 8-1: FIB Finite Element Analysis Outputs under Legal Loads (Factored Moments) [<i>kip-ft</i>].....	302
Table 8-2: FIB 45 LRF under C5 Truck Load.....	303
Table 8-3: FIB 45 LRF under SU4 Truck Load	304
Table 8-4: FIB 45 LRF under HL-93 Truck Load.....	305
Table 8-5: FIB 45 LRF under RMD Truck Load	306
Table 8-6: FIB 45 LRF under TPD Truck Load	307
Table 8-7: Finite Element Analysis Outputs under Legal Loads (Factored Moments) [<i>kip-ft</i>]	308
Table 8-8: AASHTO Type III LRF under C5 Truck Load.....	310
Table 8-9: AASHTO Type III LRF under SU4 Truck Load	311
Table 8-10: AASHTO Type III LRF under HL93 Truck Load	312

Table 8-11: AASHTO Type III LRF under RMD Truck Load	313
Table 8-12: AASHTO Type III LRF under RMD Truck Load	314
Table 8-13: Statistical values for Bridge load components	318
Table 8-14: Statistical parameters of resistance for selected bridges	319
Table 8-15: Florida I-Beam analysis results	337
Table 8-16: AASHTO type III beam results.....	338
Table 9-1: The twelve most common bridge types built between 1950-1987 and percentages classified structurally deficient [42].....	342
Table 9-2 :United States bridge count and status by construction material [44]	343
Table 9-3: United States bridge count and status by year of build [44]	344
Table 9-4: Detail category constant A and fatigue threshold $(\Delta F)_{TH}$ [38].....	351
Table 9-5: Resistance factor for evaluation minimum or mean fatigue life, R_R [47].	353
Table 9-6: Cycles per truck passage, n [2].....	353
Table 9-7: Fraction of truck traffic in single lane, P [2].....	354
Table 9-8: Partial load factors, R_{sa} , R_{st} , and R_s [2].....	356
Table 9-9: Detail Categories for Load-Induced Fatigue [46]	357
Table 9-10 :Load path factor, G [45]	364
Table 9-11: Redundancy factor, R [45]	364
Table 9-12: Importance factor, I [45]	365
Table 9-13: Fatigue rating and assessment outcomes [45]	366
Table 9-14 :Site-specific fatigue truck - stresses	376
Table 9-15: AASHTO fatigue truck - stresses	376
Table 9-16: Remaining life(Y_r), $g=2\%$	377
Table 9-17 :Remaining life (Y_r), $g=4\%$	378
Table 9-18: Remaining life (Y_r), $g=6\%$	379

Table 9-19: Remaining life (Y_r), $g=8\%$	380
Table 9-20: Site-specific fatigue truck - stresses	388
Table 9-21: AASHTO fatigue truck - stresses	389
Table 9-22: Remaining life (Y_r), $g=2\%$	390
Table 9-23: Remaining life (Y_r), $g=4\%$	391
Table 9-24: Remaining life (Y_r), $g=6\%$	392
Table 9-25: Remaining life (Y_r), $g=8\%$	393
Table 9-26: Site-specific fatigue truck (85-kip) stresses	399
Table 9-27: AASHTO fatigue truck stresses	400
Table 9-28: Remaining life (Y_r), $g=2\%$	401
Table 9-29: Remaining life (Y_r), $g=4\%$	402
Table 9-30: Remaining life (Y_r), $g=6\%$	403
Table 9-31: Remaining life (Y_r), $g=8\%$	404
Table 9-32 :RC deck slab remaining life (CT)	413
Table 9-33: RC deck slab remaining life (DTV)	415
Table 9-34: RC deck slab remaining life (DTV)	417
Table 9-35: Truck Counts Based on WisDOT Data	419
Table 9-36: FHWA Vehicle Classification.....	420
Table 9-37: Remaining Fatigue Life of the Steel Bridge Based on First and Second Scenarios	421
Table 9-42: Fatigue Serviceability Index Based on First and Second Scenarios	422
Table 9-43: Fatigue Rating Based on First and Second Scenarios	422
Table 9-44: Remaining Fatigue Life of the Steel Bridge Based on First and Third Scenarios	423
Table 9-45: Fatigue Serviceability Index Based on First and Third Scenarios	423

Table 9-46: Fatigue Rating Based on First and Third Scenarios	424
Table 9-47: Remaining Fatigue Life of the Reinforced Concrete Deck Based on First and Second Scenarios	425
Table 9-48: Remaining Fatigue Life of the Reinforced Concrete Deck Based on First and Third Scenarios	426
Table 10-1: ADTT and corresponding t(ADTT) values [48]	437
Table 10-2: Functional classification system.....	447
Table 10-3 :Cost impact for different responding actions - BC.....	454
Table 10-4: Stress range and remaining life at BC	455
Table 10-5	462
Table 10-6: Cost impact for different responding actions – AS2	463
Table 10-7: Stress range and remaining life at AS2	463
Table 10-8 :Stress range and remaining life at AS3	467
Table 10-9: Total cost impact of different scenarios	472
Table 10-10: Mean remaining life of steel bridges at different scenarios	474
Table 10-11: Mean remaining life of RC decks at different scenarios	475

LIST OF FIGURES

Figure 1-1: Turner double truck [1]	3
Figure 1-2: HL-93 Truck -AASHTO LRFD specifications [2]	3
Figure 1-3: Five-axle and six-axle Alabama legal rating loads [1]	3
Figure 1-4: Proposed 97-kip rating vehicles (left) 97-S (right) 97-TRB [1]	4
Figure 2-1: Common configuration of WIM system [4]	10
Figure 2-2: Block-maxima (left panel) and excesses over a threshold (right panel) [6]	14
Figure 2-3: Densities for the Fréchet, Weibull and Gumbel functions [6]	15
Figure 2-4: GVW histograms with parametric and semi-parametric fits [3].....	17
Figure 2-5: Traffic classification by number of axles (SOUTH).....	21
Figure 2-6: Traffic classification by number of axles (NORTH)	21
Figure 2-7: AASHTO rating truck, AL-3S2, AW to GVW percentages.....	22
Figure 2-8: 1000-year return-period GVW of 5-axle truck, (top) southbound, (bottom) northbound	26
Figure 2-9: The 1000-year characteristic heavy vehicle AW of 5-axle truck, (top) southbound and (bottom) northbound.....	27
Figure 2-10: Representative heavy vehicle - first scenario.....	28
Figure 2-11: Representative heavy vehicle - first scenario.....	29
Figure 2-12: GVW Histogram all over the year (a) Southbound (b) Northbound.....	33
Figure 2-13: Most frequent 5-axle trucks' configuration	34
Figure 3-1: AASHTO HL-93 Design loads (a) Design truck plus design lane (b) Design tandem plus design lane (17)	38
Figure 3-2: Schematic diagram of 30-ft bridge girders and diaphragms	40

Figure 3-3: Schematic diagram of 60-ft bridge girders and diaphragms	41
Figure 3-4: Schematic diagram of 90-ft bridge girders and diaphragms	42
Figure 3-5: Schematic diagram of 120-ft bridge girders and diaphragms	43
Figure 3-6: Schematic diagram of 140-ft bridge girders and diaphragms	44
Figure 3-7: Steel girder bridge typical Cross Section for (top) 30'-60'-90' (bottom) 120'-140'	46
Figure 3-8: Composite section	47
Figure 3-9: Critical traffic lane position	48
Figure 3-10: CSiBridge prospective view.....	49
Figure 3-11: AAHTOWare Bridge rating program (Virtis) schematic model	49
Figure 3-12: Bending moment of HL-93 (28-ft long) and M_n vs. bridge span – exterior girder	53
Figure 3-13: Bending moment of HL-93 (28-ft long) and M_n vs. bridge span – interior girder	53
Figure 3-14: Bending moment of HL-93 (44-ft long) and M_n vs. bridge span – exterior girder	54
Figure 3-15: Bending moment of HL-93 (44-ft long) and M_n vs. bridge span – interior girder	54
Figure 3-16: Bending moment of 170-kip truck and M_n vs. bridge span – exterior girder	55
Figure 3-17: Bending moment of 170-kip truck and M_n vs. bridge span – interior girder	55
Figure 3-18: Bending moment of 97-S truck and M_n vs. bridge span – exterior girder	56

Figure 3-19: Bending moment of 97-S truck and M_n vs. bridge span – interior girder	56
.....	
Figure 3-20: Bending moment of 97-TRB truck and M_n vs. bridge span – exterior girder	57
Figure 3-21: Bending moment of 97-TRB truck and M_n vs. bridge span – interior girder	57
Figure 3-22: Bending moment of 85-kip truck and M_n vs. bridge span – exterior girder	58
Figure 3-23: Bending moment of 85-kip truck and M_n vs. bridge span – interior girder	58
Figure 3-24: CSiBridge - Exterior girders' M_u/M_n vs. span length - Inventory Conditions	59
Figure 3-25: Virtis - Exterior girders' M_u/M_n vs. span length - Inventory Conditions	59
Figure 3-26: CSiBridge – Exterior girders' M_u/M_n vs. span length - operating conditions	60
Figure 3-27: Virtis - Exterior girders' M_u/M_n vs. span length - operating conditions	60
Figure 3-28: PSC girder bridge typical Cross Section for (top) 30'-60'-90' (bottom) 120'-140'	62
Figure 3-29: Typical AASHTO I-Girders.....	63
Figure 3-30: Girders prestressing strands' configurations.....	65
Figure 3-31: Bending moment of HL-93 (28-ft) truck and M_n vs. bridge span – exterior girder.....	69
Figure 3-32: Bending moment of HL-93 (28-ft) truck and M_n vs. bridge span – interior girder	69

Figure 3-33 :Bending moment of HL-93 (44-ft) truck and M_n vs. bridge span – exterior girder.....	70
Figure 3-34: Bending moment of HL-93 (44-ft) truck and M_n vs. bridge span – interior girder	70
Figure 3-35: Bending moment of 170-kip truck and M_n vs. bridge span – exterior girder	71
Figure 3-36: Bending moment of 170-kip truck and M_n vs. bridge span – interior girder	71
Figure 3-37: Bending moment of 97-S truck and M_n vs. bridge span – exterior girder	72
Figure 3-38: Bending moment of 97-S truck and M_n vs. bridge span – interior girder	72
Figure 3-39: Bending moment of 97-TRB truck and M_n vs. bridge span – exterior girder	73
Figure 3-40: Bending moment of 97-TB truck and M_n vs. bridge span – interior girder	73
Figure 3-41: Bending moment of 85-kip and M_n vs. bridge span – exterior girder	74
Figure 3-42: Bending moment of 85-kip and M_n vs. bridge span – interior girder	74
Figure 3-43: CSiBridge – Exterior girders' M_u/M_n vs. span length - inventory conditions	75
Figure 3-44: Virtis - Exterior girders' M_u/M_n vs. span length - inventory conditions.	75
Figure 3-45 :Grillage Element	76
Figure 3-46:Deflection Due to Dead Load for 60 ft. Steel Girder Bridge	77
Figure 3-47: Steel Bridge Mode Shapes (30' Span)	81
Figure 3-48: Steel Bridge Mode Shapes (60' Span)	82

Figure 3-49: Steel Bridge Mode Shapes (90' Span)	83
Figure 3-50: Steel Bridge Mode Shapes (120' Span)	84
Figure 3-51: Steel Bridge Mode Shapes (140' Span)	85
Figure 3-52: Prestressed Concrete Bridge Mode Shapes (30' Span).....	86
Figure 3-53: Prestressed Concrete Bridge Mode Shapes (60' Span).....	87
Figure 3-54: Prestressed Concrete Bridge Mode Shapes (90' Span).....	88
Figure 3-55: Prestressed Concrete Bridge Mode Shapes (120' Span).....	89
Figure 3-56: Prestressed Concrete Bridge Mode Shapes (140' Span).....	90
Figure 4-1: Truck Models	94
Figure 4-2: H20-44 Dynamic Model (a) Truck Side View (b) Truck Front View	97
Figure 4-3: HS20-44 Dynamic Model (a) Truck Side View (b) Truck Front View..	103
Figure 4-4: Type 3 Dynamic Model (a) Truck Side View (b) Truck Front View	111
Figure 4-5: Type 3S2 Dynamic Model (a) Truck Side View (b) Truck Front View.	116
Figure 4-6: Type 3S3 Dynamic Model (a) Truck Side View (b) Truck Front View.	127
Figure 4-7: Type 3S1 Dynamic Model (a) Truck Side View (b) Truck Front View	136
Figure 4-8: Type 2S2 Dynamic Model (a) Truck Side View (b) Truck Front View.	144
Figure 4-9: SU4 Truck Dynamic Model (a) Truck Side View (b) Truck Front View	153
Figure 4-10: Nine Axle Turnpike Double Dynamic Model (a) Truck Side View (b) Truck Front View.....	158
Figure 4-11: Seven Axle Rocky Mountain Double Dynamic Model (a) Truck Side View (b) Truck Front View	175
Figure 4-12: Eight Axle Turnpike Double Dynamic Model (a) Truck Side View (b) Truck Front View.....	188
Figure 4-13: Dodds and Robson Spectrum for Principal Roads.....	197

Figure 4-14: Road Surface Roughness for “Very Good” Condition	198
Figure 5-1: Type 2S2 Truck Impact Factors.....	202
Figure 5-2: Impact Factors of Different Truck Categories for “Very Good” Surface Condition.....	205
Figure 5-3: Impact Factors of Different Truck Categories for “Good” Surface Condition.....	206
Figure 5-4: Displacement of 30 ft. Concrete Bridge due to H-20 (“Good” Surface) 208	
Figure 5-5: Displacement of 30 ft. Concrete Bridge due to HS-20 (“Good” Surface)	209
Figure 5-6: Displacement of 30 ft. Concrete Bridge due to Type 3 (“Good” Surface)	210
Figure 5-7: Displacement of 30 ft. Concrete Bridge due to Type 3S2 (“Good” Surface)	211
Figure 5-8: Displacement of 30 ft. Concrete Bridge due to Type 3S3 (“Good” Surface)	212
Figure 5-9: Displacement of 30 ft. Concrete Bridge due to Type 3S1 (“Good” Surface)	213
Figure 5-10: Displacement of 30 ft. Concrete Bridge due to Type 2S2 (“Good” Surface)	214
Figure 5-11: Displacement of 30 ft. Concrete Bridge due to SU4 (“Good” Surface)215	
Figure 5-12: Displacement of 30 ft. Concrete Bridge due to 7-Axle Rocky Mountain Double (“Good” Surface).....	216
Figure 5-13: Displacement of 30 ft. Concrete Bridge due to 8 Axle B-Train Double (“Good” Surface)	217

Figure 5-14: Displacement of 30 ft. Concrete Bridge due to 9 Axle Turnpike Double (“Good” Surface)	218
Figure 5-15: Prestressed Concrete Bridges DAF for Different Vehicle Categories (“Good” Surface)	227
Figure 5-16: Steel Bridges DAF for Different Vehicle Categories (“Good” Surface)	228
Figure 5-17: Moment of 140 ft. Concrete Bridge due to H-20 (“Good” Surface)....	229
Figure 5-18: Moment of 140 ft. Concrete Bridge due to HS-20 (“Good” Surface) ..	230
Figure 5-19: Moment of 140 ft. Concrete Bridge due to Type 3 (“Good” Surface)...	231
Figure 5-20: Moment of 140 ft. Concrete Bridge due to Type 3S2 (“Good” Surface)	232
Figure 5-21: Moment of 140 ft. Concrete Bridge due to Type 3S3 (“Good” Surface)	233
Figure 5-22: Moment of 140 ft. Concrete Bridge due to Type 2S2 (“Good” Surface)	234
Figure 5-23: Moment of 140 ft. Concrete Bridge due to Type 3S1 (“Good” Surface)	235
Figure 5-24: Moment of 140 ft. Concrete Bridge due to Type SU4 (“Good” Surface)	236
Figure 5-25: Moment of 140 ft. Concrete Bridge due to 7-Axle Rocky Mountain Double (“Good” Surface).....	237
Figure 5-26: Moment of 140 ft. Concrete Bridge due to 8 Axle B-Train Double (“Good” Surface)	238
Figure 5-27: Moment of 140 ft. Concrete Bridge due to 9 Axle Turnpike Double (“Good” Surface)	239

Figure 5-28: Displacement of 60 ft. Steel Bridge due to H-20 (“Very Good” Surface)	240
Figure 5-29: Displacement of 60 ft. Steel Bridge due to HS-20 (“Very Good” Surface)	241
Figure 5-30: Displacement of 60 ft. Steel Bridge due to Type 3 (“Very Good” Surface)	242
Figure 5-31: Displacement of 60 ft. Steel Bridge due to Type 3S2 (“Very Good” Surface)	243
Figure 5-32: Displacement of 60 ft. Steel Bridge due to Type 3S3 (“Very Good” Surface)	244
Figure 5-33: Displacement of 60 ft. Steel Bridge due to Type 3S1 (“Very Good” Surface)	245
Figure 5-34: Displacement of 60 ft. Steel Bridge due to Type 2S2 (“Very Good” Surface)	246
Figure 5-35: Displacement of 60 ft. Steel Bridge due to SU4 (“Very Good” Surface)	247
Figure 5-36: Displacement of 60 ft. Steel Bridge due to 7-Axle Rocky Mountain Double (“Very Good” Surface)	248
Figure 5-37: Displacement of 60 ft. Steel Bridge due to 8 Axle B-Train Double (“Very Good” Surface)	249
Figure 5-38: Displacement of 60 ft. Steel Bridge due to 9 Axle Turnpike Double (“Very Good” Surface)	250
Figure 5-39: Prestressed Concrete Bridges DAF for Different Vehicle Categories (“Very good” Surface)	253

Figure 5-40: Steel Bridges DAF for Different Vehicle Categories (“Very Good” Surface)	254
Figure 5-41: Moment of 120 ft. Steel Bridge due to H-20 (“Very Good” Surface) ..	255
Figure 5-42: Moment of 120 ft. Steel Bridge due to HS-20 (“Very Good” Surface)	256
Figure 5-43: Moment of 120 ft. Steel Bridge due to Type 3 (“Very Good” Surface)	257
Figure 5-44: Moment of 120 ft. Steel Bridge due to Type 3S2 (“Very Good” Surface)	258
Figure 5-45: Moment of 120 ft. Steel Bridge due to Type 3S3 (“Very Good” Surface)	259
Figure 5-46: Moment of 120 ft. Steel Bridge due to Type 2S2 (“Very Good” Surface)	260
Figure 5-47: Moment of 120 ft. Steel Bridge due to Type 3S1 (“Very Good” Surface)	261
Figure 5-48: Moment of 120 ft. Steel Bridge due to Type SU4 (“Very Good” Surface)	262
Figure 5-49: Moment of 120 ft. Steel Bridge due to 7-Axle Rocky Mountain Double (“Very Good” Surface)	263
Figure 5-50: Moment of 120 ft. Steel Bridge due to 8 Axle B-Train Double (“Very Good” Surface)	264
Figure 5-51: Moment of 120 ft. Steel Bridge due to 9 Axle Turnpike Double (“Very Good” Surface)	265
Figure 5-52: Comparison of the "Very Good" and "Good" Surfaces Results (a) 30' Concrete (b) 30' Steel (c) 60' Concrete (d) 60' Steel	266

Figure 5-53: Comparison of the "Very Good" and "Good" Surfaces Results (a) 90' Concrete (b) 90' Steel (c) 120' Concrete (d) 120' Steel.....	267
Figure 5-54: Comparison of the "Very Good" and "Good" Surfaces Results (a) 140' Concrete (b) 140' Steel	268
Figure 6-1: Florida Legal Loads (7).....	271
Figure 6-2: Sates Allowing Various Longer Combination Vehicles [28]	272
Figure 6-3: Maximum weight of RMD and TPD [28].....	273
Figure 6-4: Seven Axle RMD with total weight of 104k [28].....	273
Figure 6-5: Nine Axle TPD with total weight of 128k [28]	273
Figure 7-1: Simply Supported 3 Span Bridge of this Study	277
Figure 7-2: Cross Section of the bridges with (a) AASHTO Type III, (b) Florida I-beam	278
Figure 7-3: FIB (left) and AASHTO Type III (right) Typical Cross Sections	279
Figure 7-4: Finite Element Models: FIB (Top) AASHTO Type (Bottom)	280
Figure 7-5: FEM Meshed Models: FIB (Top) AASHTO Type (Bottom)	283
Figure 7-6: Finite Element Model of the Link elements.....	285
Figure 7-7: Distribution of Tendons, AASHTO Type III Beam (left) and Florida I-Beams (right)	286
Figure 7-8: Elastic Shortening of the Concrete.....	289
Figure 7-9: Strain-Time Curve [27].....	293
Figure 8-1: Load rating through Entire FIB bridge under C5 truck load.....	323
Figure 8-2: Load rating through Entire FIB bridge under SU4 truck load	324
Figure 8-3: Load rating through Entire AASHTO Type bridge under C5 truck load	325
Figure 8-4: Load rating through Entire AASHTO Type bridge under SU4 truck load	326

Figure 8-5 :LRF Comparison of FIB between Legal loads	327
Figure 8-6: RI Comparison of FIB between Legal loads.....	328
Figure 8-7: LRF Comparison of AASHTO between Legal loads	329
Figure 8-8: RI Comparison of AASHTO between Legal loads.....	330
Figure 8-9: LRF Comparison of FIB between LCVs	331
Figure 8-10: RI Comparison of FIB between LCVs.....	332
Figure 8-11: LRF Comparison of AASHTO between LCVs	333
Figure 8-12 :RI Comparison of AASHTO between LCVs.....	334
Figure 8-13: LRF Comparison of FIB and AASHTO under HL-93	335
Figure 8-14: RI Comparison of FIB and AASHTO under HL-93.....	336
Figure 9-1: Age distribution of bridges in the United States [43]	339
Figure 9-2: Percentages of bridges classified structurally deficient: (a) Built 1950- 1987; and (b) Built 1980-1987 [42]	340
Figure 9-3: Definition of a stress cycle [43]	347
Figure 9-4 :Example of data from a representative fatigue test [43]	347
Figure 9-5: Change in number of cycles due to change in (a) critical crack length, (b) initial crack length, (c) stress range, and (d) type of detail [43]	349
Figure 9-6 :AASHTO S-N curves for design of steel bridges [46]	352
Figure 9-7: Lifetime average truck volume for an existing bridge [2]	354
Figure 9-8: Typical $S-N$ curve for welded joints [38]	355
Figure 9-9: Variation of $(Y-a)/N$ with remaining life for various bridge ages [45] ..	366
Figure 9-10: Shear fatigue of RC bridge deck under wheel loading [48].....	367
Figure 9-11: Negative remaining life resulting from uncertainty in fatigue life estimation (shaded area is equal to targeted failure probability) [45].....	371

Figure 9-12 :Remaining life vs. present age vs. span length, site-specific fatigue truck	383
Figure 9-13 :Remaining life vs. present age vs. span length, site-specific fatigue truck	384
Figure 9-14: Remaining life vs. present age vs. span length, AASHTO fatigue truck	385
Figure 9-15 :Remaining life vs. present age vs. span length, AASHTO fatigue truck	386
Figure 9-16 :Remaining life at age of 50-years vs. annual growth rate, fatigue truck	386
Figure 9-17 :Remaining life at age of 50-years vs. annual growth rate, AASHTO fatigue truck	387
Figure 9-18: Remaining life vs. present age vs. span length, site-specific fatigue truck	394
Figure 9-19 :Remaining life vs. present age vs. span length, site-specific fatigue truck	395
Figure 9-20: Remaining life vs. present age vs. span length, AASHTO fatigue truck	396
Figure 9-21: Remaining life vs. present age vs. span length, AASHTO fatigue truck	397
Figure 9-22.....	398
Figure 9-23: Remaining life at age 50-years vs. annual growth rate	398
Figure 9-24: Remaining life vs. present age vs. span length, site-specific fatigue truck	406

Figure 9-25: Remaining life vs. present age vs. span length, site-specific fatigue truck	407
Figure 9-26: Remaining life vs. present age vs. span length, AASHTO fatigue truck	408
Figure 9-27: Remaining life vs. present age vs. span length, AASHTO fatigue truck	409
Figure 9-28.....	409
Figure 9-29: Remaining life at age 50-years vs. annual growth rate, AASHTO fatigue truck	410
Figure 9-30: Remaining life vs. RC deck age, $fc' = 3000 \text{ psi}$	413
Figure 9-31: Remaining life vs. RC deck age, $fc' = 4000 \text{ psi}$	414
Figure 9-32: Remaining life vs. RC deck age, $fc' = 3000 \text{ psi}$	416
Figure 9-33: Remaining life vs. RC deck age, $fc' = 4000 \text{ psi}$	416
Figure 9-34: The impact of meeting the increase in freight demand on the remaining life vs. RC deck age, $fc' = 3000 \text{ psi}$, g=2%	418
Figure 10-1: Expenses accompanying the life cycle [52]	430
Figure 10-2: Worksheet “Details” to input weld detail data for sampled bridges [53]	
.....	441
Figure 10-3: Worksheet “Decks” to input deck data for sampled bridges [53].....	442
Figure 10-4: Worksheet “Cat. 3” for data input and load rating calculation [53]	443
Figure 10-5: Worksheet “Cat4” for data input and design load change factor calculation [53]	444
Figure 10-6: The BLCCA process flow chart [52].....	445

Figure 10-7: Schematic Representation of Safety Management Methodology along with Maintenance Cost Impact	446
Figure 10-8: Vehicle class definitions	448
Figure 10-9: TWH for some rural functional classes (Rural interstate, Rural other principal arterial, and Rural minor arterial)	450
Figure 10-10: TWH for some urban functional classes (Urban interstate, Urban Fwy/Expwy, and Urban other principal).....	451
Figure 10-11: Michigan most prevalent truck	452
Figure 10-12: Cost-impact categories with different responding action – AS1	457
Figure 10-13: Sensitivity analysis of ADTT on cost-impact Cat. 1 and Cat. 2 – AS1	461
Figure 10-14: Sensitivity analysis of (g) on cost-impact Cat. 1 and Cat. 2 - AS1....	461
Figure 10-15: DTV TWH for some rural functional classes (Rural interstate, Rural other principal arterial, and Rural minor arterial)	465
Figure 10-16: DTV TWH for some urban functional classes (Urban interstate, Urban Fwy/Expwy, and Urban other principal).....	466
Figure 10-17: Configurations of the proposed 97-kip trucks (97-A and 97-B	467
Figure 10-18: Cost-impact categories with different responding action – AS3	468
Figure 10-19: Sensitivity analysis of ADTT on cost-impact Cat. 1 and Cat. 2 – AS3	469
Figure 10-20: Sensitivity analysis of (g) on cost-impact Cat. 1 and Cat. 2 – AS3	470
Figure 10-21: Minimum total cost impact	473
Figure 10-22: Maximum total cost impact.....	473

1. Introduction

The use of heavy vehicles such as 18-wheelers is the backbone of freight shipment and the corner stone of economic success in the United States. National projections predict that freight shipments will double in the next ten years. Economic projections indicate that freight commodities are rapidly on the rise. In the United States, 12.8 billion tons of freight was transported by heavy vehicles in 2007. Due to lingering recession impacts, only 10.9 billion tons were moved in 2009, but 18.4 billion tons are expected in 2040 representing an increase of over 68%. Without any expansion to the national highway system, roadway congestion will increase by nearly 400% between 2007 and 2040 in already congested areas (USDOT Freight Facts 2010). Figure 1-1 thru Figure 1-3 show some ratings of heavy vehicles [1].

As freight volumes shipped by heavy vehicles in the United States continue to increase, and the weight and number of trucks are still fixed, the “trickle-down effect” will take place. Consequently, commodity prices will increase if heavy vehicle size and weight limits are not reformed. The increase in freight demand must be accommodated by increasing the number of trucks, increasing the weight of heavy vehicles, or both. It is quite obvious that increasing the number or the weight of heavy vehicles is detrimental to bridge longevity. Thus, congestion problem caused by the increased number (doubling) of heavy vehicles thus must be resolved.

Moreover, additional repetitive loading may cause fatigue cracking in bridge superstructures and limit the service life of a bridge [1].

One essential issue then is how to increase the load capacity of heavy vehicles. Today, the mass and dimensions of heavy vehicles are strictly regulated. There is an ongoing debate on this issue, with demands from several activists to allow longer and heavier vehicles on the roads. The State of Alabama is designated as “a focused state” for heavy vehicle issues. Consideration was given to the congressionally proposed rating vehicle (97-kips) replacing the current 80-kip truck (see Figure 1-4) as well as other configurations of heavy vehicles in use in Canada, a NAFTA partner of the USA [1].

The useful life of a highway bridge superstructure is directly affected by a heavy vehicle’s gross weight, axle weights, and axle configuration (typically called “heavy vehicle weight” together). Also, the damages that occur in the bridge deck and in the main superstructure elements (e.g. the floor beams and girders, the diaphragms, joints, and bearings) affect the bridge useful life. The severity of the damage is a function of structural components and construction materials used. Additionally, many of the older steel bridge girders are particularly prone to fatigue failures directly related to heavy vehicle weight. Bridge costs associated with increased heavy vehicle weights are the result of the accelerated maintenance, rehabilitation, or replacement work that is required to keep structures at an acceptable level of service.

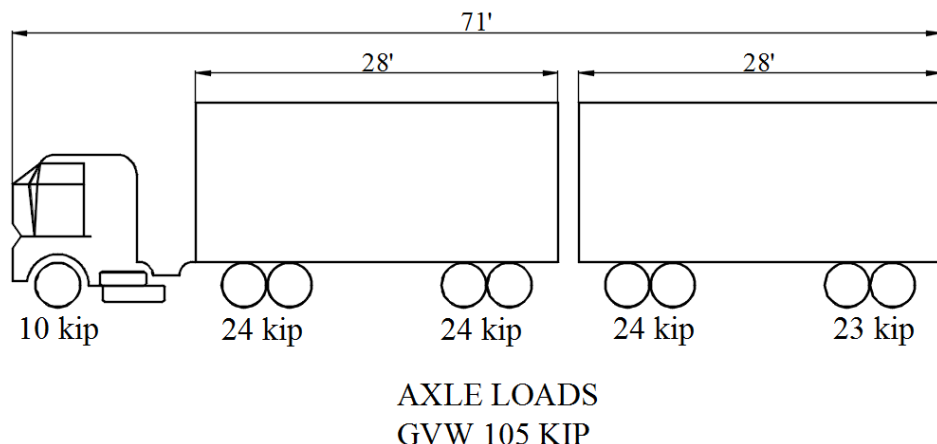


FIGURE 1-1: TURNER DOUBLE TRUCK [1]

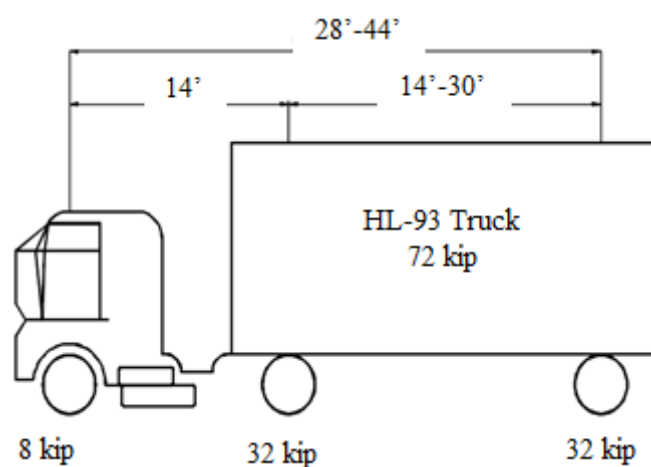


FIGURE 1-2: HL-93 TRUCK -AASHTO LRFD SPECIFICATIONS [2]

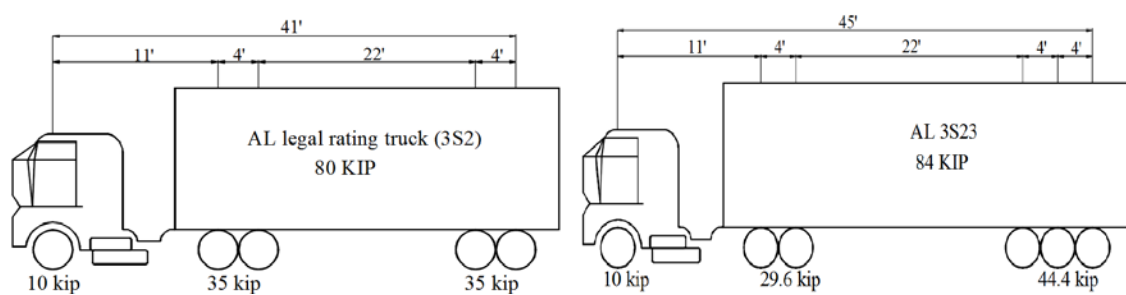
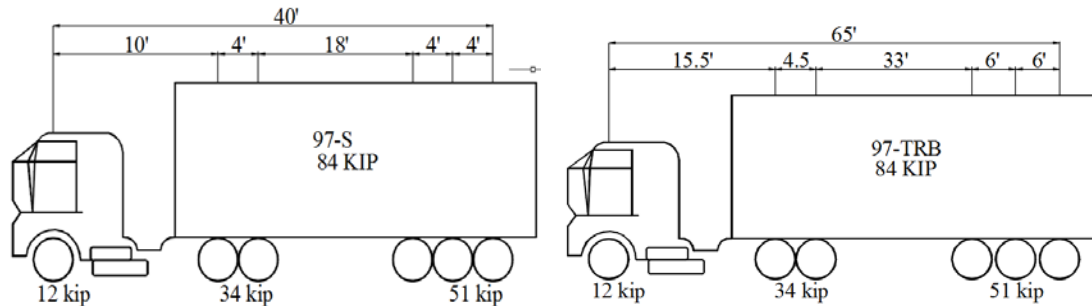


FIGURE 1-3: FIVE-AXLE AND SIX-AXLE ALABAMA LEGAL RATING LOADS [1]

1.1 Problem Statement

The bridge superstructure useful life is directly affected by the heavy vehicles configurations (gross vehicle weight, axle weight, and axle spacing) and the damages that have happened to the bridge main superstructure elements and deck.

The severity of the damage is a function of the structure's components and the construction materials used. Additionally, many of the older steel bridge girders are particularly prone to fatigue failures directly related to heavy vehicle weight. Bridge costs associated with increased heavy vehicle weight are the result of the accelerated maintenance, rehabilitation, or replacement work that is required to keep structures at an acceptable level of service.



**FIGURE 1-4: PROPOSED 97-KIP RATING VEHICLES (LEFT) 97-S (RIGHT)
97-TRB [1]**

As the severity of the damage depends on the construction material, different types of Prestressed concrete girders were studied. Two sorts of concrete girder bridges are compared in this study. The first one with AASHTO Type III girders and the other with FIB 45 girders. Aside from this difference, the other structural and

geometric components of the bridges such as number of lanes, column specifications and loads, etc. are the same.

1.2 Research Objectives

This study aimed at the following:

1. Characterizing the traffic measured by WIM data to detect the representative trucks (representative heavy vehicle and site-specific fatigue truck).
2. Characterize the bridge population sensitivity due to flexure using to evaluate the bridge safety.
3. Investigating the effect of increasing heavy vehicle loads on bridges lifespan.
4. Investigating the efficiency of using AASHTO type-III girder versus Florida I-beam 45 prestressed girder in bridges in terms of losses.
5. Investigating the changes on the performance of both girder types and reliability before and after losses using the flexural load rating and reliability index.
6. Calculating the cost effect of increasing heavy vehicle loads on bridges.

1.3 Research Approach

The useful service life of a bridge deck and girder is a random variable that is a function of a number of other variables: load magnitudes, number of load cycles, and decision as to when it should be renewed (by overlay or replacement). Also, the effects of different trucks on the bridge dynamic responses depend on many factors such as the gross vehicle weight (GVW), number and weight of truck axles, distance

between truck axles, etc. A concern of transportation agencies is the fatigue damage caused by the increasing population of heavy vehicles.

Many of the details used in older steel bridge girders are particularly prone to fatigue failures directly related to heavy vehicle weight. Repetitive loading may cause fatigue cracking in these steel members and limit the service life of a bridge. Truck-weight frequency distributions by vehicle type (i.e., heavy vehicle weight histograms) are needed to estimate the effects on a bridge's remaining life and the costs caused by changes in legal and permit heavy vehicle weights. Changing heavy vehicle weights can affect the heavy vehicle weight histograms.

Generally, a bridge's safety depends on heavy vehicle traffic, construction materials, and bridge spans. This study addresses and contributes to most of these major concerns. One main contribution was to develop a method that characterizes the representative vehicle, including the most expected extreme gross vehicle weight over a return period of interest and the site-specific fatigue truck. Furthermore, the study provides a method to characterize the bridge population sensitivity due to load effect (flexure) and fatigue. In addition, to capture the bridge behavior under the traffic, a wide range of trucks needs to be considered. To achieve this goal, many trucks with different lengths and weights have been chosen. These trucks include H20-44, HS20-44, Type 3, Type 3S2, Type 3S3, 4-axle single truck (SU4), Type 2S2 and Type 3S1. In addition to these trucks, some longer combination vehicles (LCV) including 7 Axle Rocky Mountain Double, 8 Axle B-Train Double and 9 Axle Turnpike Double were selected. Finally, this research investigated an innovative bridge safety maintenance and management tool kit based on a planning period (PP) of interest.

The characteristics of two different sets of trucks were determined to evaluate the safety of a practical range of Prestressed concrete and steel girder bridge. The first set characteristics were determined using WIM data of a specific WIM station. It was used for the application of static loads on bridges. The other set was used for dynamic load applications. The dynamic characteristics (equation of motion) of this set were derived in the following chapter.

2. Determination of the Characteristic Truck by WIM Data

2.1 Introduction

As the presence on a single very heavy truck is one of the critical bridge loading actions, the prediction of the most expected heavy vehicle weight that induces the extreme load effects is essential in bridge structures design and assessments. Codes and specs use conservative loading models to override the predication of these load effects. Advances in Weigh-in-Motion (WIM) technology increase the use of the WIM technique for accurate site-specific records that help in effective bridge structures assessments. As the use of these techniques is less conservative than those of models developed by codes of practice, it is important to quantify the factors that affect the calculations such as the traffic growth and data inaccuracy [3].

From the WIM and Bridge-WIM (BWIM) stations, the factors that widely affect the bridge's lifespan and cause serious fatigue stress problems were detected. These factors include the vehicle configurations such as number of axles, axle weight, axle spacing, and GVW. Research included a review of literature and practice related to predicting changes in truck-weight histograms; following changes in truck weight.

Characteristics of typical heavy vehicles were processed from the data acquired from WIM stations. All the collected data was analyzed to develop the site-specific

representative truck (1000-year characteristic truck), which is the truck that occurs once in 250,000 days [3].

2.1.1 Data Collection and Analysis

- *Literature Review*

Weight-in-motion (WIM) system

As its name implies, Weigh-in-Motion is the process of weighing trucks while they are travelling at full highway speeds. Due to the deficiency of the traditional static weigh stations, the WIM systems were introduced. The traditional stations have lengthy weighing processes that result in minimizing the number of vehicles being weighed. Also, heavy vehicle traffic volume often exceeds the weigh station capacity.

All of these caused resulting in the introducing of the WIM system [4] .

This system includes piezoelectric sensors, bending plate scales, inductance loops, and pressure cell scales as shown in Figure 2-1. These systems record not only the dynamic gross vehicle weight (GVW), but also the other truck configurations (axle weight, axle spacing, and number of axles) in addition to the date, time, and direction of travel. The accuracy of these systems is primarily dependent on the vehicle's dynamics and the different technologies used in the WIM system [4].

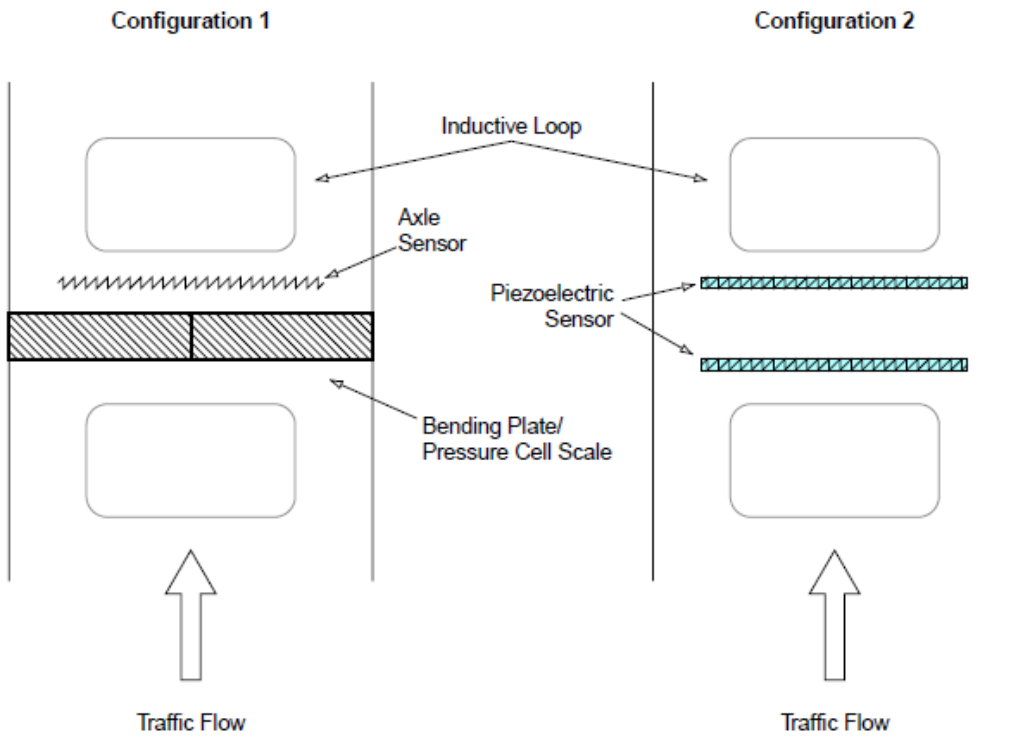


FIGURE 2-1: COMMON CONFIGURATION OF WIM SYSTEM [4]

- *Weigh-in-motion (WIM) Technology*

Lately (20 years ago), highway agencies have recognized the advantages of using automated data collection systems. This data helps for economic analysis, traffic management, and various other purposes. As the WIM technology develops, the trucks data are being collected in large quantity; that increase the use of WIM data. There are many WIM systems that ease weighing of trucks on high speeds. These systems include but are not limited to bending plates, load cells, piezoelectric cables, and bridge WIM systems. The development in sensor technology takes place in pace with the storage technologies of WIM data loggers [5].

Weigh-in-motion equipment currently used in the United States can collect data on heavy vehicle volumes, axle configurations, heavy vehicle arrival times, and load spectra. Permanent WIM station is one of the major techniques in WIM data

collection that provide more extensive data sets at geographically diverse locations over long periods of time. The portable WIM systems are utilized in case of site-specific data is required. Portable devices allow flexibility in collecting site-specific traffic data at locations of interest, such as bridges where significant illegal overloads are suspected [5].

Table 2-1 shows several types of WIM technologies. These technologies vary in performance and cost. Piezoelectric sensor-based systems are relatively cheap and offer acceptable accuracy. Strain-based WIM scales and load cell WIM systems provide more accuracy at a higher cost. Strain- and load cell-based systems are used primarily in permanent applications. Piezoquartz sensors were one of the new WIM technologies with the advantage of less sensitive to changes in temperature than the piezo-style sensors, and therefore, are generally more accurate [5].

TABLE 2-1: COMMONLY USED SENSORS FOR PERMANENT WIM SITES
[5]

Type of Sensor	Strength	Concerns
Piezoelectric (BL)	<ul style="list-style-type: none"> - Easier, faster installation than many other WIM systems. - Generally lower cost than most other WIM sensors. - Well supported by industry. - Can be used for temporary WIM systems. 	<ul style="list-style-type: none"> - Sensitive to temperature change. - Accuracy affected by structural response of roadway. - Above average maintenance requirement. - Requires multiple sensors per lane.
Piezoquartz	<ul style="list-style-type: none"> - Easier, faster installation than many other WIM systems. - May be more cost-effective (long term) if sensors prove to be long lived. <ul style="list-style-type: none"> - Very accurate sensor. - Sensor is not temperature sensitive. - Growing support by industry. 	<ul style="list-style-type: none"> - More expensive than other piezo technologies. - Requires multiple sensors per lane. - Above average maintenance requirement. - Sensor longevity data not available. - Accuracy affected by structural response of roadway.
Bending plate	<ul style="list-style-type: none"> - Frame separates sensors from pavement structure. - Entire tire fits onto sensor. <ul style="list-style-type: none"> - Moderate sensor cost. - Sensor is not temperature sensitive. - Extensive industry experience with the technology. 	<ul style="list-style-type: none"> - Longer installation time required than piezo systems. - Some systems have experienced premature failure, while others have been very long lived.
Load cell	<ul style="list-style-type: none"> - Entire tire fits onto sensor. - Frequently considered the “most accurate” of conventional WIM technologies. - Some systems have demonstrated very long lifespan 	<ul style="list-style-type: none"> - Most expensive WIM system. - Requires significant construction effort to install. - Cost-effective if constructed and maintained for long lifespan

2.1.2 Detection of Characteristic Heavy Vehicle - Approach

In many fields of modern science, engineering, and insurance, extreme value theory is well established [6]. In the following section the extreme value theory is discussed.

- *Extreme Value Theory*

Extreme value theory has the same important role as the central limit theory when modeling sums of random variables. In both cases, the theory tells the limiting distributions. In general, there are two related ways of identifying extremes in real data. The first approach considers the maximum value of a variable observed in successive periods, (i.e. days of the months). These selected observations represent the extreme events, also called block (or per period) maxima. Figure 2-2, left panel, depicts the observations X_2 , X_5 , X_7 and X_{11} represent the block maxima for four periods of three observations each. The second approach considers only the data exceeding a predefined (given) threshold. The observations X_1 , X_2 , X_7 , X_8 , X_9 and X_{11} in the right panel of Figure 2-2, exceed the threshold u and represent extreme events. The block maxima method is the traditional method used to analyze data. However, the threshold method uses data more efficiently [6].

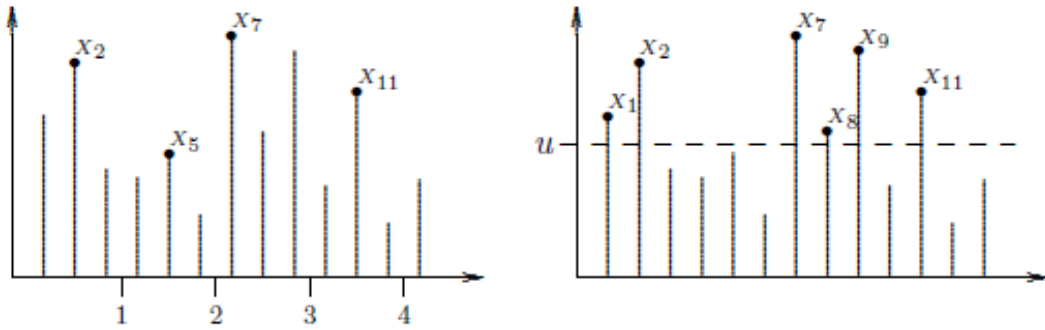


FIGURE 2-2: BLOCK-MAXIMA (LEFT PANEL) AND EXCESSES OVER A THRESHOLD (RIGHT PANEL) [6]

Distribution of Maxima

The limit law for the block maxima, which is denoted by M_n , with n the size of the subsample (block), is given by the following theorem:

Theorem 1: let (X_n) be a sequence of random variables. If there exist constants $c_n > 0$,

$d_n \in \mathbb{R}$ and some non-degenerate distribution function H such that

$$\frac{M_n - d_n}{c_n} \xrightarrow{d} H \quad (2.1)$$

Then H belongs to one of the three standard extreme value distributions:

$$\text{Fr\'echet: } \Phi_\alpha(x) = \begin{cases} 0 & x \leq 0 \\ e^{-x^{-\alpha}} & x > 0 \end{cases} \quad \alpha > 0 \quad (2.2)$$

$$\text{Weibull: } \Psi_\alpha(x) = \begin{cases} e^{-(x)^{\alpha}} & x \leq 0 \\ 1 & x > 0 \end{cases} \quad \alpha > 0 \quad (2.3)$$

$$\text{Gumbel: } \Lambda(x) = e^{-e^{-x}} \quad x \in R \quad (2.4)$$

The shape of the probability density functions for the standard Fréchet, Weibull and Gumbel distributions is given in Figure 2-3.

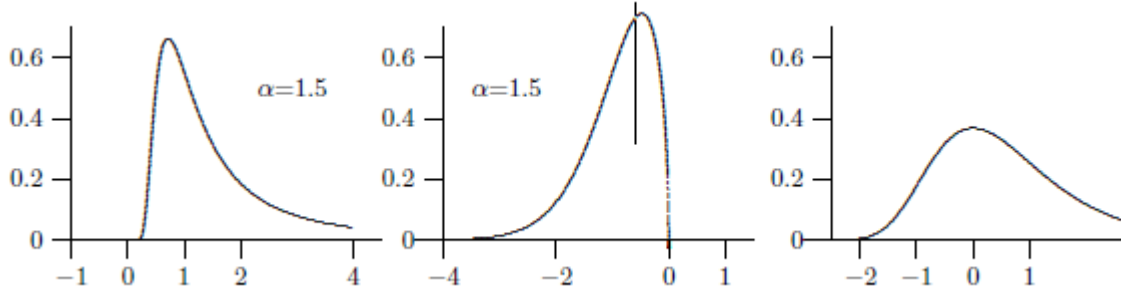


FIGURE 2-3: DENSITIES FOR THE FRÉCHET, WEIBULL AND GUMBEL FUNCTIONS [6]

As shown in Figure 2.3, the Fréchet distribution has a decaying tail in a polynomial pattern (fat tail), so it fits for heavy tailed distributions. The Weibull distribution represents the asymptotic distribution of finite endpoint distributions. The third pattern of distribution is the Gumbel distribution, which best characterizes thin tailed distributions (exponential).

The following one-parameter representation of these three standard distributions has been suggested, with x such that $1 + \xi x > 0$. This generalization, known as the generalized extreme value (GEV) distribution, is obtained by setting $\xi = \alpha - 1$ for the Fréchet distribution, $\xi = -\alpha - 1$ for the Weibull distribution, and by interpreting the Gumbel distribution as the limit case for $\xi = 0$.

$$H_\xi(x) = \begin{cases} e^{-(1+\xi)x}^{\frac{-1}{\xi}} & \text{if } \xi \neq 0 \\ e^{-e^{-x}} & \text{if } \xi = 0 \end{cases} \quad (2.5)$$

Generally speaking, it is unknown in advance what type of limiting distribution (Fréchet, Weibull, or Gumbel) the sample maxima will show. When the maximum

likelihood estimates have to be calculated, the generalized representation is useful. Moreover, the formerly defined standard GEV is the limiting distribution of normalized extrema. Practically, the exact distribution of the returns is unknown, and the norming constants c_n and d_n are unknowns accordingly. As a result, the three parameter specifications of the GEV are used, which is the limiting distribution of the unnormalized maxima. The two additional parameters μ and σ are the location and the scale parameters representing the unknown norming constants as shown in Eq. 2-6.

$$H_{\xi,\sigma,\mu}(x) = H_\xi \left(\frac{x - \mu}{\sigma} \right) \quad x \in D, D = \begin{cases}] -\infty, \mu - \frac{\sigma}{\xi} [& \xi < 0 \\] -\infty, \infty [& \xi = 0 \\] \mu - \frac{\sigma}{\xi}, \infty [& \xi > 0 \end{cases} \quad (2.6)$$

The quantities of interest are not the parameters themselves, but the quantiles, also called return levels, of the estimated GEV, see Eq. 2-7.

$$R^k = H_{\xi,\sigma,\mu}^{-1} \left(1 - \frac{1}{k} \right) \quad (2.7)$$

Substituting the parameters ξ , σ , and μ by their estimates $\hat{\xi}$, $\hat{\sigma}$, and $\hat{\mu}$ to get Eq. 2-8

$$\hat{R}^k = \begin{cases} \hat{\mu} - \frac{\hat{\sigma}}{\hat{\xi}} \left(1 - \left(-\log \left(1 - \frac{1}{k} \right) \right)^{-\hat{\xi}} \right) & \hat{\xi} \neq 0 \\ \hat{\mu} - \hat{\sigma} \log \left(-\log \left(1 - \frac{1}{k} \right) \right) & \hat{\xi} = 0 \end{cases} \quad (2.8)$$

For Example, a value of the \hat{R}^{10} of 7 means that the maximum loss observed during a period of one year will exceed 7% once in ten years on average [7].

- *Gross Vehicle Weight (GVW) Modeling*

A single truck with a very heavy load or a combination of trucks with different loads crossing the bridge at the same time may cause the critical loading condition of a bridge. Therefore, it is important to model accurately the complete range of GVWs.

Three different methods of modeling GVW (parametric fitting, nonparametric, and semi-parametric fitting), see Figure 2-4, may be considered to best define the typical truck's characteristics. All these methods are based on histograms distribution of the observed GVWs, either by field investigation or using the bridge weight-in-motion (WIM) data, and a reasonable interval (bin) size [3].

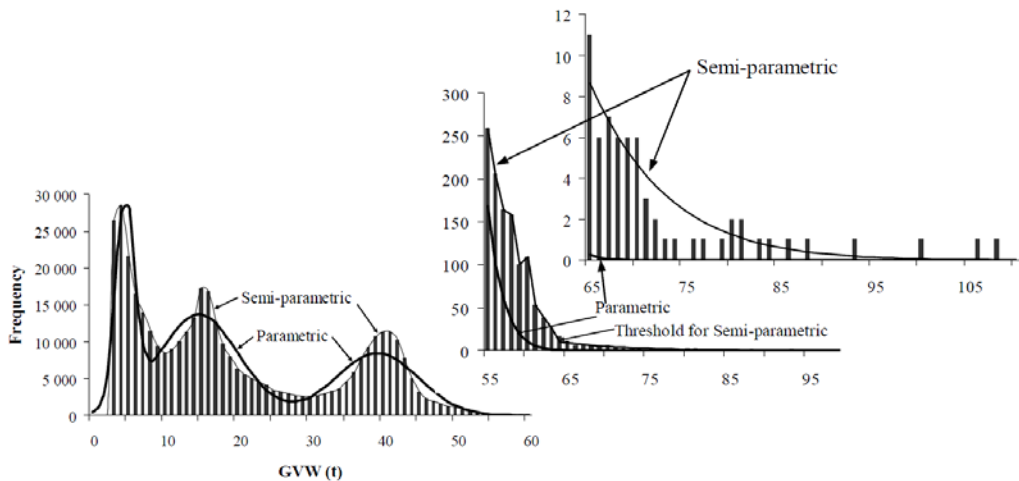


FIGURE 2-4: GVW HISTOGRAMS WITH PARAMETRIC AND SEMI-PARAMETRIC FITS [3]

2.1.3 Typical Truck Characteristics

Traffic data has been collected continuously at site 915 from January 2008 to December 2008 on South and Northbound lanes separately. During this period, the data included 275,032 heavy vehicles Southbound and 319,951 heavy vehicles Northbound. Table 2-2 and Table 2-3 illustrate respectively the total number of heavy vehicles classified by the number of axles in southbound and northbound recorded monthly during the specified duration.

Histograms of the frequency of trucks were developed to detect the most prevalent heavy vehicle in both directions. For the southbound, Figure 2-5 and indicated that the

average percentage of heavy vehicle traffic of two-axle and five-axle heavy vehicles, over the course of the year, is 41% and 36% respectively. On the Northbound, Figure 2-6 showed that 48% of trucks had two axles, while 37% had five axles. This indicates that most truck traffic is from two-axle and five-axle trucks and the most prevalent heavy truck is the five-axle truck.

TABLE 2-2: NO. OF AXLES AND TRUCKS AT SITE 915 (SOUTH BOUND)

No. of vehicles	2-axle truck	3-axle truck	4-axle truck	5-axle truck	6-axle truck	7-axle truck	8-axle truck	9-axle truck	10-axle truck	11-axle truck	12-axle truck	13-axle truck	Total
Jan	13695	2264	1156	8529	1312	13	2	1	1	0	0	0	26973
Feb	10774	1657	959	8386	1068	16	2	1	0	0	0	0	22863
March	12038	1758	1101	8841	1530	17	8	0	3	1	0	0	25297
April	11982	1682	939	8645	2148	16	11	0	0	1	0	0	25424
May	9283	1583	1145	8280	2446	22	6	2	1	0	1	0	22769
June	8381	1530	1409	7851	2560	24	3	0	2	1	1	0	21762
July	7883	1663	926	7876	3087	33	7	1	2	1	0	0	21479
August	7625	1615	991	7681	2150	20	8	4	7	1	0	0	20102
Sep	7770	1672	1270	7902	2951	49	6	5	2	0	1	0	21628
Oct	8532	1680	1227	8460	4476	32	7	1	4	1	0	0	24420
Nov	7769	1536	1313	7044	3961	10	10	0	0	0	1	0	21644
Dec	7572	1458	1171	6774	3685	9	2	0	0	0	0	0	20671

TABLE 2-3: NO. OF AXLES AND TRUCKS AT SITE 915 (NORTH BOUND)

No. of vehicles	2-axle truck	3-axle truck	4-axle truck	5-axle truck	6-axle truck	7-axle truck	8-axle truck	9-axle truck	10-axle truck	11-axle truck	12-axle truck	13-axle truck	Total
Jan	15260	2992	1312	9909	184	11	4	1	3	0	0	0	29676
Feb	12378	2079	1167	9430	182	12	2	0	0	0	0	0	25250
March	13901	2416	1585	9579	187	9	5	4	1	0	0	0	27687
April	13312	2330	1843	10055	216	16	9	0	0	0	0	0	27781
May	13820	2399	1589	9752	280	27	3	0	1	0	1	0	27872
June	13456	2560	1697	9563	271	17	3	0	2	0	1	0	27570
July	14032	2261	2016	10154	313	14	12	3	1	0	0	0	28806
August	11159	2112	1459	9002	398	14	12	3	3	4	0	0	24166
Sep	9916	2178	1564	9789	300	9	3	3	2	0	0	0	23764
Oct	11397	2371	1900	11733	282	15	8	0	1	2	0	0	27709
Nov	11269	2112	2057	8951	223	13	9	0	1	0	0	0	24635
Dec	11718	2280	2216	8620	196	3	2	0	0	0	0	0	25035

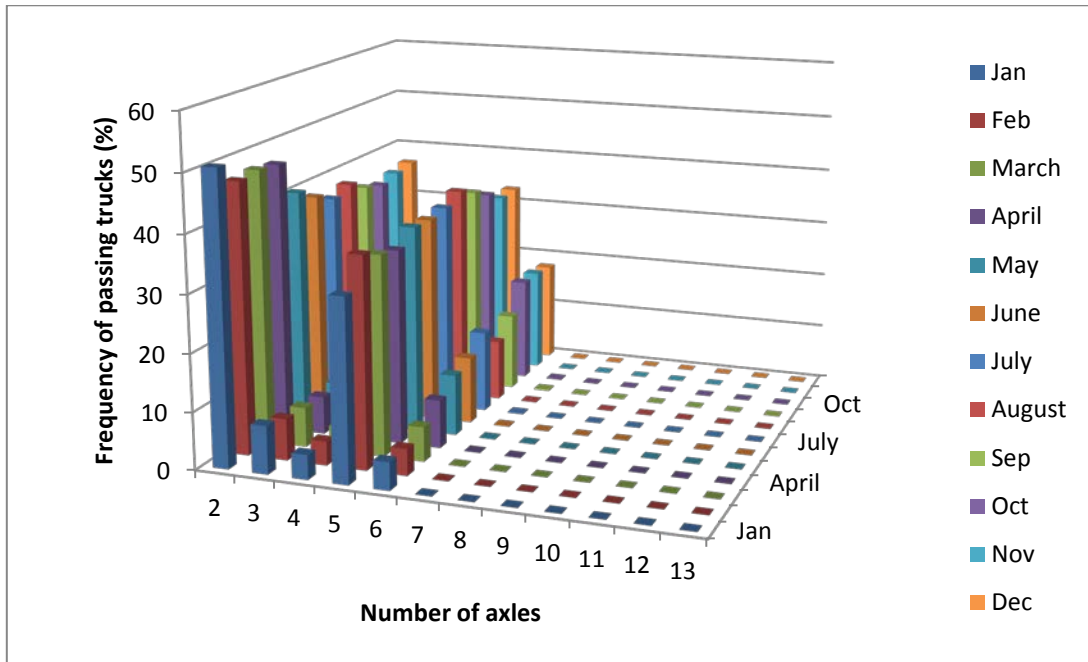


FIGURE 2-5: TRAFFIC CLASSIFICATION BY NUMBER OF AXLES (SOUTH)

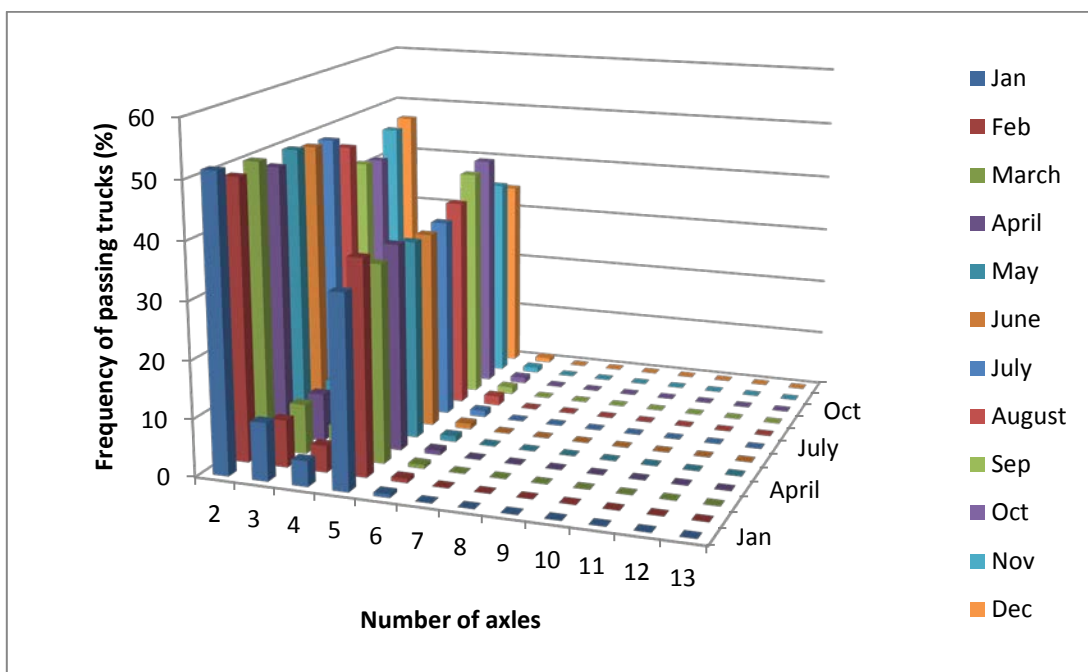


FIGURE 2-6: TRAFFIC CLASSIFICATION BY NUMBER OF AXLES (NORTH)

2.1.4 Prediction of the Representative Heavy Vehicle

The recorded WIM data (GVW and axle weight) was processed using MATLAB programming to estimate the 1000-year characteristic heavy vehicle. To estimate this representative heavy vehicle configurations (GVW, AW, and axle spacing) based on the recorded WIM data, two different scenarios were used. Both scenarios depend on the recorded WIM data of the 5-axle truck (most prevalent), the parametric modelling of maxima daily recoded data, and the first approach of the extreme value theory.

As the heaviest prevalent truck is the five-axle truck, the AASHTO rating truck 3S2 (80 kip), as shown in Figure 5, was considered as a reference truck for the relative weights of axles to the GVW.

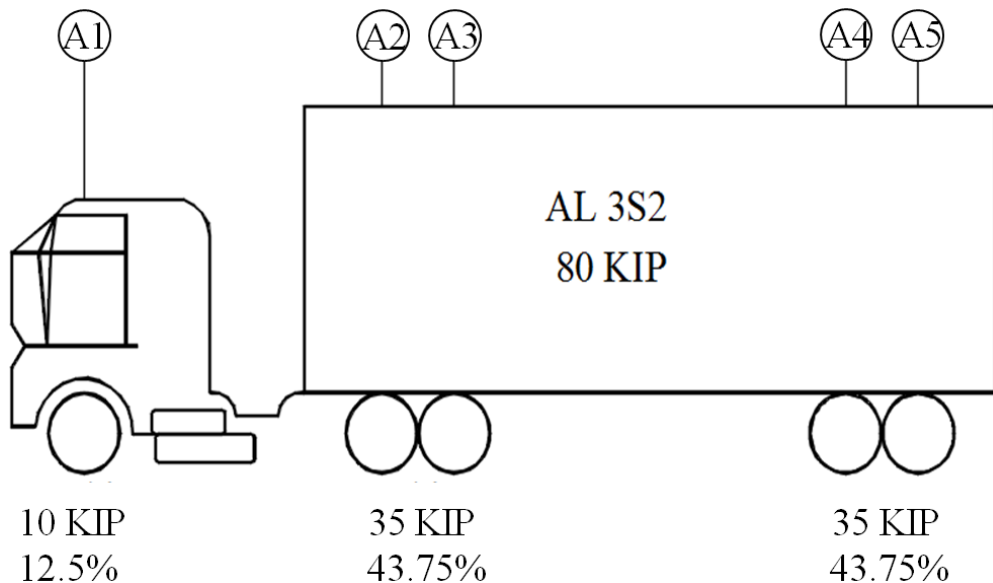


FIGURE 2-7: AASHTO RATING TRUCK, AL-3S2, AW TO GVW PERCENTAGES

Two different scenarios were used to estimate the 1000-year characteristic truck. The characteristic truck is the one that has the greatest load effect of both scenarios.

- *First Scenario*

This scenario depends only on the recorded GVW. Accordingly, only the recorded GVW of the 5-axle truck will be processed to detect the representative heavy vehicle in 1000-year return period.

1. Predict the most expected extreme GVW.
 - a. Only, consider the maximum daily GVW of 5-axle truck for each month.
 - b. Utilizing MATLAB program, build a chart of the maximum daily recorded GVW against the standard extremal variate (SEV). Extrapolate this chart curve to a value of 12.43 on the SEV axis to detect the corresponding most-expected extreme GVW. The SEV of 12.43 was calculated based on equation (2.9). Where 1000 in the denominator of the equation refers to the return period of interest that can be changed from model to model.

$$-\ln \left[-\ln \left(1 - \frac{1}{250 \times 1000} \right) \right] = 12.43 \quad (2.9)$$
 - c. The representative heavy vehicle GVW is the maximum predicted GVW all over the acquired WIM data duration that
2. Based on the AW to GVW percentage of the AASHTO rating truck (Figure 5) and the predicted extreme GVW, compute the representative heavy vehicle axle weights.

Using a MATLAB model, the acquired GVW data of the 5-axle truck were processed to predict the 1000-year representative heavy vehicle GVW at site 915 in Alabama. For the whole recorded WIM data, Figure 2.8 shows the most expected GEV of the GVW in the southbound and northbound lanes.

As shown in Figure 6 (a), the GEV of the GVW on the bridge in both directions is 743.1-kn (167 kip). Consequently, the representative truck axle weights were as follow: axle A1 weights 21 kip, axles A2, A3, A4, and A5 weights 73 kip each.

- *Second Scenario*

It is similar to the first scenario but depends on the recorded AW of the 5-axle truck. Only, the AW data was processed to predict the representative heavy vehicle over 1000-year return period.

- 1- Predict the most expected extreme GVW.
 - a. Consider only the maximum daily AW of 5-axle truck for each month.
 - b. As in step (b) of the first scenario, use MATLAB program to predict the most expected extreme AW.
 - c. The greatest predicted AW represents the representative heavy vehicle rear axles (A2, A3, A4, and A5).
- 2- Based on the AW to GVW percentage of the AASHTO rating truck and the predicted extreme AW, compute the front axle weight. Consequently, the representative heavy vehicle weight is the sum of all the computed AW.

Figure 2.9 shows most expected GEV of the AW in the southbound and northbound lanes. The GEV of the AW is 164.3 kn (37 kip). Based on the assumed reference truck, the representative heavy vehicle axle weights were as follow: A1 weights 22

kip and axle A2, A3, A4, and A5 weights 37 kip each. Adding the axles weight together, the 1000-year representative heavy vehicle GVW equals 170-kip.

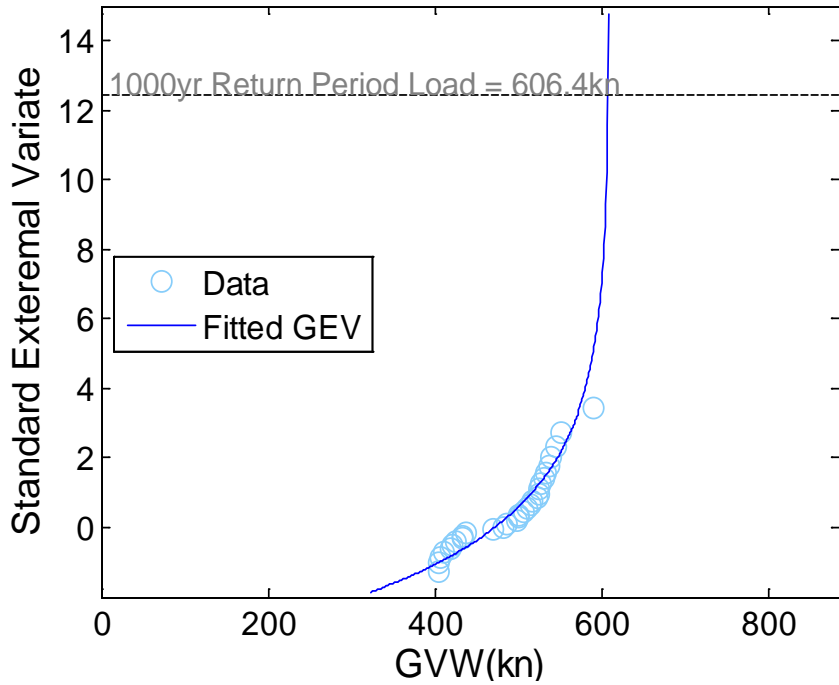
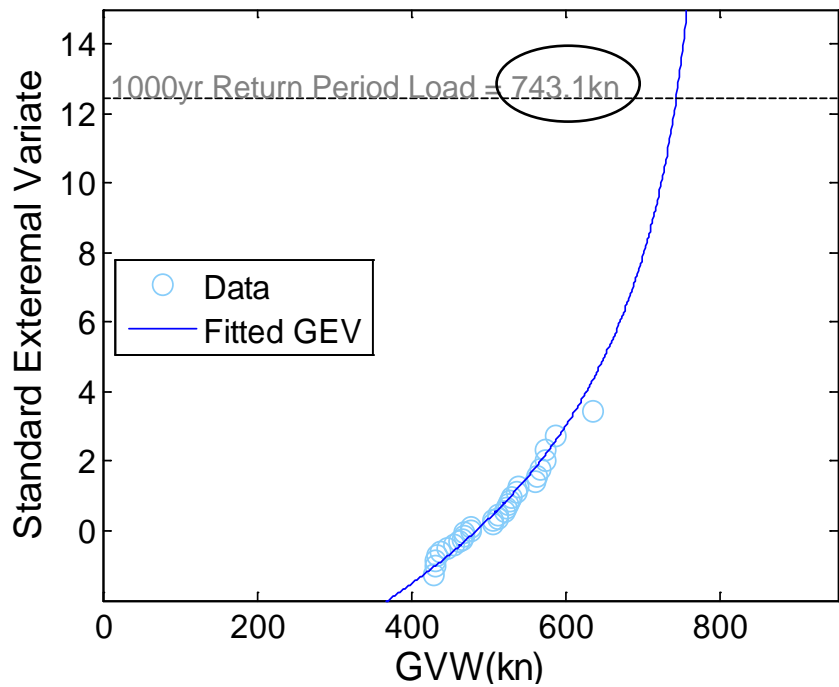


**FIGURE 2-8: 1000-YEAR RETURN-PERIOD GVW OF 5-AXLE TRUCK,
(TOP) SOUTHBOUND, (BOTTOM) NORTHBOUND**

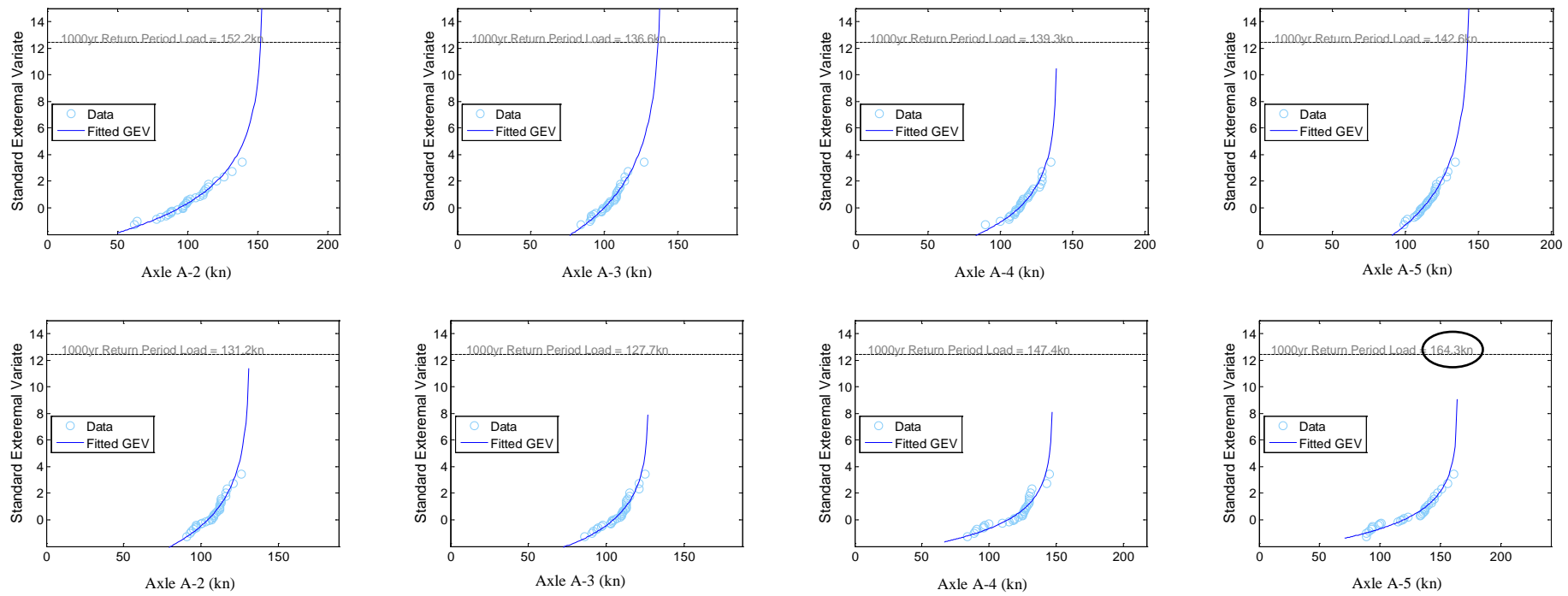


FIGURE 2-9: THE 1000-YEAR CHARACTERISTIC HEAVY VEHICLE AW OF 5-AXLE TRUCK, (TOP) SOUTHBOUND AND (BOTTOM) NORTHBBOUND

As the standard deviations of the axle spacing are low, so it is reasonable to assume mean values of the recorded WIM data for axle spacing of the 1000-year representative heavy vehicle [8]. The mean values of the recorded axle spacing are as follow: the spacing between axle A1 and axle A2 (A1-A2) equals 16 ft., A2-A3 spacing equals 5 ft., A3-A4 spacing equals 31 ft., and A4-A5 spacing equals 5 ft. the total length of the representative vehicle (A1-A5) equals 57 ft. Figure 2.10 and Figure 2.11 illustrates the representative heavy vehicles on both scenarios.

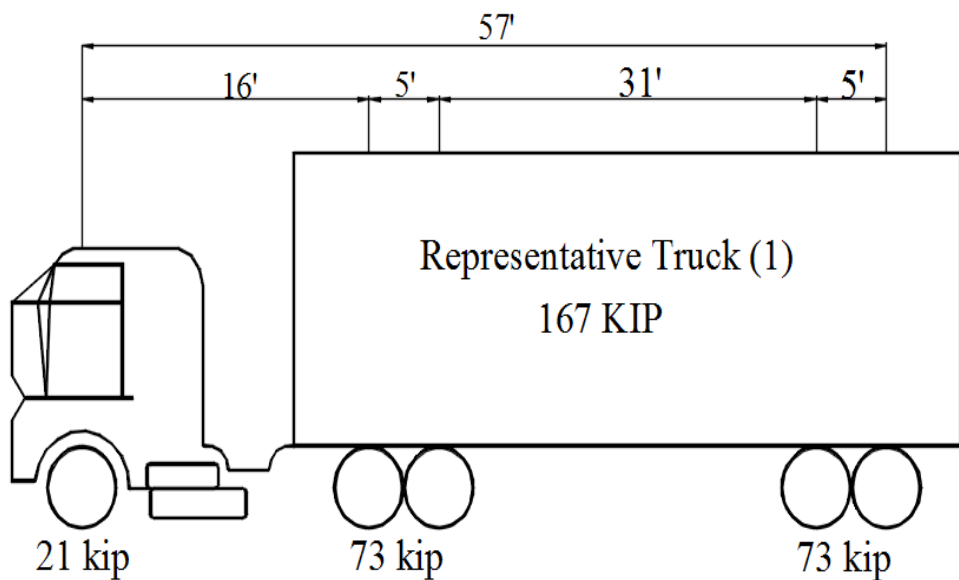


FIGURE 2-10: REPRESENTATIVE HEAVY VEHICLE - FIRST SCENARIO

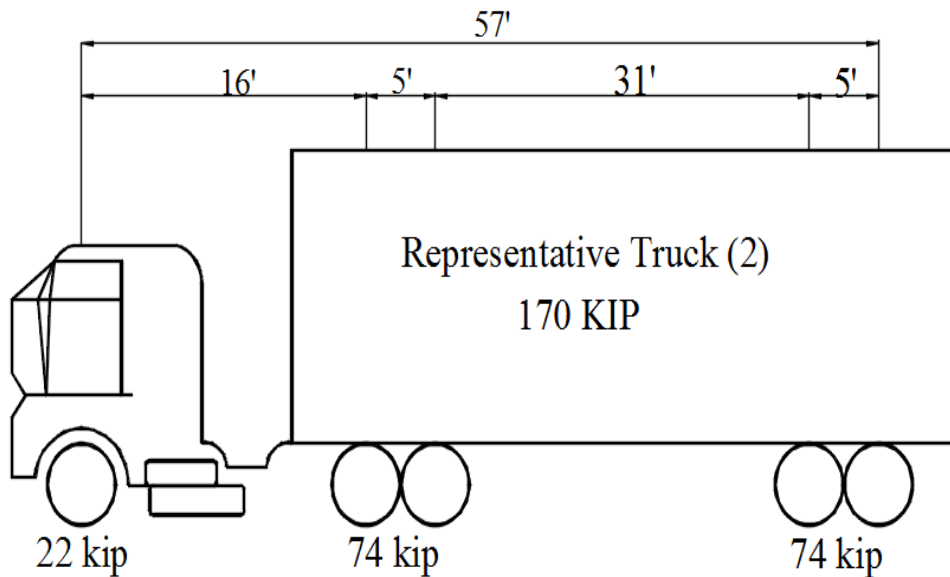


FIGURE 2-11: REPRESENTATIVE HEAVY VEHICLE - FIRST SCENARIO

2.1.5 *Prediction of Representative Fatigue Truck*

Maximizing the benefits of the WIM data, WIM data may be processed and analyzed to detect the most frequent GVW. Build histograms of the frequency of the number of trucks classified by the GVW to detect the most frequent GVW. Along with the most prevalent truck at the same WIM station, the GVW, number of axles, and axle spacing of the site-specific fatigue truck can be predicted.

According to the recorded WIM data at site 915 in Alabama, Table 2.4 and Table 2.5 shows the number of trucks in south and north bounds classified by the GVW to an interval (bin) size of 25 kn. Histograms were built for both bounds as shown in Figure 9. As illustrated in Figure 9, the GVW of the heaviest most frequent truck is 350-375kn (79-85 kip). The explored GVW of the most frequent truck was read in conjunction with the information given by Figure 4 (5-axle truck is the heaviest most prevalent truck). Consequently, the most frequent truck (site-specific fatigue truck)

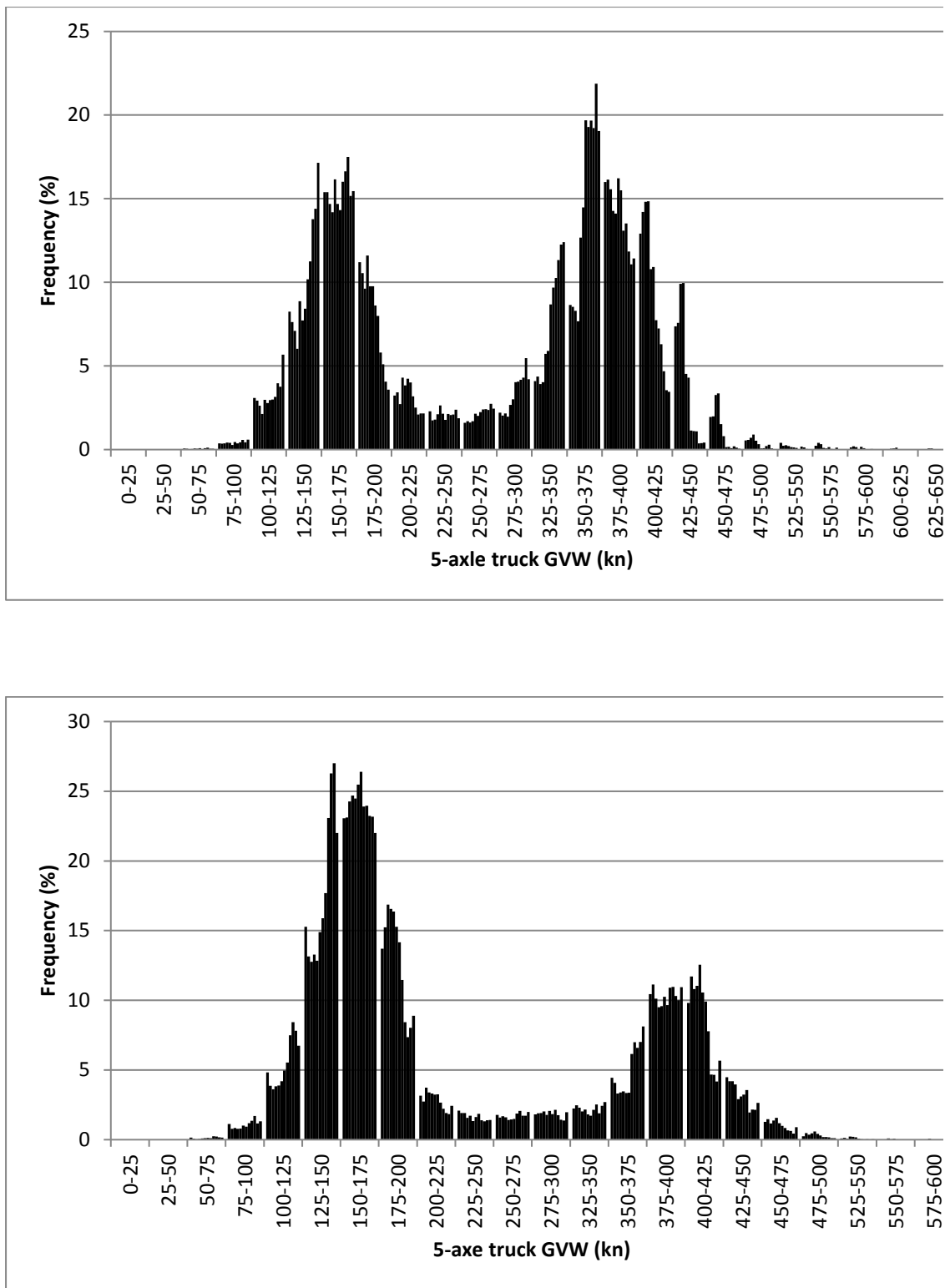
configuration was reasonable assumed as a 5-axle truck with GVW of 85 kip. Based on the configuration of the AASHTO legal truck (3S2), the axle loads and spacing of the site-specific fatigue truck were extracted and presented in Figure 10.

TABLE 2-4 :NO. OF TRUCKS IN NORTHBOUND CLASSIFIED BY GVW

GVW (kn)	Jan	Feb	Mar.	April	May	June	July	Aug	Sep	Oct	Nov	Dec
0-25	11	14	16	12	16	20	20	17	17	18	13	14
25-50	12767	9565	10910	10692	8058	7327	6834	6451	6597	7235	6920	6662
50-75	982	753	794	859	805	725	715	679	794	788	638	652
75-100	861	835	846	814	843	805	886	944	987	1070	802	897
100-125	796	807	748	712	729	635	703	684	759	905	736	821
125-150	1221	1081	1073	942	1200	1041	1193	1429	1460	1745	1480	1569
150-175	1715	1645	1636	1617	1665	1506	1464	1517	1590	1753	1279	1210
175-200	1107	1048	1043	1201	986	931	813	750	602	589	390	321
200-225	390	384	343	495	414	408	407	325	263	265	239	204
225-250	240	207	213	235	298	210	186	208	203	241	220	178
250-275	186	176	198	198	241	194	209	217	249	244	233	209
275-300	236	234	265	259	287	315	395	366	410	456	459	359
300-325	419	434	452	468	607	589	794	886	988	1153	1139	1146
325-350	934	851	915	833	1400	1578	1880	1870	2106	2210	2296	2032
350-375	1822	1696	1801	1560	1680	2114	1662	1412	1578	1644	1422	1382
375-400	1517	1514	1796	1875	1571	1489	1796	1499	1978	2907	2677	2682
400-425	996	911	1227	1270	1201	1325	1301	753	925	1091	652	313
425-450	593	516	757	962	525	455	185	76	62	47	29	11
450-475	78	108	171	333	172	58	12	11	23	37	12	7
475-500	57	26	28	47	23	13	8	2	16	15	4	1
500-525	27	35	33	9	9	13	9	2	12	2	1	0
525-550	13	17	16	4	14	7	2	2	4	1	1	0
550-575	0	2	7	6	13	2	1	0	1	1	1	0
575-600	1	0	2	9	6	0	0	0	1	0	0	1
600-625	0	2	3	4	3	0	0	0	1	0	0	0
625-650	1	0	1	2	0	0	0	0	0	1	0	0
650-675	0	1	1	2	1	0	1	0	0	1	0	0
675-700	0	0	0	1	0	1	0	0	0	0	0	0
700-725	1	0	0	0	0	0	1	1	0	0	0	0
725-750	1	0	0	0	1	1	1	1	1	0	0	0
750-775	0	1	1	3	1	0	0	0	0	0	0	0
775-800	0	0	1	0	0	0	0	0	1	1	1	0
800-825	1	0	0	0	0	0	1	0	0	0	0	0
Total	26973	22863	25297	25424	22769	21762	21479	2010	21628	24420	2164	2067

TABLE 2-5: NO. OF TRUCKS IN NORTHBOUND CLASSIFIED BY GVW

GVW (kn)	Jan	Feb	Mar.	April	May	June	July	Aug	Sep	Oct	Nov	Dec
0-25	28	31	55	34	54	52	66	38	32	38	42	32
25-50	14275	11071	12616	11931	12353	12238	12836	9912	8745	10090	1040	1083
50-75	1097	858	925	1023	1116	964	970	920	873	978	831	769
75-100	995	904	959	961	963	960	955	1007	1104	1292	979	1034
100-125	1268	1095	1154	1206	1156	1135	1233	1229	1547	1953	1465	1415
125-150	2773	2235	2469	2664	2432	2845	2978	2829	3687	4785	4166	3858
150-175	3043	2902	3322	3538	3355	3400	3657	2705	2865	3242	2590	2603
175-200	1543	1636	1779	1855	1802	1665	1675	1194	970	1041	848	893
200-225	412	363	465	464	457	429	468	346	317	338	284	294
225-250	272	240	270	241	264	193	238	250	210	231	194	169
250-275	214	181	205	210	194	185	209	225	251	227	190	195
275-300	204	207	219	238	207	231	254	242	207	195	144	192
300-325	287	252	241	227	243	209	208	243	284	257	243	241
325-350	530	430	350	365	373	367	392	638	740	820	665	711
350-375	1070	1086	990	990	971	1056	1052	1066	1108	1244	919	954
375-400	996	1112	1051	1128	1260	1061	1038	776	492	582	383	503
400-425	477	423	425	439	325	342	366	374	227	278	214	242
425-450	147	158	135	155	216	153	141	119	72	81	47	79
450-475	26	46	40	48	66	48	38	23	23	24	15	14
475-500	11	14	7	26	22	20	17	5	1	7	3	3
500-525	4	1	2	10	7	10	5	5	2	4	2	1
525-550	1	2	1	7	10	2	5	1	0	1	3	1
550-575	1	1	1	6	5	0	0	0	1	0	1	1
575-600	0	1	2	1	3	2	2	1	0	1	1	0
600-625	0	1	2	0	3	2	0	0	3	0	0	0
625-650	0	0	0	1	4	1	0	0	1	0	2	1
650-675	0	0	0	3	1	0	0	3	0	0	0	0
675-700	1	0	0	3	5	0	0	0	1	0	0	0
700-725	1	0	0	2	1	0	0	3	0	0	0	0
725-750	0	0	0	0	1	0	1	2	0	0	0	0
750-775	0	0	1	2	1	0	2	6	0	0	0	0
775-800	0	0	0	2	1	0	0	1	1	0	0	0
800-825	0	0	0	0	0	0	0	2	0	0	0	0
Total	29676	25250	27687	27781	27872	27570	28806	2416	23764	27709	2463	2503



**FIGURE 2-12: GVW HISTOGRAM ALL OVER THE YEAR (A)
SOUTHBOUND (B) NORTHBOUND**

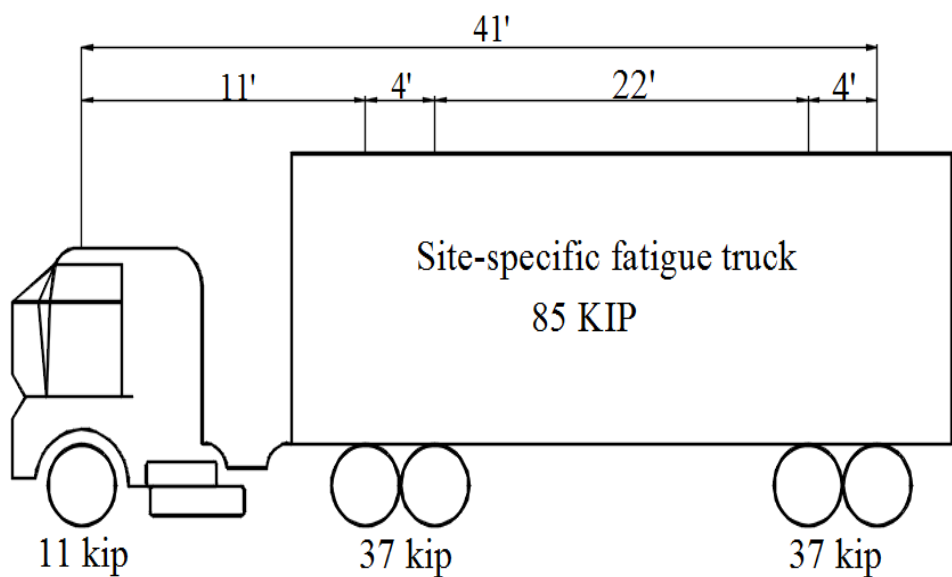


FIGURE 2-13: MOST FREQUENT 5-AXLE TRUCKS' CONFIGURATION

3. Characteristic Bridge Traffic Load Effects

3.1 Introduction

Heavy truck traffic affects the service life of highway bridge superstructures. Damage typically occurs in the bridge deck and in the superstructure's main elements. This damage may be mainly due to a bending moment (BM) that could exceed the load capacity of the bridge.

Based on the analyzed data and characteristic truck configuration in the previous section, static and dynamic analysis was performed to determine the characterization of prestressed concrete and steel bridge girders against heavy truck loading. The static analysis was performed using AASHTOWare Bridge rating program (Virtis) and CSiBridge program to 3D model. Models were subjected to the load of the AASHTO LRFD design truck (HL93), the representative heavy vehicle (170 kip), and the proposed 97-kip truck (97-TRB and 97-S) in addition to the site-specific fatigue truck (85 kip). The bending moment developed by these models at the most critical sections at the exterior and interior girders were captured and recorded.

3.2 Characteristic Bridge Load Approach

Steel and prestressed concrete girder bridges of practical different spans were used in the research. The spans lengths are 30, 60, 90, 120, and 140-ft. these bridges were subjected to different sets of truck based on the type of analysis (static – dynamic). In static analysis, finite element models (FEM) of bridges were subjected to the static load of the AASHTO LRFD design truck (HL93), the representative heavy vehicle

(170 kip), and the proposed 97-kip truck (97-TRB and 97-S) in addition to the site-specific fatigue truck (85 kip).

3.3 Vehicular Loads

3.3.1 *HL-93 Truck Load*

In order to define a specific loading that could represent the same extreme effects as the other vehicles of any type could create on a bridge while in operation, a simpler and more tractable load type called HL-93 (Highway Load, developed in 1993) was developed. This load is defined in such a way that it makes the same extreme load effects that of the exclusion vehicles. HL-93 consists of three different live loads namely, Design truck, Design tandem and Design lane (Fig 2-1). HL-93 Truck load resembles the typical semitrailer truck (Fig 2-1 (a)). The front axle load of the HL-93 truck is 8 kips, the drive axle is 32 kips with distance of 14 feet away from first axle and the rear trailer axle is 32 kips with the varying distance of 14 to 30 feet. Variable spacing range for the rear axle allows the designer to adjust the spacing so as to cause the most critical load effect. Generally, where the front and rear axles are positioned in adjacent structurally continuous spans like in continues short span bridges, long spacing of the rear axle controls.

Design tandem configuration consists of two axles with the weight of 25 kips and the spacing of 4 feet between the axles (Fig 2-1 (b)). It is similar to the tandem axle load in the previous AASHTO Standard Specifications except the load is increased from 24 kips to 25 kips.

Design lane load is a uniform load with the magnitude of 0.64 kips/ft occupying a 10 feet length. This lane load is the same as the one that has been previously used in AASHTO Standard Specifications for many years. The only difference is that LRFD lane load does not require any concentrated loads.

Although the live load modeling was developed using the exclusion vehicles, it is also compared with other weight in motion (WIM) studies.

Since the surface of the roadways is not perfectly smooth, extension and compression of the suspension creates an oscillating motion. This oscillation results in axle forces exceeding the static load. Although this phenomenon can be seen as some type of impact loading, its dynamic effects are taken into consideration under the name of dynamic load allowance (DLA). Dynamic load allowance is used by AASHTO and it is abbreviated as IM (17). Statistical studies and analytical models show that the effect of impact loads are typically less than 30%. (22)

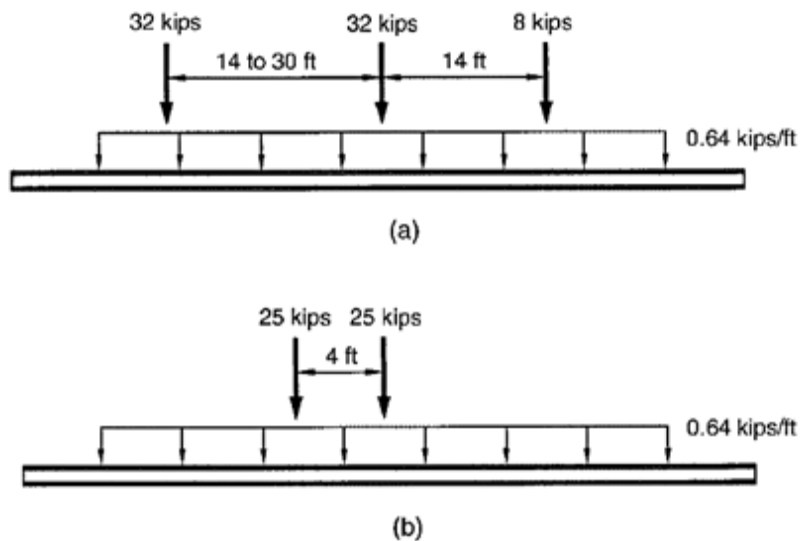


FIGURE 3-1: AASHTO HL-93 DESIGN LOADS (A) DESIGN TRUCK PLUS DESIGN LANE (B) DESIGN TANDEM PLUS DESIGN LANE (17)

AASHTO suggests the designers to use IM as 33% for all limit states except fatigue and fracture limit states. Thus, the dynamic load factor applied to static loads becomes:

$$U_{L+1} = U_L(1 + IM) \quad (3-1)$$

3.3.2 Proposed 97-kip Truck

One of the trucks that were used in the static analysis was names as the proposed 97-kip truck. The 97-kip truck is in use in Mexico (NAFTA agreement member [1]), and to maximizes the effectiveness of this agreement especially for those engaged in international trade. US truckers would only need to purchase new trailers with many components to current vehicle combination.

It is a six-axle truck. With regard to pavement, it is considered one of the least damaging truck configurations; however, the increase in GVW results in higher stress on the older (aging) highway infrastructures (bridges). As seen in Figure 1.4, it is

offered in two lengths. The shorter truck is designated as 97-S (40 feet long) while the longer one is designated as 97-TRB (65 feet long) [9].

3.3.3 170 kip truck

As developed in section 2.5, the 170 kip has five axles with a total length of 57 feet (see Figure 2-11). The front axle is 22 kips while the other five are 37 kips each. It is the heaviest truck used in this study.

3.3.4 85 kip truck

Based on the site specification, WIM data, and analyzed data, the developed site-specific fatigue truck (85 kip) is similar in effect to the 97-S truck, having a total length of 41 feet, with five axles and with the front axle at 12 kips. The other four axles are 21 kips weight each. The tandem axles are spaced 4 feet apart (see Figure 2-13).

3.4 Bridges Configurations

Five single span girder bridges with the lengths of 30', 60', 90', 120' and 140' have been selected and designed in accordance with the AASHTO LRFD Design Specifications. Figure 3.1 thru Figure 3.5 shows the schematic diagram of those bridges. The span length was decided based on the actual needs of the bridge being built. The girder, diaphragm, diaphragm spacing and other components of the structure and substructure are assumed. They were subject to change using the “trial and error method” after computing the factored applied moment and the applied factored shear.

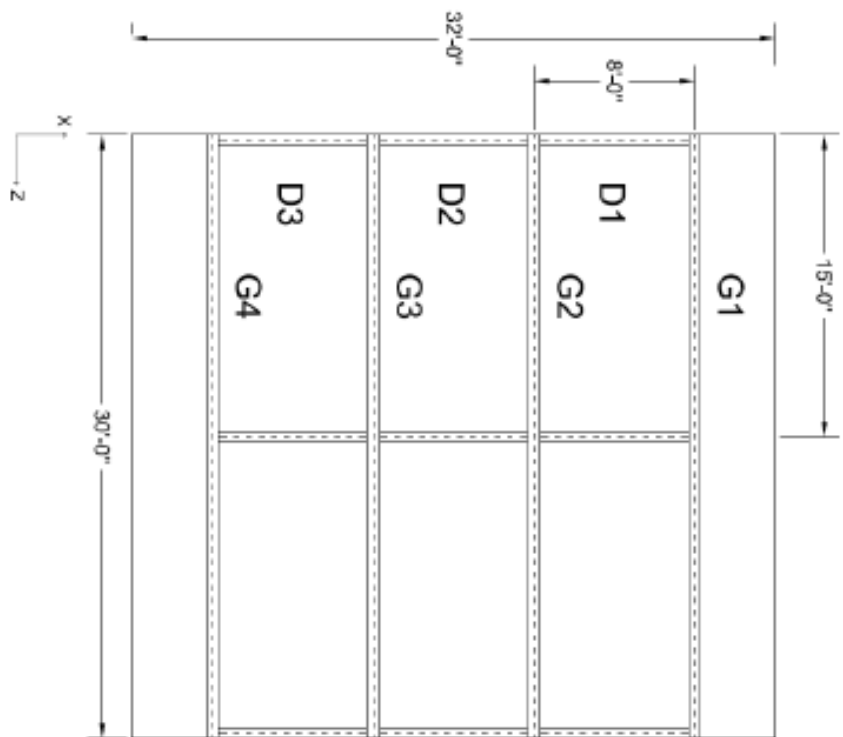


FIGURE 3-2: SCHEMATIC DIAGRAM OF 30-FT BRIDGE GIRDERS AND DIAPHRAGMS

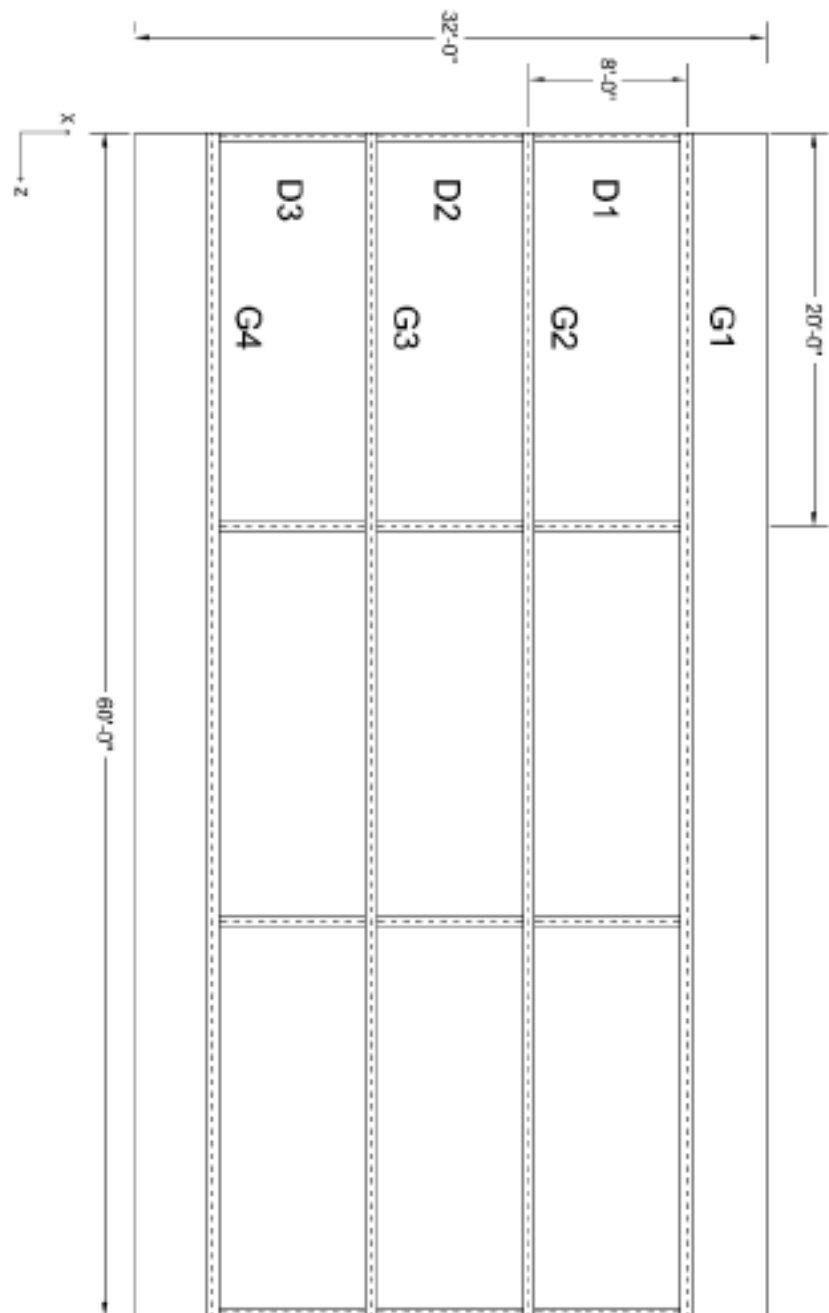


FIGURE 3-3: SCHEMATIC DIAGRAM OF 60-FT BRIDGE GIRDERS AND DIAPHRAGMS

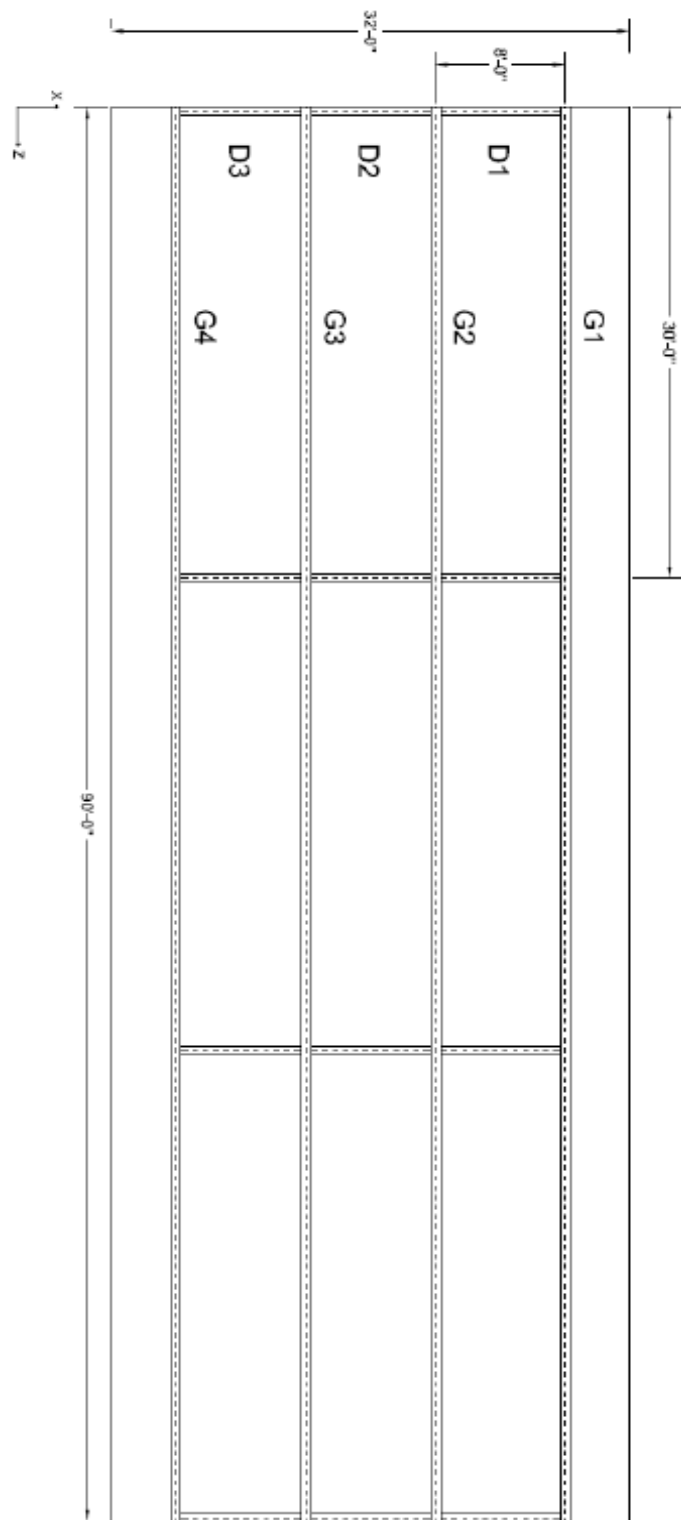


FIGURE 3-4: SCHEMATIC DIAGRAM OF 90-FT BRIDGE GIRDERS AND DIAPHRAGMS

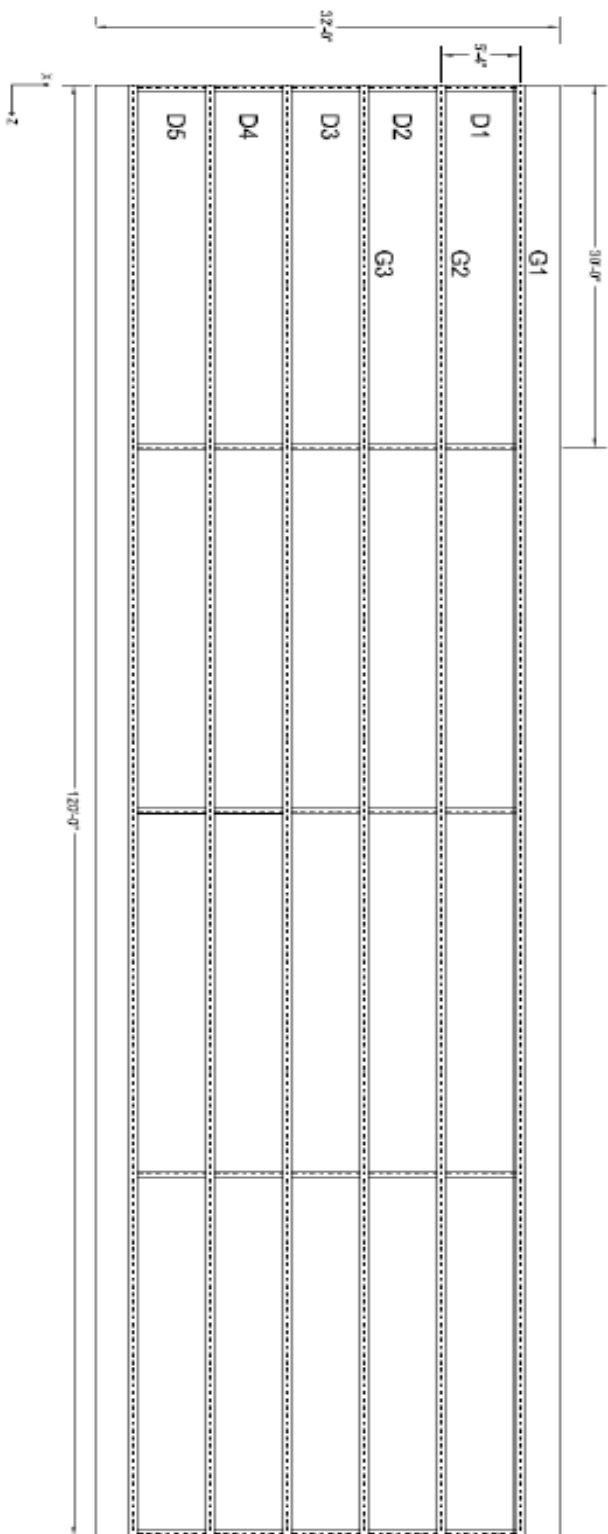


FIGURE 3-5: SCHEMATIC DIAGRAM OF 120-FT BRIDGE GIRDERS AND DIAPHRAGMS

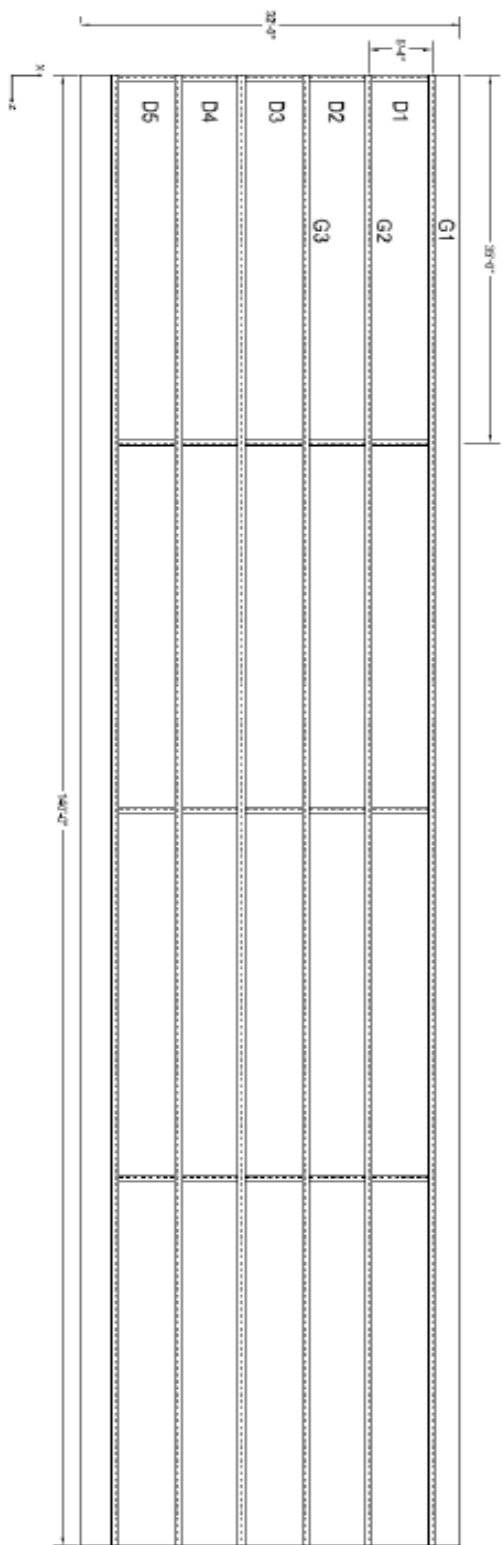


FIGURE 3-6: SCHEMATIC DIAGRAM OF 140-FT BRIDGE GIRDERS AND DIAPHRAGMS

3.5 Steel Type Bridge

Steel girder bridges of 32 ft total width and Five simply supported bridges of spans 30, 60, 90, 120, and 140 ft., with a roadway width of 24 ft. and concrete deck thickness of 6 to 9 in, were analyzed. Table 3.1and Figure 3.6 illustrate the bridge type, girder dimensions, and diaphragm sections and spacing.

TABLE 3-1: STEEL BRIDGES' CONFIGURATIONS

Span (ft)	Girder Section	Diaphragm Section	Diaphragm Spacing (ft)	Slab Thickness (in)
30	W16x57	W10x30	15	6
60	W16x77	W16x77	20	6
90	W30x292	W21x101	30	6
120	W40x392	W24x131	30	6
140	W40x431	W24x131	35	6

As shown in Figure 3.7, the provision of shear-connector between the deck and girders allowed the two structures to work together. Since the concrete deck and steel girders resist applied loads simultaneously, both applied stresses and capacities of sections at the location of maximum load effect were calculated. Accordingly, Table 3.2 shows the bending and shear capacity of girders.

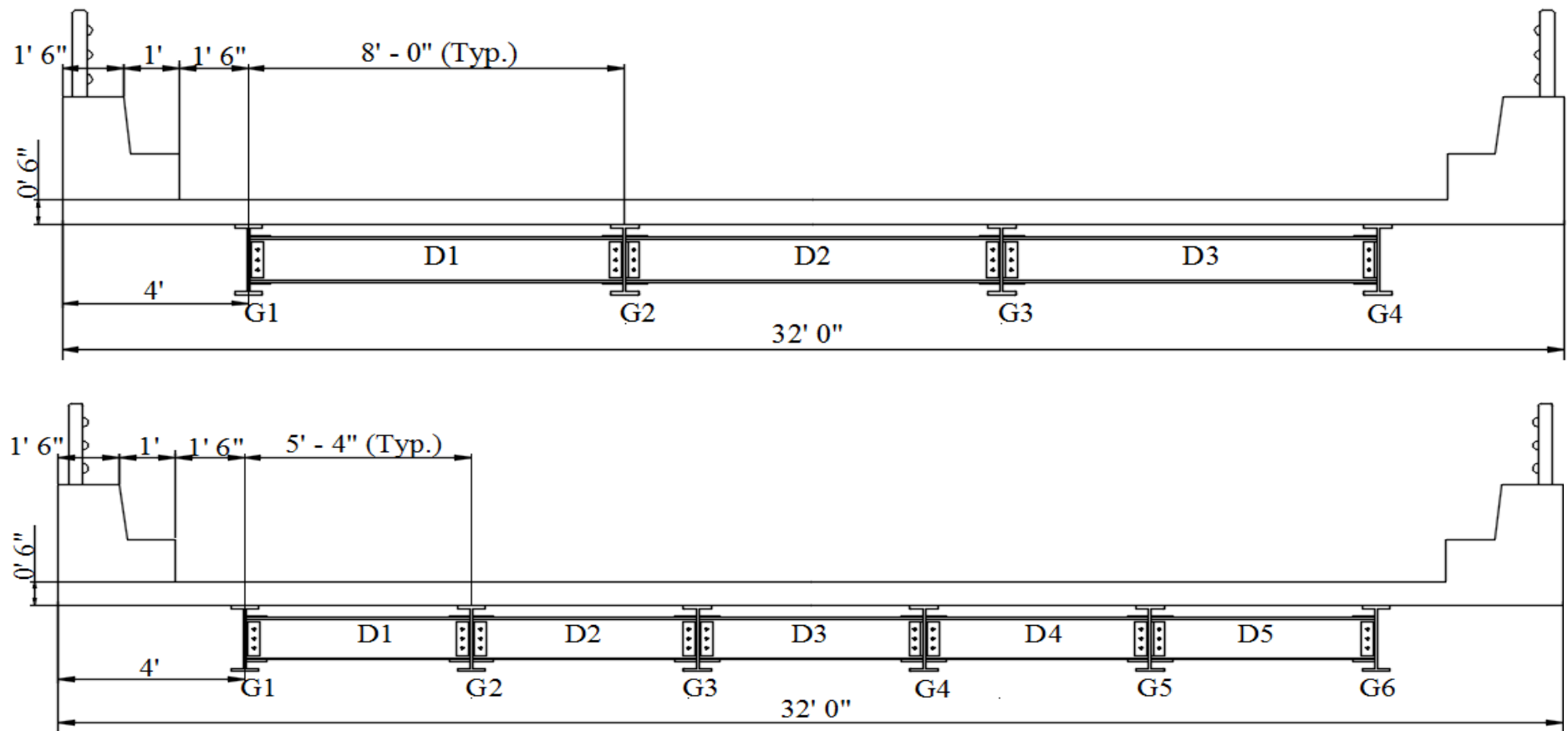


FIGURE 3-7: STEEL GIRDER BRIDGE TYPICAL CROSS SECTION FOR (TOP) 30'-60'-90' (BOTTOM) 120'-140'

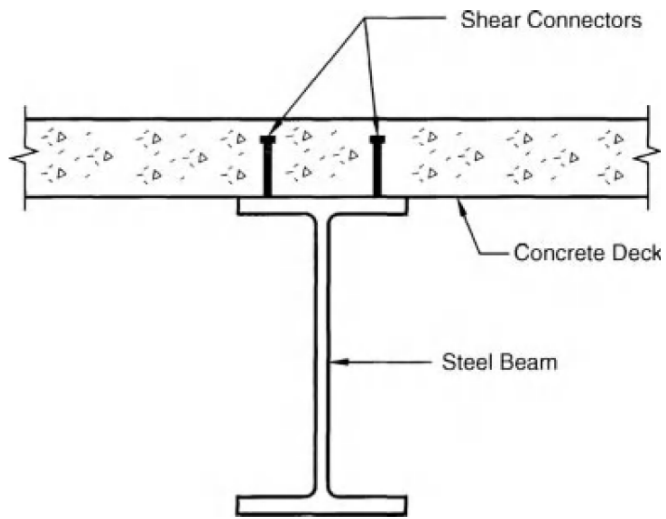


FIGURE 3-8: COMPOSITE SECTION

TABLE 3-2: STEEL GIRDERS MOMENT AND SHEAR CAPACITY

Girder	Length (ft)	Deck thick. (in)	M _n (kip.ft)	V _n (kip)
W16X57	30	6	901	187
W24X146	60	6	2914	425
W30X292	90	6	5763	837
W40X392	120	6	9535	1228
W40X431	140	6	13239	1421

All five bridges were modeled under the application of the predefined trucks (HL-93, 170-kip truck, 85-kip, 97-S, and 97-RB) using CSiBridge and AASHTOWare bridge rating (Virtis) programs. The traffic lane was positioned in the location to induce the maximum flexure, see Figure 3.8 [10].

The induced bending moment by each truck was captured and recorded based on strength-I limit state load factors for dead and live loads ($\gamma_{DC} = 1.25$, $\gamma_{DW} = 1.35$, $\gamma_{LL} = 1.75$) [2].

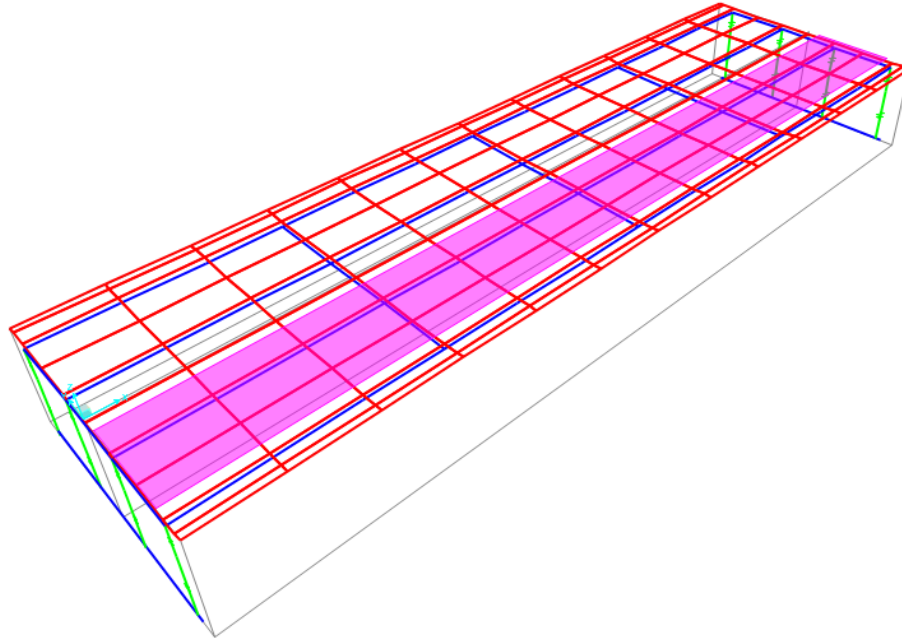


FIGURE 3-9: CRITICAL TRAFFIC LANE POSITION

Figure 3.9 and Figure 3.10 respectively shows the CSiBridge and virtis programs schematic diagram of the modeled structure illustrating the deck, girder and diaphragm arrangement..

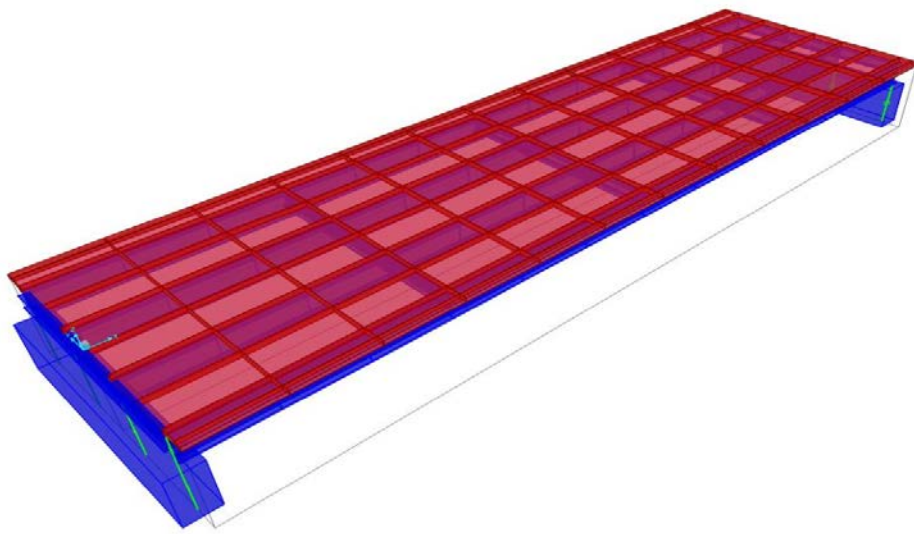
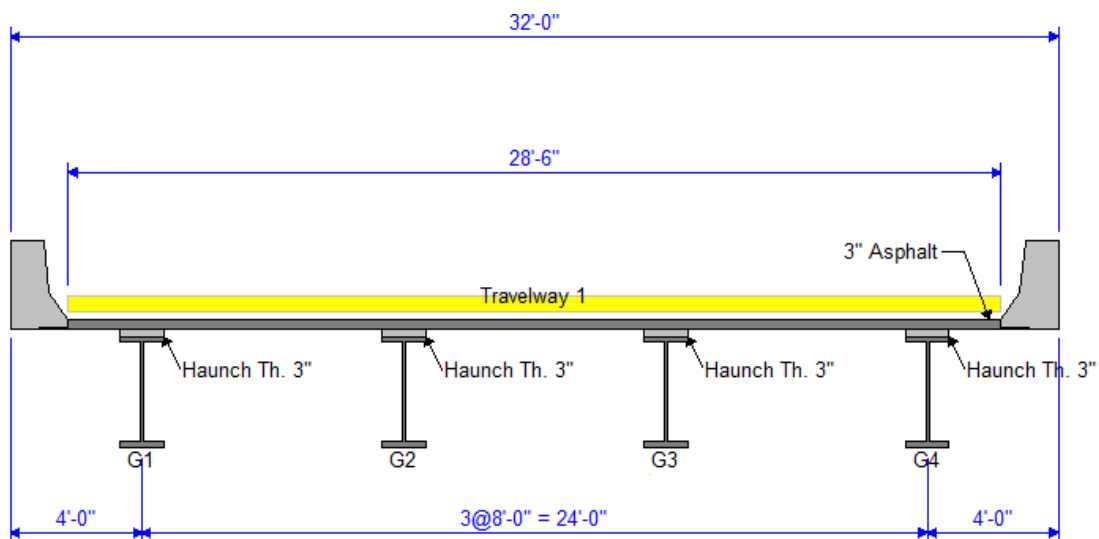


FIGURE 3-10: CSIBRIDGE PROSPECTIVE VIEW



**FIGURE 3-11: AAHTOWARE BRIDGE RATING PROGRAM (VIRTIS)
SCHEMATIC MODEL**

Bending moments of exterior and interior girders have been captured and recorder for different span lengths and live loads, and recorded as shown in Table 3.3 and Table 3.4 CSiBridge and Virtis models respectively. All the recorded data was depicted in Figure 3.11 thru Figure 3.22. These figures show the relationship between the bending moment induced by different truck loads at both interior and exterior bridge girders

and the bending capacity of those girders. Figures show that the exterior girders in most of the cases experience a higher bending moment.

3.5.1 Results and Discussion

In most cases, the bending moment induced in the exterior girder is greater than those induced in the interior girders. Also, for longer bridges ($> 30\text{-ft long}$), the AASHTO LRDF design trucks (28-ft and 44-ft long) develop bending moment greater than that developed under the application of the representative heavy vehicle (170 kip). Moreover, the shorter HL-93 truck (28 ft) induced bending moments greater than those induced under the application of the longer HL-93 truck (44 ft).

All bending moments extracted from the CSiBridge and Virtis models for different spans and trucks were normalized to the girders' moment capacity. The bending moment of lesser weight trucks (85 and 97-kip) have been eliminated because of their relatively low load effect compared to those of heavier trucks (HL-93 and 170-kip). Figure 3.23 and Figure 3.24 show the normalized bending moments of the heaviest trucks (HL-93 and 170 kip truck) in both FE programs. Under the application of the inventory load effect (strength I, $\gamma_p = 1.75$), only the 30-ft-long bridge was unsafe under the effect of the 170-ft truck. As the 170-kip truck is the representative heavy vehicle that may present once in 1000 year, very rare loading case, so the operating load factors ($\gamma_p = 1.35$) were applied. Under these load factors, the unsafe bridge turns to safe as shown in Figure 3.25 and Figure 3.26.

TABLE 3-3: CSIBRIDGE PROGRAM – BENDING MOMENT INDUCED IN EXTERIOR AND INTERIOR GIRDERS

Span (ft)	Bending Moment (kip.ft)											
	HL-93 (28-ft.)		HL-93 (44-ft.)		170-kip		97-S		97-TRB		85-kip	
	Ext.	Int.	Ext.	Int.	Ext.	Int.	Ext.	Int.	Ext.	Int.	Ext.	Int.
30	724.3	734.8	722.0	727.9	945.1	892.8	707.7	688.0	654.2	641.4	624.0	620.5
60	1670.9	1548.7	1466.1	1367.1	1499.7	1344.9	1197.2	1065.6	1059.8	946.9	1085.5	974.8
90	3621.6	3420.2	3416.7	3238.7	3397.6	3000.8	2708.7	2437.5	2359.6	2151.2	2517.8	2281.6
120	7481.2	7442.7	7232.1	7258.9	7029.2	6739.4	5851.5	5713.0	5434.9	5405.8	5567.6	5480.3
140	10628.6	9909.6	10293.4	9711.7	10554.2	8974.0	8515.3	7628.8	7973.0	7279.6	8059.1	7321.5

TABLE 3-4: AASHTOWARE BRIDGE RATING PROGRAM (VIRTIS) – BENDING MOMENT INDUCED IN EXTERIOR AND INTERIOR GIRDERS

Span (ft)	Bending Moment (kip.ft)											
	HL-93 (28-ft.)		HL-93 (44-ft.)		170-kip		97-S		97-TRB		85-kip	
	Ext.	Int.	Ext.	Int.	Ext.	Int.	Ext.	Int.	Ext.	Int.	Ext.	Int.
30	835	742	773	715	914	820	638	572	576	514	542	488
60	2758	2535	2295	2114	2390	2182	1823	1590	1485	1339	1602	1400
90	5382	5037	4940	4577	4721	4222	3474	3129	2841	2547	3128	2825
120	9186	8412	7868	7903	8045	6978	5755	5076	5033	4388	5236	4629
140	11205	11001	11475	10048	10184	8920	7290	6516	6585	5839	6674	5990

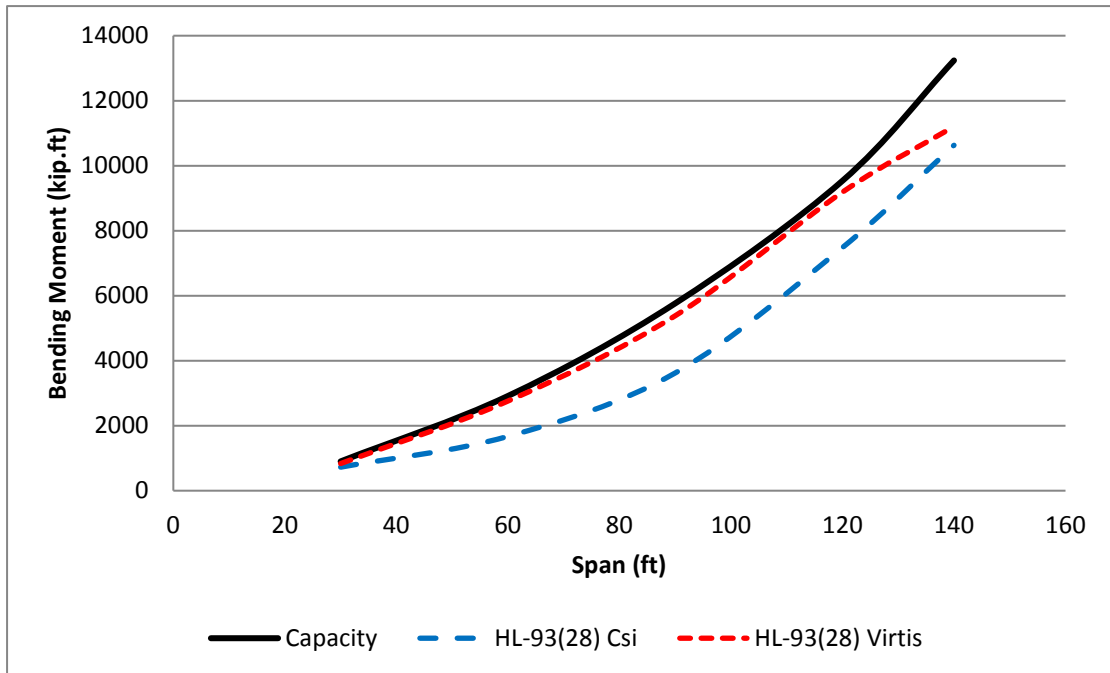


FIGURE 3-12: BENDING MOMENT OF HL-93 (28-FT LONG) AND M_N VS. BRIDGE SPAN – EXTERIOR GIRDER

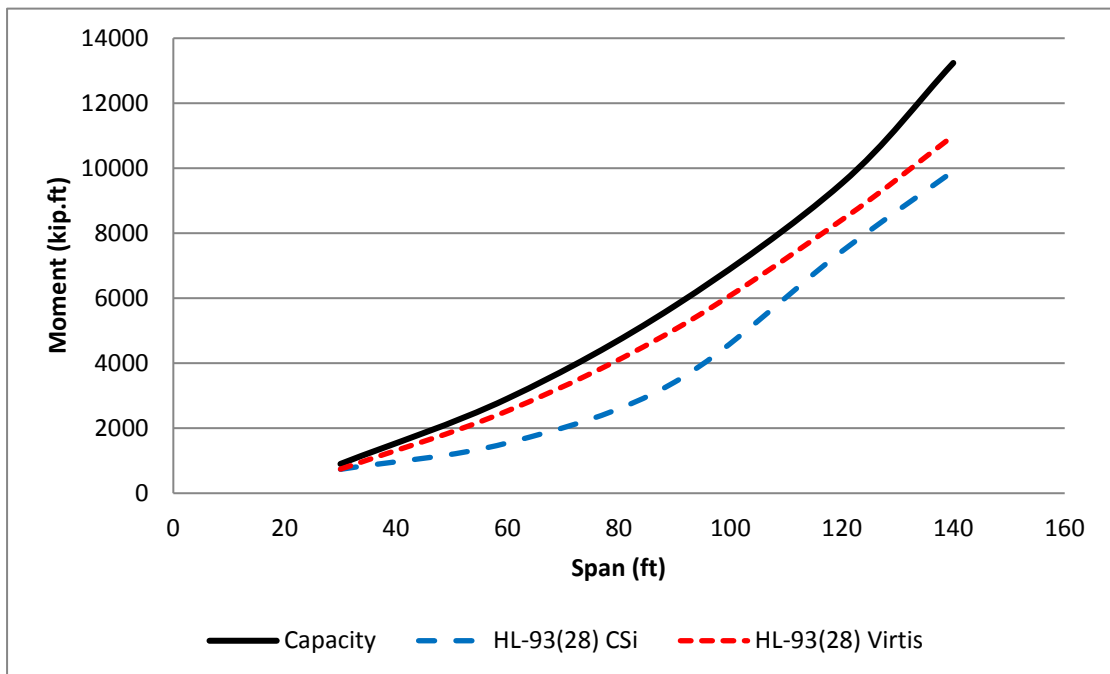


FIGURE 3-13: BENDING MOMENT OF HL-93 (28-FT LONG) AND M_N VS. BRIDGE SPAN – INTERIOR GIRDER

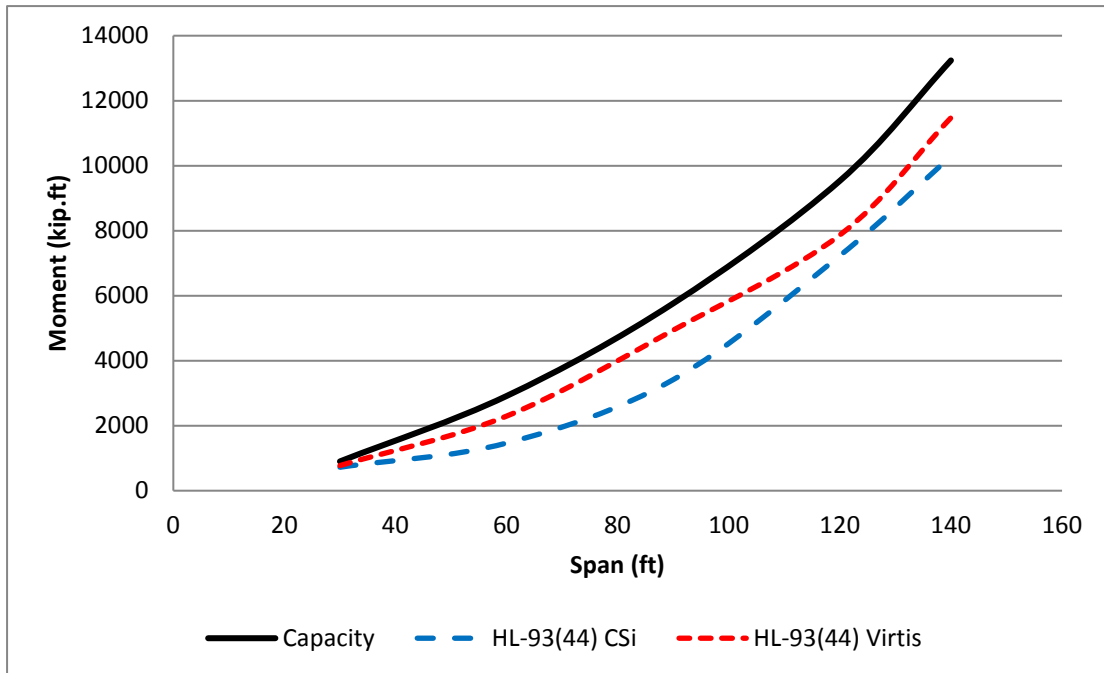


FIGURE 3-14: BENDING MOMENT OF HL-93 (44-FT LONG) AND M_N VS. BRIDGE SPAN – EXTERIOR GIRDER

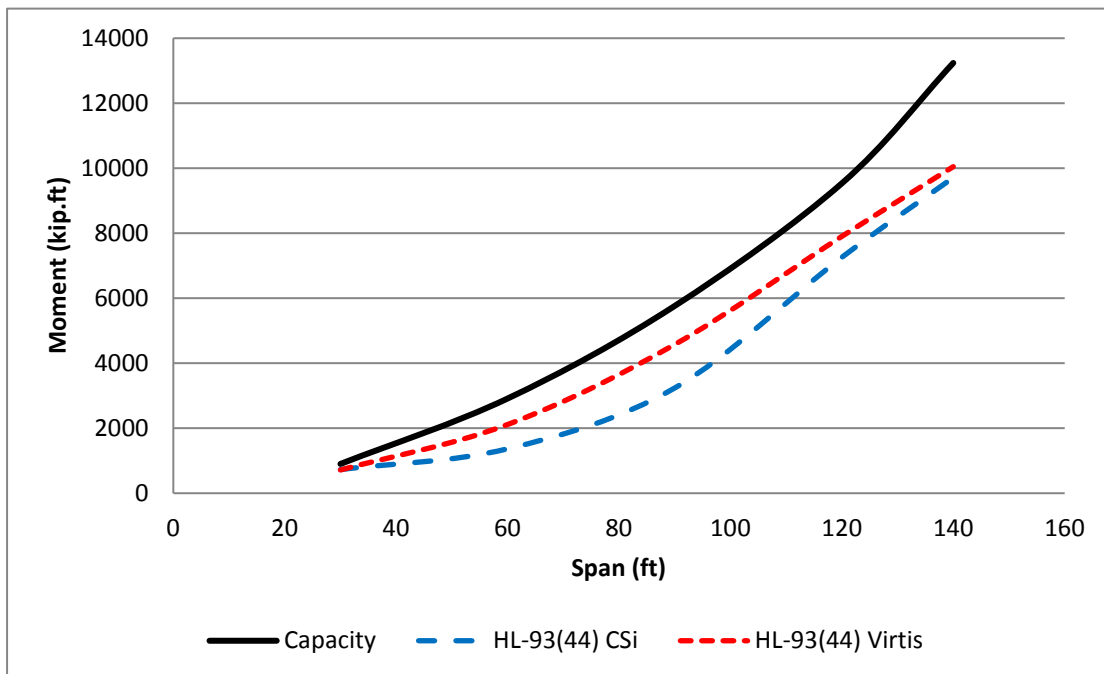


FIGURE 3-15: BENDING MOMENT OF HL-93 (44-FT LONG) AND M_N VS. BRIDGE SPAN – INTERIOR GIRDER

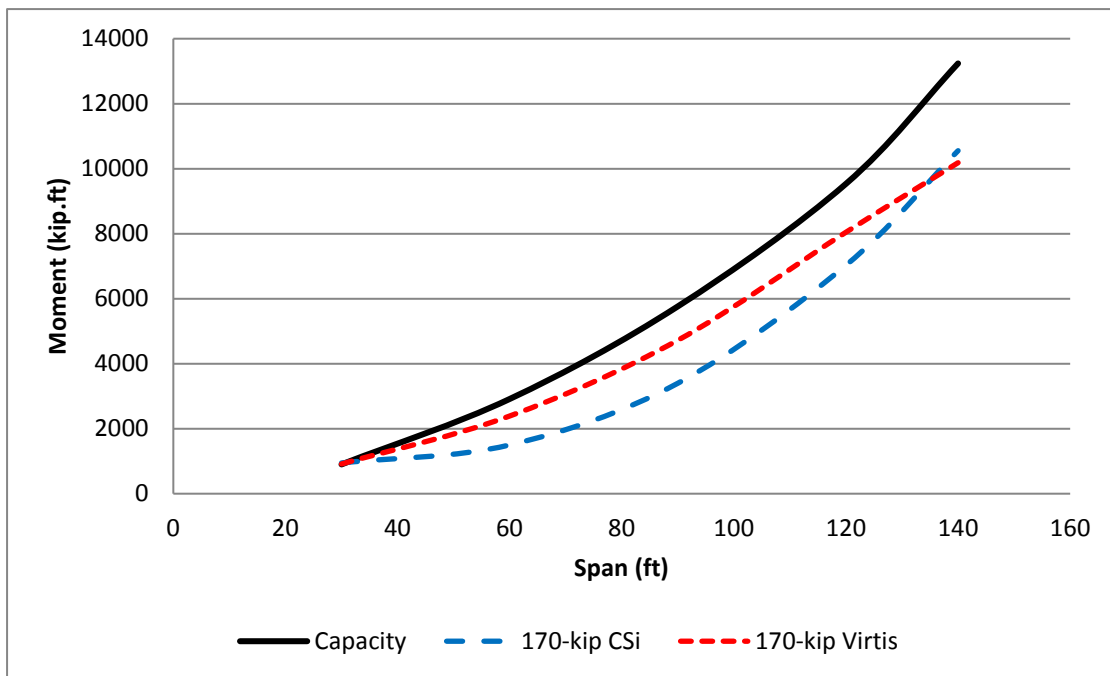


FIGURE 3-16: BENDING MOMENT OF 170-KIP TRUCK AND M_N VS. BRIDGE SPAN – EXTERIOR GIRDER

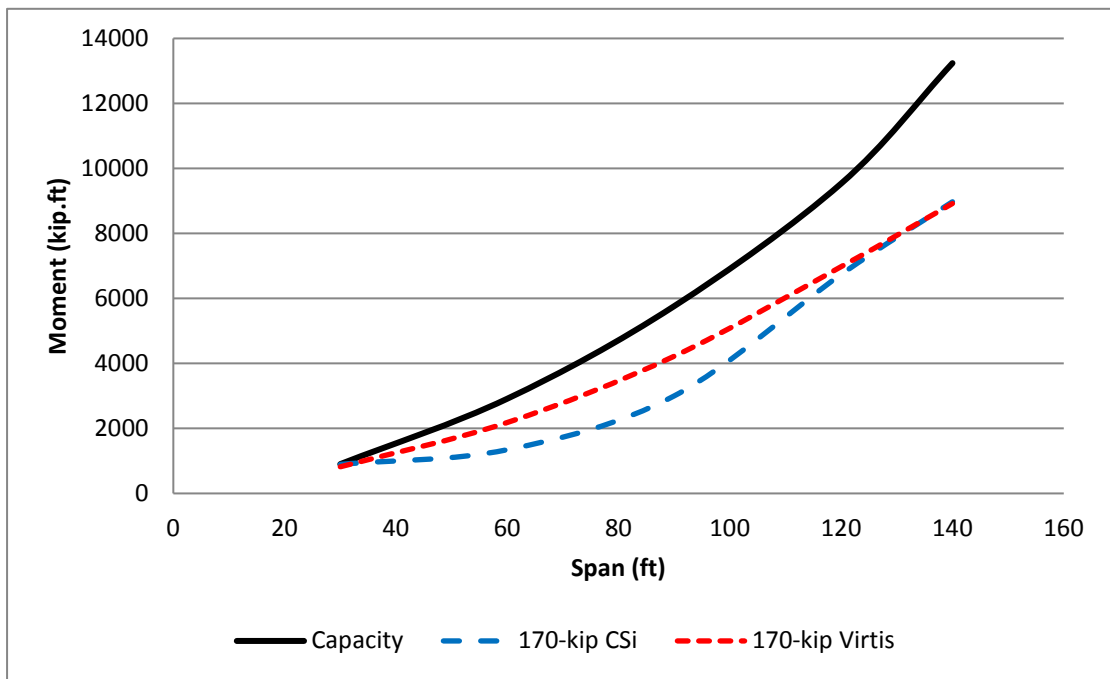


FIGURE 3-17: BENDING MOMENT OF 170-KIP TRUCK AND M_N VS. BRIDGE SPAN – INTERIOR GIRDER

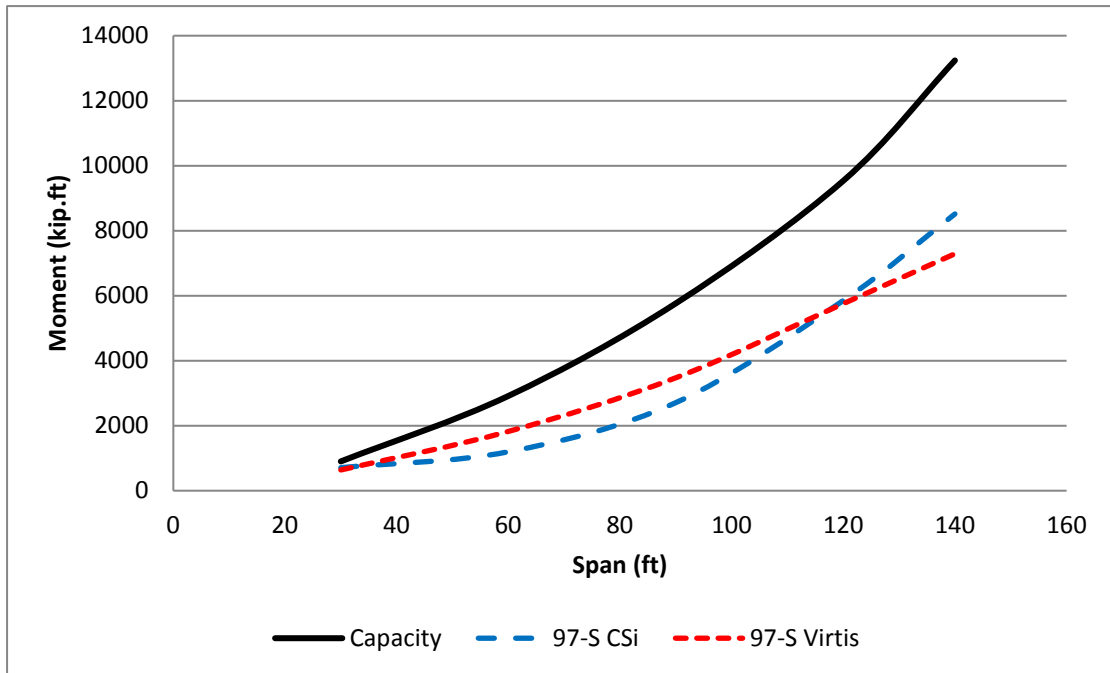


FIGURE 3-18: BENDING MOMENT OF 97-S TRUCK AND M_N VS. BRIDGE SPAN – EXTERIOR GIRDER

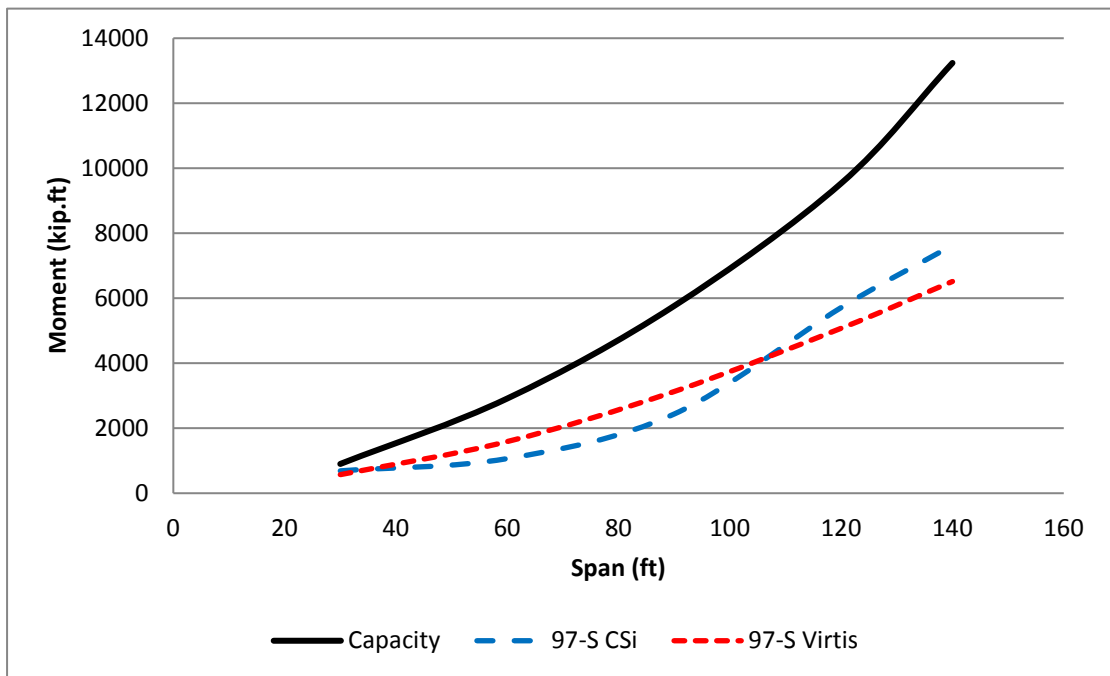


FIGURE 3-19: BENDING MOMENT OF 97-S TRUCK AND M_N VS. BRIDGE SPAN – INTERIOR GIRDER

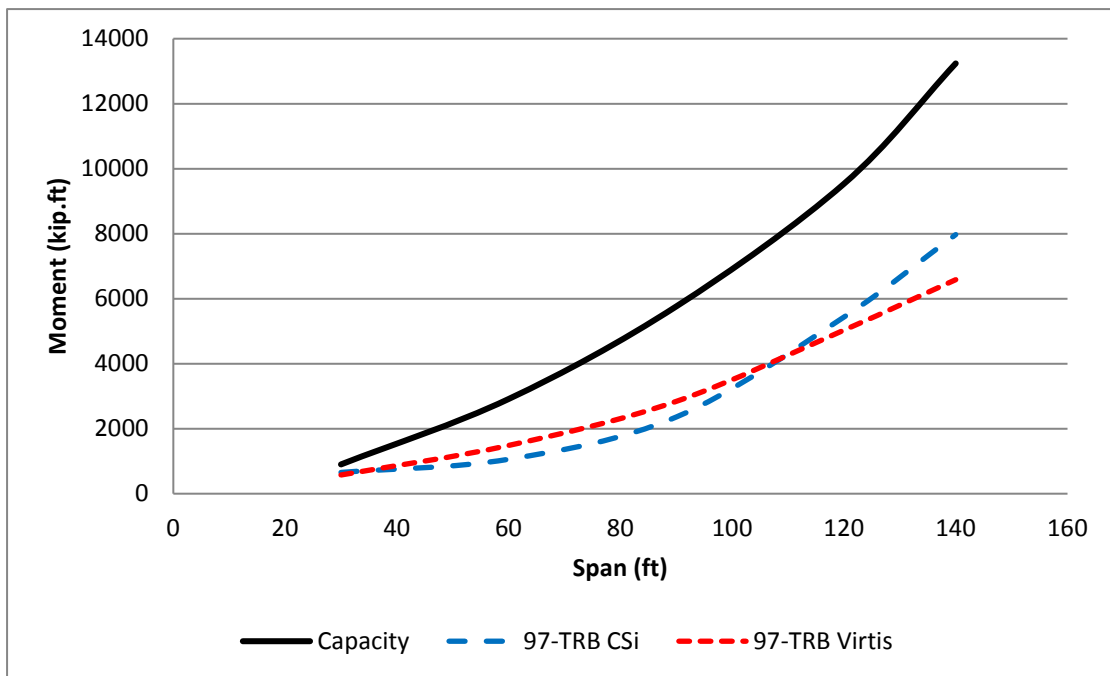


FIGURE 3-20: BENDING MOMENT OF 97-TRB TRUCK AND M_N VS. BRIDGE SPAN – EXTERIOR GIRDER

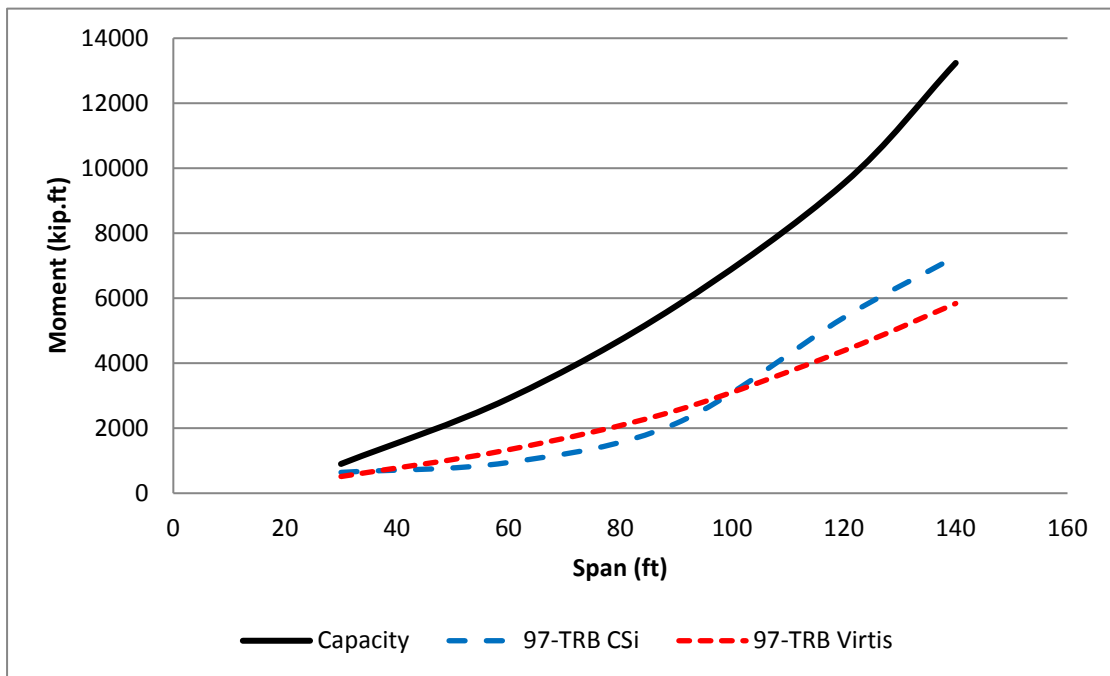


FIGURE 3-21: BENDING MOMENT OF 97-TRB TRUCK AND M_N VS. BRIDGE SPAN – INTERIOR GIRDER

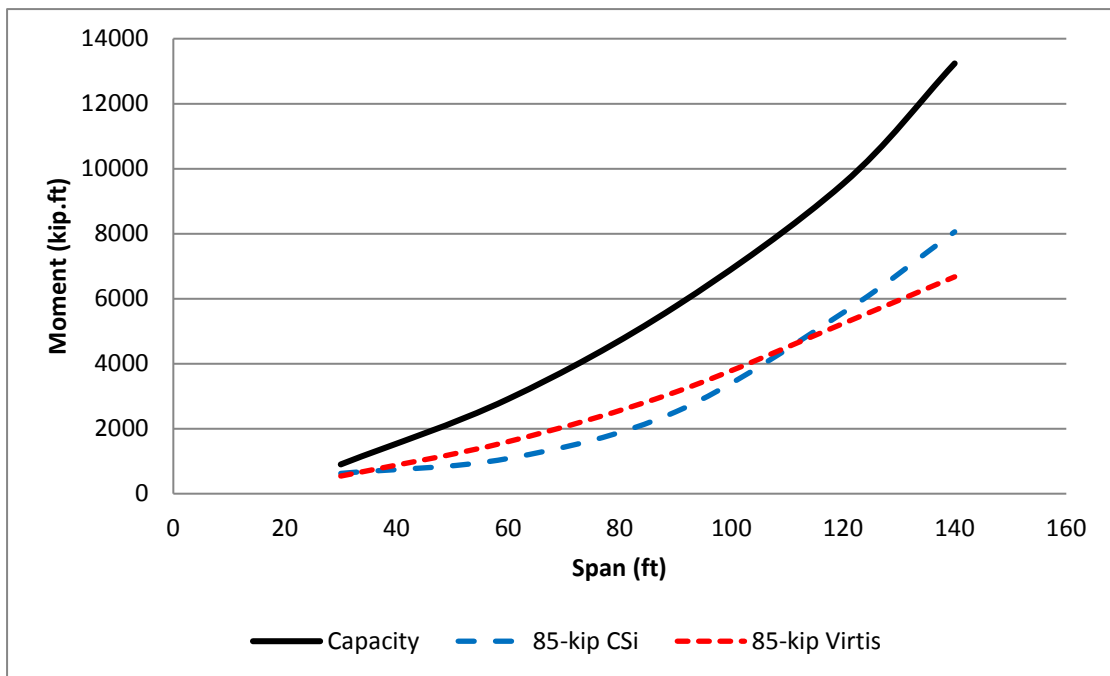


FIGURE 3-22: BENDING MOMENT OF 85-KIP TRUCK AND M_N VS. BRIDGE SPAN – EXTERIOR GIRDER

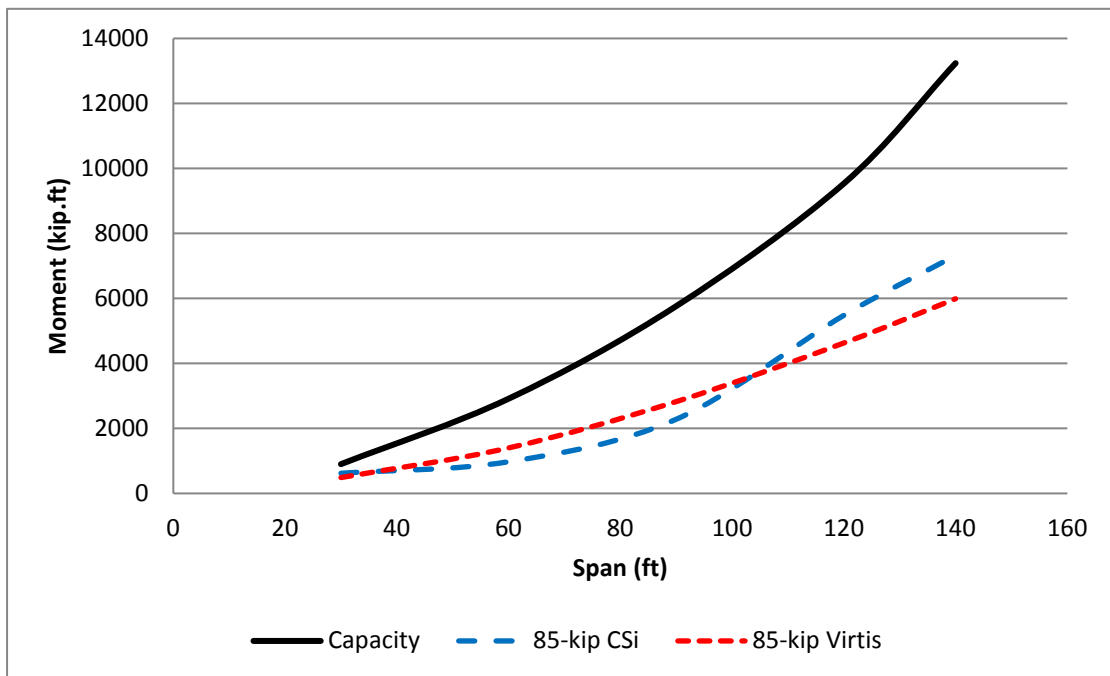


FIGURE 3-23: BENDING MOMENT OF 85-KIP TRUCK AND M_N VS. BRIDGE SPAN – INTERIOR GIRDER

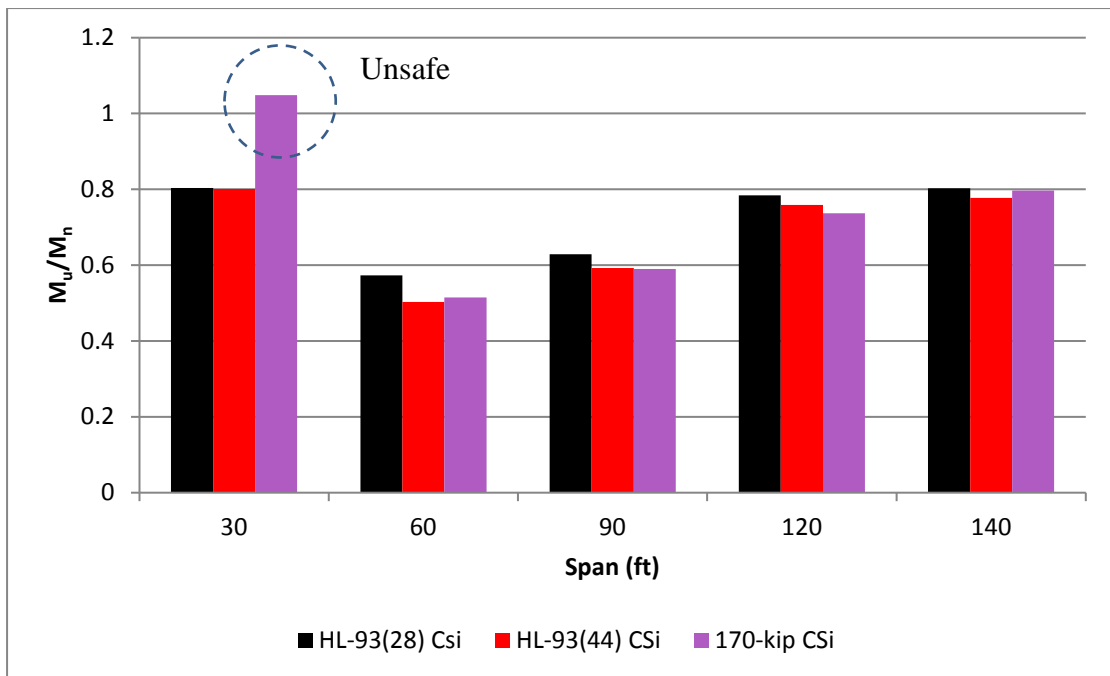


FIGURE 3-24: CSIBRIDGE - EXTERIOR GIRDERS' M_u/M_n VS. SPAN LENGTH - INVENTORY CONDITIONS

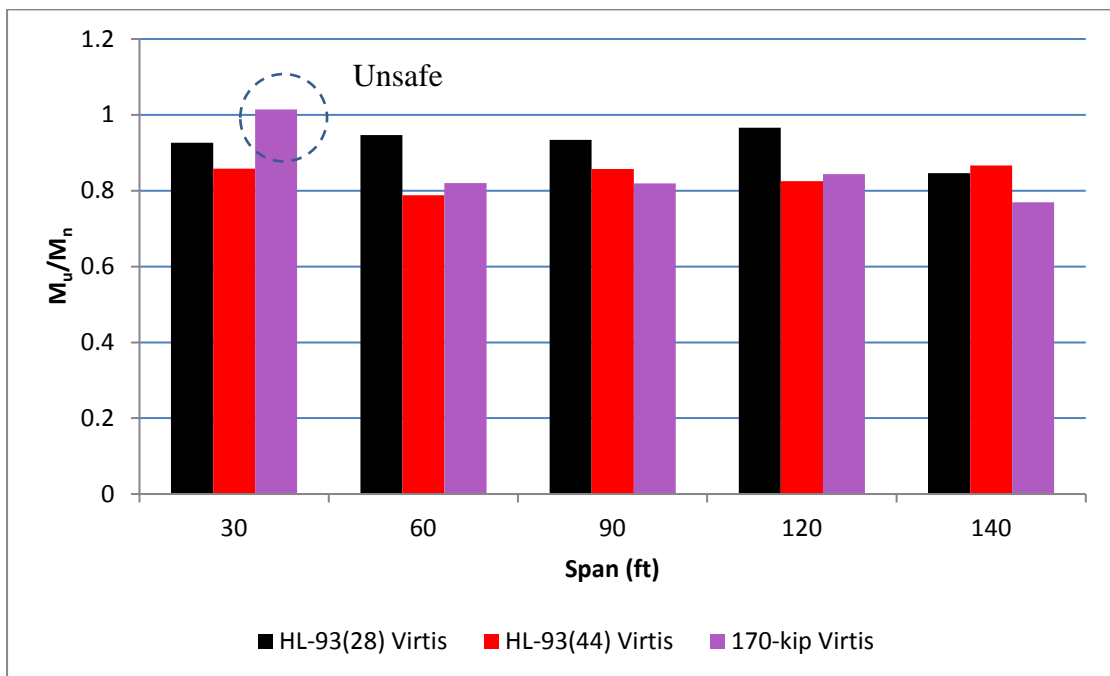


FIGURE 3-25: VIRTIS - EXTERIOR GIRDERS' M_u/M_n VS. SPAN LENGTH - INVENTORY CONDITIONS

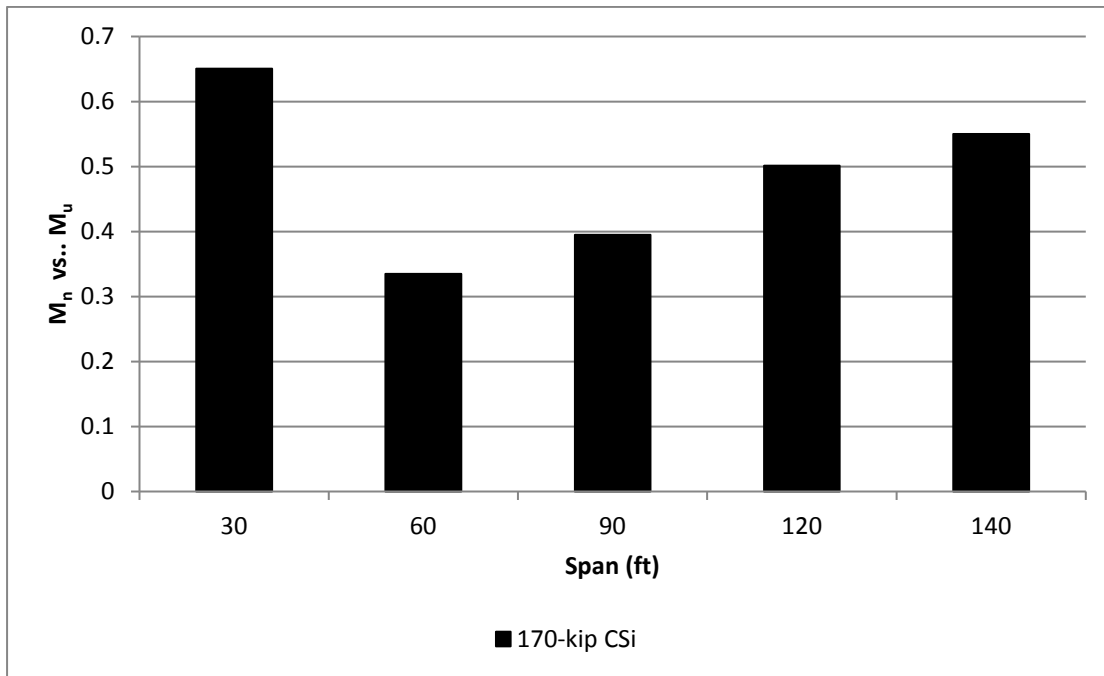


FIGURE 3-26: CSIBRIDGE – EXTERIOR GIRDERS' M_u /M_n VS. SPAN LENGTH - OPERATING CONDITIONS

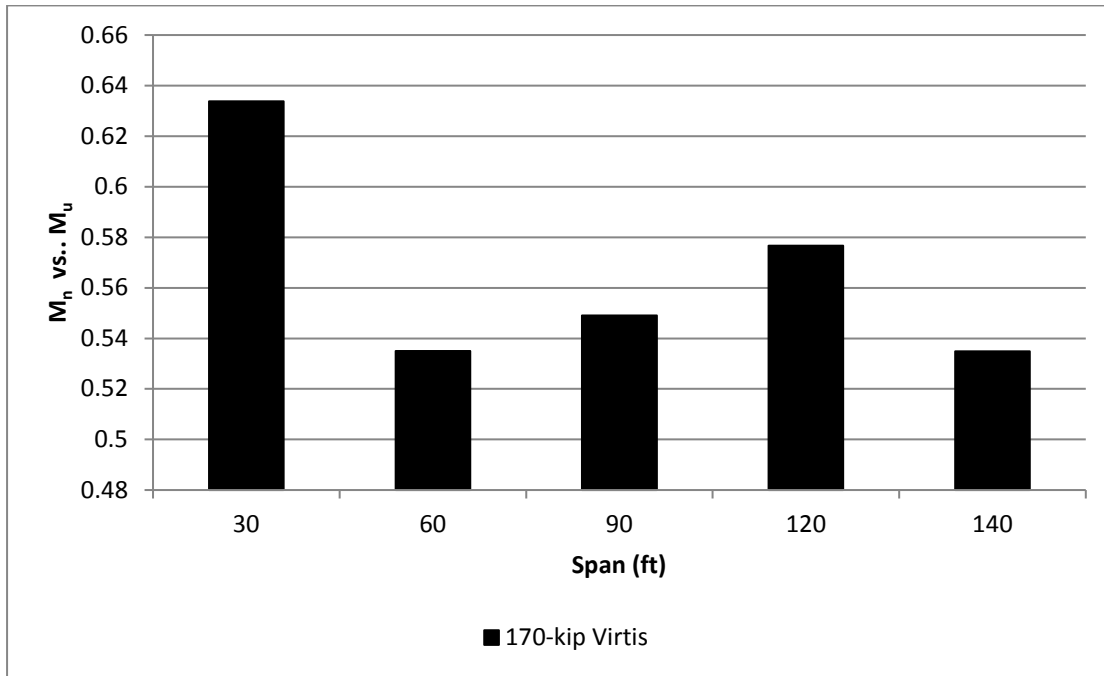


FIGURE 3-27: VIRTIS - EXTERIOR GIRDERS' M_u /M_n VS. SPAN LENGTH - OPERATING CONDITIONS

3.6 Prestressed Girder Type Bridge

Similar to the steel bridge's simulation and analysis, FEM models have been developed to investigate the BM on a concrete bridge of 30, 60, 90, 120, and 140-ft span lengths. The configurations, properties, and capacities of the typical cross section of the bridges and are illustrated in Figure 3.27 thru Figure 3.29, and Table 3.5 and Table 3.7.

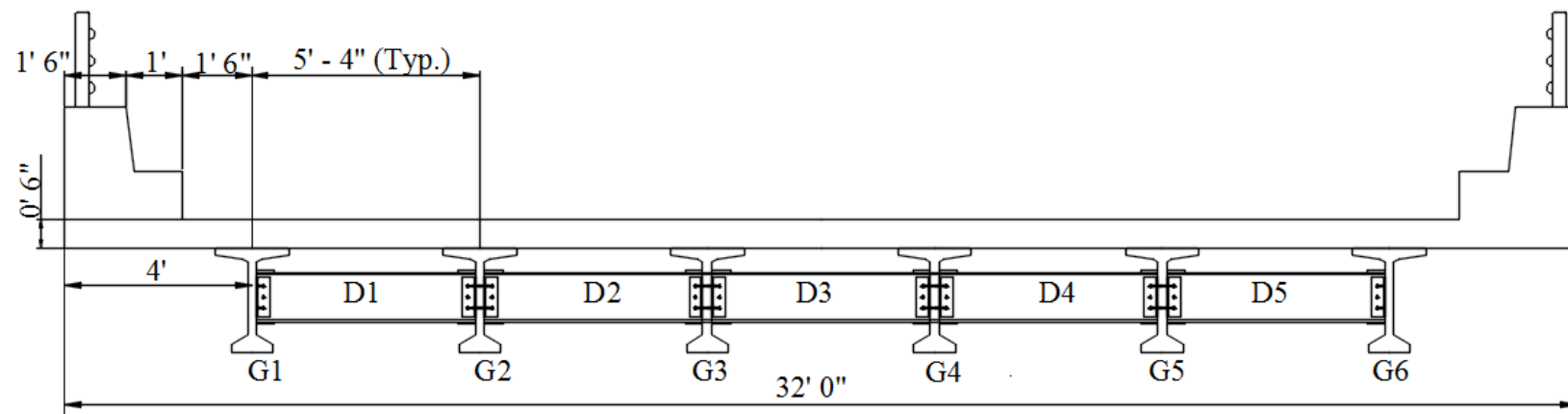
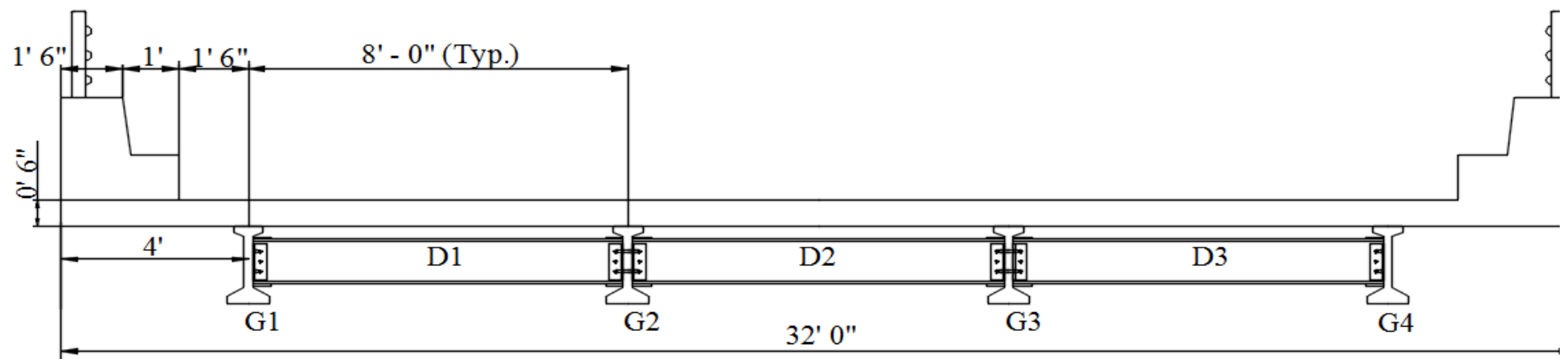
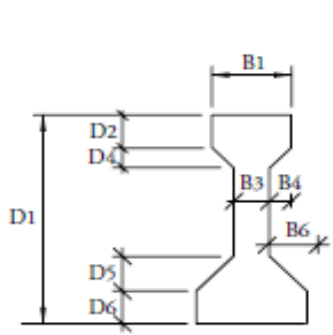


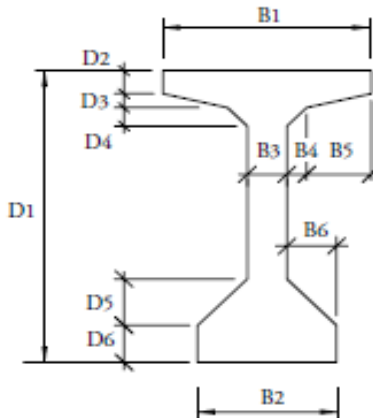
FIGURE 3-28: PSC GIRDER BRIDGE TYPICAL CROSS SECTION FOR (TOP) 30'-60'-90' (BOTTOM) 120'-140'

TABLE 3-5: PRESTRESSED CONCRETE BRIDGE GIRDERS' CONFIGURATION

Span (ft)	Girder Sec.	Diaph. Sec.	Diaph. Spacing (ft)	No. of Strands	No. of Harped Strands	Slab Th. (in)	Concrete f'_c (psi)	Moment Capacity (kip.ft)
30	III	W10X30	15	12	4	8	5000	2041
60	III	W16X77	20	20	6	8	5000	3274
90	V	W21X101	30	32	6	8	5000	7049
120	VI	W24X131	30	38	8	9	6000	9429
140	VI	W24X131	35	56	10	9	6000	13203



Type I-IV



Type V-VI

FIGURE 3-29: TYPICAL AASHTO I-GIRDERS

TABLE 3-6: DIMENSIONS OF AASHTO I-GIRDER (INCHES)

Type	D1	D2	D3	D4	D5	D6	B1	B2	B3	B4	B5	B6
III	45.0	7.0	0.0	4.5	7.5	7.0	16.0	22.0	7.0	4.5	0.0	7.5
V	63.0	5.0	3.0	4.0	10.0	8.0	42.0	28.0	8.0	4.0	13.0	10.0
VI	72.0	5.0	3.0	4.0	10.0	8.0	42.0	28.0	8.0	4.0	13.0	10.0

TABLE 3-7: PROPERTIES OF AASHTO I-GIRDER

Type	Area (in ²)	Y _{bottom} (in)	Inertia (in ⁴)	Weight (kip/ft)	Max. Span (ft)
III	560	20.27	125,390	0.583	100
V	1013	31.96	521,180	1.055	145
VI	1085	36.38	733,320	1.130	167

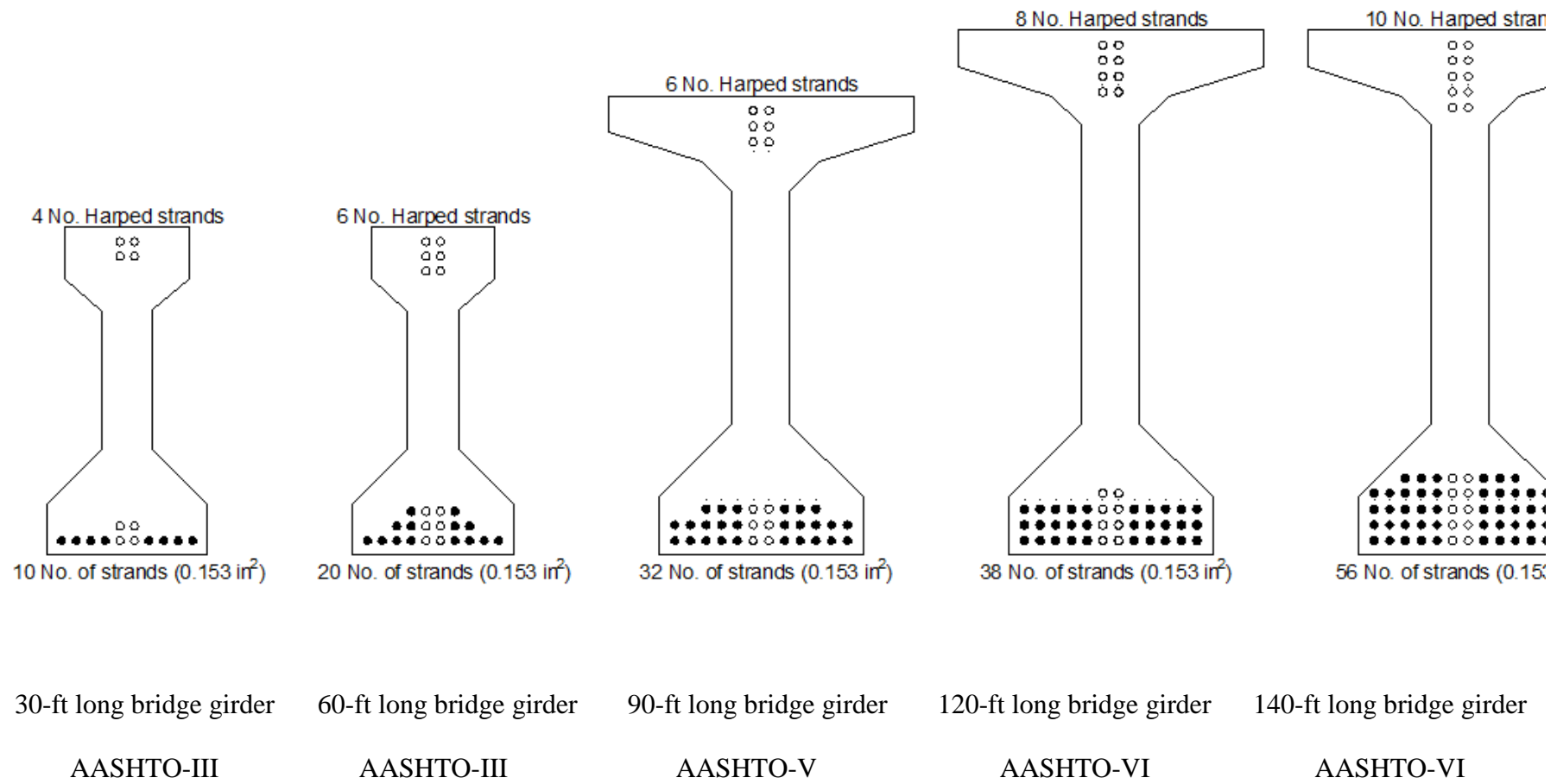


FIGURE 3-30: GIRDERS PRESTRESSING STRANDS' CONFIGURATIONS

TABLE 3-8: CSIBRIDGE PROGRAM – BENDING MOMENT INDUCED IN EXTERIOR AND INTERIOR GIRDERS

Span (ft)	Bending Moment (kip.ft)											
	HL-93 (28-ft.)		HL-93 (44-ft.)		170-kip		97-S		97-TRB		85-kip	
	Ext.	Int.	Ext.	Int.	Ext.	Int.	Ext.	Int.	Ext.	Int.	Ext.	Int.
30	719	555	614	492	837	603	639	455	595	482	579	457
60	2092	1759	1810	1777	2301	1807	1877	1390	1674	1525	1730	1430
90	4639	4090	4362	4536	5229	4284	4228	3392	3884	3690	4091	3530
120	9163	8053	8065	8059	8860	7548	7431	6294	6996	6582	6866	6359
140	10340	9569	10080	11580	11263	9782	9085	8581	9522	8288	9140	8321

TABLE 3-9: AASHTOWARE BRIDGE RATING PROGRAM (VIRTIS) – BENDING MOMENT INDUCED IN EXTERIOR AND INTERIOR GIRDERS

Span (ft)	Bending Moment (kip.ft)											
	HL-93 (28-ft.)		HL-93 (44-ft.)		170-kip		97-S		97-TRB		85-kip	
	Ext.	Int.	Ext.	Int.	Ext.	Int.	Ext.	Int.	Ext.	Int.	Ext.	Int.
30	1091	1166	1124	1111	1107	1300	842	933	782	850	751	807
60	3206	2886	2983	2686	3063	3116	2477	2409	2182	2080	2268	2166
90	6791	6017	6218	5530	7000	6608	5758	5352	5103	4673	5415	4998
120	8280	7701	7916	7386	8835	8538	7417	7071	6957	6600	7096	6734
140	10950	8696	10592	10110	11824	11408	10015	9579	9570	9116	9633	9183

3.6.1 Results and Discussion

All the captured and recorded value of bending moment was listed in Table 3.8 and Table 3.9. Figure 3.30 thru Figure 3.41 illustrate the extracted BM of exterior and interior girders of those five bridges under the application of the different trucks loads. As in steel bridges, the AASHTO design vehicle (HL-93 28-ft long) developed BM in exterior and interior girders greater than those developed by heavier vehicle (170 kip). Also the Virtis program shows very good results comparing to the CSiBridge program results. Due to the limited variety of prestressed girders, the design of short bridges (<50-ft) as well as the relatively longer bridges (>100-ft) may be over designed. Those figures show also that the optimum design of this set of PSC bridges occurred for bridges of span range 60 to 100 ft.

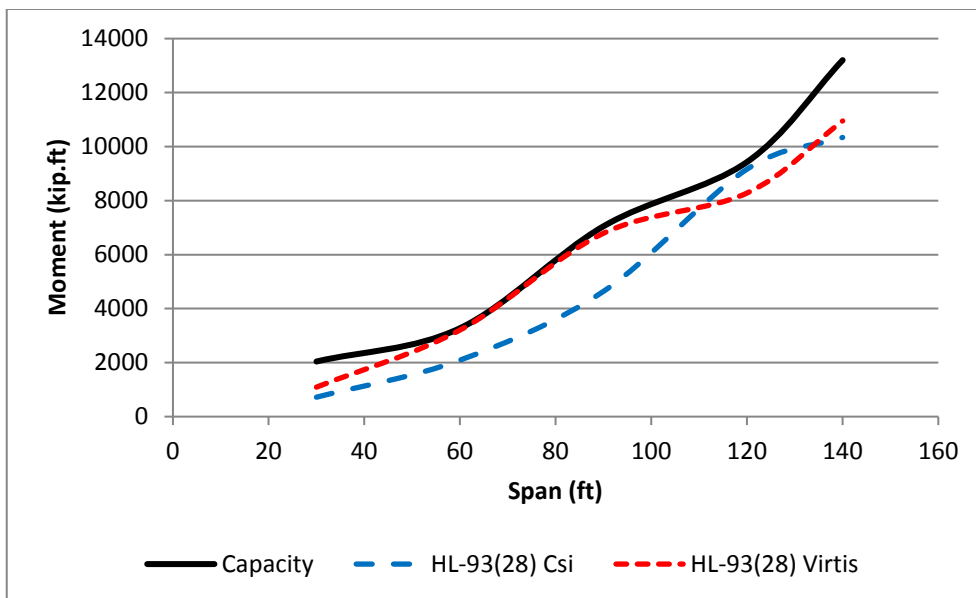


FIGURE 3-31: BENDING MOMENT OF HL-93 (28-FT) TRUCK AND M_N VS. BRIDGE SPAN – EXTERIOR GIRDER

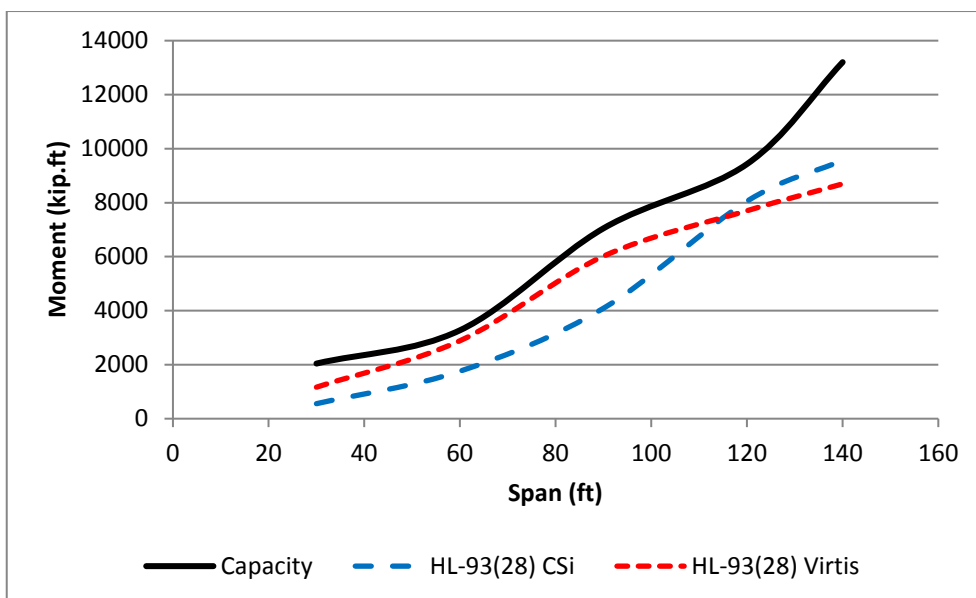


FIGURE 3-32: BENDING MOMENT OF HL-93 (28-FT) TRUCK AND M_N VS. BRIDGE SPAN – INTERIOR GIRDER

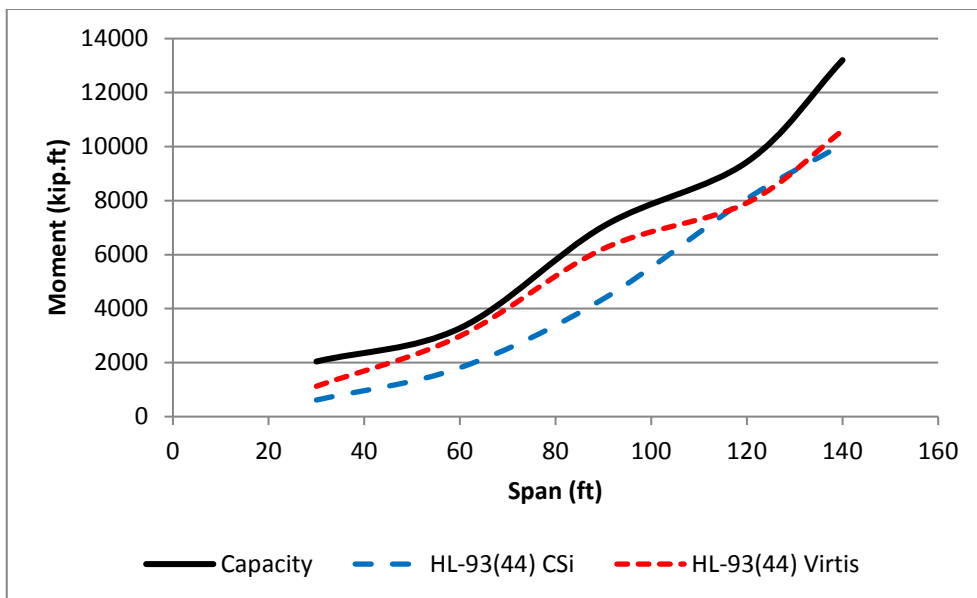


FIGURE 3-33 :BENDING MOMENT OF HL-93 (44-FT) TRUCK AND M_N VS. BRIDGE SPAN – EXTERIOR GIRDER

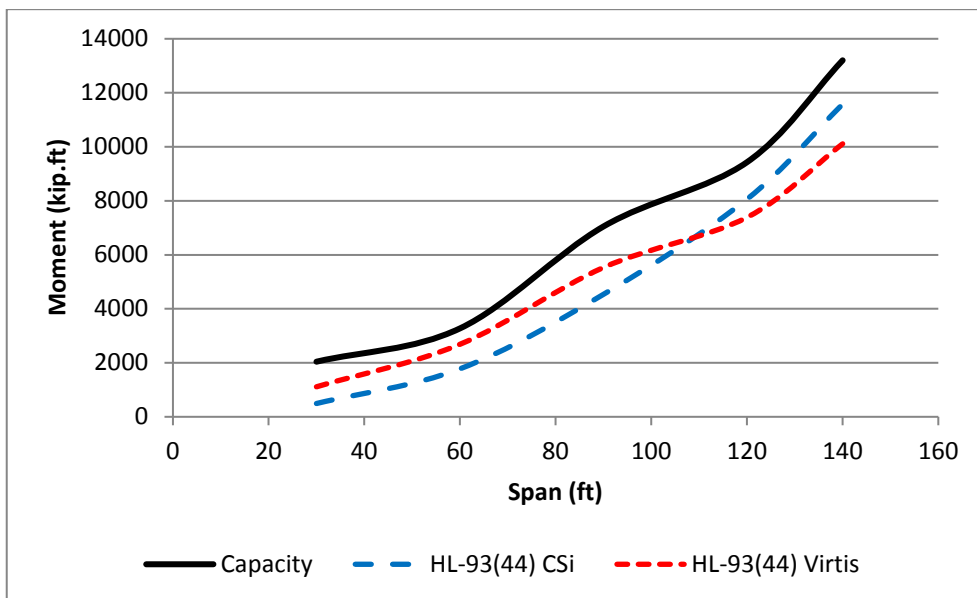


FIGURE 3-34: BENDING MOMENT OF HL-93 (44-FT) TRUCK AND M_N VS. BRIDGE SPAN – INTERIOR GIRDER

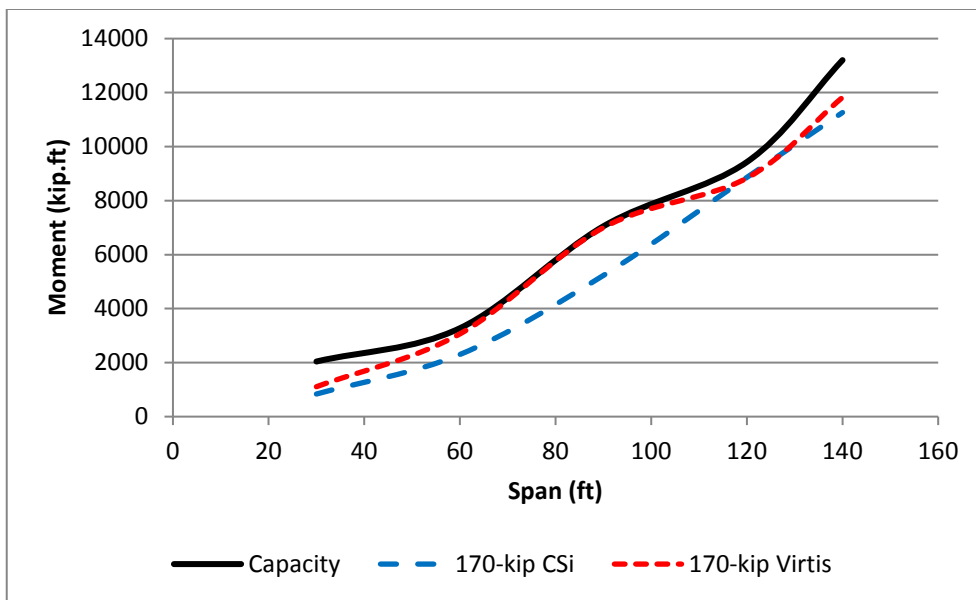


FIGURE 3-35: BENDING MOMENT OF 170-KIP TRUCK AND M_N VS. BRIDGE SPAN – EXTERIOR GIRDER

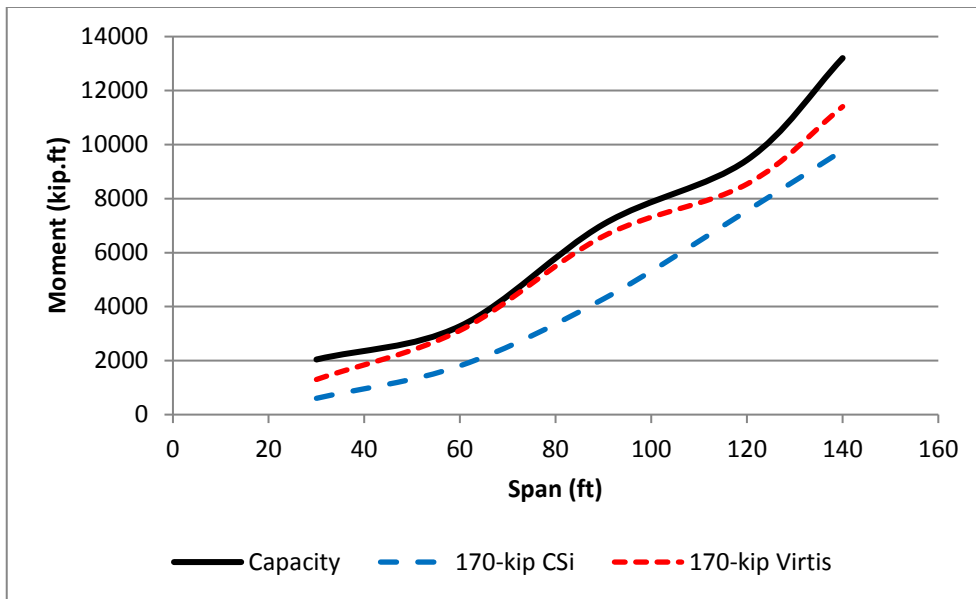


FIGURE 3-36: BENDING MOMENT OF 170-KIP TRUCK AND M_N VS. BRIDGE SPAN – INTERIOR GIRDER

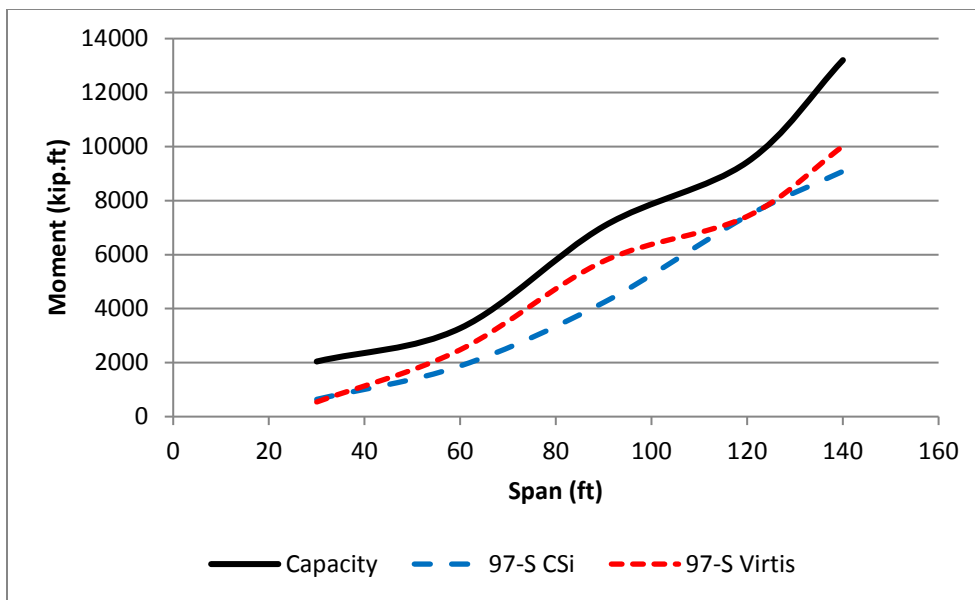


FIGURE 3-37: BENDING MOMENT OF 97-S TRUCK AND M_N VS. BRIDGE SPAN – EXTERIOR GIRDER

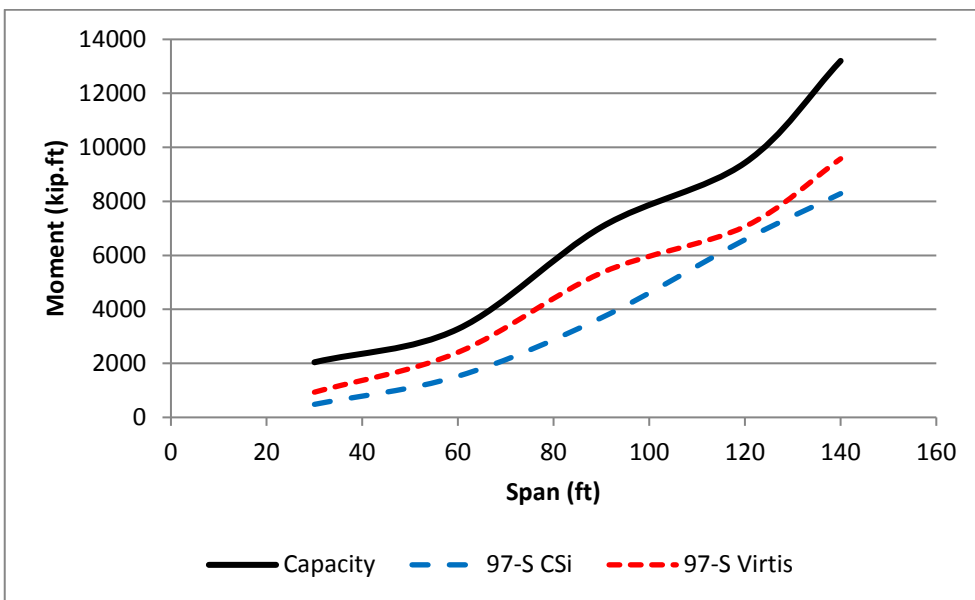


FIGURE 3-38: BENDING MOMENT OF 97-S TRUCK AND M_N VS. BRIDGE SPAN – INTERIOR GIRDER

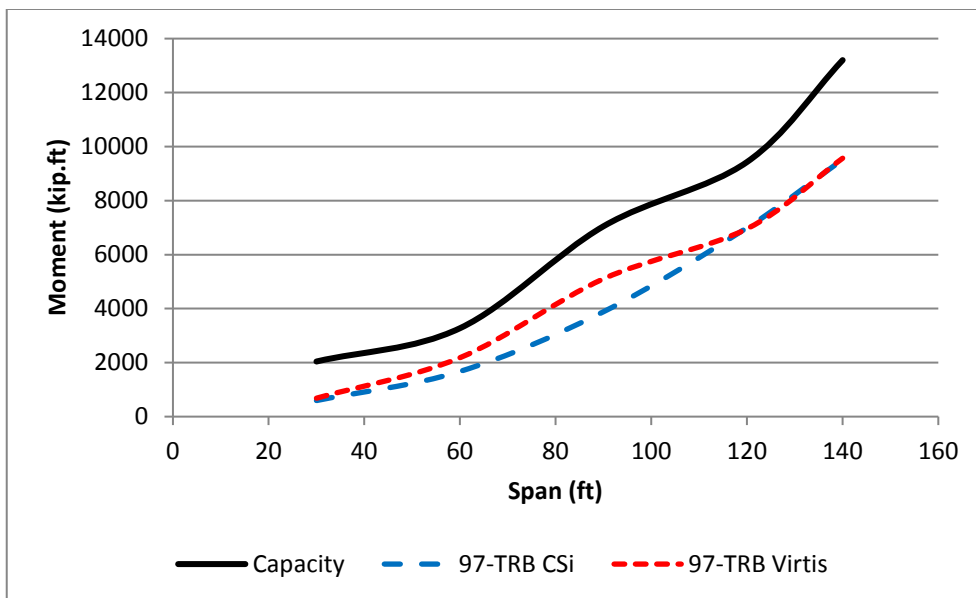


FIGURE 3-39: BENDING MOMENT OF 97-TRB TRUCK AND M_N VS. BRIDGE SPAN – EXTERIOR GIRDER

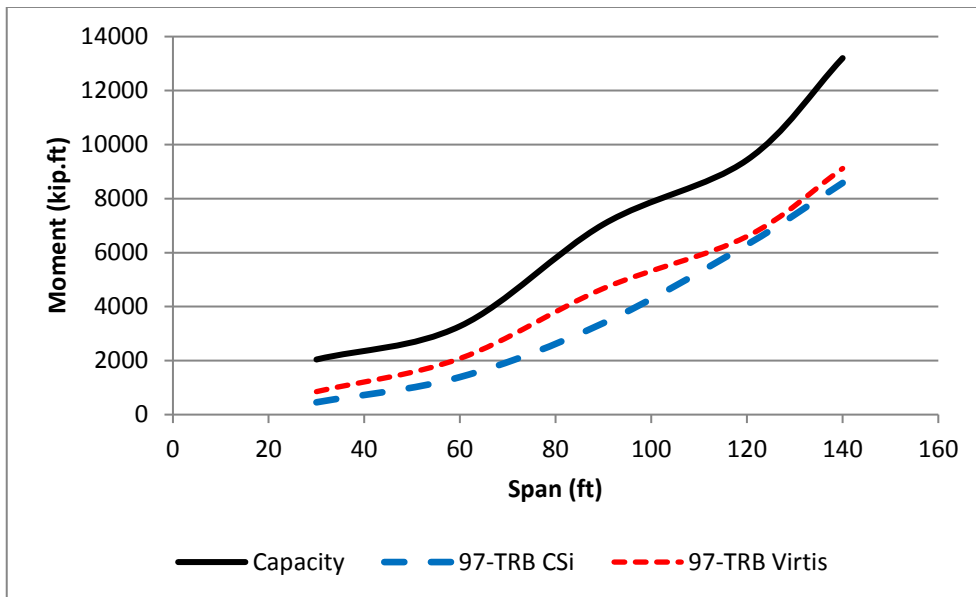


FIGURE 3-40: BENDING MOMENT OF 97-TB TRUCK AND M_N VS. BRIDGE SPAN – INTERIOR GIRDER

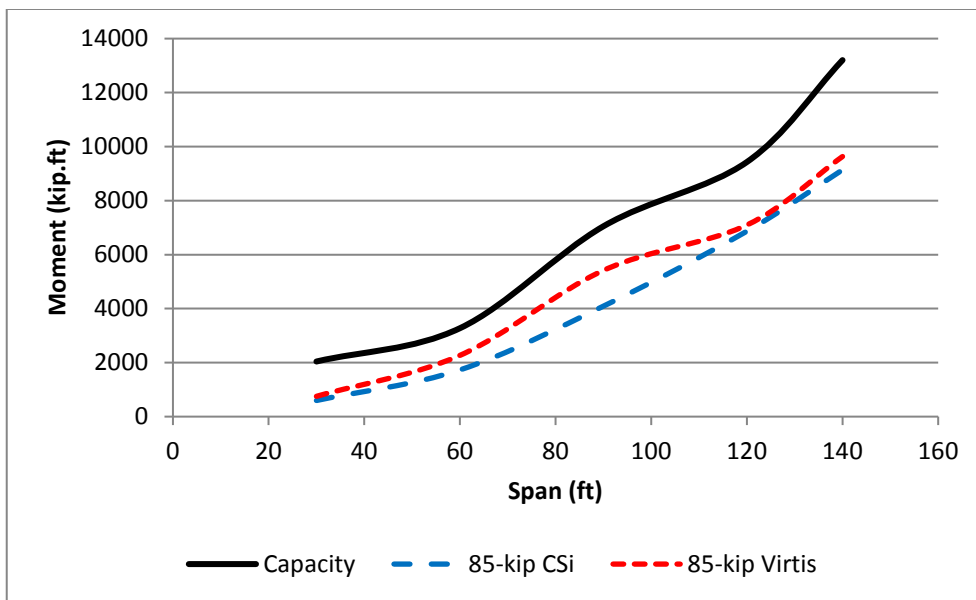


FIGURE 3-41: BENDING MOMENT OF 85-KIP AND M_N VS. BRIDGE SPAN – EXTERIOR GIRDER

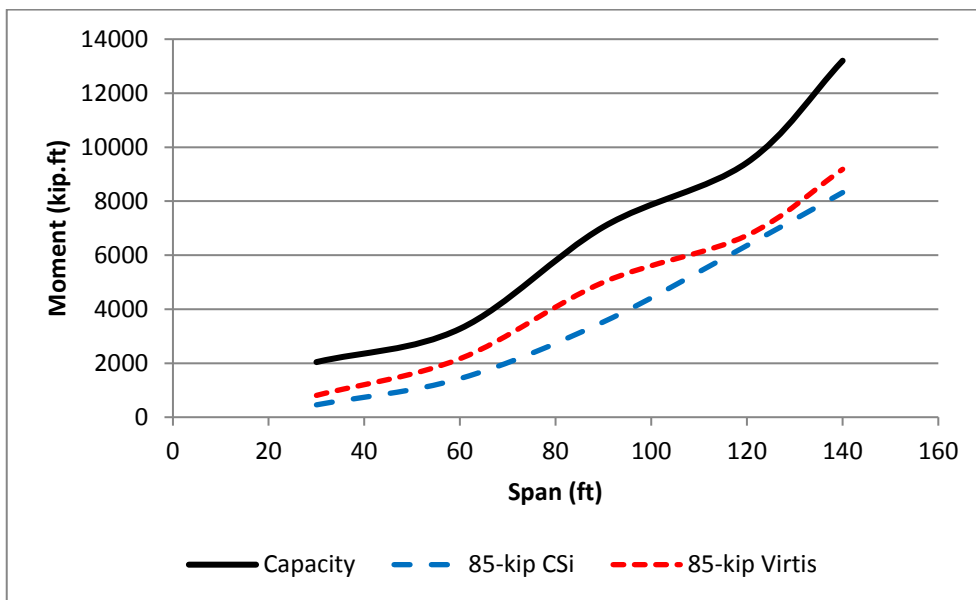


FIGURE 3-42: BENDING MOMENT OF 85-KIP AND M_N VS. BRIDGE SPAN – INTERIOR GIRDER

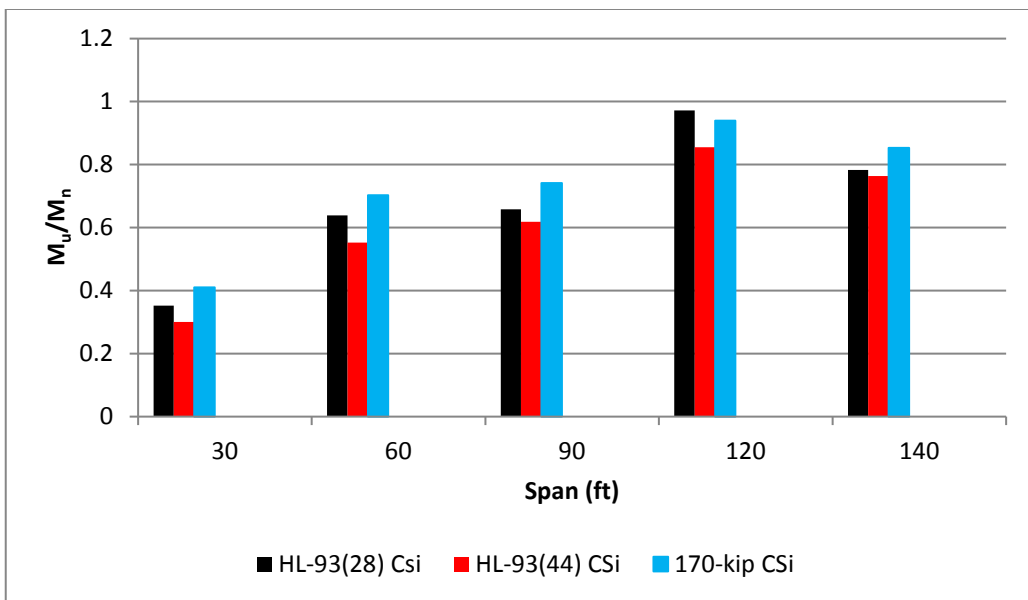


FIGURE 3-43: CSIBRIDGE – EXTERIOR GIRDERS’ M_u/M_n VS. SPAN LENGTH - INVENTORY CONDITIONS

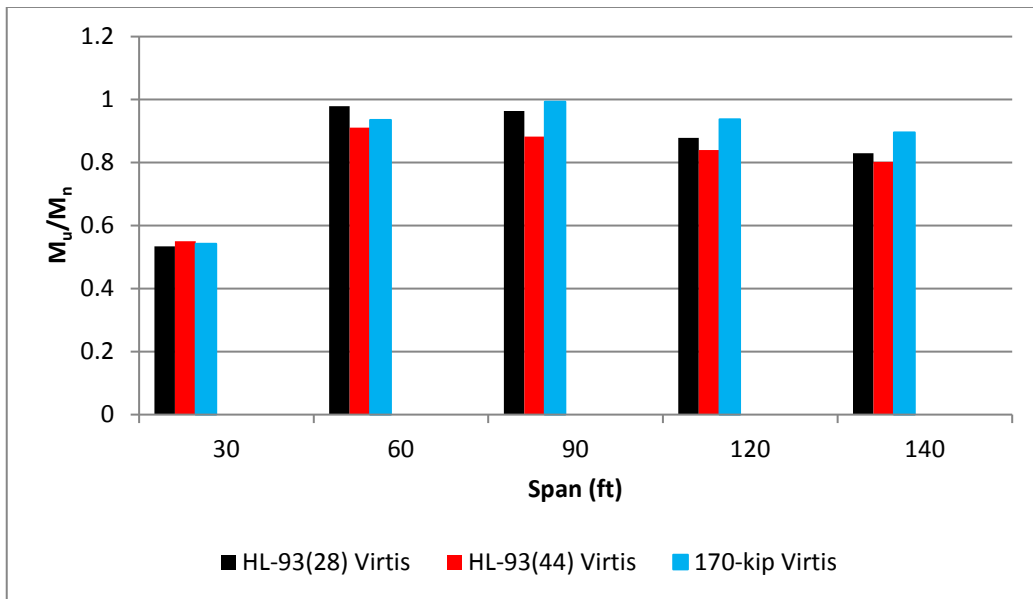


FIGURE 3-44: VIRTIS - EXTERIOR GIRDERS’ M_u/M_n VS. SPAN LENGTH - INVENTORY CONDITIONS

3.7 Bridge-Vehicle Interaction and Numerical Methods

Designed bridges in the previous two sections are modeled as grillage beam systems. The grillage model (also called Grid Model) is a group of beam elements put together as one system. These elements are defined with two nodes as shown in Figure 3.44 and they are connected at their joints.

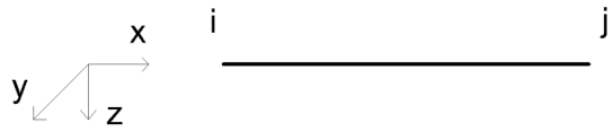


FIGURE 3-45 :GRILLAGE ELEMENT

The node parameters are:

$$\boldsymbol{\delta}^e = \{\boldsymbol{\delta}_i \quad \boldsymbol{\delta}_j\}^T \quad (3.1)$$

Where,

$\boldsymbol{\delta}_i = \{w_{zi} \quad \theta_{xi} \quad \theta_{yi}\}^T$ is the left joint displacement vector.

$\boldsymbol{\delta}_j = \{w_{zj} \quad \theta_{xj} \quad \theta_{yj}\}^T$ is the right joint displacement vector.

w_z is the vertical displacement in the z direction.

θ_x and θ_y are the rotational displacements about the x and y direction, respectively.

Each beam element represents the moment of inertia and torsional stiffness of the girder and the deck above the girder and these elements are usually chosen in a way that they coincide with the girders. The starting and the ending elements are restrained by hinged supports at each node. Since the axial component of the elements or the force along the x-axis is not usually modeled in the grillage model, using hinged or roller supports would not make any difference. The transverse elements are modeled in a manner to represent the flexural and torsional behavior of the concrete deck in the transverse direction but at

the place of the diaphragms, these elements also include the properties of the diaphragm section in addition to the concrete deck. As for the spacing of the transverse elements, they should be around 1.5 to 2 times the distance between the longitudinal members.

Matrix structural analysis method has been used here to model the bridge system. First, the local mass and stiffness matrices of each element are formed and then these matrices are assembled together using the transfer matrices to form the global stiffness and mass matrices. Then the force matrix will be formed based on the degree of freedom in which the load is being applied to and finally the displacements, moments and stresses at each node can be calculated. The deflection of the bridge due to the dead load weight of the bridge is shown in Figure 3.45 for the case of 60 ft. concrete bridge,

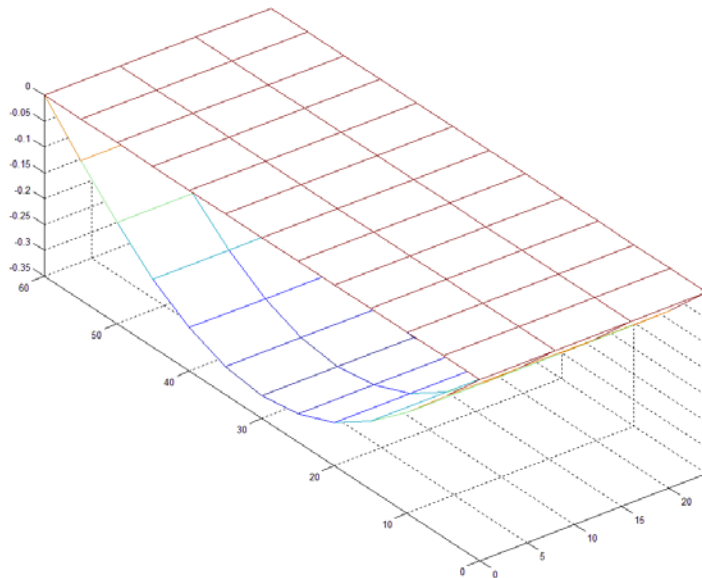


FIGURE 3-46:DEFLECTION DUE TO DEAD LOAD FOR 60 FT. STEEL GIRDER BRIDGE

For the dynamic analysis of the bridge, damping matrix for the bridge needs to be determined. Rayleigh Damping has been used in this research, to model the damping behavior of the bridge. In this type of damping, the damping matrix can be obtained from

the mass matrix or the stiffness matrix. It can also be found using the combination of the stiffness and the mass matrices which is shown in equation (3.2),

$$[C] = \alpha[M] + \beta[K] \quad (3.2)$$

α and β can be calculated using the frequency values of two selected modes,

$$\alpha = \frac{2\xi w_i w_j}{w_i + w_j} \quad (3.3)$$

$$\beta = \frac{2\xi}{w_i + w_j} \quad (3.4)$$

Fixed value of 5% damping has been selected for the bridge and the frequencies of the first two modes have been used to find the damping matrix.

The equation of motion for bridge-vehicle system is:

$$[M_b]\{\ddot{\delta}\} + [C_b]\{\dot{\delta}\} + [K_b]\{\delta\} = F_b \quad (3.5)$$

Where,

M_b is the global mass matrix of the bridge.

C_b is the global damping matrix of the bridge.

K_b is the global stiffness matrix of the bridge.

δ is the nodal displacement.

And F_b is the global load vector due to the bridge-vehicle interaction. This interaction force can be calculated using equation (3.6).

$$F_{bt}^i = K_{tzi}U_{tzi} + C_{tzi}\dot{U}_{tzi} \quad (3.6)$$

Where,

F_{bt}^i is the force between the i^{th} wheel and the bridge.

K_{tzi} is the tire stiffness of the i^{th} wheel.

C_{tzi} is the tire damping of the i^{th} wheel.

\dot{U}_{tzi} is the relative velocity between the bridge and the i^{th} wheel.

$U_{tzi} = z_{wi} - (-u_{sri}) - (-z_{bi})$ is the relative displacement of the bridge and the i^{th} wheel.

z_{wi} is the vertical displacement of the i^{th} wheel.

u_{sri} is the road surface roughness under the i^{th} wheel. (Positive upwards)

And z_{bi} is the bridge vertical displacement under the i^{th} wheel. (Positive upwards)

Numerical methods need to be used to solve the equations of motion given in equation (2-308). Fourth order Runge-Kutta (with 0.00025 second integration time step) has been used to solve the equations of motion for the trucks at each time step to get the tire forces.

Then the tire forces have been used as the forcing vector in equation (3.5). Now the equation (3.5), which is a coupled system of second degree differential equations, needs to be solved. The number of equations in this system is equal to the number of the degrees of freedom of the bridge grid model. These equations can be solved using the “ODE Solver” in MATLAB and the results would be the deflection, velocity and acceleration of the bridge for each degree of freedom. In the next step, the new state of the bridge will be imposed on the vehicle which changes the initial values for solving the equations of motion of the vehicle. These equations will be solved using the new initial state and the results for the tire forces will be applied to the bridge in the next step. This cycle of interaction between the bridge and the vehicle will be continued until the vehicle passes the bridge and at that time the bridge starts to vibrate and the damping of the bridge will eventually stop the bridge movement.

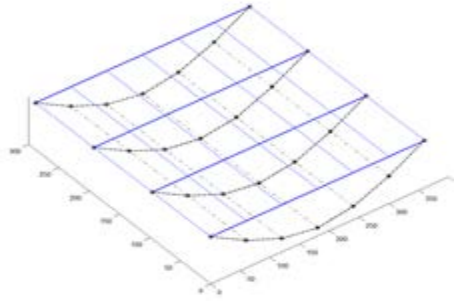
Modal analysis of the bridge models was performed and the first five frequencies of the bridges were calculated. The results have been shown in Table 3.10. It can be observed

from this table that the prestressed concrete bridges have higher frequencies comparing to the steel bridges which shows the higher stiffness to mass ratio in these bridges. All the mode shapes can be seen in Figure 3.46 to Figure 3.55.

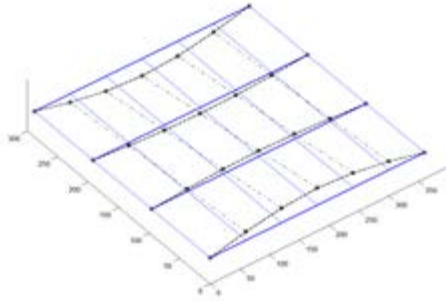
TABLE 3-10: BRIDGE MODELS FREQUENCIES

Mode Number	Steel Bridge				
	Mode Number				
	30	60	90	120	140
1 st	8.81	4.24	3.17	2.52	2.31
2 nd	9.03	4.34	3.21	2.52	2.33
3 rd	11.87	9.55	9.05	8.25	4.51
4 th	22.85	17.39	12.81	10.00	9.11
5 th	38.95	17.46	12.87	10.17	9.28
6 th	39.10	19.38	15.03	12.30	9.38

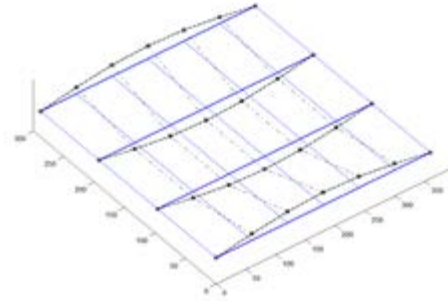
Mode Number	Steel Bridge				
	Mode Number				
	30	60	90	120	140
1 st	14.76	6.35	4.07	2.77	2.05
2 nd	15.16	6.64	4.31	3.03	2.32
3 rd	17.18	9.11	6.74	5.86	5.13
4 th	24.22	16.93	13.29	11.20	8.23
5 th	61.30	26.04	16.47	11.21	8.33
6 th	63.56	26.10	16.55	12.09	9.53



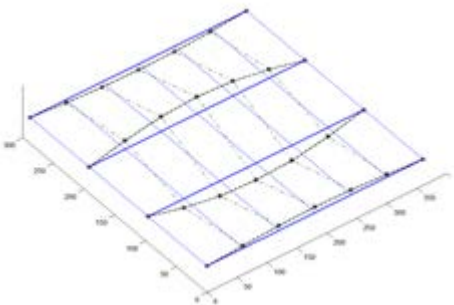
(a) 1st Mode ($f_1=8.81$ Hz)



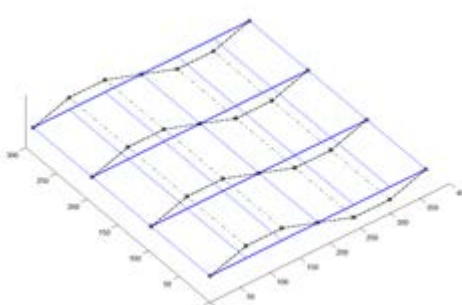
(b) 2nd Mode ($f_2=9.03$ Hz)



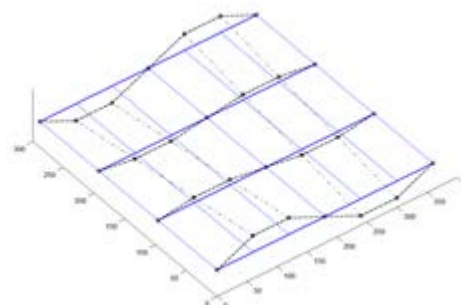
(c) 3rd Mode ($f_3=11.87$ Hz)



(d) 4th Mode ($f_4=22.85$ Hz)



(e) 5th Mode ($f_5=38.95$ Hz)



(f) 6th Mode ($f_6=39.10$ Hz)

FIGURE 3-47: STEEL BRIDGE MODE SHAPES (30' SPAN)

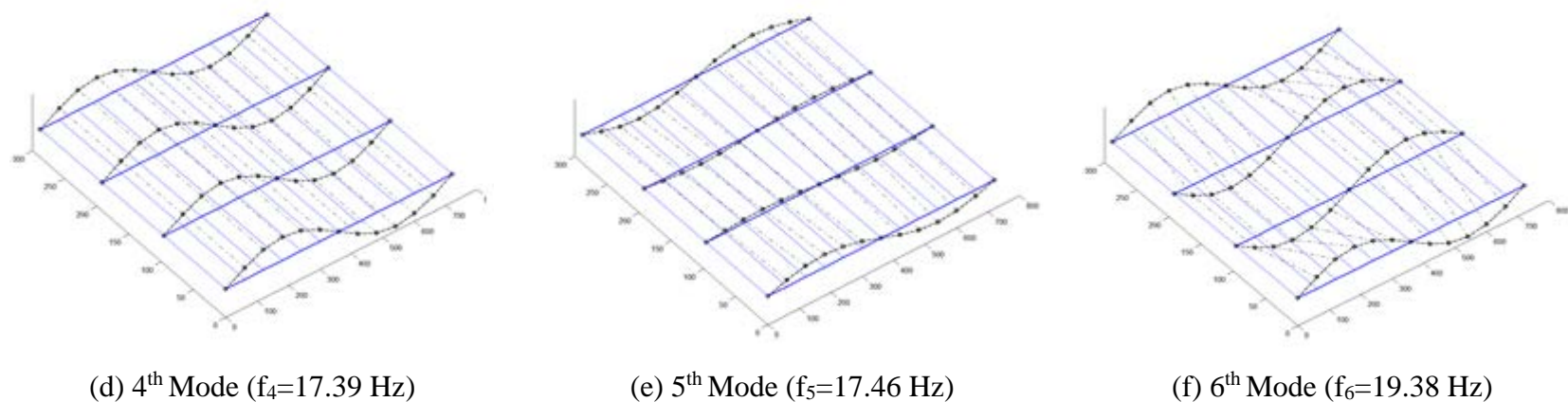
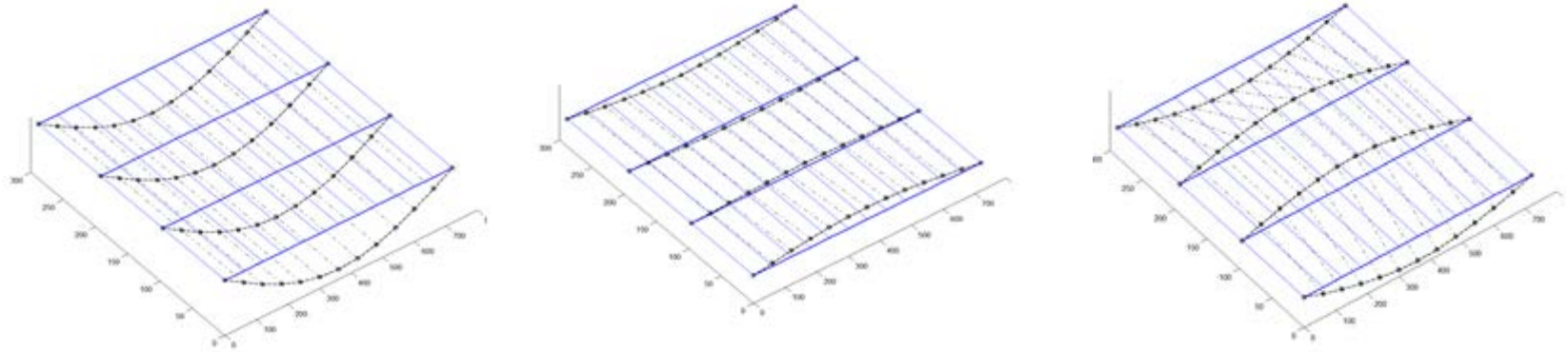
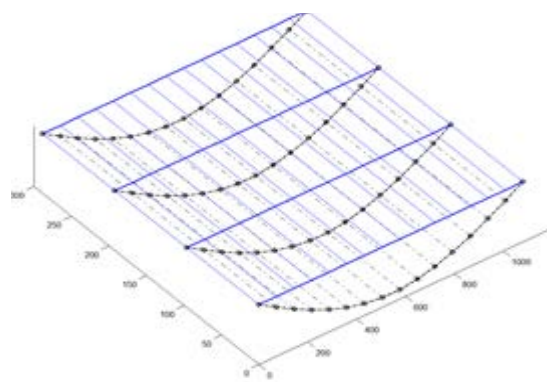
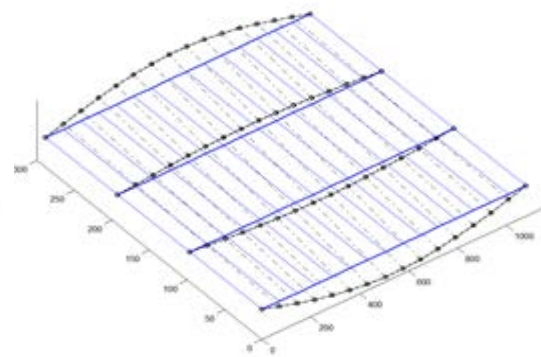


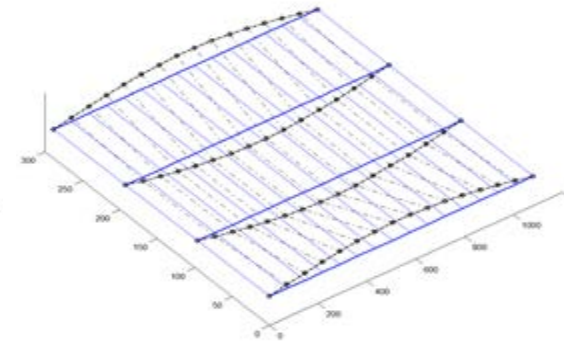
FIGURE 3-48: STEEL BRIDGE MODE SHAPES (60' SPAN)



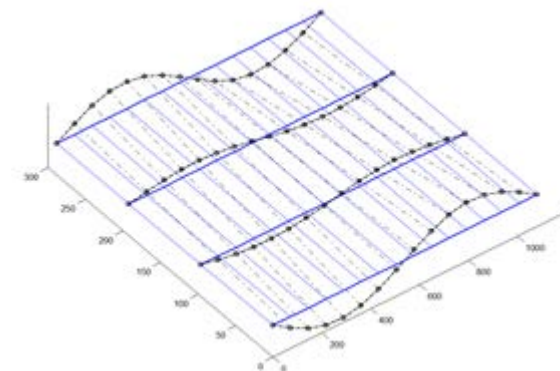
(a) 1st Mode ($f_1=3.17$ Hz)



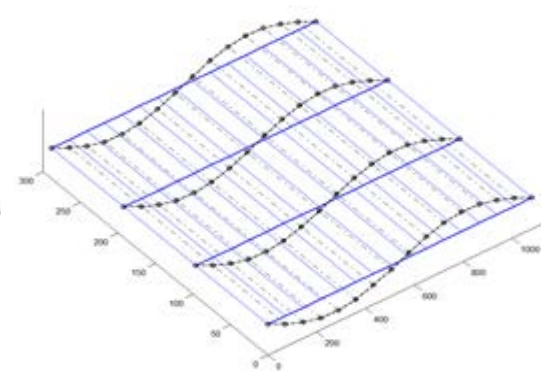
(b) 2nd Mode ($f_2=3.21$ Hz)



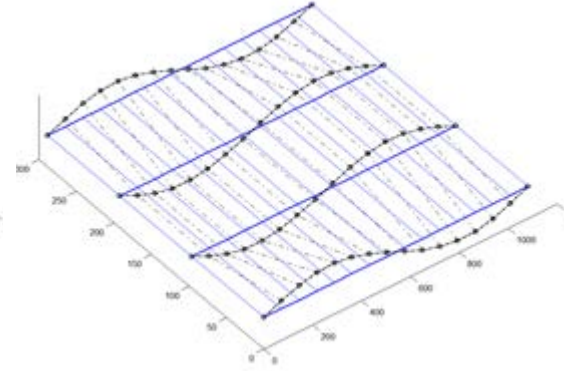
(c) 3rd Mode ($f_3=9.05$ Hz)



(d) 4th Mode ($f_4=12.81$ Hz)

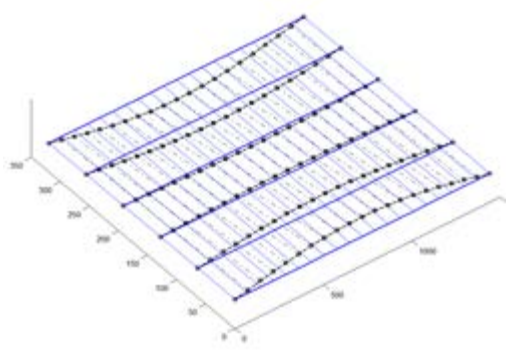


(e) 5th Mode ($f_5=12.87$ Hz)

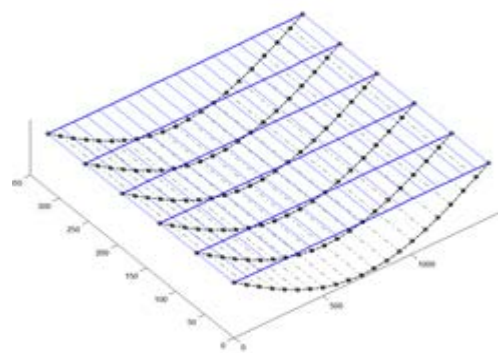


(f) 6th Mode ($f_6=15.03$ Hz)

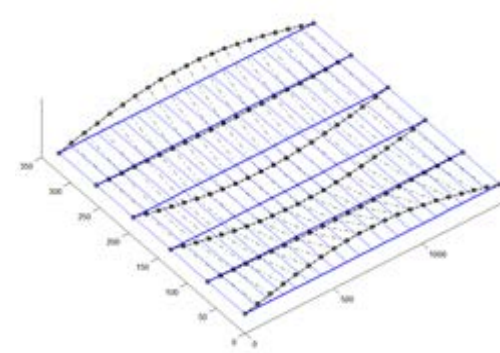
FIGURE 3-49: STEEL BRIDGE MODE SHAPES (90' SPAN)



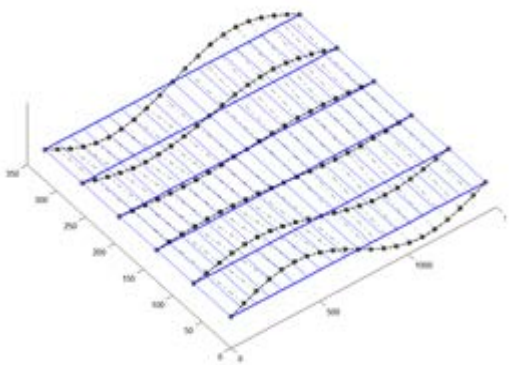
(a) 1st Mode ($f_1=2.52$ Hz)



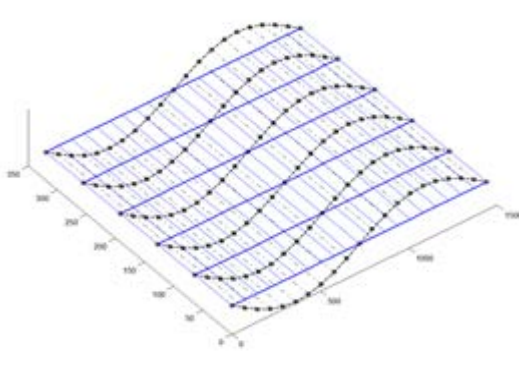
(b) 2nd Mode ($f_2=2.52$ Hz)



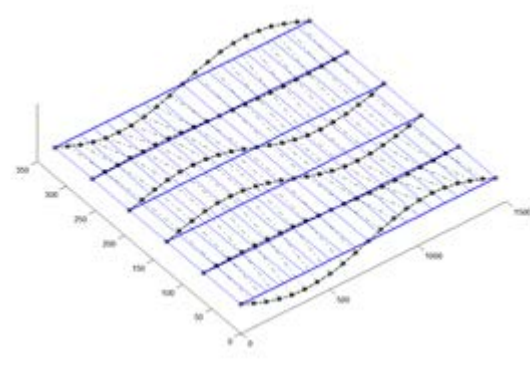
(c) 3rd Mode ($f_3=8.25$ Hz)



(d) 4th Mode ($f_4=10.00$ Hz)

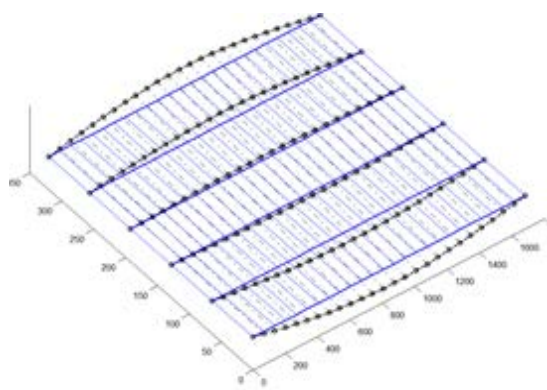


(e) 5th Mode ($f_5=10.17$ Hz)

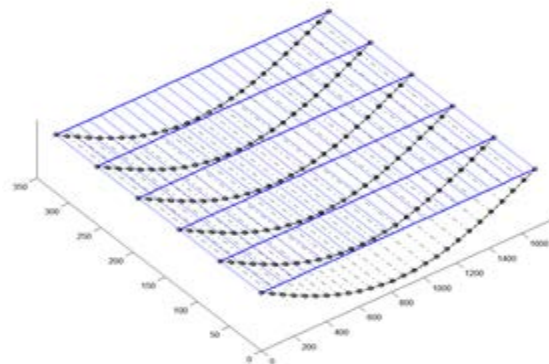


(f) 6th Mode ($f_6=12.30$ Hz)

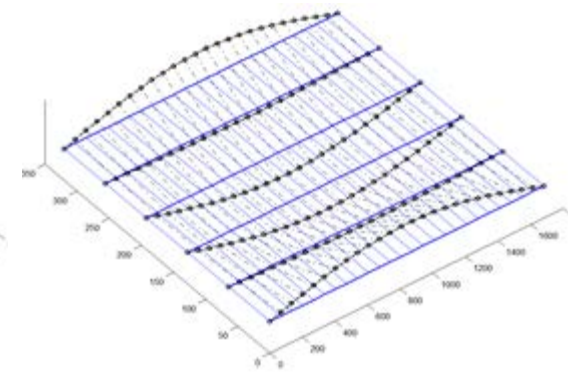
FIGURE 3-50: STEEL BRIDGE MODE SHAPES (120' SPAN)



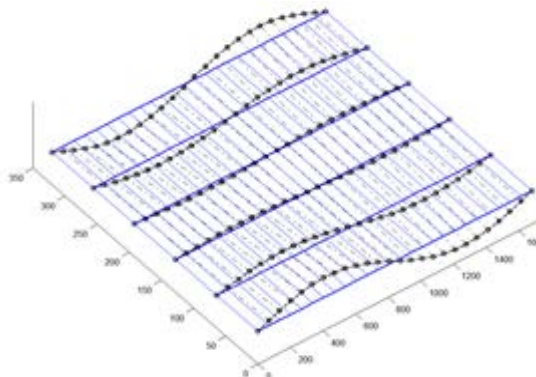
(a) 1st Mode ($f_1=2.31$ Hz)



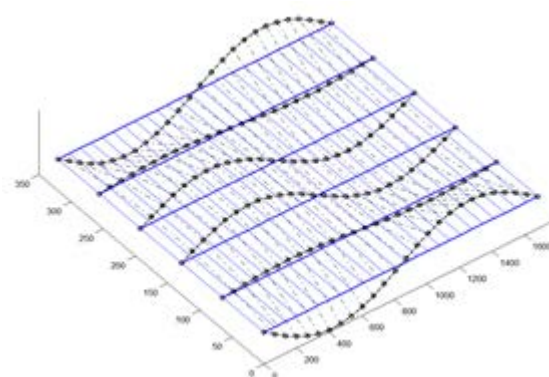
(b) 2nd Mode ($f_2=2.33$ Hz)



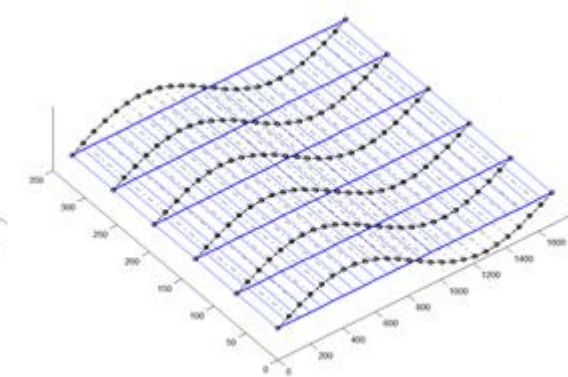
(c) 3rd Mode ($f_3=4.51$ Hz)



(d) 4th Mode ($f_4=9.11$ Hz)



(e) 5th Mode ($f_5=9.28$ Hz)



(f) 6th Mode ($f_6=9.38$ Hz)

FIGURE 3-51: STEEL BRIDGE MODE SHAPES (140' SPAN)

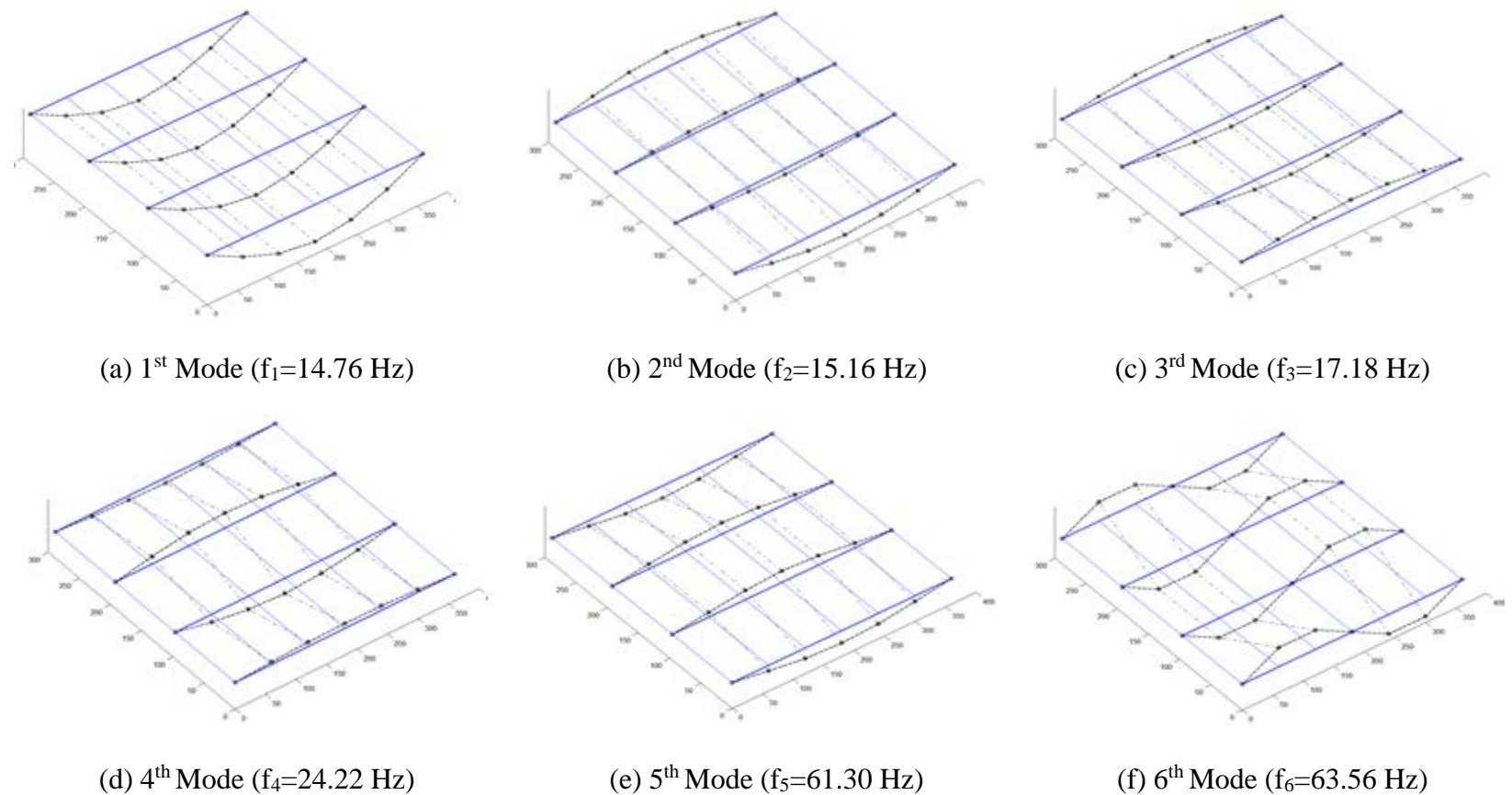
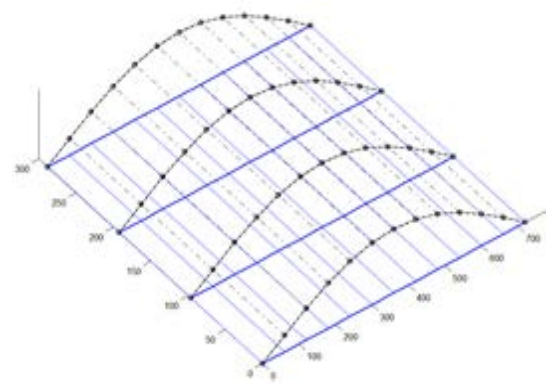
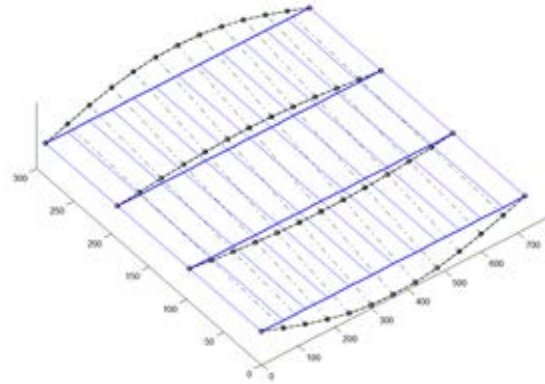


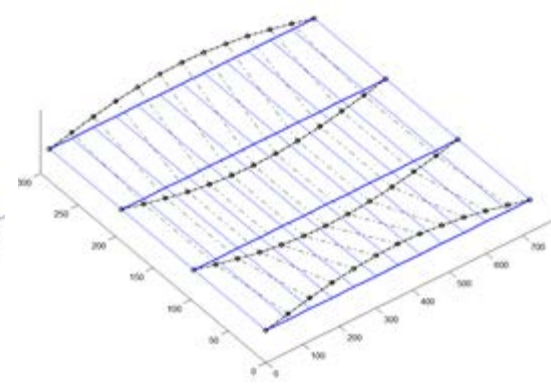
FIGURE 3-52: PRESTRESSED CONCRETE BRIDGE MODE SHAPES (30' SPAN)



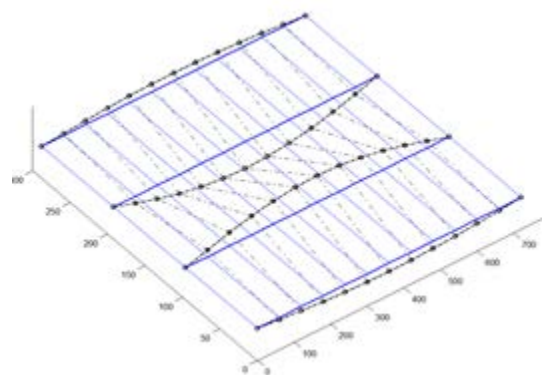
(a) 1st Mode ($f_1=6.35$ Hz)



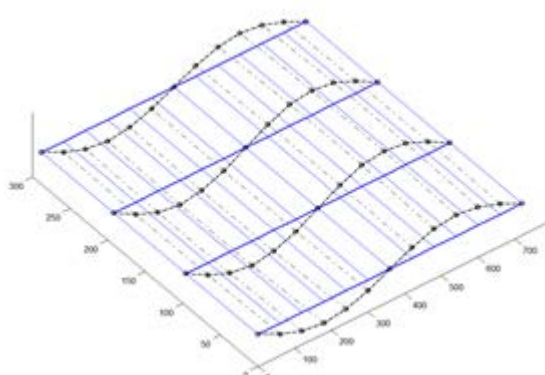
(b) 2nd Mode ($f_2=6.64$ Hz)



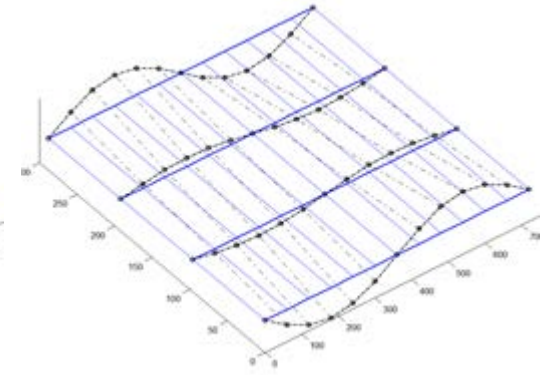
(c) 3rd Mode ($f_3=9.11$ Hz)



(d) 4th Mode ($f_4=16.93$ Hz)

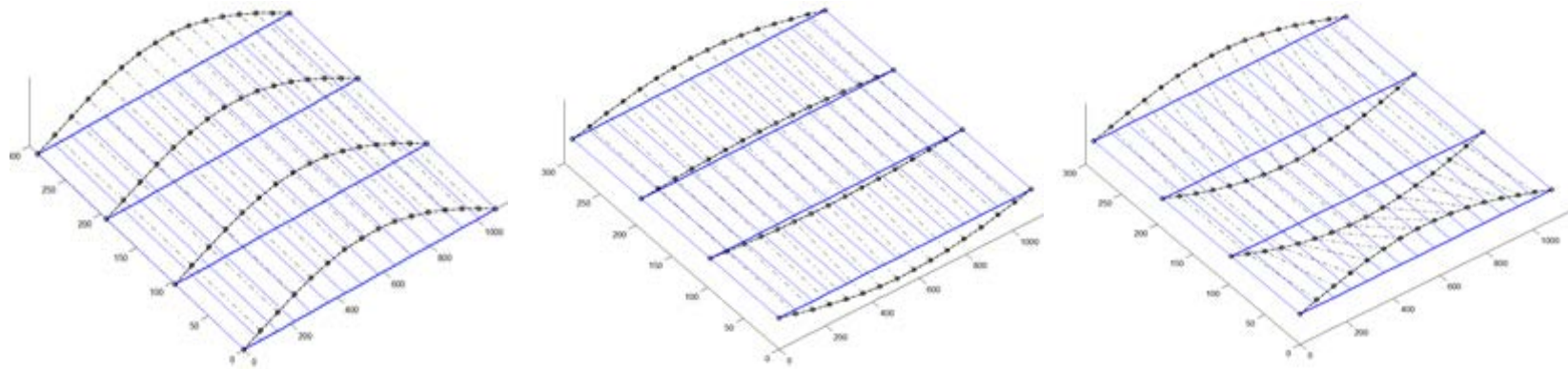


(e) 5th Mode ($f_5=26.04$ Hz)



(f) 6th Mode ($f_6=26.10$ Hz)

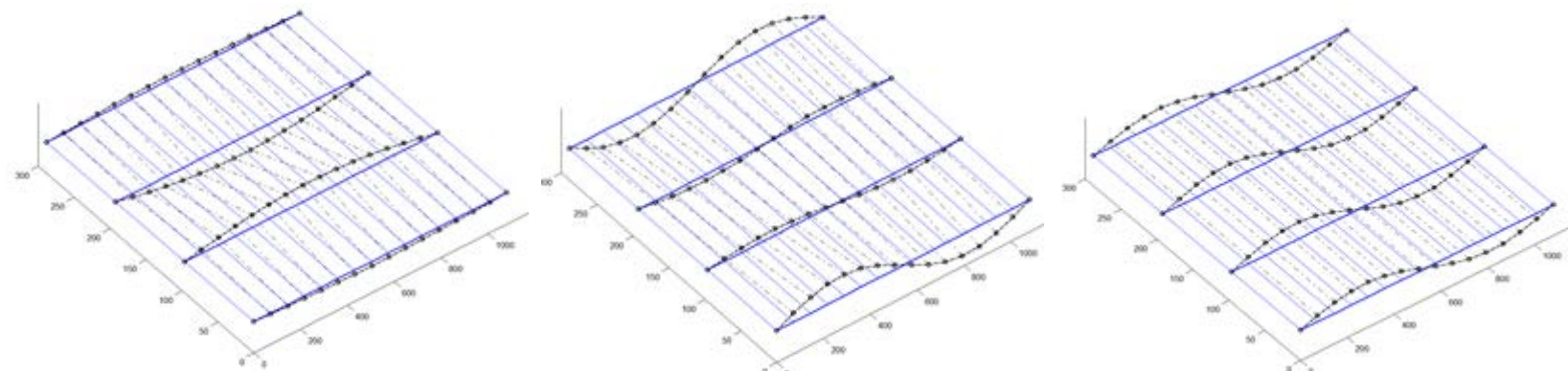
FIGURE 3-53: PRESTRESSED CONCRETE BRIDGE MODE SHAPES (60' SPAN)



(a) 1st Mode ($f_1=4.07$ Hz)

(b) 2nd Mode ($f_2=4.31$ Hz)

(c) 3rd Mode ($f_3=6.74$ Hz)

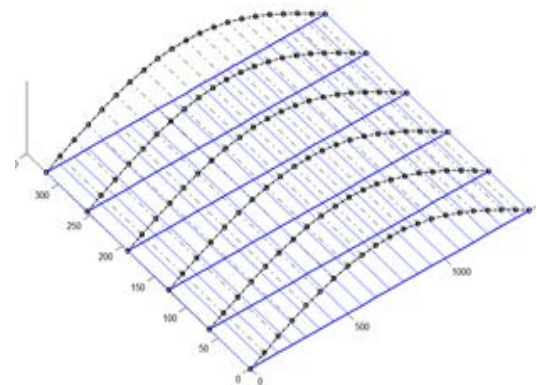


(d) 4th Mode ($f_4=13.29$ Hz)

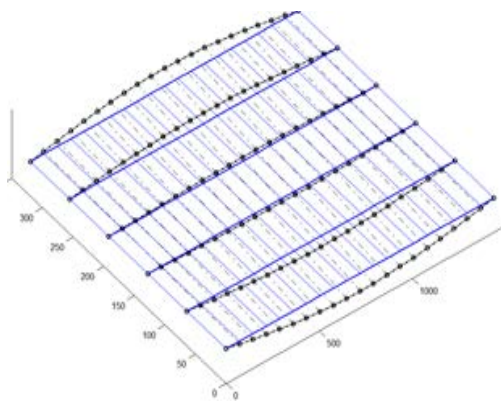
(e) 5th Mode ($f_5=16.47$ Hz)

(f) 6th Mode ($f_6=16.55$ Hz)

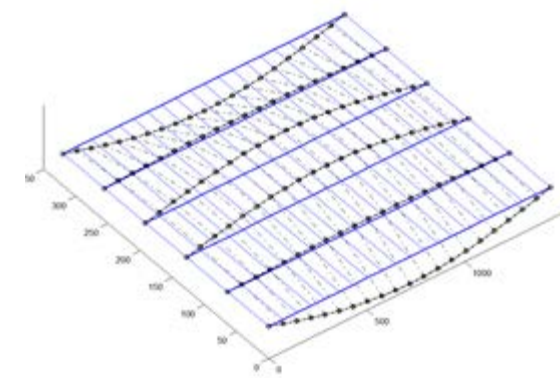
FIGURE 3-54: PRESTRESSED CONCRETE BRIDGE MODE SHAPES (90' SPAN)



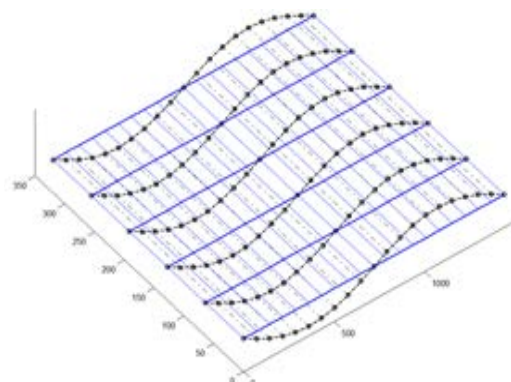
(a) 1st Mode ($f_1=2.77$ Hz)



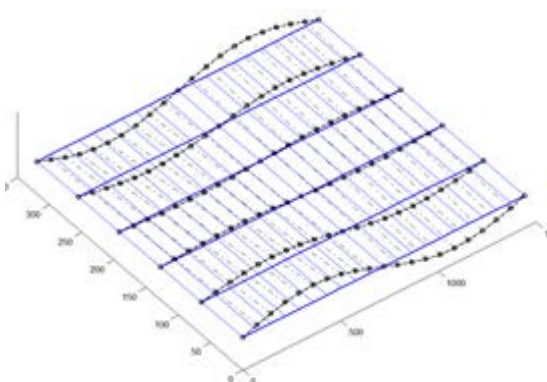
(b) 2nd Mode ($f_2=3.03$ Hz)



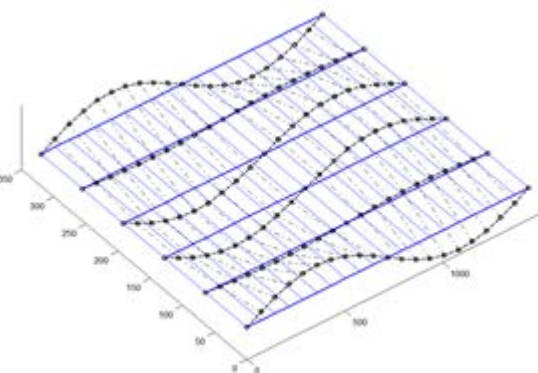
(c) 3rd Mode ($f_3=5.86$ Hz)



(d) 4th Mode ($f_4=11.20$ Hz)

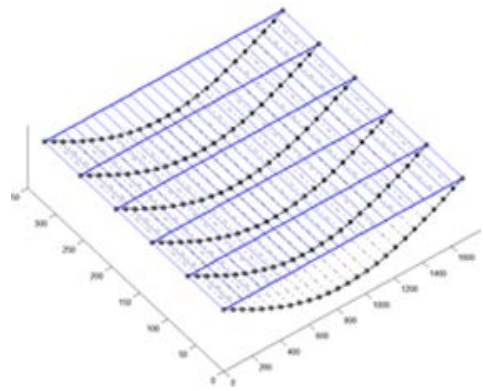


(e) 5th Mode ($f_5=11.21$ Hz)

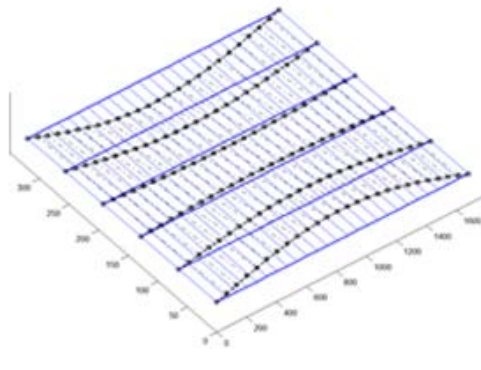


(f) 6th Mode ($f_6=12.09$ Hz)

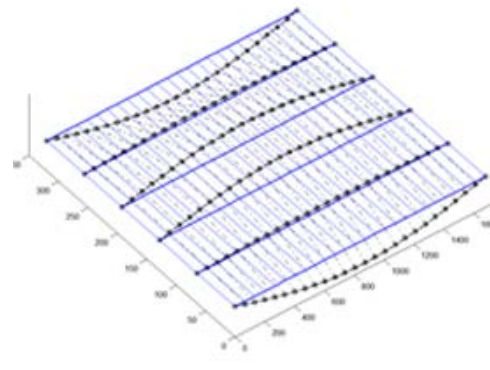
FIGURE 3-55: PRESTRESSED CONCRETE BRIDGE MODE SHAPES (120' SPAN)



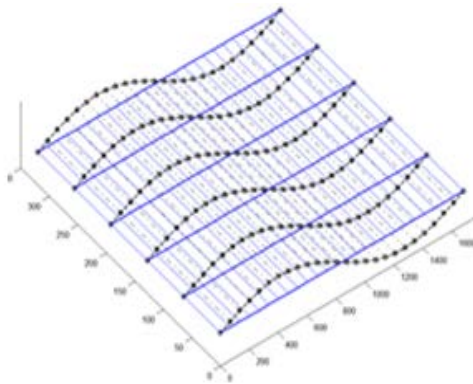
(a) 1st Mode ($f_1=2.05$ Hz)



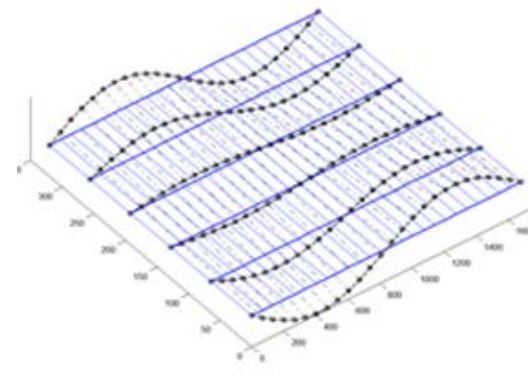
(b) 2nd Mode ($f_2=2.32$ Hz)



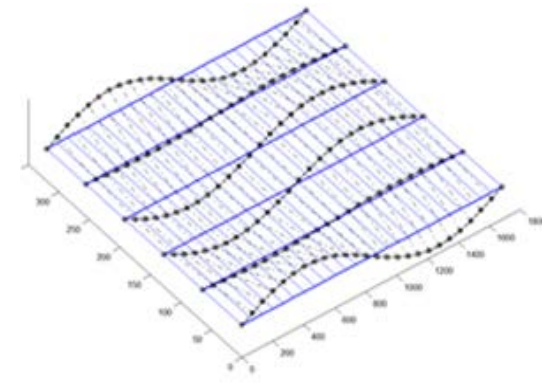
(c) 3rd Mode ($f_3=5.13$ Hz)



(d) 4th Mode ($f_4=8.23$ Hz)



(e) 5th Mode ($f_5=8.33$ Hz)



(f) 6th Mode ($f_6=9.53$ Hz)

FIGURE 3-56: PRESTRESSED CONCRETE BRIDGE MODE SHAPES (140' SPAN)

4. Dynamic characteristics of Different Group of Trucks

4.1 Introduction

Bridge vibration problems due to a moving vehicle have been a subject of many studies in the past. From a general point of view, these studies can be categorized into nine groups: the suspension systems effects, road surface roughness, bridge span length, vehicle braking, axle spacing, gross vehicle weight, vehicle speed, bridge mass and bridge damping. In order to investigate different factors on the bridge dynamic behavior a lot of numerical methods have been developed [11].

There are different approaches to the way that vehicles are modeled. Quarter truck vehicle is the simplest model [12]. The other two common models are the two-dimensional models [13]; and the three-dimensional models [11, 14, 15].

Also, different ways to model bridge structures have been proposed. Some of them are: grillage method [16], eight-node quadrilateral Kirchhoff plate/shell element and three-node Euler–Bernoulli beam [14], plate elements [15], and assemblage of beam and plate elements [11, 13]

Using the above models, the bridge–vehicle system is formed with the constant interaction between the bridge and the vehicle. The equations of motion of the bridge and the vehicle can be solved separately using iterative procedures or as coupled equations of motion by some methods such as the central difference method [17].

Dynamic load allowance (dynamic impact factor (DAF)) is the dynamic effect of moving vehicles on bridges and is defined as the ratio of the maximum dynamic response to the maximum static response. It can be evaluated from the displacements, strains, or

reactions which result in different numbers. In most of the experimental studies published, the computation of DAF is based on the displacements [14]. The AASHTO LRFD design manual suggests a value of 0.33 for the dynamic load allowance [2]. In AASHTO standard specifications, it is expressed as a function of the bridge length [18]. Some other codes, like Canada's Ontario Bridge Design Code, define DAF as a function of the first flexural frequency of the bridge [19]. There has been a huge effort in the past decades to investigate the effects of dynamic loading on the bridges through both analytical and field testing methods; the codes' underestimation when it comes to the dynamic load allowance has been suggested in some studies. A reason for this problem might be that, the codes consider good road surface condition, where in fact some of the bridges in the US might experience bad surface conditions at times.

A complete investigation of the factors affecting DAF, using analytical and experimental methods, was performed by Paultre et al. [20] and they concluded that DAF is related to the surface condition, vehicle suspension system and the fundamental frequency.

A series of investigations using analytical methods were carried out and the results showed that the vehicle speed does not have a big effect on the impact factor when vehicles travel on “Good” and “Very Good” surface conditions. Also the impact factors for short span bridges were larger than the impact factors of the long span bridges. It was also observed that an increase in the vehicle weight would result in smaller impact factors [21-23].

In a research by Brady et al. [24] the DAF was investigated using one simple model as well as another more complicated 3D model. It was observed that the values of DAF for two vehicles on the bridge were smaller than those for one vehicle. In addition, DAF

values were larger in a lane in which there is no vehicle comparing to the lane where the vehicle is traveling.

The effects of different trucks on the bridge dynamic responses depend on many factors such as the gross vehicle weight (GVW), number and weight of truck axles, distance between truck axles, etc. To capture the bridge behavior under the traffic, a wide range of trucks needs to be considered. To achieve this goal, many trucks with different lengths and weights have been chosen. These trucks include H20-44, HS20-44, Type 3, Type 3S2, Type 3S3, 4-axle single truck (SU4), Type 2S2 and Type 3S1. In addition to these trucks, some longer combination vehicles (LCV) including 7 Axle Rocky Mountain Double, 8 Axle B-Train Double and 9 Axle Turnpike Double were selected. All these trucks can be seen in Figure 4-1.

The next step is to develop the equations of motion for these trucks. This was done for HS20-44 by Huang et al. [21] and in this research the derivation has been done and extended for the other types of trucks in addition to the three longer combination vehicles (LCV). The details of the derivation of equations for the simplest (H20-44) and the most complicated case (9 Axle Turnpike Double) are provided here. Data of tractor and trailer lengths in addition to the weights on different axles were gathered from different reports and sources online and for the other cases that no data were found, reasonable assumptions based on the similar cases were made in order to complete the model.

The axle weights and the gross vehicle weight of all the trucks which is the sum of the Tare weight and the maximum load that the truck can carry are shown in Table 4-1.

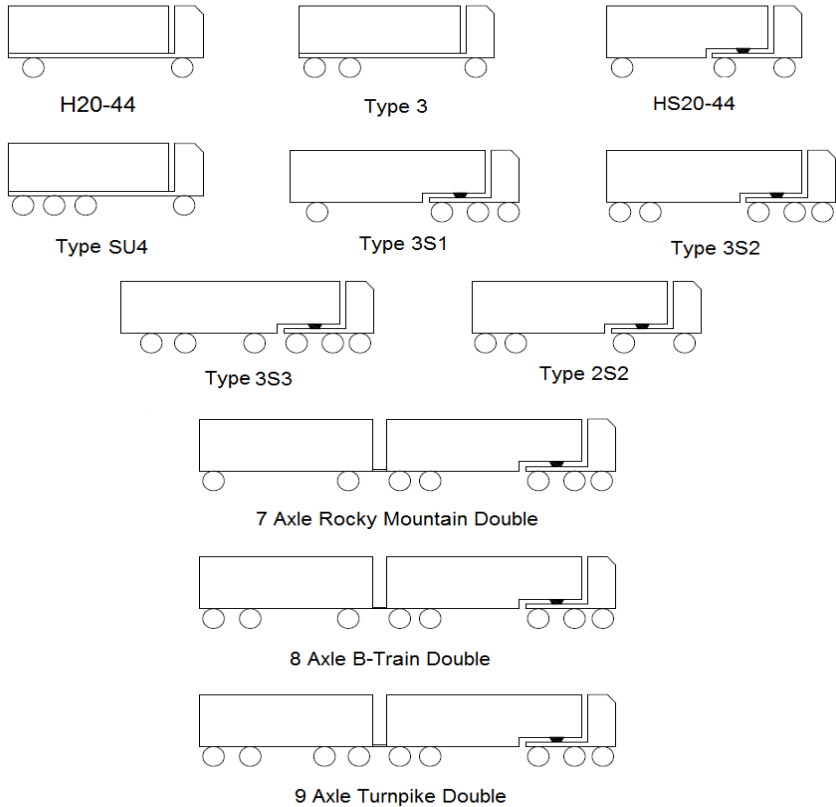


FIGURE 4-1: TRUCK MODELS

4.2 Derivation of Equations of Motion for “H20-44 Truck”

Parallel springs and dampers have been used to model the suspension systems and tires of the truck. Rigid masses were used to model the axles and the truck. Three degrees of freedom for vertical, roll, and pitch displacements of the truck have been defined. Also each of the two axles has two degrees of freedom for vertical and roll displacements. There are seven degrees of freedom in total for this type of truck. The degrees of freedom can be seen in Figure 4-2 and the description of those degrees of freedom can be found in Table 4-2. Relative Displacements at the locations of the springs are also calculated using the values given in Table 4-3.

TABLE 4-1: AXLE WEIGHTS AND GROSS VEHICLE WEIGHT OF TRUCKS

Aisle	Vehicle Type											
	Number	H-20	HS-20	Type 3	Type 3S2	Type 3S3	Type 2S2	Type 3S1	SU4	7-Axle Rocky Mountain	8 Axle B-Train Double	9 Axle Turnpike Double
1	8	8	16	12	12	12	12	13.9	14	12	15	
2	32	32	17	17	17	24	18	18.7	18	15	17	
3		32	17	17	17	18	18	18.7	18	15	17	
4				17	17	18	24	18.7	17	14	16	
5					17	17			17	14	16	
6						17			18	19	16	
7									18	17.5	16	
8										17.5	17	
9											17	
Gross Vehicle Weight [Kips]		40	72	50	80	97	72	72	70	120	124	147

4.3 Derivation of Equations of Motion for “H20-44 Truck”

Parallel springs and dampers have been used to model the suspension systems and tires of the truck. Rigid masses were used to model the axles and the truck. Three degrees of freedom for vertical, roll, and pitch displacements of the truck have been defined. Also each of the two axles has two degrees of freedom for vertical and roll displacements. There are seven degrees of freedom in total for this type of truck. The degrees of freedom can be seen in Figure 4-2 and the description of those degrees of freedom can be found in Table 4-2. Relative Displacements at the locations of the springs are also calculated using the values given in Table 4-3.

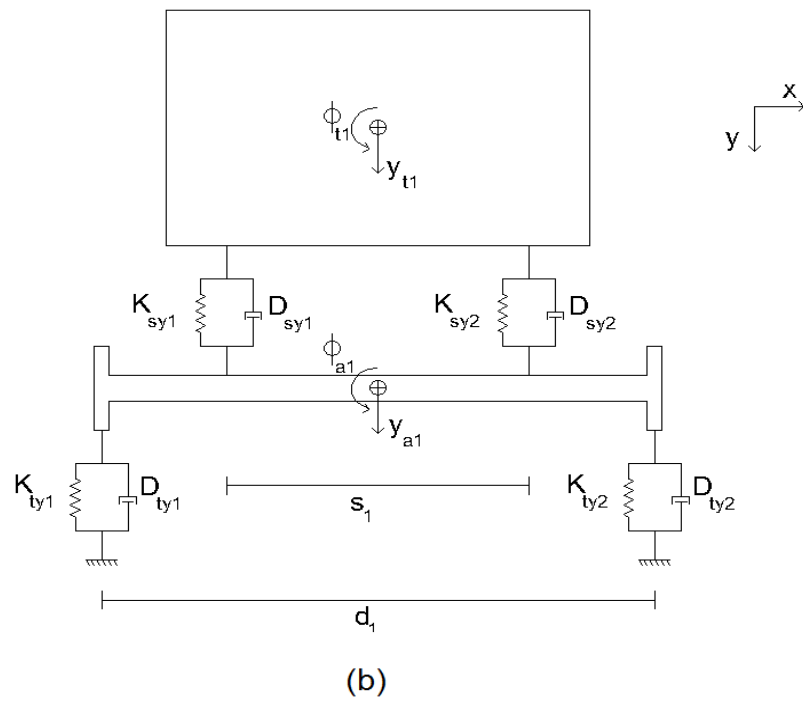
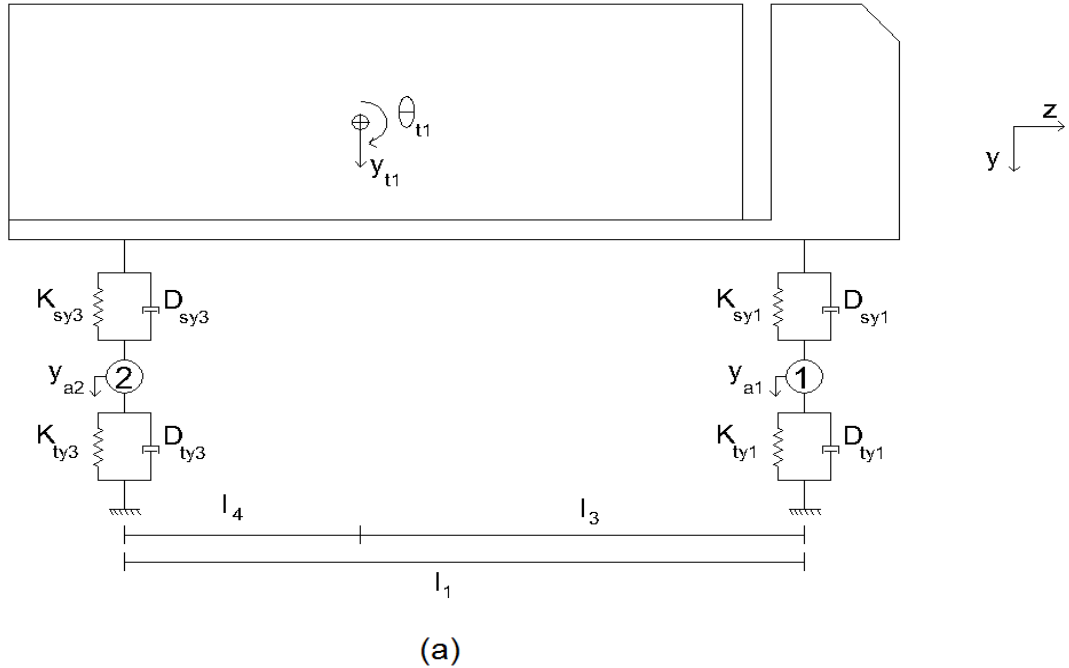


FIGURE 4-2: H20-44 DYNAMIC MODEL (A) TRUCK SIDE VIEW (B) TRUCK FRONT VIEW

TABLE 4-2: DEGREES OF FREEDOM OF H20-44 TRUCK

No.	Degree of Freedom	Contributed Mass	Description
1	y_{t1}	m_{t1}	Truck vertical displacement and mass
2	φ_{t1}	I_{xt1}	Truck roll displacement and mass moment of inertia
3	θ_{t1}	I_{zt1}	Truck pitch displacement and mass moment of inertia
4	y_{a1}	m_{a1}	Front axle vertical displacement and mass
5	φ_{a1}	I_{xa1}	Front axle roll displacement and mass moment of inertia
6	y_{a2}	m_{a2}	Rear axle vertical displacement and mass
7	φ_{a2}	I_{xa2}	Rear axle roll displacement and mass moment of inertia

TABLE 4-3: RELATIVE DISPLACEMENTS AT SPRING LOCATIONS OF H20-44 TRUCK

Suspension springs	
U_{sy1}	$(y_{t1} - y_{a1}) + (S_1/2)(\varphi_{t1} - \varphi_{a1}) + l_3\theta_{t1}$
U_{sy2}	$(y_{t1} - y_{a1}) - (S_1/2)(\varphi_{t1} - \varphi_{a1}) + l_3\theta_{t1}$
U_{sy3}	$(y_{t1} - y_{a2}) + (S_2/2)(\varphi_{t1} - \varphi_{a2}) - l_4\theta_{t1}$
U_{sy4}	$(y_{t1} - y_{a2}) - (S_2/2)(\varphi_{t1} - \varphi_{a2}) - l_4\theta_{t1}$

Tire springs	
U_{ty1}	$y_{a1} + (d_1/2)\varphi_{a1} + u_{SR1}$
U_{ty2}	$y_{a1} - (d_1/2)\varphi_{a1} + u_{SR2}$
U_{ty3}	$y_{a2} + (d_2/2)\varphi_{a2} + u_{SR3}$
U_{ty4}	$y_{a2} - (d_2/2)\varphi_{a2} + u_{SR4}$

In this table u_{SRi} is the road surface roughness under the i^{th} wheel.

F_{syi} and F_{dsyi} are defined as the i^{th} suspension spring force and suspension damper force, respectively:

$$F_{syi} = K_{syi}U_{syi} + F_{yi} \quad (4-1)$$

$$F_{dsyi} = D_{syi}\dot{U}_{syi} \quad (4-2)$$

Where F_{yi} is the friction force at the i^{th} suspension. Similarly F_{tyi} and F_{dtyi} are defined as the spring force and the damper force under the i^{th} wheel:

$$F_{tyi} = K_{tyi}U_{tyi} \quad (4-3)$$

$$F_{dtyi} = D_{tyi}\dot{U}_{tyi} \quad (4-4)$$

Lagrange's equation has been used to generate the equations of motion of the system:

$$\frac{d}{dt} \left(\frac{\partial T}{\partial \dot{q}_i} \right) - \frac{\partial T}{\partial q_i} + \frac{\partial V}{\partial q_i} + \frac{\partial D}{\partial \dot{q}_i} = 0 \quad (4-5)$$

Where, T is the Kinetic Energy of the system:

$$T = \frac{1}{2}m_{t1}\dot{y}_{t1}^2 + \frac{1}{2}m_{a1}\dot{y}_{a1}^2 + \frac{1}{2}m_{a2}\dot{y}_{a2}^2 + \frac{1}{2}I_{xt1}\dot{\phi}_{t1}^2 + \frac{1}{2}I_{zt1}\dot{\theta}_{t1}^2 + \frac{1}{2}I_{xa1}\dot{\phi}_{a1}^2 + \frac{1}{2}I_{xa2}\dot{\phi}_{a2}^2 \quad (4-6)$$

V is the Potential Energy of the system.

$$V = \frac{1}{2}K_{sy1}U_{sy1}^2 + \frac{1}{2}K_{sy2}U_{sy2}^2 + \frac{1}{2}K_{sy3}U_{sy3}^2 + \frac{1}{2}K_{sy4}U_{sy4}^2 + \frac{1}{2}K_{ty1}U_{ty1}^2 + \frac{1}{2}K_{ty2}U_{ty2}^2 + \frac{1}{2}K_{ty3}U_{ty3}^2 + \frac{1}{2}K_{ty4}U_{ty4}^2 - ((m_{t1}g)y_{t1} + (m_{a1}g)y_{a1} + (m_{a2}g)y_{a2}) + (F_{y1}U_{sy1} + F_{y2}U_{sy2} + F_{y3}U_{sy3} + F_{y4}U_{sy4}) \quad (4-7)$$

D is the Damping Energy of the system.

$$D = \frac{1}{2} D_{sy1} \dot{U}_{sy1}^2 + \frac{1}{2} D_{sy2} \dot{U}_{sy2}^2 + \frac{1}{2} D_{sy3} \dot{U}_{sy3}^2 + \frac{1}{2} D_{sy4} \dot{U}_{sy4}^2 + \frac{1}{2} D_{ty1} \dot{U}_{ty1}^2 + \frac{1}{2} D_{ty2} \dot{U}_{ty2}^2 + \frac{1}{2} D_{ty3} \dot{U}_{ty3}^2 + \frac{1}{2} D_{ty4} \dot{U}_{ty4}^2 \quad (4-8)$$

And q_i is one of the degrees of freedom.

Now the Lagrange's equation is applied to y_{t1} :

$$m_{t1}\ddot{y}_{t1} + [(F_{sy1} + F_{sy2} + F_{sy3} + F_{sy4}) + (F_{dsy1} + F_{dsy2} + F_{dsy3} + F_{dsy4})] = m_{t1}g \quad (4-9)$$

$$m_{t1}g$$

Also, by applying the Lagrange's equation to θ_{t1} :

$$I_{zt1}\ddot{\theta}_{t1} + [l_3(F_{sy1} + F_{sy2}) - l_4(F_{sy3} + F_{sy4})] + [l_3(F_{dsy1} + F_{dsy2}) - l_4(F_{dsy3} + F_{dsy4})] = 0 \quad (4-10)$$

By applying the Lagrange's equation to φ_{t1} :

$$I_{xt1}\ddot{\varphi}_{t1} + \left[\left(\frac{s_1}{2}\right)(F_{sy1} - F_{sy2}) + \left(\frac{s_2}{2}\right)(F_{sy3} - F_{sy4}) \right] + \left[\left(\frac{s_1}{2}\right)(F_{dsy1} - F_{dsy2}) + \left(\frac{s_2}{2}\right)(F_{dsy3} - F_{dsy4}) \right] = 0 \quad (4-11)$$

Also the rest of degrees of freedom will be as follows:

$$m_{a1}\ddot{y}_{a1} - (F_{sy1} + F_{sy2}) + (F_{ty1} + F_{ty2}) - (F_{dsy1} + F_{dsy2}) + (F_{dty1} + F_{dty2}) = m_{a1}g \quad (4-12)$$

$$I_{xa1}\ddot{\varphi}_{a1} - \left(\frac{s_1}{2}\right)(F_{sy1} - F_{sy2}) + \left(\frac{d_1}{2}\right)(F_{ty1} - F_{ty2}) - \left(\frac{s_1}{2}\right)(F_{dsy1} - F_{dsy2}) + \left(\frac{d_1}{2}\right)(F_{dty1} - F_{dty2}) = 0 \quad (4-13)$$

$$m_{a2}\ddot{y}_{a2} - (F_{sy3} + F_{sy4}) + (F_{ty3} + F_{ty4}) - (F_{dsy3} + F_{dsy4}) + (F_{dty3} + F_{dty4}) = m_{a2}g \quad (4-14)$$

$$\begin{aligned}
I_{xa2} \ddot{\phi}_{a2} - (\frac{s_2}{2})(F_{sy3} - F_{sy4}) + (\frac{d_2}{2})(F_{ty3} - F_{ty4}) - (\frac{s_2}{2})(F_{dsy3} - F_{dsy4}) + \\
(\frac{d_2}{2})(F_{dty3} - F_{dty4}) = 0
\end{aligned} \tag{4-15}$$

In total there are seven equations of motion for the seven degrees of freedom and these equations will be solved using fourth order Runge-Kutta to determine the state of the vehicle at each instant.

4.4 Derivation of Equations of Motion for “HS20-44 Truck”

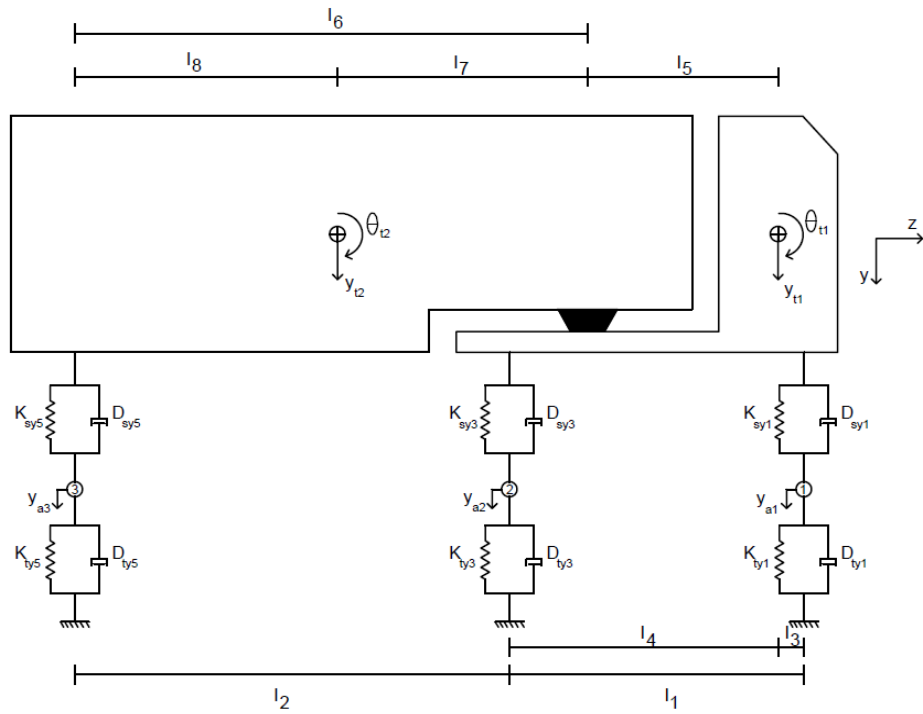
Same modeling approach as in previous section has been used to formulate the other types of trucks. The only difference of the larger vehicles is the so-called “Pivot Point” which changes the number of equations of the motion of the whole system by reducing one equation with each pivot point.

Pivot point acts like a vertical restraint between the trailer and the tractor and a relation between the pitch displacements of the trailer and the tractor is generated to deal with this point.

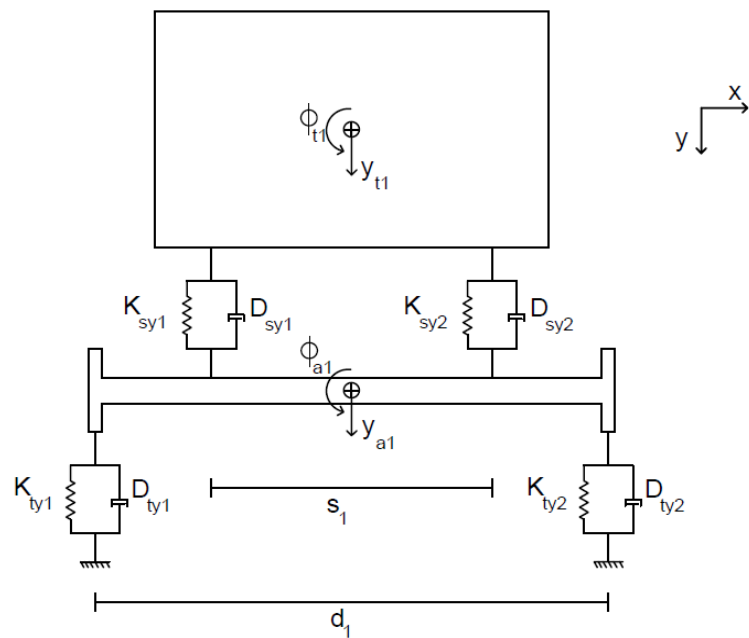
There are twelve degrees of freedom in total for this type of truck. The degrees of freedom can be seen in Figure 4-3 and the description of those degrees of freedom can be found in Table 4-4. Relative Displacements at the locations of the springs are also calculated using the values given in Table 4-5.

TABLE 4-4
Degrees of Freedom of HS20-44 Truck

No.	Degree of Freedom	Contributed Mass	Description
1	y_{t1}	m_{t1}	Tractor vertical displacement and mass
2	φ_{t1}	I_{xt1}	Tractor roll displacement and mass moment of inertia
3	θ_{t1}	I_{zt1}	Tractor pitch displacement and mass moment of inertia
4	y_{t2}	m_{t2}	Trailer vertical displacement and mass
5	φ_{t2}	I_{xt2}	Trailer roll displacement and mass moment of inertia
6	θ_{t2}	I_{zt2}	Trailer pitch displacement and mass moment of inertia
7	y_{a1}	m_{a1}	Steer axle vertical displacement and mass
8	φ_{a1}	I_{xa1}	Steer axle roll displacement and mass moment of inertia
9	y_{a2}	m_{a2}	Tractor axle vertical displacement and mass
10	φ_{a2}	I_{xa2}	Tractor axle roll displacement and mass moment of inertia
11	y_{a3}	m_{a3}	Trailer axle vertical displacement and mass
12	φ_{a3}	I_{xa3}	Trailer axle roll displacement and mass moment of inertia



(a)



(b)

FIGURE 4-3: HS20-44 DYNAMIC MODEL (A) TRUCK SIDE VIEW (B) TRUCK FRONT VIEW

TABLE 4-5: RELATIVE DISPLACEMENTS AT SPRING LOCATIONS OF HS20-44 TRUCK

Suspension springs	
\mathbf{U}_{sy1}	$(y_{t1} - y_{a1}) + (S_1/2)(\varphi_{t1} - \varphi_{a1}) + l_3\theta_{t1}$
\mathbf{U}_{sy2}	$(y_{t1} - y_{a1}) - (S_1/2)(\varphi_{t1} - \varphi_{a1}) + l_3\theta_{t1}$
\mathbf{U}_{sy3}	$(y_{t1} - y_{a2}) + (S_2/2)(\varphi_{t1} - \varphi_{a2}) - l_4\theta_{t1}$
\mathbf{U}_{sy4}	$(y_{t1} - y_{a2}) - (S_2/2)(\varphi_{t1} - \varphi_{a2}) - l_4\theta_{t1}$
\mathbf{U}_{sy5}	$(y_{t2} - y_{a3}) + (S_3/2)(\varphi_{t2} - \varphi_{a3}) - l_8\theta_{t2}$
\mathbf{U}_{sy6}	$(y_{t2} - y_{a3}) - (S_3/2)(\varphi_{t2} - \varphi_{a3}) - l_8\theta_{t2}$
Tire springs	
\mathbf{U}_{ty1}	$y_{a1} + (d_1/2)\varphi_{a1} + u_{SR1}$
\mathbf{U}_{ty2}	$y_{a1} - (d_1/2)\varphi_{a1} + u_{SR2}$
\mathbf{U}_{ty3}	$y_{a2} + (d_2/2)\varphi_{a2} + u_{SR3}$
\mathbf{U}_{ty4}	$y_{a2} - (d_2/2)\varphi_{a2} + u_{SR4}$
\mathbf{U}_{ty5}	$y_{a3} + (d_3/2)\varphi_{a3} + u_{SR5}$
\mathbf{U}_{ty6}	$y_{a3} - (d_3/2)\varphi_{a3} + u_{SR6}$

In this table u_{SRi} is the road surface roughness under the i^{th} wheel.

F_{syi} , F_{dsyi} , F_{tyi} and F_{dtyi} have been defined in equations (4-1) to (4-4). Similarly

Lagrange's equation (4-5) has been used to generate the equations of motion.

Kinetic Energy of the system:

$$\begin{aligned}
 T = & \frac{1}{2}m_{t1}\dot{y}_{t1}^2 + \frac{1}{2}m_{a1}\dot{y}_{a1}^2 + \frac{1}{2}m_{a2}\dot{y}_{a2}^2 + \frac{1}{2}m_{a3}\dot{y}_{a3}^2 + \frac{1}{2}I_{xt1}\dot{\varphi}_{t1}^2 + \\
 & \frac{1}{2}I_{zt1}\dot{\theta}_{t1}^2 + \frac{1}{2}I_{xt2}\dot{\varphi}_{t2}^2 + \frac{1}{2}I_{zt2}\dot{\theta}_{t2}^2 + \frac{1}{2}I_{xa1}\dot{\varphi}_{a1}^2 + \frac{1}{2}I_{xa2}\dot{\varphi}_{a2}^2 + \frac{1}{2}I_{xa3}\dot{\varphi}_{a3}^2 + \quad (4-16) \\
 & \frac{1}{2}m_{t2}\dot{y}_{t2}^2
 \end{aligned}$$

Potential Energy of the system:

$$\begin{aligned}
V = & \frac{1}{2} K_{sy1} U_{sy1}^2 + \frac{1}{2} K_{sy2} U_{sy2}^2 + \frac{1}{2} K_{sy3} U_{sy3}^2 + \frac{1}{2} K_{sy4} U_{sy4}^2 + \frac{1}{2} K_{sy5} U_{sy5}^2 + \\
& \frac{1}{2} K_{sy6} U_{sy6}^2 + \frac{1}{2} K_{ty1} U_{ty1}^2 + \frac{1}{2} K_{ty2} U_{ty2}^2 + \frac{1}{2} K_{ty3} U_{ty3}^2 + \frac{1}{2} K_{ty4} U_{ty4}^2 + \\
& \frac{1}{2} K_{ty5} U_{ty5}^2 + \frac{1}{2} K_{ty6} U_{ty6}^2 - ((m_{t1}g)y_{t1} + (m_{t2}g)y_{t2} + (m_{a1}g)y_{a1} + \\
& (m_{a2}g)y_{a2} + (m_{a3}g)y_{a3}) + (F_{y1}U_{sy1} + F_{y2}U_{sy2} + F_{y3}U_{sy3} + F_{y4}U_{sy4} + \\
& F_{y5}U_{sy5} + F_{y6}U_{sy6})
\end{aligned} \quad (4-17)$$

Damping Energy of the system:

$$\begin{aligned}
D = & \frac{1}{2} D_{sy1} \dot{U}_{sy1}^2 + \frac{1}{2} D_{sy2} \dot{U}_{sy2}^2 + \frac{1}{2} D_{sy3} \dot{U}_{sy3}^2 + \frac{1}{2} D_{sy4} \dot{U}_{sy4}^2 + \frac{1}{2} D_{sy5} \dot{U}_{sy5}^2 + \\
& \frac{1}{2} D_{sy6} \dot{U}_{sy6}^2 + \frac{1}{2} D_{ty1} \dot{U}_{ty1}^2 + \frac{1}{2} D_{ty2} \dot{U}_{ty2}^2 + \frac{1}{2} D_{ty3} \dot{U}_{ty3}^2 + \frac{1}{2} D_{ty4} \dot{U}_{ty4}^2 + \\
& \frac{1}{2} D_{ty5} \dot{U}_{ty5}^2 + \frac{1}{2} D_{ty6} \dot{U}_{ty6}^2
\end{aligned} \quad (4-18)$$

The displacement at the pivot point should stay the same, whether it is calculated from the trailer part or the tractor part,

$$y_{t2} + \theta_{t2} l_7 = y_{t1} - \theta_{t1} l_5 \quad (4-19)$$

Thus, by calculating θ_{t2} from equation (4-19) and substituting in equation (4-16),

$$\begin{aligned}
T = & \frac{1}{2} m_{t1} \dot{y}_{t1}^2 + \frac{1}{2} m_{a1} \dot{y}_{a1}^2 + \frac{1}{2} m_{a2} \dot{y}_{a2}^2 + \frac{1}{2} m_{a3} \dot{y}_{a3}^2 + \frac{1}{2} I_{xt1} \dot{\phi}_{t1}^2 + \\
& \frac{1}{2} I_{zt1} \dot{\theta}_{t1}^2 + \frac{1}{2} I_{xt2} \dot{\phi}_{t2}^2 + \frac{1}{2} I_{zt2} \left(\frac{\dot{y}_{t1} - \dot{y}_{t2} - \dot{\theta}_{t1} l_5}{l_7} \right)^2 + \frac{1}{2} I_{xa1} \dot{\phi}_{a1}^2 + \frac{1}{2} I_{xa2} \dot{\phi}_{a2}^2 + \\
& \frac{1}{2} I_{xa3} \dot{\phi}_{a3}^2 + \frac{1}{2} m_{t2} \dot{y}_{t2}^2
\end{aligned} \quad (4-20)$$

Same substitution will be applied to the equations (4-17) and (4-18). Now the Lagrange's equation is applied to y_{t2} :

$$\left[m_{t2} \ddot{y}_{t2} - \frac{l_{zt2}}{l_7^2} (\ddot{y}_{t1} - \ddot{y}_{t2} - \ddot{\theta}_{t1} l_5) \right] + \left[\left(1 + \frac{l_8}{l_7} \right) (F_{sy5} + F_{sy6}) - (m_{t2}g) \right] + \quad (4-21)$$

$$\left[\left(1 + \frac{l_8}{l_7} \right) (F_{dsy5} + F_{dsy6}) \right] = 0$$

To simplify the equation some variables are defined as follows:

$$S_{a2} = \frac{I_{zt2}}{l_7^2}$$

$$S_{c2} = \frac{I_{zt2}}{l_7^2} + m_{t2}$$

$$S_{a3} = \frac{I_{zt2}}{l_7^2} l_5$$

$$B_{t4} = m_{t2}g - \left(1 + \frac{l_8}{l_7} \right) (F_{sy5} + F_{sy6} + F_{dsy5} + F_{dsy6})$$

Therefore equation (4-21) will be simplified to:

$$-S_{a2}\ddot{y}_{t1} + S_{c2}\ddot{y}_{t2} + S_{a3}\dot{\theta}_{t1} = B_{t4} \quad (4-22)$$

By applying the Lagrange's equation to y_{t1} :

$$\begin{aligned} & \left[m_{t1}\ddot{y}_{t1} + \frac{I_{zt2}}{l_7^2} (\dot{y}_{t1} - \dot{y}_{t2} - \dot{\theta}_{t1}l_5) \right] + \left[(F_{sy1} + F_{sy2} + F_{sy3} + F_{sy4}) - \right. \\ & \left. \frac{l_8}{l_7} (F_{sy5} + F_{sy6}) - (m_{t1}g) \right] + \left[(F_{dsy1} + F_{dsy2} + F_{dsy3} + F_{dsy4}) - \right. \\ & \left. \frac{l_8}{l_7} (F_{dsy5} + F_{dsy6}) \right] = 0 \end{aligned} \quad (4-23)$$

Again to simplify the equation some variables are defined as follows:

$$S_{a1} = \frac{I_{zt2}}{l_7^2} + m_{t1}$$

$$\begin{aligned} B_{t1} = m_{t1}g - & \left[(F_{sy1} + F_{sy2} + F_{sy3} + F_{sy4}) - \frac{l_8}{l_7} (F_{sy5} + F_{sy6}) + (F_{dsy1} + F_{dsy2} + \right. \\ & \left. F_{dsy3} + F_{dsy4}) - \frac{l_8}{l_7} (F_{dsy5} + F_{dsy6}) \right] \end{aligned}$$

Therefore equation (4-23) will be simplified to:

$$S_{a1}\ddot{y}_{t1} - S_{a2}\ddot{y}_{t2} - S_{a3}\dot{\theta}_{t1} = B_{t1} \quad (4-24)$$

Also, by applying the Lagrange's equation to θ_{t1} :

$$\begin{aligned} & \left[I_{zt1} \ddot{\theta}_{t1} - \frac{l_{zt2} l_5}{l_7^2} (\ddot{y}_{t1} - \ddot{y}_{t2} - \ddot{\theta}_{t1} l_5) \right] + \left[l_3 (F_{sy1} + F_{sy2}) - l_4 (F_{sy3} + F_{sy4}) + \right. \\ & \left. \frac{l_5 l_8}{l_7} (F_{sy5} + F_{sy6}) \right] + \left[l_3 (F_{dsy1} + F_{dsy2}) - l_4 (F_{dsy3} + F_{dsy4}) + \frac{l_5 l_8}{l_7} (F_{dsy5} + \right. \\ & \left. F_{dsy6}) \right] = 0 \end{aligned} \quad (4-25)$$

Once again to simplify the equation some variables need to be defined as follows:

$$\begin{aligned} S_{b3} &= I_{zt1} + \frac{I_{zt2} l_5^2}{l_7^2} \\ B_{t3} &= - \left[\left[l_3 (F_{sy1} + F_{sy2}) - l_4 (F_{sy3} + F_{sy4}) + \frac{l_5 l_8}{l_7} (F_{sy5} + F_{sy6}) \right] + \left[l_3 (F_{dsy1} + F_{dsy2}) - \right. \right. \\ &\quad \left. \left. l_4 (F_{dsy3} + F_{dsy4}) + \frac{l_5 l_8}{l_7} (F_{dsy5} + F_{dsy6}) \right] \right] \end{aligned}$$

Therefore equation (4-25) will be simplified to:

$$-S_{a3} \ddot{y}_{t1} + S_{a3} \ddot{y}_{t2} + S_{b3} \ddot{\theta}_{t1} = B_{t3} \quad (4-26)$$

By adding equations (4-22) and (4-24),

$$(S_{a1} - S_{a2}) \ddot{y}_{t1} - (S_{a2} - S_{c2}) \ddot{y}_{t2} = B_{t1} + B_{t4} \quad (4-27)$$

Also by multiplying S_{b3} and S_{a3} to equations (4-24) and (4-26) respectively,

$$(S_{a1} S_{b3} - S_{a3}^2) \ddot{y}_{t1} - (S_{a2} S_{b3} - S_{a3}^2) \ddot{y}_{t2} = S_{b3} B_{t1} + S_{a3} B_{t3} \quad (4-28)$$

By defining the following expressions, equations (4-27) and (4-28) are simplified to equations (4-29) and (4-30) respectively,

$$e_1 = S_{a1} - S_{a2}$$

$$e_2 = S_{a2} - S_{c2}$$

$$e_3 = S_{a1} S_{b3} - S_{a3}^2$$

$$e_4 = S_{a2} S_{b3} - S_{a3}^2$$

$$e_1 \ddot{y}_{t1} - e_2 \ddot{y}_{t2} = B_{t1} + B_{t4} \quad (4-29)$$

$$e_3 \ddot{y}_{t1} - e_4 \ddot{y}_{t2} = S_{b3}B_{t1} + S_{a3}B_{t3} \quad (4-30)$$

Solving equations (2-29) and (2-30) for \ddot{y}_{t1} and \ddot{y}_{t2} will lead to:

$$\ddot{y}_{t1} = \frac{e_4(B_{t1}+B_{t4})-e_2(S_{b3}B_{t1}+S_{a3}B_{t3})}{e_1e_4-e_2e_3} \quad (4-31)$$

$$\ddot{y}_{t2} = \frac{e_1\left(\frac{e_4(B_{t1}+B_{t4})-e_2(S_{b3}B_{t1}+S_{a3}B_{t3})}{e_1e_4-e_2e_3}\right) - \frac{B_{t1}+B_{t4}}{e_2}}{e_2} \quad (4-32)$$

Substituting equations (2-31) and (2-32) into equation (2-26) will give,

$$\begin{aligned} \ddot{\theta}_{t1} = & \frac{B_{t3}}{S_{b3}} + \frac{S_{a3}}{S_{b3}}\left(\frac{e_4(B_{t1}+B_{t4})-e_2(S_{b3}B_{t1}+S_{a3}B_{t3})}{e_1e_4-e_2e_3}\right) - \\ & \frac{S_{a3}}{S_{b3}}\left(\frac{e_1\left(\frac{e_4(B_{t1}+B_{t4})-e_2(S_{b3}B_{t1}+S_{a3}B_{t3})}{e_1e_4-e_2e_3}\right) - \frac{B_{t1}+B_{t4}}{e_2}}{e_2}\right) \end{aligned} \quad (4-33)$$

By applying the Lagrange's equation to $\varphi_{t1}, \varphi_{t2}$:

$$\begin{aligned} I_{xt1} \ddot{\varphi}_{t1} + & \left[\left(\frac{s_1}{2} \right) (F_{sy1} - F_{sy2}) + \left(\frac{s_2}{2} \right) (F_{sy3} - F_{sy4}) \right] + \left[\left(\frac{s_1}{2} \right) (F_{dsy1} - F_{dsy2}) + \right. \\ & \left. \left(\frac{s_2}{2} \right) (F_{dsy3} - F_{dsy4}) \right] = 0 \end{aligned} \quad (4-34)$$

$$I_{xt2} \ddot{\varphi}_{t2} + \left[\left(\frac{s_3}{2} \right) (F_{sy5} - F_{sy6}) \right] + \left[\left(\frac{s_3}{2} \right) (F_{dsy5} - F_{dsy6}) \right] = 0 \quad (4-35)$$

Also the rest of degrees of freedom will be as follows:

$$\begin{aligned} m_{a1} \ddot{y}_{a1} - (F_{sy1} + F_{sy2}) + (F_{ty1} + F_{ty2}) - (F_{dsy1} + F_{dsy2}) + (F_{dty1} + \\ F_{dty2}) = m_{a1}g \end{aligned} \quad (4-36)$$

$$\begin{aligned} I_{xa1} \ddot{\varphi}_{a1} - \left(\frac{s_1}{2} \right) (F_{sy1} - F_{sy2}) + \left(\frac{d_1}{2} \right) (F_{ty1} - F_{ty2}) - \left(\frac{s_1}{2} \right) (F_{dsy1} - F_{dsy2}) + \\ \left(\frac{d_1}{2} \right) (F_{dty1} - F_{dty2}) = 0 \end{aligned} \quad (4-37)$$

$$\begin{aligned} m_{a2} \ddot{y}_{a2} - (F_{sy3} + F_{sy4}) + (F_{ty3} + F_{ty4}) - (F_{dsy3} + F_{dsy4}) + (F_{dty3} + \\ F_{dty4}) = m_{a2}g \end{aligned} \quad (4-38)$$

$$I_{xa2}\ddot{\varphi}_{a2} - \left(\frac{s_2}{2}\right)(F_{sy3} - F_{sy4}) + \left(\frac{d_2}{2}\right)(F_{ty3} - F_{ty4}) - \left(\frac{s_2}{2}\right)(F_{dsy3} - F_{dsy4}) + \left(\frac{d_2}{2}\right)(F_{dty3} - F_{dty4}) = 0 \quad (4-39)$$

$$m_{a3}\ddot{y}_{a3} - (F_{sy5} + F_{sy6}) + (F_{ty5} + F_{ty6}) - (F_{dsy5} + F_{dsy6}) + (F_{dty5} + F_{dty6}) = m_{a3}g \quad (4-40)$$

$$I_{xa3}\ddot{\varphi}_{a3} - \left(\frac{s_3}{2}\right)(F_{sy5} - F_{sy6}) + \left(\frac{d_3}{2}\right)(F_{ty5} - F_{ty6}) - \left(\frac{s_3}{2}\right)(F_{dsy5} - F_{dsy6}) + \left(\frac{d_3}{2}\right)(F_{dty5} - F_{dty6}) = 0 \quad (4-41)$$

4.5 Derivation of Equations of Motion for “Type 3 Truck”

There are nine degrees of freedom in total for this type of truck. The degrees of freedom

TABLE 4-6: DEGREES OF FREEDOM OF TYPE 3 TRUCK

No.	Degree of Freedom	Contributed Mass	Description
1	y_{t1}	m_{t1}	Truck vertical displacement and mass
2	φ_{t1}	I_{xt1}	Truck roll displacement and mass moment of inertia
3	θ_{t1}	I_{zt1}	Truck pitch displacement and mass moment of inertia
4	y_{a1}	m_{a1}	First axle vertical displacement and mass
5	φ_{a1}	I_{xa1}	First axle roll displacement and mass moment of inertia
6	y_{a2}	m_{a2}	Second axle vertical displacement and mass
7	φ_{a2}	I_{xa2}	Second axle roll displacement and mass moment of inertia
8	y_{a3}	m_{a3}	Third axle vertical displacement and mass
9	φ_{a3}	I_{xa3}	Third axle roll displacement and mass moment of inertia

can be seen in Figure 4-4 and the description of those degrees of freedom can be found in Table 4-6. Relative Displacements at the locations of the springs are also calculated using the values given in Table 4-7.

Kinetic Energy of the system:

$$T = \frac{1}{2}m_{t1}\dot{y}_{t1}^2 + \frac{1}{2}m_{a1}\dot{y}_{a1}^2 + \frac{1}{2}m_{a2}\dot{y}_{a2}^2 + \frac{1}{2}m_{a3}\dot{y}_{a3}^2 + \frac{1}{2}I_{xt1}\dot{\phi}_{t1}^2 + \frac{1}{2}I_{zt1}\dot{\theta}_{t1}^2 + \frac{1}{2}I_{xa1}\dot{\phi}_{a1}^2 + \frac{1}{2}I_{xa2}\dot{\phi}_{a2}^2 + \frac{1}{2}I_{xa3}\dot{\phi}_{a3}^2 \quad (4-42)$$

Potential Energy of the system:

$$V = \frac{1}{2}K_{sy1}U_{sy1}^2 + \frac{1}{2}K_{sy2}U_{sy2}^2 + \frac{1}{2}K_{sy3}U_{sy3}^2 + \frac{1}{2}K_{sy4}U_{sy4}^2 + \frac{1}{2}K_{sy5}U_{sy5}^2 + \frac{1}{2}K_{sy6}U_{sy6}^2 + \frac{1}{2}K_{ty1}U_{ty1}^2 + \frac{1}{2}K_{ty2}U_{ty2}^2 + \frac{1}{2}K_{ty3}U_{ty3}^2 + \frac{1}{2}K_{ty4}U_{ty4}^2 + \frac{1}{2}K_{ty5}U_{ty5}^2 + \frac{1}{2}K_{ty6}U_{ty6}^2 - ((m_{t1}g)y_{t1} + (m_{a1}g)y_{a1} + (m_{a2}g)y_{a2} + (m_{a3}g)y_{a3}) + (F_{y1}U_{sy1} + F_{y2}U_{sy2} + F_{y3}U_{sy3} + F_{y4}U_{sy4} + F_{y5}U_{sy5} + F_{y6}U_{sy6}) \quad (4-43)$$

Damping Energy of the system:

$$D = \frac{1}{2}D_{sy1}\dot{U}_{sy1}^2 + \frac{1}{2}D_{sy2}\dot{U}_{sy2}^2 + \frac{1}{2}D_{sy3}\dot{U}_{sy3}^2 + \frac{1}{2}D_{sy4}\dot{U}_{sy4}^2 + \frac{1}{2}D_{sy5}\dot{U}_{sy5}^2 + \frac{1}{2}D_{sy6}\dot{U}_{sy6}^2 + \frac{1}{2}D_{ty1}\dot{U}_{ty1}^2 + \frac{1}{2}D_{ty2}\dot{U}_{ty2}^2 + \frac{1}{2}D_{ty3}\dot{U}_{ty3}^2 + \frac{1}{2}D_{ty4}\dot{U}_{ty4}^2 + \frac{1}{2}D_{ty5}\dot{U}_{ty5}^2 + \frac{1}{2}D_{ty6}\dot{U}_{ty6}^2 \quad (4-44)$$

Now the Lagrange's equation is applied to y_{t1} :

$$m_{t1}\ddot{y}_{t1} + [(F_{sy1} + F_{sy2} + F_{sy3} + F_{sy4} + F_{sy5} + F_{sy6}) + (F_{dsy1} + F_{dsy2} + F_{dsy3} + F_{dsy4} + F_{dsy5} + F_{dsy6})] = m_{t1}g \quad (4-45)$$

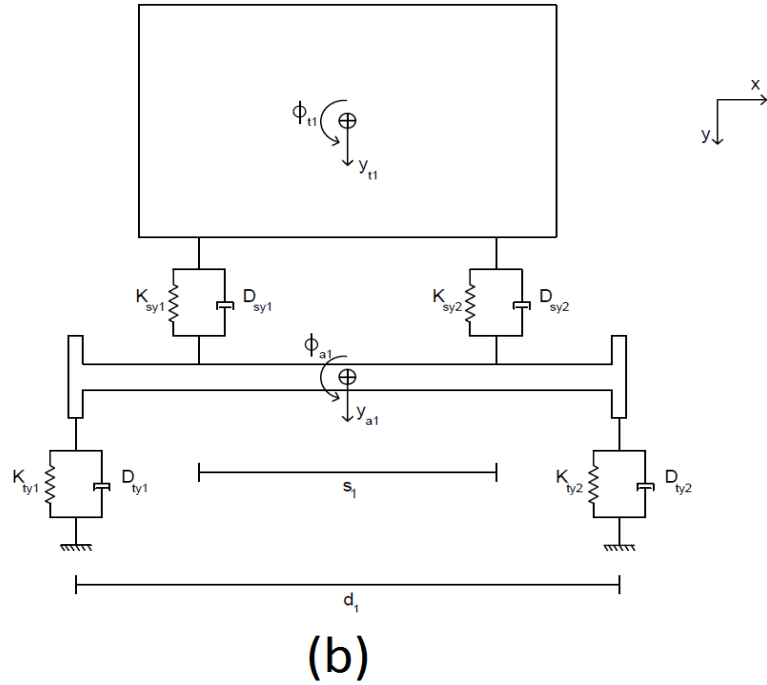
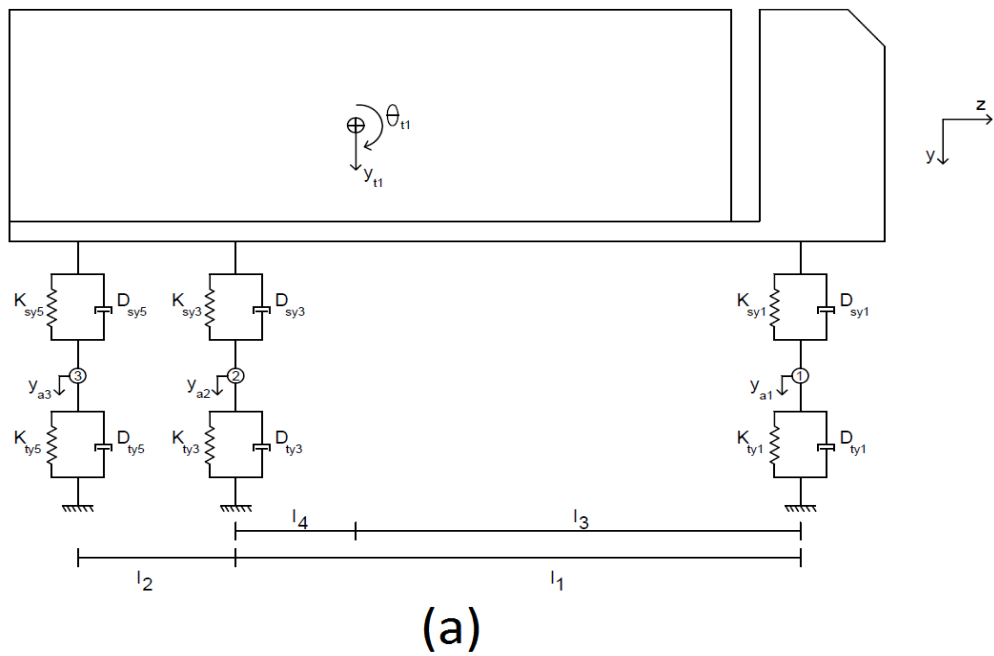


FIGURE 4-4: TYPE 3 DYNAMIC MODEL (A) TRUCK SIDE VIEW (B) TRUCK FRONT VIEW

TABLE 4-7: RELATIVE DISPLACEMENTS AT SPRING LOCATIONS OF TYPE 3 TRUCK

Suspension springs	
\mathbf{U}_{sy1}	$(y_{t1} - y_{a1}) + (S_1/2)(\varphi_{t1} - \varphi_{a1}) + l_3\theta_{t1}$
\mathbf{U}_{sy2}	$(y_{t1} - y_{a1}) - (S_1/2)(\varphi_{t1} - \varphi_{a1}) + l_3\theta_{t1}$
\mathbf{U}_{sy3}	$(y_{t1} - y_{a2}) + (S_2/2)(\varphi_{t1} - \varphi_{a2}) - l_4\theta_{t1}$
\mathbf{U}_{sy4}	$(y_{t1} - y_{a2}) - (S_2/2)(\varphi_{t1} - \varphi_{a2}) - l_4\theta_{t1}$
\mathbf{U}_{sy5}	$(y_{t1} - y_{a3}) + (S_3/2)(\varphi_{t1} - \varphi_{a3}) - (l_2 + l_4)\theta_{t1}$
\mathbf{U}_{sy6}	$(y_{t1} - y_{a3}) - (S_3/2)(\varphi_{t1} - \varphi_{a3}) - (l_2 + l_4)\theta_{t1}$
Tire springs	
\mathbf{U}_{ty1}	$y_{a1} + (d_1/2)\varphi_{a1} + u_{SR1}$
\mathbf{U}_{ty2}	$y_{a1} - (d_1/2)\varphi_{a1} + u_{SR2}$
\mathbf{U}_{ty3}	$y_{a2} + (d_2/2)\varphi_{a2} + u_{SR3}$
\mathbf{U}_{ty4}	$y_{a2} - (d_2/2)\varphi_{a2} + u_{SR4}$
\mathbf{U}_{ty5}	$y_{a3} + (d_3/2)\varphi_{a3} + u_{SR5}$
\mathbf{U}_{ty6}	$y_{a3} - (d_3/2)\varphi_{a3} + u_{SR6}$

Also, by applying the Lagrange's equation to θ_{t1} :

$$I_{zt1}\ddot{\theta}_{t1} + [l_3(F_{sy1} + F_{sy2}) - l_4(F_{sy3} + F_{sy4}) - (l_2 + l_4)(F_{sy5} + F_{sy6})] + [l_3(F_{dsy1} + F_{dsy2}) - l_4(F_{dsy3} + F_{dsy4}) - (l_2 + l_4)(F_{dsy5} + F_{dsy6})] = 0 \quad (4-46)$$

By applying the Lagrange's equation to φ_{t1} :

$$I_{xt1}\ddot{\varphi}_{t1} + \left[\left(\frac{s_1}{2}\right)(F_{sy1} - F_{sy2}) + \left(\frac{s_2}{2}\right)(F_{sy3} - F_{sy4}) + \left(\frac{s_3}{2}\right)(F_{sy5} - F_{sy6}) \right] + \left[\left(\frac{s_1}{2}\right)(F_{dsy1} - F_{dsy2}) + \left(\frac{s_2}{2}\right)(F_{dsy3} - F_{dsy4}) + \left(\frac{s_3}{2}\right)(F_{dsy5} - F_{dsy6}) \right] = 0 \quad (4-47)$$

Also the rest of degrees of freedom will be as follows:

$$m_{a1}\ddot{y}_{a1} - (F_{sy1} + F_{sy2}) + (F_{ty1} + F_{ty2}) - (F_{dsy1} + F_{dsy2}) + (F_{dty1} + F_{dty2}) = 0 \quad (4-48)$$

$$F_{dty2}) = m_{a1}g$$

$$I_{xa1}\ddot{\varphi}_{a1} - (\frac{s_1}{2})(F_{sy1} - F_{sy2}) + (\frac{d_1}{2})(F_{ty1} - F_{ty2}) - (\frac{s_1}{2})(F_{dsy1} - F_{dsy2}) + \\ (\frac{d_1}{2})(F_{dty1} - F_{dty2}) = 0 \quad (4-49)$$

$$m_{a2}\ddot{y}_{a2} - (F_{sy3} + F_{sy4}) + (F_{ty3} + F_{ty4}) - (F_{dsy3} + F_{dsy4}) + (F_{dty3} + \\ F_{dty4}) = m_{a2}g \quad (4-50)$$

$$I_{xa2}\ddot{\varphi}_{a2} - (\frac{s_2}{2})(F_{sy3} - F_{sy4}) + (\frac{d_2}{2})(F_{ty3} - F_{ty4}) - (\frac{s_2}{2})(F_{dsy3} - F_{dsy4}) + \\ (\frac{d_2}{2})(F_{dty3} - F_{dty4}) = 0 \quad (4-51)$$

$$m_{a3}\ddot{y}_{a3} - (F_{sy5} + F_{sy6}) + (F_{ty5} + F_{ty6}) - (F_{dsy5} + F_{dsy6}) + (F_{dty5} + \\ F_{dty6}) = m_{a3}g \quad (4-52)$$

$$I_{xa3}\ddot{\varphi}_{a3} - (\frac{s_3}{2})(F_{sy5} - F_{sy6}) + (\frac{d_3}{2})(F_{ty5} - F_{ty6}) - (\frac{s_3}{2})(F_{dsy5} - F_{dsy6}) + \\ (\frac{d_3}{2})(F_{dty5} - F_{dty6}) = 0 \quad (4-53)$$

4.6 Derivation of Equations of Motion for “Type 3S2 Truck (FDOT Truck)”

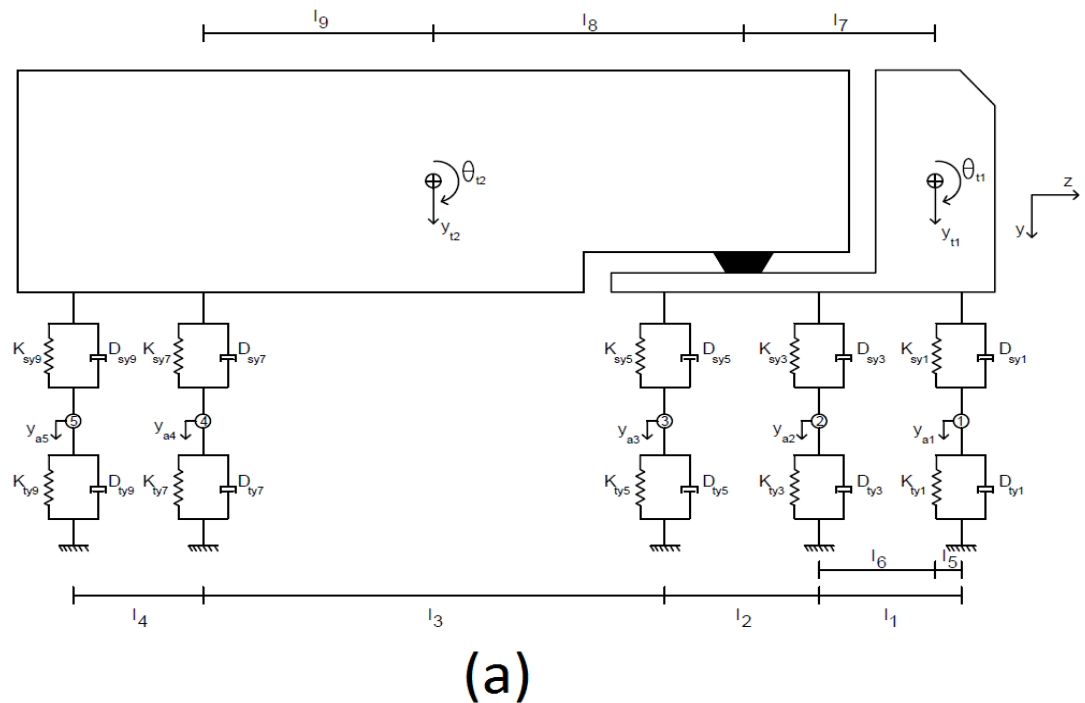
There are sixteen degrees of freedom in total for this type of truck. The degrees of freedom can be seen in Figure 4-5 and the description of those degrees of freedom can be found in Table 4-8. Relative Displacements at the locations of the springs are also calculated using the values given in Table 4-9.

Kinetic Energy of the system:

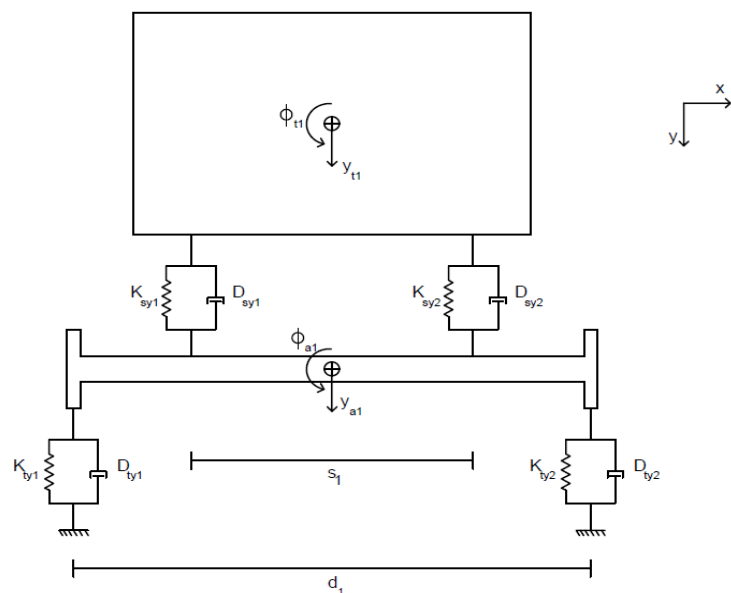
$$\begin{aligned}
 T = & \frac{1}{2}m_{t1}\dot{y}_{t1}^2 + \frac{1}{2}m_{a1}\dot{y}_{a1}^2 + \frac{1}{2}m_{a2}\dot{y}_{a2}^2 + \frac{1}{2}m_{a3}\dot{y}_{a3}^2 + \frac{1}{2}m_{a4}\dot{y}_{a4}^2 + \\
 & \frac{1}{2}m_{a5}\dot{y}_{a5}^2 + \frac{1}{2}I_{xt1}\dot{\phi}_{t1}^2 + \frac{1}{2}I_{zt1}\dot{\theta}_{t1}^2 + \frac{1}{2}I_{xt2}\dot{\phi}_{t2}^2 + \frac{1}{2}I_{zt2}\dot{\theta}_{t2}^2 + \frac{1}{2}I_{xa1}\dot{\phi}_{a1}^2 + \\
 & \frac{1}{2}I_{xa2}\dot{\phi}_{a2}^2 + \frac{1}{2}I_{xa3}\dot{\phi}_{a3}^2 + \frac{1}{2}I_{xa4}\dot{\phi}_{a4}^2 + \frac{1}{2}I_{xa5}\dot{\phi}_{a5}^2 + \frac{1}{2}m_{t2}\dot{y}_{t2}^2
 \end{aligned} \quad (4-54)$$

TABLE 4-8: DEGREES OF FREEDOM OF TYPE 3S2 TRUCK

No.	Degree of Freedom	Contributed Mass	Description
1	y_{t1}	m_{t1}	Tractor vertical displacement and mass
2	φ_{t1}	I_{xt1}	Tractor roll displacement and mass moment of inertia
3	θ_{t1}	I_{zt1}	Tractor pitch displacement and mass moment of inertia
4	y_{t2}	m_{t2}	Trailer vertical displacement and mass
5	φ_{t2}	I_{xt2}	Trailer roll displacement and mass moment of inertia
6	θ_{t2}	I_{zt2}	Trailer pitch displacement and mass moment of inertia
7	y_{a1}	m_{a1}	Steer axle vertical displacement and mass
8	φ_{a1}	I_{xa1}	Steer axle roll displacement and mass moment of inertia
9	y_{a2}	m_{a2}	Vertical displacement and mass of forward axle of tractor tandem
10	φ_{a2}	I_{xa2}	Roll displacement and mass moment of inertia of forward axle of tractor tandem
11	y_{a3}	m_{a3}	Vertical displacement and mass of aft axle of tractor tandem
12	φ_{a3}	I_{xa3}	Roll displacement and mass moment of inertia of aft axle of tractor tandem
13	y_{a4}	m_{a4}	Vertical displacement and mass of forward axle of trailer tandem
14	φ_{a4}	I_{xa4}	Roll displacement and mass moment of inertia of forward axle of trailer tandem
15	y_{a5}	m_{a5}	Vertical displacement and mass of aft axle of trailer tandem
16	φ_{a5}	I_{xa5}	Roll displacement and mass moment of inertia of aft axle of trailer tandem



(a)



(b)

FIGURE 4-5: TYPE 3S2 DYNAMIC MODEL (A) TRUCK SIDE VIEW (B) TRUCK FRONT VIEW

TABLE 4-9: RELATIVE DISPLACEMENTS AT SPRING LOCATIONS OF TYPE 3S2 TRUCK

Suspension springs	
\mathbf{U}_{sy1}	$(y_{t1} - y_{a1}) + (S_1/2)(\varphi_{t1} - \varphi_{a1}) + l_5\theta_{t1}$
\mathbf{U}_{sy2}	$(y_{t1} - y_{a1}) - (S_1/2)(\varphi_{t1} - \varphi_{a1}) + l_5\theta_{t1}$
\mathbf{U}_{sy3}	$(y_{t1} - y_{a2}) + (S_2/2)(\varphi_{t1} - \varphi_{a2}) - l_6\theta_{t1}$
\mathbf{U}_{sy4}	$(y_{t1} - y_{a2}) - (S_2/2)(\varphi_{t1} - \varphi_{a2}) - l_6\theta_{t1}$
\mathbf{U}_{sy5}	$(y_{t1} - y_{a3}) + (S_3/2)(\varphi_{t1} - \varphi_{a3}) - (l_2 + l_6)\theta_{t1}$
\mathbf{U}_{sy6}	$(y_{t1} - y_{a3}) - (S_3/2)(\varphi_{t1} - \varphi_{a3}) - (l_2 + l_6)\theta_{t1}$
\mathbf{U}_{sy7}	$(y_{t2} - y_{a4}) + (S_4/2)(\varphi_{t2} - \varphi_{a4}) - l_9\theta_{t2}$
\mathbf{U}_{sy8}	$(y_{t2} - y_{a4}) - (S_4/2)(\varphi_{t2} - \varphi_{a4}) - l_9\theta_{t2}$
\mathbf{U}_{sy9}	$(y_{t2} - y_{a5}) + (S_5/2)(\varphi_{t2} - \varphi_{a5}) - (l_4 + l_9)\theta_{t2}$
\mathbf{U}_{sy10}	$(y_{t2} - y_{a5}) - (S_5/2)(\varphi_{t2} - \varphi_{a5}) - (l_4 + l_9)\theta_{t2}$
Tire springs	
\mathbf{U}_{ty1}	$y_{a1} + (d_1/2)\varphi_{a1} + u_{SR1}$
\mathbf{U}_{ty2}	$y_{a1} - (d_1/2)\varphi_{a1} + u_{SR2}$
\mathbf{U}_{ty3}	$y_{a2} + (d_2/2)\varphi_{a2} + u_{SR3}$
\mathbf{U}_{ty4}	$y_{a2} - (d_2/2)\varphi_{a2} + u_{SR4}$
\mathbf{U}_{ty5}	$y_{a3} + (d_3/2)\varphi_{a3} + u_{SR5}$
\mathbf{U}_{ty6}	$y_{a3} - (d_3/2)\varphi_{a3} + u_{SR6}$
\mathbf{U}_{ty7}	$y_{a4} + (d_4/2)\varphi_{a4} + u_{SR7}$
\mathbf{U}_{ty8}	$y_{a4} - (d_4/2)\varphi_{a4} + u_{SR8}$
\mathbf{U}_{ty9}	$y_{a5} + (d_5/2)\varphi_{a5} + u_{SR9}$
\mathbf{U}_{ty10}	$y_{a5} - (d_5/2)\varphi_{a5} + u_{SR10}$

Potential Energy of the system:

$$\begin{aligned}
V = & \frac{1}{2}K_{sy1}U_{sy1}^2 + \frac{1}{2}K_{sy2}U_{sy2}^2 + \frac{1}{2}K_{sy3}U_{sy3}^2 + \frac{1}{2}K_{sy4}U_{sy4}^2 + \\
& \frac{1}{2}K_{sy5}U_{sy5}^2 + \frac{1}{2}K_{sy6}U_{sy6}^2 + \frac{1}{2}K_{sy7}U_{sy7}^2 + \frac{1}{2}K_{sy8}U_{sy8}^2 + \frac{1}{2}K_{sy9}U_{sy9}^2 + \\
& \frac{1}{2}K_{sy10}U_{sy10}^2 + \frac{1}{2}K_{ty1}U_{ty1}^2 + \frac{1}{2}K_{ty2}U_{ty2}^2 + \frac{1}{2}K_{ty3}U_{ty3}^2 + \frac{1}{2}K_{ty4}U_{ty4}^2 + \\
& \frac{1}{2}K_{ty5}U_{ty5}^2 + \frac{1}{2}K_{ty6}U_{ty6}^2 + \frac{1}{2}K_{ty7}U_{sy7}^2 + \frac{1}{2}K_{ty8}U_{ty8}^2 + \frac{1}{2}K_{ty9}U_{ty9}^2 + \\
& \frac{1}{2}K_{ty10}U_{ty10}^2 - ((m_{t1}g)y_{t1} + (m_{t2}g)y_{t2} + (m_{a1}g)y_{a1} + (m_{a2}g)y_{a2} + \\
& (m_{a3}g)y_{a3} + (m_{a4}g)y_{a4} + (m_{a5}g)y_{a5}) + (F_{y1}U_{sy1} + F_{y2}U_{sy2} + \\
& F_{y3}U_{sy3} + F_{y4}U_{sy4} + F_{y5}U_{sy5} + F_{y6}U_{sy6} + F_{y7}U_{sy7} + F_{y8}U_{sy8} + F_{y9}U_{sy9} + \\
& F_{y10}U_{sy10})
\end{aligned} \tag{4-55}$$

Damping Energy of the system:

$$\begin{aligned}
D = & \frac{1}{2}D_{sy1}\dot{U}_{sy1}^2 + \frac{1}{2}D_{sy2}\dot{U}_{sy2}^2 + \frac{1}{2}D_{sy3}\dot{U}_{sy3}^2 + \frac{1}{2}D_{sy4}\dot{U}_{sy4}^2 + \\
& \frac{1}{2}D_{sy5}\dot{U}_{sy5}^2 + \frac{1}{2}D_{sy6}\dot{U}_{sy6}^2 + \frac{1}{2}D_{sy7}\dot{U}_{sy7}^2 + \frac{1}{2}D_{sy8}\dot{U}_{sy8}^2 + \frac{1}{2}D_{sy9}\dot{U}_{sy9}^2 + \\
& \frac{1}{2}D_{sy10}\dot{U}_{sy10}^2 + \frac{1}{2}D_{ty1}\dot{U}_{ty1}^2 + \frac{1}{2}D_{ty2}\dot{U}_{ty2}^2 + \frac{1}{2}D_{ty3}\dot{U}_{ty3}^2 + \frac{1}{2}D_{ty4}\dot{U}_{ty4}^2 + \\
& \frac{1}{2}D_{ty5}\dot{U}_{ty5}^2 + \frac{1}{2}D_{ty6}\dot{U}_{ty6}^2 + \frac{1}{2}D_{ty7}\dot{U}_{ty7}^2 + \frac{1}{2}D_{ty8}\dot{U}_{ty8}^2 + \frac{1}{2}D_{ty9}\dot{U}_{ty9}^2 + \\
& \frac{1}{2}D_{ty10}\dot{U}_{ty10}^2
\end{aligned} \tag{4-56}$$

The displacement at the pivot point should stay the same, whether it is calculated from the trailer part or the tractor part,

$$y_{t2} + \theta_{t2}l_8 = y_{t1} - \theta_{t1}l_7 \tag{4-57}$$

Thus, by calculating θ_{t2} from equation (4-57) and substituting in equation (4-54),

$$\begin{aligned}
T = & \frac{1}{2}m_{t1}\dot{y}_{t1}^2 + \frac{1}{2}m_{a1}\dot{y}_{a1}^2 + \frac{1}{2}m_{a2}\dot{y}_{a2}^2 + \frac{1}{2}m_{a3}\dot{y}_{a3}^2 + \frac{1}{2}m_{a4}\dot{y}_{a4}^2 + \\
& \frac{1}{2}m_{a5}\dot{y}_{a5}^2 + \frac{1}{2}I_{xt1}\dot{\phi}_{t1}^2 + \frac{1}{2}I_{zt1}\dot{\theta}_{t1}^2 + \frac{1}{2}I_{xt2}\dot{\phi}_{t2}^2 + \frac{1}{2}I_{zt2}\left(\frac{\dot{y}_{t1}-\dot{y}_{t2}-\dot{\theta}_{t1}l_7}{l_8}\right)^2 + \quad (4-58) \\
& \frac{1}{2}I_{xa1}\dot{\phi}_{a1}^2 + \frac{1}{2}I_{xa2}\dot{\phi}_{a2}^2 + \frac{1}{2}I_{xa3}\dot{\phi}_{a3}^2 + \frac{1}{2}I_{xa4}\dot{\phi}_{a4}^2 + \frac{1}{2}I_{xa5}\dot{\phi}_{a5}^2 + \frac{1}{2}m_{t2}\dot{y}_{t2}^2
\end{aligned}$$

Same substitution will be applied to the equations (4-55) and (4-56). Now the Lagrange's equation is applied to y_{t2} :

$$\begin{aligned}
& \left[m_{t2}\ddot{y}_{t2} - \frac{I_{zt2}}{l_8^2}(\ddot{y}_{t1} - \ddot{y}_{t2} - \ddot{\theta}_{t1}l_7) \right] + \left[\left(1 + \frac{l_9}{l_8}\right)(K_{sy7}U_{sy7} + K_{sy8}U_{sy8} + \right. \\
& \left. F_{y7} + F_{y8}) + \left(1 + \frac{l_4+l_9}{l_8}\right)(K_{sy9}U_{sy9} + K_{sy10}U_{sy10} + F_{y9} + F_{y10}) - (m_{t2}g) \right] + \quad (4-59) \\
& \left[\left(1 + \frac{l_9}{l_8}\right)(D_{sy7}\dot{U}_{sy7} + D_{sy8}\dot{U}_{sy8}) + \left(1 + \frac{l_4+l_9}{l_8}\right)(D_{sy9}\dot{U}_{sy9} + D_{sy10}\dot{U}_{sy10}) \right] = \\
& 0
\end{aligned}$$

To simplify the equation some variables are defined as follows:

$$S_{a2} = \frac{I_{zt2}}{l_8^2}$$

$$S_{c2} = \frac{I_{zt2}}{l_8^2} + m_{t2}$$

$$S_{a3} = \frac{I_{zt2}}{l_8^2}l_7$$

$$\begin{aligned}
B_{t4} = & m_{t2}g - \left(1 + \frac{l_9}{l_8}\right)(F_{sy7} + F_{sy8} + F_{dsy7} + F_{dsy8}) - \left(1 + \frac{l_4+l_9}{l_8}\right)(F_{sy9} + F_{sy10} + \\
& F_{dsy9} + F_{dsy10})
\end{aligned}$$

Therefore equation (4-59) will be simplified to:

$$-S_{a2}\ddot{y}_{t1} + S_{c2}\ddot{y}_{t2} + S_{a3}\ddot{\theta}_{t1} = B_{t4} \quad (4-60)$$

By applying the Lagrange's equation to y_{t1} :

$$\begin{aligned} & \left[m_{t1} \ddot{y}_{t1} + \frac{I_{zt2}}{l_8^2} (\ddot{y}_{t1} - \ddot{y}_{t2} - \ddot{\theta}_{t1} l_7) \right] + \left[(F_{sy1} + F_{sy2} + F_{sy3} + F_{sy4} + F_{sy5} + \right. \\ & F_{sy6}) - \frac{l_9}{l_8} (F_{sy7} + F_{sy8}) - \frac{l_9 + l_4}{l_8} (F_{sy9} + F_{sy10}) - (m_{t1} g) \left. \right] + \left[(F_{dsy1} + \right. \\ & F_{dsy2} + F_{dsy3} + F_{dsy4} + F_{dsy5} + F_{dsy6}) - \frac{l_9}{l_8} (F_{dsy7} + F_{dsy8}) - \frac{l_9 + l_4}{l_8} (F_{dsy9} + \right. \\ & \left. F_{dsy10}) \right] = 0 \end{aligned} \quad (4-61)$$

Again to simplify the equation some variables are defined as follows:

$$S_{a1} = \frac{I_{zt2}}{l_8^2} + m_{t1}$$

$$\begin{aligned} B_{t1} = & m_{t1} g - [(F_{sy1} + F_{sy2} + F_{sy3} + F_{sy4} + F_{sy5} + F_{sy6}) - \frac{l_9}{l_8} (F_{sy7} + F_{sy8}) - \\ & \frac{l_9 + l_4}{l_8} (F_{sy9} + F_{sy10}) + (F_{dsy1} + F_{dsy2} + F_{dsy3} + F_{dsy4} + F_{dsy5} + F_{dsy6}) - \frac{l_9}{l_8} (F_{dsy7} + \\ & F_{dsy8}) - \frac{l_9 + l_4}{l_8} (F_{dsy9} + F_{dsy10})] \end{aligned}$$

Therefore equation (2-61) will be simplified to:

$$S_{a1} \ddot{y}_{t1} - S_{a2} \ddot{y}_{t2} - S_{a3} \ddot{\theta}_{t1} = B_{t1} \quad (4-62)$$

Also, by applying the Lagrange's equation to θ_{t1} :

$$\begin{aligned} & \left[I_{zt1} \ddot{\theta}_{t1} - \frac{I_{zt2} l_7}{l_8^2} (\ddot{y}_{t1} - \ddot{y}_{t2} - \ddot{\theta}_{t1} l_7) \right] + \left[l_5 (F_{sy1} + F_{sy2}) - l_6 (F_{sy3} + F_{sy4}) - \right. \\ & (l_2 + l_6) (F_{sy5} + F_{sy6}) + \frac{l_7 l_9}{l_8} (F_{sy7} + F_{sy8}) + \frac{l_7 (l_4 + l_9)}{l_8} (F_{sy9} + F_{sy10}) \left. \right] + \\ & \left[l_5 (F_{dsy1} + F_{dsy2}) - l_6 (F_{dsy3} + F_{dsy4}) - (l_2 + l_6) (F_{dsy5} + F_{dsy6}) + \right. \\ & \left. \frac{l_7 l_9}{l_8} (F_{dsy7} + F_{dsy8}) + \frac{l_7 (l_4 + l_9)}{l_8} (F_{dsy9} + F_{dsy10}) \right] = 0 \end{aligned} \quad (4-63)$$

Once again to simplify the equation some variables need to be defined as follows:

$$S_{b3} = I_{zt1} + \frac{I_{zt2}l_7^2}{l_8^2}$$

$$\begin{aligned} B_{t3} = & - \left[\left[l_5(F_{sy1} + F_{sy2}) - l_6(F_{sy3} + F_{sy4}) - (l_2 + l_6)(F_{sy5} + F_{sy6}) + \frac{l_7l_9}{l_8}(F_{sy7} + \right. \right. \\ & F_{sy8}) + \frac{l_7(l_4+l_9)}{l_8}(F_{sy9} + F_{sy10}) \left. \right] + \left[l_5(F_{dsy1} + F_{dsy2}) - l_6(F_{dsy3} + F_{dsy4}) - (l_2 + \right. \\ & l_6)(F_{dsy5} + F_{dsy6}) + \frac{l_7l_9}{l_8}(F_{dsy7} + F_{dsy8}) + \frac{l_7(l_4+l_9)}{l_8}(F_{dsy9} + F_{dsy10}) \left. \right] \left. \right] \end{aligned}$$

Therefore equation (2-63) will be simplified to:

$$-S_{a3}\ddot{y}_{t1} + S_{a3}\ddot{y}_{t2} + S_{b3}\ddot{\theta}_{t1} = B_{t3} \quad (4-64)$$

By adding equations (2-60) and (2-62),

$$(S_{a1} - S_{a2})\ddot{y}_{t1} - (S_{a2} - S_{c2})\ddot{y}_{t2} = B_{t1} + B_{t4} \quad (4-65)$$

Also by multiplying S_{b3} and S_{a3} to equations (2-62) and (2-64) respectively,

$$(S_{a1}S_{b3} - S_{a3}^2)\ddot{y}_{t1} - (S_{a2}S_{b3} - S_{a3}^2)\ddot{y}_{t2} = S_{b3}B_{t1} + S_{a3}B_{t3} \quad (4-66)$$

By defining the following expressions, equations (2-65) and (2-66) are simplified to equations (2-67) and (2-68) respectively,

$$e_1 = S_{a1} - S_{a2}$$

$$e_2 = S_{a2} - S_{c2}$$

$$e_3 = S_{a1}S_{b3} - S_{a3}^2$$

$$e_4 = S_{a2}S_{b3} - S_{a3}^2$$

$$e_1\ddot{y}_{t1} - e_2\ddot{y}_{t2} = B_{t1} + B_{t4} \quad (4-67)$$

$$e_3\ddot{y}_{t1} - e_4\ddot{y}_{t2} = S_{b3}B_{t1} + S_{a3}B_{t3} \quad (4-68)$$

Solving equations (2-67) and (2-68) for \ddot{y}_{t1} and \ddot{y}_{t2} will lead to:

$$\ddot{y}_{t1} = \frac{e_4(B_{t1} + B_{t4}) - e_2(S_{b3}B_{t1} + S_{a3}B_{t3})}{e_1e_4 - e_2e_3} \quad (4-69)$$

$$\ddot{y}_{t2} = \frac{e_1}{e_2} \left(\frac{e_4(B_{t1}+B_{t4}) - e_2(S_{b3}B_{t1} + S_{a3}B_{t3})}{e_1e_4 - e_2e_3} \right) - \frac{B_{t1}+B_{t4}}{e_2} \quad (4-70)$$

Substituting equations (4-69) and (4-70) into equation (4-64) will give,

$$\begin{aligned} \ddot{\theta}_{t1} &= \frac{B_{t3}}{S_{b3}} + \frac{S_{a3}}{S_{b3}} \left(\frac{e_4(B_{t1}+B_{t4}) - e_2(S_{b3}B_{t1} + S_{a3}B_{t3})}{e_1e_4 - e_2e_3} \right) - \\ &\quad \frac{S_{a3}}{S_{b3}} \left(\frac{e_1 \left(e_4(B_{t1}+B_{t4}) - e_2(S_{b3}B_{t1} + S_{a3}B_{t3}) \right)}{e_1e_4 - e_2e_3} - \frac{B_{t1}+B_{t4}}{e_2} \right) \end{aligned} \quad (4-71)$$

By applying the Lagrange's equation to $\varphi_{t1}, \varphi_{t2}$:

$$I_{xt1} \ddot{\varphi}_{t1} + \left[\left(\frac{s_1}{2} \right) (F_{sy1} - F_{sy2}) + \left(\frac{s_2}{2} \right) (F_{sy3} - F_{sy4}) + \left(\frac{s_3}{2} \right) (F_{sy5} - F_{sy6}) \right] + \quad (4-72)$$

$$\begin{aligned} &\left[\left(\frac{s_1}{2} \right) (F_{dsy1} - F_{dsy2}) + \left(\frac{s_2}{2} \right) (F_{dsy3} - F_{dsy4}) + \left(\frac{s_3}{2} \right) (F_{dsy5} - F_{dsy6}) \right] = 0 \\ I_{xt2} \ddot{\varphi}_{t2} + &\left[\left(\frac{s_4}{2} \right) (F_{sy7} - F_{sy8}) + \left(\frac{s_5}{2} \right) (F_{sy9} - F_{sy10}) \right] + \left[\left(\frac{s_4}{2} \right) (F_{dsy7} - \right. \\ &\left. F_{dsy8}) + \left(\frac{s_5}{2} \right) (F_{dsy9} - F_{dsy10}) \right] = 0 \end{aligned} \quad (4-73)$$

Also the rest of degrees of freedom will be as follows:

$$\begin{aligned} m_{a1} \ddot{y}_{a1} - (F_{sy1} + F_{sy2}) + (F_{ty1} + F_{ty2}) - (F_{dsy1} + F_{dsy2}) + (F_{dty1} + \\ F_{dty2}) = m_{a1}g \end{aligned} \quad (4-74)$$

$$\begin{aligned} I_{xa1} \ddot{\varphi}_{a1} - \left(\frac{s_1}{2} \right) (F_{sy1} - F_{sy2}) + \left(\frac{d_1}{2} \right) (F_{ty1} - F_{ty2}) - \left(\frac{s_1}{2} \right) (F_{dsy1} - F_{dsy2}) + \\ \left(\frac{d_1}{2} \right) (F_{dty1} - F_{dty2}) = 0 \end{aligned} \quad (4-75)$$

$$\begin{aligned} m_{a2} \ddot{y}_{a2} - (F_{sy3} + F_{sy4}) + (F_{ty3} + F_{ty4}) - (F_{dsy3} + F_{dsy4}) + (F_{dty3} + \\ F_{dty4}) = m_{a2}g \end{aligned} \quad (4-76)$$

$$\begin{aligned} I_{xa2} \ddot{\varphi}_{a2} - \left(\frac{s_2}{2} \right) (F_{sy3} - F_{sy4}) + \left(\frac{d_2}{2} \right) (F_{ty3} - F_{ty4}) - \left(\frac{s_2}{2} \right) (F_{dsy3} - F_{dsy4}) + \\ \left(\frac{d_2}{2} \right) (F_{dty3} - F_{dty4}) = 0 \end{aligned} \quad (4-77)$$

$$m_{a3} \ddot{y}_{a3} - (F_{sy5} + F_{sy6}) + (F_{ty5} + F_{ty6}) - (F_{dsy5} + F_{dsy6}) + (F_{dty5} + \quad (4-78)$$

$$F_{dty6}) = m_{a3}g$$

$$I_{xa3}\ddot{\varphi}_{a3} - (\frac{s_3}{2})(F_{sy5} - F_{sy6}) + (\frac{d_3}{2})(F_{ty5} - F_{ty6}) - (\frac{s_3}{2})(F_{dsy5} - F_{dsy6}) + \\ (\frac{d_3}{2})(F_{dty5} - F_{dty6}) = 0 \quad (4-79)$$

$$m_{a4}\ddot{y}_{a4} - (F_{sy7} + F_{sy8}) + (F_{ty7} + F_{ty8}) - (F_{dsy7} + F_{dsy8}) + (F_{dty7} + \\ F_{dty8}) = m_{a4}g \quad (4-80)$$

$$I_{xa4}\ddot{\varphi}_{a4} - (\frac{s_4}{2})(F_{sy7} - F_{sy8}) + (\frac{d_4}{2})(F_{ty7} - F_{ty8}) - (\frac{s_4}{2})(F_{dsy7} - F_{dsy8}) + \\ (\frac{d_4}{2})(F_{dty7} - F_{dty8}) = 0 \quad (4-81)$$

$$m_{a5}\ddot{y}_{a5} - (F_{sy9} + F_{sy10}) + (F_{ty9} + F_{ty10}) - (F_{dsy9} + F_{dsy10}) + (F_{dty9} + \\ F_{dty10}) = m_{a5}g \quad (4-82)$$

$$I_{xa5}\ddot{\varphi}_{a5} - (\frac{s_5}{2})(F_{sy9} - F_{sy10}) + (\frac{d_5}{2})(F_{ty9} - F_{ty10}) - (\frac{s_5}{2})(F_{dsy9} - F_{dsy10}) + \\ (\frac{d_5}{2})(F_{dty9} - F_{dty10}) = 0 \quad (4-83)$$

4.7 Derivation of Equations of Motion for “Type 3S3 Truck”

There are eighteen degrees of freedom in total for this type of truck. The degrees of freedom can be seen in Figure 2-6 and the description of those degrees of freedom can be found in

Table 4-10. Relative displacements at the locations of the springs are also calculated using the values given in Table 4-11.

Kinetic Energy of the system:

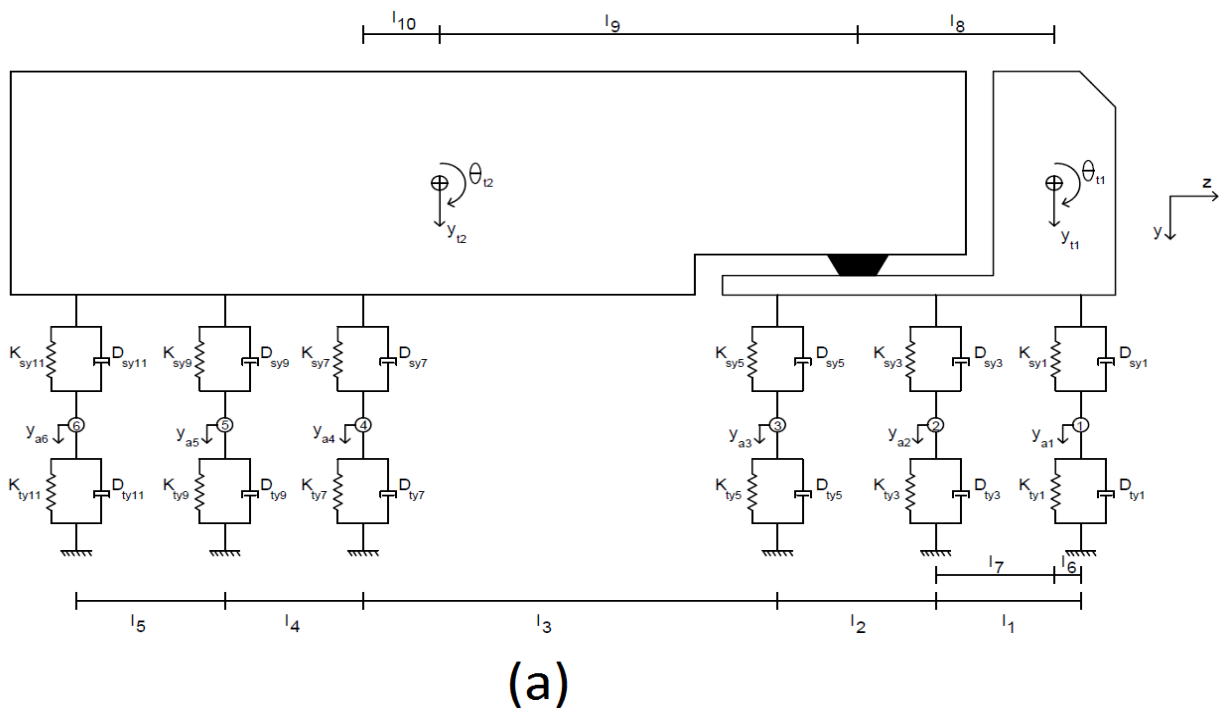
$$\begin{aligned}
T = & \frac{1}{2}m_{t1}\dot{y}_{t1}^2 + \frac{1}{2}m_{a1}\dot{y}_{a1}^2 + \frac{1}{2}m_{a2}\dot{y}_{a2}^2 + \frac{1}{2}m_{a3}\dot{y}_{a3}^2 + \frac{1}{2}m_{a4}\dot{y}_{a4}^2 + \\
& \frac{1}{2}m_{a5}\dot{y}_{a5}^2 + \frac{1}{2}m_{a6}\dot{y}_{a6}^2 + \frac{1}{2}I_{xt1}\dot{\phi}_{t1}^2 + \frac{1}{2}I_{zt1}\dot{\theta}_{t1}^2 + \frac{1}{2}I_{xt2}\dot{\phi}_{t2}^2 + \frac{1}{2}I_{zt2}\dot{\theta}_{t2}^2 + \\
& \frac{1}{2}I_{xa1}\dot{\phi}_{a1}^2 + \frac{1}{2}I_{xa2}\dot{\phi}_{a2}^2 + \frac{1}{2}I_{xa3}\dot{\phi}_{a3}^2 + \frac{1}{2}I_{xa4}\dot{\phi}_{a4}^2 + \frac{1}{2}I_{xa5}\dot{\phi}_{a5}^2 + \\
& \frac{1}{2}I_{xa6}\dot{\phi}_{a6}^2 + \frac{1}{2}m_{t2}\dot{y}_{t2}^2
\end{aligned} \tag{4-84}$$

TABLE 4-10: DEGREES OF FREEDOM OF TYPE 3S3 TRUCK

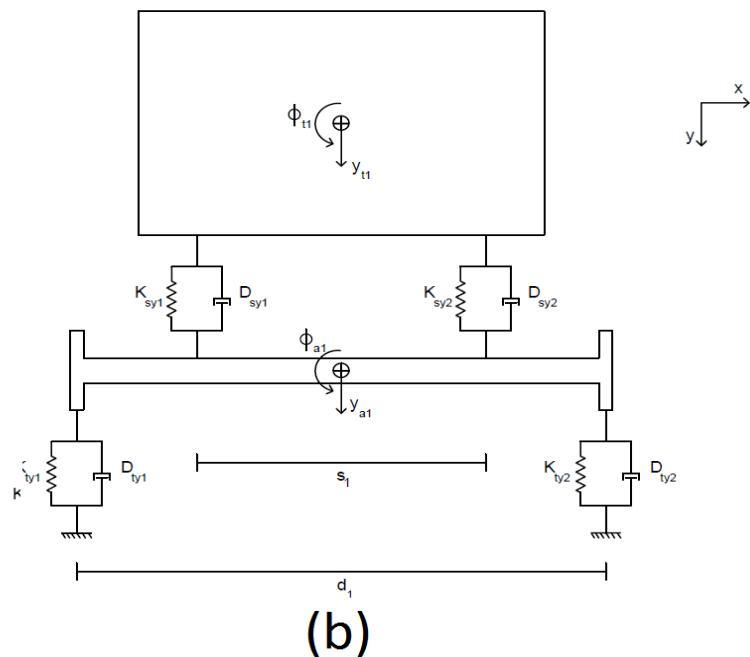
No.	Degree of Freedom	Contributed Mass	Description
1	y_{t1}	m_{t1}	Tractor vertical displacement and mass
2	φ_{t1}	I_{xt1}	Tractor roll displacement and mass moment of inertia
3	θ_{t1}	I_{zt1}	Tractor pitch displacement and mass moment of inertia
4	y_{t2}	m_{t2}	Trailer vertical displacement and mass
5	φ_{t2}	I_{xt2}	Trailer roll displacement and mass moment of inertia
6	θ_{t2}	I_{zt2}	Trailer pitch displacement and mass moment of inertia
7	y_{a1}	m_{a1}	Steer axle vertical displacement and mass
8	φ_{a1}	I_{xa1}	Steer axle roll displacement and mass moment of inertia
9	y_{a2}	m_{a2}	Vertical displacement and mass of forward axle of tractor tandem
10	φ_{a2}	I_{xa2}	Roll displacement and mass moment of inertia of forward axle of tractor tandem
11	y_{a3}	m_{a3}	Vertical displacement and mass of aft axle of tractor tandem
12	φ_{a3}	I_{xa3}	Roll displacement and mass moment of inertia of aft axle of tractor tandem
13	y_{a4}	m_{a4}	Vertical displacement and mass of first axle of trailer
14	φ_{a4}	I_{xa4}	Roll disp. and mass moment of inertia of first axle of trailer
15	y_{a5}	m_{a5}	Vertical disp. and mass of forward axle of trailer tandem
16	φ_{a5}	I_{xa5}	Roll displacement and mass moment of inertia of forward axle of trailer tandem
17	y_{a6}	m_{a6}	Vertical displacement and mass of aft axle of trailer tandem
18	φ_{a6}	I_{xa6}	Roll displacement and mass moment of inertia of aft axle of trailer tandem

TABLE 4-11: RELATIVE DISPLACEMENTS AT SPRING LOCATIONS OF TYPE 3S3 TRUCK

Suspension springs	
\mathbf{U}_{sy1}	$(y_{t1} - y_{a1}) + (S_1/2)(\varphi_{t1} - \varphi_{a1}) + l_6\theta_{t1}$
\mathbf{U}_{sy2}	$(y_{t1} - y_{a1}) - (S_1/2)(\varphi_{t1} - \varphi_{a1}) + l_6\theta_{t1}$
\mathbf{U}_{sy3}	$(y_{t1} - y_{a2}) + (S_2/2)(\varphi_{t1} - \varphi_{a2}) - l_7\theta_{t1}$
\mathbf{U}_{sy4}	$(y_{t1} - y_{a2}) - (S_2/2)(\varphi_{t1} - \varphi_{a2}) - l_7\theta_{t1}$
\mathbf{U}_{sy5}	$(y_{t1} - y_{a3}) + (S_3/2)(\varphi_{t1} - \varphi_{a3}) - (l_2 + l_7)\theta_{t1}$
\mathbf{U}_{sy6}	$(y_{t1} - y_{a3}) - (S_3/2)(\varphi_{t1} - \varphi_{a3}) - (l_2 + l_7)\theta_{t1}$
\mathbf{U}_{sy7}	$(y_{t2} - y_{a4}) + (S_4/2)(\varphi_{t2} - \varphi_{a4}) - l_{10}\theta_{t2}$
\mathbf{U}_{sy8}	$(y_{t2} - y_{a4}) - (S_4/2)(\varphi_{t2} - \varphi_{a4}) - l_{10}\theta_{t2}$
\mathbf{U}_{sy9}	$(y_{t2} - y_{a5}) + (S_5/2)(\varphi_{t2} - \varphi_{a5}) - (l_4 + l_{10})\theta_{t2}$
\mathbf{U}_{sy10}	$(y_{t2} - y_{a5}) - (S_5/2)(\varphi_{t2} - \varphi_{a5}) - (l_4 + l_{10})\theta_{t2}$
\mathbf{U}_{sy11}	$(y_{t2} - y_{a6}) + (S_6/2)(\varphi_{t2} - \varphi_{a6}) - (l_5 + l_4 + l_{10})\theta_{t2}$
\mathbf{U}_{sy12}	$(y_{t2} - y_{a6}) - (S_6/2)(\varphi_{t2} - \varphi_{a6}) - (l_5 + l_4 + l_{10})\theta_{t2}$
Tire springs	
\mathbf{U}_{ty1}	$y_{a1} + (d_1/2)\varphi_{a1} + u_{SR1}$
\mathbf{U}_{ty2}	$y_{a1} - (d_1/2)\varphi_{a1} + u_{SR2}$
\mathbf{U}_{ty3}	$y_{a2} + (d_2/2)\varphi_{a2} + u_{SR3}$
\mathbf{U}_{ty4}	$y_{a2} - (d_2/2)\varphi_{a2} + u_{SR4}$
\mathbf{U}_{ty5}	$y_{a3} + (d_3/2)\varphi_{a3} + u_{SR5}$
\mathbf{U}_{ty6}	$y_{a3} - (d_3/2)\varphi_{a3} + u_{SR6}$
\mathbf{U}_{ty7}	$y_{a4} + (d_4/2)\varphi_{a4} + u_{SR7}$
\mathbf{U}_{ty8}	$y_{a4} - (d_4/2)\varphi_{a4} + u_{SR8}$
\mathbf{U}_{ty9}	$y_{a5} + (d_5/2)\varphi_{a5} + u_{SR9}$
\mathbf{U}_{ty10}	$y_{a5} - (d_5/2)\varphi_{a5} + u_{SR10}$
\mathbf{U}_{ty11}	$y_{a6} + (d_6/2)\varphi_{a6} + u_{SR11}$
\mathbf{U}_{ty12}	$y_{a6} - (d_6/2)\varphi_{a6} + u_{SR12}$



(a)



(b)

FIGURE 4-6: TYPE 3S3 DYNAMIC MODEL (A) TRUCK SIDE VIEW (B) TRUCK FRONT VIEW

Potential Energy of the system:

$$\begin{aligned}
V = & \frac{1}{2}K_{sy1}U_{sy1}^2 + \frac{1}{2}K_{sy2}U_{sy2}^2 + \frac{1}{2}K_{sy3}U_{sy3}^2 + \frac{1}{2}K_{sy4}U_{sy4}^2 + \\
& \frac{1}{2}K_{sy5}U_{sy5}^2 + \frac{1}{2}K_{sy6}U_{sy6}^2 + \frac{1}{2}K_{sy7}U_{sy7}^2 + \frac{1}{2}K_{sy8}U_{sy8}^2 + \frac{1}{2}K_{sy9}U_{sy9}^2 + \\
& \frac{1}{2}K_{sy10}U_{sy10}^2 + \frac{1}{2}K_{sy11}U_{sy11}^2 + \frac{1}{2}K_{sy12}U_{sy12}^2 + \frac{1}{2}K_{ty1}U_{ty1}^2 + \\
& \frac{1}{2}K_{ty2}U_{ty2}^2 + \frac{1}{2}K_{ty3}U_{ty3}^2 + \frac{1}{2}K_{ty4}U_{ty4}^2 + \frac{1}{2}K_{ty5}U_{ty5}^2 + \frac{1}{2}K_{ty6}U_{ty6}^2 + \\
& \frac{1}{2}K_{ty7}U_{sy7}^2 + \frac{1}{2}K_{ty8}U_{ty8}^2 + \frac{1}{2}K_{ty9}U_{ty9}^2 + \frac{1}{2}K_{ty10}U_{ty10}^2 + \frac{1}{2}K_{ty11}U_{ty11}^2 + \quad (4-85) \\
& \frac{1}{2}K_{ty12}U_{ty12}^2 - ((m_{t1}g)y_{t1} + (m_{t2}g)y_{t2} + (m_{a1}g)y_{a1} + (m_{a2}g)y_{a2} + \\
& (m_{a3}g)y_{a3} + (m_{a4}g)y_{a4} + (m_{a5}g)y_{a5} + (m_{a6}g)y_{a6}) + (F_{y1}U_{sy1} + \\
& F_{y2}U_{sy2} + F_{y3}U_{sy3} + F_{y4}U_{sy4} + F_{y5}U_{sy5} + F_{y6}U_{sy6} + F_{y7}U_{sy7} + F_{y8}U_{sy8} + \\
& F_{y9}U_{sy9} + F_{y10}U_{sy10} + F_{y11}U_{sy11} + F_{y12}U_{sy12})
\end{aligned}$$

Damping Energy of the system:

$$\begin{aligned}
D = & \frac{1}{2}D_{sy1}\dot{U}_{sy1}^2 + \frac{1}{2}D_{sy2}\dot{U}_{sy2}^2 + \frac{1}{2}D_{sy3}\dot{U}_{sy3}^2 + \frac{1}{2}D_{sy4}\dot{U}_{sy4}^2 + \frac{1}{2}D_{sy5}\dot{U}_{sy5}^2 + \\
& \frac{1}{2}D_{sy6}\dot{U}_{sy6}^2 + \frac{1}{2}D_{sy7}\dot{U}_{sy7}^2 + \frac{1}{2}D_{sy8}\dot{U}_{sy8}^2 + \frac{1}{2}D_{sy9}\dot{U}_{sy9}^2 + \frac{1}{2}D_{sy10}\dot{U}_{sy10}^2 + \\
& \frac{1}{2}D_{sy11}\dot{U}_{sy11}^2 + \frac{1}{2}D_{sy12}\dot{U}_{sy12}^2 + \frac{1}{2}D_{ty1}\dot{U}_{ty1}^2 + \frac{1}{2}D_{ty2}\dot{U}_{ty2}^2 + \frac{1}{2}D_{ty3}\dot{U}_{ty3}^2 + \quad (4-86) \\
& \frac{1}{2}D_{ty4}\dot{U}_{ty4}^2 + \frac{1}{2}D_{ty5}\dot{U}_{ty5}^2 + \frac{1}{2}D_{ty6}\dot{U}_{ty6}^2 + \frac{1}{2}D_{ty7}\dot{U}_{ty7}^2 + \frac{1}{2}D_{ty8}\dot{U}_{ty8}^2 + \\
& \frac{1}{2}D_{ty9}\dot{U}_{ty9}^2 + \frac{1}{2}D_{ty10}\dot{U}_{ty10}^2 + \frac{1}{2}D_{ty11}\dot{U}_{ty11}^2 + \frac{1}{2}D_{ty12}\dot{U}_{ty12}^2
\end{aligned}$$

The displacement at the pivot point should stay the same, whether it is calculated from the trailer part or the tractor part,

$$y_{t2} + \theta_{t2}l_8 = y_{t1} - \theta_{t1}l_7 \quad (4-87)$$

Thus, by calculating θ_{t2} from equation (4-86) and substituting in equation (4-83),

$$\begin{aligned}
T = & \frac{1}{2}m_{t1}\dot{y}_{t1}^2 + \frac{1}{2}m_{a1}\dot{y}_{a1}^2 + \frac{1}{2}m_{a2}\dot{y}_{a2}^2 + \frac{1}{2}m_{a3}\dot{y}_{a3}^2 + \frac{1}{2}m_{a4}\dot{y}_{a4}^2 + \\
& \frac{1}{2}m_{a5}\dot{y}_{a5}^2 + \frac{1}{2}m_{a6}\dot{y}_{a6}^2 + \frac{1}{2}I_{xt1}\dot{\phi}_{t1}^2 + \frac{1}{2}I_{zt1}\dot{\theta}_{t1}^2 + \frac{1}{2}I_{xt2}\dot{\phi}_{t2}^2 + \\
& \frac{1}{2}I_{zt2}\left(\frac{\dot{y}_{t1}-\dot{y}_{t2}-\dot{\theta}_{t1}l_8}{l_9}\right)^2 + \frac{1}{2}I_{xa1}\dot{\phi}_{a1}^2 + \frac{1}{2}I_{xa2}\dot{\phi}_{a2}^2 + \frac{1}{2}I_{xa3}\dot{\phi}_{a3}^2 + \frac{1}{2}I_{xa4}\dot{\phi}_{a4}^2 + \\
& \frac{1}{2}I_{xa5}\dot{\phi}_{a5}^2 + \frac{1}{2}I_{xa6}\dot{\phi}_{a6}^2 + \frac{1}{2}m_{t2}\dot{y}_{t2}^2
\end{aligned} \tag{4-88}$$

Same substitution will be applied to the equations (4-84) and (4-85). Now the Lagrange's equation is applied to y_{t2} :

$$\begin{aligned}
& \left[m_{t2}\ddot{y}_{t2} - \frac{I_{zt2}}{l_9^2}(\ddot{y}_{t1} - \ddot{y}_{t2} - \ddot{\theta}_{t1}l_8) \right] + \left[\left(1 + \frac{l_{10}}{l_9}\right)(K_{sy7}U_{sy7} + K_{sy8}U_{sy8} + \right. \\
& F_{y7} + F_{y8}) + \left(1 + \frac{l_4+l_{10}}{l_9}\right)(K_{sy9}U_{sy9} + K_{sy10}U_{sy10} + F_{y9} + F_{y10}) + \\
& \left. \left(1 + \frac{l_4+l_5+l_{10}}{l_9}\right)(K_{sy11}U_{sy11} + K_{sy12}U_{sy12} + F_{y11} + F_{y12}) - (m_{t2}g) \right] + \\
& \left[\left(1 + \frac{l_{10}}{l_9}\right)(D_{sy7}\dot{U}_{sy7} + D_{sy8}\dot{U}_{sy8}) + \left(1 + \frac{l_4+l_{10}}{l_9}\right)(D_{sy9}\dot{U}_{sy9} + \right. \\
& D_{sy10}\dot{U}_{sy10}) + \left. \left(1 + \frac{l_4+l_5+l_{10}}{l_9}\right)(D_{sy11}\dot{U}_{sy11} + D_{sy12}\dot{U}_{sy12}) \right] = 0
\end{aligned} \tag{4-89}$$

To simplify the equation some variables are defined as follows:

$$S_{a2} = \frac{I_{zt2}}{l_8^2}$$

$$S_{c2} = \frac{I_{zt2}}{l_8^2} + m_{t2}$$

$$S_{a3} = \frac{I_{zt2}}{l_8^2}l_7$$

$$\begin{aligned}
B_{t4} = & m_{t2}g - \left(1 + \frac{l_9}{l_8}\right)(F_{sy7} + F_{sy8} + F_{dsy7} + F_{dsy8}) - \left(1 + \frac{l_4+l_9}{l_8}\right)(F_{sy9} + F_{sy10} + \\
& F_{dsy9} + F_{dsy10})
\end{aligned}$$

Therefore equation (2-88) will be simplified to:

$$-S_{a2}\ddot{y}_{t1} + S_{c2}\ddot{y}_{t2} + S_{a3}\ddot{\theta}_{t1} = B_{t4} \quad (4-90)$$

By applying the Lagrange's equation to y_{t1} :

$$\begin{aligned} & \left[m_{t1}\ddot{y}_{t1} + \frac{l_{zt2}}{l_9^2}(\ddot{y}_{t1} - \ddot{y}_{t2} - \ddot{\theta}_{t1}l_8) \right] + \left[(F_{sy1} + F_{sy2} + F_{sy3} + F_{sy4} + F_{sy5} + \right. \\ & F_{sy6}) - \frac{l_{10}}{l_9}(F_{sy7} + F_{sy8}) - \frac{l_4+l_{10}}{l_9}(F_{sy9} + F_{sy10}) - \frac{l_4+l_5+l_{10}}{l_9}(F_{sy11} + \right. \\ & F_{sy12}) - (m_{t1}g) \Big] + \left[(F_{dsy1} + F_{dsy2} + F_{dsy3} + F_{dsy4} + F_{dsy5} + F_{dsy6}) - \right. \\ & \left. \frac{l_{10}}{l_9}(F_{dsy7} + F_{dsy8}) - \frac{l_4+l_{10}}{l_9}(F_{dsy9} + F_{dsy10}) - \frac{l_4+l_5+l_{10}}{l_9}(F_{dsy11} + F_{dsy12}) \right] = \\ & 0 \end{aligned} \quad (4-91)$$

Again to simplify the equation some variables are defined as follows:

$$S_{a1} = \frac{l_{zt2}}{l_9^2} + m_{t1}$$

$$\begin{aligned} B_{t1} = & m_{t1}g - \left[(F_{sy1} + F_{sy2} + F_{sy3} + F_{sy4} + F_{sy5} + F_{sy6}) - \frac{l_{10}}{l_9}(F_{sy7} + F_{sy8}) - \right. \\ & \frac{l_4+l_{10}}{l_9}(F_{sy9} + F_{sy10}) - \frac{l_4+l_5+l_{10}}{l_9}(F_{sy11} + F_{sy12}) + (F_{dsy1} + F_{dsy2} + F_{dsy3} + F_{dsy4} + \\ & F_{dsy5} + F_{dsy6}) - \frac{l_{10}}{l_9}(F_{dsy7} + F_{dsy8}) - \frac{l_4+l_{10}}{l_9}(F_{dsy9} + F_{dsy10}) - \frac{l_4+l_5+l_{10}}{l_9}(F_{dsy11} + \\ & \left. F_{dsy12}) \right] \end{aligned}$$

Therefore equation (4-90) will be simplified to:

$$S_{a1}\ddot{y}_{t1} - S_{a2}\ddot{y}_{t2} - S_{a3}\ddot{\theta}_{t1} = B_{t1} \quad (4-92)$$

Also, by applying the Lagrange's equation to θ_{t1} :

$$\begin{aligned} & \left[I_{zt1}\ddot{\theta}_{t1} - \frac{l_{zt2}l_8}{l_9^2}(\ddot{y}_{t1} - \ddot{y}_{t2} - \ddot{\theta}_{t1}l_8) \right] + \left[l_6(F_{sy1} + F_{sy2}) - l_7(F_{sy3} + F_{sy4}) - \right. \\ & (l_2 + l_7)(F_{sy5} + F_{sy6}) + \frac{l_8l_{10}}{l_9}(F_{sy7} + F_{sy8}) + \frac{l_8(l_4+l_{10})}{l_9}(F_{sy9} + F_{sy10}) + \\ & \left. \right] \end{aligned} \quad (4-93)$$

$$\begin{aligned} & \left[\frac{l_8(l_4+l_5+l_{10})}{l_9} (F_{sy11} + F_{sy12}) \right] + \left[l_6(F_{dsy1} + F_{dsy2}) - l_7(F_{dsy3} + F_{dsy4}) - \right. \\ & (l_2 + l_7)(F_{dsy5} + F_{dsy6}) + \frac{l_8l_{10}}{l_9}(F_{dsy7} + F_{dsy8}) + \frac{l_8(l_4+l_{10})}{l_9}(F_{dsy9} + \\ & \left. F_{dsy10}) + \frac{l_8(l_4+l_5+l_{10})}{l_9}(F_{dsy11} + F_{dsy12}) \right] = 0 \end{aligned}$$

Once again to simplify the equation some variables need to be defined as follows:

$$\begin{aligned} S_{b3} &= I_{zt1} + \frac{I_{zt2}l_8^2}{l_9^2} \\ B_{t3} &= - \left[\left[l_6(F_{sy1} + F_{sy2}) - l_7(F_{sy3} + F_{sy4}) - (l_2 + l_7)(F_{sy5} + F_{sy6}) + \frac{l_8l_{10}}{l_9}(F_{sy7} + \right. \right. \\ & F_{sy8}) + \frac{l_8(l_4+l_{10})}{l_9}(F_{sy9} + F_{sy10}) + \frac{l_8(l_4+l_5+l_{10})}{l_9}(F_{sy11} + F_{sy12}) \left. \right] + \left[l_6(F_{dsy1} + F_{dsy2}) - \right. \\ & l_7(F_{dsy3} + F_{dsy4}) - (l_2 + l_7)(F_{dsy5} + F_{dsy6}) + \frac{l_8l_{10}}{l_9}(F_{dsy7} + F_{dsy8}) + \frac{l_8(l_4+l_{10})}{l_9}(F_{dsy9} + \\ & \left. F_{dsy10}) + \frac{l_8(l_4+l_5+l_{10})}{l_9}(F_{dsy11} + F_{dsy12}) \right] \left. \right] \end{aligned}$$

Therefore equation (4-92) will be simplified to:

$$-S_{a3}\ddot{y}_{t1} + S_{a3}\ddot{y}_{t2} + S_{b3}\ddot{\theta}_{t1} = B_{t3} \quad (4-94)$$

By adding equations (4-89) and (4-91),

$$(S_{a1} - S_{a2})\ddot{y}_{t1} - (S_{a2} - S_{c2})\ddot{y}_{t2} = B_{t1} + B_{t4} \quad (4-95)$$

Also by multiplying S_{b3} and S_{a3} to equations (4-91) and (4-93) respectively,

$$(S_{a1}S_{b3} - S_{a3}^2)\ddot{y}_{t1} - (S_{a2}S_{b3} - S_{a3}^2)\ddot{y}_{t2} = S_{b3}B_{t1} + S_{a3}B_{t3} \quad (4-96)$$

By defining the following expressions, equations (4-94) and (4-95) are simplified to equations (4-96) and (4-97) respectively,

$$e_1 = S_{a1} - S_{a2}$$

$$e_2 = S_{a2} - S_{c2}$$

$$\begin{aligned}
e_3 &= S_{a1}S_{b3} - S_{a3}^2 \\
e_4 &= S_{a2}S_{b3} - S_{a3}^2 \\
e_1\ddot{y}_{t1} - e_2\ddot{y}_{t2} &= B_{t1} + B_{t4} \quad (4-97)
\end{aligned}$$

$$e_3\ddot{y}_{t1} - e_4\ddot{y}_{t2} = S_{b3}B_{t1} + S_{a3}B_{t3} \quad (4-98)$$

Solving equations (4-96) and (4-97) for \ddot{y}_{t1} and \ddot{y}_{t2} will lead to:

$$\ddot{y}_{t1} = \frac{e_4(B_{t1} + B_{t4}) - e_2(S_{b3}B_{t1} + S_{a3}B_{t3})}{e_1e_4 - e_2e_3} \quad (4-99)$$

$$\ddot{y}_{t2} = \frac{e_1\left(\frac{e_4(B_{t1} + B_{t4}) - e_2(S_{b3}B_{t1} + S_{a3}B_{t3})}{e_1e_4 - e_2e_3}\right) - \frac{B_{t1} + B_{t4}}{e_2}}{e_2} \quad (4-100)$$

Substituting equations (4-98) and (4-99) into equation (4-93) will give,

$$\begin{aligned}
\ddot{\theta}_{t1} &= \frac{B_{t3}}{S_{b3}} + \frac{S_{a3}}{S_{b3}} \left(\frac{e_4(B_{t1} + B_{t4}) - e_2(S_{b3}B_{t1} + S_{a3}B_{t3})}{e_1e_4 - e_2e_3} \right) \\
&\quad - \frac{S_{a3}}{S_{b3}} \left(\frac{e_1\left(\frac{e_4(B_{t1} + B_{t4}) - e_2(S_{b3}B_{t1} + S_{a3}B_{t3})}{e_1e_4 - e_2e_3}\right) - \frac{B_{t1} + B_{t4}}{e_2}}{e_2} \right) \\
&\quad - \frac{B_{t1} + B_{t4}}{e_2} \quad (4-101)
\end{aligned}$$

By applying the Lagrange's equation to $\varphi_{t1}, \varphi_{t2}$:

$$\begin{aligned}
I_{xt1}\ddot{\varphi}_{t1} + \left[\left(\frac{s_1}{2}\right)(F_{sy1} - F_{sy2}) + \left(\frac{s_2}{2}\right)(F_{sy3} - F_{sy4}) + \left(\frac{s_3}{2}\right)(F_{sy5} - F_{sy6}) \right] + \\
\left[\left(\frac{s_1}{2}\right)(F_{dsy1} - F_{dsy2}) + \left(\frac{s_2}{2}\right)(F_{dsy3} - F_{dsy4}) + \left(\frac{s_3}{2}\right)(F_{dsy5} - F_{dsy6}) \right] = 0 \quad (4-102)
\end{aligned}$$

$$\begin{aligned}
I_{xt2}\ddot{\varphi}_{t2} + \left[\left(\frac{s_4}{2}\right)(F_{sy7} - F_{sy8}) + \left(\frac{s_5}{2}\right)(F_{sy9} - F_{sy10}) + \left(\frac{s_6}{2}\right)(F_{sy11} - \right. \\
\left. F_{sy12}) \right] + \left[\left(\frac{s_4}{2}\right)(F_{dsy7} - F_{dsy8}) + \left(\frac{s_5}{2}\right)(F_{dsy9} - F_{dsy10}) + \left(\frac{s_6}{2}\right)(F_{dsy11} - \right. \\
\left. F_{dsy12}) \right] = 0 \quad (4-103)
\end{aligned}$$

Also the rest of degrees of freedom will be as follows:

$$m_{a1}\ddot{y}_{a1} - (F_{sy1} + F_{sy2}) + (F_{ty1} + F_{ty2}) - (F_{dsy1} + F_{dsy2}) + (F_{dty1} + F_{dty2}) = m_{a1}g \quad (4-104)$$

$$I_{xa1}\ddot{\varphi}_{a1} - (\frac{s_1}{2})(F_{sy1} - F_{sy2}) + (\frac{d_1}{2})(F_{ty1} - F_{ty2}) - (\frac{s_1}{2})(F_{dsy1} - F_{dsy2}) + (\frac{d_1}{2})(F_{dty1} - F_{dty2}) = 0 \quad (4-105)$$

$$m_{a2}\ddot{y}_{a2} - (F_{sy3} + F_{sy4}) + (F_{ty3} + F_{ty4}) - (F_{dsy3} + F_{dsy4}) + (F_{dty3} + F_{dty4}) = m_{a2}g \quad (4-106)$$

$$I_{xa2}\ddot{\varphi}_{a2} - (\frac{s_2}{2})(F_{sy3} - F_{sy4}) + (\frac{d_2}{2})(F_{ty3} - F_{ty4}) - (\frac{s_2}{2})(F_{dsy3} - F_{dsy4}) + (\frac{d_2}{2})(F_{dty3} - F_{dty4}) = 0 \quad (4-107)$$

$$m_{a3}\ddot{y}_{a3} - (F_{sy5} + F_{sy6}) + (F_{ty5} + F_{ty6}) - (F_{dsy5} + F_{dsy6}) + (F_{dty5} + F_{dty6}) = m_{a3}g \quad (4-108)$$

$$I_{xa3}\ddot{\varphi}_{a3} - (\frac{s_3}{2})(F_{sy5} - F_{sy6}) + (\frac{d_3}{2})(F_{ty5} - F_{ty6}) - (\frac{s_3}{2})(F_{dsy5} - F_{dsy6}) + (\frac{d_3}{2})(F_{dty5} - F_{dty6}) = 0 \quad (4-109)$$

$$m_{a4}\ddot{y}_{a4} - (F_{sy7} + F_{sy8}) + (F_{ty7} + F_{ty8}) - (F_{dsy7} + F_{dsy8}) + (F_{dty7} + F_{dty8}) = m_{a4}g \quad (4-110)$$

$$I_{xa4}\ddot{\varphi}_{a4} - (\frac{s_4}{2})(F_{sy7} - F_{sy8}) + (\frac{d_4}{2})(F_{ty7} - F_{ty8}) - (\frac{s_4}{2})(F_{dsy7} - F_{dsy8}) + (\frac{d_4}{2})(F_{dty7} - F_{dty8}) = 0 \quad (4-111)$$

$$m_{a5}\ddot{y}_{a5} - (F_{sy9} + F_{sy10}) + (F_{ty9} + F_{ty10}) - (F_{dsy9} + F_{dsy10}) + (F_{dty9} + F_{dty10}) = m_{a5}g \quad (4-112)$$

$$I_{xa5}\ddot{\varphi}_{a5} - (\frac{s_5}{2})(F_{sy9} - F_{sy10}) + (\frac{d_5}{2})(F_{ty9} - F_{ty10}) - (\frac{s_5}{2})(F_{dsy9} - F_{dsy10}) = 0 \quad (4-113)$$

$$F_{dsy10}) + \left(\frac{d_5}{2}\right)(F_{dty9} - F_{dty10}) = 0$$

$$m_{a6}\ddot{y}_{a6} - (F_{sy11} + F_{sy12}) + (F_{ty11} + F_{ty12}) - (F_{dsy11} + F_{dsy12}) + (F_{dty11} + F_{dty12}) = m_{a6}g \quad (4-114)$$

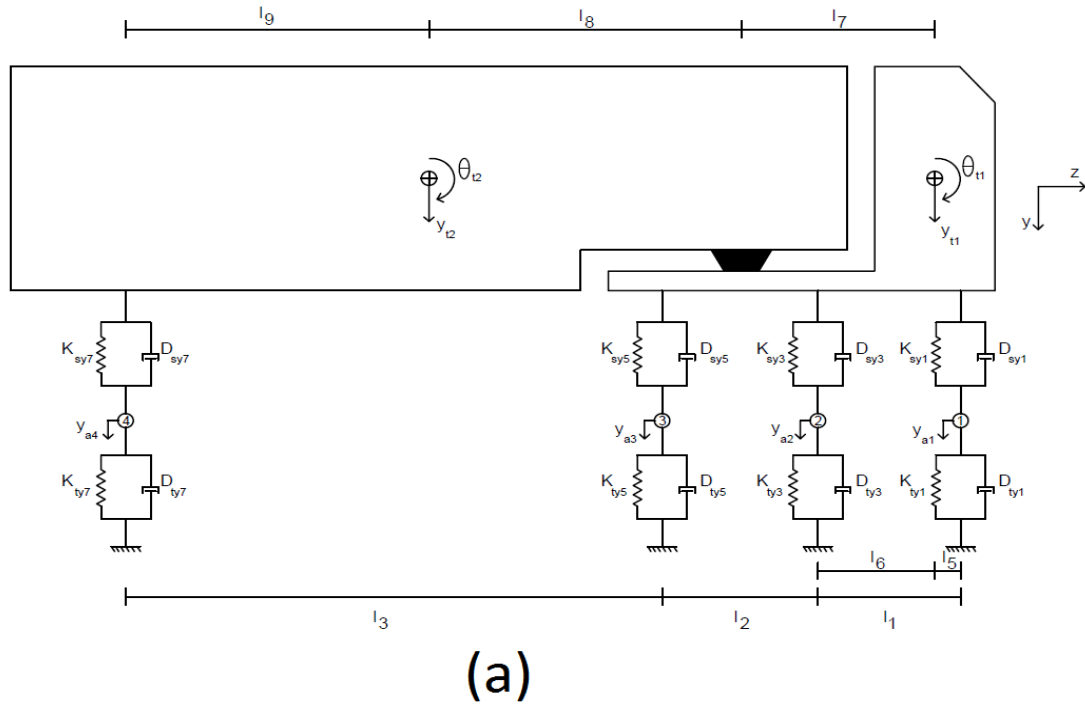
$$I_{xa6}\ddot{\varphi}_{a6} - \left(\frac{s_6}{2}\right)(F_{sy11} - F_{sy12}) + \left(\frac{d_6}{2}\right)(F_{ty11} - F_{ty12}) - \left(\frac{s_6}{2}\right)(F_{dsy11} - F_{dsy12}) + \left(\frac{d_6}{2}\right)(F_{dty11} - F_{dty12}) = 0 \quad (4-115)$$

4.8 Derivation of Equations of Motion for “Type 3S1 Truck”

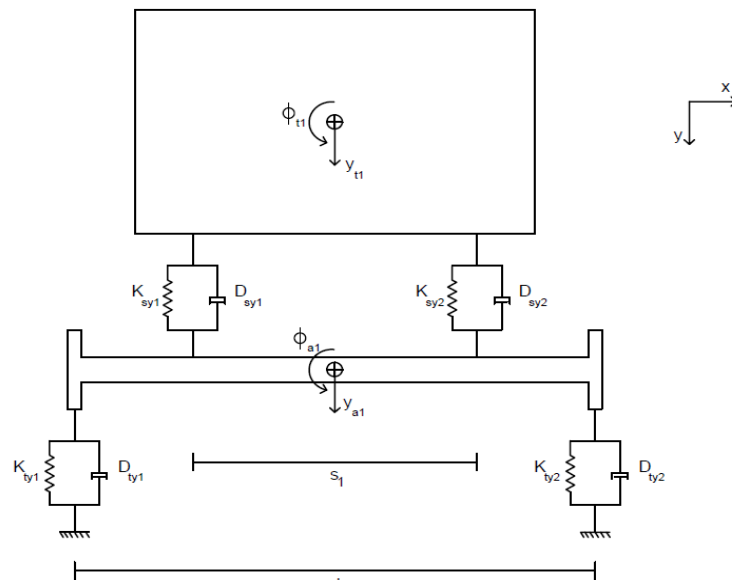
There are fourteen degrees of freedom in total for this type of truck. The degrees of freedom can be seen in Figure 4-7 and the description of those degrees of freedom can be found in Table 4-12. Relative Displacements at the locations of the springs are also calculated using the values given in Table 4-13.

TABLE 4-12: DEGREES OF FREEDOM OF TYPE 3S1 TRUCK

No.	Degree of Freedom	Contributed Mass	Description
1	y_{t1}	m_{t1}	Tractor vertical displacement and mass
2	φ_{t1}	I_{xt1}	Tractor roll displacement and mass moment of inertia
3	θ_{t1}	I_{zt1}	Tractor pitch displacement and mass moment of inertia
4	y_{t2}	m_{t2}	Trailer vertical displacement and mass
5	φ_{t2}	I_{xt2}	Trailer roll displacement and mass moment of inertia
6	θ_{t2}	I_{zt2}	Trailer pitch displacement and mass moment of inertia
7	y_{a1}	m_{a1}	Steer axle vertical displacement and mass
8	φ_{a1}	I_{xa1}	Steer axle roll displacement and mass moment of inertia
9	y_{a2}	m_{a2}	Vertical displacement and mass of forward axle of tractor tandem
10	φ_{a2}	I_{xa2}	Roll displacement and mass moment of inertia of forward axle of tractor tandem
11	y_{a3}	m_{a3}	Vertical displacement and mass of aft axle of tractor tandem
12	φ_{a3}	I_{xa3}	Roll displacement and mass moment of inertia of aft axle of tractor tandem
13	y_{a4}	m_{a4}	Trailer axle vertical displacement and mass
14	φ_{a4}	I_{xa4}	Trailer axle roll displacement and mass moment of inertia



(a)



(b)

FIGURE 4-7: TYPE 3S1 DYNAMIC MODEL (A) TRUCK SIDE VIEW (B) TRUCK FRONT VIEW

TABLE 4-13: RELATIVE DISPLACEMENTS AT SPRING LOCATIONS OF TYPE 3S1 TRUCK

Suspension springs	
U_{sy1}	$(y_{t1} - y_{a1}) + (S_1/2)(\varphi_{t1} - \varphi_{a1}) + l_5\theta_{t1}$
U_{sy2}	$(y_{t1} - y_{a1}) - (S_1/2)(\varphi_{t1} - \varphi_{a1}) + l_5\theta_{t1}$
U_{sy3}	$(y_{t1} - y_{a2}) + (S_2/2)(\varphi_{t1} - \varphi_{a2}) - l_6\theta_{t1}$
U_{sy4}	$(y_{t1} - y_{a2}) - (S_2/2)(\varphi_{t1} - \varphi_{a2}) - l_6\theta_{t1}$
U_{sy5}	$(y_{t1} - y_{a3}) + (S_3/2)(\varphi_{t1} - \varphi_{a3}) - (l_2 + l_6)\theta_{t1}$
U_{sy6}	$(y_{t1} - y_{a3}) - (S_3/2)(\varphi_{t1} - \varphi_{a3}) - (l_2 + l_6)\theta_{t1}$
U_{sy7}	$(y_{t2} - y_{a4}) + (S_4/2)(\varphi_{t2} - \varphi_{a4}) - l_9\theta_{t2}$
U_{sy8}	$(y_{t2} - y_{a4}) - (S_4/2)(\varphi_{t2} - \varphi_{a4}) - l_9\theta_{t2}$
Tire springs	
U_{ty1}	$y_{a1} + (d_1/2)\varphi_{a1} + u_{SR1}$
U_{ty2}	$y_{a1} - (d_1/2)\varphi_{a1} + u_{SR2}$
U_{ty3}	$y_{a2} + (d_2/2)\varphi_{a2} + u_{SR3}$
U_{ty4}	$y_{a2} - (d_2/2)\varphi_{a2} + u_{SR4}$
U_{ty5}	$y_{a3} + (d_3/2)\varphi_{a3} + u_{SR5}$
U_{ty6}	$y_{a3} - (d_3/2)\varphi_{a3} + u_{SR6}$
U_{ty7}	$y_{a4} + (d_4/2)\varphi_{a4} + u_{SR7}$
U_{ty8}	$y_{a4} - (d_4/2)\varphi_{a4} + u_{SR8}$

Kinetic Energy of the system:

$$\begin{aligned}
 T = & \frac{1}{2}m_{t1}\dot{y}_{t1}^2 + \frac{1}{2}m_{a1}\dot{y}_{a1}^2 + \frac{1}{2}m_{a2}\dot{y}_{a2}^2 + \frac{1}{2}m_{a3}\dot{y}_{a3}^2 + \frac{1}{2}m_{a4}\dot{y}_{a4}^2 + \\
 & \frac{1}{2}I_{xt1}\dot{\varphi}_{t1}^2 + \frac{1}{2}I_{zt1}\dot{\theta}_{t1}^2 + \frac{1}{2}I_{xt2}\dot{\varphi}_{t2}^2 + \frac{1}{2}I_{zt2}\dot{\theta}_{t2}^2 + \frac{1}{2}I_{xa1}\dot{\varphi}_{a1}^2 + \frac{1}{2}I_{xa2}\dot{\varphi}_{a2}^2 + \quad (4-116) \\
 & \frac{1}{2}I_{xa3}\dot{\varphi}_{a3}^2 + \frac{1}{2}I_{xa4}\dot{\varphi}_{a4}^2 + \frac{1}{2}m_{t2}\dot{y}_{t2}^2
 \end{aligned}$$

Potential Energy of the system:

$$\begin{aligned}
V = & \frac{1}{2} K_{sy1} U_{sy1}^2 + \frac{1}{2} K_{sy2} U_{sy2}^2 + \frac{1}{2} K_{sy3} U_{sy3}^2 + \frac{1}{2} K_{sy4} U_{sy4}^2 + \\
& \frac{1}{2} K_{sy5} U_{sy5}^2 + \frac{1}{2} K_{sy6} U_{sy6}^2 + \frac{1}{2} K_{sy7} U_{sy7}^2 + \frac{1}{2} K_{sy8} U_{sy8}^2 + \frac{1}{2} K_{ty1} U_{ty1}^2 + \\
& \frac{1}{2} K_{ty2} U_{ty2}^2 + \frac{1}{2} K_{ty3} U_{ty3}^2 + \frac{1}{2} K_{ty4} U_{ty4}^2 + \frac{1}{2} K_{ty5} U_{ty5}^2 + \frac{1}{2} K_{ty6} U_{ty6}^2 + \\
& \frac{1}{2} K_{ty7} U_{sy7}^2 + \frac{1}{2} K_{ty8} U_{ty8}^2 - ((m_{t1}g)y_{t1} + (m_{t2}g)y_{t2} + (m_{a1}g)y_{a1} + \\
& (m_{a2}g)y_{a2} + (m_{a3}g)y_{a3} + (m_{a4}g)y_{a4}) + (F_{y1}U_{sy1} + F_{y2}U_{sy2} + \\
& F_{y3}U_{sy3} + F_{y4}U_{sy4} + F_{y5}U_{sy5} + F_{y6}U_{sy6} + F_{y7}U_{sy7} + F_{y8}U_{sy8})
\end{aligned} \tag{4-117}$$

Damping Energy of the system:

$$\begin{aligned}
D = & \frac{1}{2} D_{sy1} \dot{U}_{sy1}^2 + \frac{1}{2} D_{sy2} \dot{U}_{sy2}^2 + \frac{1}{2} D_{sy3} \dot{U}_{sy3}^2 + \frac{1}{2} D_{sy4} \dot{U}_{sy4}^2 + \\
& \frac{1}{2} D_{sy5} \dot{U}_{sy5}^2 + \frac{1}{2} D_{sy6} \dot{U}_{sy6}^2 + \frac{1}{2} D_{sy7} \dot{U}_{sy7}^2 + \frac{1}{2} D_{sy8} \dot{U}_{sy8}^2 + \frac{1}{2} D_{ty1} \dot{U}_{ty1}^2 + \\
& \frac{1}{2} D_{ty2} \dot{U}_{ty2}^2 + \frac{1}{2} D_{ty3} \dot{U}_{ty3}^2 + \frac{1}{2} D_{ty4} \dot{U}_{ty4}^2 + \frac{1}{2} D_{ty5} \dot{U}_{ty5}^2 + \frac{1}{2} D_{ty6} \dot{U}_{ty6}^2 + \\
& \frac{1}{2} D_{ty7} \dot{U}_{ty7}^2 + \frac{1}{2} D_{ty8} \dot{U}_{ty8}^2
\end{aligned} \tag{4-118}$$

Whether it is calculated from the trailer part or the tractor part, the displacement at the pivot point should be the same,

$$y_{t2} + \theta_{t2} l_8 = y_{t1} - \theta_{t1} l_7 \tag{4-119}$$

Thus, by calculating θ_{t2} from equation (4-119) and substituting in equation (4-116),

$$\begin{aligned}
T = & \frac{1}{2} m_{t1} \dot{y}_{t1}^2 + \frac{1}{2} m_{a1} \dot{y}_{a1}^2 + \frac{1}{2} m_{a2} \dot{y}_{a2}^2 + \frac{1}{2} m_{a3} \dot{y}_{a3}^2 + \frac{1}{2} m_{a4} \dot{y}_{a4}^2 + \\
& \frac{1}{2} I_{xt1} \dot{\phi}_{t1}^2 + \frac{1}{2} I_{zt1} \dot{\theta}_{t1}^2 + \frac{1}{2} I_{xt2} \dot{\phi}_{t2}^2 + \frac{1}{2} I_{zt2} \left(\frac{\dot{y}_{t1} - \dot{y}_{t2} - \dot{\theta}_{t1} l_7}{l_8} \right)^2 + \frac{1}{2} I_{xa1} \dot{\phi}_{a1}^2 + \\
& \frac{1}{2} I_{xa2} \dot{\phi}_{a2}^2 + \frac{1}{2} I_{xa3} \dot{\phi}_{a3}^2 + \frac{1}{2} I_{xa4} \dot{\phi}_{a4}^2 + \frac{1}{2} m_{t2} \dot{y}_{t2}^2
\end{aligned} \tag{4-120}$$

Same substitution will be applied to the equations (4-117) and (4-118). Now the Lagrange's equation is applied to y_{t2} :

$$\left[m_{t2} \ddot{y}_{t2} - \frac{I_{zt2}}{l_8^2} (\dot{y}_{t1} - \dot{y}_{t2} - \ddot{\theta}_{t1} l_7) \right] + \left[\left(1 + \frac{l_9}{l_8}\right) (K_{sy7} U_{sy7} + K_{sy8} U_{sy8} + F_{y7} + F_{y8}) \right] + \left[\left(1 + \frac{l_9}{l_8}\right) (D_{sy7} \dot{U}_{sy7} + D_{sy8} \dot{U}_{sy8}) \right] = 0 \quad (4-121)$$

To simplify the equation some variables are defined as follows:

$$S_{a2} = \frac{I_{zt2}}{l_8^2}$$

$$S_{c2} = \frac{I_{zt2}}{l_8^2} + m_{t2}$$

$$S_{a3} = \frac{I_{zt2}}{l_8^2} l_7$$

$$B_{t4} = m_{t2} g - \left(1 + \frac{l_9}{l_8}\right) (F_{sy7} + F_{sy8} + F_{dsy7} + F_{dsy8})$$

Therefore equation (4-121) will be simplified to:

$$-S_{a2} \ddot{y}_{t1} + S_{c2} \ddot{y}_{t2} + S_{a3} \ddot{\theta}_{t1} = B_{t4} \quad (4-122)$$

By applying the Lagrange's equation to y_{t1} :

$$\begin{aligned} & \left[m_{t1} \ddot{y}_{t1} + \frac{I_{zt2}}{l_8^2} (\dot{y}_{t1} - \dot{y}_{t2} - \ddot{\theta}_{t1} l_7) \right] + \left[(F_{sy1} + F_{sy2} + F_{sy3} + F_{sy4} + F_{sy5} + F_{sy6}) - \frac{l_9}{l_8} (F_{sy7} + F_{sy8}) - (m_{t1} g) \right] + \left[(F_{dsy1} + F_{dsy2} + F_{dsy3} + F_{dsy4} + F_{dsy5} + F_{dsy6}) - \frac{l_9}{l_8} (F_{dsy7} + F_{dsy8}) \right] = 0 \end{aligned} \quad (4-123)$$

Again to simplify the equation some variables are defined as follows:

$$S_{a1} = \frac{I_{zt2}}{l_8^2} + m_{t1}$$

$$\begin{aligned} B_{t1} = m_{t1} g - & [(F_{sy1} + F_{sy2} + F_{sy3} + F_{sy4} + F_{sy5} + F_{sy6}) - \frac{l_9}{l_8} (F_{sy7} + F_{sy8}) + \\ & (F_{dsy1} + F_{dsy2} + F_{dsy3} + F_{dsy4} + F_{dsy5} + F_{dsy6}) - \frac{l_9}{l_8} (F_{dsy7} + F_{dsy8})] \end{aligned}$$

Therefore equation (4-123) will be simplified to:

$$S_{a1}\ddot{y}_{t1} - S_{a2}\ddot{y}_{t2} - S_{a3}\ddot{\theta}_{t1} = B_{t1} \quad (4-124)$$

Also, by applying the Lagrange's equation to θ_{t1} :

$$\begin{aligned} & \left[I_{zt1}\ddot{\theta}_{t1} - \frac{I_{zt2}l_7}{l_8^2}(\ddot{y}_{t1} - \ddot{y}_{t2} - \ddot{\theta}_{t1}l_7) \right] + \left[l_5(F_{sy1} + F_{sy2}) - l_6(F_{sy3} + F_{sy4}) - \right. \\ & (l_2 + l_6)(F_{sy5} + F_{sy6}) + \frac{l_7l_9}{l_8}(F_{sy7} + F_{sy8}) \Big] + \left[l_5(F_{dsy1} + F_{dsy2}) - \right. \\ & l_6(F_{dsy3} + F_{dsy4}) - (l_2 + l_6)(F_{dsy5} + F_{dsy6}) + \frac{l_7l_9}{l_8}(F_{dsy7} + F_{dsy8}) \Big] = 0 \end{aligned} \quad (4-125)$$

Once again to simplify the equation some variables need to be defined as follows:

$$\begin{aligned} S_{b3} &= I_{zt1} + \frac{I_{zt2}l_7^2}{l_8^2} \\ B_{t3} &= - \left[\left[l_5(F_{sy1} + F_{sy2}) - l_6(F_{sy3} + F_{sy4}) - (l_2 + l_6)(F_{sy5} + F_{sy6}) + \frac{l_7l_9}{l_8}(F_{sy7} + \right. \right. \\ & F_{sy8}) \Big] + \left[l_5(F_{dsy1} + F_{dsy2}) - l_6(F_{dsy3} + F_{dsy4}) - (l_2 + l_6)(F_{dsy5} + F_{dsy6}) + \right. \\ & \left. \left. \frac{l_7l_9}{l_8}(F_{dsy7} + F_{dsy8}) \right] \right] \end{aligned}$$

Therefore equation (4-125) will be simplified to:

$$-S_{a3}\ddot{y}_{t1} + S_{a3}\ddot{y}_{t2} + S_{b3}\ddot{\theta}_{t1} = B_{t3} \quad (4-126)$$

By adding equations (4-122) and (4-124),

$$(S_{a1} - S_{a2})\ddot{y}_{t1} - (S_{a2} - S_{c2})\ddot{y}_{t2} = B_{t1} + B_{t4} \quad (4-127)$$

Also by multiplying S_{b3} and S_{a3} to equations (2-124) and (2-126) respectively,

$$(S_{a1}S_{b3} - S_{a3}^2)\ddot{y}_{t1} - (S_{a2}S_{b3} - S_{a3}^2)\ddot{y}_{t2} = S_{b3}B_{t1} + S_{a3}B_{t3} \quad (4-128)$$

By defining the following expressions, equations (4-127) and (4-128) are simplified to equations (4-129) and (4-130) respectively,

$$e_1 = S_{a1} - S_{a2}$$

$$e_2 = S_{a2} - S_{c2}$$

$$e_3 = S_{a1}S_{b3} - S_{a3}^2$$

$$e_4 = S_{a2}S_{b3} - S_{a3}^2$$

$$e_1\ddot{y}_{t1} - e_2\ddot{y}_{t2} = B_{t1} + B_{t4} \quad (4-129)$$

$$e_3\ddot{y}_{t1} - e_4\ddot{y}_{t2} = S_{b3}B_{t1} + S_{a3}B_{t3} \quad (4-130)$$

Solving equations (4-129) and (4-130) for \ddot{y}_{t1} and \ddot{y}_{t2} will lead to:

$$\ddot{y}_{t1} = \frac{e_4(B_{t1}+B_{t4})-e_2(S_{b3}B_{t1}+S_{a3}B_{t3})}{e_1e_4-e_2e_3} \quad (4-131)$$

$$\ddot{y}_{t2} = \frac{e_1\left(\frac{e_4(B_{t1}+B_{t4})-e_2(S_{b3}B_{t1}+S_{a3}B_{t3})}{e_1e_4-e_2e_3}\right)}{e_2} - \frac{B_{t1}+B_{t4}}{e_2} \quad (4-132)$$

Substituting equations (2-131) and (2-132) into equation (2-126) will give,

$$\ddot{\theta}_{t1} = \frac{B_{t3}}{S_{b3}} + \frac{S_{a3}}{S_{b3}}\left(\frac{e_4(B_{t1}+B_{t4})-e_2(S_{b3}B_{t1}+S_{a3}B_{t3})}{e_1e_4-e_2e_3}\right) - \frac{B_{t1}+B_{t4}}{e_2} \quad (4-133)$$

$$\frac{S_{a3}}{S_{b3}}\left(\frac{e_1\left(\frac{e_4(B_{t1}+B_{t4})-e_2(S_{b3}B_{t1}+S_{a3}B_{t3})}{e_1e_4-e_2e_3}\right)}{e_2} - \frac{B_{t1}+B_{t4}}{e_2}\right)$$

By applying the Lagrange's equation to $\varphi_{t1}, \varphi_{t2}$:

$$I_{xt1}\ddot{\varphi}_{t1} + \left[\left(\frac{s_1}{2}\right)(F_{sy1} - F_{sy2}) + \left(\frac{s_2}{2}\right)(F_{sy3} - F_{sy4}) + \left(\frac{s_3}{2}\right)(F_{sy5} - F_{sy6})\right] + \quad (4-134)$$

$$\left[\left(\frac{s_1}{2}\right)(F_{dsy1} - F_{dsy2}) + \left(\frac{s_2}{2}\right)(F_{dsy3} - F_{dsy4}) + \left(\frac{s_3}{2}\right)(F_{dsy5} - F_{dsy6})\right] = 0$$

$$I_{xt2}\ddot{\varphi}_{t2} + \left(\frac{s_4}{2}\right)(F_{sy7} - F_{sy8}) + \left(\frac{s_4}{2}\right)(F_{dsy7} - F_{dsy8}) = 0 \quad (4-135)$$

Also the rest of degrees of freedom will be as follows:

$$m_{a1}\ddot{y}_{a1} - (F_{sy1} + F_{sy2}) + (F_{ty1} + F_{ty2}) - (F_{dsy1} + F_{dsy2}) + (F_{dty1} + F_{dty2}) = m_{a1}g \quad (4-136)$$

$$I_{xa1}\ddot{\varphi}_{a1} - \left(\frac{s_1}{2}\right)(F_{sy1} - F_{sy2}) + \left(\frac{d_1}{2}\right)(F_{ty1} - F_{ty2}) - \left(\frac{s_1}{2}\right)(F_{dsy1} - F_{dsy2}) + \left(\frac{d_1}{2}\right)(F_{dty1} - F_{dty2}) = 0 \quad (4-137)$$

$$m_{a2}\ddot{y}_{a2} - (F_{sy3} + F_{sy4}) + (F_{ty3} + F_{ty4}) - (F_{dsy3} + F_{dsy4}) + (F_{dty3} + F_{dty4}) = m_{a2}g \quad (4-138)$$

$$I_{xa2}\ddot{\phi}_{a2} - (\frac{s_2}{2})(F_{sy3} - F_{sy4}) + (\frac{d_2}{2})(F_{ty3} - F_{ty4}) - (\frac{s_2}{2})(F_{dsy3} - F_{dsy4}) + (\frac{d_2}{2})(F_{dty3} - F_{dty4}) = 0 \quad (4-139)$$

$$m_{a3}\ddot{y}_{a3} - (F_{sy5} + F_{sy6}) + (F_{ty5} + F_{ty6}) - (F_{dsy5} + F_{dsy6}) + (F_{dty5} + F_{dty6}) = m_{a3}g \quad (4-140)$$

$$I_{xa3}\ddot{\phi}_{a3} - (\frac{s_3}{2})(F_{sy5} - F_{sy6}) + (\frac{d_3}{2})(F_{ty5} - F_{ty6}) - (\frac{s_3}{2})(F_{dsy5} - F_{dsy6}) + (\frac{d_3}{2})(F_{dty5} - F_{dty6}) = 0 \quad (4-141)$$

$$m_{a4}\ddot{y}_{a4} - (F_{sy7} + F_{sy8}) + (F_{ty7} + F_{ty8}) - (F_{dsy7} + F_{dsy8}) + (F_{dty7} + F_{dty8}) = m_{a4}g \quad (4-142)$$

$$I_{xa4}\ddot{\phi}_{a4} - (\frac{s_4}{2})(F_{sy7} - F_{sy8}) + (\frac{d_4}{2})(F_{ty7} - F_{ty8}) - (\frac{s_4}{2})(F_{dsy7} - F_{dsy8}) + (\frac{d_4}{2})(F_{dty7} - F_{dty8}) = 0 \quad (4-143)$$

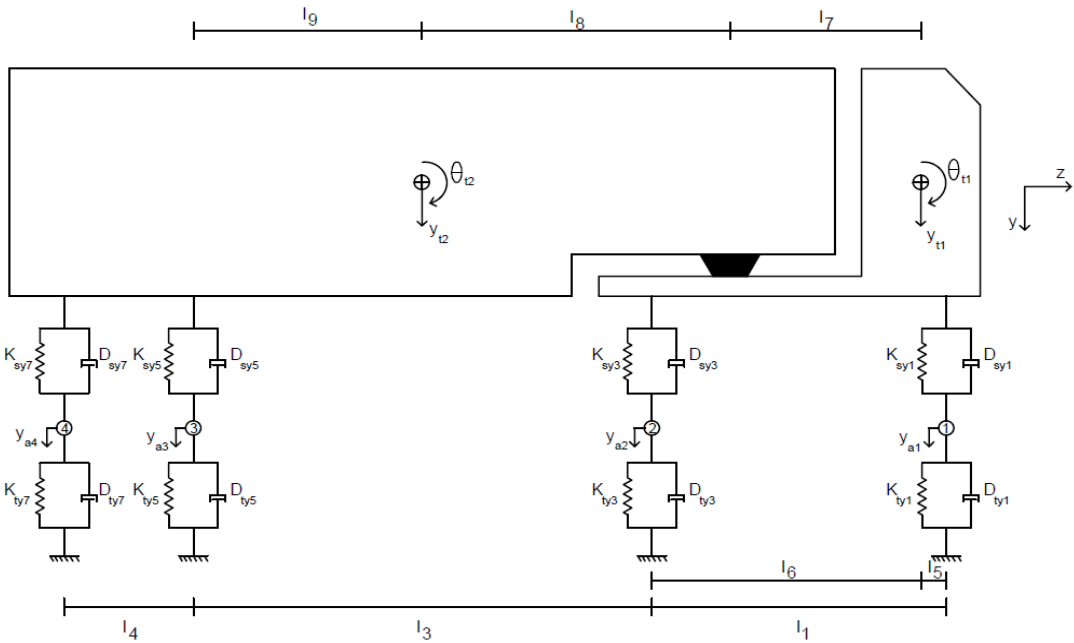
4.9 Derivation of Equations of Motion for “Type 2S2 Truck”

There are fourteen degrees of freedom in total for this type of truck. The degrees of freedom can be seen in Figure 2-8 and the description of those degrees of freedom can be found in Table 4-14.

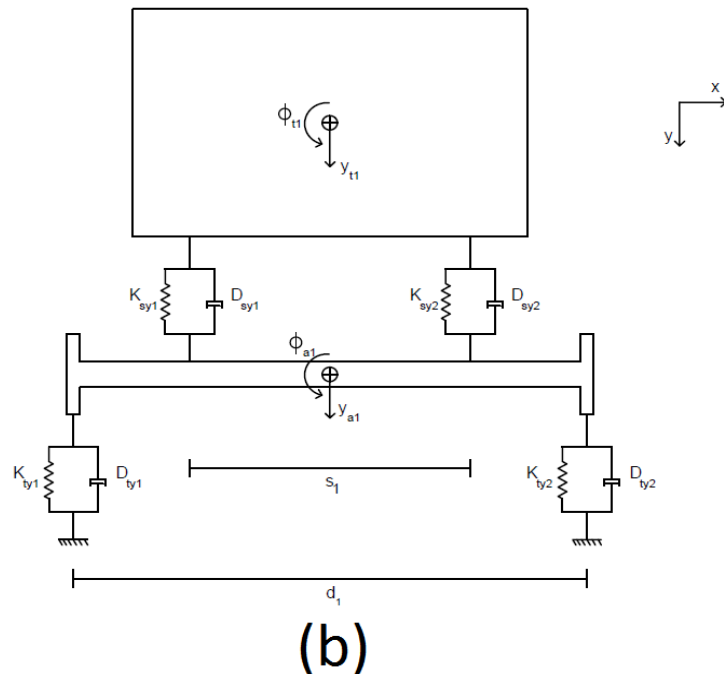
TABLE 4-14: DEGREES OF FREEDOM OF TYPE 2S2 TRUCK

No.	Degree of Freedom	Contributed Mass	Description
1	y_{t1}	m_{t1}	Tractor vertical displacement and mass
2	φ_{t1}	I_{xt1}	Tractor roll displacement and mass moment of inertia
3	θ_{t1}	I_{zt1}	Tractor pitch displacement and mass moment of inertia

4	y_{t2}	m_{t2}	Trailer vertical displacement and mass
5	φ_{t2}	I_{xt2}	Trailer roll displacement and mass moment of inertia
6	θ_{t2}	I_{zt2}	Trailer pitch displacement and mass moment of inertia
7	y_{a1}	m_{a1}	Steer axle vertical displacement and mass
8	φ_{a1}	I_{xa1}	Steer axle roll displacement and mass moment of inertia
9	y_{a2}	m_{a2}	Tractor second axle vertical displacement and mass
10	φ_{a2}	I_{xa2}	Tractor second axle roll displacement and mass moment of inertia
11	y_{a3}	m_{a3}	Vertical displacement and mass of forward axle of trailer tandem
12	φ_{a3}	I_{xa3}	Roll displacement and mass moment of inertia of forward axle of trailer tandem
13	y_{a4}	m_{a4}	Vertical displacement and mass of aft axle of trailer tandem
14	φ_{a4}	I_{xa4}	Roll displacement and mass moment of inertia of aft axle of trailer tandem



(a)



(b)

FIGURE 4-8: TYPE 2S2 DYNAMIC MODEL (A) TRUCK SIDE VIEW (B) TRUCK FRONT VIEW

Relative Displacements at the locations of the springs are also calculated using the values given in Table 2-15.

TABLE 4-15: RELATIVE DISPLACEMENTS AT SPRING LOCATIONS OF TYPE 2S2 TRUCK

Suspension springs	
U_{sy1}	$(y_{t1} - y_{a1}) + (S_1/2)(\varphi_{t1} - \varphi_{a1}) + l_5\theta_{t1}$
U_{sy2}	$(y_{t1} - y_{a1}) - (S_1/2)(\varphi_{t1} - \varphi_{a1}) + l_5\theta_{t1}$
U_{sy3}	$(y_{t1} - y_{a2}) + (S_2/2)(\varphi_{t1} - \varphi_{a2}) - l_6\theta_{t1}$
U_{sy4}	$(y_{t1} - y_{a2}) - (S_2/2)(\varphi_{t1} - \varphi_{a2}) - l_6\theta_{t1}$
U_{sy5}	$(y_{t2} - y_{a3}) + (S_3/2)(\varphi_{t2} - \varphi_{a3}) - l_9\theta_{t2}$
U_{sy6}	$(y_{t2} - y_{a3}) - (S_3/2)(\varphi_{t2} - \varphi_{a3}) - l_9\theta_{t2}$
U_{sy7}	$(y_{t2} - y_{a4}) + (S_4/2)(\varphi_{t2} - \varphi_{a4}) - (l_4 + l_9)\theta_{t2}$
U_{sy8}	$(y_{t2} - y_{a4}) - (S_4/2)(\varphi_{t2} - \varphi_{a4}) - (l_4 + l_9)\theta_{t2}$
Tire springs	
U_{ty1}	$y_{a1} + (d_1/2)\varphi_{a1} + u_{SR1}$
U_{ty2}	$y_{a1} - (d_1/2)\varphi_{a1} + u_{SR2}$
U_{ty3}	$y_{a2} + (d_2/2)\varphi_{a2} + u_{SR3}$
U_{ty4}	$y_{a2} - (d_2/2)\varphi_{a2} + u_{SR4}$
U_{ty5}	$y_{a3} + (d_3/2)\varphi_{a3} + u_{SR5}$
U_{ty6}	$y_{a3} - (d_3/2)\varphi_{a3} + u_{SR6}$
U_{ty7}	$y_{a4} + (d_4/2)\varphi_{a4} + u_{SR7}$
U_{ty8}	$y_{a4} - (d_4/2)\varphi_{a4} + u_{SR8}$

Kinetic Energy of the system:

$$T = \frac{1}{2}m_{t1}\dot{y}_{t1}^2 + \frac{1}{2}m_{a1}\dot{y}_{a1}^2 + \frac{1}{2}m_{a2}\dot{y}_{a2}^2 + \frac{1}{2}m_{a3}\dot{y}_{a3}^2 + \frac{1}{2}m_{a4}\dot{y}_{a4}^2 + \frac{1}{2}I_{xt1}\dot{\phi}_{t1}^2 + \frac{1}{2}I_{zt1}\dot{\theta}_{t1}^2 + \frac{1}{2}I_{xt2}\dot{\phi}_{t2}^2 + \frac{1}{2}I_{zt2}\dot{\theta}_{t2}^2 + \frac{1}{2}I_{xa1}\dot{\phi}_{a1}^2 + \frac{1}{2}I_{xa2}\dot{\phi}_{a2}^2 + \frac{1}{2}I_{xa3}\dot{\phi}_{a3}^2 + \frac{1}{2}I_{xa4}\dot{\phi}_{a4}^2 + \frac{1}{2}m_{t2}\dot{y}_{t2}^2 \quad (4-144)$$

Potential Energy of the system:

$$V = \frac{1}{2}K_{sy1}U_{sy1}^2 + \frac{1}{2}K_{sy2}U_{sy2}^2 + \frac{1}{2}K_{sy3}U_{sy3}^2 + \frac{1}{2}K_{sy4}U_{sy4}^2 + \frac{1}{2}K_{sy5}U_{sy5}^2 + \frac{1}{2}K_{sy6}U_{sy6}^2 + \frac{1}{2}K_{sy7}U_{sy7}^2 + \frac{1}{2}K_{sy8}U_{sy8}^2 + \frac{1}{2}K_{ty1}U_{ty1}^2 + \frac{1}{2}K_{ty2}U_{ty2}^2 + \frac{1}{2}K_{ty3}U_{ty3}^2 + \frac{1}{2}K_{ty4}U_{ty4}^2 + \frac{1}{2}K_{ty5}U_{ty5}^2 + \frac{1}{2}K_{ty6}U_{ty6}^2 + \frac{1}{2}K_{ty7}U_{sy7}^2 + \frac{1}{2}K_{ty8}U_{ty8}^2 - ((m_{t1}g)y_{t1} + (m_{t2}g)y_{t2} + (m_{a1}g)y_{a1} + (m_{a2}g)y_{a2} + (m_{a3}g)y_{a3} + (m_{a4}g)y_{a4}) + (F_{y1}U_{sy1} + F_{y2}U_{sy2} + F_{y3}U_{sy3} + F_{y4}U_{sy4} + F_{y5}U_{sy5} + F_{y6}U_{sy6} + F_{y7}U_{sy7} + F_{y8}U_{sy8}) \quad (4-145)$$

Damping Energy of the system:

$$D = \frac{1}{2}D_{sy1}\dot{U}_{sy1}^2 + \frac{1}{2}D_{sy2}\dot{U}_{sy2}^2 + \frac{1}{2}D_{sy3}\dot{U}_{sy3}^2 + \frac{1}{2}D_{sy4}\dot{U}_{sy4}^2 + \frac{1}{2}D_{sy5}\dot{U}_{sy5}^2 + \frac{1}{2}D_{sy6}\dot{U}_{sy6}^2 + \frac{1}{2}D_{sy7}\dot{U}_{sy7}^2 + \frac{1}{2}D_{sy8}\dot{U}_{sy8}^2 + \frac{1}{2}D_{ty1}\dot{U}_{ty1}^2 + \frac{1}{2}D_{ty2}\dot{U}_{ty2}^2 + \frac{1}{2}D_{ty3}\dot{U}_{ty3}^2 + \frac{1}{2}D_{ty4}\dot{U}_{ty4}^2 + \frac{1}{2}D_{ty5}\dot{U}_{ty5}^2 + \frac{1}{2}D_{ty6}\dot{U}_{ty6}^2 + \frac{1}{2}D_{ty7}\dot{U}_{ty7}^2 + \frac{1}{2}D_{ty8}\dot{U}_{ty8}^2 \quad (4-146)$$

Whether it is calculated from the trailer part or the tractor part, the displacement at the pivot point should be the same,

$$y_{t2} + \theta_{t2}l_8 = y_{t1} - \theta_{t1}l_7 \quad (4-147)$$

Thus, by calculating θ_{t2} from equation (4-147) and substituting in equation (4-144),

$$\begin{aligned}
T = & \frac{1}{2}m_{t1}\dot{y}_{t1}^2 + \frac{1}{2}m_{a1}\dot{y}_{a1}^2 + \frac{1}{2}m_{a2}\dot{y}_{a2}^2 + \frac{1}{2}m_{a3}\dot{y}_{a3}^2 + \frac{1}{2}m_{a4}\dot{y}_{a4}^2 + \\
& \frac{1}{2}I_{xt1}\dot{\phi}_{t1}^2 + \frac{1}{2}I_{zt1}\dot{\theta}_{t1}^2 + \frac{1}{2}I_{xt2}\dot{\phi}_{t2}^2 + \frac{1}{2}I_{zt2}\left(\frac{\dot{y}_{t1}-\dot{y}_{t2}-\dot{\theta}_{t1}l_7}{l_8}\right)^2 + \frac{1}{2}I_{xa1}\dot{\phi}_{a1}^2 + \\
& \frac{1}{2}I_{xa2}\dot{\phi}_{a2}^2 + \frac{1}{2}I_{xa3}\dot{\phi}_{a3}^2 + \frac{1}{2}I_{xa4}\dot{\phi}_{a4}^2 + \frac{1}{2}m_{t2}\dot{y}_{t2}^2
\end{aligned} \quad (4-148)$$

Same substitution will be applied to the equations (4-145) and (4-146). Now the Lagrange's equation is applied to y_{t2} :

$$\begin{aligned}
& \left[m_{t2}\ddot{y}_{t2} - \frac{I_{zt2}}{l_8^2}(\ddot{y}_{t1} - \ddot{y}_{t2} - \ddot{\theta}_{t1}l_7)\right] + \left[\left(1 + \frac{l_9}{l_8}\right)(F_{sy5} + F_{sy6}) + \right. \\
& \left.\left(1 + \frac{l_4+l_9}{l_8}\right)(F_{sy7} + F_{sy8}) - (m_{t2}g)\right] + \left[\left(1 + \frac{l_9}{l_8}\right)(F_{dsy5} + F_{dsy6}) + \right. \\
& \left.\left(1 + \frac{l_4+l_9}{l_8}\right)(F_{dsy7} + F_{dsy8})\right] = 0
\end{aligned} \quad (4-149)$$

To simplify the equation some variables are defined as follows:

$$S_{a2} = \frac{I_{zt2}}{l_8^2}$$

$$S_{c2} = \frac{I_{zt2}}{l_8^2} + m_{t2}$$

$$S_{a3} = \frac{I_{zt2}}{l_8^2}l_7$$

$$\begin{aligned}
B_{t4} = & m_{t2}g - \left(1 + \frac{l_9}{l_8}\right)(F_{sy5} + F_{sy6} + F_{dsy5} + F_{dsy6}) - \left(1 + \frac{l_4+l_9}{l_8}\right)(F_{sy7} + F_{sy8} + \\
& F_{dsy7} + F_{dsy8})
\end{aligned}$$

Therefore equation (4-149) will be simplified to:

$$-S_{a2}\ddot{y}_{t1} + S_{c2}\ddot{y}_{t2} + S_{a3}\ddot{\theta}_{t1} = B_{t4} \quad (4-150)$$

By applying the Lagrange's equation to y_{t1} :

$$\begin{aligned} & \left[m_{t1} \ddot{y}_{t1} + \frac{I_{zt2}}{l_8^2} (\ddot{y}_{t1} - \ddot{y}_{t2} - \ddot{\theta}_{t1} l_7) \right] + \left[(F_{sy1} + F_{sy2} + F_{sy3} + F_{sy4}) - \right. \\ & \left. \frac{l_9}{l_8} (F_{sy5} + F_{sy6}) - \frac{l_9 + l_4}{l_8} (F_{sy7} + F_{sy8}) - (m_{t1} g) \right] + \left[(F_{dsy1} + F_{dsy2} + \right. \\ & \left. F_{dsy3} + F_{dsy4}) - \frac{l_9}{l_8} (F_{dsy5} + F_{dsy6}) - \frac{l_9 + l_4}{l_8} (F_{dsy7} + F_{dsy8}) \right] = 0 \end{aligned} \quad (4-151)$$

Again to simplify the equation some variables are defined as follows:

$$S_{a1} = \frac{I_{zt2}}{l_8^2} + m_{t1}$$

$$\begin{aligned} B_{t1} = m_{t1} g - & [(F_{sy1} + F_{sy2} + F_{sy3} + F_{sy4}) - \frac{l_9}{l_8} (F_{sy5} + F_{sy6}) - \frac{l_9 + l_4}{l_8} (F_{sy7} + F_{sy8}) + \\ & (F_{dsy1} + F_{dsy2} + F_{dsy3} + F_{dsy4}) - \frac{l_9}{l_8} (F_{dsy5} + F_{dsy6}) - \frac{l_9 + l_4}{l_8} (F_{dsy7} + F_{dsy8})] \end{aligned}$$

Therefore equation (4-151) will be simplified to:

$$S_{a1} \ddot{y}_{t1} - S_{a2} \ddot{y}_{t2} - S_{a3} \ddot{\theta}_{t1} = B_{t1} \quad (4-152)$$

Also, by applying the Lagrange's equation to θ_{t1} :

$$\begin{aligned} & \left[I_{zt1} \ddot{\theta}_{t1} - \frac{I_{zt2} l_7}{l_8^2} (\ddot{y}_{t1} - \ddot{y}_{t2} - \ddot{\theta}_{t1} l_7) \right] + \left[l_5 (F_{sy1} + F_{sy2}) - l_6 (F_{sy3} + \right. \\ & \left. F_{sy4}) + \frac{l_7 l_9}{l_8} (F_{sy5} + F_{sy6}) + \frac{l_7 (l_4 + l_9)}{l_8} (F_{sy7} + F_{sy8}) \right] + \left[l_5 (F_{dsy1} + F_{dsy2}) - \right. \\ & \left. l_6 (F_{dsy3} + F_{dsy4}) + \frac{l_7 l_9}{l_8} (F_{dsy5} + F_{dsy6}) + \frac{l_7 (l_4 + l_9)}{l_8} (F_{dsy7} + F_{dsy8}) \right] = 0 \end{aligned} \quad (4-153)$$

Once again to simplify the equation some variables need to be defined as follows:

$$S_{b3} = I_{zt1} + \frac{I_{zt2} l_7^2}{l_8^2}$$

$$\begin{aligned} B_{t3} = - & \left[\left[l_5 (F_{sy1} + F_{sy2}) - l_6 (F_{sy3} + F_{sy4}) + \frac{l_7 l_9}{l_8} (F_{sy5} + F_{sy6}) + \frac{l_7 (l_4 + l_9)}{l_8} (F_{sy7} + \right. \right. \\ & \left. \left. F_{sy8}) \right] + \left[l_5 (F_{dsy1} + F_{dsy2}) - l_6 (F_{dsy3} + F_{dsy4}) + \frac{l_7 l_9}{l_8} (F_{dsy5} + F_{dsy6}) + \frac{l_7 (l_4 + l_9)}{l_8} (F_{dsy7} + \right. \right. \\ & \left. \left. F_{dsy8}) \right] \right] \end{aligned}$$

Therefore equation (4-153) will be simplified to:

$$-S_{a3}\ddot{y}_{t1} + S_{a3}\ddot{y}_{t2} + S_{b3}\ddot{\theta}_{t1} = B_{t3} \quad (4-154)$$

By adding equations (2-150) and (2-152),

$$(S_{a1} - S_{a2})\ddot{y}_{t1} - (S_{a2} - S_{c2})\ddot{y}_{t2} = B_{t1} + B_{t4} \quad (4-155)$$

Also by multiplying S_{b3} and S_{a3} to equations (2-152) and (2-154) respectively,

$$(S_{a1}S_{b3} - S_{a3}^2)\ddot{y}_{t1} - (S_{a2}S_{b3} - S_{a3}^2)\ddot{y}_{t2} = S_{b3}B_{t1} + S_{a3}B_{t3} \quad (4-156)$$

By defining the following expressions, equations (4-155) and (4-156) are simplified to equations (4-157) and (4-158) respectively,

$$e_1 = S_{a1} - S_{a2}$$

$$e_2 = S_{a2} - S_{c2}$$

$$e_3 = S_{a1}S_{b3} - S_{a3}^2$$

$$e_4 = S_{a2}S_{b3} - S_{a3}^2$$

$$e_1\ddot{y}_{t1} - e_2\ddot{y}_{t2} = B_{t1} + B_{t4} \quad (4-157)$$

$$e_3\ddot{y}_{t1} - e_4\ddot{y}_{t2} = S_{b3}B_{t1} + S_{a3}B_{t3} \quad (4-158)$$

Solving equations (4-157) and (4-158) for \ddot{y}_{t1} and \ddot{y}_{t2} will lead to:

$$\ddot{y}_{t1} = \frac{e_4(B_{t1} + B_{t4}) - e_2(S_{b3}B_{t1} + S_{a3}B_{t3})}{e_1e_4 - e_2e_3} \quad (4-159)$$

$$\ddot{y}_{t2} = \frac{e_1 \left(\frac{e_4(B_{t1} + B_{t4}) - e_2(S_{b3}B_{t1} + S_{a3}B_{t3})}{e_1e_4 - e_2e_3} \right) - \frac{B_{t1} + B_{t4}}{e_2}}{e_2} \quad (4-160)$$

Substituting equations (4-159) and (4-160) into equation (4-154) will give,

$$\begin{aligned}
\ddot{\theta}_{t1} = & \frac{B_{t3}}{S_{b3}} + \frac{S_{a3}}{S_{b3}} \left(\frac{e_4(B_{t1} + B_{t4}) - e_2(S_{b3}B_{t1} + S_{a3}B_{t3})}{e_1e_4 - e_2e_3} \right) \\
& - \frac{S_{a3}}{S_{b3}} \left(\frac{e_1}{e_2} \left(\frac{e_4(B_{t1} + B_{t4}) - e_2(S_{b3}B_{t1} + S_{a3}B_{t3})}{e_1e_4 - e_2e_3} \right) \right. \\
& \left. - \frac{B_{t1} + B_{t4}}{e_2} \right)
\end{aligned} \tag{4-161}$$

By applying the Lagrange's equation to $\varphi_{t1}, \varphi_{t2}$:

$$I_{xt1}\ddot{\varphi}_{t1} + \left[\left(\frac{s_1}{2}\right)(F_{sy1} - F_{sy2}) + \left(\frac{s_2}{2}\right)(F_{sy3} - F_{sy4}) \right] + \left[\left(\frac{s_1}{2}\right)(F_{dsy1} - F_{dsy2}) + \left(\frac{s_2}{2}\right)(F_{dsy3} - F_{dsy4}) \right] = 0 \tag{4-162}$$

$$I_{xt2}\ddot{\varphi}_{t2} + \left[\left(\frac{s_3}{2}\right)(F_{sy5} - F_{sy6}) + \left(\frac{s_4}{2}\right)(F_{sy7} - F_{sy8}) \right] + \left[\left(\frac{s_3}{2}\right)(F_{dsy5} - F_{dsy6}) + \left(\frac{s_4}{2}\right)(F_{dsy7} - F_{dsy8}) \right] = 0 \tag{4-163}$$

Also the rest of degrees of freedom will be as follows:

$$m_{a1}\ddot{y}_{a1} - (F_{sy1} + F_{sy2}) + (F_{ty1} + F_{ty2}) - (F_{dsy1} + F_{dsy2}) + (F_{dty1} + F_{dty2}) = m_{a1}g \tag{4-164}$$

$$\begin{aligned}
I_{xa1}\ddot{\varphi}_{a1} - \left(\frac{s_1}{2}\right)(F_{sy1} - F_{sy2}) + \left(\frac{d_1}{2}\right)(F_{ty1} - F_{ty2}) - \left(\frac{s_1}{2}\right)(F_{dsy1} - F_{dsy2}) + \\
\left(\frac{d_1}{2}\right)(F_{dty1} - F_{dty2}) = 0
\end{aligned} \tag{4-165}$$

$$\begin{aligned}
m_{a2}\ddot{y}_{a2} - (F_{sy3} + F_{sy4}) + (F_{ty3} + F_{ty4}) - (F_{dsy3} + F_{dsy4}) + (F_{dty3} + F_{dty4}) = m_{a2}g
\end{aligned} \tag{4-166}$$

$$\begin{aligned}
I_{xa2}\ddot{\varphi}_{a2} - \left(\frac{s_2}{2}\right)(F_{sy3} - F_{sy4}) + \left(\frac{d_2}{2}\right)(F_{ty3} - F_{ty4}) - \left(\frac{s_2}{2}\right)(F_{dsy3} - F_{dsy4}) + \\
\left(\frac{d_2}{2}\right)(F_{dty3} - F_{dty4}) = 0
\end{aligned} \tag{4-167}$$

$$m_{a3}\ddot{y}_{a3} - (F_{sy5} + F_{sy6}) + (F_{ty5} + F_{ty6}) - (F_{dsy5} + F_{dsy6}) + (F_{dty5} + F_{dty6}) = m_{a3}g \tag{4-168}$$

$$F_{dty6}) = m_{a3}g$$

$$I_{xa3}\ddot{\varphi}_{a3} - (\frac{s_3}{2})(F_{sy5} - F_{sy6}) + (\frac{d_3}{2})(F_{ty5} - F_{ty6}) - (\frac{s_3}{2})(F_{dsy5} - F_{dsy6}) + \\ (4-169)$$

$$(\frac{d_3}{2})(F_{dty5} - F_{dty6}) = 0$$

$$m_{a4}\ddot{y}_{a4} - (F_{sy7} + F_{sy8}) + (F_{ty7} + F_{ty8}) - (F_{dsy7} + F_{dsy8}) + (F_{dty7} + \\ (4-170)$$

$$F_{dty8}) = m_{a4}g$$

$$I_{xa4}\ddot{\varphi}_{a4} - (\frac{s_4}{2})(F_{sy7} - F_{sy8}) + (\frac{d_4}{2})(F_{ty7} - F_{ty8}) - (\frac{s_4}{2})(F_{dsy7} - F_{dsy8}) + \\ (4-171)$$

$$(\frac{d_4}{2})(F_{dty7} - F_{dty8}) = 0$$

4.10 Derivation of Equations of Motion for “SU4 Truck”

There are eleven degrees of freedom in total for this type of truck. The degrees of freedom can be seen in Figure 4-9 and the description of those degrees of freedom can be found in Table 4-16. Relative Displacements at the locations of the springs are also calculated using the values given in Table 4-17.

TABLE 4-16: DEGREES OF FREEDOM OF SU4 TRUCK

No.	Degree of Freedom	Contributed Mass	Description
1	y_{t1}	m_{t1}	Truck vertical displacement and mass
2	φ_{t1}	I_{xt1}	Truck roll displacement and mass moment of inertia
3	θ_{t1}	I_{zt1}	Truck pitch displacement and mass moment of inertia
4	y_{a1}	m_{a1}	Steer axle vertical displacement and mass
5	φ_{a1}	I_{xa1}	Steer axle roll displacement and mass moment of inertia
6	y_{a2}	m_{a2}	Vertical displacement and mass of first axle of truck tridem
7	φ_{a2}	I_{xa2}	Roll displacement and mass moment of inertia of first axle of truck tridem
8	y_{a3}	m_{a3}	Vertical displacement and mass of second axle of truck tridem
9	φ_{a3}	I_{xa3}	Roll displacement and mass moment of inertia of second axle of truck tridem
10	y_{a4}	m_{a4}	Fourth axle vertical displacement and mass of third axle of truck tridem
11	φ_{a4}	I_{xa4}	Roll displacement and mass moment of inertia of third axle of truck tridem

Kinetic Energy of the system:

$$T = \frac{1}{2}m_{t1}\dot{y}_{t1}^2 + \frac{1}{2}m_{a1}\dot{y}_{a1}^2 + \frac{1}{2}m_{a2}\dot{y}_{a2}^2 + \frac{1}{2}m_{a3}\dot{y}_{a3}^2 + \frac{1}{2}m_{a4}\dot{y}_{a4}^2 + \frac{1}{2}I_{xt1}\dot{\varphi}_{t1}^2 + \frac{1}{2}I_{zt1}\dot{\theta}_{t1}^2 + \frac{1}{2}I_{xa1}\dot{\varphi}_{a1}^2 + \frac{1}{2}I_{xa2}\dot{\varphi}_{a2}^2 + \frac{1}{2}I_{xa3}\dot{\varphi}_{a3}^2 + \frac{1}{2}I_{xa4}\dot{\varphi}_{a4}^2 \quad (4-172)$$

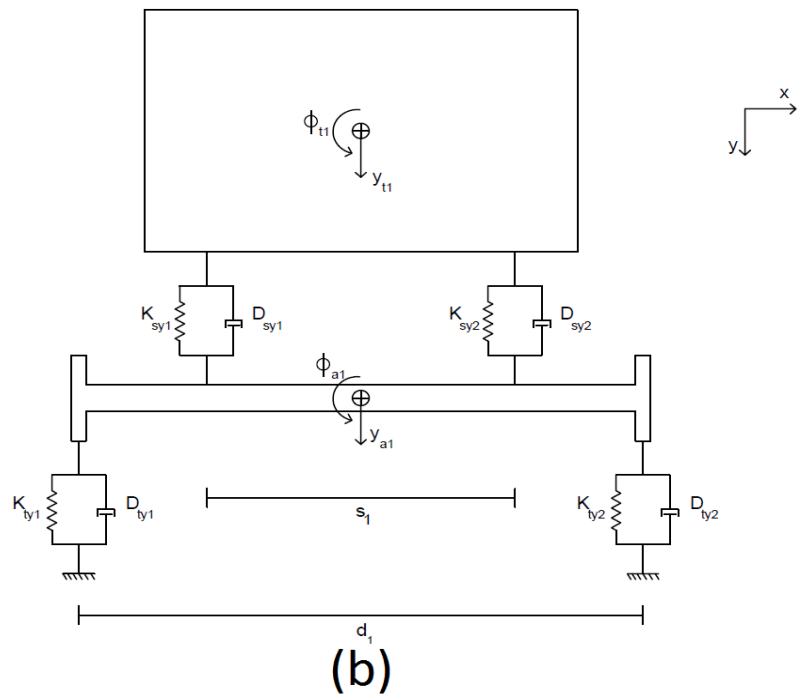
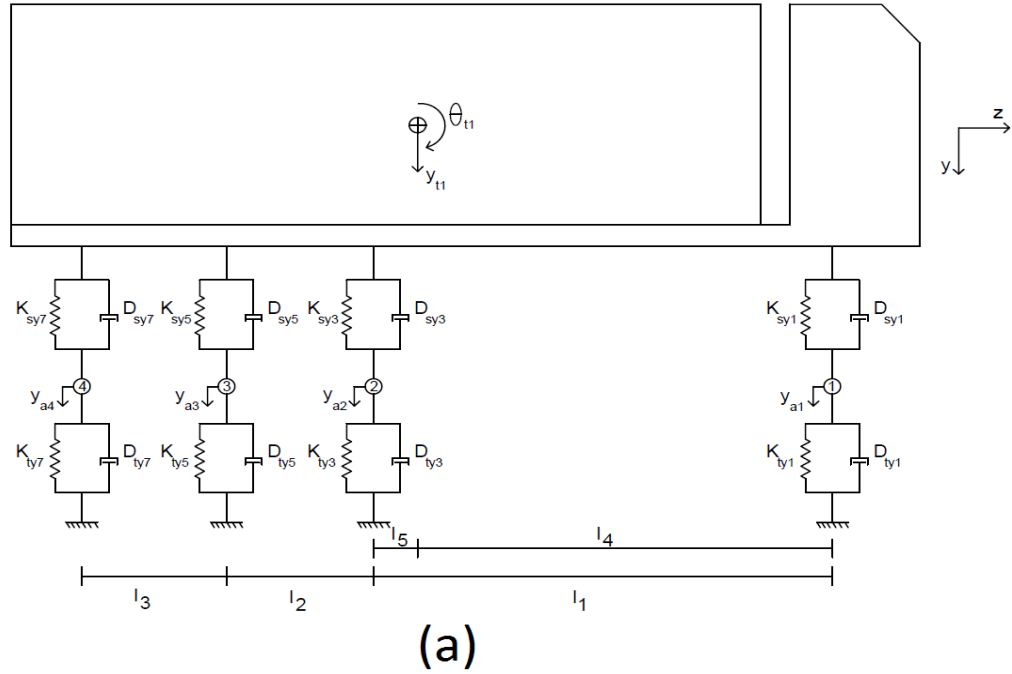


FIGURE 4-9: SU4 TRUCK DYNAMIC MODEL (A) TRUCK SIDE VIEW (B) TRUCK FRONT VIEW

TABLE 4-17: RELATIVE DISPLACEMENTS AT SPRING LOCATIONS OF SU4 TRUCK

Suspension springs	
\mathbf{U}_{sy1}	$(y_{t1} - y_{a1}) + (S_1/2)(\varphi_{t1} - \varphi_{a1}) + l_4\theta_{t1}$
\mathbf{U}_{sy2}	$(y_{t1} - y_{a1}) - (S_1/2)(\varphi_{t1} - \varphi_{a1}) + l_4\theta_{t1}$
\mathbf{U}_{sy3}	$(y_{t1} - y_{a2}) + (S_2/2)(\varphi_{t1} - \varphi_{a2}) - l_5\theta_{t1}$
\mathbf{U}_{sy4}	$(y_{t1} - y_{a2}) - (S_2/2)(\varphi_{t1} - \varphi_{a2}) - l_5\theta_{t1}$
\mathbf{U}_{sy5}	$(y_{t1} - y_{a3}) + (S_3/2)(\varphi_{t1} - \varphi_{a3}) - (l_2 + l_5)\theta_{t1}$
\mathbf{U}_{sy6}	$(y_{t1} - y_{a3}) - (S_3/2)(\varphi_{t1} - \varphi_{a3}) - (l_2 + l_5)\theta_{t1}$
\mathbf{U}_{sy7}	$(y_{t1} - y_{a4}) + (S_4/2)(\varphi_{t1} - \varphi_{a4}) - (l_2 + l_3 + l_5)\theta_{t1}$
\mathbf{U}_{sy8}	$(y_{t1} - y_{a4}) - (S_4/2)(\varphi_{t1} - \varphi_{a4}) - (l_2 + l_3 + l_5)\theta_{t1}$
Tire springs	
\mathbf{U}_{ty1}	$y_{a1} + (d_1/2)\varphi_{a1} + u_{SR1}$
\mathbf{U}_{ty2}	$y_{a1} - (d_1/2)\varphi_{a1} + u_{SR2}$
\mathbf{U}_{ty3}	$y_{a2} + (d_2/2)\varphi_{a2} + u_{SR3}$
\mathbf{U}_{ty4}	$y_{a2} - (d_2/2)\varphi_{a2} + u_{SR4}$
\mathbf{U}_{ty5}	$y_{a3} + (d_3/2)\varphi_{a3} + u_{SR5}$
\mathbf{U}_{ty6}	$y_{a3} - (d_3/2)\varphi_{a3} + u_{SR6}$
\mathbf{U}_{ty7}	$y_{a4} + (d_4/2)\varphi_{a4} + u_{SR7}$
\mathbf{U}_{ty8}	$y_{a4} - (d_4/2)\varphi_{a4} + u_{SR8}$

Potential Energy of the system:

$$\begin{aligned}
V = & \frac{1}{2}K_{sy1}U_{sy1}^2 + \frac{1}{2}K_{sy2}U_{sy2}^2 + \frac{1}{2}K_{sy3}U_{sy3}^2 + \frac{1}{2}K_{sy4}U_{sy4}^2 + \\
& \frac{1}{2}K_{sy5}U_{sy5}^2 + \frac{1}{2}K_{sy6}U_{sy6}^2 + \frac{1}{2}K_{sy7}U_{sy7}^2 + \frac{1}{2}K_{sy8}U_{sy8}^2 + \frac{1}{2}K_{ty1}U_{ty1}^2 + \\
& \frac{1}{2}K_{ty2}U_{ty2}^2 + \frac{1}{2}K_{ty3}U_{ty3}^2 + \frac{1}{2}K_{ty4}U_{ty4}^2 + \frac{1}{2}K_{ty5}U_{ty5}^2 + \frac{1}{2}K_{ty6}U_{ty6}^2 + \\
& \frac{1}{2}K_{ty7}U_{ty7}^2 + \frac{1}{2}K_{ty8}U_{ty8}^2 - ((m_{t1}g)y_{t1} + (m_{a1}g)y_{a1} + (m_{a2}g)y_{a2} + \\
& (m_{a3}g)y_{a3} + (m_{a4}g)y_{a4}) + (F_{y1}U_{sy1} + F_{y2}U_{sy2} + F_{y3}U_{sy3} + F_{y4}U_{sy4} + \\
& F_{y5}U_{sy5} + F_{y6}U_{sy6} + F_{y7}U_{sy7} + F_{y8}U_{sy8})
\end{aligned} \tag{4-173}$$

Damping Energy of the system:

$$\begin{aligned}
D = & \frac{1}{2}D_{sy1}\dot{U}_{sy1}^2 + \frac{1}{2}D_{sy2}\dot{U}_{sy2}^2 + \frac{1}{2}D_{sy3}\dot{U}_{sy3}^2 + \frac{1}{2}D_{sy4}\dot{U}_{sy4}^2 + \\
& \frac{1}{2}D_{sy5}\dot{U}_{sy5}^2 + \frac{1}{2}D_{sy6}\dot{U}_{sy6}^2 + \frac{1}{2}D_{sy7}\dot{U}_{sy7}^2 + \frac{1}{2}D_{sy8}\dot{U}_{sy8}^2 + \frac{1}{2}D_{ty1}\dot{U}_{ty1}^2 + \\
& \frac{1}{2}D_{ty2}\dot{U}_{ty2}^2 + \frac{1}{2}D_{ty3}\dot{U}_{ty3}^2 + \frac{1}{2}D_{ty4}\dot{U}_{ty4}^2 + \frac{1}{2}D_{ty5}\dot{U}_{ty5}^2 + \frac{1}{2}D_{ty6}\dot{U}_{ty6}^2 + \\
& \frac{1}{2}D_{ty7}\dot{U}_{ty7}^2 + \frac{1}{2}D_{ty8}\dot{U}_{ty8}^2
\end{aligned} \tag{4-174}$$

Now the Lagrange's equation is applied to y_{t1} :

$$\begin{aligned}
m_{t1}\ddot{y}_{t1} + & [(F_{sy1} + F_{sy2} + F_{sy3} + F_{sy4} + F_{sy5} + F_{sy6} + F_{sy7} + F_{sy8}) + \\
& (F_{dsy1} + F_{dsy2} + F_{dsy3} + F_{dsy4} + F_{dsy5} + F_{dsy6} + F_{dsy7} + F_{dsy8})] = m_{t1}g
\end{aligned} \tag{4-175}$$

Also, by applying the Lagrange's equation to θ_{t1} :

$$I_{zt1}\ddot{\theta}_{t1} + [l_4(F_{sy1} + F_{sy2}) - l_5(F_{sy3} + F_{sy4}) - (l_2 + l_5)(F_{sy5} + F_{sy6}) - (l_2 + l_3 + l_5)(F_{sy7} + F_{sy8})] + [l_4(F_{dsy1} + F_{dsy2}) - l_5(F_{dsy3} + F_{dsy4}) - (l_2 + l_5)(F_{dsy5} + F_{dsy6}) - (l_2 + l_3 + l_5)(F_{dsy7} + F_{dsy8})] = 0 \quad (4-176)$$

By applying the Lagrange's equation to φ_{t1} :

$$I_{xt1}\ddot{\varphi}_{t1} + \left[\left(\frac{s_1}{2}\right)(F_{sy1} - F_{sy2}) + \left(\frac{s_2}{2}\right)(F_{sy3} - F_{sy4}) + \left(\frac{s_3}{2}\right)(F_{sy5} - F_{sy6}) + \left(\frac{s_4}{2}\right)(F_{sy7} - F_{sy8}) \right] + \left[\left(\frac{s_1}{2}\right)(F_{dsy1} - F_{dsy2}) + \left(\frac{s_2}{2}\right)(F_{dsy3} - F_{dsy4}) + \left(\frac{s_3}{2}\right)(F_{dsy5} - F_{dsy6}) + \left(\frac{s_4}{2}\right)(F_{dsy7} - F_{dsy8}) \right] = 0 \quad (4-177)$$

Also the rest of degrees of freedom will be as follows:

$$m_{a1}\ddot{y}_{a1} - (F_{sy1} + F_{sy2}) + (F_{ty1} + F_{ty2}) - (F_{dsy1} + F_{dsy2}) + (F_{dty1} + F_{dty2}) = m_{a1}g \quad (4-178)$$

$$I_{xa1}\ddot{\varphi}_{a1} - \left(\frac{s_1}{2}\right)(F_{sy1} - F_{sy2}) + \left(\frac{d_1}{2}\right)(F_{ty1} - F_{ty2}) - \left(\frac{s_1}{2}\right)(F_{dsy1} - F_{dsy2}) + \left(\frac{d_1}{2}\right)(F_{dty1} - F_{dty2}) = 0 \quad (4-179)$$

$$m_{a2}\ddot{y}_{a2} - (F_{sy3} + F_{sy4}) + (F_{ty3} + F_{ty4}) - (F_{dsy3} + F_{dsy4}) + (F_{dty3} + F_{dty4}) = m_{a2}g \quad (4-180)$$

$$I_{xa2}\ddot{\varphi}_{a2} - \left(\frac{s_2}{2}\right)(F_{sy3} - F_{sy4}) + \left(\frac{d_2}{2}\right)(F_{ty3} - F_{ty4}) - \left(\frac{s_2}{2}\right)(F_{dsy3} - F_{dsy4}) + \left(\frac{d_2}{2}\right)(F_{dty3} - F_{dty4}) = 0 \quad (4-181)$$

$$m_{a3}\ddot{y}_{a3} - (F_{sy5} + F_{sy6}) + (F_{ty5} + F_{ty6}) - (F_{dsy5} + F_{dsy6}) + (F_{dty5} + F_{dty6}) = m_{a3}g \quad (4-182)$$

$$I_{xa3}\ddot{\varphi}_{a3} - \left(\frac{s_3}{2}\right)(F_{sy5} - F_{sy6}) + \left(\frac{d_3}{2}\right)(F_{ty5} - F_{ty6}) - \left(\frac{s_3}{2}\right)(F_{dsy5} - F_{dsy6}) + \left(\frac{d_3}{2}\right)(F_{dty5} - F_{dty6}) = 0 \quad (4-183)$$

$$m_{a4}\ddot{y}_{a4} - (F_{sy7} + F_{sy8}) + (F_{ty7} + F_{ty8}) - (F_{dsy7} + F_{dsy8}) + (F_{dty7} + F_{dty8}) = m_{a4}g \quad (4-184)$$

$$I_{xa4}\ddot{\varphi}_{a4} - \left(\frac{s_4}{2}\right)(F_{sy7} - F_{sy8}) + \left(\frac{d_4}{2}\right)(F_{ty7} - F_{ty8}) - \left(\frac{s_4}{2}\right)(F_{dsy7} - F_{dsy8}) + \left(\frac{d_4}{2}\right)(F_{dty7} - F_{dty8}) = 0 \quad (4-185)$$

4.11 Derivation of Equations of Motion for “9 Axle Turnpike Double”

The dynamic model of 9 Axle Turnpike Double can be seen in Figure 2-10. Degrees of freedom of this truck and the relative displacements at the spring locations are given in Table 2-18 and Table 2-19, respectively. Twenty seven degrees of freedom in total have been chosen for this type of truck.

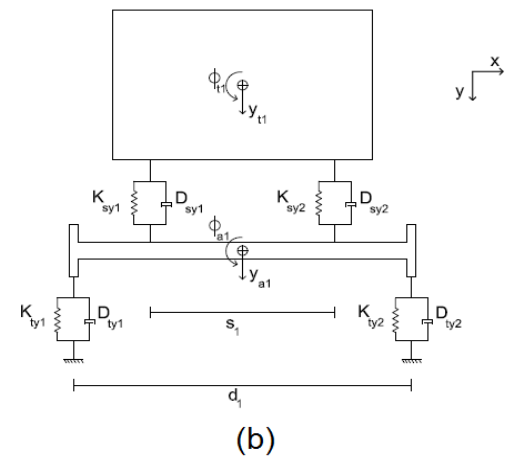
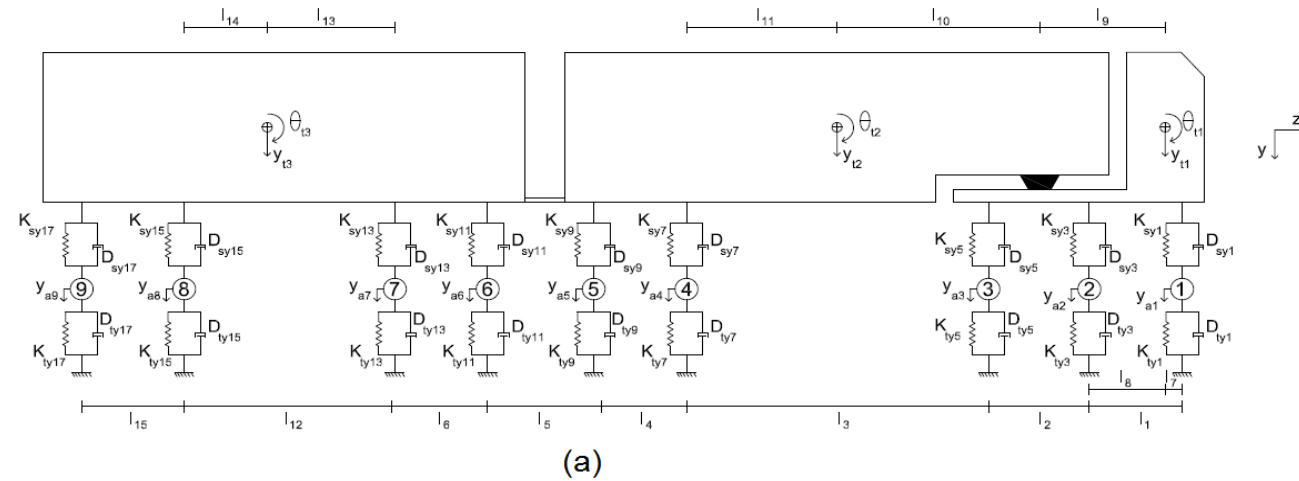


FIGURE 4-10: NINE AXLE TURNPIKE DOUBLE DYNAMIC MODEL (A) TRUCK SIDE VIEW (B) TRUCK FRONT VIEW

TABLE 4-18: DEGREES OF FREEDOM OF 9 AXLE TURNPIKE DOUBLE

No.	Degree of Freedom	Contrib. Mass	Description
1	y_{t1}	m_{t1}	Tractor vertical displacement and mass
2	φ_{t1}	I_{xt1}	Tractor roll displacement and mass moment of inertia
3	θ_{t1}	I_{zt1}	Tractor pitch displacement and mass moment of inertia
4	y_{t2}	m_{t2}	Semi-trailer vertical displacement and mass
5	φ_{t2}	I_{xt2}	Semi-trailer roll displacement and mass moment of inertia
6	θ_{t2}	I_{zt2}	Semi-trailer pitch displacement and mass moment of inertia
7	y_{t3}	m_{t3}	Trailer vertical displacement and mass
8	φ_{t3}	I_{xt3}	Trailer roll displacement and mass moment of inertia
9	θ_{t3}	I_{zt3}	Trailer pitch displacement and mass moment of inertia
10	y_{a1}	m_{a1}	Steer axle vertical displacement and mass
11	φ_{a1}	I_{xa1}	Steer axle roll displacement and mass moment of inertia
12	y_{a2}	m_{a2}	Vertical displacement and mass of forward axle of tractor tandem
13	φ_{a2}	I_{xa2}	Roll displacement and mass moment of inertia of forward axle of tractor tandem
14	y_{a3}	m_{a3}	Vertical displacement and mass of aft axle of tractor tandem
15	φ_{a3}	I_{xa3}	Roll displacement and mass moment of inertia of aft axle of tractor tandem
16	y_{a4}	m_{a4}	Vertical displacement and mass of first axle of semi-trailer
17	φ_{a4}	I_{xa4}	Roll displacement and mass moment of inertia of first axle of semi-trailer
18	y_{a5}	m_{a5}	Vertical displacement and mass of second axle of semi-trailer
19	φ_{a5}	I_{xa5}	Roll displacement and mass moment of inertia of second axle of semi-trailer
20	y_{a6}	m_{a6}	Vertical displacement and mass of first axle of trailer
21	φ_{a6}	I_{xa6}	Roll displacement and mass moment of inertia of first axle of trailer
22	y_{a7}	m_{a7}	Vertical displacement and mass of second axle of trailer
23	φ_{a7}	I_{xa7}	Roll displacement and mass moment of inertia of second axle of trailer
24	y_{a8}	m_{a8}	Vertical displacement and mass of third axle of trailer
25	φ_{a8}	I_{xa8}	Roll displacement and mass moment of inertia of third axle of trailer
26	y_{a9}	m_{a9}	Vertical displacement and mass of fourth axle of trailer
27	φ_{a9}	I_{xa9}	Roll displacement and mass moment of inertia of fourth axle of trailer

TABLE 4-19: RELATIVE DISPLACEMENTS AT SPRING LOCATIONS OF 9 AXLE TURNPIKE DOUBLE

Suspension springs	
\mathbf{U}_{sy1}	$(y_{t1} - y_{a1}) + (S_1/2)(\varphi_{t1} - \varphi_{a1}) + l_7\theta_{t1}$
\mathbf{U}_{sy2}	$(y_{t1} - y_{a1}) - (S_1/2)(\varphi_{t1} - \varphi_{a1}) + l_7\theta_{t1}$
\mathbf{U}_{sy3}	$(y_{t1} - y_{a2}) + (S_2/2)(\varphi_{t1} - \varphi_{a2}) - l_8\theta_{t1}$
\mathbf{U}_{sy4}	$(y_{t1} - y_{a2}) - (S_2/2)(\varphi_{t1} - \varphi_{a2}) - l_8\theta_{t1}$
\mathbf{U}_{sy5}	$(y_{t1} - y_{a3}) + (S_3/2)(\varphi_{t1} - \varphi_{a3}) - (l_2 + l_8)\theta_{t1}$
\mathbf{U}_{sy6}	$(y_{t1} - y_{a3}) - (S_3/2)(\varphi_{t1} - \varphi_{a3}) - (l_2 + l_8)\theta_{t1}$
\mathbf{U}_{sy7}	$(y_{t2} - y_{a4}) + (S_4/2)(\varphi_{t2} - \varphi_{a4}) - l_{11}\theta_{t2}$
\mathbf{U}_{sy8}	$(y_{t2} - y_{a4}) - (S_4/2)(\varphi_{t2} - \varphi_{a4}) - l_{11}\theta_{t2}$
\mathbf{U}_{sy9}	$(y_{t2} - y_{a5}) + (S_5/2)(\varphi_{t2} - \varphi_{a5}) - (l_4 + l_{11})\theta_{t2}$
\mathbf{U}_{sy10}	$(y_{t2} - y_{a5}) - (S_5/2)(\varphi_{t2} - \varphi_{a5}) - (l_4 + l_{11})\theta_{t2}$
\mathbf{U}_{sy11}	$(y_{t3} - y_{a6}) + (S_6/2)(\varphi_{t3} - \varphi_{a6}) + (l_6 + l_{13})\theta_{t3}$
\mathbf{U}_{sy12}	$(y_{t3} - y_{a6}) - (S_6/2)(\varphi_{t3} - \varphi_{a6}) + (l_6 + l_{13})\theta_{t3}$
\mathbf{U}_{sy13}	$(y_{t3} - y_{a7}) + (S_7/2)(\varphi_{t3} - \varphi_{a7}) + l_{13}\theta_{t3}$
\mathbf{U}_{sy14}	$(y_{t3} - y_{a7}) - (S_7/2)(\varphi_{t3} - \varphi_{a7}) + l_{13}\theta_{t3}$
\mathbf{U}_{sy15}	$(y_{t3} - y_{a8}) + (S_8/2)(\varphi_{t3} - \varphi_{a8}) - l_{14}\theta_{t3}$
\mathbf{U}_{sy16}	$(y_{t3} - y_{a8}) - (S_8/2)(\varphi_{t3} - \varphi_{a8}) - l_{14}\theta_{t3}$
\mathbf{U}_{sy17}	$(y_{t3} - y_{a9}) + (S_9/2)(\varphi_{t3} - \varphi_{a9}) - (l_{14} + l_{15})\theta_{t3}$
\mathbf{U}_{sy18}	$(y_{t3} - y_{a9}) - (S_9/2)(\varphi_{t3} - \varphi_{a9}) - (l_{14} + l_{15})\theta_{t3}$

Table 4-19 (Cont.)

Tire springs	
U_{ty1}	$y_{a1} + (d_1/2)\varphi_{a1} + u_{SR1}$
U_{ty2}	$y_{a1} - (d_1/2)\varphi_{a1} + u_{SR2}$
U_{ty3}	$y_{a2} + (d_2/2)\varphi_{a2} + u_{SR3}$
U_{ty4}	$y_{a2} - (d_2/2)\varphi_{a2} + u_{SR4}$
U_{ty5}	$y_{a3} + (d_3/2)\varphi_{a3} + u_{SR5}$
U_{ty6}	$y_{a3} - (d_3/2)\varphi_{a3} + u_{SR6}$
U_{ty7}	$y_{a4} + (d_4/2)\varphi_{a4} + u_{SR7}$
U_{ty8}	$y_{a4} - (d_4/2)\varphi_{a4} + u_{SR8}$
U_{ty9}	$y_{a5} + (d_5/2)\varphi_{a5} + u_{SR9}$
U_{ty10}	$y_{a5} - (d_5/2)\varphi_{a5} + u_{SR10}$
U_{ty11}	$y_{a6} + (d_6/2)\varphi_{a6} + u_{SR11}$
U_{ty12}	$y_{a6} - (d_6/2)\varphi_{a6} + u_{SR12}$
U_{ty13}	$y_{a7} + (d_7/2)\varphi_{a7} + u_{SR13}$
U_{ty14}	$y_{a7} - (d_7/2)\varphi_{a7} + u_{SR14}$
U_{ty15}	$y_{a8} + (d_8/2)\varphi_{a8} + u_{SR15}$
U_{ty16}	$y_{a8} - (d_8/2)\varphi_{a8} + u_{SR16}$
U_{ty17}	$y_{a9} + (d_9/2)\varphi_{a9} + u_{SR17}$
U_{ty18}	$y_{a9} - (d_9/2)\varphi_{a9} + u_{SR18}$

In this table u_{SRi} is the road surface roughness under the i th wheel.

For the LCV's, it is assumed that the second trailer is traveling at the same speed as the truck and it is connected through a horizontal link to the first trailer which assures the same speed for the second trailer but since the horizontal acceleration of the vehicle is assumed to be zero, this constraint cannot be seen in the equations.

F_{syi} , F_{dsyi} , F_{tyi} and F_{dtyi} have been defined in equations (4-1) to (4-4). Similarly Lagrange's equation (4-5) has been used to generate the equations of motion.

Kinetic Energy of the system:

$$\begin{aligned}
 T = & \frac{1}{2}m_{t1}\dot{y}_{t1}^2 + \frac{1}{2}m_{a1}\dot{y}_{a1}^2 + \frac{1}{2}m_{a2}\dot{y}_{a2}^2 + \frac{1}{2}m_{a3}\dot{y}_{a3}^2 + \frac{1}{2}m_{a4}\dot{y}_{a4}^2 + \\
 & \frac{1}{2}m_{a5}\dot{y}_{a5}^2 + \frac{1}{2}m_{a6}\dot{y}_{a6}^2 + \frac{1}{2}m_{a7}\dot{y}_{a7}^2 + \frac{1}{2}m_{a8}\dot{y}_{a8}^2 + \frac{1}{2}m_{a9}\dot{y}_{a9}^2 + \frac{1}{2}I_{xt1}\dot{\phi}_{t1}^2 + \\
 & \frac{1}{2}I_{zt1}\dot{\theta}_{t1}^2 + \frac{1}{2}I_{xt2}\dot{\phi}_{t2}^2 + \frac{1}{2}I_{zt2}\dot{\theta}_{t2}^2 + \frac{1}{2}I_{xt3}\dot{\phi}_{t3}^2 + \frac{1}{2}I_{zt3}\dot{\theta}_{t3}^2 + \frac{1}{2}I_{xa1}\dot{\phi}_{a1}^2 + \quad (4-186) \\
 & \frac{1}{2}I_{xa2}\dot{\phi}_{a2}^2 + \frac{1}{2}I_{xa3}\dot{\phi}_{a3}^2 + \frac{1}{2}I_{xa4}\dot{\phi}_{a4}^2 + \frac{1}{2}I_{xa5}\dot{\phi}_{a5}^2 + \frac{1}{2}I_{xa6}\dot{\phi}_{a6}^2 + \\
 & \frac{1}{2}I_{xa7}\dot{\phi}_{a7}^2 + \frac{1}{2}I_{xa8}\dot{\phi}_{a8}^2 + \frac{1}{2}I_{xa9}\dot{\phi}_{a9}^2 + \frac{1}{2}m_{t2}\dot{y}_{t2}^2 + \frac{1}{2}m_{t3}\dot{y}_{t3}^2
 \end{aligned}$$

Potential Energy of the system:

$$\begin{aligned}
V = & \frac{1}{2}K_{sy1}U_{sy1}^2 + \frac{1}{2}K_{sy2}U_{sy2}^2 + \frac{1}{2}K_{sy3}U_{sy3}^2 + \frac{1}{2}K_{sy4}U_{sy4}^2 + \\
& \frac{1}{2}K_{sy5}U_{sy5}^2 + \frac{1}{2}K_{sy6}U_{sy6}^2 + \frac{1}{2}K_{sy7}U_{sy7}^2 + \frac{1}{2}K_{sy8}U_{sy8}^2 + \frac{1}{2}K_{sy9}U_{sy9}^2 + \\
& \frac{1}{2}K_{sy10}U_{sy10}^2 + \frac{1}{2}K_{sy11}U_{sy11}^2 + \frac{1}{2}K_{sy12}U_{sy12}^2 + \frac{1}{2}K_{sy13}U_{sy13}^2 + \\
& \frac{1}{2}K_{sy14}U_{sy14}^2 + \frac{1}{2}K_{sy15}U_{sy15}^2 + \frac{1}{2}K_{sy16}U_{sy16}^2 + \frac{1}{2}K_{sy17}U_{sy17}^2 + \\
& \frac{1}{2}K_{sy18}U_{sy18}^2 + \frac{1}{2}K_{ty1}U_{ty1}^2 + \frac{1}{2}K_{ty2}U_{ty2}^2 + \frac{1}{2}K_{ty3}U_{ty3}^2 + \frac{1}{2}K_{ty4}U_{ty4}^2 + \\
& \frac{1}{2}K_{ty5}U_{ty5}^2 + \frac{1}{2}K_{ty6}U_{ty6}^2 + \frac{1}{2}K_{ty7}U_{ty7}^2 + \frac{1}{2}K_{ty8}U_{ty8}^2 + \frac{1}{2}K_{ty9}U_{ty9}^2 + \\
& \frac{1}{2}K_{ty10}U_{ty10}^2 + \frac{1}{2}K_{ty11}U_{ty11}^2 + \frac{1}{2}K_{ty12}U_{ty12}^2 + \frac{1}{2}K_{ty13}U_{ty13}^2 + \\
& \frac{1}{2}K_{ty14}U_{ty14}^2 + \frac{1}{2}K_{ty15}U_{ty15}^2 + \frac{1}{2}K_{ty16}U_{ty16}^2 + \frac{1}{2}K_{ty17}U_{ty17}^2 + \\
& \frac{1}{2}K_{ty18}U_{ty18}^2 - ((m_{t1}g)y_{t1} + (m_{t2}g)y_{t2} + (m_{t3}g)y_{t3} + (m_{a1}g)y_{a1} + \\
& (m_{a2}g)y_{a2} + (m_{a3}g)y_{a3} + (m_{a4}g)y_{a4} + (m_{a5}g)y_{a5} + (m_{a6}g)y_{a6} + \\
& (m_{a7}g)y_{a7} + (m_{a8}g)y_{a8} + (m_{a9}g)y_{a9}) + (F_{y1}U_{sy1} + F_{y2}U_{sy2} + F_{y3}U_{sy3} + \\
& F_{y4}U_{sy4} + F_{y5}U_{sy5} + F_{y6}U_{sy6} + F_{y7}U_{sy7} + F_{y8}U_{sy8} + F_{y9}U_{sy9} + \\
& F_{y10}U_{sy10} + F_{y11}U_{sy11} + F_{y12}U_{sy12} + F_{y13}U_{sy13} + F_{y14}U_{sy14} + \\
& F_{y15}U_{sy15} + F_{y16}U_{sy16} + F_{y17}U_{sy17} + F_{y18}U_{sy18})
\end{aligned} \tag{4-187}$$

Damping Energy of the system:

$$\begin{aligned}
D = & \frac{1}{2} D_{sy1} \dot{U}_{sy1}^2 + \frac{1}{2} D_{sy2} \dot{U}_{sy2}^2 + \frac{1}{2} D_{sy3} \dot{U}_{sy3}^2 + \frac{1}{2} D_{sy4} \dot{U}_{sy4}^2 + \\
& \frac{1}{2} D_{sy5} \dot{U}_{sy5}^2 + \frac{1}{2} D_{sy6} \dot{U}_{sy6}^2 + \frac{1}{2} D_{sy7} \dot{U}_{sy7}^2 + \frac{1}{2} D_{sy8} \dot{U}_{sy8}^2 + \frac{1}{2} D_{sy9} \dot{U}_{sy9}^2 + \\
& \frac{1}{2} D_{sy10} \dot{U}_{sy10}^2 + \frac{1}{2} D_{sy11} \dot{U}_{sy11}^2 + \frac{1}{2} D_{sy12} \dot{U}_{sy12}^2 + \frac{1}{2} D_{sy13} \dot{U}_{sy13}^2 + \\
& \frac{1}{2} D_{sy14} \dot{U}_{sy14}^2 + \frac{1}{2} D_{sy15} \dot{U}_{sy15}^2 + \frac{1}{2} D_{sy16} \dot{U}_{sy16}^2 + \frac{1}{2} D_{sy17} \dot{U}_{sy17}^2 + \\
& \frac{1}{2} D_{sy18} \dot{U}_{sy18}^2 + \frac{1}{2} D_{ty1} \dot{U}_{ty1}^2 + \frac{1}{2} D_{ty2} \dot{U}_{ty2}^2 + \frac{1}{2} D_{ty3} \dot{U}_{ty3}^2 + \frac{1}{2} D_{ty4} \dot{U}_{ty4}^2 + \quad (4-188) \\
& \frac{1}{2} D_{ty5} \dot{U}_{ty5}^2 + \frac{1}{2} D_{ty6} \dot{U}_{ty6}^2 + \frac{1}{2} D_{ty7} \dot{U}_{ty7}^2 + \frac{1}{2} D_{ty8} \dot{U}_{ty8}^2 + \frac{1}{2} D_{ty9} \dot{U}_{ty9}^2 + \\
& \frac{1}{2} D_{ty10} \dot{U}_{ty10}^2 + \frac{1}{2} D_{ty11} \dot{U}_{ty11}^2 + \frac{1}{2} D_{ty12} \dot{U}_{ty12}^2 + \frac{1}{2} D_{ty13} \dot{U}_{ty13}^2 + \\
& \frac{1}{2} D_{ty14} \dot{U}_{ty14}^2 + \frac{1}{2} D_{ty15} \dot{U}_{ty15}^2 + \frac{1}{2} D_{ty16} \dot{U}_{ty16}^2 + \frac{1}{2} D_{ty17} \dot{U}_{ty17}^2 + \\
& \frac{1}{2} D_{ty18} \dot{U}_{ty18}^2
\end{aligned}$$

The displacement at the pivot point should stay the same, whether it is calculated from the trailer part or the tractor part,

$$y_{t2} + \theta_{t2} l_{10} = y_{t1} - \theta_{t1} l_9 \quad (4-189)$$

Thus, by substituting θ_{t2} from equation (4-189) in equation (4-186),

$$\begin{aligned}
 T = & \frac{1}{2}m_{t1}\dot{y}_{t1}^2 + \frac{1}{2}m_{a1}\dot{y}_{a1}^2 + \frac{1}{2}m_{a2}\dot{y}_{a2}^2 + \frac{1}{2}m_{a3}\dot{y}_{a3}^2 + \frac{1}{2}m_{a4}\dot{y}_{a4}^2 + \\
 & \frac{1}{2}m_{a5}\dot{y}_{a5}^2 + \frac{1}{2}m_{a6}\dot{y}_{a6}^2 + \frac{1}{2}m_{a7}\dot{y}_{a7}^2 + \frac{1}{2}m_{a8}\dot{y}_{a8}^2 + \frac{1}{2}m_{a9}\dot{y}_{a9}^2 + \frac{1}{2}I_{xt1}\dot{\phi}_{t1}^2 + \\
 & \frac{1}{2}I_{zt1}\dot{\theta}_{t1}^2 + \frac{1}{2}I_{xt2}\dot{\phi}_{t2}^2 + \frac{1}{2}I_{zt2}\left(\frac{\dot{y}_{t1}-\dot{y}_{t2}-\dot{\theta}_{t1}l_9}{l_{10}}\right)^2 + \frac{1}{2}I_{xt3}\dot{\phi}_{t3}^2 + \frac{1}{2}I_{zt3}\dot{\theta}_{t3}^2 + \quad (4-190) \\
 & \frac{1}{2}I_{xa1}\dot{\phi}_{a1}^2 + \frac{1}{2}I_{xa2}\dot{\phi}_{a2}^2 + \frac{1}{2}I_{xa3}\dot{\phi}_{a3}^2 + \frac{1}{2}I_{xa4}\dot{\phi}_{a4}^2 + \frac{1}{2}I_{xa5}\dot{\phi}_{a5}^2 + \\
 & \frac{1}{2}I_{xa6}\dot{\phi}_{a6}^2 + \frac{1}{2}I_{xa7}\dot{\phi}_{a7}^2 + \frac{1}{2}I_{xa8}\dot{\phi}_{a8}^2 + \frac{1}{2}I_{xa9}\dot{\phi}_{a9}^2 + \frac{1}{2}m_{t2}\dot{y}_{t2}^2 + \frac{1}{2}m_{t3}\dot{y}_{t3}^2
 \end{aligned}$$

Same substitution will be applied to the equations (4-187) and (4-188). Now the Lagrange's equation is applied to y_{t2} :

$$\begin{aligned}
 & \left[m_{t2}\ddot{y}_{t2} - \frac{I_{zt2}}{l_{10}^2}(\dot{y}_{t1} - \dot{y}_{t2} - \dot{\theta}_{t1}l_9)\right] + \left[\left(1 + \frac{l_{11}}{l_{10}}\right)(F_{sy7} + F_{sy8}) + \right. \\
 & \left.\left(1 + \frac{l_4+l_{11}}{l_{10}}\right)(F_{sy9} + F_{sy10}) - (m_{t2}g)\right] + \left[\left(1 + \frac{l_{11}}{l_{10}}\right)(F_{dsy7} + F_{dsy8}) + \right. \\
 & \left.\left(1 + \frac{l_4+l_{11}}{l_{10}}\right)(F_{dsy9} + F_{dsy10})\right] = 0 \quad (4-191)
 \end{aligned}$$

To simplify the equation some variables are defined as follows:

$$S_{a2} = \frac{I_{zt2}}{l_{10}^2}$$

$$S_{c2} = \frac{I_{zt2}}{l_{10}^2} + m_{t2}$$

$$S_{a3} = \frac{I_{zt2}}{l_{10}^2}l_9$$

$$\begin{aligned}
 B_{t4} = & m_{t2}g - \left(1 + \frac{l_{11}}{l_{10}}\right)(F_{sy7} + F_{sy8} + F_{dsy7} + F_{dsy8}) - \left(1 + \frac{l_4+l_{11}}{l_{10}}\right)(F_{sy9} + F_{sy10} + \\
 & F_{dsy9} + F_{dsy10})
 \end{aligned}$$

Therefore equation (4-191) will be simplified to:

$$-S_{a2}\ddot{y}_{t1} + S_{c2}\ddot{y}_{t2} + S_{a3}\ddot{\theta}_{t1} = B_{t4} \quad (4-192)$$

By applying the Lagrange's equation to y_{t1} :

$$\begin{aligned} & \left[m_{t1} \ddot{y}_{t1} + \frac{I_{zt2}}{l_{10}^2} (\ddot{y}_{t1} - \ddot{y}_{t2} - \ddot{\theta}_{t1} l_9) \right] + \left[(F_{sy1} + F_{sy2} + F_{sy3} + F_{sy4} + F_{sy5} + \right. \\ & \left. F_{sy6}) - \frac{l_{11}}{l_{10}} (F_{sy7} + F_{sy8}) - \frac{l_4 + l_{11}}{l_{10}} (F_{sy9} + F_{sy10}) - (m_{t1}g) \right] + \left[(F_{dsy1} + \right. \\ & \left. F_{dsy2} + F_{dsy3} + F_{dsy4} + F_{dsy5} + F_{dsy6}) - \frac{l_{11}}{l_{10}} (F_{dsy7} + F_{dsy8}) - \right. \\ & \left. \frac{l_4 + l_{11}}{l_{10}} (F_{dsy9} + F_{dsy10}) \right] = 0 \end{aligned} \quad (4-193)$$

Again to simplify the equation some variables are defined as follows:

$$S_{a1} = \frac{I_{zt2}}{l_{10}^2} + m_{t1}$$

$$\begin{aligned} B_{t1} = m_{t1}g - & \left[(F_{sy1} + F_{sy2} + F_{sy3} + F_{sy4} + F_{sy5} + F_{sy6}) - \frac{l_{11}}{l_{10}} (F_{sy7} + F_{sy8}) - \right. \\ & \left. \frac{l_4 + l_{11}}{l_{10}} (F_{sy9} + F_{sy10}) + (F_{dsy1} + F_{dsy2} + F_{dsy3} + F_{dsy4} + F_{dsy5} + F_{dsy6}) - \frac{l_{11}}{l_{10}} (F_{dsy7} + \right. \\ & \left. F_{dsy8}) - \frac{l_4 + l_{11}}{l_{10}} (F_{dsy9} + F_{dsy10}) \right] \end{aligned}$$

Therefore equation (2-193) will be simplified to:

$$S_{a1}\ddot{y}_{t1} - S_{a2}\ddot{y}_{t2} - S_{a3}\ddot{\theta}_{t1} = B_{t1} \quad (4-194)$$

Also, by applying the Lagrange's equation to θ_{t1} :

$$\begin{aligned} & \left[I_{zt1} \ddot{\theta}_{t1} - \frac{I_{zt2} l_9}{l_{10}^2} (\ddot{y}_{t1} - \ddot{y}_{t2} - \ddot{\theta}_{t1} l_9) \right] + \left[l_7 (F_{sy1} + F_{sy2}) - l_8 (F_{sy3} + F_{sy4}) - \right. \\ & \left. (l_2 + l_8) (F_{sy5} + F_{sy6}) + \frac{l_9 l_{11}}{l_{10}} (F_{sy7} + F_{sy8}) + \frac{l_9 (l_4 + l_{11})}{l_{10}} (F_{sy9} + F_{sy10}) \right] + \\ & \left[l_7 (F_{dsy1} + F_{dsy2}) - l_8 (F_{dsy3} + F_{dsy4}) - (l_2 + l_8) (F_{dsy5} + F_{dsy6}) + \right. \\ & \left. \frac{l_9 l_{11}}{l_{10}} (F_{dsy7} + F_{dsy8}) + \frac{l_9 (l_4 + l_{11})}{l_{10}} (F_{dsy9} + F_{dsy10}) \right] = 0 \end{aligned} \quad (4-195)$$

Once again to simplify the equation some variables need to be defined as follows:

$$S_{b3} = I_{zt1} + \frac{I_{zt2}l_9}{l_{10}^2}$$

$$B_{t3} = - \left[l_7(F_{sy1} + F_{sy2}) - l_8(F_{sy3} + F_{sy4}) - (l_2 + l_8)(F_{sy5} + F_{sy6}) + \frac{l_9 l_{11}}{l_{10}}(F_{sy7} + F_{sy8}) + \frac{l_9(l_4 + l_{11})}{l_{10}}(F_{sy9} + F_{sy10}) \right] + \left[l_7(F_{dsy1} + F_{dsy2}) - l_8(F_{dsy3} + F_{dsy4}) - (l_2 + l_8)(F_{dsy5} + F_{dsy6}) + \frac{l_9 l_{11}}{l_{10}}(F_{dsy7} + F_{dsy8}) + \frac{l_9(l_4 + l_{11})}{l_{10}}(F_{dsy9} + F_{dsy10}) \right]$$

Therefore equation (4-195) will be simplified to:

$$-S_{a3}\ddot{y}_{t1} + S_{a3}\ddot{y}_{t2} + S_{b3}\ddot{\theta}_{t1} = B_{t3} \quad (4-196)$$

By adding equations (4-192) and (4-194),

$$(S_{a1} - S_{a2})\ddot{y}_{t1} - (S_{a2} - S_{c2})\ddot{y}_{t2} = B_{t1} + B_{t4} \quad (4-197)$$

Also by multiplying S_{b3} and S_{a3} to equations (2-194) and (2-196), respectively,

$$(S_{a1}S_{b3} - S_{a3}^2)\ddot{y}_{t1} - (S_{a2}S_{b3} - S_{a3}^2)\ddot{y}_{t2} = S_{b3}B_{t1} + S_{a3}B_{t3} \quad (4-198)$$

By defining the following expressions, equations (4-197) and (4-198) are simplified to equations (4-199) and (4-200), respectively,

$$e_1 = S_{a1} - S_{a2}$$

$$e_2 = S_{a2} - S_{c2}$$

$$e_3 = S_{a1}S_{b3} - S_{a3}^2$$

$$e_4 = S_{a2}S_{b3} - S_{a3}^2$$

$$e_1\ddot{y}_{t1} - e_2\ddot{y}_{t2} = B_{t1} + B_{t4} \quad (4-199)$$

$$e_3\ddot{y}_{t1} - e_4\ddot{y}_{t2} = S_{b3}B_{t1} + S_{a3}B_{t3} \quad (4-200)$$

Solving equations (4-199) and (4-200) for \ddot{y}_{t1} and \ddot{y}_{t2} will lead to:

$$\ddot{y}_{t1} = \frac{e_4(B_{t1} + B_{t4}) - e_2(S_{b3}B_{t1} + S_{a3}B_{t3})}{e_1e_4 - e_2e_3} \quad (4-201)$$

$$\ddot{y}_{t2} = \frac{e_1}{e_2} \left(\frac{e_4(B_{t1} + B_{t4}) - e_2(S_{b3}B_{t1} + S_{a3}B_{t3})}{e_1e_4 - e_2e_3} \right) - \frac{B_{t1} + B_{t4}}{e_2} \quad (4-202)$$

Substituting equations (4-201) and (4-202) into equation (4-196) will give,

$$\begin{aligned} \ddot{\theta}_{t1} = & \\ & \frac{B_{t3}}{S_{b3}} + \frac{S_{a3}}{S_{b3}} \left(\frac{e_4(B_{t1} + B_{t4}) - e_2(S_{b3}B_{t1} + S_{a3}B_{t3})}{e_1e_4 - e_2e_3} \right) \\ & - \frac{S_{a3}}{S_{b3}} \left(\frac{e_1}{e_2} \left(\frac{e_4(B_{t1} + B_{t4}) - e_2(S_{b3}B_{t1} + S_{a3}B_{t3})}{e_1e_4 - e_2e_3} \right) \right. \\ & \left. - \frac{B_{t1} + B_{t4}}{e_2} \right) \end{aligned} \quad (4-203)$$

By applying the Lagrange's equation to $\varphi_{t1}, \varphi_{t2}, \varphi_{t3}, y_{t3}, \theta_{t3}$:

$$I_{xt1}\ddot{\varphi}_{t1} + \left[\left(\frac{s_1}{2}\right)(F_{sy1} - F_{sy2}) + \left(\frac{s_2}{2}\right)(F_{sy3} - F_{sy4}) + \left(\frac{s_3}{2}\right)(F_{sy5} - F_{sy6}) \right] + \quad (4-204)$$

$$\left[\left(\frac{s_1}{2}\right)(F_{dsy1} - F_{dsy2}) + \left(\frac{s_2}{2}\right)(F_{dsy3} - F_{dsy4}) + \left(\frac{s_3}{2}\right)(F_{dsy5} - F_{dsy6}) \right] = 0$$

$$I_{xt2}\ddot{\varphi}_{t2} + \left[\left(\frac{s_4}{2}\right)(F_{sy7} - F_{sy8}) + \left(\frac{s_5}{2}\right)(F_{sy9} - F_{sy10}) \right] + \left[\left(\frac{s_4}{2}\right)(F_{dsy7} - \right. \quad (4-205)$$

$$\left. F_{dsy8} \right) + \left(\frac{s_5}{2}\right)(F_{dsy9} - F_{dsy10}) \right] = 0$$

$$I_{xt3}\ddot{\varphi}_{t3} + \left[\left(\frac{s_6}{2}\right)(F_{sy11} - F_{sy12}) + \left(\frac{s_7}{2}\right)(F_{sy13} - F_{sy14}) + \left(\frac{s_8}{2}\right)(F_{sy15} - \quad (4-206)$$

$$F_{sy16}) + \left(\frac{s_9}{2}\right)(F_{sy17} - F_{sy18}) \right] + \left[\left(\frac{s_6}{2}\right)(F_{dsy11} - F_{dsy12}) + \left(\frac{s_7}{2}\right)(F_{dsy13} - \right.$$

$$\left. F_{dsy14}) + \left(\frac{s_8}{2}\right)(F_{dsy15} - F_{dsy16}) + \left(\frac{s_9}{2}\right)(F_{dsy17} - F_{dsy18}) \right] = 0$$

$$m_{t3}\ddot{y}_{t3} + (F_{sy11} + F_{sy12} + F_{sy13} + F_{sy14} + F_{sy15} + F_{sy16} + F_{sy17} + F_{sy18}) + \quad (4-207)$$

$$(F_{dsy11} + F_{dsy12} + F_{dsy13} + F_{dsy14} + F_{dsy15} + F_{dsy16} + F_{dsy17} + F_{dsy18}) =$$

$$m_{t3}g$$

$$\begin{aligned}
I_{zt3} \ddot{\theta}_{t3} + & [(l_6 + l_{13})(F_{sy11} + F_{sy12}) + l_{13}(F_{sy13} + F_{sy14}) - l_{14}(F_{sy15} + \\
& F_{sy16}) - (l_{14} + l_{15})(F_{sy17} + F_{sy18})] + [(l_6 + l_{13})(F_{dsy11} + F_{dsy12}) + \\
& l_{13}(F_{dsy13} + F_{dsy14}) - l_{14}(F_{dsy15} + F_{dsy16}) - (l_{14} + l_{15})(F_{dsy17} + \\
& F_{dsy18})] = 0
\end{aligned} \tag{4-208}$$

The rest of degrees of freedom will be as follows:

$$\begin{aligned}
m_{a1}\ddot{y}_{a1} - (F_{sy1} + F_{sy2}) + (F_{ty1} + F_{ty2}) - (F_{dsy1} + F_{dsy2}) + (F_{dty1} + F_{dty2}) = \\
m_{a1}g
\end{aligned} \tag{4-209}$$

$$\begin{aligned}
I_{xa1}\ddot{\phi}_{a1} - (\frac{s_1}{2})(F_{sy1} - F_{sy2}) + (\frac{d_1}{2})(F_{ty1} - F_{ty2}) - (\frac{s_1}{2})(F_{dsy1} - F_{dsy2}) + \\
(\frac{d_1}{2})(F_{dty1} - F_{dty2}) = 0
\end{aligned} \tag{4-210}$$

$$\begin{aligned}
m_{a2}\ddot{y}_{a2} - (F_{sy3} + F_{sy4}) + (F_{ty3} + F_{ty4}) - (F_{dsy3} + F_{dsy4}) + (F_{dty3} + F_{dty4}) = \\
m_{a2}g
\end{aligned} \tag{4-211}$$

$$\begin{aligned}
I_{xa2}\ddot{\phi}_{a2} - (\frac{s_2}{2})(F_{sy3} - F_{sy4}) + (\frac{d_2}{2})(F_{ty3} - F_{ty4}) - (\frac{s_2}{2})(F_{dsy3} - F_{dsy4}) + \\
(\frac{d_2}{2})(F_{dty3} - F_{dty4}) = 0
\end{aligned} \tag{4-212}$$

$$\begin{aligned}
m_{a3}\ddot{y}_{a3} - (F_{sy5} + F_{sy6}) + (F_{ty5} + F_{ty6}) - (F_{dsy5} + F_{dsy6}) + (F_{dty5} + F_{dty6}) = \\
m_{a3}g
\end{aligned} \tag{4-213}$$

$$\begin{aligned}
I_{xa3}\ddot{\phi}_{a3} - (\frac{s_3}{2})(F_{sy5} - F_{sy6}) + (\frac{d_3}{2})(F_{ty5} - F_{ty6}) - (\frac{s_3}{2})(F_{dsy5} - F_{dsy6}) + \\
(\frac{d_3}{2})(F_{dty5} - F_{dty6}) = 0
\end{aligned} \tag{4-214}$$

$$\begin{aligned}
m_{a4}\ddot{y}_{a4} - (F_{sy7} + F_{sy8}) + (F_{ty7} + F_{ty8}) - (F_{dsy7} + F_{dsy8}) + (F_{dty7} + F_{dty8}) = \\
m_{a4}g
\end{aligned} \tag{4-215}$$

$$I_{xa4}\ddot{\phi}_{a4} - \left(\frac{s_4}{2}\right)(F_{sy7} - F_{sy8}) + \left(\frac{d_4}{2}\right)(F_{ty7} - F_{ty8}) - \left(\frac{s_4}{2}\right)(F_{dsy7} - F_{dsy8}) + \left(\frac{d_4}{2}\right)(F_{dty7} - F_{dty8}) = 0 \quad (4-216)$$

$$m_{a5}\ddot{y}_{a5} - (F_{sy9} + F_{sy10}) + (F_{ty9} + F_{ty10}) - (F_{dsy9} + F_{dsy10}) + (F_{dty9} + F_{dty10}) = m_{a5}g \quad (4-217)$$

$$I_{xa5}\ddot{\phi}_{a5} - \left(\frac{s_5}{2}\right)(F_{sy9} - F_{sy10}) + \left(\frac{d_5}{2}\right)(F_{ty9} - F_{ty10}) - \left(\frac{s_5}{2}\right)(F_{dsy9} - F_{dsy10}) + \left(\frac{d_5}{2}\right)(F_{dty9} - F_{dty10}) = 0 \quad (4-218)$$

$$m_{a6}\ddot{y}_{a6} - (F_{sy11} + F_{sy12}) + (F_{ty11} + F_{ty12}) - (F_{dsy11} + F_{dsy12}) + (F_{dty11} + F_{dty12}) = m_{a6}g \quad (4-219)$$

$$I_{xa6}\ddot{\phi}_{a6} - \left(\frac{s_6}{2}\right)(F_{sy11} - F_{sy12}) + \left(\frac{d_6}{2}\right)(F_{ty11} - F_{ty12}) - \left(\frac{s_6}{2}\right)(F_{dsy11} - F_{dsy12}) + \left(\frac{d_6}{2}\right)(F_{dty11} - F_{dty12}) = 0 \quad (4-220)$$

$$m_{a7}\ddot{y}_{a7} - (F_{sy13} + F_{sy14}) + (F_{ty13} + F_{ty14}) - (F_{dsy13} + F_{dsy14}) + (F_{dty13} + F_{dty14}) = m_{a7}g \quad (4-221)$$

$$I_{xa7}\ddot{\phi}_{a7} - \left(\frac{s_7}{2}\right)(F_{sy13} - F_{sy14}) + \left(\frac{d_7}{2}\right)(F_{ty13} - F_{ty14}) - \left(\frac{s_7}{2}\right)(F_{dsy13} - F_{dsy14}) + \left(\frac{d_7}{2}\right)(F_{dty13} - F_{dty14}) = 0 \quad (4-222)$$

$$m_{a8}\ddot{y}_{a8} - (F_{sy15} + F_{sy16}) + (F_{ty15} + F_{ty16}) - (F_{dsy15} + F_{dsy16}) + (F_{dty15} + F_{dty16}) = m_{a8}g \quad (4-223)$$

$$I_{xa8}\ddot{\phi}_{a8} - \left(\frac{s_8}{2}\right)(F_{sy15} - F_{sy16}) + \left(\frac{d_8}{2}\right)(F_{ty15} - F_{ty16}) - \left(\frac{s_8}{2}\right)(F_{dsy15} - F_{dsy16}) + \left(\frac{d_8}{2}\right)(F_{dty15} - F_{dty16}) = 0 \quad (4-224)$$

$$m_{a9}\ddot{y}_{a9} - (F_{sy17} + F_{sy18}) + (F_{ty17} + F_{ty18}) - (F_{dsy17} + F_{dsy18}) + (F_{dty17} + F_{dty18}) = m_{a9}g \quad (4-225)$$

$$\begin{aligned}
I_{xa9}\ddot{\phi}_{a9} - \left(\frac{s_9}{2}\right)(F_{sy17} - F_{sy18}) + \left(\frac{d_9}{2}\right)(F_{ty17} - F_{ty18}) - \left(\frac{s_9}{2}\right)(F_{dsy17} - F_{dsy18}) + \\
\left(\frac{d_9}{2}\right)(F_{dty17} - F_{dty18}) = 0
\end{aligned} \tag{4-226}$$

Twenty seven equations of motion were developed here to capture the real behavior of the 9-Axle Turnpike Double.

4.12 Derivation of Equations of Motion for “7-Axle Rocky Mountain Double”

There are twenty three degrees of freedom in total for this type of truck. The degrees of freedom can be seen in Figure 2-11 and the description of those degrees of freedom can be found in Table 2-20. Relative Displacements at the locations of the springs are also calculated using the values given in Table 2-21.

Kinetic Energy of the system:

$$\begin{aligned}
T = & \frac{1}{2}m_{t1}\dot{y}_{t1}^2 + \frac{1}{2}m_{a1}\dot{y}_{a1}^2 + \frac{1}{2}m_{a2}\dot{y}_{a2}^2 + \frac{1}{2}m_{a3}\dot{y}_{a3}^2 + \frac{1}{2}m_{a4}\dot{y}_{a4}^2 + \\
& \frac{1}{2}m_{a5}\dot{y}_{a5}^2 + \frac{1}{2}m_{a6}\dot{y}_{a6}^2 + \frac{1}{2}m_{a7}\dot{y}_{a7}^2 + \frac{1}{2}I_{xt1}\dot{\phi}_{t1}^2 + \frac{1}{2}I_{zt1}\dot{\theta}_{t1}^2 + \frac{1}{2}I_{xt2}\dot{\phi}_{t2}^2 + \\
& \frac{1}{2}I_{zt2}\dot{\theta}_{t2}^2 + \frac{1}{2}I_{xt3}\dot{\phi}_{t3}^2 + \frac{1}{2}I_{zt3}\dot{\theta}_{t3}^2 + \frac{1}{2}I_{xa1}\dot{\phi}_{a1}^2 + \frac{1}{2}I_{xa2}\dot{\phi}_{a2}^2 + \frac{1}{2}I_{xa3}\dot{\phi}_{a3}^2 + \\
& \frac{1}{2}I_{xa4}\dot{\phi}_{a4}^2 + \frac{1}{2}I_{xa5}\dot{\phi}_{a5}^2 + \frac{1}{2}I_{xa6}\dot{\phi}_{a6}^2 + \frac{1}{2}I_{xa7}\dot{\phi}_{a7}^2 + \frac{1}{2}m_{t2}\dot{y}_{t2}^2 + \frac{1}{2}m_{t3}\dot{y}_{t3}^2
\end{aligned} \tag{4-227}$$

TABLE 4-20: DEGREES OF FREEDOM OF 7-AXLE ROCKY MOUNTAIN DOUBLE

No.	Degree of Freedom	Contrib. Mass	Description
1	y_{t1}	m_{t1}	Tractor vertical displacement and mass
2	φ_{t1}	I_{xt1}	Tractor roll displacement and mass moment of inertia
3	θ_{t1}	I_{zt1}	Tractor pitch displacement and mass moment of inertia
4	y_{t2}	m_{t2}	Semi-trailer vertical displacement and mass
5	φ_{t2}	I_{xt2}	Semi-trailer roll displacement and mass moment of inertia
6	θ_{t2}	I_{zt2}	Semi-trailer pitch displacement and mass moment of inertia
7	y_{t3}	m_{t3}	Trailer vertical displacement and mass
8	φ_{t3}	I_{xt3}	Trailer roll displacement and mass moment of inertia
9	θ_{t3}	I_{zt3}	Trailer pitch displacement and mass moment of inertia
10	y_{a1}	m_{a1}	Steer axle vertical displacement and mass
11	φ_{a1}	I_{xa1}	Steer axle roll displacement and mass moment of inertia
12	y_{a2}	m_{a2}	Vertical displacement and mass of forward axle of tractor tandem
13	φ_{a2}	I_{xa2}	Roll displacement and mass moment of inertia of forward axle of tractor tandem
14	y_{a3}	m_{a3}	Vertical displacement and mass of aft axle of tractor tandem
15	φ_{a3}	I_{xa3}	Roll displacement and mass moment of inertia of aft axle of tractor tandem
16	y_{a4}	m_{a4}	Vertical displacement and mass of first axle of first trailer
17	φ_{a4}	I_{xa4}	Roll displacement and mass moment of inertia of first axle of first trailer
18	y_{a5}	m_{a5}	Vertical displacement and mass of second axle of first trailer
19	φ_{a5}	I_{xa5}	Roll displacement and mass moment of inertia of second axle of first trailer
20	y_{a6}	m_{a6}	Vertical displacement and mass of first axle of second trailer
21	φ_{a6}	I_{xa6}	Roll displacement and mass moment of inertia of first axle of second trailer
22	y_{a7}	m_{a7}	Vertical displacement and mass of second axle of second trailer
23	φ_{a7}	I_{xa7}	Roll displacement and mass moment of inertia of second axle of second trailer

TABLE 4-21: RELATIVE DISPLACEMENTS AT SPRING LOCATIONS OF 7-AXLE ROCKY MOUNTAIN DOUBLE

Suspension springs	
U_{sy1}	$(y_{t1} - y_{a1}) + (S_1/2)(\varphi_{t1} - \varphi_{a1}) + l_7\theta_{t1}$
U_{sy2}	$(y_{t1} - y_{a1}) - (S_1/2)(\varphi_{t1} - \varphi_{a1}) + l_7\theta_{t1}$
U_{sy3}	$(y_{t1} - y_{a2}) + (S_2/2)(\varphi_{t1} - \varphi_{a2}) - l_8\theta_{t1}$
U_{sy4}	$(y_{t1} - y_{a2}) - (S_2/2)(\varphi_{t1} - \varphi_{a2}) - l_8\theta_{t1}$
U_{sy5}	$(y_{t1} - y_{a3}) + (S_3/2)(\varphi_{t1} - \varphi_{a3}) - (l_2 + l_8)\theta_{t1}$
U_{sy6}	$(y_{t1} - y_{a3}) - (S_3/2)(\varphi_{t1} - \varphi_{a3}) - (l_2 + l_8)\theta_{t1}$
U_{sy7}	$(y_{t2} - y_{a4}) + (S_4/2)(\varphi_{t2} - \varphi_{a4}) - l_{11}\theta_{t2}$
U_{sy8}	$(y_{t2} - y_{a4}) - (S_4/2)(\varphi_{t2} - \varphi_{a4}) - l_{11}\theta_{t2}$
U_{sy9}	$(y_{t2} - y_{a5}) + (S_5/2)(\varphi_{t2} - \varphi_{a5}) - (l_4 + l_{11})\theta_{t2}$
U_{sy10}	$(y_{t2} - y_{a5}) - (S_5/2)(\varphi_{t2} - \varphi_{a5}) - (l_4 + l_{11})\theta_{t2}$
U_{sy11}	$(y_{t3} - y_{a6}) + (S_6/2)(\varphi_{t3} - \varphi_{a6}) + l_{12}\theta_{t3}$
U_{sy12}	$(y_{t3} - y_{a6}) - (S_6/2)(\varphi_{t3} - \varphi_{a6}) + l_{12}\theta_{t3}$
U_{sy13}	$(y_{t3} - y_{a7}) + (S_7/2)(\varphi_{t3} - \varphi_{a7}) - l_{13}\theta_{t3}$
U_{sy14}	$(y_{t3} - y_{a7}) - (S_7/2)(\varphi_{t3} - \varphi_{a7}) - l_{13}\theta_{t3}$

Table 4-21 (Cont.)

Tire springs	
U_{ty1}	$y_{a1} + (d_1/2)\varphi_{a1} + u_{SR1}$
U_{ty2}	$y_{a1} - (d_1/2)\varphi_{a1} + u_{SR2}$
U_{ty3}	$y_{a2} + (d_2/2)\varphi_{a2} + u_{SR3}$
U_{ty4}	$y_{a2} - (d_2/2)\varphi_{a2} + u_{SR4}$
U_{ty5}	$y_{a3} + (d_3/2)\varphi_{a3} + u_{SR5}$
U_{ty6}	$y_{a3} - (d_3/2)\varphi_{a3} + u_{SR6}$
U_{ty7}	$y_{a4} + (d_4/2)\varphi_{a4} + u_{SR7}$
U_{ty8}	$y_{a4} - (d_4/2)\varphi_{a4} + u_{SR8}$
U_{ty9}	$y_{a5} + (d_5/2)\varphi_{a5} + u_{SR9}$
U_{ty10}	$y_{a5} - (d_5/2)\varphi_{a5} + u_{SR10}$
U_{ty11}	$y_{a6} + (d_6/2)\varphi_{a6} + u_{SR11}$
U_{ty12}	$y_{a6} - (d_6/2)\varphi_{a6} + u_{SR12}$
U_{ty13}	$y_{a7} + (d_7/2)\varphi_{a7} + u_{SR13}$
U_{ty14}	$y_{a7} - (d_7/2)\varphi_{a7} + u_{SR14}$

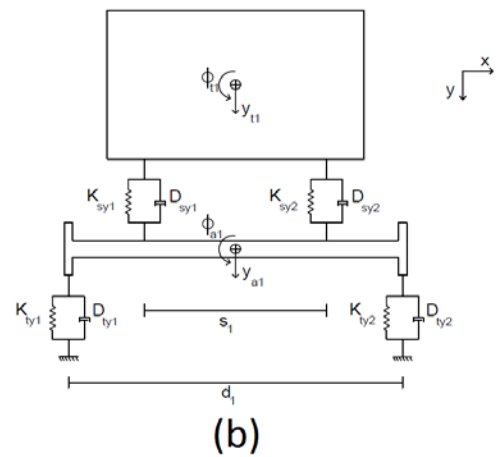
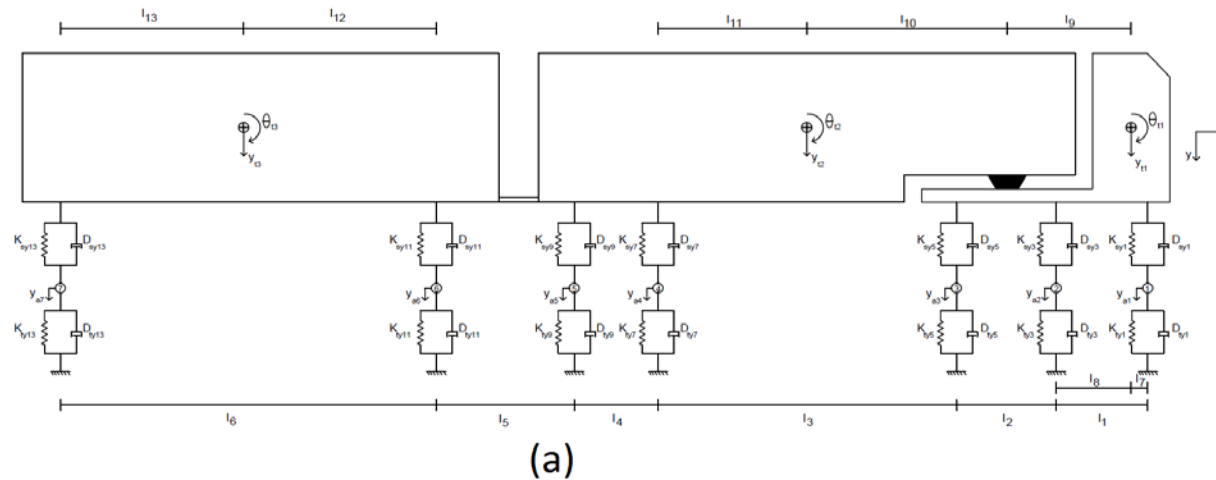


FIGURE 4-11: SEVEN AXLE ROCKY MOUNTAIN DOUBLE DYNAMIC MODEL (A) TRUCK SIDE VIEW (B) TRUCK FRONT VIEW

Potential Energy of the system:

$$\begin{aligned}
V = & \frac{1}{2}K_{sy1}U_{sy1}^2 + \frac{1}{2}K_{sy2}U_{sy2}^2 + \frac{1}{2}K_{sy3}U_{sy3}^2 + \frac{1}{2}K_{sy4}U_{sy4}^2 + \\
& \frac{1}{2}K_{sy5}U_{sy5}^2 + \frac{1}{2}K_{sy6}U_{sy6}^2 + \frac{1}{2}K_{sy7}U_{sy7}^2 + \frac{1}{2}K_{sy8}U_{sy8}^2 + \frac{1}{2}K_{sy9}U_{sy9}^2 + \\
& \frac{1}{2}K_{sy10}U_{sy10}^2 + \frac{1}{2}K_{sy11}U_{sy11}^2 + \frac{1}{2}K_{sy12}U_{sy12}^2 + \frac{1}{2}K_{sy13}U_{sy13}^2 + \\
& \frac{1}{2}K_{sy14}U_{sy14}^2 + \frac{1}{2}K_{ty1}U_{ty1}^2 + \frac{1}{2}K_{ty2}U_{ty2}^2 + \frac{1}{2}K_{ty3}U_{ty3}^2 + \frac{1}{2}K_{ty4}U_{ty4}^2 + \\
& \frac{1}{2}K_{ty5}U_{ty5}^2 + \frac{1}{2}K_{ty6}U_{ty6}^2 + \frac{1}{2}K_{ty7}U_{sy7}^2 + \frac{1}{2}K_{ty8}U_{ty8}^2 + \frac{1}{2}K_{ty9}U_{ty9}^2 + \\
& \frac{1}{2}K_{ty10}U_{ty10}^2 + \frac{1}{2}K_{ty11}U_{ty11}^2 + \frac{1}{2}K_{ty12}U_{ty12}^2 + \frac{1}{2}K_{ty13}U_{ty13}^2 + \quad (4-228) \\
& \frac{1}{2}K_{ty14}U_{ty14}^2 - ((m_{t1}g)y_{t1} + (m_{t2}g)y_{t2} + (m_{t3}g)y_{t3} + (m_{a1}g)y_{a1} + \\
& (m_{a2}g)y_{a2} + (m_{a3}g)y_{a3} + (m_{a4}g)y_{a4} + (m_{a5}g)y_{a5} + (m_{a6}g)y_{a6} + \\
& (m_{a7}g)y_{a7}) + (F_{y1}U_{sy1} + F_{y2}U_{sy2} + F_{y3}U_{sy3} + F_{y4}U_{sy4} + F_{y5}U_{sy5} + \\
& F_{y6}U_{sy6} + F_{y7}U_{sy7} + F_{y8}U_{sy8} + F_{y9}U_{sy9} + F_{y10}U_{sy10} + F_{y11}U_{sy11} + \\
& F_{y12}U_{sy12} + F_{y13}U_{sy13} + F_{y14}U_{sy14})
\end{aligned}$$

Damping Energy of the system:

$$\begin{aligned}
D = & \frac{1}{2} D_{sy1} \dot{U}_{sy1}^2 + \frac{1}{2} D_{sy2} \dot{U}_{sy2}^2 + \frac{1}{2} D_{sy3} \dot{U}_{sy3}^2 + \frac{1}{2} D_{sy4} \dot{U}_{sy4}^2 + \\
& \frac{1}{2} D_{sy5} \dot{U}_{sy5}^2 + \frac{1}{2} D_{sy6} \dot{U}_{sy6}^2 + \frac{1}{2} D_{sy7} \dot{U}_{sy7}^2 + \frac{1}{2} D_{sy8} \dot{U}_{sy8}^2 + \frac{1}{2} D_{sy9} \dot{U}_{sy9}^2 + \\
& \frac{1}{2} D_{sy10} \dot{U}_{sy10}^2 + \frac{1}{2} D_{sy11} \dot{U}_{sy11}^2 + \frac{1}{2} D_{sy12} \dot{U}_{sy12}^2 + \frac{1}{2} D_{sy13} \dot{U}_{sy13}^2 + \\
& \frac{1}{2} D_{sy14} \dot{U}_{sy14}^2 + \frac{1}{2} D_{ty1} \dot{U}_{ty1}^2 + \frac{1}{2} D_{ty2} \dot{U}_{ty2}^2 + \frac{1}{2} D_{ty3} \dot{U}_{ty3}^2 + \frac{1}{2} D_{ty4} \dot{U}_{ty4}^2 + \quad (4-229) \\
& \frac{1}{2} D_{ty5} \dot{U}_{ty5}^2 + \frac{1}{2} D_{ty6} \dot{U}_{ty6}^2 + \frac{1}{2} D_{ty7} \dot{U}_{ty7}^2 + \frac{1}{2} D_{ty8} \dot{U}_{ty8}^2 + \frac{1}{2} D_{ty9} \dot{U}_{ty9}^2 + \\
& \frac{1}{2} D_{ty10} \dot{U}_{ty10}^2 + \frac{1}{2} D_{ty11} \dot{U}_{ty11}^2 + \frac{1}{2} D_{ty12} \dot{U}_{ty12}^2 + \frac{1}{2} D_{ty13} \dot{U}_{ty13}^2 + \\
& \frac{1}{2} D_{ty14} \dot{U}_{ty14}^2
\end{aligned}$$

The displacement at the pivot point should stay the same, whether it is calculated from the trailer part or the tractor part,

$$y_{t2} + \theta_{t2} l_{10} = y_{t1} - \theta_{t1} l_9 \quad (4-230)$$

Thus, by substituting θ_{t2} from equation (4-230) in equation (4-227),

$$\begin{aligned}
T = & \frac{1}{2} m_{t1} \dot{y}_{t1}^2 + \frac{1}{2} m_{a1} \dot{y}_{a1}^2 + \frac{1}{2} m_{a2} \dot{y}_{a2}^2 + \frac{1}{2} m_{a3} \dot{y}_{a3}^2 + \frac{1}{2} m_{a4} \dot{y}_{a4}^2 + \\
& \frac{1}{2} m_{a5} \dot{y}_{a5}^2 + \frac{1}{2} m_{a6} \dot{y}_{a6}^2 + \frac{1}{2} m_{a7} \dot{y}_{a7}^2 + \frac{1}{2} I_{xt1} \dot{\phi}_{t1}^2 + \frac{1}{2} I_{zt1} \dot{\theta}_{t1}^2 + \frac{1}{2} I_{xt2} \dot{\phi}_{t2}^2 + \\
& \frac{1}{2} I_{zt2} \left(\frac{\dot{y}_{t1} - \dot{y}_{t2} - \dot{\theta}_{t1} l_9}{l_{10}} \right)^2 + \frac{1}{2} I_{xt3} \dot{\phi}_{t3}^2 + \frac{1}{2} I_{zt3} \dot{\theta}_{t3}^2 + \frac{1}{2} I_{xa1} \dot{\phi}_{a1}^2 + \frac{1}{2} I_{xa2} \dot{\phi}_{a2}^2 + \quad (4-231) \\
& \frac{1}{2} I_{xa3} \dot{\phi}_{a3}^2 + \frac{1}{2} I_{xa4} \dot{\phi}_{a4}^2 + \frac{1}{2} I_{xa5} \dot{\phi}_{a5}^2 + \frac{1}{2} I_{xa6} \dot{\phi}_{a6}^2 + \frac{1}{2} I_{xa7} \dot{\phi}_{a7}^2 + \\
& \frac{1}{2} m_{t2} \dot{y}_{t2}^2 + \frac{1}{2} m_{t3} \dot{y}_{t3}^2
\end{aligned}$$

Same substitution will be applied to the equations (4-228) and (4-229). Now the Lagrange's equation is applied to y_{t2} :

$$\begin{aligned}
& \left[m_{t2} \ddot{y}_{t2} - \frac{l_{zt2}}{l_{10}^2} (\ddot{y}_{t1} - \ddot{y}_{t2} - \ddot{\theta}_{t1} l_9) \right] + \left[\left(1 + \frac{l_{11}}{l_{10}} \right) (F_{sy7} + F_{sy8}) + \right. \\
& \left. \left(1 + \frac{l_4 + l_{11}}{l_{10}} \right) (F_{sy9} + F_{sy10}) - (m_{t2} g) \right] + \left[\left(1 + \frac{l_{11}}{l_{10}} \right) (F_{dsy7} + F_{dsy8}) + \right. \\
& \left. \left(1 + \frac{l_4 + l_{11}}{l_{10}} \right) (F_{dsy9} + F_{dsy10}) \right] = 0
\end{aligned} \tag{4-232}$$

To simplify the equation some variables are defined as follows:

$$S_{a2} = \frac{I_{zt2}}{l_{10}^2}$$

$$S_{c2} = \frac{I_{zt2}}{l_{10}^2} + m_{t2}$$

$$S_{a3} = \frac{I_{zt2}}{l_{10}^2} l_9$$

$$\begin{aligned}
B_{t4} = & m_{t2} g - \left(1 + \frac{l_{11}}{l_{10}} \right) (F_{sy7} + F_{sy8} + F_{dsy7} + F_{dsy8}) - \left(1 + \frac{l_4 + l_{11}}{l_{10}} \right) (F_{sy9} + F_{sy10} + \\
& F_{dsy9} + F_{dsy10})
\end{aligned}$$

Therefore equation (4-232) will be simplified to:

$$-S_{a2} \ddot{y}_{t1} + S_{c2} \ddot{y}_{t2} + S_{a3} \ddot{\theta}_{t1} = B_{t4} \tag{4-233}$$

By applying the Lagrange's equation to y_{t1} :

$$\begin{aligned}
& \left[m_{t1} \ddot{y}_{t1} + \frac{l_{zt2}}{l_{10}^2} (\ddot{y}_{t1} - \ddot{y}_{t2} - \ddot{\theta}_{t1} l_9) \right] + \left[(F_{sy1} + F_{sy2} + F_{sy3} + F_{sy4} + F_{sy5} + \right. \\
& \left. F_{sy6}) - \frac{l_{11}}{l_{10}} (F_{sy7} + F_{sy8}) - \frac{l_4 + l_{11}}{l_{10}} (F_{sy9} + F_{sy10}) - (m_{t1} g) \right] + \\
& \left[(F_{dsy1} + F_{dsy2} + F_{dsy3} + F_{dsy4} + F_{dsy5} + F_{dsy6}) - \frac{l_{11}}{l_{10}} (F_{dsy7} + F_{dsy8}) - \right. \\
& \left. \frac{l_4 + l_{11}}{l_{10}} (F_{dsy9} + F_{dsy10}) \right] = 0
\end{aligned} \tag{4-234}$$

Again to simplify the equation some variables are defined as follows:

$$S_{a1} = \frac{I_{zt2}}{l_{10}^2} + m_{t1}$$

$$B_{t1} = m_{t1}g - [(F_{sy1} + F_{sy2} + F_{sy3} + F_{sy4} + F_{sy5} + F_{sy6}) - \frac{l_{11}}{l_{10}}(F_{sy7} + F_{sy8}) - \frac{l_4 + l_{11}}{l_{10}}(F_{sy9} + F_{sy10}) + (F_{dsy1} + F_{dsy2} + F_{dsy3} + F_{dsy4} + F_{dsy5} + F_{dsy6}) - \frac{l_{11}}{l_{10}}(F_{dsy7} + F_{dsy8}) - \frac{l_4 + l_{11}}{l_{10}}(F_{dsy9} + F_{dsy10})]$$

Therefore equation (4-234) will be simplified to:

$$S_{a1}\ddot{y}_{t1} - S_{a2}\ddot{y}_{t2} - S_{a3}\ddot{\theta}_{t1} = B_{t1} \quad (4-235)$$

Also, by applying the Lagrange's equation to θ_{t1} :

$$\begin{aligned} & \left[I_{zt1}\ddot{\theta}_{t1} - \frac{I_{zt2}l_9}{l_{10}^2}(\ddot{y}_{t1} - \ddot{y}_{t2} - \dot{\theta}_{t1}l_9) \right] + \left[l_7(F_{sy1} + F_{sy2}) - l_8(F_{sy3} + F_{sy4}) - \right. \\ & (l_2 + l_8)(F_{sy5} + F_{sy6}) + \frac{l_9l_{11}}{l_{10}}(F_{sy7} + F_{sy8}) + \frac{l_9(l_4 + l_{11})}{l_{10}}(F_{sy9} + F_{sy10}) \Big] + \\ & \left[l_7(F_{dsy1} + F_{dsy2}) - l_8(F_{dsy3} + F_{dsy4}) - (l_2 + l_8)(F_{dsy5} + F_{dsy6}) + \right. \\ & \left. \frac{l_9l_{11}}{l_{10}}(F_{dsy7} + F_{dsy8}) + \frac{l_9(l_4 + l_{11})}{l_{10}}(F_{dsy9} + F_{dsy10}) \right] = 0 \end{aligned} \quad (4-236)$$

Once again to simplify the equation some variables need to be defined as follows:

$$\begin{aligned} S_{b3} &= I_{zt1} + \frac{I_{zt2}l_9}{l_{10}^2} \\ B_{t3} &= - \left[\left[l_7(F_{sy1} + F_{sy2}) - l_8(F_{sy3} + F_{sy4}) - (l_2 + l_8)(F_{sy5} + F_{sy6}) + \frac{l_9l_{11}}{l_{10}}(F_{sy7} + \right. \right. \\ & F_{sy8}) + \frac{l_9(l_4 + l_{11})}{l_{10}}(F_{sy9} + F_{sy10}) \Big] + \left[l_7(F_{dsy1} + F_{dsy2}) - l_8(F_{dsy3} + F_{dsy4}) - (l_2 + \right. \\ & l_8)(F_{dsy5} + F_{dsy6}) + \frac{l_9l_{11}}{l_{10}}(F_{dsy7} + F_{dsy8}) + \frac{l_9(l_4 + l_{11})}{l_{10}}(F_{dsy9} + F_{dsy10}) \Big] \Big] \end{aligned}$$

Therefore equation (4-236) will be simplified to:

$$-S_{a3}\ddot{y}_{t1} + S_{a3}\ddot{y}_{t2} + S_{b3}\ddot{\theta}_{t1} = B_{t3} \quad (4-237)$$

By adding equations (2-233) and (2-235),

$$(S_{a1} - S_{a2})\ddot{y}_{t1} - (S_{a2} - S_{c2})\ddot{y}_{t2} = B_{t1} + B_{t4} \quad (4-238)$$

Also by multiplying S_{b3} and S_{a3} to equations (2-237) and (2-238), respectively,

$$(S_{a1}S_{b3} - S_{a3}^2)\ddot{y}_{t1} - (S_{a2}S_{b3} - S_{a3}^2)\ddot{y}_{t2} = S_{b3}B_{t1} + S_{a3}B_{t3} \quad (4-239)$$

By defining the following expressions, equations (4-238) and (4-239) are simplified to equations (4-240) and (4-241), respectively,

$$e_1 = S_{a1} - S_{a2}$$

$$e_2 = S_{a2} - S_{c2}$$

$$e_3 = S_{a1}S_{b3} - S_{a3}^2$$

$$e_4 = S_{a2}S_{b3} - S_{a3}^2$$

$$e_1\ddot{y}_{t1} - e_2\ddot{y}_{t2} = B_{t1} + B_{t4} \quad (4-240)$$

$$e_3\ddot{y}_{t1} - e_4\ddot{y}_{t2} = S_{b3}B_{t1} + S_{a3}B_{t3} \quad (4-241)$$

Solving equations (4-240) and (4-241) for \ddot{y}_{t1} and \ddot{y}_{t2} will lead to:

$$\ddot{y}_{t1} = \frac{e_4(B_{t1} + B_{t4}) - e_2(S_{b3}B_{t1} + S_{a3}B_{t3})}{e_1e_4 - e_2e_3} \quad (4-242)$$

$$\ddot{y}_{t2} = \frac{e_1\left(\frac{e_4(B_{t1} + B_{t4}) - e_2(S_{b3}B_{t1} + S_{a3}B_{t3})}{e_1e_4 - e_2e_3}\right) - \frac{B_{t1} + B_{t4}}{e_2}}{e_2} \quad (4-243)$$

Substituting equations (4-242) and (4-243) into equation (4-237) will give,

$$\begin{aligned} \ddot{\theta}_{t1} &= \frac{B_{t3}}{S_{b3}} + \frac{S_{a3}}{S_{b3}}\left(\frac{e_4(B_{t1} + B_{t4}) - e_2(S_{b3}B_{t1} + S_{a3}B_{t3})}{e_1e_4 - e_2e_3}\right) - \\ &\quad \frac{S_{a3}}{S_{b3}}\left(\frac{e_1\left(\frac{e_4(B_{t1} + B_{t4}) - e_2(S_{b3}B_{t1} + S_{a3}B_{t3})}{e_1e_4 - e_2e_3}\right) - \frac{B_{t1} + B_{t4}}{e_2}}{e_2}\right) \end{aligned} \quad (4-244)$$

By applying the Lagrange's equation to $\varphi_{t1}, \varphi_{t2}, \varphi_{t3}, y_{t3}, \theta_{t3}$:

$$\begin{aligned} I_{xt1}\ddot{\varphi}_{t1} + \left[\left(\frac{s_1}{2}\right)(F_{sy1} - F_{sy2}) + \left(\frac{s_2}{2}\right)(F_{sy3} - F_{sy4}) + \left(\frac{s_3}{2}\right)(F_{sy5} - F_{sy6})\right] + \\ \left[\left(\frac{s_1}{2}\right)(F_{dsy1} - F_{dsy2}) + \left(\frac{s_2}{2}\right)(F_{dsy3} - F_{dsy4}) + \left(\frac{s_3}{2}\right)(F_{dsy5} - F_{dsy6})\right] = 0 \end{aligned} \quad (4-245)$$

$$I_{xt2}\ddot{\varphi}_{t2} + \left[\left(\frac{s_4}{2}\right)(F_{sy7} - F_{sy8}) + \left(\frac{s_5}{2}\right)(F_{sy9} - F_{sy10}) \right] + \left[\left(\frac{s_4}{2}\right)(F_{dsy7} - F_{dsy8}) + \left(\frac{s_5}{2}\right)(F_{dsy9} - F_{dsy10}) \right] = 0 \quad (4-246)$$

$$I_{xt3}\ddot{\varphi}_{t3} + \left[\left(\frac{s_6}{2}\right)(F_{sy11} - F_{sy12}) + \left(\frac{s_7}{2}\right)(F_{sy13} - F_{sy14}) \right] + \left[\left(\frac{s_6}{2}\right)(F_{dsy11} - F_{dsy12}) + \left(\frac{s_7}{2}\right)(F_{dsy13} - F_{dsy14}) \right] = 0 \quad (4-247)$$

$$m_{t3}\ddot{y}_{t3} + (F_{sy11} + F_{sy12} + F_{sy13} + F_{sy14}) + (F_{dsy11} + F_{dsy12} + F_{dsy13} + F_{dsy14}) - m_{t3}g = 0 \quad (4-248)$$

$$I_{zt3}\ddot{\theta}_{t3} + [l_{12}(F_{sy11} + F_{sy12}) - l_{13}(F_{sy13} + F_{sy14})] + [l_{12}(F_{dsy11} + F_{dsy12}) - l_{13}(F_{dsy13} + F_{dsy14})] = 0 \quad (4-249)$$

The rest of degrees of freedom will be as follows:

$$m_{a1}\ddot{y}_{a1} - (F_{sy1} + F_{sy2}) + (F_{ty1} + F_{ty2}) - (F_{dsy1} + F_{dsy2}) + (F_{dty1} + F_{dty2}) = m_{a1}g \quad (4-250)$$

$$I_{xa1}\ddot{\varphi}_{a1} - \left(\frac{s_1}{2}\right)(F_{sy1} - F_{sy2}) + \left(\frac{d_1}{2}\right)(F_{ty1} - F_{ty2}) - \left(\frac{s_1}{2}\right)(F_{dsy1} - F_{dsy2}) + \left(\frac{d_1}{2}\right)(F_{dty1} - F_{dty2}) = \mathbf{0} \quad (4-251)$$

$$m_{a2}\ddot{y}_{a2} - (F_{sy3} + F_{sy4}) + (F_{ty3} + F_{ty4}) - (F_{dsy3} + F_{dsy4}) + (F_{dty3} + F_{dty4}) = m_{a2}g \quad (4-252)$$

$$I_{xa2}\ddot{\varphi}_{a2} - \left(\frac{s_2}{2}\right)(F_{sy3} - F_{sy4}) + \left(\frac{d_2}{2}\right)(F_{ty3} - F_{ty4}) - \left(\frac{s_2}{2}\right)(F_{dsy3} - F_{dsy4}) + \left(\frac{d_2}{2}\right)(F_{dty3} - F_{dty4}) = 0 \quad (4-253)$$

$$m_{a3}\ddot{y}_{a3} - (F_{sy5} + F_{sy6}) + (F_{ty5} + F_{ty6}) - (F_{dsy5} + F_{dsy6}) + (F_{dty5} + F_{dty6}) = m_{a3}g \quad (4-254)$$

$$I_{xa3}\ddot{\varphi}_{a3} - \left(\frac{s_3}{2}\right)(F_{sy5} - F_{sy6}) + \left(\frac{d_3}{2}\right)(F_{ty5} - F_{ty6}) - \left(\frac{s_3}{2}\right)(F_{dsy5} - F_{dsy6}) + \left(\frac{d_3}{2}\right)(F_{dty5} - F_{dty6}) = 0 \quad (4-255)$$

$$(\frac{d_3}{2})(F_{dty5} - F_{dty6}) = 0$$

$$m_{a4}\ddot{y}_{a4} - (F_{sy7} + F_{sy8}) + (F_{ty7} + F_{ty8}) - (F_{dsy7} + F_{dsy8}) + (F_{dty7} + F_{dty8}) = m_{a4}g \quad (4-256)$$

$$I_{xa4}\ddot{\varphi}_{a4} - (\frac{s_4}{2})(F_{sy7} - F_{sy8}) + (\frac{d_4}{2})(F_{ty7} - F_{ty8}) - (\frac{s_4}{2})(F_{dsy7} - F_{dsy8}) + (\frac{d_4}{2})(F_{dty7} - F_{dty8}) = 0 \quad (4-257)$$

$$m_{a5}\ddot{y}_{a5} - (F_{sy9} + F_{sy10}) + (F_{ty9} + F_{ty10}) - (F_{dsy9} + F_{dsy10}) + (F_{dty9} + F_{dty10}) = m_{a5}g \quad (4-258)$$

$$I_{xa5}\ddot{\varphi}_{a5} - (\frac{s_5}{2})(F_{sy9} - F_{sy10}) + (\frac{d_5}{2})(F_{ty9} - F_{ty10}) - (\frac{s_5}{2})(F_{dsy9} - F_{dsy10}) + (\frac{d_5}{2})(F_{dty9} - F_{dty10}) = 0 \quad (4-259)$$

$$m_{a6}\ddot{y}_{a6} - (F_{sy11} + F_{sy12}) + (F_{ty11} + F_{ty12}) - (F_{dsy11} + F_{dsy12}) + (F_{dty11} + F_{dty12}) = m_{a6}g \quad (4-260)$$

$$I_{xa6}\ddot{\varphi}_{a6} - (\frac{s_6}{2})(F_{sy11} - F_{sy12}) + (\frac{d_6}{2})(F_{ty11} - F_{ty12}) - (\frac{s_6}{2})(F_{dsy11} - F_{dsy12}) + (\frac{d_6}{2})(F_{dty11} - F_{dty12}) = 0 \quad (4-261)$$

$$m_{a7}\ddot{y}_{a7} - (F_{sy13} + F_{sy14}) + (F_{ty13} + F_{ty14}) - (F_{dsy13} + F_{dsy14}) + (F_{dty13} + F_{dty14}) = m_{a7}g \quad (4-262)$$

$$I_{xa7}\ddot{\varphi}_{a7} - (\frac{s_7}{2})(F_{sy13} - F_{sy14}) + (\frac{d_7}{2})(F_{ty13} - F_{ty14}) - (\frac{s_7}{2})(F_{dsy13} - F_{dsy14}) + (\frac{d_7}{2})(F_{dty13} - F_{dty14}) = 0 \quad (4-263)$$

4.13 Derivation of Equations of Motion for “8 Axle B-Train Double”

There are twenty five degrees of freedom in total for this type of truck. The degrees of freedom can be seen in Figure 2-12 and the description of those degrees of freedom can be found in Table 2-22. Relative Displacements at the locations of the springs are also calculated using the values given in Table 2-23.

TABLE 4-22: DEGREES OF FREEDOM OF 8 AXLE B-TRAIN DOUBLE

No.	Degree of Freedom	Contrib. Mass	Description
1	y_{t1}	m_{t1}	Tractor vertical displacement and mass
2	φ_{t1}	I_{xt1}	Tractor roll displacement and mass moment of inertia
3	θ_{t1}	I_{zt1}	Tractor pitch displacement and mass moment of inertia
4	y_{t2}	m_{t2}	Semi-trailer vertical displacement and mass
5	φ_{t2}	I_{xt2}	Semi-trailer roll displacement and mass moment of inertia
6	θ_{t2}	I_{zt2}	Semi-trailer pitch displacement and mass moment of inertia
7	y_{t3}	m_{t3}	Trailer vertical displacement and mass
8	φ_{t3}	I_{xt3}	Trailer roll displacement and mass moment of inertia
9	θ_{t3}	I_{zt3}	Trailer pitch displacement and mass moment of inertia
10	y_{a1}	m_{a1}	Steer axle vertical displacement and mass
11	φ_{a1}	I_{xa1}	Steer axle roll displacement and mass moment of inertia
12	y_{a2}	m_{a2}	Vertical displacement and mass of forward axle of tractor tandem
13	φ_{a2}	I_{xa2}	Roll displacement and mass moment of inertia of forward axle of tractor tandem
14	y_{a3}	m_{a3}	Vertical displacement and mass of aft axle of tractor tandem
15	φ_{a3}	I_{xa3}	Roll displacement and mass moment of inertia of aft axle of tractor tandem
16	y_{a4}	m_{a4}	Vertical displacement and mass of first axle of first trailer
17	φ_{a4}	I_{xa4}	Roll displacement and mass moment of inertia of first axle of first trailer
18	y_{a5}	m_{a5}	Vertical displacement and mass of second axle of first trailer
19	φ_{a5}	I_{xa5}	Roll displacement and mass moment of inertia of second axle of first trailer
20	y_{a6}	m_{a6}	Vertical displacement and mass of first axle of second trailer
21	φ_{a6}	I_{xa6}	Roll displacement and mass moment of inertia of first axle of second trailer
22	y_{a7}	m_{a7}	Vertical displacement and mass of second axle of second trailer
23	φ_{a7}	I_{xa7}	Roll displacement and mass moment of inertia of second axle of second trailer
24	y_{a8}	m_{a8}	Vertical displacement and mass of third axle of second trailer
25	φ_{a8}	I_{xa8}	Roll displacement and mass moment of inertia of third axle of second trailer

TABLE 4-23: RELATIVE DISPLACEMENTS AT SPRING LOCATIONS OF 8 AXLE TURNPIKE DOUBLE

Suspension springs	
U_{sy1}	$(y_{t1} - y_{a1}) + (S_1/2)(\varphi_{t1} - \varphi_{a1}) + l_7\theta_{t1}$
U_{sy2}	$(y_{t1} - y_{a1}) - (S_1/2)(\varphi_{t1} - \varphi_{a1}) + l_7\theta_{t1}$
U_{sy3}	$(y_{t1} - y_{a2}) + (S_2/2)(\varphi_{t1} - \varphi_{a2}) - l_8\theta_{t1}$
U_{sy4}	$(y_{t1} - y_{a2}) - (S_2/2)(\varphi_{t1} - \varphi_{a2}) - l_8\theta_{t1}$
U_{sy5}	$(y_{t1} - y_{a3}) + (S_3/2)(\varphi_{t1} - \varphi_{a3}) - (l_2 + l_8)\theta_{t1}$
U_{sy6}	$(y_{t1} - y_{a3}) - (S_3/2)(\varphi_{t1} - \varphi_{a3}) - (l_2 + l_8)\theta_{t1}$
U_{sy7}	$(y_{t2} - y_{a4}) + (S_4/2)(\varphi_{t2} - \varphi_{a4}) - l_{11}\theta_{t2}$
U_{sy8}	$(y_{t2} - y_{a4}) - (S_4/2)(\varphi_{t2} - \varphi_{a4}) - l_{11}\theta_{t2}$
U_{sy9}	$(y_{t2} - y_{a5}) + (S_5/2)(\varphi_{t2} - \varphi_{a5}) - (l_4 + l_{11})\theta_{t2}$
U_{sy10}	$(y_{t2} - y_{a5}) - (S_5/2)(\varphi_{t2} - \varphi_{a5}) - (l_4 + l_{11})\theta_{t2}$
U_{sy11}	$(y_{t3} - y_{a6}) + (S_6/2)(\varphi_{t3} - \varphi_{a6}) + l_{13}\theta_{t3}$
U_{sy12}	$(y_{t3} - y_{a6}) - (S_6/2)(\varphi_{t3} - \varphi_{a6}) + l_{13}\theta_{t3}$
U_{sy13}	$(y_{t3} - y_{a7}) + (S_7/2)(\varphi_{t3} - \varphi_{a7}) - l_{14}\theta_{t3}$
U_{sy14}	$(y_{t3} - y_{a7}) - (S_7/2)(\varphi_{t3} - \varphi_{a7}) - l_{14}\theta_{t3}$
U_{sy15}	$(y_{t3} - y_{a8}) + (S_8/2)(\varphi_{t3} - \varphi_{a8}) - (l_{14} + l_{12})\theta_{t3}$
U_{sy16}	$(y_{t3} - y_{a8}) - (S_8/2)(\varphi_{t3} - \varphi_{a8}) - (l_{14} + l_{12})\theta_{t3}$

Table 4-23 (Cont.)

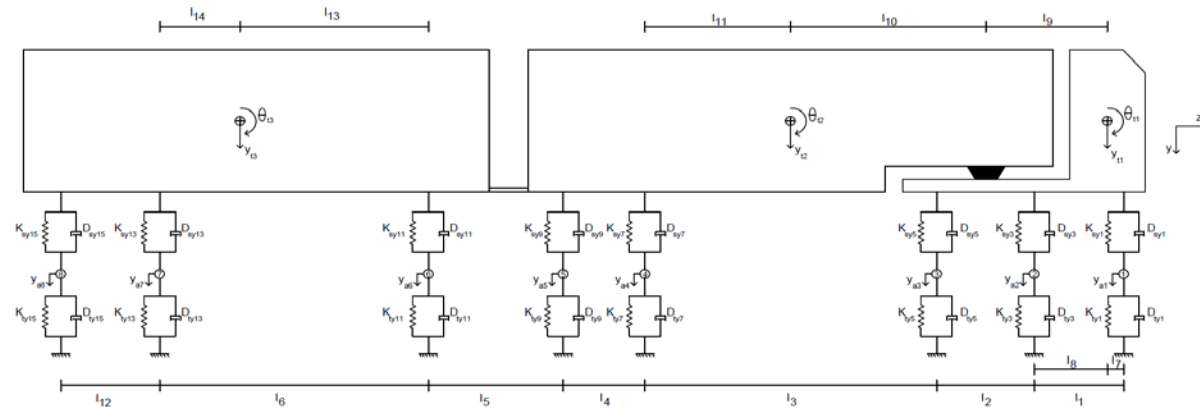
Tire springs	
U_{ty1}	$y_{a1} + (d_1/2)\varphi_{a1} + u_{SR1}$
U_{ty2}	$y_{a1} - (d_1/2)\varphi_{a1} + u_{SR2}$
U_{ty3}	$y_{a2} + (d_2/2)\varphi_{a2} + u_{SR3}$
U_{ty4}	$y_{a2} - (d_2/2)\varphi_{a2} + u_{SR4}$
U_{ty5}	$y_{a3} + (d_3/2)\varphi_{a3} + u_{SR5}$
U_{ty6}	$y_{a3} - (d_3/2)\varphi_{a3} + u_{SR6}$
U_{ty7}	$y_{a4} + (d_4/2)\varphi_{a4} + u_{SR7}$
U_{ty8}	$y_{a4} - (d_4/2)\varphi_{a4} + u_{SR8}$
U_{ty9}	$y_{a5} + (d_5/2)\varphi_{a5} + u_{SR9}$
U_{ty10}	$y_{a5} - (d_5/2)\varphi_{a5} + u_{SR10}$
U_{ty11}	$y_{a6} + (d_6/2)\varphi_{a6} + u_{SR11}$
U_{ty12}	$y_{a6} - (d_6/2)\varphi_{a6} + u_{SR12}$
U_{ty13}	$y_{a7} + (d_7/2)\varphi_{a7} + u_{SR13}$
U_{ty14}	$y_{a7} - (d_7/2)\varphi_{a7} + u_{SR14}$
U_{ty15}	$y_{a8} + (d_8/2)\varphi_{a8} + u_{SR15}$
U_{ty16}	$y_{a8} - (d_8/2)\varphi_{a8} + u_{SR16}$

Kinetic Energy of the system:

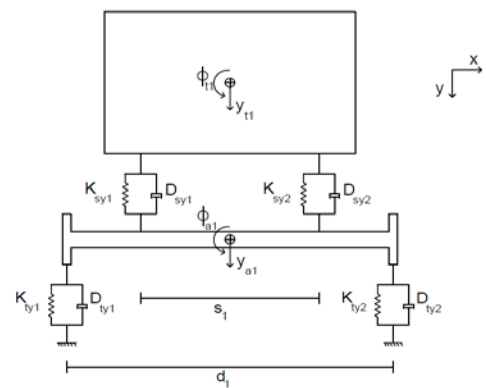
$$\begin{aligned}
T = & \frac{1}{2}m_{t1}\dot{y}_{t1}^2 + \frac{1}{2}m_{a1}\dot{y}_{a1}^2 + \frac{1}{2}m_{a2}\dot{y}_{a2}^2 + \frac{1}{2}m_{a3}\dot{y}_{a3}^2 + \frac{1}{2}m_{a4}\dot{y}_{a4}^2 + \\
& \frac{1}{2}m_{a5}\dot{y}_{a5}^2 + \frac{1}{2}m_{a6}\dot{y}_{a6}^2 + \frac{1}{2}m_{a7}\dot{y}_{a7}^2 + \frac{1}{2}m_{a8}\dot{y}_{a8}^2 + \frac{1}{2}I_{xt1}\dot{\phi}_{t1}^2 + \\
& \frac{1}{2}I_{zt1}\dot{\theta}_{t1}^2 + \frac{1}{2}I_{xt2}\dot{\phi}_{t2}^2 + \frac{1}{2}I_{zt2}\dot{\theta}_{t2}^2 + \frac{1}{2}I_{xt3}\dot{\phi}_{t3}^2 + \frac{1}{2}I_{zt3}\dot{\theta}_{t3}^2 + \frac{1}{2}I_{xa1}\dot{\phi}_{a1}^2 + \quad (4-264) \\
& \frac{1}{2}I_{xa2}\dot{\phi}_{a2}^2 + \frac{1}{2}I_{xa3}\dot{\phi}_{a3}^2 + \frac{1}{2}I_{xa4}\dot{\phi}_{a4}^2 + \frac{1}{2}I_{xa5}\dot{\phi}_{a5}^2 + \frac{1}{2}I_{xa6}\dot{\phi}_{a6}^2 + \\
& \frac{1}{2}I_{xa7}\dot{\phi}_{a7}^2 + \frac{1}{2}I_{xa8}\dot{\phi}_{a8}^2 + \frac{1}{2}m_{t2}\dot{y}_{t2}^2 + \frac{1}{2}m_{t3}\dot{y}_{t3}^2
\end{aligned}$$

Damping Energy of the system:

$$\begin{aligned}
D = & \frac{1}{2}D_{sy1}\dot{U}_{sy1}^2 + \frac{1}{2}D_{sy2}\dot{U}_{sy2}^2 + \frac{1}{2}D_{sy3}\dot{U}_{sy3}^2 + \frac{1}{2}D_{sy4}\dot{U}_{sy4}^2 + \\
& \frac{1}{2}D_{sy5}\dot{U}_{sy5}^2 + \frac{1}{2}D_{sy6}\dot{U}_{sy6}^2 + \frac{1}{2}D_{sy7}\dot{U}_{sy7}^2 + \frac{1}{2}D_{sy8}\dot{U}_{sy8}^2 + \frac{1}{2}D_{sy9}\dot{U}_{sy9}^2 + \\
& \frac{1}{2}D_{sy10}\dot{U}_{sy10}^2 + \frac{1}{2}D_{sy11}\dot{U}_{sy11}^2 + \frac{1}{2}D_{sy12}\dot{U}_{sy12}^2 + \frac{1}{2}D_{sy13}\dot{U}_{sy13}^2 + \\
& \frac{1}{2}D_{sy14}\dot{U}_{sy14}^2 + \frac{1}{2}D_{sy15}\dot{U}_{sy15}^2 + \frac{1}{2}D_{sy16}\dot{U}_{sy16}^2 + \frac{1}{2}D_{ty1}\dot{U}_{ty1}^2 + \quad (4-265) \\
& \frac{1}{2}D_{ty2}\dot{U}_{ty2}^2 + \frac{1}{2}D_{ty3}\dot{U}_{ty3}^2 + \frac{1}{2}D_{ty4}\dot{U}_{ty4}^2 + \frac{1}{2}D_{ty5}\dot{U}_{ty5}^2 + \frac{1}{2}D_{ty6}\dot{U}_{ty6}^2 + \\
& \frac{1}{2}D_{ty7}\dot{U}_{ty7}^2 + \frac{1}{2}D_{ty8}\dot{U}_{ty8}^2 + \frac{1}{2}D_{ty9}\dot{U}_{ty9}^2 + \frac{1}{2}D_{ty10}\dot{U}_{ty10}^2 + \frac{1}{2}D_{ty11}\dot{U}_{ty11}^2 + \\
& \frac{1}{2}D_{ty12}\dot{U}_{ty12}^2 + \frac{1}{2}D_{ty13}\dot{U}_{ty13}^2 + \frac{1}{2}D_{ty14}\dot{U}_{ty14}^2 + \frac{1}{2}D_{ty15}\dot{U}_{ty15}^2 + \\
& \frac{1}{2}D_{ty16}\dot{U}_{ty16}^2
\end{aligned}$$



(a)



(b)

FIGURE 4-12: EIGHT AXLE TURNPIKE DOUBLE DYNAMIC MODEL (A) TRUCK SIDE VIEW (B) TRUCK FRONT VIEW

Potential Energy of the system:

$$\begin{aligned}
V = & \frac{1}{2}K_{sy1}U_{sy1}^2 + \frac{1}{2}K_{sy2}U_{sy2}^2 + \frac{1}{2}K_{sy3}U_{sy3}^2 + \frac{1}{2}K_{sy4}U_{sy4}^2 + \\
& \frac{1}{2}K_{sy5}U_{sy5}^2 + \frac{1}{2}K_{sy6}U_{sy6}^2 + \frac{1}{2}K_{sy7}U_{sy7}^2 + \frac{1}{2}K_{sy8}U_{sy8}^2 + \frac{1}{2}K_{sy9}U_{sy9}^2 + \\
& \frac{1}{2}K_{sy10}U_{sy10}^2 + \frac{1}{2}K_{sy11}U_{sy11}^2 + \frac{1}{2}K_{sy12}U_{sy12}^2 + \frac{1}{2}K_{sy13}U_{sy13}^2 + \\
& \frac{1}{2}K_{sy14}U_{sy14}^2 + \frac{1}{2}K_{sy15}U_{sy15}^2 + \frac{1}{2}K_{sy16}U_{sy16}^2 + \frac{1}{2}K_{ty1}U_{ty1}^2 + \\
& \frac{1}{2}K_{ty2}U_{ty2}^2 + \frac{1}{2}K_{ty3}U_{ty3}^2 + \frac{1}{2}K_{ty4}U_{ty4}^2 + \frac{1}{2}K_{ty5}U_{ty5}^2 + \frac{1}{2}K_{ty6}U_{ty6}^2 + \\
& \frac{1}{2}K_{ty7}U_{sy7}^2 + \frac{1}{2}K_{ty8}U_{ty8}^2 + \frac{1}{2}K_{ty9}U_{ty9}^2 + \frac{1}{2}K_{ty10}U_{ty10}^2 + \frac{1}{2}K_{ty11}U_{ty11}^2 + \quad (4-266) \\
& \frac{1}{2}K_{ty12}U_{ty12}^2 + \frac{1}{2}K_{ty13}U_{ty13}^2 + \frac{1}{2}K_{ty14}U_{ty14}^2 + \frac{1}{2}K_{ty15}U_{ty15}^2 + \\
& \frac{1}{2}K_{ty16}U_{ty16}^2 - ((m_{t1}g)y_{t1} + (m_{t2}g)y_{t2} + (m_{t3}g)y_{t3} + (m_{a1}g)y_{a1} + \\
& (m_{a2}g)y_{a2} + (m_{a3}g)y_{a3} + (m_{a4}g)y_{a4} + (m_{a5}g)y_{a5} + (m_{a6}g)y_{a6} + \\
& (m_{a7}g)y_{a7} + (m_{a8}g)y_{a8}) + (F_{y1}U_{sy1} + F_{y2}U_{sy2} + F_{y3}U_{sy3} + F_{y4}U_{sy4} + \\
& F_{y5}U_{sy5} + F_{y6}U_{sy6} + F_{y7}U_{sy7} + F_{y8}U_{sy8} + F_{y9}U_{sy9} + F_{y10}U_{sy10} + \\
& F_{y11}U_{sy11} + F_{y12}U_{sy12} + F_{y13}U_{sy13} + F_{y14}U_{sy14} + F_{y15}U_{sy15} + F_{y16}U_{sy16})
\end{aligned}$$

The displacement at the pivot point should stay the same, whether it is calculated from the trailer part or the tractor part,

$$y_{t2} + \theta_{t2}l_{10} = y_{t1} - \theta_{t1}l_9 \quad (4-267)$$

Thus, by substituting θ_{t2} from equation (4-267) in equation (4-264),

$$\begin{aligned}
T = & \frac{1}{2}m_{t1}\dot{y}_{t1}^2 + \frac{1}{2}m_{a1}\dot{y}_{a1}^2 + \frac{1}{2}m_{a2}\dot{y}_{a2}^2 + \frac{1}{2}m_{a3}\dot{y}_{a3}^2 + \frac{1}{2}m_{a4}\dot{y}_{a4}^2 + \\
& \frac{1}{2}m_{a5}\dot{y}_{a5}^2 + \frac{1}{2}m_{a6}\dot{y}_{a6}^2 + \frac{1}{2}m_{a7}\dot{y}_{a7}^2 + \frac{1}{2}m_{a8}\dot{y}_{a8}^2 + \frac{1}{2}I_{xt1}\dot{\phi}_{t1}^2 + \frac{1}{2}I_{zt1}\dot{\theta}_{t1}^2 + \quad (4-268)
\end{aligned}$$

$$\begin{aligned} & \frac{1}{2} I_{xt2} \dot{\phi}_{t2}^2 + \frac{1}{2} I_{zt2} \left(\frac{\ddot{y}_{t1} - \ddot{y}_{t2} - \dot{\theta}_{t1} l_9}{l_{10}} \right)^2 + \frac{1}{2} I_{xt3} \dot{\phi}_{t3}^2 + \frac{1}{2} I_{zt3} \dot{\theta}_{t3}^2 + \frac{1}{2} I_{xa1} \dot{\phi}_{a1}^2 + \\ & \frac{1}{2} I_{xa2} \dot{\phi}_{a2}^2 + \frac{1}{2} I_{xa3} \dot{\phi}_{a3}^2 + \frac{1}{2} I_{xa4} \dot{\phi}_{a4}^2 + \frac{1}{2} I_{xa5} \dot{\phi}_{a5}^2 + \frac{1}{2} I_{xa6} \dot{\phi}_{a6}^2 + \\ & \frac{1}{2} I_{xa7} \dot{\phi}_{a7}^2 + \frac{1}{2} I_{xa8} \dot{\phi}_{a8}^2 + \frac{1}{2} m_{t2} \dot{y}_{t2}^2 + \frac{1}{2} m_{t3} \dot{y}_{t3}^2 \end{aligned}$$

Same substitution will be applied to the equations (4-265) and (4-266). Now the Lagrange's equation is applied to y_{t2} :

$$\begin{aligned} & \left[m_{t2} \ddot{y}_{t2} - \frac{I_{zt2}}{l_{10}^2} (\ddot{y}_{t1} - \ddot{y}_{t2} - \dot{\theta}_{t1} l_9) \right] + \left[\left(1 + \frac{l_{11}}{l_{10}} \right) (F_{sy7} + F_{sy8}) + \right. \\ & \left. \left(1 + \frac{l_4 + l_{11}}{l_{10}} \right) (F_{sy9} + F_{sy10}) - (m_{t2} g) \right] + \left[\left(1 + \frac{l_{11}}{l_{10}} \right) (F_{dsy7} + F_{dsy8}) + \right. \\ & \left. \left(1 + \frac{l_4 + l_{11}}{l_{10}} \right) (F_{dsy9} + F_{dsy10}) \right] = 0 \end{aligned} \quad (4-269)$$

To simplify the equation some variables are defined as follows:

$$S_{a2} = \frac{I_{zt2}}{l_{10}^2}$$

$$S_{c2} = \frac{I_{zt2}}{l_{10}^2} + m_{t2}$$

$$S_{a3} = \frac{I_{zt2}}{l_{10}^2} l_9$$

$$\begin{aligned} B_{t4} = m_{t2} g - & \left[\left(1 + \frac{l_{11}}{l_{10}} \right) (F_{sy7} + F_{sy8} + F_{dsy7} + F_{dsy8}) + \left(1 + \frac{l_4 + l_{11}}{l_{10}} \right) (F_{sy9} + F_{sy10} + \right. \\ & \left. F_{dsy9} + F_{dsy10}) \right] \end{aligned}$$

Therefore equation (4-269) will be simplified to:

$$-S_{a2} \ddot{y}_{t1} + S_{c2} \ddot{y}_{t2} + S_{a3} \ddot{\theta}_{t1} = B_{t4} \quad (4-270)$$

By applying the Lagrange's equation to y_{t1} :

$$\left[m_{t1} \ddot{y}_{t1} + \frac{I_{zt2}}{l_{10}^2} (\ddot{y}_{t1} - \ddot{y}_{t2} - \dot{\theta}_{t1} l_9) \right] + \left[(F_{sy1} + F_{sy2} + F_{sy3} + F_{sy4} + F_{sy5} + \right. \quad (4-271)$$

$$\begin{aligned}
& F_{sy6} \Big) - \frac{l_{11}}{l_{10}} (F_{sy7} + F_{sy8}) - \frac{l_4+l_{11}}{l_{10}} (F_{sy9} + F_{sy10}) - (m_{t1}g) \Big] + \\
& \Big[(F_{dsy1} + F_{dsy2} + F_{dsy3} + F_{dsy4} + F_{dsy5} + F_{dsy6}) - \frac{l_{11}}{l_{10}} (F_{dsy7} + F_{dsy8}) - \\
& \frac{l_4+l_{11}}{l_{10}} (F_{dsy9} + F_{dsy10}) \Big] = 0
\end{aligned}$$

Again to simplify the equation some variables are defined as follows:

$$S_{a1} = \frac{I_{zt2}}{l_{10}^2} + m_{t1}$$

$$\begin{aligned}
B_{t1} = & m_{t1}g - \Big[(F_{sy1} + F_{sy2} + F_{sy3} + F_{sy4} + F_{sy5} + F_{sy6}) - \frac{l_{11}}{l_{10}} (F_{sy7} + F_{sy8}) - \\
& \frac{l_4+l_{11}}{l_{10}} (F_{sy9} + F_{sy10}) + (F_{dsy1} + F_{dsy2} + F_{dsy3} + F_{dsy4} + F_{dsy5} + F_{dsy6}) - \frac{l_{11}}{l_{10}} (F_{dsy7} + \\
& F_{dsy8}) - \frac{l_4+l_{11}}{l_{10}} (F_{dsy9} + F_{dsy10}) \Big]
\end{aligned}$$

Therefore equation (4-271) will be simplified to:

$$S_{a1}\ddot{y}_{t1} - S_{a2}\ddot{y}_{t2} - S_{a3}\ddot{\theta}_{t1} = B_{t1} \quad (4-272)$$

Also, by applying the Lagrange's equation to θ_{t1} :

$$\begin{aligned}
& \Big[I_{zt1}\ddot{\theta}_{t1} - \frac{I_{zt2}l_9}{l_{10}^2} (\ddot{y}_{t1} - \ddot{y}_{t2} - \ddot{\theta}_{t1}l_9) \Big] + \Big[l_7(F_{sy1} + F_{sy2}) - l_8(F_{sy3} + F_{sy4}) - \\
& (l_2 + l_8)(F_{sy5} + F_{sy6}) + \frac{l_9l_{11}}{l_{10}} (F_{sy7} + F_{sy8}) + \frac{l_9(l_4+l_{11})}{l_{10}} (F_{sy9} + F_{sy10}) \Big] + \\
& \Big[l_7(F_{dsy1} + F_{dsy2}) - l_8(F_{dsy3} + F_{dsy4}) - (l_2 + l_8)(F_{dsy5} + F_{dsy6}) + \\
& \frac{l_9l_{11}}{l_{10}} (F_{dsy7} + F_{dsy8}) + \frac{l_9(l_4+l_{11})}{l_{10}} (F_{dsy9} + F_{dsy10}) \Big] = 0
\end{aligned} \quad (4-273)$$

Once again to simplify the equation some variables need to be defined as follows:

$$S_{b3} = I_{zt1} + \frac{I_{zt2}l_9}{l_{10}^2}$$

$$B_{t3} = - \left[\left[l_7(F_{sy1} + F_{sy2}) - l_8(F_{sy3} + F_{sy4}) - (l_2 + l_8)(F_{sy5} + F_{sy6}) + \frac{l_9 l_{11}}{l_{10}}(F_{sy7} + F_{sy8}) + \frac{l_9(l_4 + l_{11})}{l_{10}}(F_{sy9} + F_{sy10}) \right] + \left[l_7(F_{dsy1} + F_{dsy2}) - l_8(F_{dsy3} + F_{dsy4}) - (l_2 + l_8)(F_{dsy5} + F_{dsy6}) + \frac{l_9 l_{11}}{l_{10}}(F_{dsy7} + F_{dsy8}) + \frac{l_9(l_4 + l_{11})}{l_{10}}(F_{dsy9} + F_{dsy10}) \right] \right]$$

Therefore equation (4-273) will be simplified to:

$$-S_{a3}\ddot{y}_{t1} + S_{a3}\ddot{y}_{t2} + S_{b3}\ddot{\theta}_{t1} = B_{t3} \quad (4-274)$$

By adding equations (2-270) and (2-272),

$$(S_{a1} - S_{a2})\ddot{y}_{t1} - (S_{a2} - S_{c2})\ddot{y}_{t2} = B_{t1} + B_{t4} \quad (4-275)$$

Also by multiplying S_{b3} and S_{a3} to equations (4-274) and (4-275), respectively,

$$(S_{a1}S_{b3} - S_{a3}^2)\ddot{y}_{t1} - (S_{a2}S_{b3} - S_{a3}^2)\ddot{y}_{t2} = S_{b3}B_{t1} + S_{a3}B_{t3} \quad (4-276)$$

By defining the following expressions, equations (4-275) and (4-276) are simplified to equations (4-277) and (4-278), respectively,

$$e_1 = S_{a1} - S_{a2}$$

$$e_2 = S_{a2} - S_{c2}$$

$$e_3 = S_{a1}S_{b3} - S_{a3}^2$$

$$e_4 = S_{a2}S_{b3} - S_{a3}^2$$

$$e_1\ddot{y}_{t1} - e_2\ddot{y}_{t2} = B_{t1} + B_{t4} \quad (4-277)$$

$$e_3\ddot{y}_{t1} - e_4\ddot{y}_{t2} = S_{b3}B_{t1} + S_{a3}B_{t3} \quad (4-278)$$

Solving equations (4-277) and (4-278) for \ddot{y}_{t1} and \ddot{y}_{t2} will lead to:

$$\ddot{y}_{t1} = \frac{e_4(B_{t1} + B_{t4}) - e_2(S_{b3}B_{t1} + S_{a3}B_{t3})}{e_1e_4 - e_2e_3} \quad (4-279)$$

$$\ddot{y}_{t2} = \frac{e_1 \left(\frac{e_4(B_{t1} + B_{t4}) - e_2(S_{b3}B_{t1} + S_{a3}B_{t3})}{e_1e_4 - e_2e_3} \right) - \frac{B_{t1} + B_{t4}}{e_2}}{e_2} \quad (4-280)$$

Substituting equations (4-279) and (4-280) into equation (4-274) will give,

$$\ddot{\theta}_{t1} = \frac{B_{t3}}{S_{b3}} + \frac{S_{a3}}{S_{b3}} \left(\frac{e_4(B_{t1}+B_{t4}) - e_2(S_{b3}B_{t1}+S_{a3}B_{t3})}{e_1e_4 - e_2e_3} \right) - \frac{S_{a3}}{S_{b3}} \left(\frac{e_1 \left(\frac{e_4(B_{t1}+B_{t4}) - e_2(S_{b3}B_{t1}+S_{a3}B_{t3})}{e_1e_4 - e_2e_3} \right)}{e_2} - \frac{B_{t1}+B_{t4}}{e_2} \right)$$
(4-281)

By applying the Lagrange's equation to φ_{t1} , φ_{t2} , φ_{t3} , y_{t3} , θ_{t3} :

$$I_{xt1}\ddot{\varphi}_{t1} + \left[\left(\frac{s_1}{2} \right) (F_{sy1} - F_{sy2}) + \left(\frac{s_2}{2} \right) (F_{sy3} - F_{sy4}) + \left(\frac{s_3}{2} \right) (F_{sy5} - F_{sy6}) \right] + \left[\left(\frac{s_1}{2} \right) (F_{dsy1} - F_{dsy2}) + \left(\frac{s_2}{2} \right) (F_{dsy3} - F_{dsy4}) + \left(\frac{s_3}{2} \right) (F_{dsy5} - F_{dsy6}) \right] = 0$$
(4-282)

$$I_{xt2}\ddot{\varphi}_{t2} + \left[\left(\frac{s_4}{2} \right) (F_{sy7} - F_{sy8}) + \left(\frac{s_5}{2} \right) (F_{sy9} - F_{sy10}) \right] + \left[\left(\frac{s_4}{2} \right) (F_{dsy7} - F_{dsy8}) + \left(\frac{s_5}{2} \right) (F_{dsy9} - F_{dsy10}) \right] = 0$$
(4-283)

$$I_{xt3}\ddot{\varphi}_{t3} + \left[\left(\frac{s_6}{2} \right) (F_{sy11} - F_{sy12}) + \left(\frac{s_7}{2} \right) (F_{sy13} - F_{sy14}) + \left(\frac{s_8}{2} \right) (F_{sy15} - F_{sy16}) \right] + \left[\left(\frac{s_6}{2} \right) (F_{dsy11} - F_{dsy12}) + \left(\frac{s_7}{2} \right) (F_{dsy13} - F_{dsy14}) + \left(\frac{s_8}{2} \right) (F_{dsy15} - F_{dsy16}) \right] = 0$$
(4-284)

$$m_{t3}\ddot{y}_{t3} + (F_{sy11} + F_{sy12} + F_{sy13} + F_{sy14} + F_{sy15} + F_{sy16}) + (F_{dsy11} + F_{dsy12} + F_{dsy13} + F_{dsy14} + F_{dsy15} + F_{dsy16}) - m_{t3}g = 0$$
(4-285)

$$I_{zt3}\ddot{\theta}_{t3} + [l_{13}(F_{sy11} + F_{sy12}) - l_{14}(F_{sy13} + F_{sy14}) - (l_{14} + l_{12})(F_{sy15} + F_{sy16})] + [l_{13}(F_{dsy11} + F_{dsy12}) - l_{14}(F_{dsy13} + F_{dsy14}) - (l_{14} + l_{12})(F_{dsy15} + F_{dsy16})] = 0$$
(4-286)

The rest of degrees of freedom will be as follows:

$$m_{a1}\ddot{y}_{a1} - (F_{sy1} + F_{sy2}) + (F_{ty1} + F_{ty2}) - (F_{dsy1} + F_{dsy2}) + (F_{dty1} + F_{dty2}) = m_{a1}g$$
(4-287)

$$I_{xa1}\ddot{\varphi}_{a1} - (\frac{s_1}{2})(F_{sy1} - F_{sy2}) + (\frac{d_1}{2})(F_{ty1} - F_{ty2}) - (\frac{s_1}{2})(F_{dsy1} - F_{dsy2}) +$$
(4-288)

$$(\frac{d_1}{2})(F_{dty1} - F_{dty2}) = 0$$

$$m_{a2}\ddot{y}_{a2} - (F_{sy3} + F_{sy4}) + (F_{ty3} + F_{ty4}) - (F_{dsy3} + F_{dsy4}) + (F_{dty3} + F_{dty4}) = m_{a2}g \quad (4-289)$$

$$I_{xa2}\ddot{\phi}_{a2} - (\frac{s_2}{2})(F_{sy3} - F_{sy4}) + (\frac{d_2}{2})(F_{ty3} - F_{ty4}) - (\frac{s_2}{2})(F_{dsy3} - F_{dsy4}) + (\frac{d_2}{2})(F_{dty3} - F_{dty4}) = 0 \quad (4-290)$$

$$m_{a3}\ddot{y}_{a3} - (F_{sy5} + F_{sy6}) + (F_{ty5} + F_{ty6}) - (F_{dsy5} + F_{dsy6}) + (F_{dty5} + F_{dty6}) = m_{a3}g \quad (4-291)$$

$$I_{xa3}\ddot{\phi}_{a3} - (\frac{s_3}{2})(F_{sy5} - F_{sy6}) + (\frac{d_3}{2})(F_{ty5} - F_{ty6}) - (\frac{s_3}{2})(F_{dsy5} - F_{dsy6}) + (\frac{d_3}{2})(F_{dty5} - F_{dty6}) = 0 \quad (4-292)$$

$$m_{a4}\ddot{y}_{a4} - (F_{sy7} + F_{sy8}) + (F_{ty7} + F_{ty8}) - (F_{dsy7} + F_{dsy8}) + (F_{dty7} + F_{dty8}) = m_{a4}g \quad (4-293)$$

$$I_{xa4}\ddot{\phi}_{a4} - (\frac{s_4}{2})(F_{sy7} - F_{sy8}) + (\frac{d_4}{2})(F_{ty7} - F_{ty8}) - (\frac{s_4}{2})(F_{dsy7} - F_{dsy8}) + (\frac{d_4}{2})(F_{dty7} - F_{dty8}) = 0 \quad (4-294)$$

$$m_{a5}\ddot{y}_{a5} - (F_{sy9} + F_{sy10}) + (F_{ty9} + F_{ty10}) - (F_{dsy9} + F_{dsy10}) + (F_{dty9} + F_{dty10}) = m_{a5}g \quad (4-295)$$

$$I_{xa5}\ddot{\phi}_{a5} - (\frac{s_5}{2})(F_{sy9} - F_{sy10}) + (\frac{d_5}{2})(F_{ty9} - F_{ty10}) - (\frac{s_5}{2})(F_{dsy9} - F_{dsy10}) + (\frac{d_5}{2})(F_{dty9} - F_{dty10}) = 0 \quad (4-296)$$

$$m_{a6}\ddot{y}_{a6} - (F_{sy11} + F_{sy12}) + (F_{ty11} + F_{ty12}) - (F_{dsy11} + F_{dsy12}) + (F_{dty11} + F_{dty12}) = m_{a6}g \quad (4-297)$$

$$I_{xa6}\ddot{\varphi}_{a6} - \left(\frac{s_6}{2}\right)(F_{sy11} - F_{sy12}) + \left(\frac{d_6}{2}\right)(F_{ty11} - F_{ty12}) - \left(\frac{s_6}{2}\right)(F_{dsy11} - F_{dsy12}) + \left(\frac{d_6}{2}\right)(F_{dty11} - F_{dty12}) = 0 \quad (4-298)$$

$$m_{a7}\ddot{y}_{a7} - (F_{sy13} + F_{sy14}) + (F_{ty13} + F_{ty14}) - (F_{dsy13} + F_{dsy14}) + (F_{dty13} + F_{dty14}) = m_{a7}g \quad (4-299)$$

$$I_{xa7}\ddot{\varphi}_{a7} - \left(\frac{s_7}{2}\right)(F_{sy13} - F_{sy14}) + \left(\frac{d_7}{2}\right)(F_{ty13} - F_{ty14}) - \left(\frac{s_7}{2}\right)(F_{dsy13} - F_{dsy14}) + \left(\frac{d_7}{2}\right)(F_{dty13} - F_{dty14}) = 0 \quad (4-300)$$

$$m_{a8}\ddot{y}_{a8} - (F_{sy15} + F_{sy16}) + (F_{ty15} + F_{ty16}) - (F_{dsy15} + F_{dsy16}) + (F_{dty15} + F_{dty16}) = m_{a8}g \quad (4-301)$$

$$I_{xa8}\ddot{\varphi}_{a8} - \left(\frac{s_8}{2}\right)(F_{sy15} - F_{sy16}) + \left(\frac{d_8}{2}\right)(F_{ty15} - F_{ty16}) - \left(\frac{s_8}{2}\right)(F_{dsy15} - F_{dsy16}) + \left(\frac{d_8}{2}\right)(F_{dty15} - F_{dty16}) = 0 \quad (4-302)$$

4.14 Road Surface Roughness

Road surface roughness is an important factor when it comes to the dynamic response of bridges and their interaction with the moving vehicles. Many different methods for road profile generation have been proposed during the past decades but there have been two main methods used by the most of researchers trying to capture the real behavior of bridge-vehicle interaction.

The first method which will be used in this research was proposed by Dodds and Robson [25]. These researchers basically developed power spectral density (PSD) functions and validated these functions with the data recorded at the field. The function that they came up with is,

$$\varphi(n) = \begin{cases} \varphi(n_0) \left(\frac{n}{n_0}\right)^{-w_1}, & n \leq n_0 \\ \varphi(n_0) \left(\frac{n}{n_0}\right)^{-w_2}, & n \geq n_0 \end{cases} \quad (4-303)$$

In this equation,

$\varphi(n)$ is the PSD and has the unit of $m^2/\text{cycle}/m$

n is the wave number and has the unit of cycle/m

n_0 is the discontinuity frequency and has the value of $n_0 = \frac{1}{2\pi}$ cycle/m

$\varphi(n_0)$ is the roughness coefficient or the value of the power spectral density at the discontinuity frequency point (n_0) and has the unit of $m^2/\text{cycle}/m$

And w_1 and w_2 are roughness exponents.

According to Dodds and Robson [25], $\varphi(n_0)$ depends on the road type and road surface condition and the values of w_1 and w_2 are only related to the type of the road.

In this study, “Good” surface condition for the “Principal Roads” is assumed and mean values of 20, 2.05, 1.44 are chosen for $\varphi(n_0)$, w_1 and w_2 , respectively.

By plugging the values of n_0 , $\varphi(n_0)$, w_1 and w_2 in to the equation (4-303) and drawing the graph of the given function in a log-log scale Figure 4-13 is obtained which is a bilinear presentation of the PSD and the point of discontinuity is shown on the graph [26].

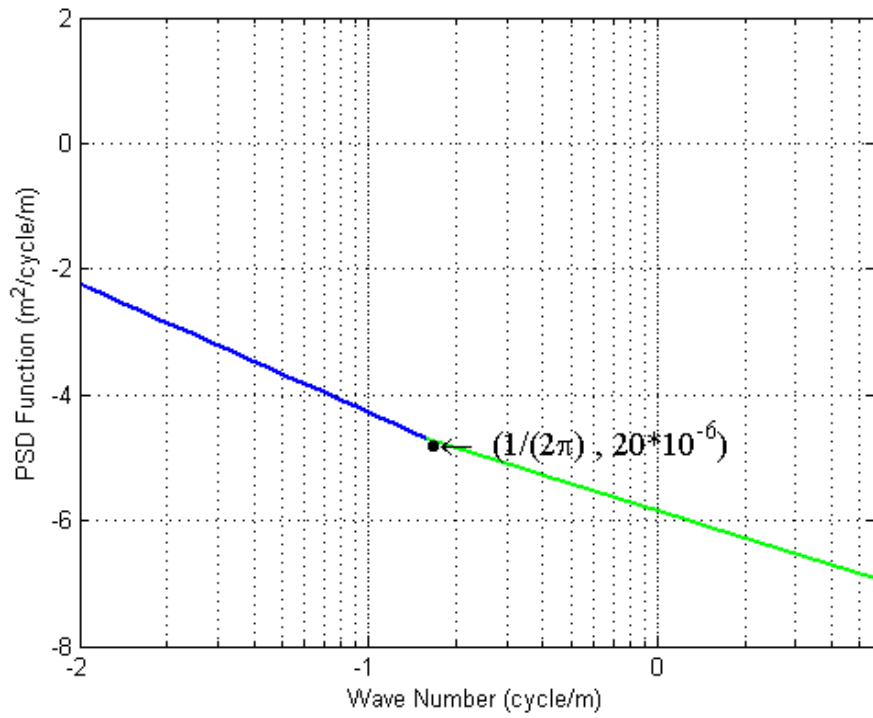


FIGURE 4-13: DODDS AND ROBSON SPECTRUM FOR PRINCIPAL ROADS

In order to create road profiles, some random numbers with Gaussian distribution and zero mean should be generated. This can be done by different methods such as the random numbers generation tools in Matlab software. These numbers then should be passed through some filters to get the form of equation (4-303). The obtained numbers show the road surface profile of the bridge and they can present the actual behavior of a bridge surface. The result for one of the surface conditions (“Very Good” Condition”) using this method is shown in Figure 4-14. This profile is only used for the left wheels and a different profile will be used for the right wheel.

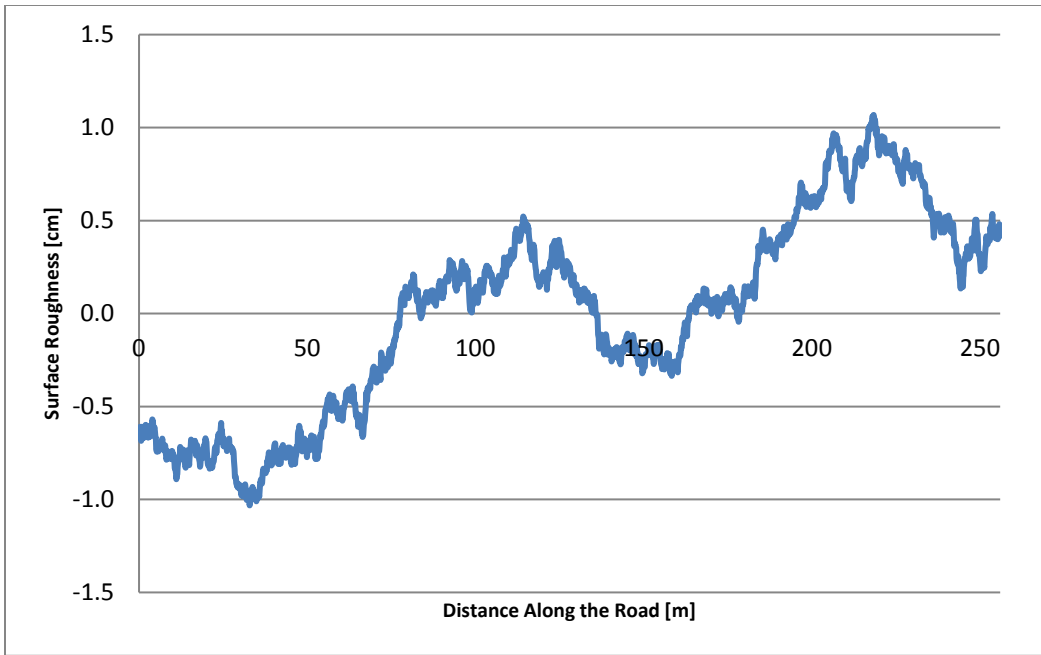


FIGURE 4-14: ROAD SURFACE ROUGHNESS FOR “VERY GOOD” CONDITION

The second method which was proposed by Honda et al. [26] involves a different power spectral density (PSD) function with different values for the exponent and the coefficient which were calculated using least square method. It should also be noted that recently some new methods using non-Gaussian process and also using Laplace model have been proposed by some researchers in Sweden but since the reliability of these models have not been verified by any other researchers around the world they are not used in this research.

All the methods so far can be used to generate a road profile for a bridge in the longitudinal direction but there have been some studies such as Liu et al. [23] in which efforts have been made to investigate the effects of transverse undulation in bridges. But since no significant effects have been reported by these studies on the importance of

considering transverse road surface, only one direction road surface profile has been taken into consideration in this research.

5. Dynamic Amplification Factor Analysis

5.1 Tire Truck Forces on the Road

Equations of motion for the trucks given in section 4.3.1 due to effects of different levels of road surface roughness described in section 4.4 were solved using the ODE45 function in MATLAB. This function which uses Runge-Kutta method (with 0.005 second integration time step) is the most common MATLAB function to solve “Ordinary Differential Equations”. The impact factors for the suspensions and tires were also calculated for different truck speeds as the ratio of the maximum dynamic force to the static force in the suspension or the tire. The results for the impact factors of tires and suspensions of the H-20 truck front and rear axles can be seen in Table 5.1 and Table 5.2, respectively.

TABLE 5-1: TIRE IMPACT FACTORS OF H-20 TRUCK

Vehicle Speed [mph]	Tire Impact Factor [%]			
	"Very Good" Surface Condition		"Good" Surface Condition	
	Front Axle	Rear Axle	Front Axle	Rear Axle
15	11.7	13.2	10.1	27.9
25	10.2	11.9	9.5	28.1
35	6.6	10.2	14.5	20.0
45	5.8	25.3	19.1	22.6
55	6.8	15.9	22.9	40.7
65	9.4	16.2	22.9	25.2
75	8.6	16.4	24.4	23.3

It can be observed from the above table that the values of impact factor for the rear axle (16 kips) are generally higher than those values of the front axle (4 kips) which is lighter. Also the impact factor values for the tires are in some cases close or higher than 33%.

TABLE 5-2: SUSPENSION IMPACT FACTORS OF H-20 TRUCK

Vehicle Speed [mph]	Suspension Impact Factor [%]			
	"Very Good" Surface Condition		"Good" Surface Condition	
	Front Axle	Rear Axle	Front Axle	Rear Axle
15	23.7	51.7	26.7	80.7
25	21.7	52.4	23.9	80.4
35	14.6	56.3	29.4	58.6
45	15.8	77.0	32.9	68.2
55	17.5	58.1	31.7	98.6
65	20.9	59.7	32.8	73.0
75	15.7	58.4	31.9	80.9

Higher impact factors for the rear axle can also be observed in Table 5.2 but the impact factors of the suspension are much higher than the impact factors calculated from the tire responses.

To obtain a better understanding of the road surface roughness effects on the truck responses, the results of the analyses for “Type 2S2” truck for all four levels of the road surface is shown in Figure 5.1. From this figure it can be pointed out that in the case of trucks traveling on the road, the vehicle speed seems to have more effects on the impact factor when the road surface roughness is “Average” or “Poor” comparing to the cases of “Very Good” and “Good” surface conditions. It can also be seen that as the road surface undulations increase, (i.e. moving from the “Very Good” surface condition to “Poor” surface condition) the impact factor which is the ratio between the dynamic response and

the static response of the vehicle rises significantly. This increase can be more than 100% at times. It should be noted that this value is different from the dynamic load allowance which is 33% by the AASHTO LRFD Bridge Design Specifications [11] and the dynamic load allowance results will be calculated in the next section using the interaction of the vehicle and the bridge.

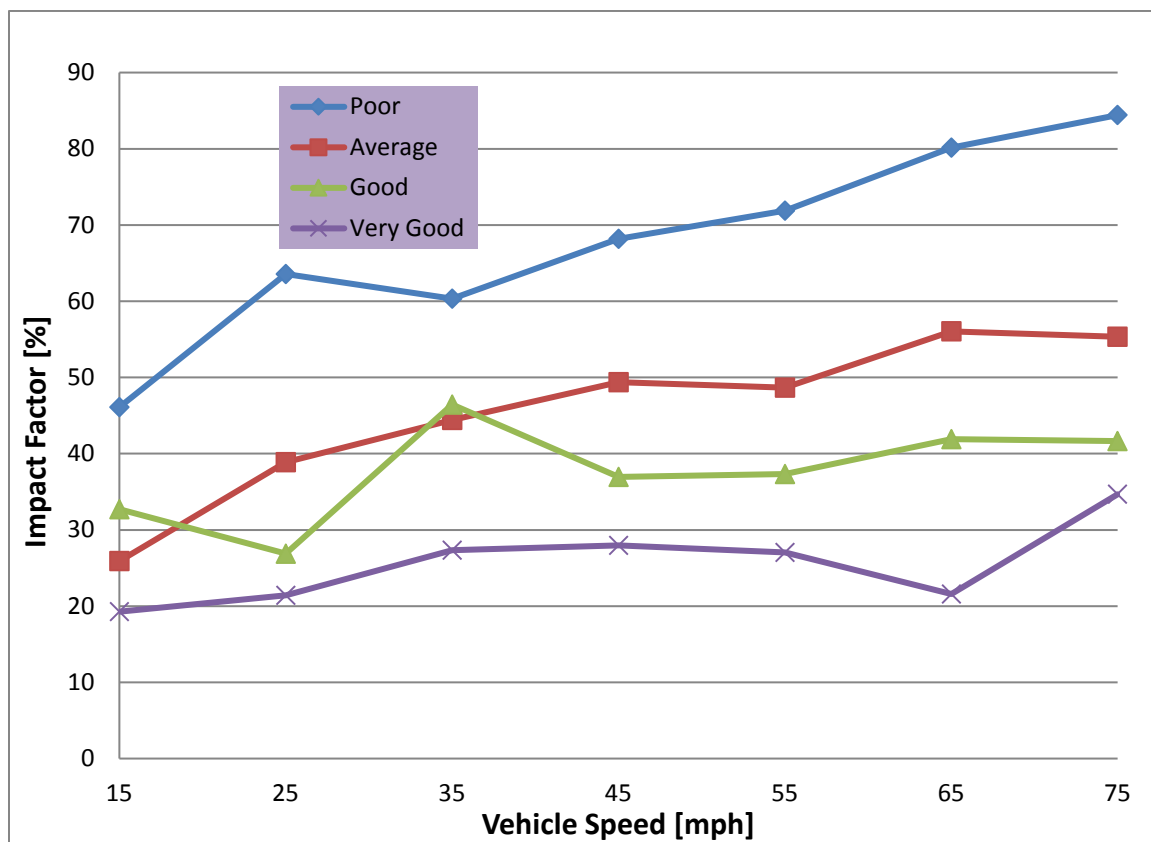


FIGURE 5-1: TYPE 2S2 TRUCK IMPACT FACTORS

In order to comprehend the effects of different trucks on the bridges it is necessary to compare the results of all different trucks but it should be noted the gross vehicle weight should also be taken into account. Also determining that which truck has more detrimental effects on the bridges without actually putting the loads on the bridge and calculating resulted moments, shears and stresses is not possible.

Table 5.3 shows the maximum tire impact factors for all the trucks when the truck is traveling at 35 mph. The impact factor is defined as the ratio of the dynamic force to the static force.

TABLE 5-3: TIRE IMPACT FACTORS FOR ALL TRUCKS [35 MPH SPEED]

Truck Type	Road Surface Condition	
	"Very Good"	"Good"
H-20	10.2	20.0
HS-20	15.7	28.3
Type 3	30.8	38.1
Type 3S2	24.9	47.4
Type 3S3	38.9	53.9
Type 2S2	27.3	46.4
Type 3S1	41.1	34.8
SU4	42.9	47.3
7 Axle Rocky Mountain Double	37.7	48.8
8 Axle B-Train Double	41.0	52.1
9 Axle Turnpike Double	41.5	51.6

The same information can be found in Table 5.4 regarding the maximum tire impact factors recorded for different trucks when traveling at 25 mph.

TABLE 5-4: TIRE IMPACT FACTORS FOR ALL TRUCKS [25 MPH SPEED]

Truck Type	Road Surface Condition	
	"Very Good"	"Good"
H-20	25.7	22.6
HS-20	23.9	23.5
Type 3	26.8	41.4
Type 3S2	25.7	35.2
Type 3S3	24.1	63.5
Type 2S2	28.0	37.0
Type 3S1	36.1	44.2
SU4	42.4	49.7
7 Axle Rocky Mountain Double	40.0	40.3
8 Axle B-Train Double	40.8	50.6
9 Axle Turnpike Double	40.6	56.3

It can be seen that in many cases the impact factors for the “Very Good” and “Good” surface condition is higher than 33%.

In order to understand the effects of number of trailers, the results have been categorized into three different groups of “Single Unit Truck”, “Truck and Trailer” and “Truck and Double Trailer”. The results for the “Very Good” and “Good” surface condition can be seen in Figure 5.2 and Figure 5.3, respectively.

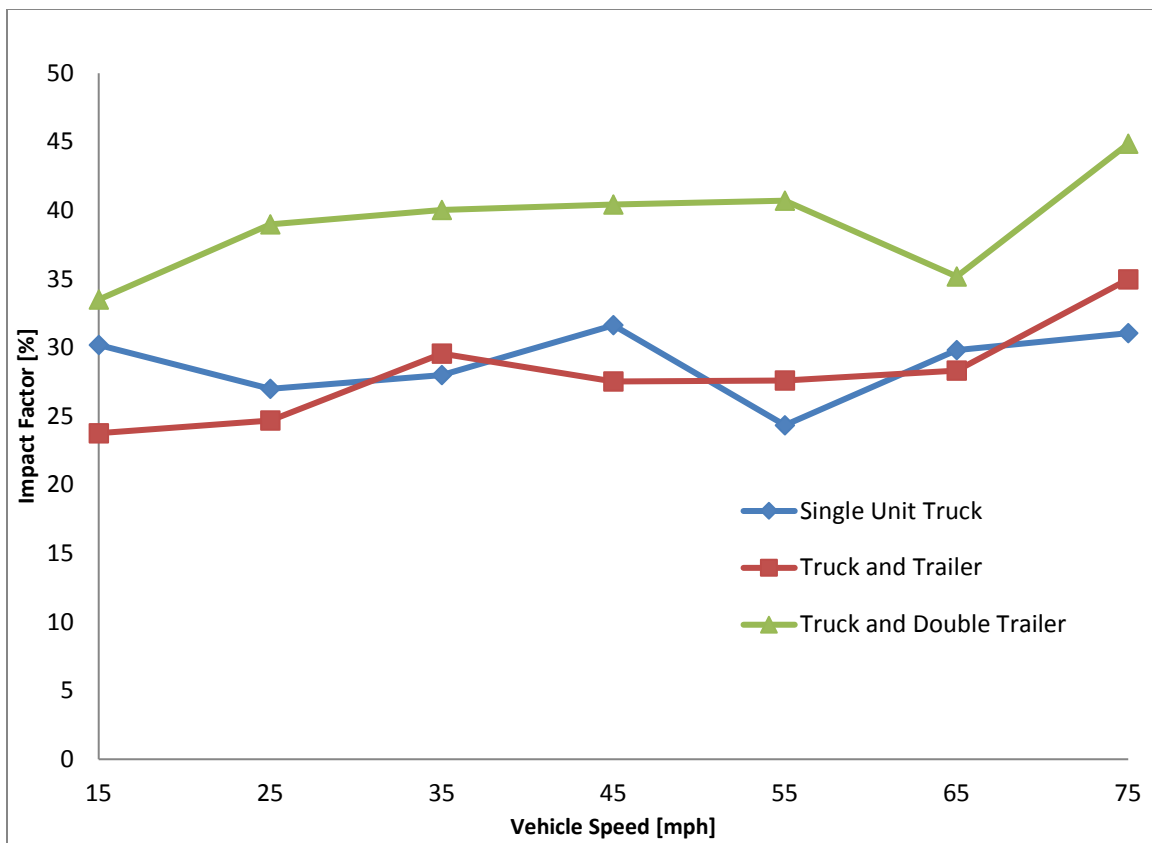


FIGURE 5-2: IMPACT FACTORS OF DIFFERENT TRUCK CATEGORIES FOR “VERY GOOD” SURFACE CONDITION

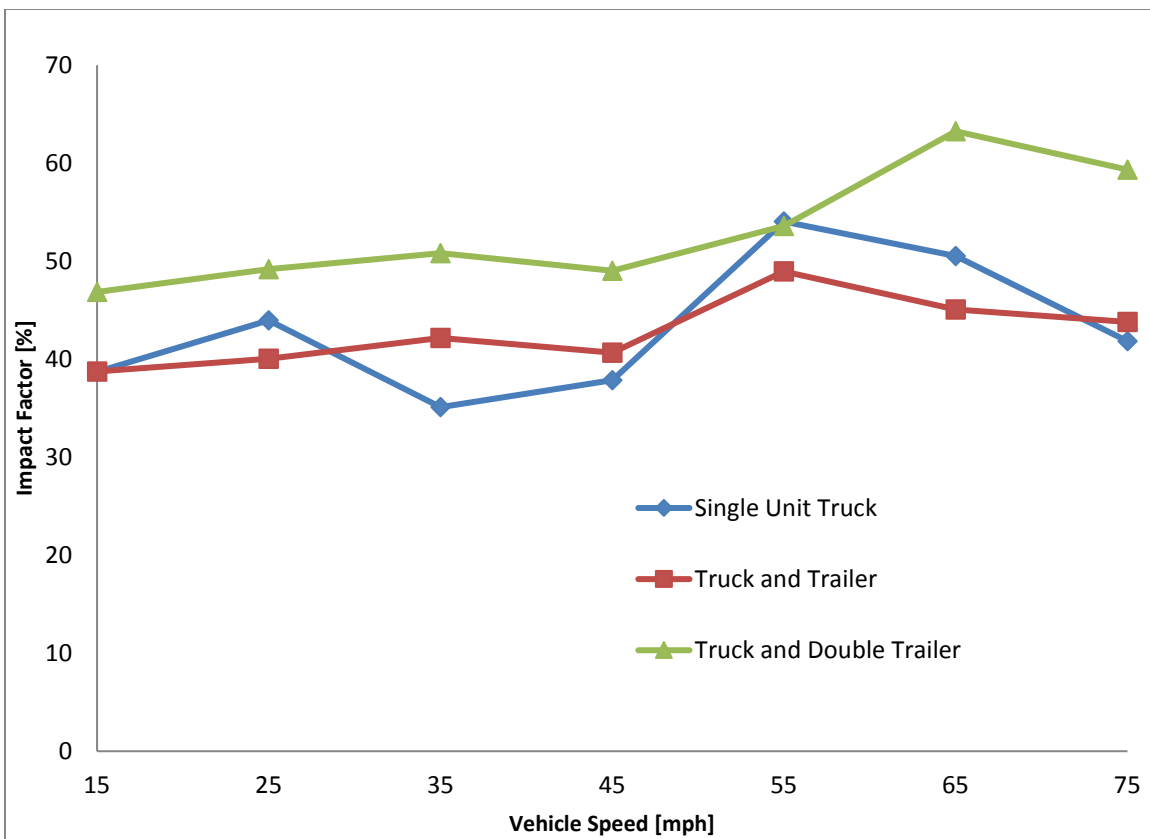


FIGURE 5-3: IMPACT FACTORS OF DIFFERENT TRUCK CATEGORIES FOR “GOOD” SURFACE CONDITION

It can be seen in these two figures that the “Truck and Double Trailer” case has the highest values of impact factor.

5.2 Tire Truck Forces on the Bridge

In this section, the effects of different types of vehicles on different types of bridges will be studied and the Dynamic Amplification Factor (DAF) i.e. the Dynamic Load Allowance will be calculated and compared for different cases of analysis.

The cases here are based on the “Good” and “very Good” road surface condition and four different vehicle speeds of 15, 35, 55, 75 mph have been considered. The analysis was

carried out for two different types of bridges (Steel Bridge and Prestressed Concrete Bridge) with five different span lengths of 30, 60, 90, 120, 140 feet. In order to eliminate the effects of initial vibrations of trucks, it was assumed that each truck started to move from a distance of five times its length before reaching the bridge.

The results of the deflection for the case of "Good" surface condition at a middle point of the bridge (one of the grid points) which has the highest displacement are shown in Figure 5.4 to Figure 5.14 for all eleven types of trucks traveling on the prestressed concrete bridge with the span length of 30 feet. The transverse vehicle location was assumed to be at the far right end of the bridge with a distance of 30 inches from the curb.

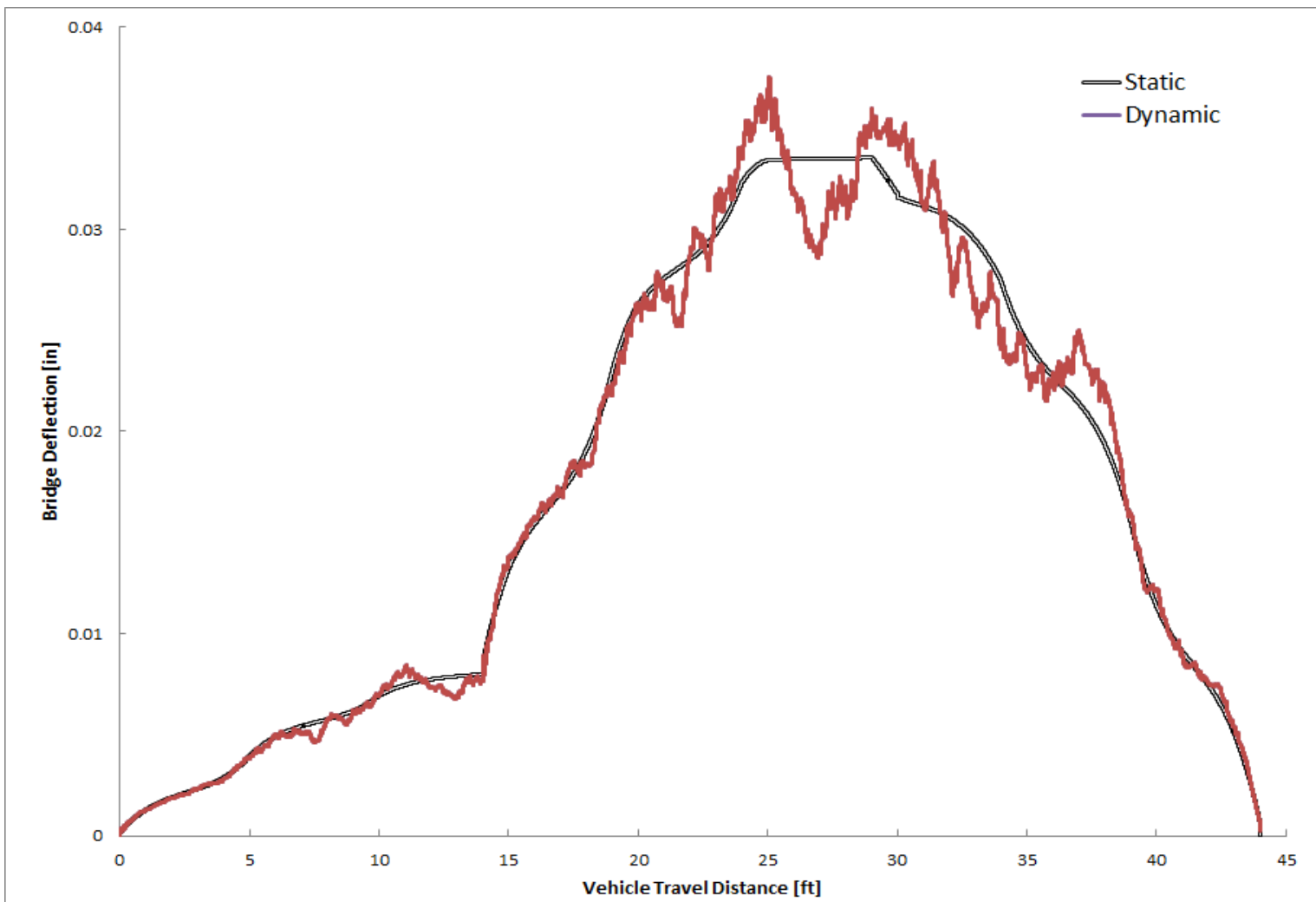


FIGURE 5-4: DISPLACEMENT OF 30 FT. CONCRETE BRIDGE DUE TO H-20 (“GOOD” SURFACE)

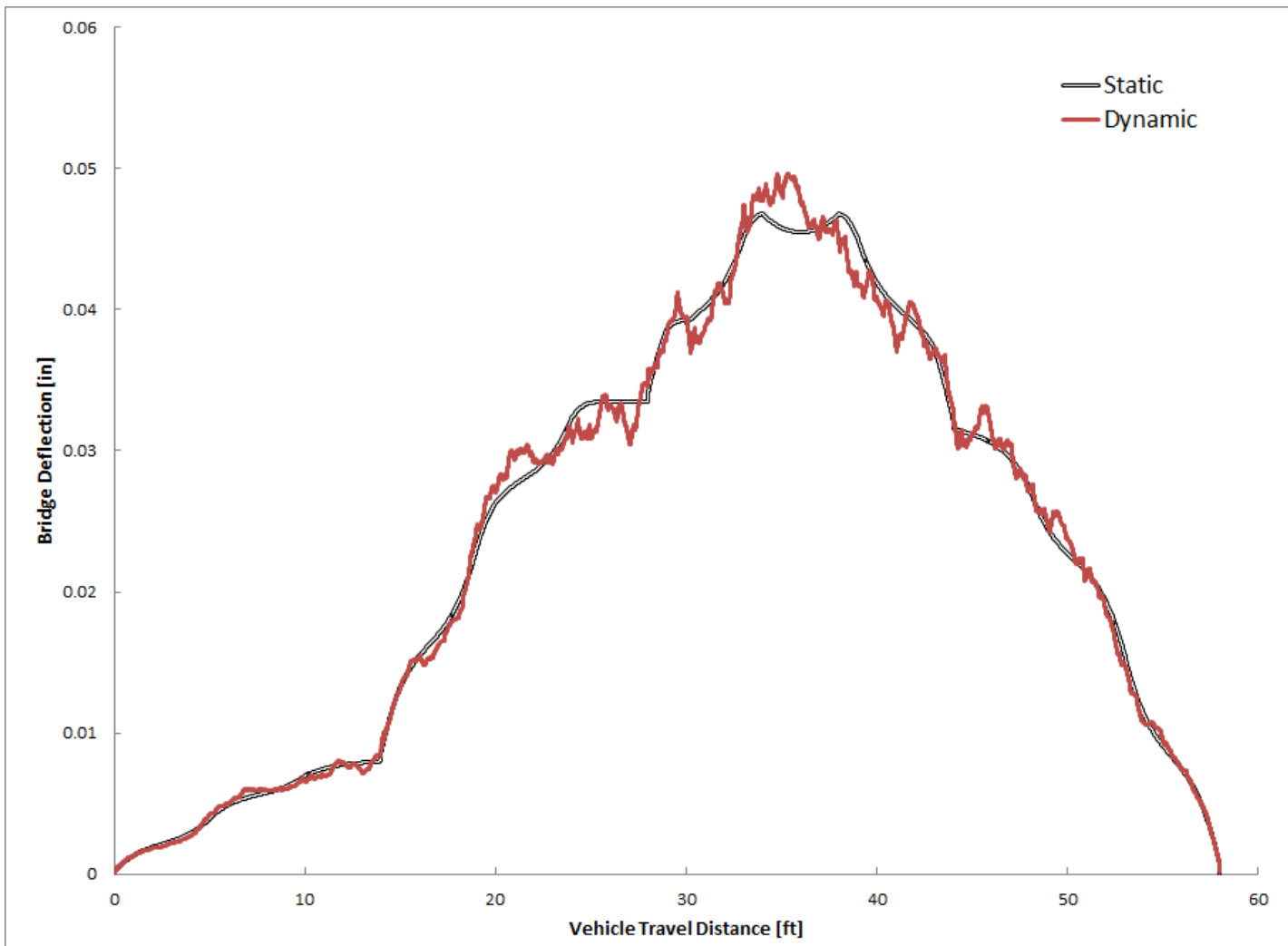


FIGURE 5-5: DISPLACEMENT OF 30 FT. CONCRETE BRIDGE DUE TO HS-20 (“GOOD” SURFACE)

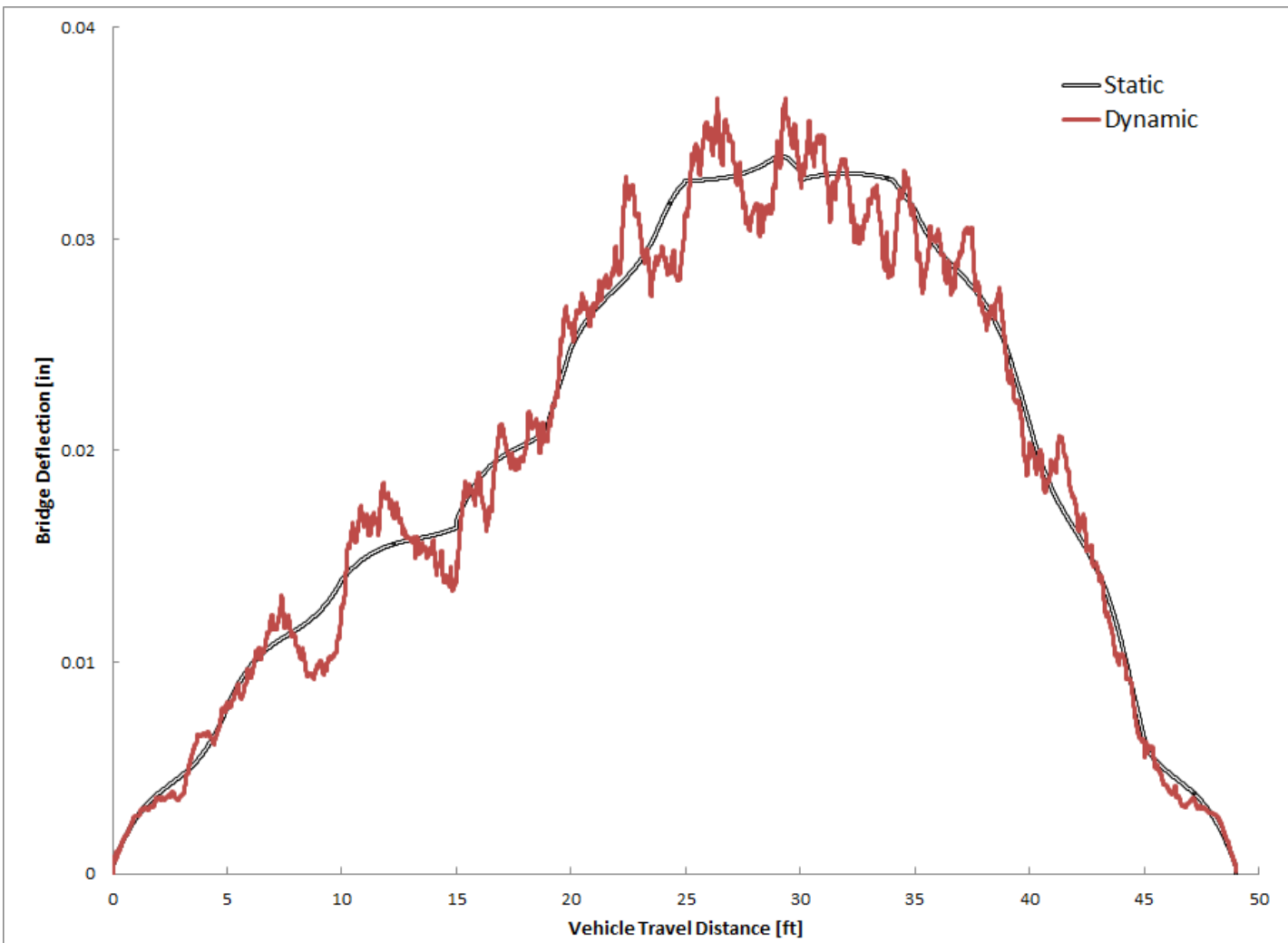


FIGURE 5-6: DISPLACEMENT OF 30 FT. CONCRETE BRIDGE DUE TO TYPE 3 (“GOOD” SURFACE)

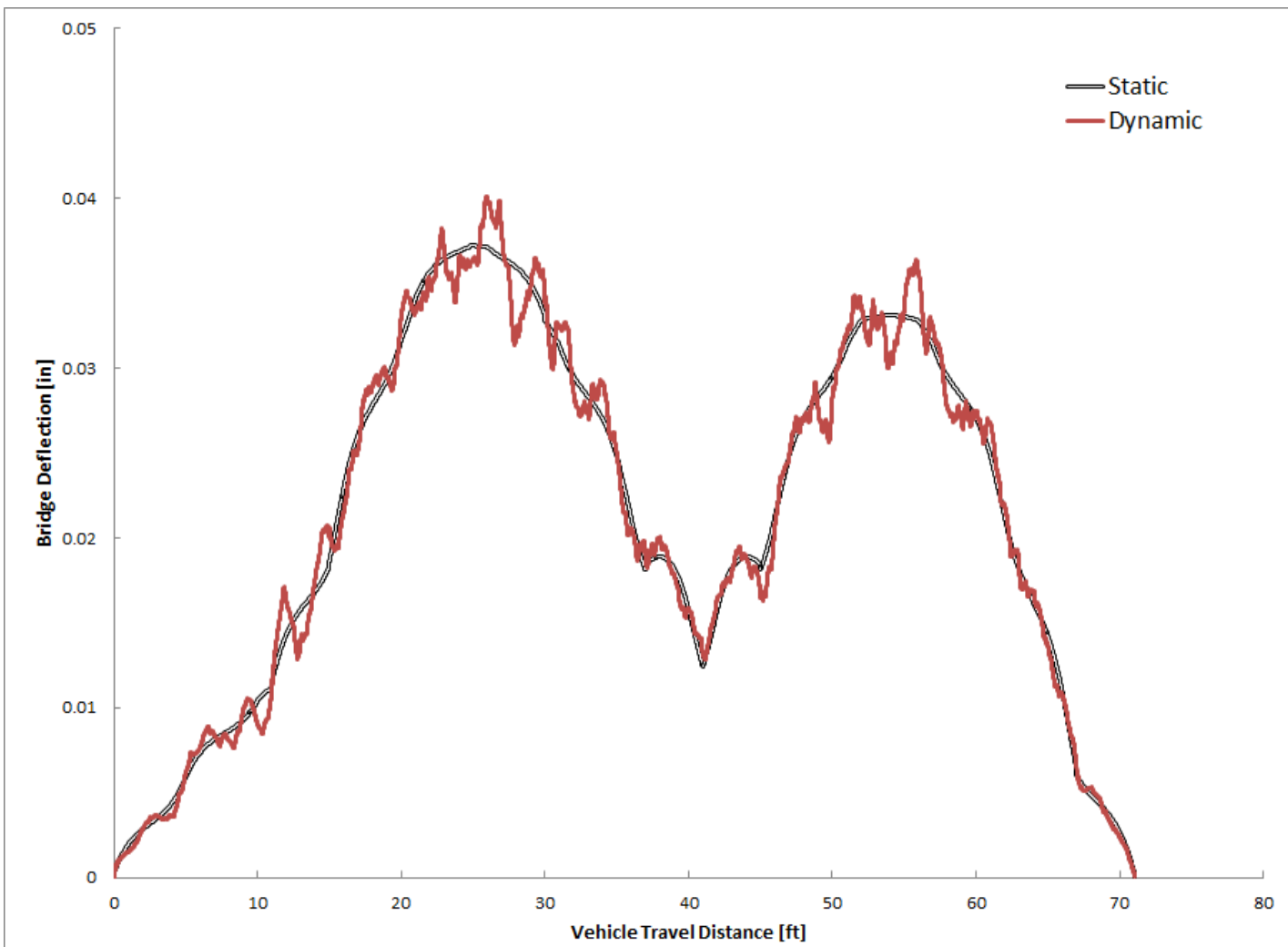


FIGURE 5-7: DISPLACEMENT OF 30 FT. CONCRETE BRIDGE DUE TO TYPE 3S2 (“GOOD” SURFACE)

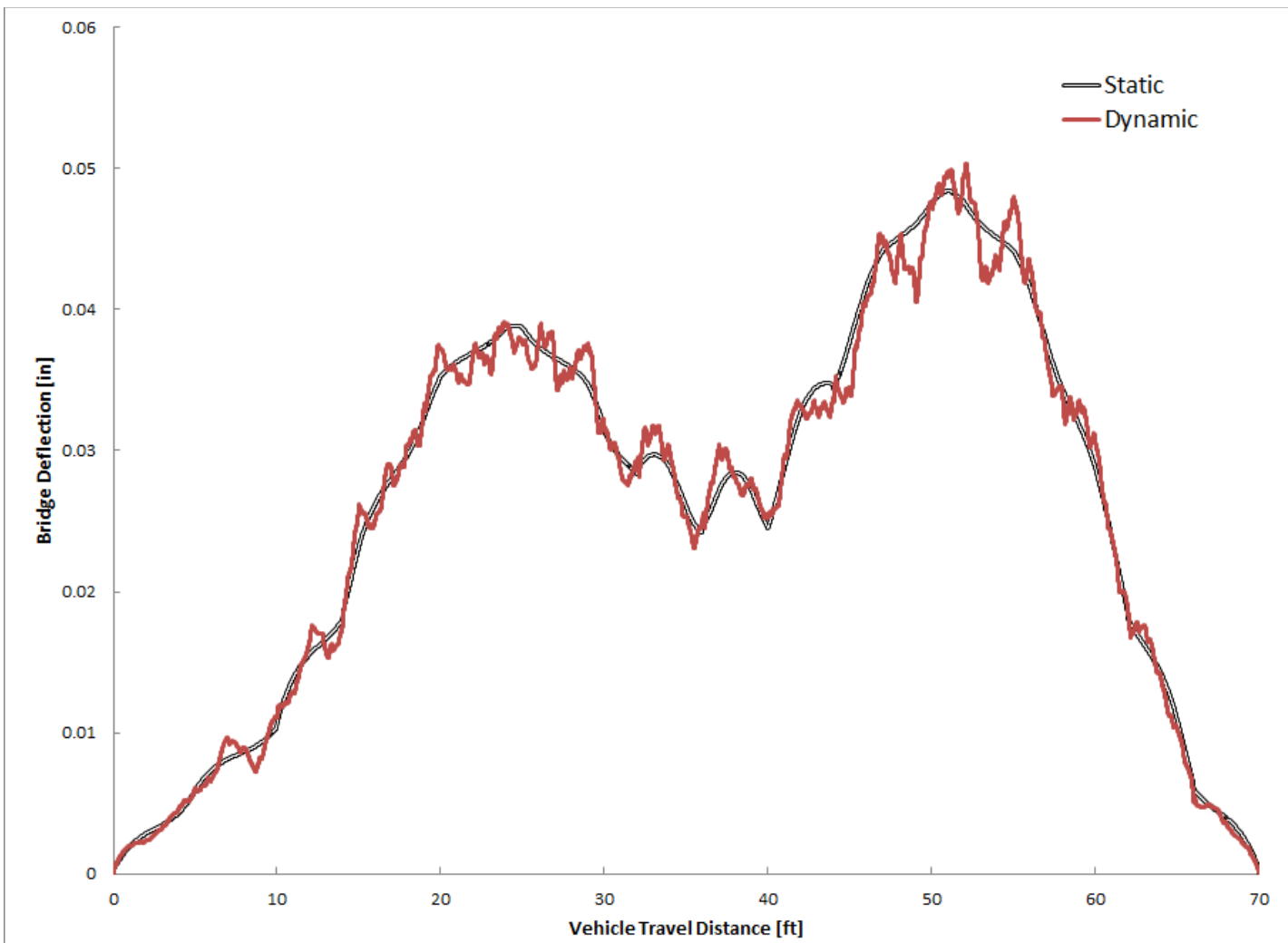


FIGURE 5-8: DISPLACEMENT OF 30 FT. CONCRETE BRIDGE DUE TO TYPE 3S3 (“GOOD” SURFACE)

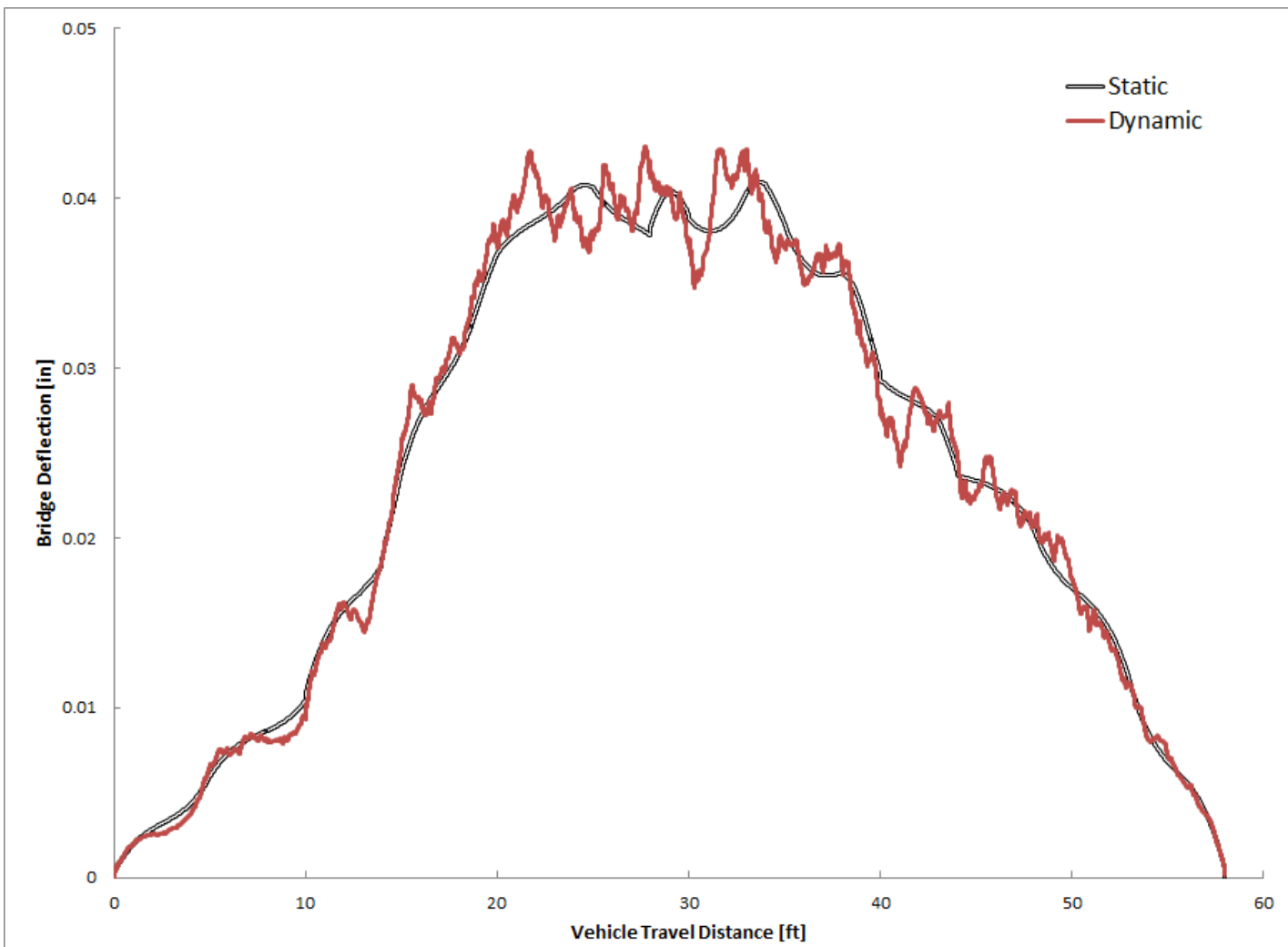


FIGURE 5-9: DISPLACEMENT OF 30 FT. CONCRETE BRIDGE DUE TO TYPE 3S1 (“GOOD” SURFACE)

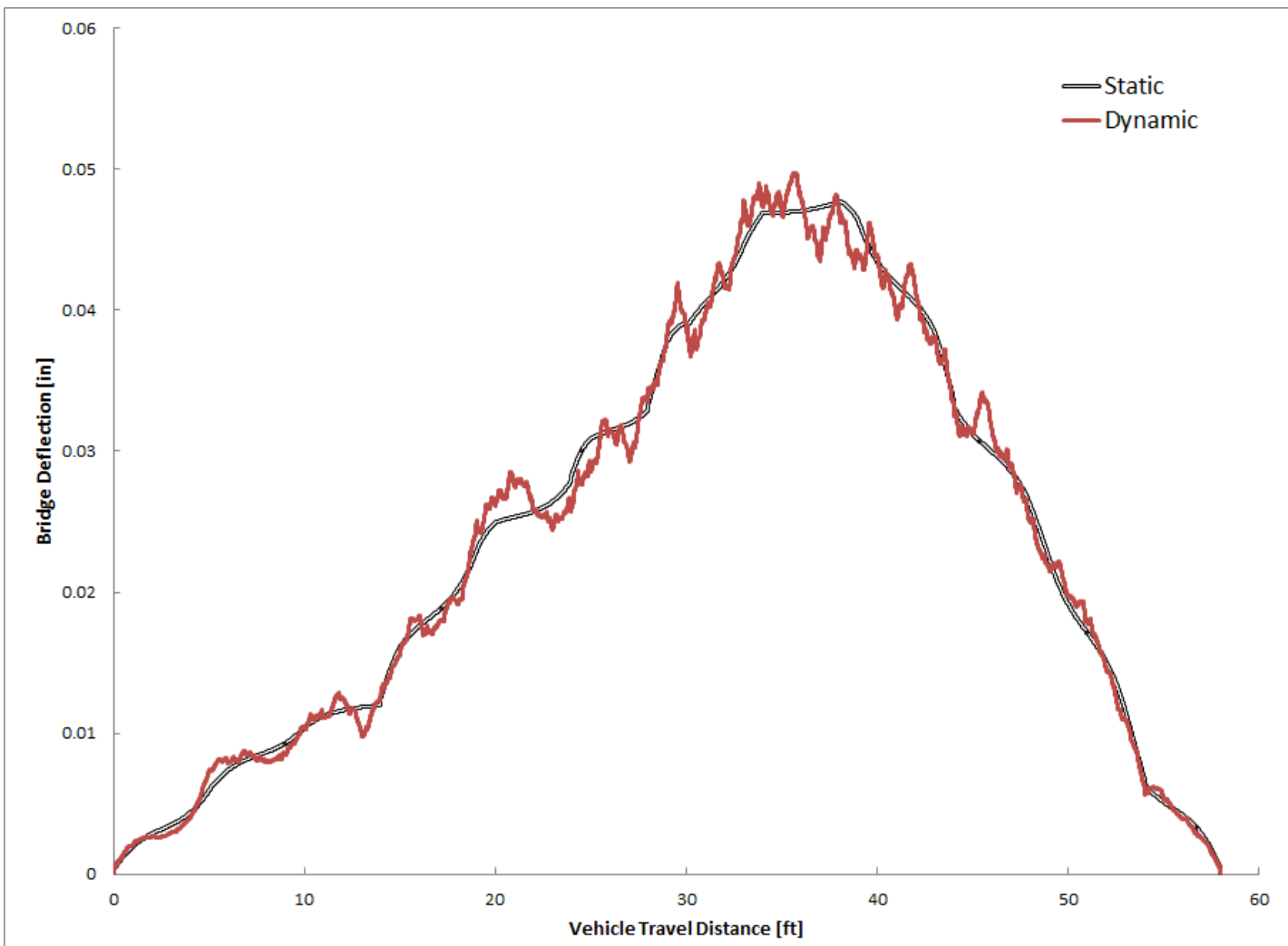


FIGURE 5-10: DISPLACEMENT OF 30 FT. CONCRETE BRIDGE DUE TO TYPE 2S2 (“GOOD” SURFACE)

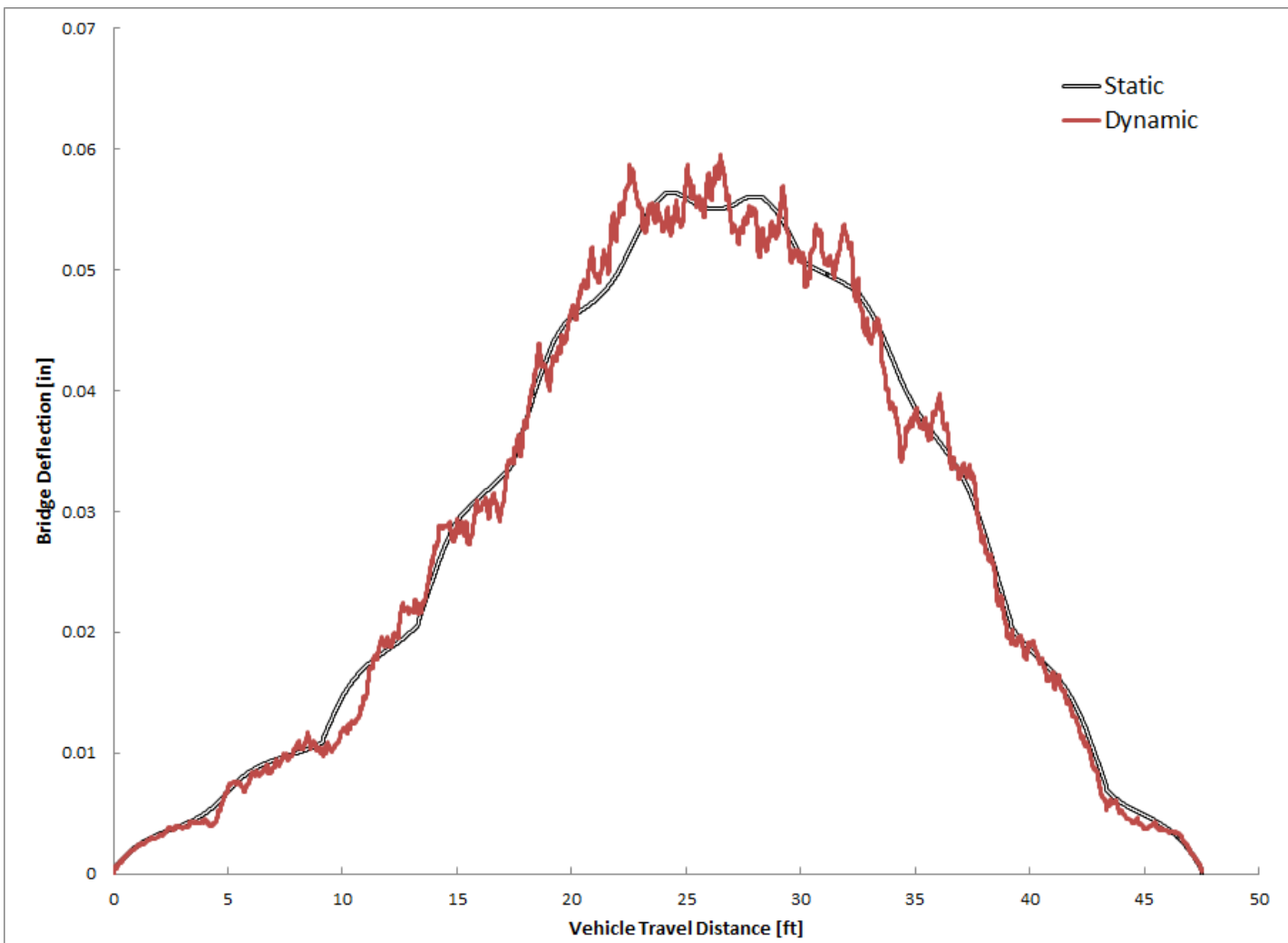


FIGURE 5-11: DISPLACEMENT OF 30 FT. CONCRETE BRIDGE DUE TO SU4 (“GOOD” SURFACE)

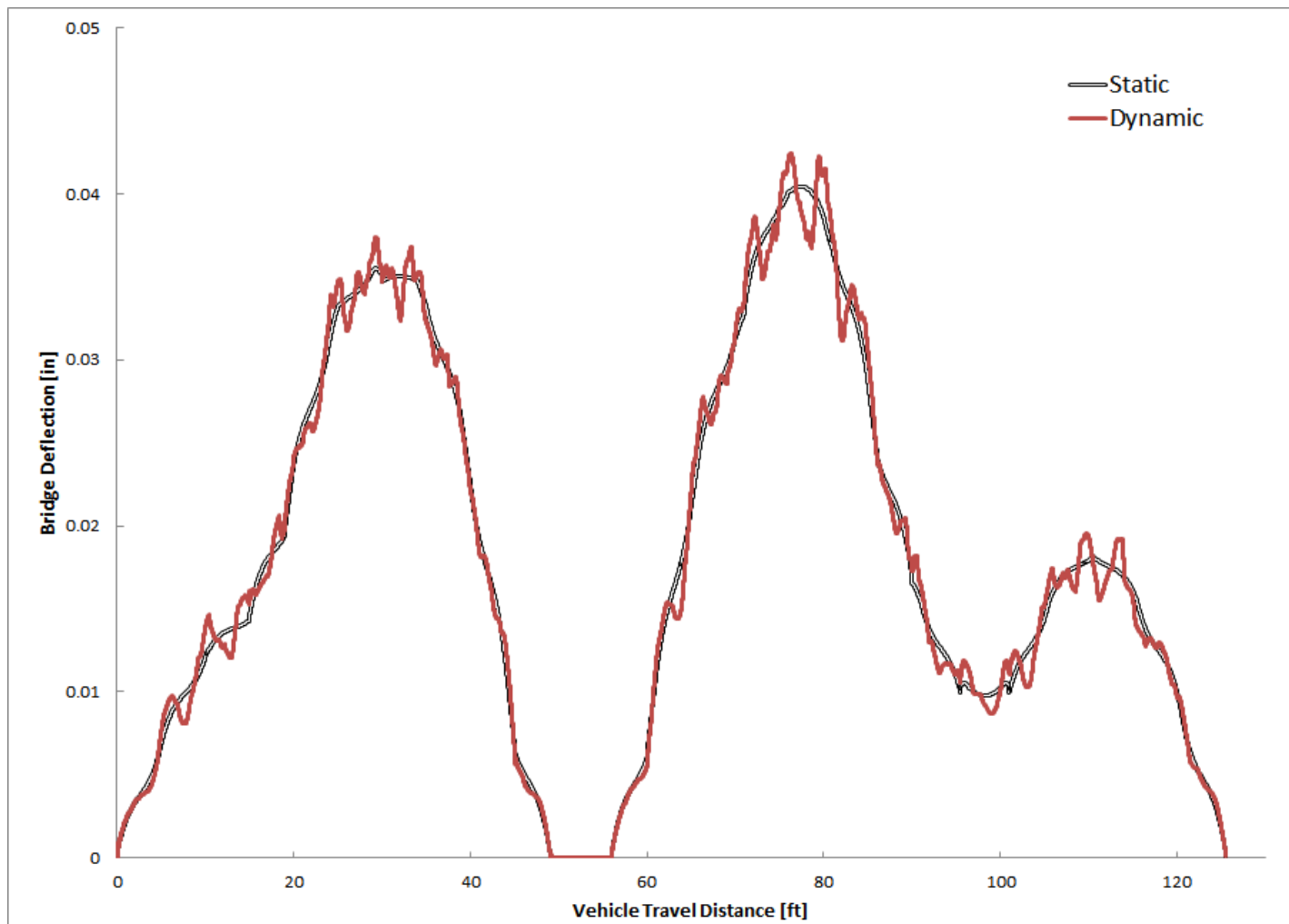


FIGURE 5-12: DISPLACEMENT OF 30 FT. CONCRETE BRIDGE DUE TO 7-AXLE ROCKY MOUNTAIN DOUBLE (“GOOD” SURFACE)

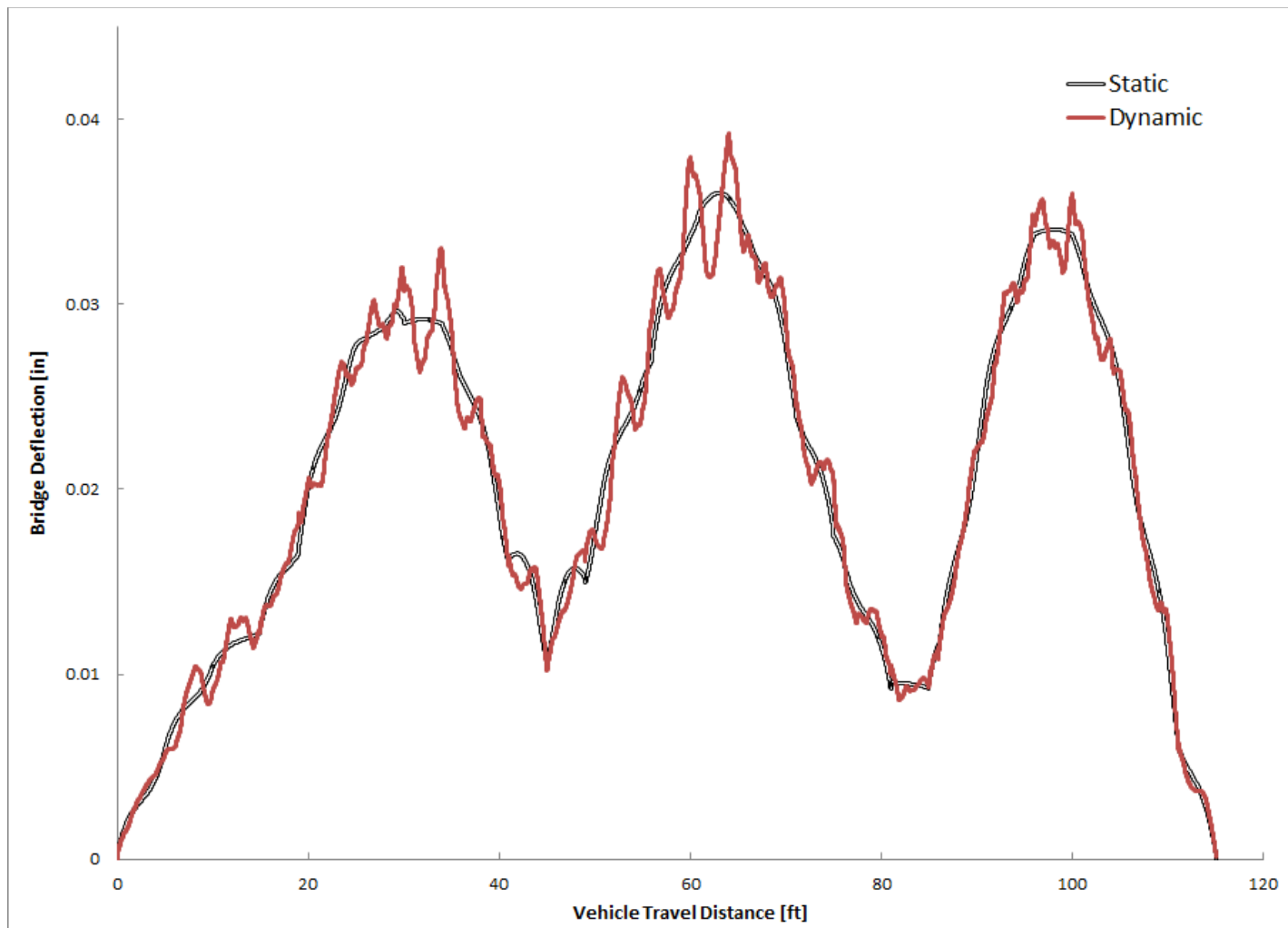


FIGURE 5-13: DISPLACEMENT OF 30 FT. CONCRETE BRIDGE DUE TO 8 AXLE B-TRAIN DOUBLE (“GOOD” SURFACE)

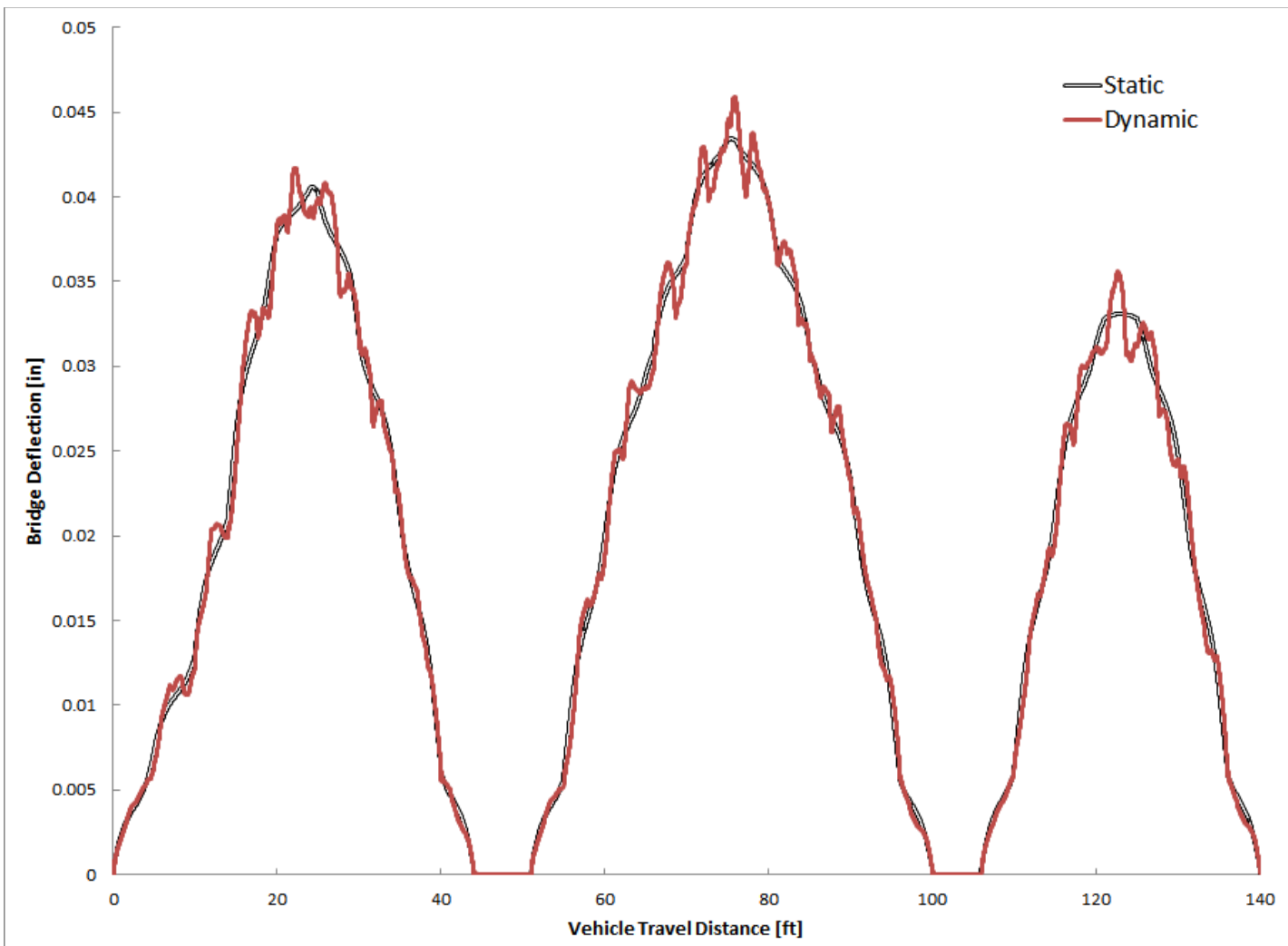


FIGURE 5-14: DISPLACEMENT OF 30 FT. CONCRETE BRIDGE DUE TO 9 AXLE TURNPIKE DOUBLE (“GOOD” SURFACE)

The results are shown as the static and dynamic response of the bridge. The static response of the bridge means that the vehicle is moving along the bridge without vibrating due to the effects of suspensions and tires so the loading would be static and the interaction of the bridge and vehicle does not have a role in this case while in the case of dynamic response of the bridge, the interaction of the bridge and vehicle has a significant role in the response of the bridge.

The horizontal axis which shows the vehicle travel distance is the distance which the truck travels when it has at least one set of wheels on the bridge. The total vehicle distance would be equal to the length of the bridge plus the length of the vehicle.

Dynamic Amplification Factor (DAF) or the dynamic load allowance is defined as,

$$DAF(\%) = \frac{\text{Maximum Dynamic Response} - \text{Maximum Static Response}}{\text{Maximum Static Response}} * 100 \quad (5.1)$$

The values of DAF for different vehicle speeds are given in Table 3-5 and Table 3-6 for Steel and Prestressed Concrete bridges, respectively. All these numbers shown here are for the case of “Good” road surface condition. The reason for choosing the “Good” road surface condition is that the maintenance of road surface of bridges is an important issue and usually the old surfaces are replaced by new surfaces before their complete deterioration. It can be observed that almost all these numbers are below 33% which was suggested by the AASHTO LRFD Bridge Design Specification [2]. In order to understand the effects of different trucks on bridges in terms of the dynamic amplification factor, all the trucks have been categorized into three groups of “Single Unit Truck”, “Tractor Semitrailer” and “Twin (Double) Trailers”. These categories can be seen in Table 5-7. Now by averaging the values of dynamic amplification factor for

each of these categories for all the vehicle speeds and bridge lengths, a comparison can be made.

TABLE 5-5: DYNAMIC AMPLIFICATION FACTOR FOR PRESTREESED CONCRETE BRIDGES (“GOOD” SURFACE)

Bridge Type	Span Length [feet]	Speed [mph]	Vehicle Type										
			T-1	T-2	T-3	T-4	T-5	T-6	T-7	T-8	T-9	T-10	T-11
Concrete	30	15	11.8	6.1	8.0	7.6	3.9	4.3	5.1	5.6	5.0	8.9	5.8
		35	12.3	10.7	7.7	3.0	8.8	14.5	13.5	10.4	2.4	4.6	3.7
		55	9.5	10.1	10.8	1.1	0.9	13.8	9.3	9.5	2.3	9.0	4.3
	60	75	6.4	7.4	7.7	3.2	3.0	11.5	7.5	3.8	6.0	15.7	1.3
		15	6.6	2.8	14.9	5.9	5.1	4.4	6.8	14.6	3.7	5.3	4.5
		35	6.9	7.8	12.5	5.9	6.9	14.7	12.8	17.1	5.1	3.3	6.0
Steel	90	55	4.4	6.9	8.7	6.1	10.9	10.3	8.5	13.3	7.1	1.9	10.6
		75	1.9	7.0	5.5	3.8	8.6	10.2	2.3	13.1	10.3	3.0	13.1
		15	5.9	8.4	12.9	10.1	10.4	8.6	6.4	14.5	3.3	3.9	5.5
	120	35	5.9	7.5	18.4	7.9	7.4	14.1	12.2	14.3	4.7	6.3	4.5
		55	7.4	7.6	12.5	12.1	8.3	8.2	6.4	9.5	5.5	8.7	9.3
		75	8.7	3.5	18.9	7.8	9.6	4.9	3.9	10.8	8.1	8.9	11.0
Composite	140	15	8.2	9.0	13.0	18.5	11.7	8.8	9.8	9.7	4.0	4.1	5.6
		35	8.2	9.0	11.1	9.3	11.4	13.7	17.7	8.7	6.8	6.6	6.0
		55	10.5	8.3	12.6	14.2	10.3	10.3	6.8	10.7	8.2	5.8	5.2
	160	75	16.7	6.0	21.1	15.9	14.4	11.0	7.9	20.2	14.3	6.9	9.2
		15	9.8	9.6	16.7	12.8	19.5	12.7	12.5	10.2	6.4	4.9	8.5
		35	7.7	7.5	13.6	11.7	21.4	12.6	16.2	13.7	5.8	4.8	6.1
	180	55	13.6	9.7	22.8	11.8	17.2	12.6	11.5	15.7	5.6	6.9	7.7
		75	6.7	9.5	12.9	14.7	18.0	13.3	14.2	11.1	7.3	4.5	4.6

TABLE 5-6: DYNAMIC AMPLIFICATION FACTOR FOR STEEL BRIDGES (“GOOD” SURFACE)

Bridge Type	Span Length [feet]	Speed [mph]	Vehicle Type										
			T-1	T-2	T-3	T-4	T-5	T-6	T-7	T-8	T-9	T-10	T-11
Steel	30	Good	15	11.3	6.3	9.6	8.4	3.8	5.3	8.5	9.6	5.8	9.6
		35	35	12.9	11.1	14.1	4.3	6.8	13.3	15.7	12.9	1.6	5.1
		55	55	9.2	11.0	13.6	1.8	2.1	15.9	10.5	7.0	2.4	9.3
	60	75	75	1.7	6.6	7.1	3.6	3.0	14.3	6.1	6.0	6.4	16.7
		Good	15	7.1	5.5	18.9	8.4	8.0	13.7	9.6	16.6	5.7	5.5
		35	35	5.5	10.3	13.3	12.2	8.9	14.0	17.4	21.8	5.5	3.5
90	60	55	55	8.9	5.5	13.0	8.7	12.7	17.0	8.6	14.1	6.2	4.5
		75	75	5.4	7.6	15.7	12.6	9.5	11.4	4.6	15.8	9.3	8.2
		Good	15	5.8	10.1	16.5	15.7	9.5	12.7	10.7	18.6	6.1	6.4
	90	35	35	8.5	10.3	15.7	16.9	14.7	16.8	15.2	26.7	8.0	10.3
		55	55	13.0	5.5	22.1	22.4	14.0	22.7	7.9	21.8	12.3	13.1
		75	75	14.9	6.8	20.6	24.7	24.2	10.8	9.2	22.8	12.9	10.7
120	90	Good	15	8.1	10.1	13.4	18.9	16.6	11.9	12.0	18.5	9.0	6.1
		35	35	8.8	9.2	18.4	15.1	18.0	11.9	15.3	18.4	10.3	9.1
		55	55	17.2	5.8	26.3	16.4	18.1	15.2	11.2	18.2	11.9	10.0
	120	75	75	15.3	11.7	23.5	16.9	21.0	14.5	13.7	18.8	13.1	10.2
		Good	15	10.3	9.2	19.9	13.2	19.0	14.4	13.2	12.9	6.7	5.0
		35	35	9.9	7.5	15.4	11.3	20.8	12.1	14.5	20.2	6.0	6.1
140	120	55	55	16.1	8.5	21.0	14.6	21.5	16.9	11.6	14.7	7.0	6.6
		75	75	8.0	10.8	21.0	14.5	14.0	9.8	10.0	13.3	8.1	4.6

Where:

- T-1 : H-20
- T-2 : HS-20
- T-3 : Type 3
- T-4 : Type 3S2
- T-5 : Type 3S3
- T-6 : Type 2S2
- T-7 : Type 3S1
- T-8 : SU4
- T-9 : 7-axle rocky mountain double
- T-10 : 8-axle B-train double
- T-11 : 9-axle turnpike double

The results of this averaging have been shown in Figure 5-15 and Figure 5-16.

TABLE 5-7: DIFFERENT TRUCK CATEGORIES

Single Unit Truck	Tractor Semitrailer	Twin (Double) Trailers
H-20	HS-20	7-Axle Rocky Mountain Double
Type 3	Type 3S2	8 Axle B-Train Double
SU4	Type 3S3	9 Axle Turnpike Double
	Type 2S2	
	Type 3S1	

It can be observed from the results of these two figures that the dynamic amplification factor is always below 33% when considering the “Good” surface condition for the bridge.

It can also be said that the highest values of the dynamic amplification factor belong to the cases of “Single Unit Truck”. Cases of “Tractor Semitrailer” also have higher dynamic amplification factor comparing to the cases of “Twin (Double) Trailers”. These results show consistency with the results obtained from the previous section where the heavier trucks generated the lowest dynamic amplification factors.

Another observation from these results is that the increase in the vehicle speed does not always result in higher dynamic amplification. For the case of “Twin (Double) Trailers” in most cases there is a direct relation between the vehicle speed and the dynamic amplification factor and the highest values of the DAF are achieved when the vehicle speed is at its most. (i.e. 75mph) For the case of “Tractor Semitrailer” the increasing trend for the DAF cannot be seen but the maximum values of DAF in this case mostly happen when the vehicle speed is around the average speed of 35 mph.

A closer look at the results for different span lengths also shows that as the span length increases, the values of dynamic amplification factor also increase which is consistent with the common sense.

The reason for this increase is that, with the increase in the span length, the maximum deflection in the middle of the bridge also increases and more fluctuations of the bridge would happen. These extra vibrations would result in larger differences between the cases of static and dynamic responses.

Value of moment at different grid points of the bridge was also calculated as a measure to calculate the stresses which were endured by the bridge. These values were recorded for the static and dynamic truck loading at each time step and the results for the prestressed concrete bridge with the span length of 140 ft. for the “Good” road surface condition and 15 mph vehicle speed is shown in Figure 5-17 to Figure 5-27.

It can be observed from these graphs that the maximum moment in the bridge is resulted when the heaviest trucks (Longer Combination Vehicles such as 9 Axle Turnpike Double and 8 Axle B-Train Double) pass the bridge.

The results when “Very Good” road surface condition was used, is also shown here to make a comparison between the two cases of surface condition. The displacement at the midspan of the 60 ft. span Steel Bridge when different trucks travel on the bridge is shown in Figure 3-28 to Figure 3-38. All these figures show the static and dynamic responses as it was explained before and these responses have been recorded for a point in the middle of the bridge which has the largest deflection.

Using the relationship given in equation 3.2 , the Dynamic Amplification Factor (DAF) for all the vehicle speeds and all the bridge cases were calculated. The summary of all the DAFs for the case of “Very Good” surface condition is given in Table 5.8 and Table 5.9.

It can be observed from these tables that the DAF values are still smaller than the 0.33 suggested by AASHTO LRFD and these numbers are even smaller comparing to the case of “Good” surface condition.

Using the same truck categories which were given in Table 5.7, the results for all the eleven trucks were summarized and shown in the graphs of Figure 5.39 and Figure 5.40. Comparing the results in those figures and the results shown in Figure 5.15 and Figure

5.16 shows that the values of the Dynamic Amplification Factor for the case of “Very Good” road surface condition are generally smaller than the values of DAF for the case of “Good” surface condition which is sensible.

The results for the moment at the midpoint of 120 ft. steel bridge was also recorded for the case of “Very Good” surface condition and the comparison between the static and dynamic responses are shown in Figure 5.41 to Figure 5.51.

Finally, all results for the discussed cases were grouped and shown in Figure 5.52 to Figure 5.54. It can be seen that in the majority of cases the Dynamic Amplification Factor (DAF) is higher in the case of “Good” surface condition and the values are below 33%.

Also the highest values of DAF happen when the “Single Unit Truck” is on the road.

One reason that can be mentioned for getting the highest values of DAF for the “Single Unit Truck” group is that the weight of a single axle in the trucks under this category can be as high as 34 kips and also the distance between the axles are smaller because the total length of the truck is small comparing to the other two cases. So with the heavy trucks, the distribution of the loads over more number of axles and more distance between these axles result in smaller values for DAF.

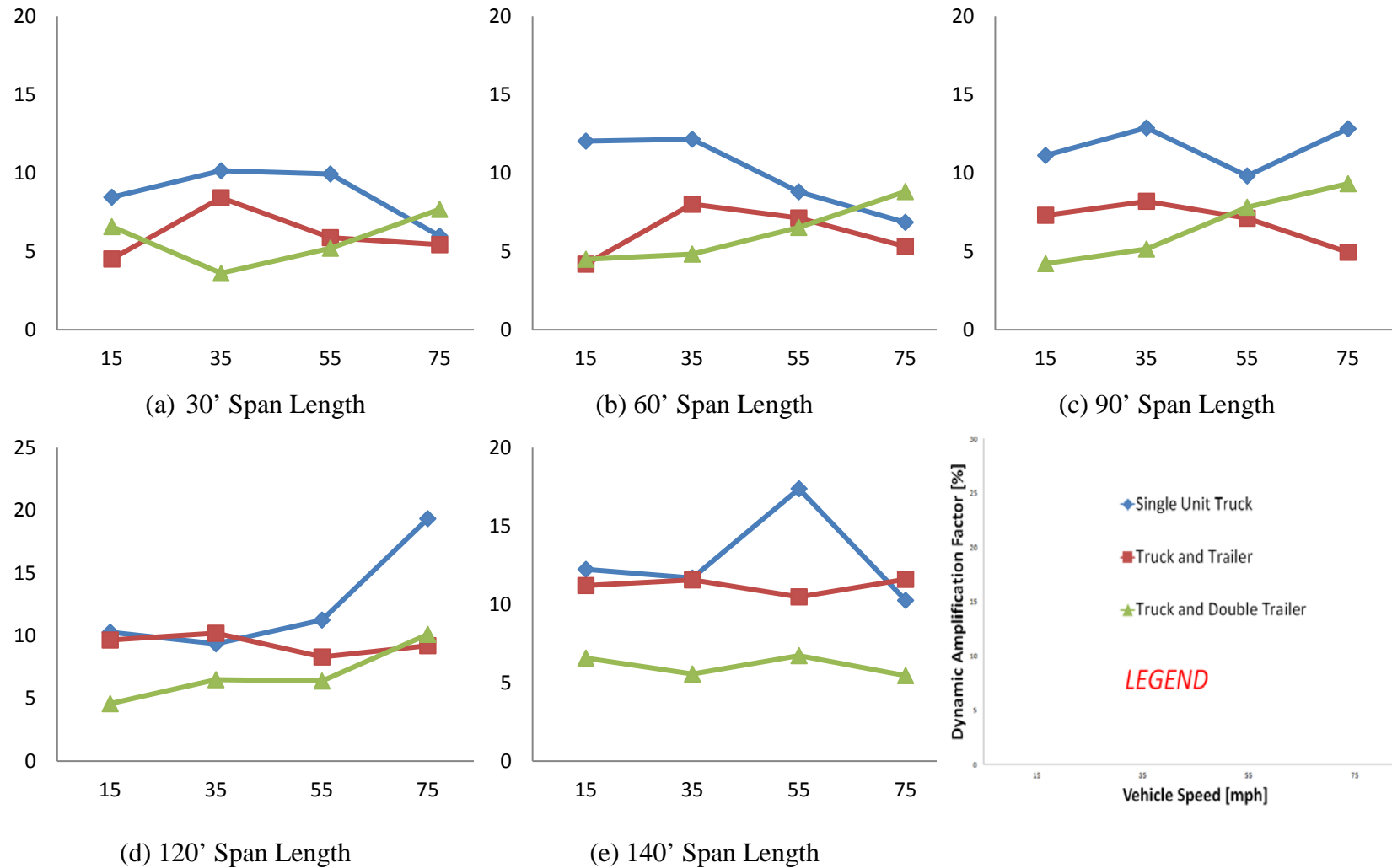


FIGURE 5-15: PRESTRESSED CONCRETE BRIDGES DAF FOR DIFFERENT VEHICLE CATEGORIES (“GOOD” SURFACE)

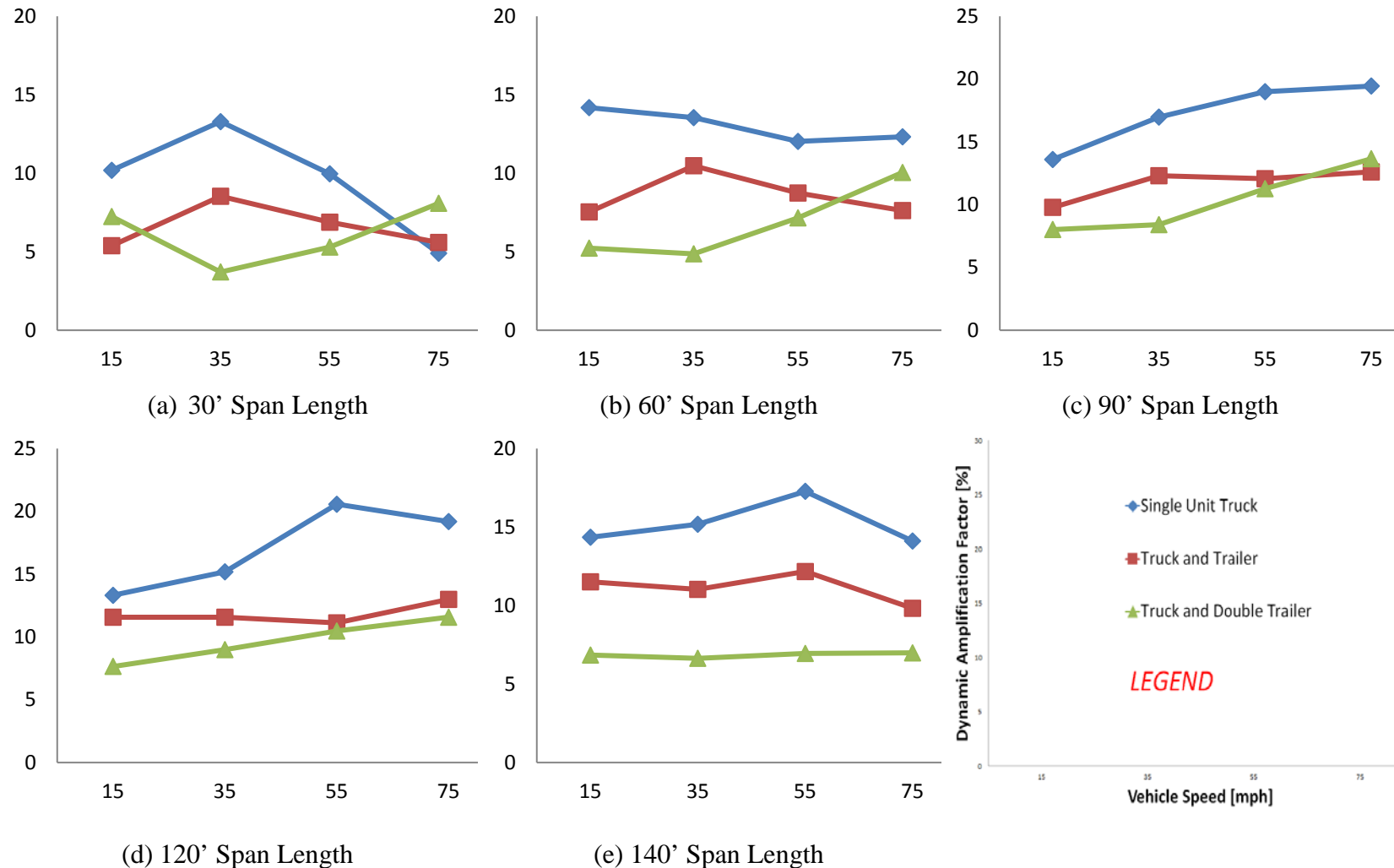


FIGURE 5-16: STEEL BRIDGES DAF FOR DIFFERENT VEHICLE CATEGORIES (“GOOD” SURFACE)

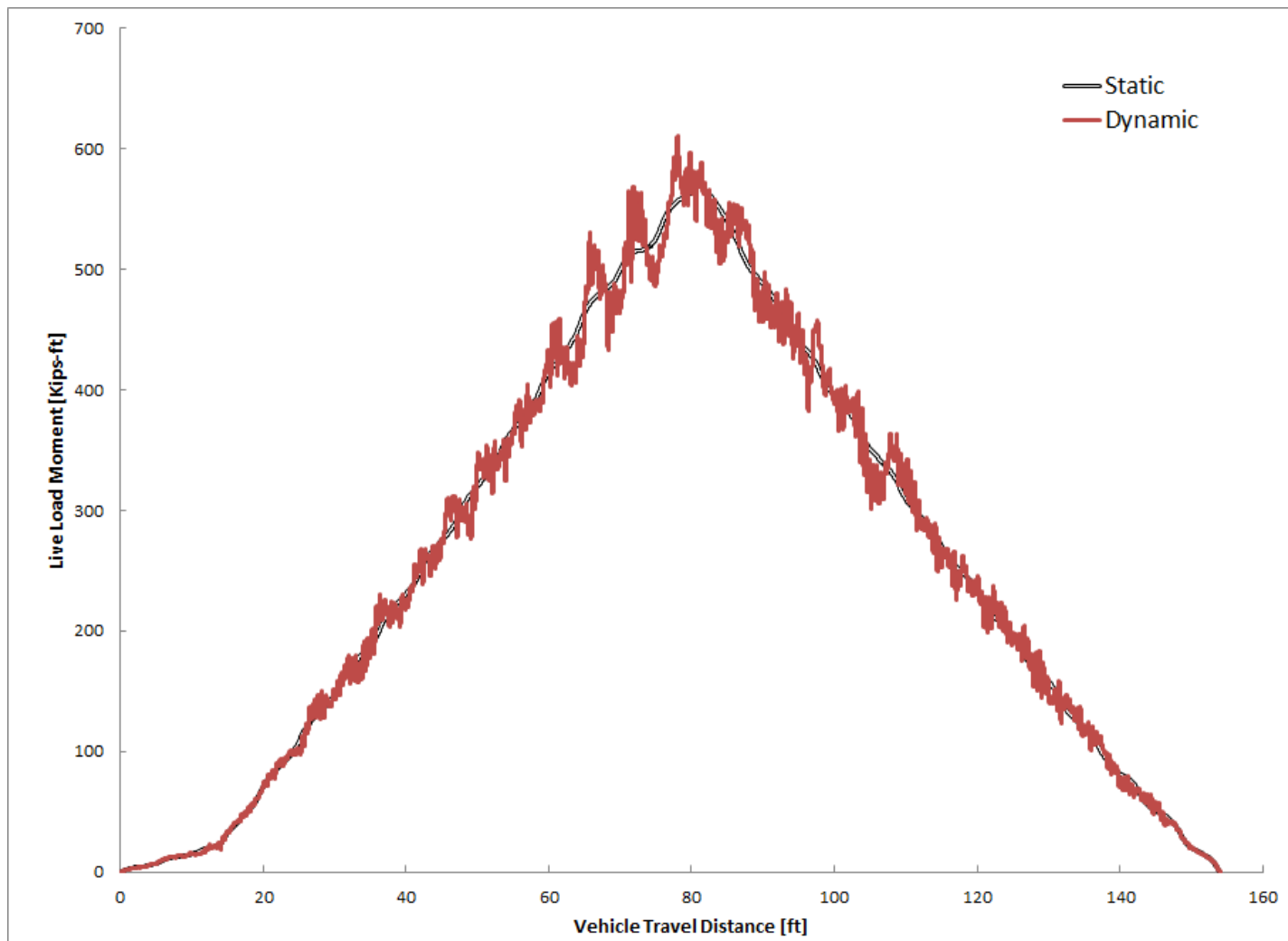


FIGURE 5-17: MOMENT OF 140 FT. CONCRETE BRIDGE DUE TO H-20 (“GOOD” SURFACE)

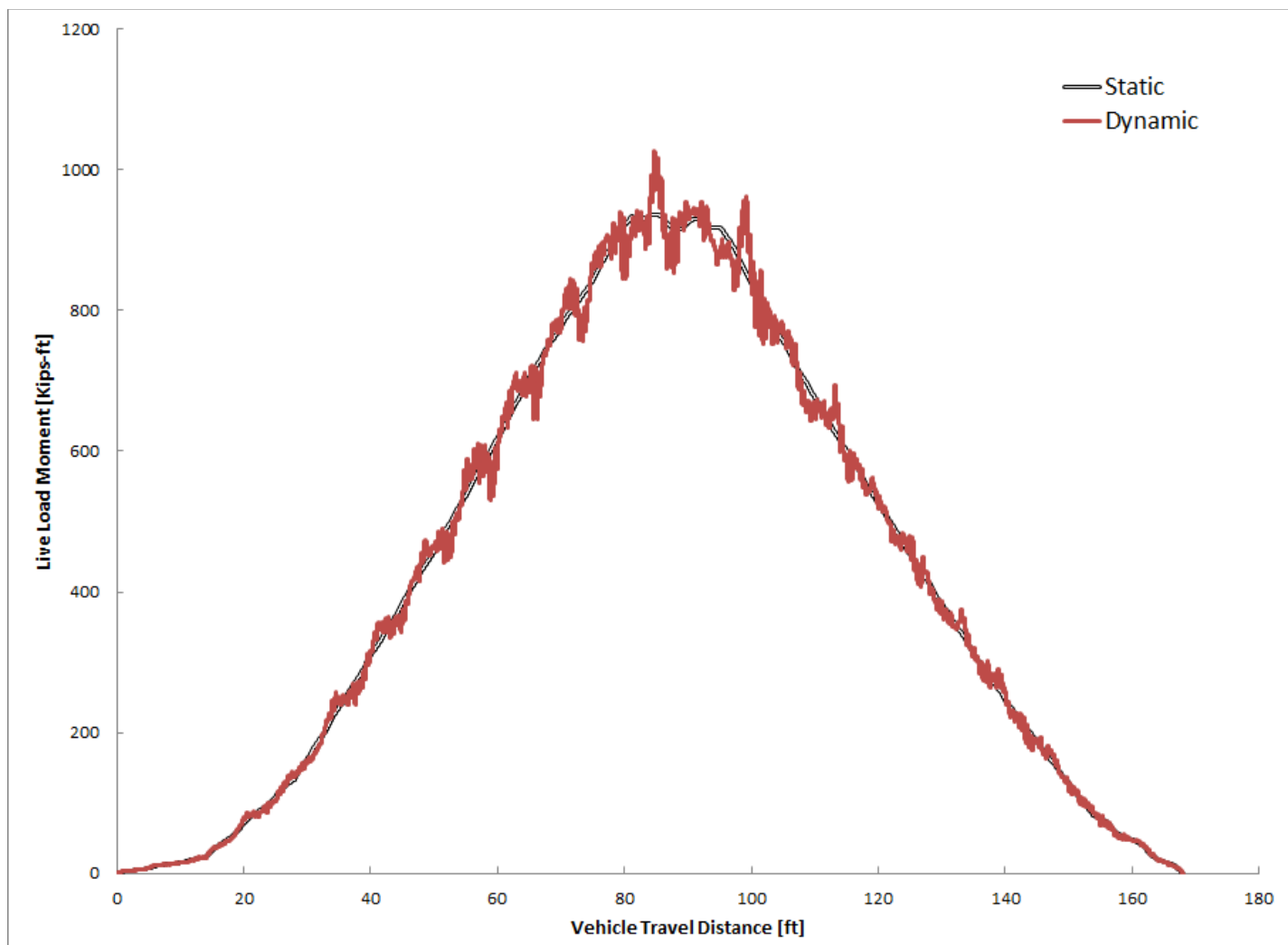


FIGURE 5-18: MOMENT OF 140 FT. CONCRETE BRIDGE DUE TO HS-20 (“GOOD” SURFACE)

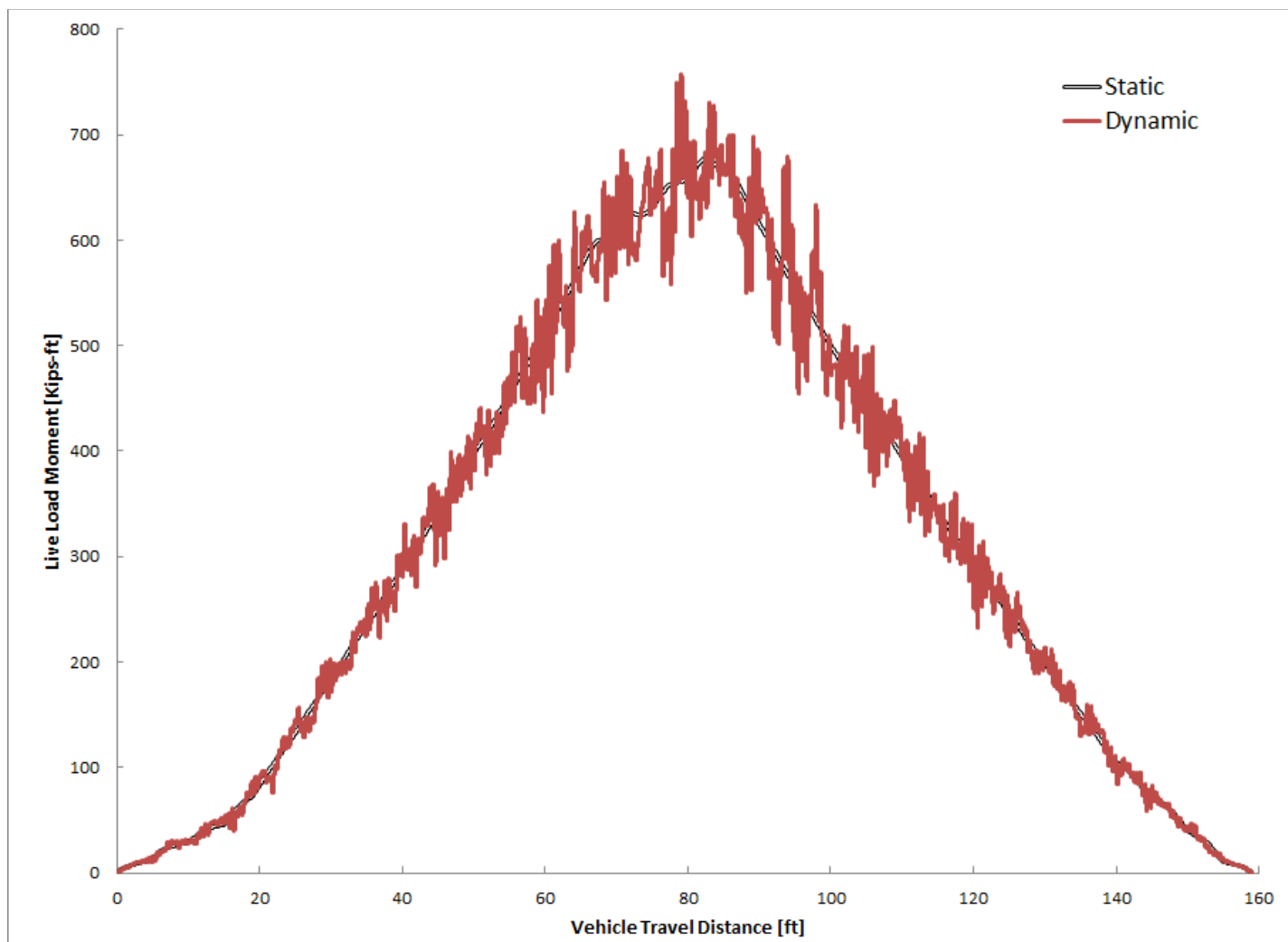


FIGURE 5-19:MOMENT OF 140 FT. CONCRETE BRIDGE DUE TO TYPE 3 (“GOOD” SURFACE)

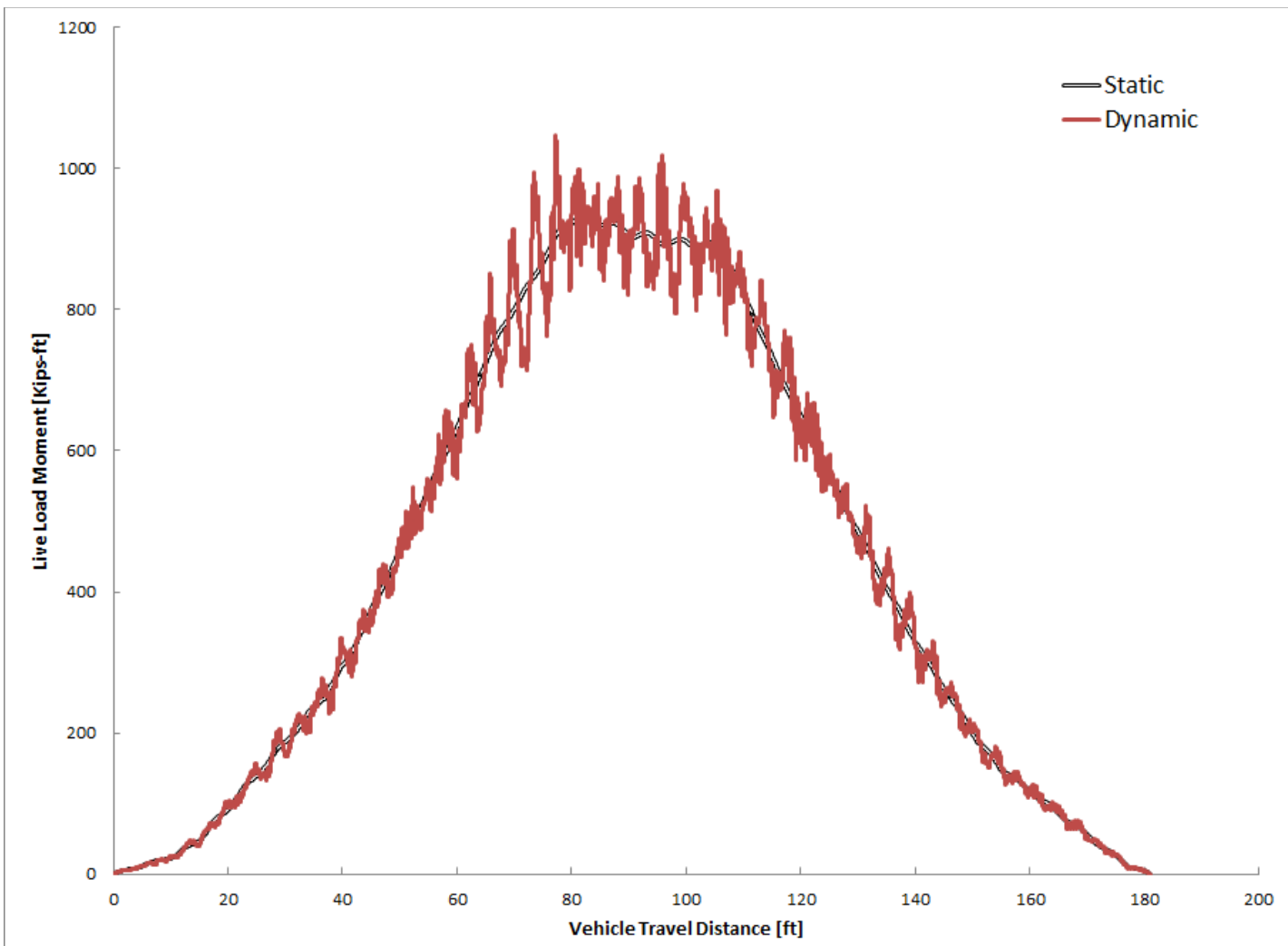


FIGURE 5-20: MOMENT OF 140 FT. CONCRETE BRIDGE DUE TO TYPE 3S2 (“GOOD” SURFACE)

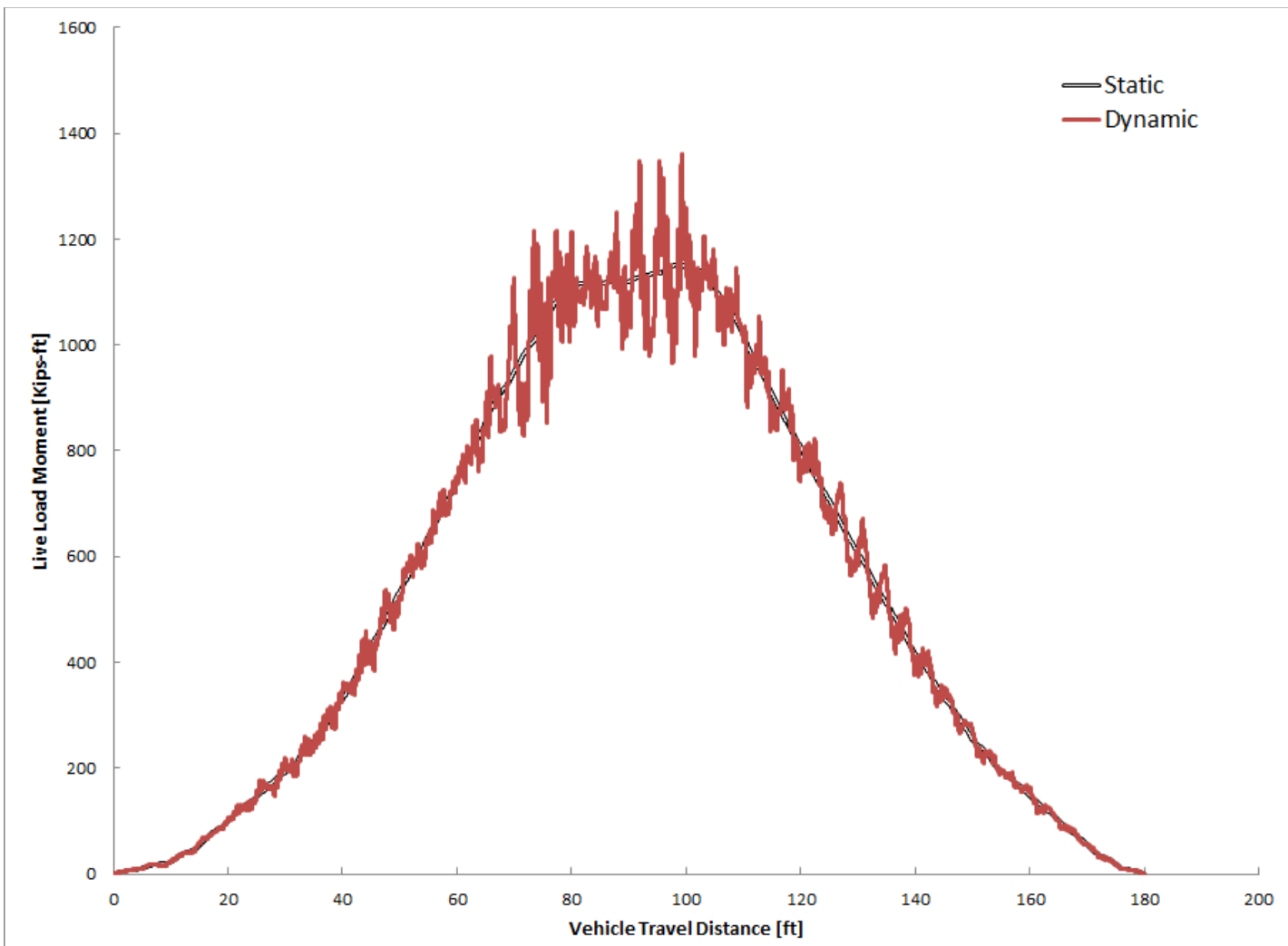


FIGURE 5-21: MOMENT OF 140 FT. CONCRETE BRIDGE DUE TO TYPE 3S3 (“GOOD” SURFACE)

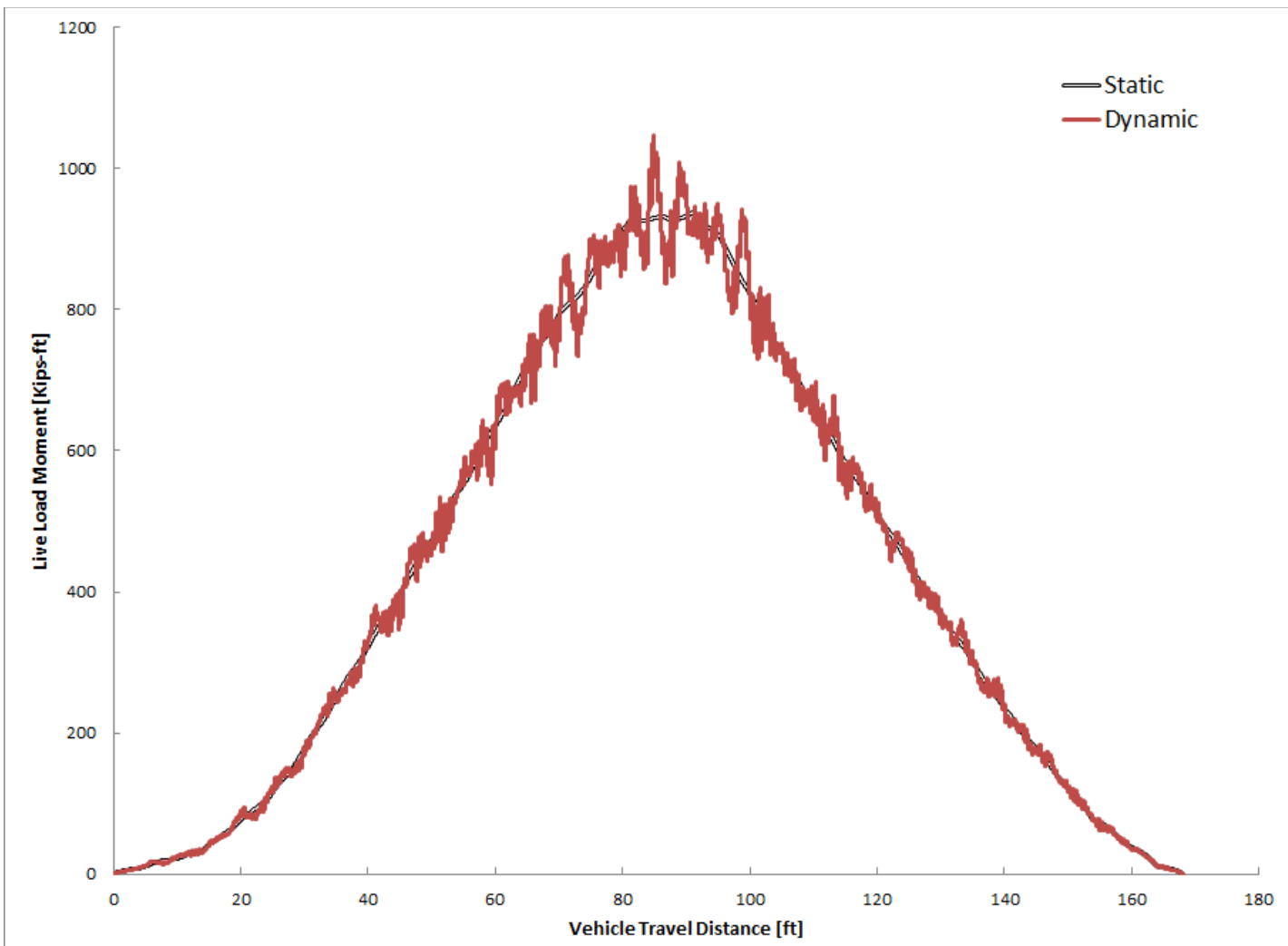


FIGURE 5-22: MOMENT OF 140 FT. CONCRETE BRIDGE DUE TO TYPE 2S2 (“GOOD” SURFACE)

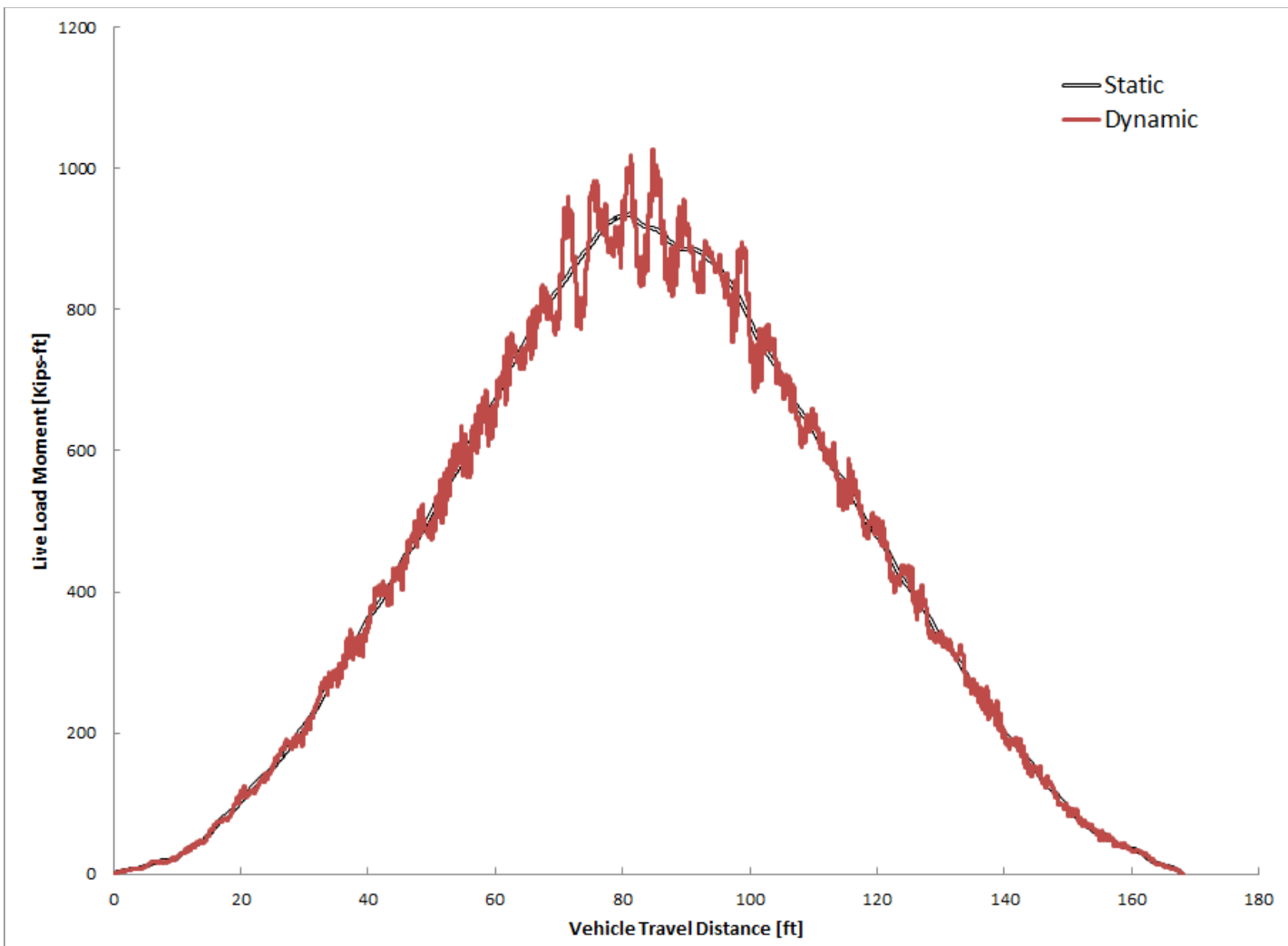


FIGURE 5-23: MOMENT OF 140 FT. CONCRETE BRIDGE DUE TO TYPE 3S1 (“GOOD” SURFACE)

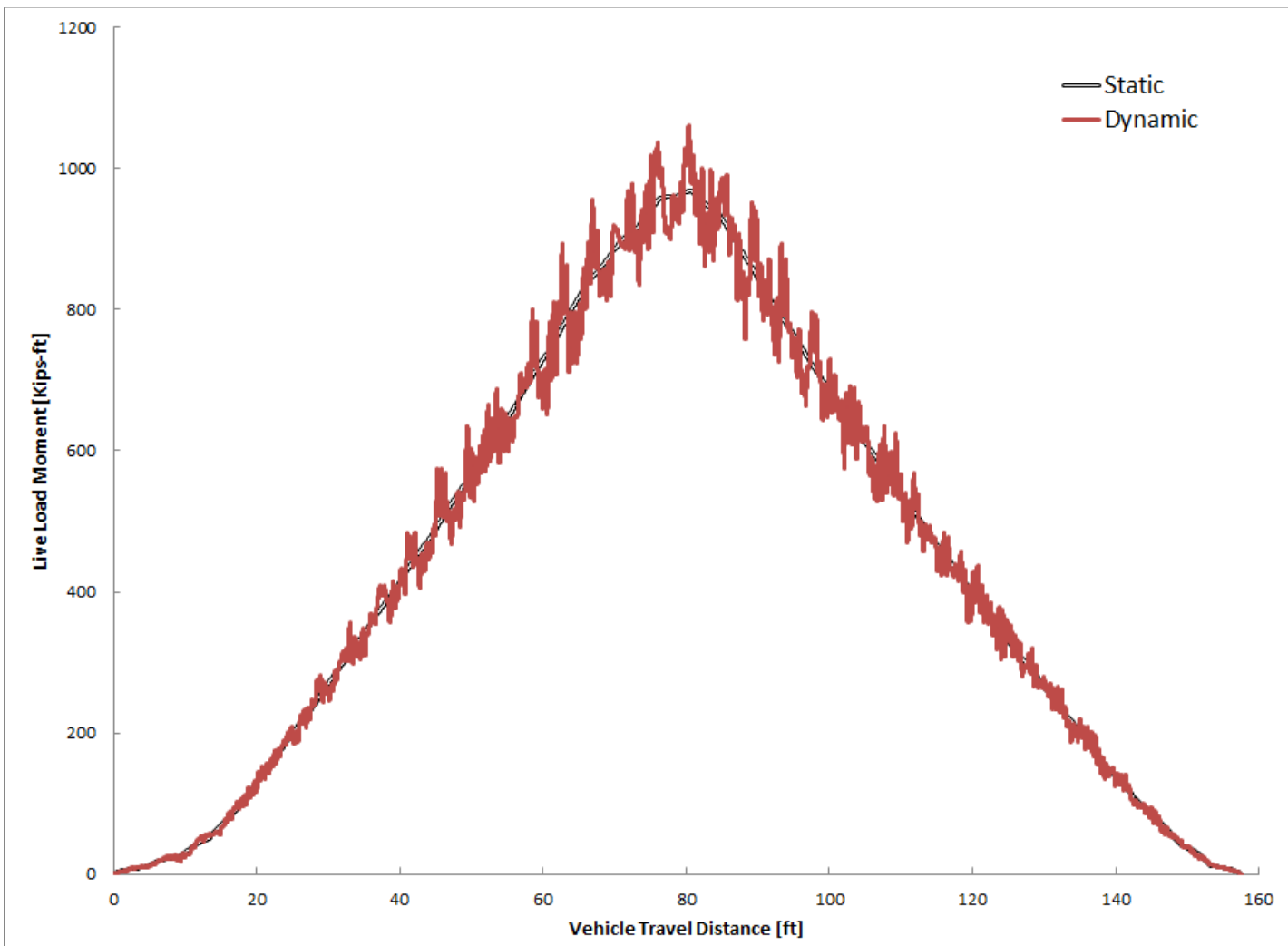


FIGURE 5-24: MOMENT OF 140 FT. CONCRETE BRIDGE DUE TO TYPE SU4 (“GOOD” SURFACE)

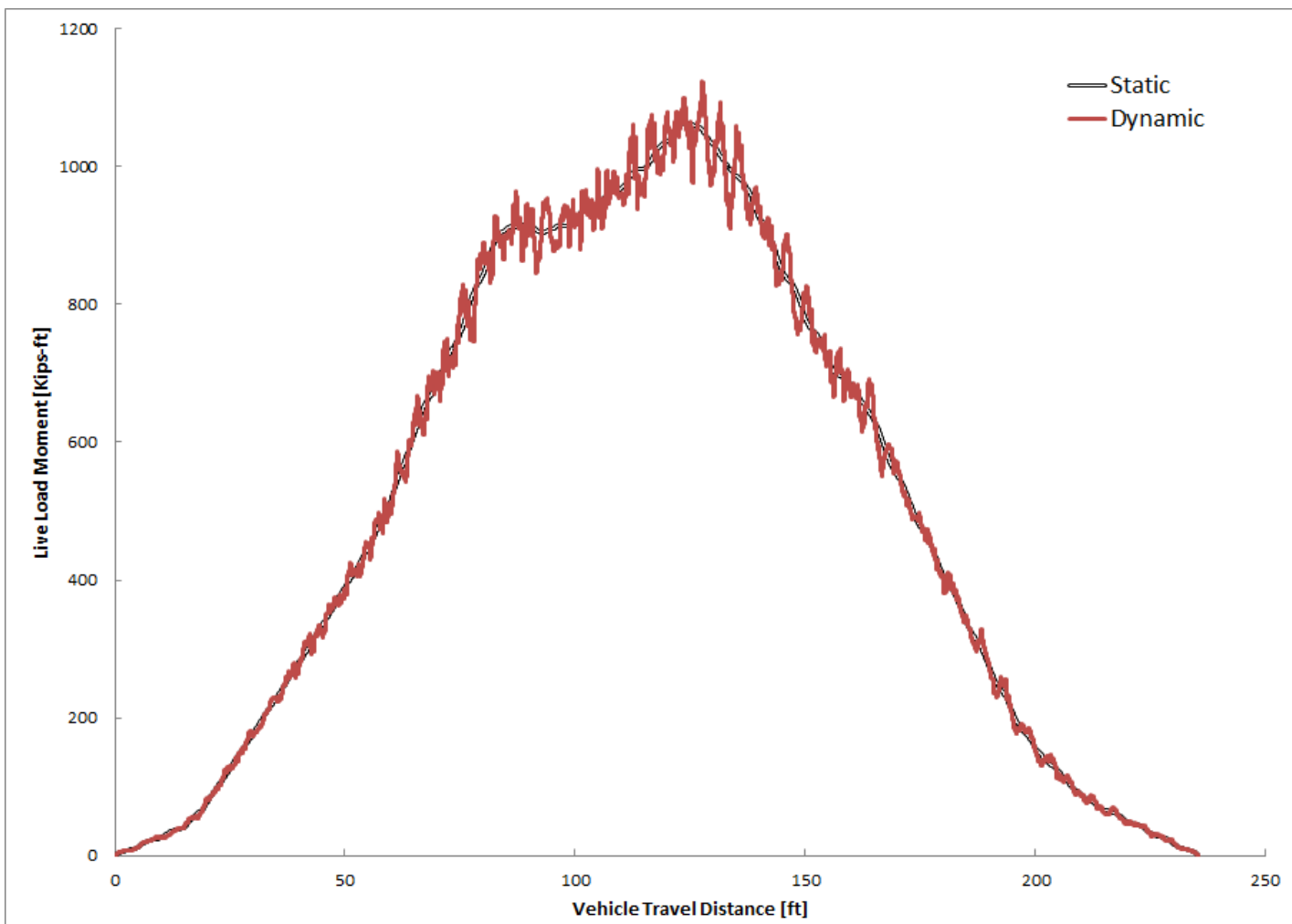


FIGURE 5-25: MOMENT OF 140 FT. CONCRETE BRIDGE DUE TO 7-AXLE ROCKY MOUNTAIN DOUBLE (“GOOD” SURFACE)

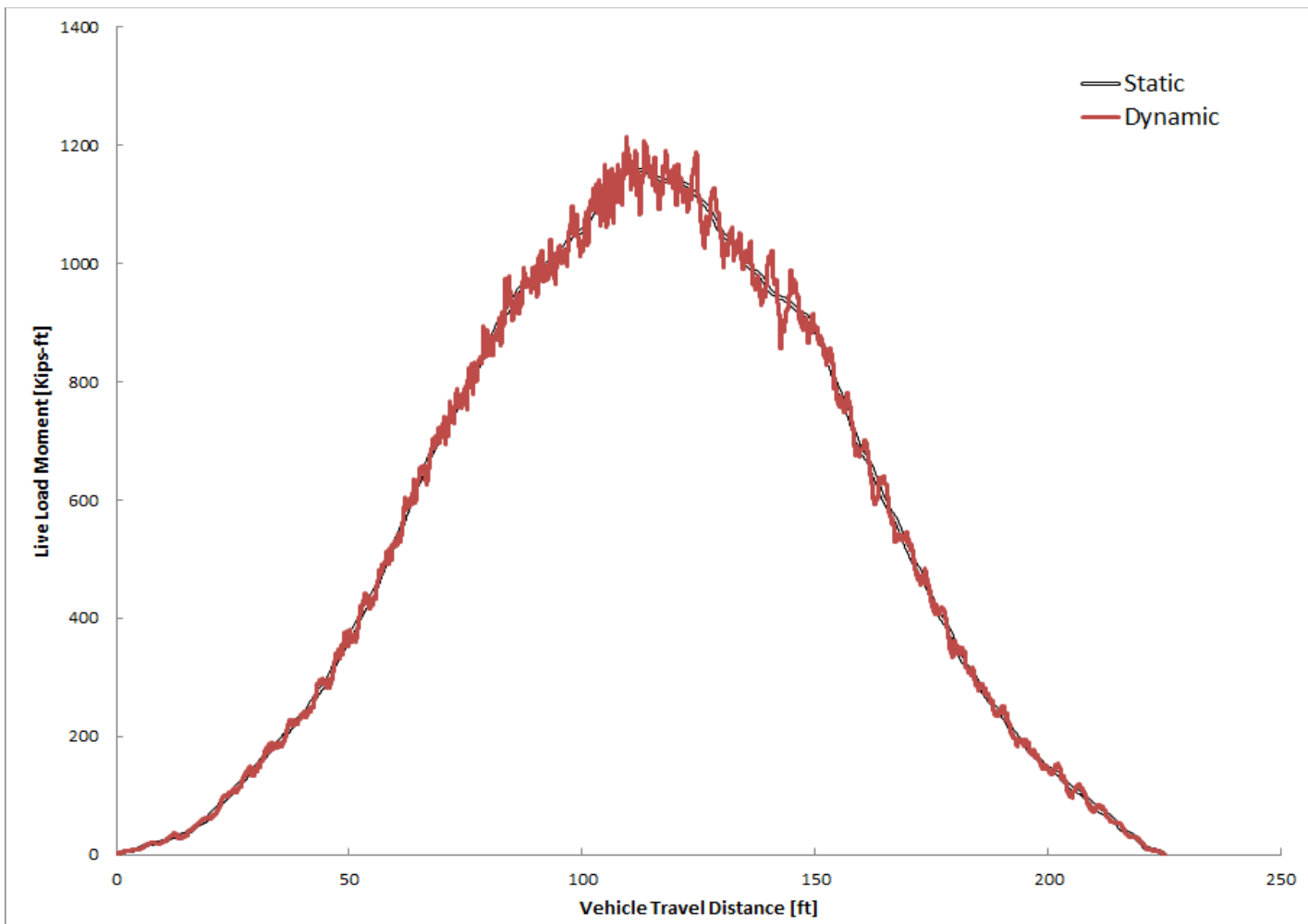


FIGURE 5-26: MOMENT OF 140 FT. CONCRETE BRIDGE DUE TO 8 AXLE B-TRAIN DOUBLE (“GOOD” SURFACE)

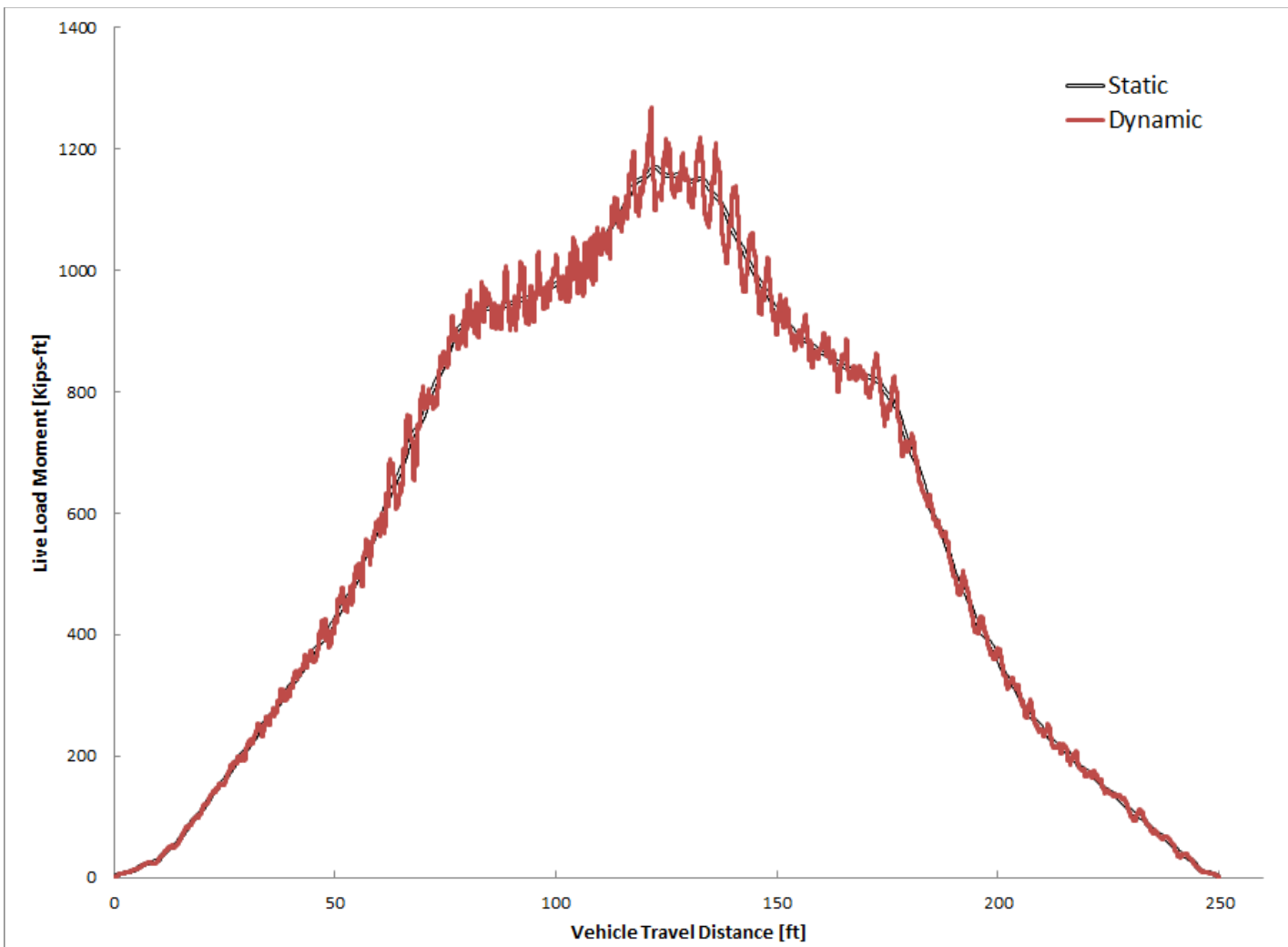


FIGURE 5-27: MOMENT OF 140 FT. CONCRETE BRIDGE DUE TO 9 AXLE TURNPIKE DOUBLE (“GOOD” SURFACE)

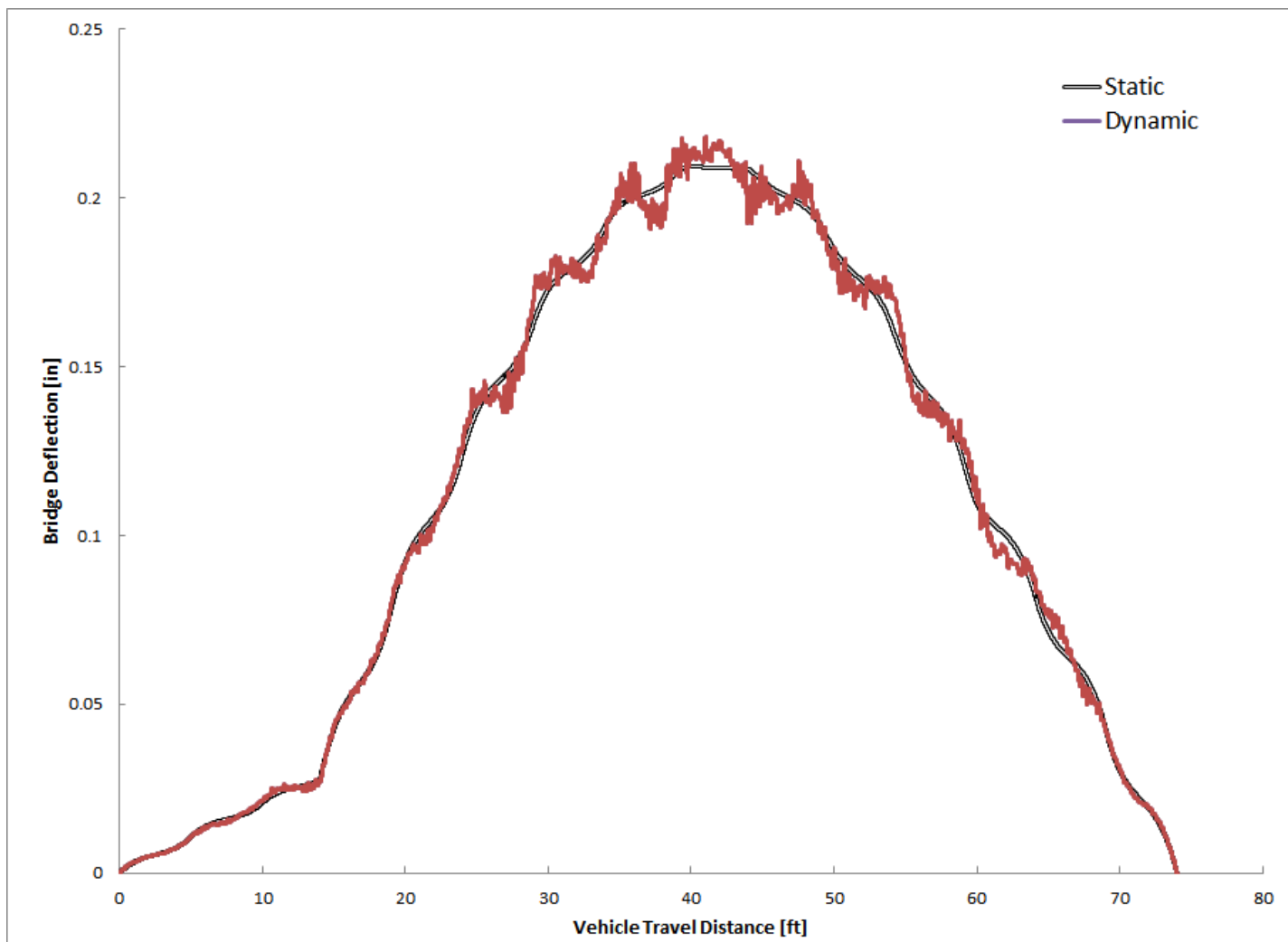


FIGURE 5-28: DISPLACEMENT OF 60 FT. STEEL BRIDGE DUE TO H-20 (“VERY GOOD” SURFACE)

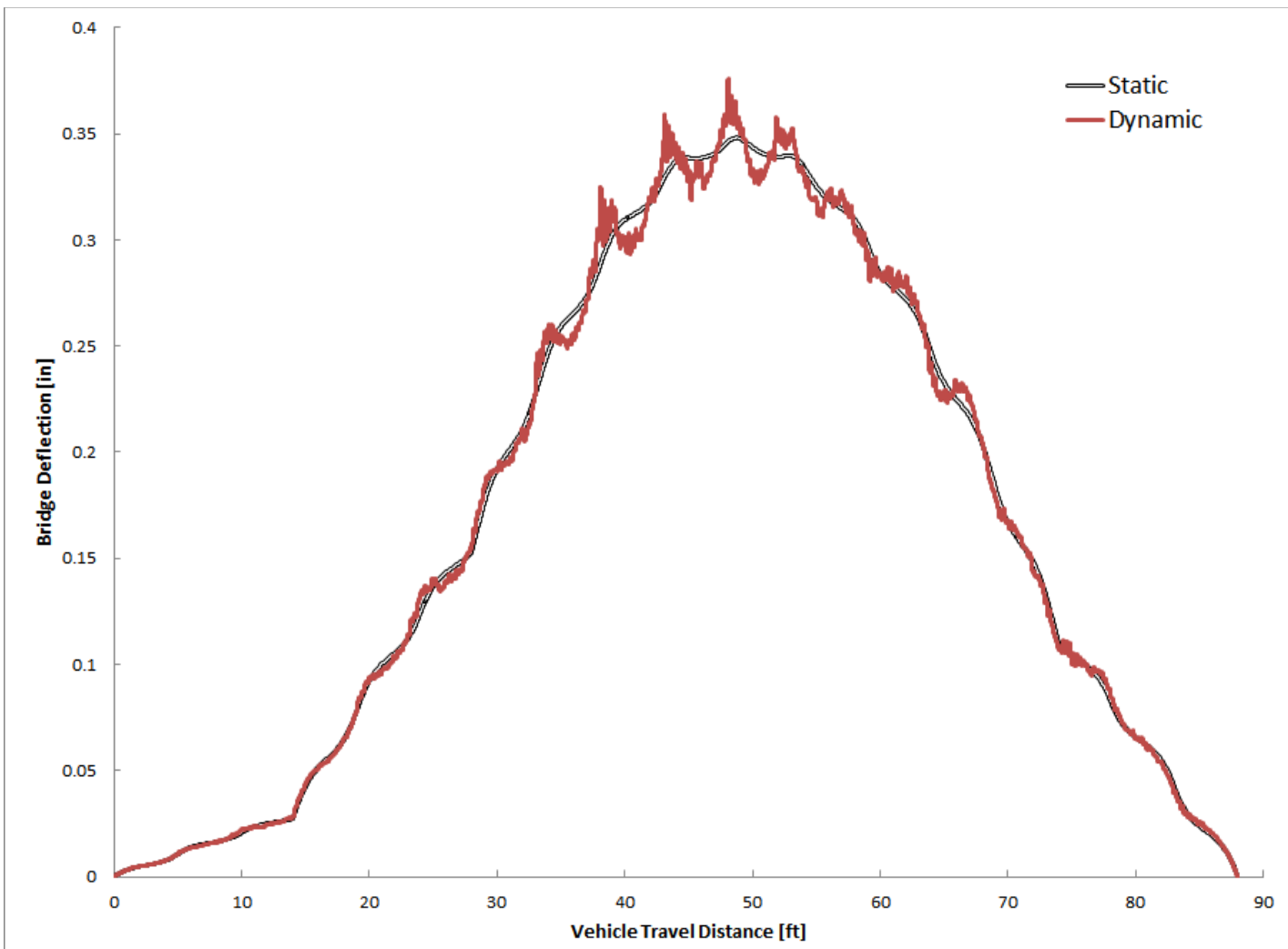


FIGURE 5-29: DISPLACEMENT OF 60 FT. STEEL BRIDGE DUE TO HS-20 (“VERY GOOD” SURFACE)

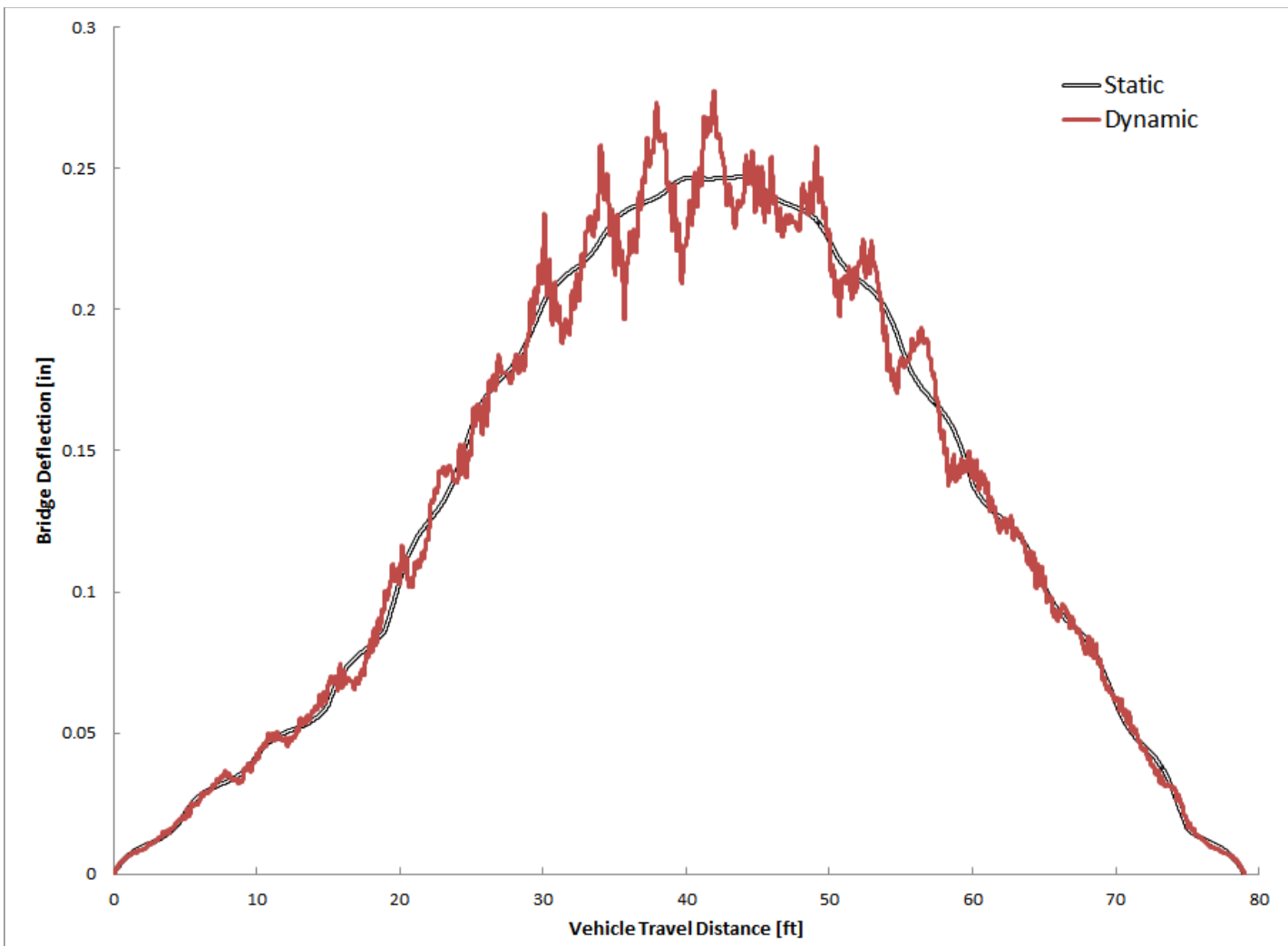


FIGURE 5-30: DISPLACEMENT OF 60 FT. STEEL BRIDGE DUE TO TYPE 3 (“VERY GOOD” SURFACE)

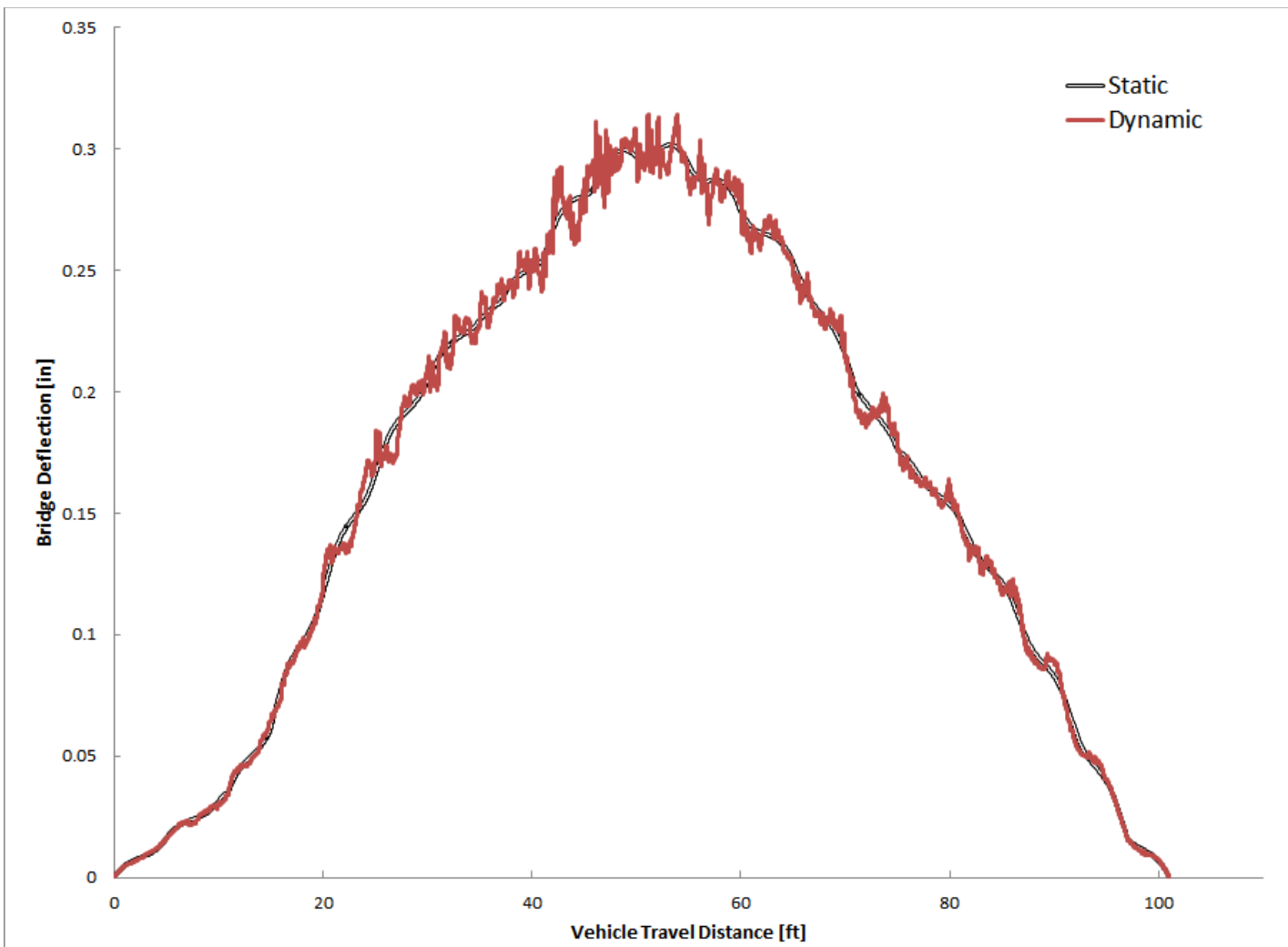


FIGURE 5-31: DISPLACEMENT OF 60 FT. STEEL BRIDGE DUE TO TYPE 3S2 (“VERY GOOD” SURFACE)

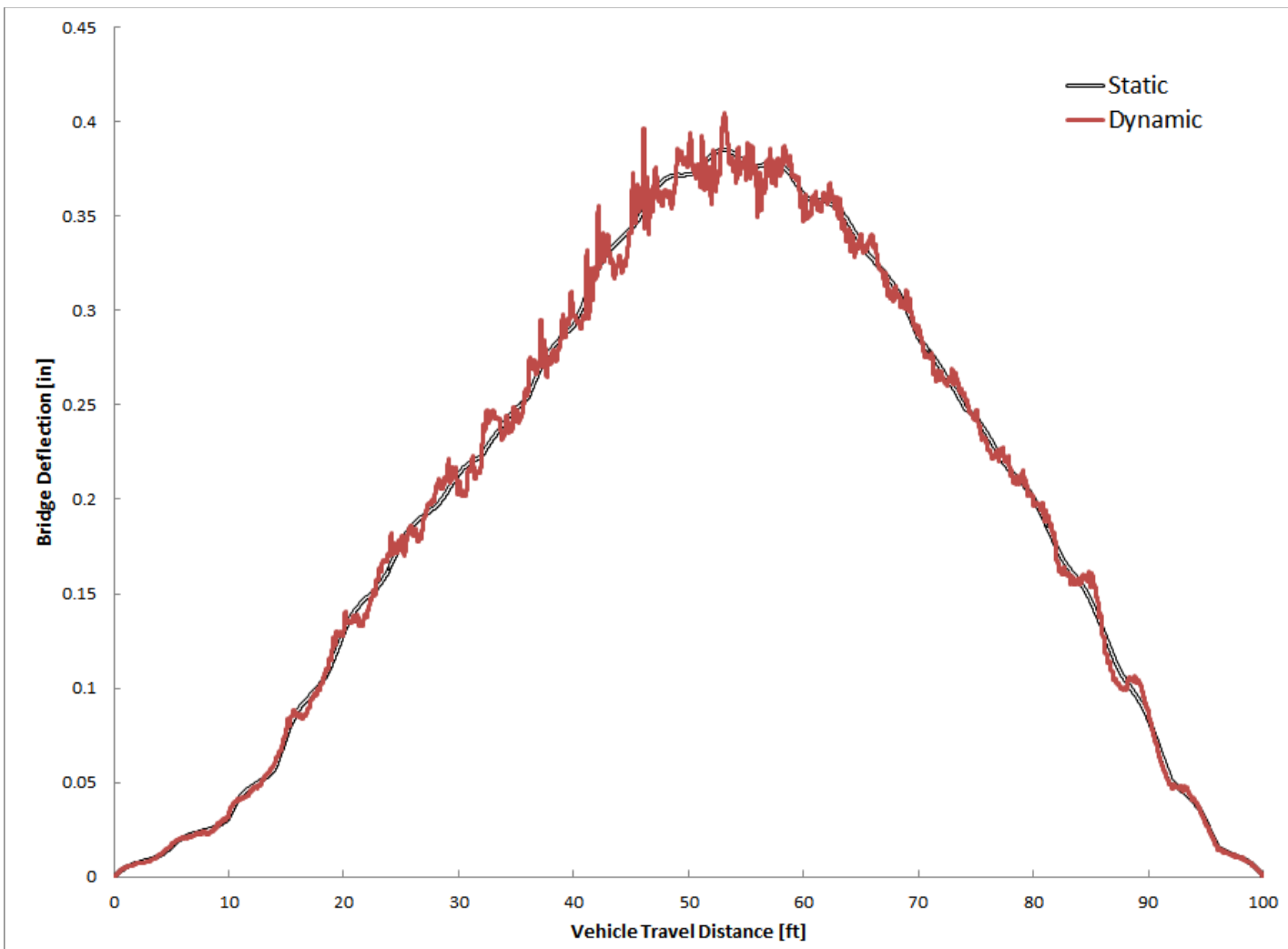


FIGURE 5-32: DISPLACEMENT OF 60 FT. STEEL BRIDGE DUE TO TYPE 3S3 (“VERY GOOD” SURFACE)

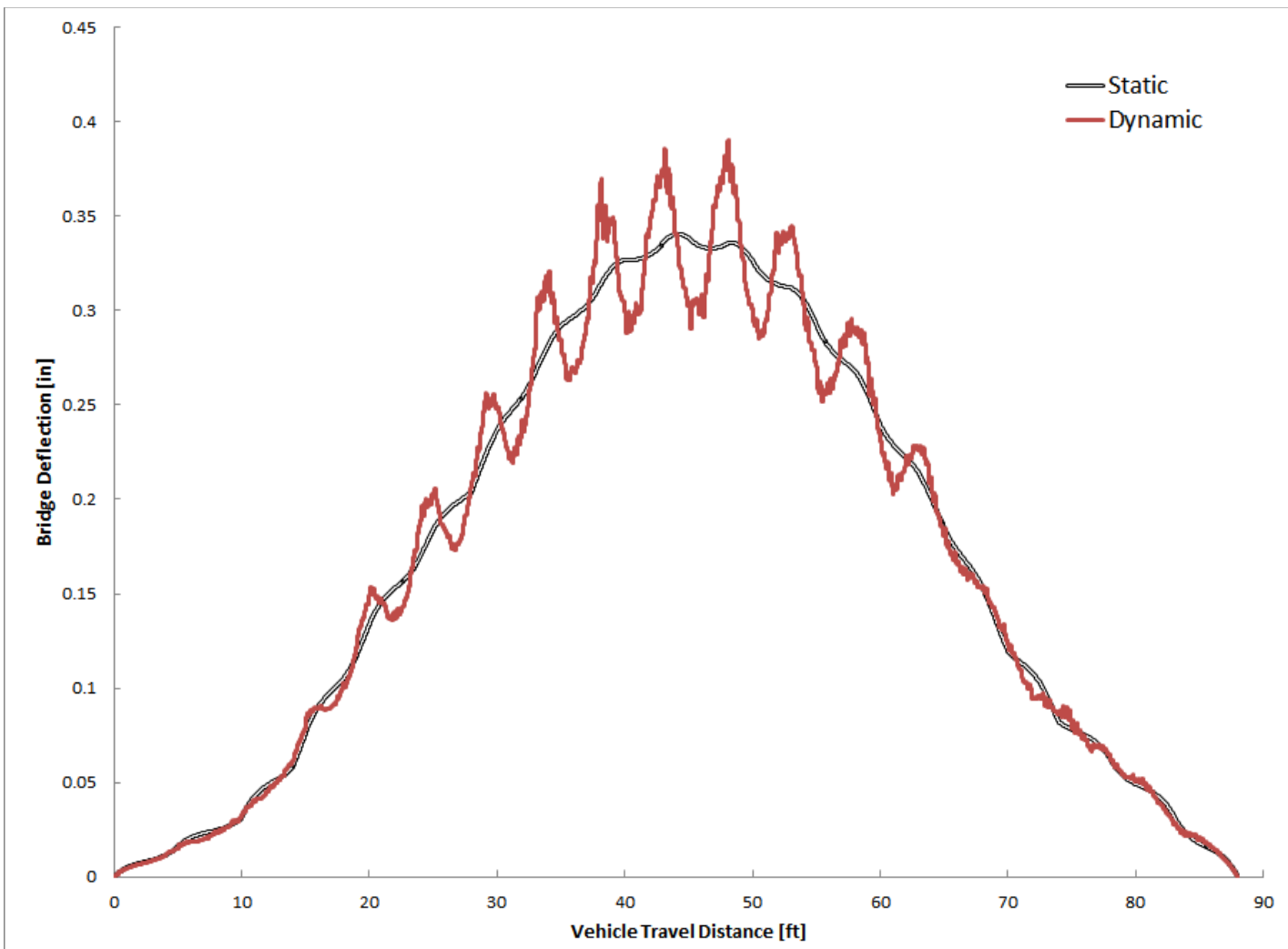


FIGURE 5-33: DISPLACEMENT OF 60 FT. STEEL BRIDGE DUE TO TYPE 3S1 (“VERY GOOD” SURFACE)

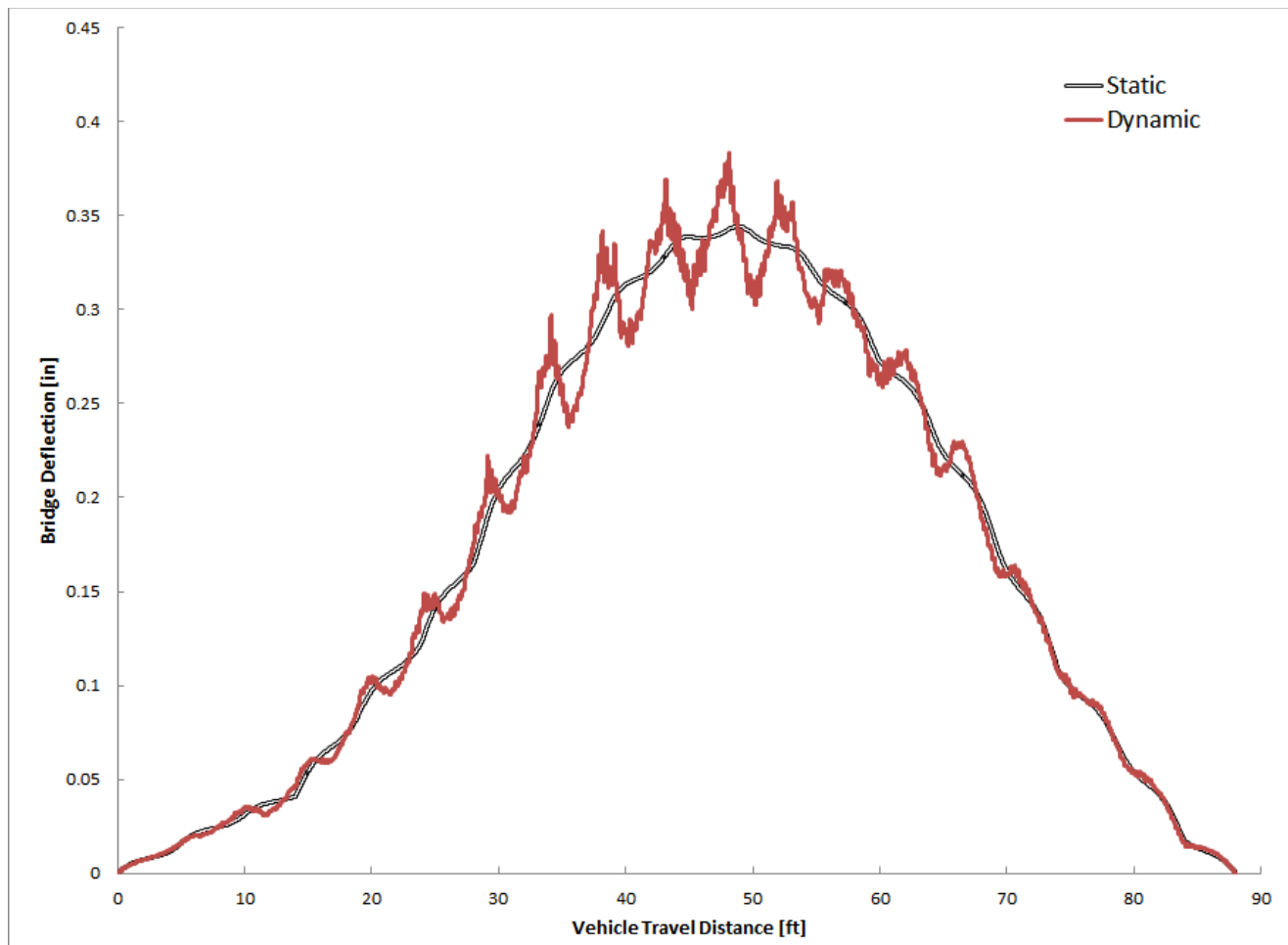


FIGURE 5-34: DISPLACEMENT OF 60 FT. STEEL BRIDGE DUE TO TYPE 2S2 (“VERY GOOD” SURFACE)

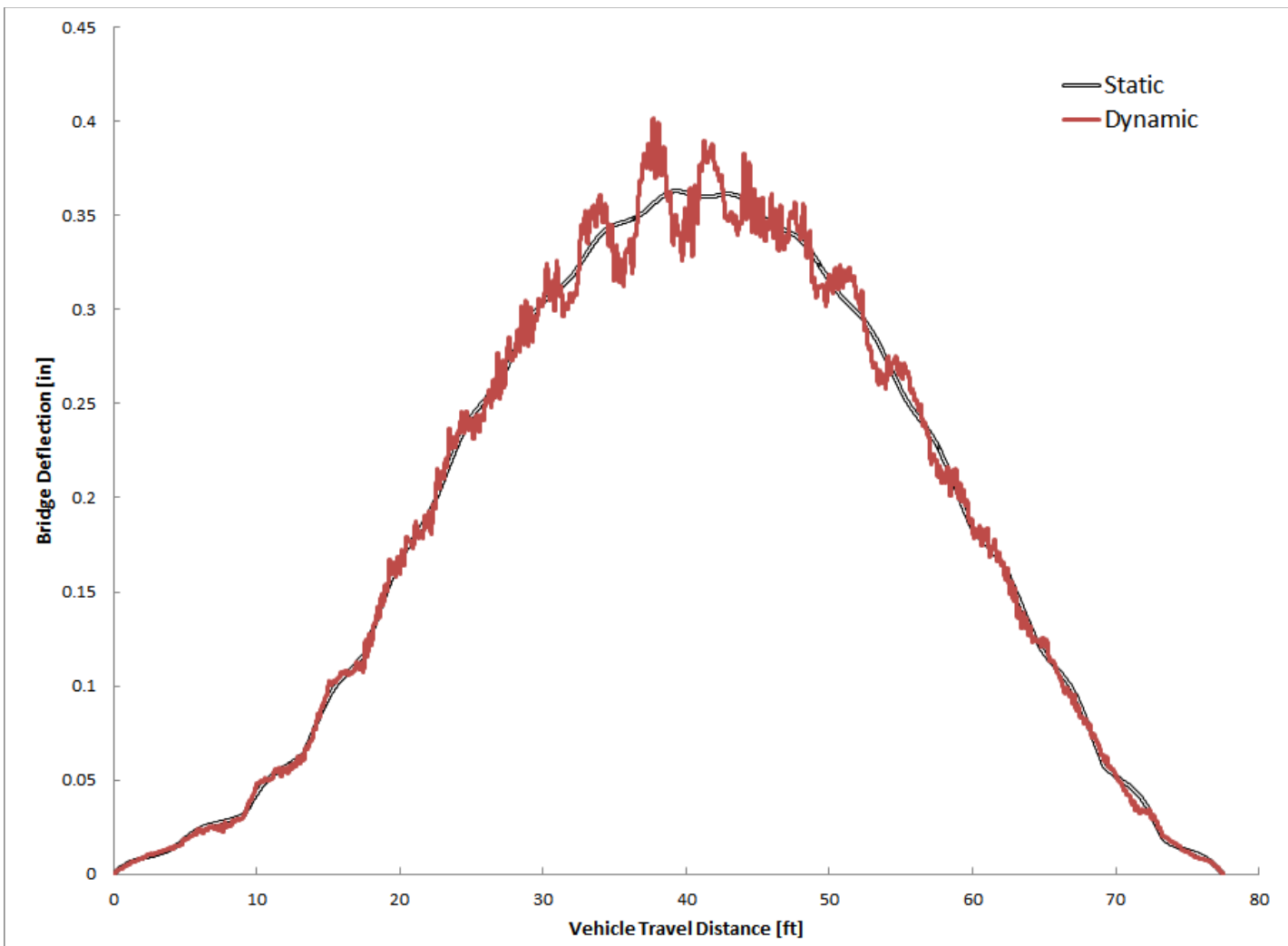


FIGURE 5-35: DISPLACEMENT OF 60 FT. STEEL BRIDGE DUE TO SU4 (“VERY GOOD” SURFACE)

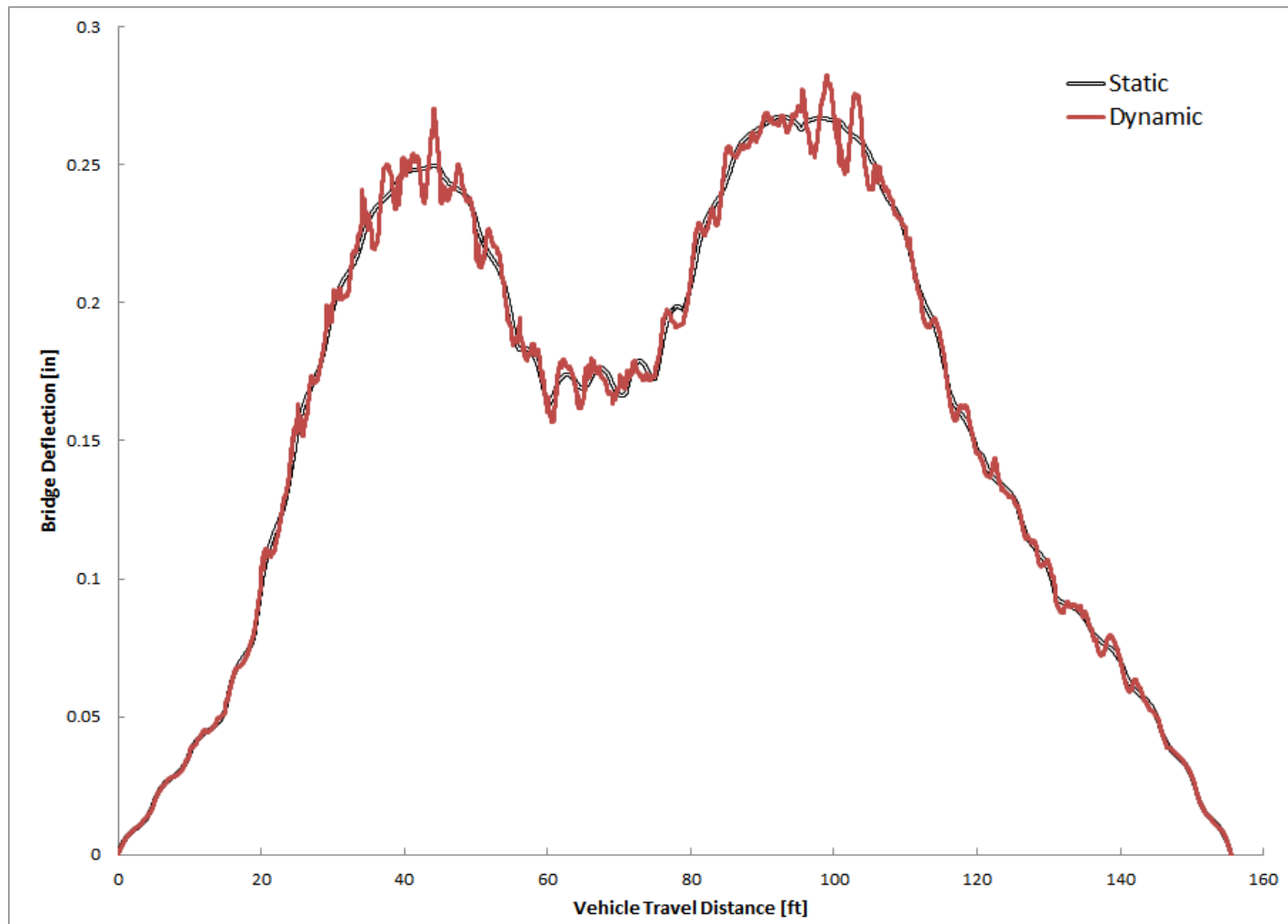


FIGURE 5-36: DISPLACEMENT OF 60 FT. STEEL BRIDGE DUE TO 7-AXLE ROCKY MOUNTAIN DOUBLE (“VERY GOOD” SURFACE)

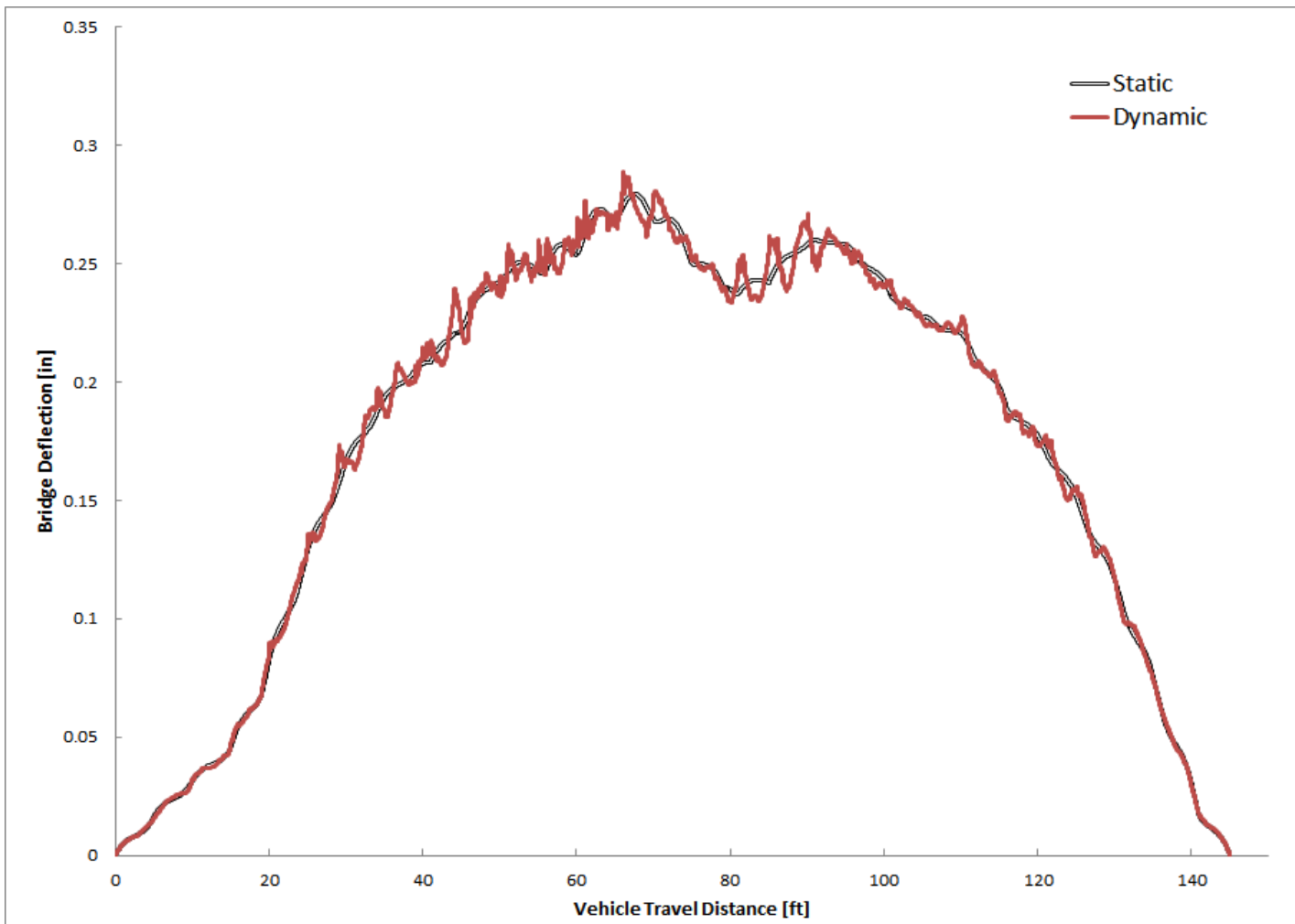


FIGURE 5-37: DISPLACEMENT OF 60 FT. STEEL BRIDGE DUE TO 8 AXLE B-TRAIN DOUBLE (“VERY GOOD” SURFACE)

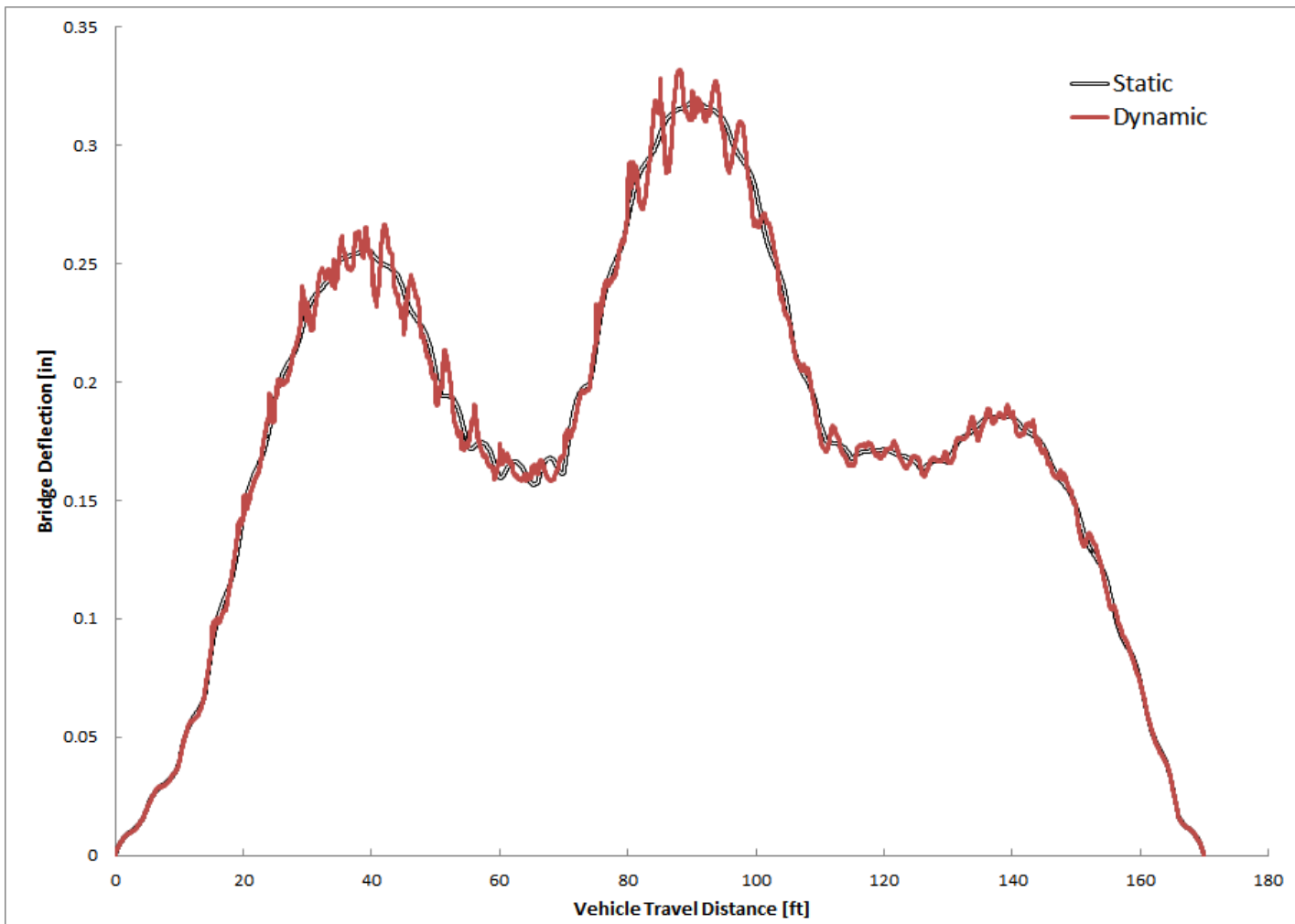


FIGURE 5-38: DISPLACEMENT OF 60 FT. STEEL BRIDGE DUE TO 9 AXLE TURNPIKE DOUBLE (“VERY GOOD” SURFACE)

TABLE 5-8: DYNAMIC AMPLIFICATION FACTOR FOR PRESTRESSED CONCRETE BRIDGES (“VERY GOOD” SURFACE)

Bridge Type	Span Length [feet]	Speed [mph]	Vehicle Type								
			T-1	T-2	T-3	T-4	T-5	T-6	T-7	T-8	T-9
Concrete	30	15	4.0	4.0	2.9	5.5	6.5	4.4	5.7	5.5	1.7
		35	6.6	1.5	5.0	9.4	0.7	1.5	5.7	3.3	1.9
		55	10.9	5.1	4.3	6.7	1.1	1.6	2.4	2.5	6.2
	60	75	17.8	5.2	1.6	3.4	7.3	1.9	6.4	4.1	1.6
		15	3.6	3.7	9.5	3.4	2.2	7.7	9.1	7.3	4.0
		35	3.6	3.7	8.3	5.8	2.5	3.1	6.6	5.6	4.0
90	60	55	4.1	2.9	9.6	5.4	5.0	4.1	2.2	5.0	4.5
		75	8.9	0.9	7.9	1.8	1.5	2.4	5.3	4.3	3.1
		15	5.3	2.0	8.1	4.6	4.0	3.7	6.6	9.7	2.1
	90	35	4.6	3.0	6.9	5.3	4.1	5.7	8.0	8.3	2.7
		55	7.3	3.1	6.3	10.7	6.1	4.0	3.2	5.2	6.2
		75	11.0	1.4	4.2	9.1	6.0	4.1	2.0	4.8	5.4
120	90	15	4.6	4.9	9.3	4.3	4.1	4.0	5.5	7.5	4.7
		35	4.6	4.4	10.4	6.4	5.8	5.1	9.5	6.6	3.2
		55	4.1	3.2	6.8	7.7	6.5	4.1	4.0	5.2	5.3
	120	75	12.1	2.5	11.9	5.8	7.2	4.3	5.2	11.4	4.4
		15	6.0	5.4	7.2	4.8	4.0	6.4	6.6	8.3	5.6
		35	7.7	7.5	13.6	11.7	21.4	12.6	16.2	13.7	5.8
140	120	55	5.0	4.4	12.0	8.8	8.3	4.1	3.3	6.3	5.6
		75	6.9	6.1	5.8	7.1	9.5	4.9	9.1	6.7	8.4
											6.8
											6.3

TABLE 5-9: DYNAMIC AMPLIFICATION FACTOR FOR STEEL BRIDGES (“VERY GOOD” SURFACE)

Bridge Type	Span Length [feet]	Speed [mph]	Vehicle Type										
			T-1	T-2	T-3	T-4	T-5	T-6	T-7	T-8	T-9	T-10	T-11
Concrete	30	15	3.5	4.9	4.2	6.9	8.2	5.0	9.4	8.9	1.2	3.2	3.9
		35	6.8	3.5	6.0	10.5	0.2	1.6	6.4	5.1	1.8	3.5	2.4
		55	7.7	6.9	6.8	6.3	0.6	1.1	3.5	3.4	6.8	9.3	2.2
		75	18.0	7.3	5.8	2.5	6.3	7.5	5.5	4.4	1.3	0.6	2.1
	60	15	4.1	7.9	12.3	4.2	5.1	11.3	14.5	10.6	5.7	3.3	4.2
		35	5.8	6.1	9.0	6.3	4.6	8.0	9.6	8.3	6.9	3.2	5.2
90	55	3.1	3.6	9.8	10.3	7.6	6.3	5.4	7.7	7.6	7.8	11.0	
		75	7.5	3.5	10.9	3.3	1.1	4.1	7.0	4.0	6.3	7.8	4.3
		15	5.0	3.6	8.2	7.7	7.1	5.4	9.0	8.8	6.5	4.5	5.6
	35	4.9	4.2	17.0	11.0	9.1	6.4	6.3	12.4	7.9	5.2	5.9	
		75	14.2	1.5	8.8	13.2	11.2	4.6	3.3	8.7	10.5	12.5	10.0
	120	15	5.9	4.4	12.1	6.1	6.4	4.0	8.4	7.7	8.2	4.4	5.7
		35	4.8	5.5	15.0	12.6	12.7	6.7	9.1	10.6	4.4	7.1	5.2
		55	4.9	4.1	10.8	10.0	10.6	6.1	5.9	11.9	9.9	6.0	8.3
140	75	11.4	2.0	9.8	10.0	9.5	4.0	4.1	6.2	9.4	5.8	7.7	
		15	4.3	5.2	8.2	4.9	4.7	6.1	7.0	6.9	6.3	4.6	9.2
		35	5.3	6.1	7.5	12.7	7.5	5.3	8.1	11.6	4.6	7.0	5.2
	55	6.1	5.3	11.8	12.0	8.6	6.5	4.4	6.6	6.9	7.9	6.6	
	75	7.7	4.4	7.1	6.6	8.1	6.6	7.0	6.2	9.9	8.4	6.9	

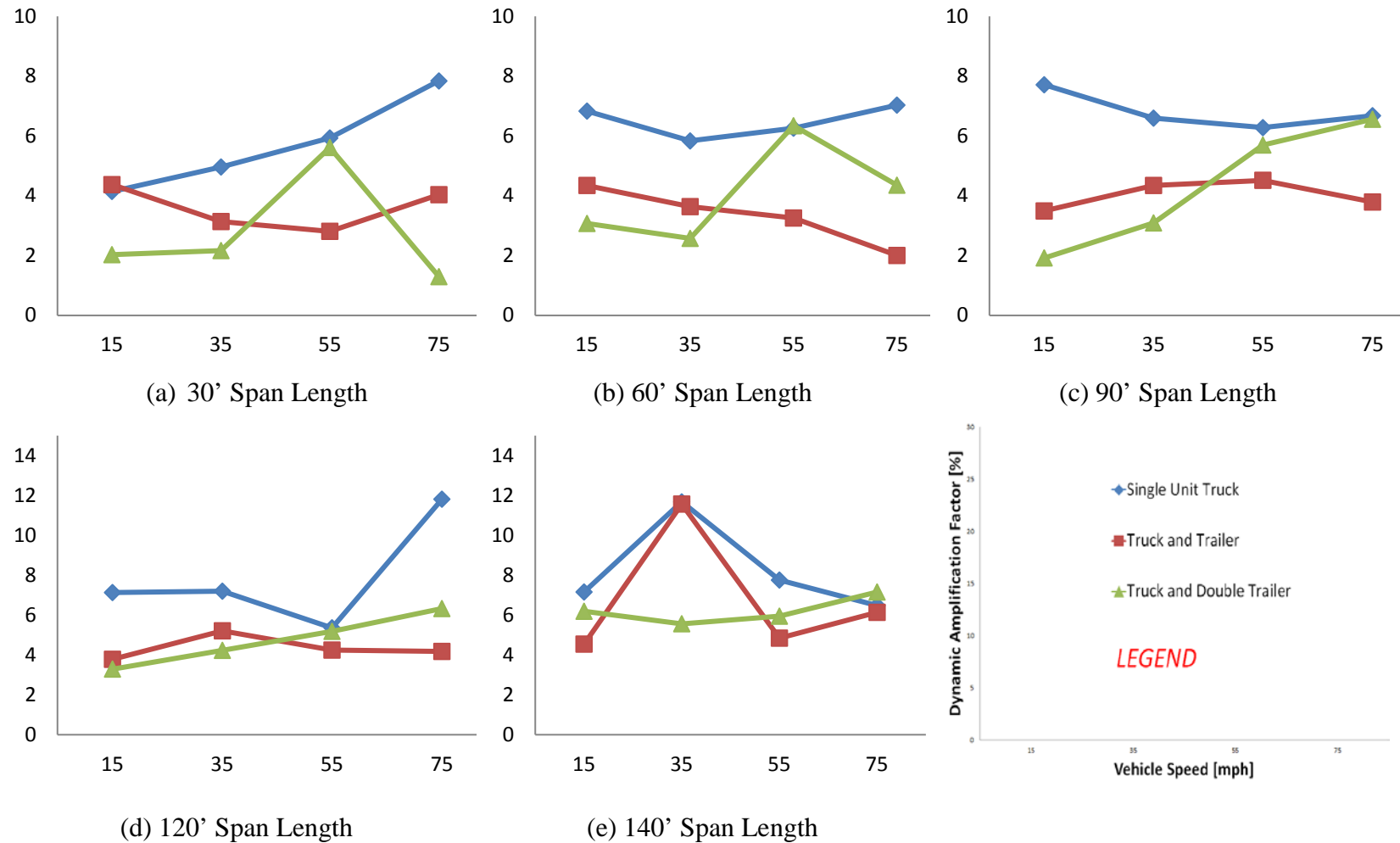


FIGURE 5-39: PRESTRESSED CONCRETE BRIDGES DAF FOR DIFFERENT VEHICLE CATEGORIES (“VERY GOOD” SURFACE)

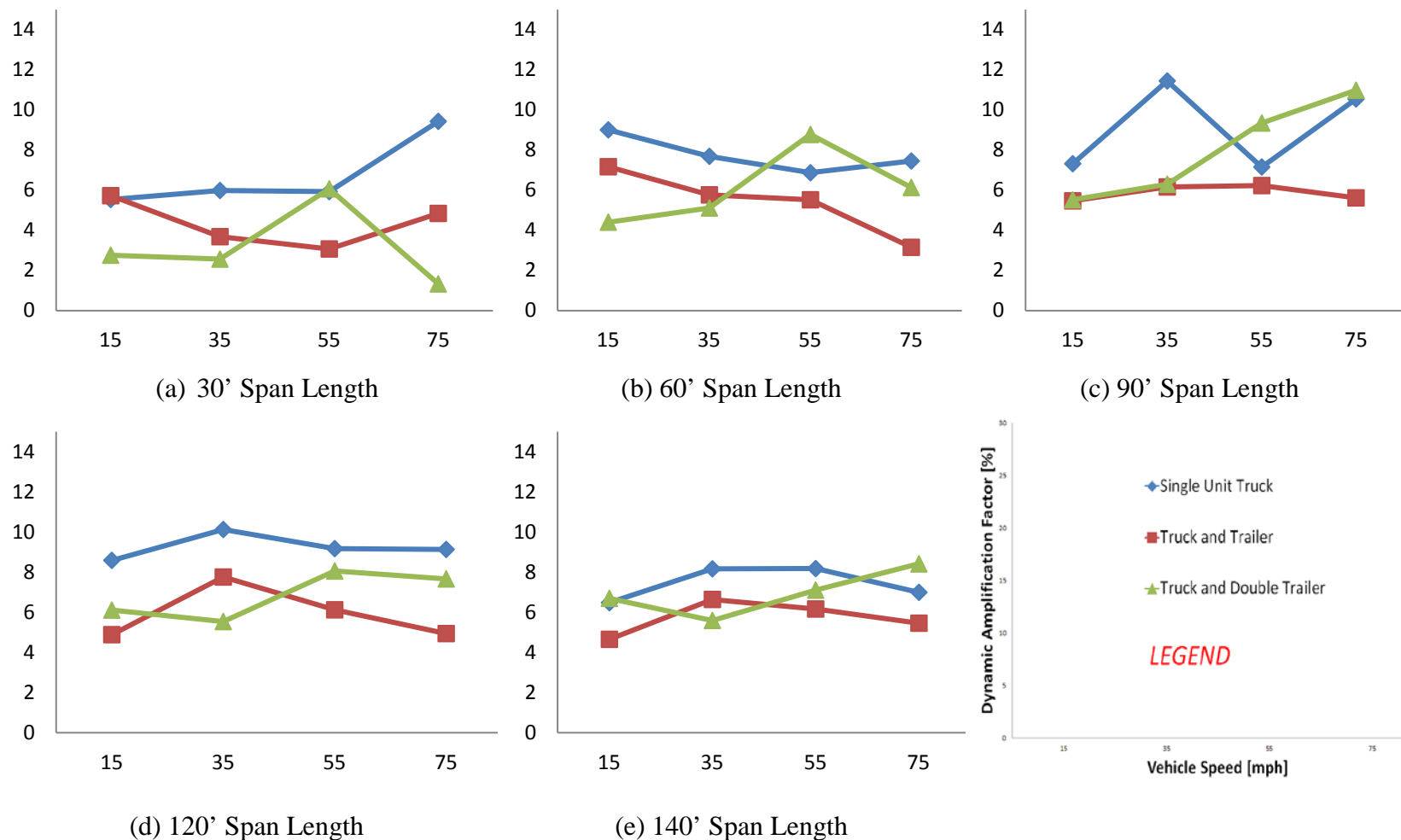


FIGURE 5-40: STEEL BRIDGES DAF FOR DIFFERENT VEHICLE CATEGORIES (“VERY GOOD” SURFACE)

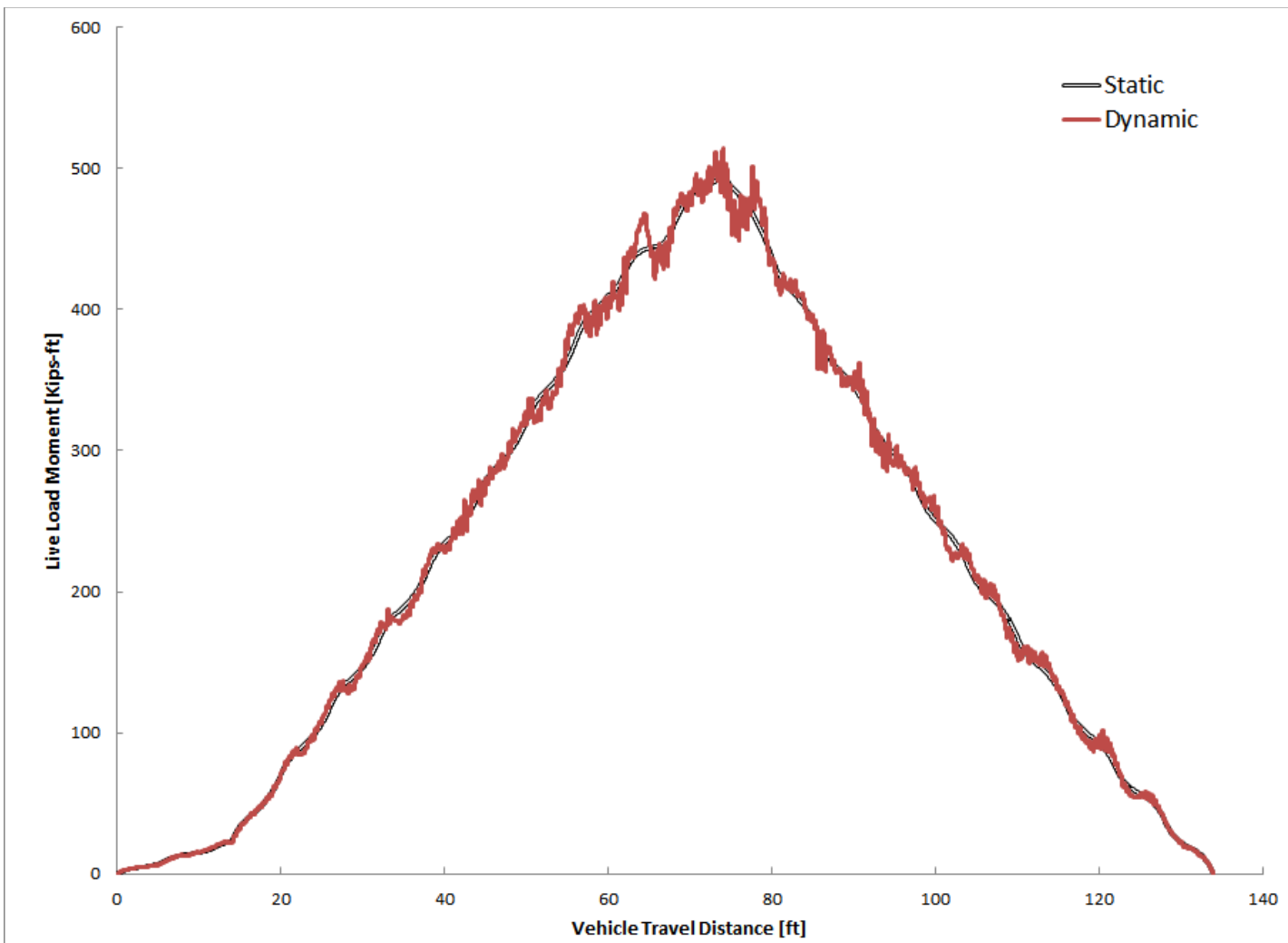


FIGURE 5-41: MOMENT OF 120 FT. STEEL BRIDGE DUE TO H-20 (“VERY GOOD” SURFACE)

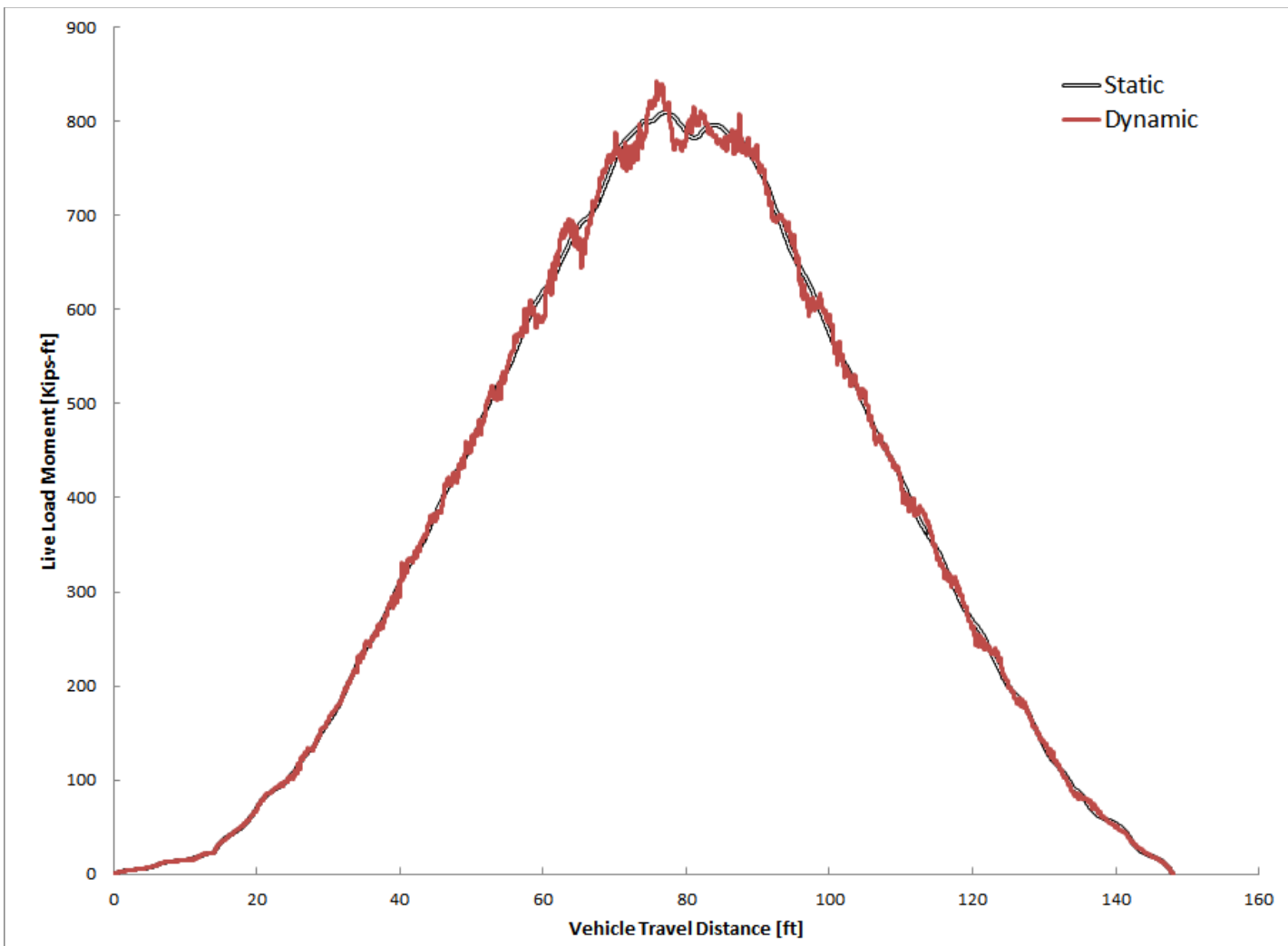


FIGURE 5-42: MOMENT OF 120 FT. STEEL BRIDGE DUE TO HS-20 (“VERY GOOD” SURFACE)

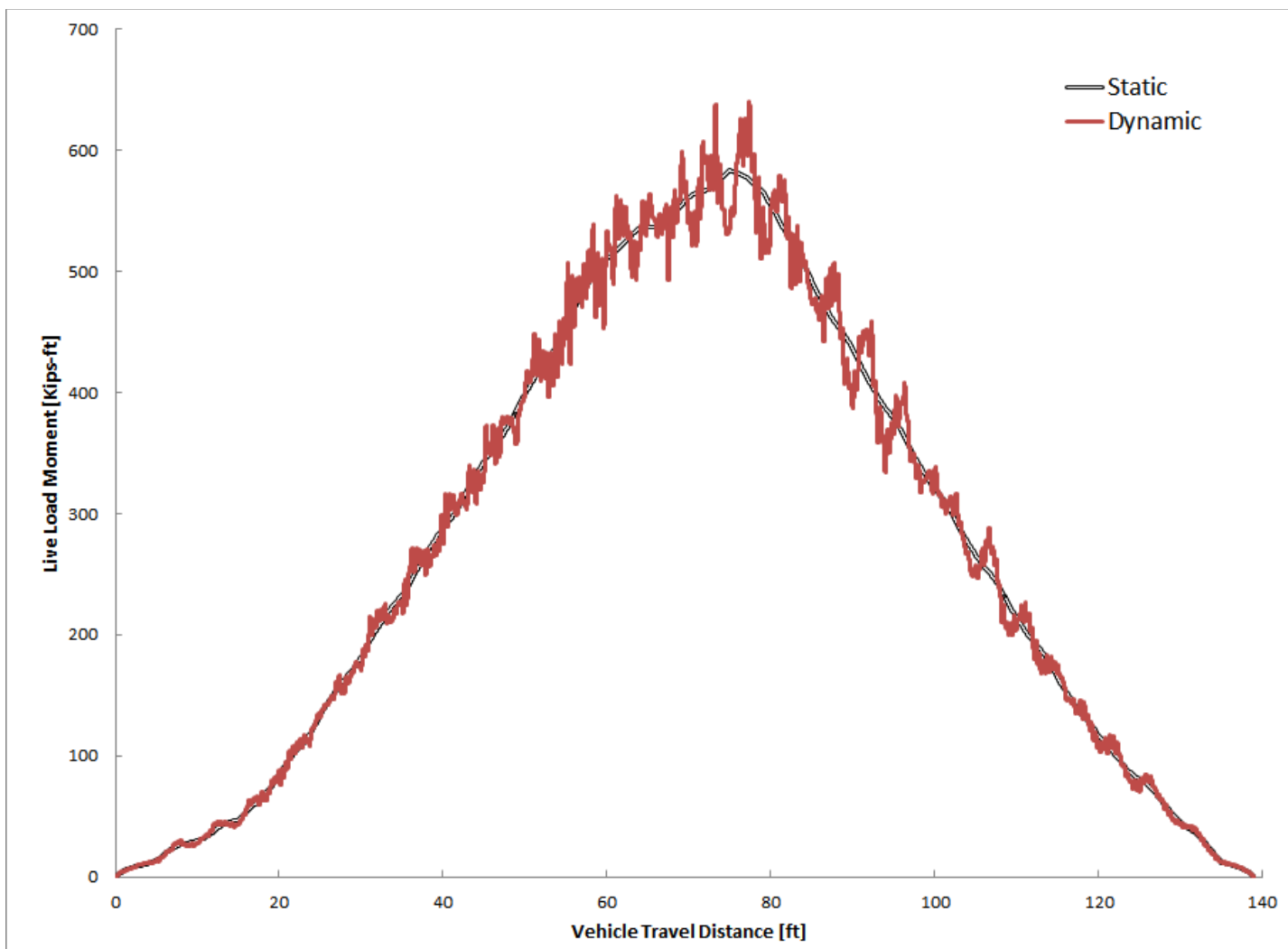


FIGURE 5-43: MOMENT OF 120 FT. STEEL BRIDGE DUE TO TYPE 3 (“VERY GOOD” SURFACE)

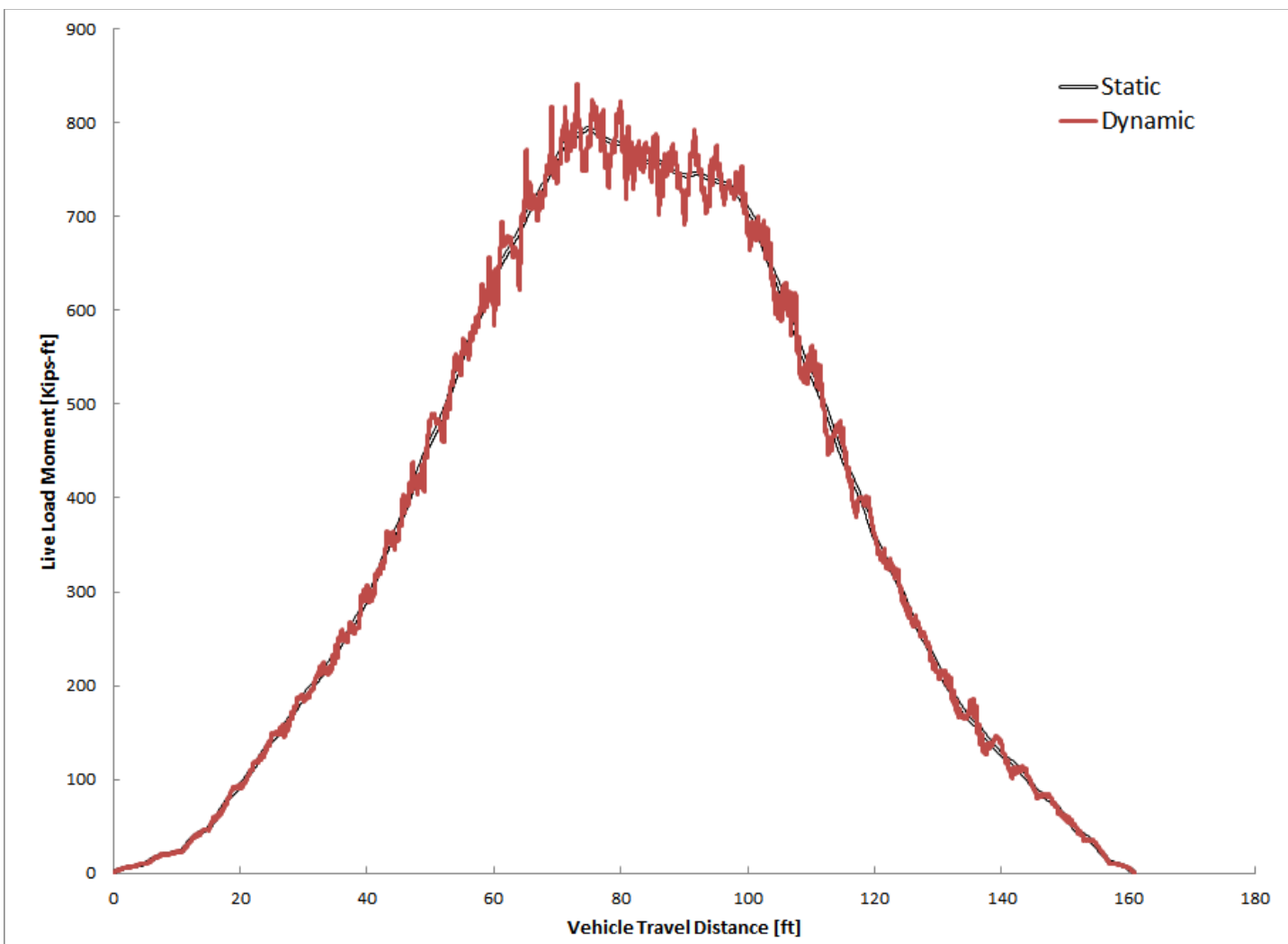


FIGURE 5-44: MOMENT OF 120 FT. STEEL BRIDGE DUE TO TYPE 3S2 (“VERY GOOD” SURFACE)

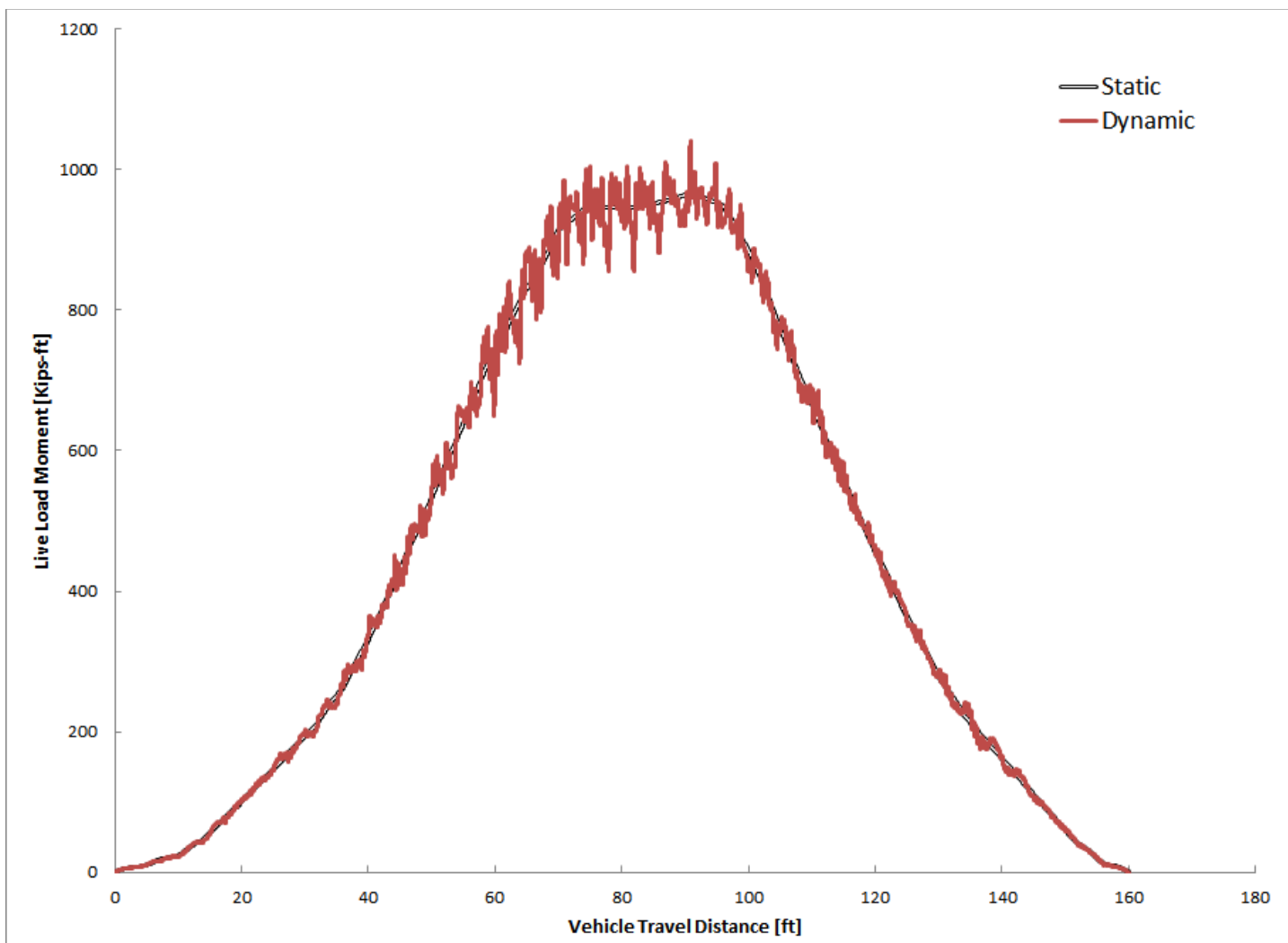


FIGURE 5-45: MOMENT OF 120 FT. STEEL BRIDGE DUE TO TYPE 3S3 (“VERY GOOD” SURFACE)

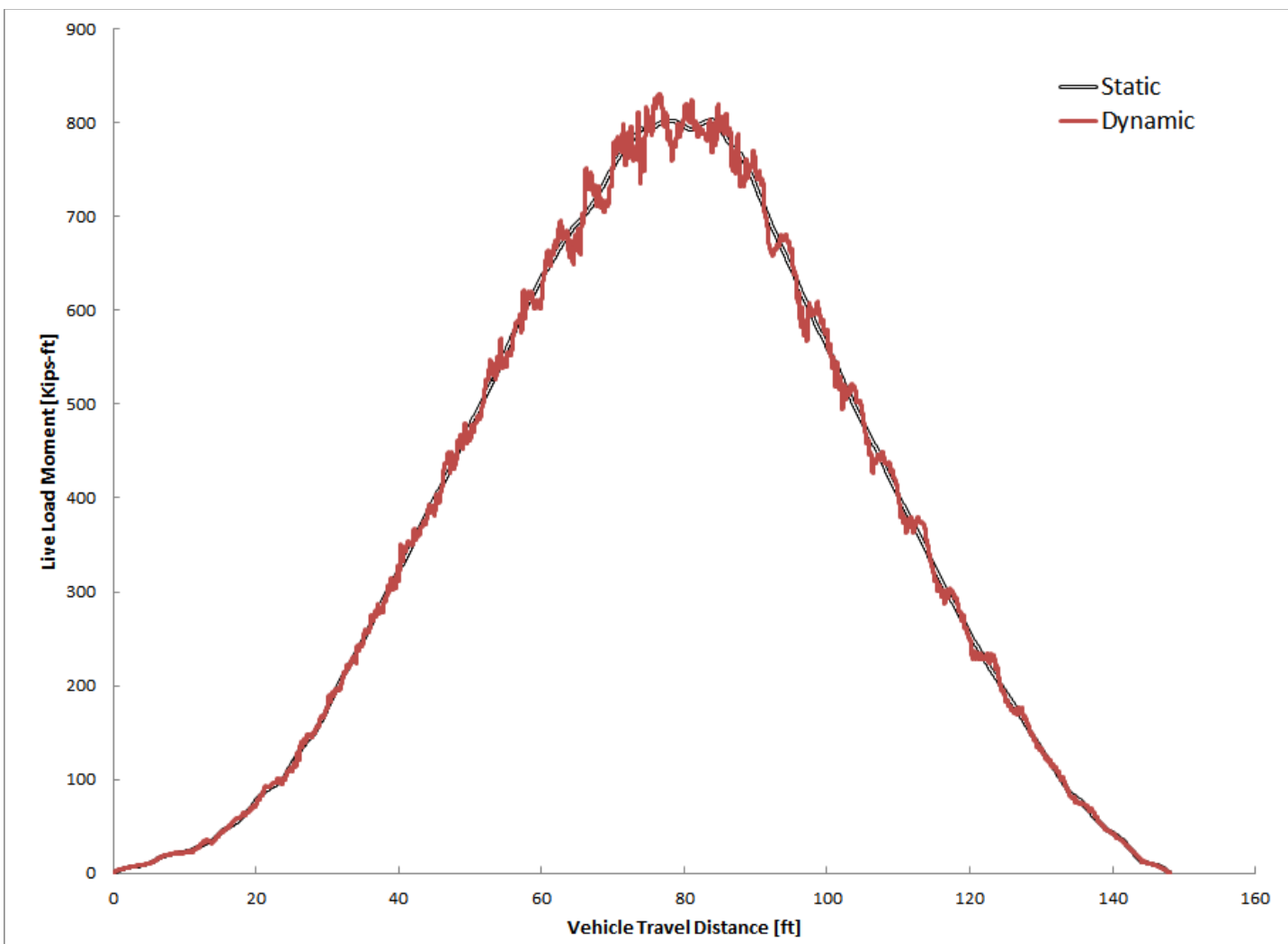


FIGURE 5-46: MOMENT OF 120 FT. STEEL BRIDGE DUE TO TYPE 2S2 (“VERY GOOD” SURFACE)

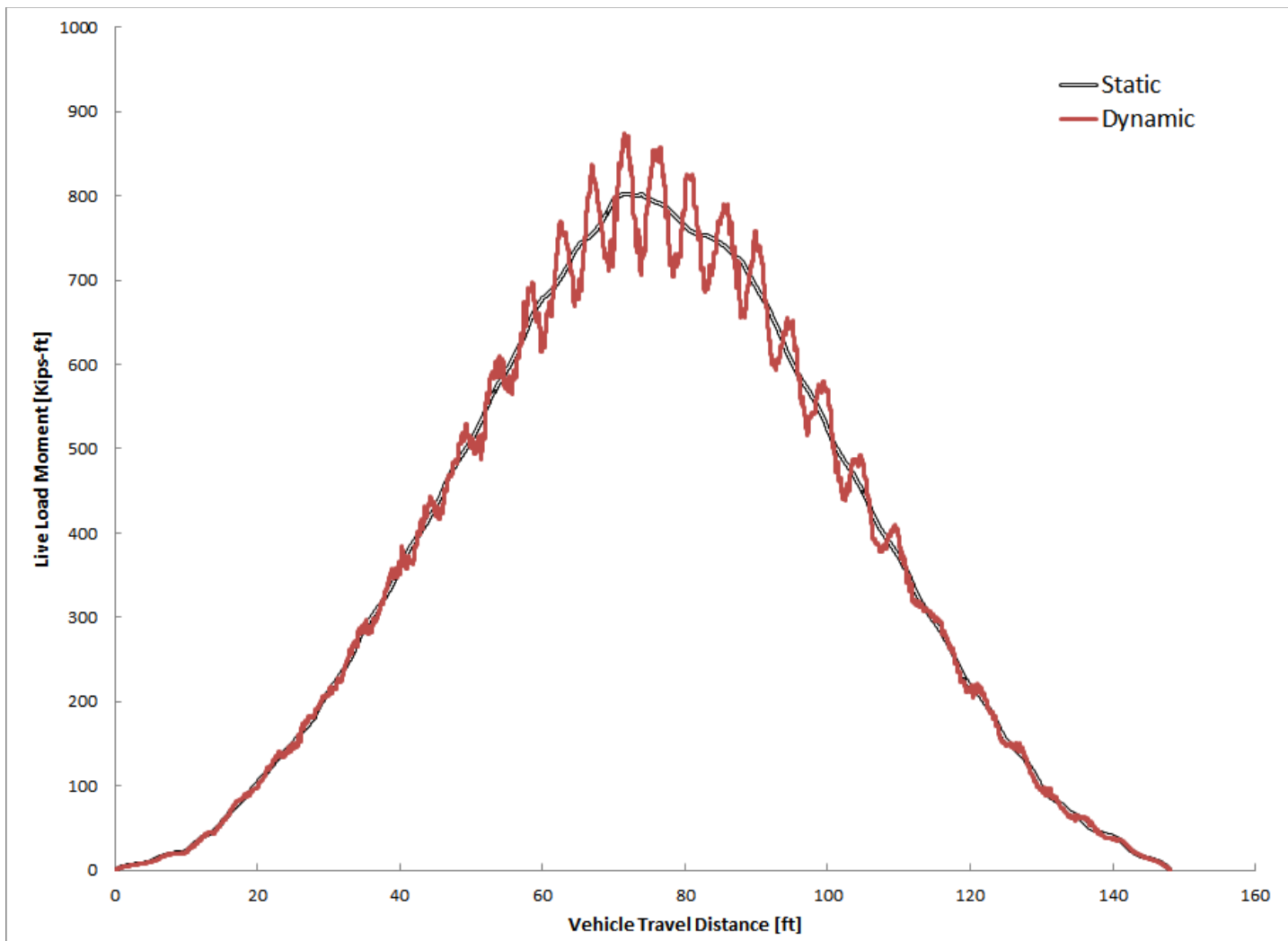


FIGURE 5-47: MOMENT OF 120 FT. STEEL BRIDGE DUE TO TYPE 3S1 (“VERY GOOD” SURFACE)

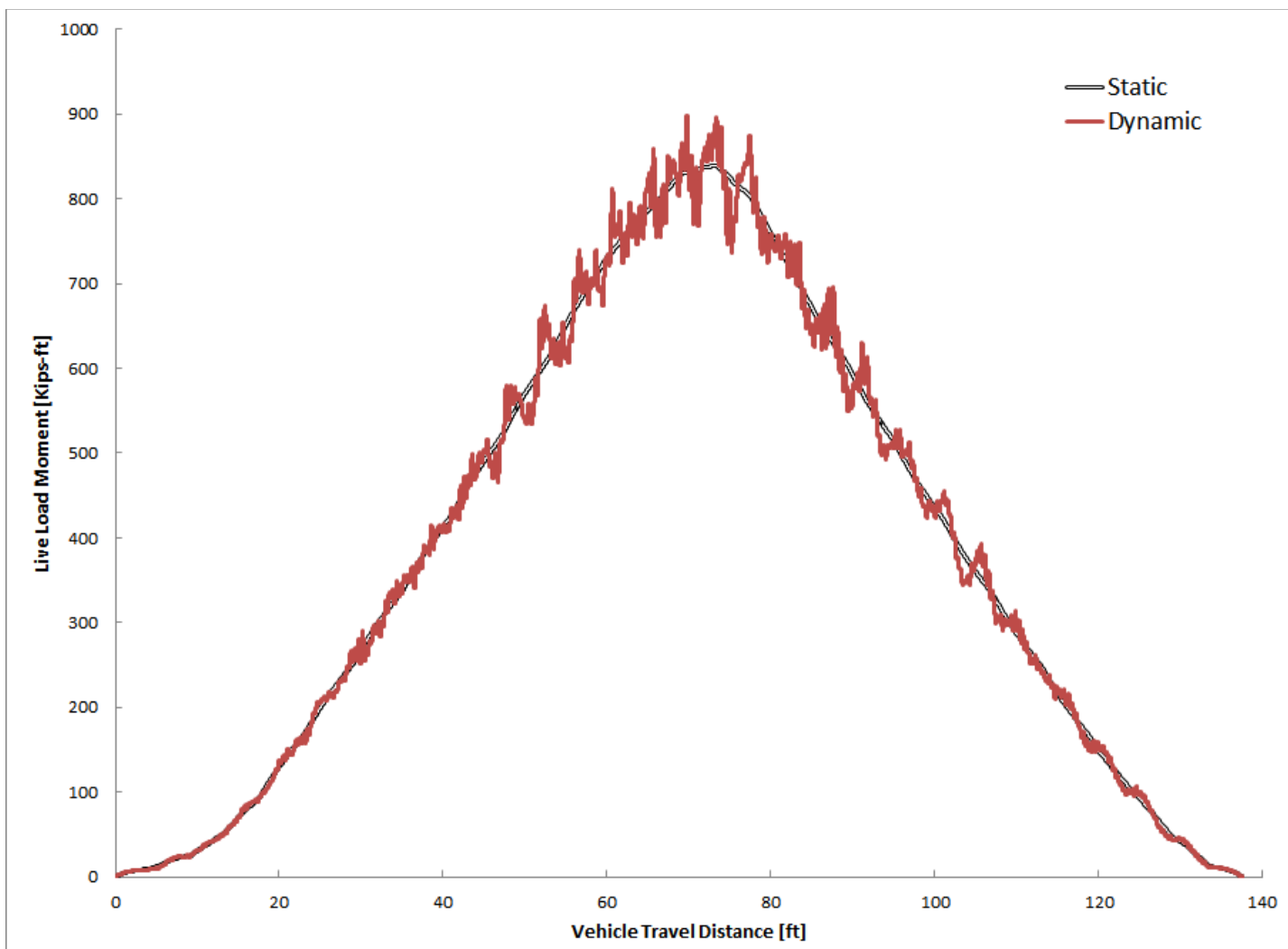


FIGURE 5-48: MOMENT OF 120 FT. STEEL BRIDGE DUE TO TYPE SU4 (“VERY GOOD” SURFACE)

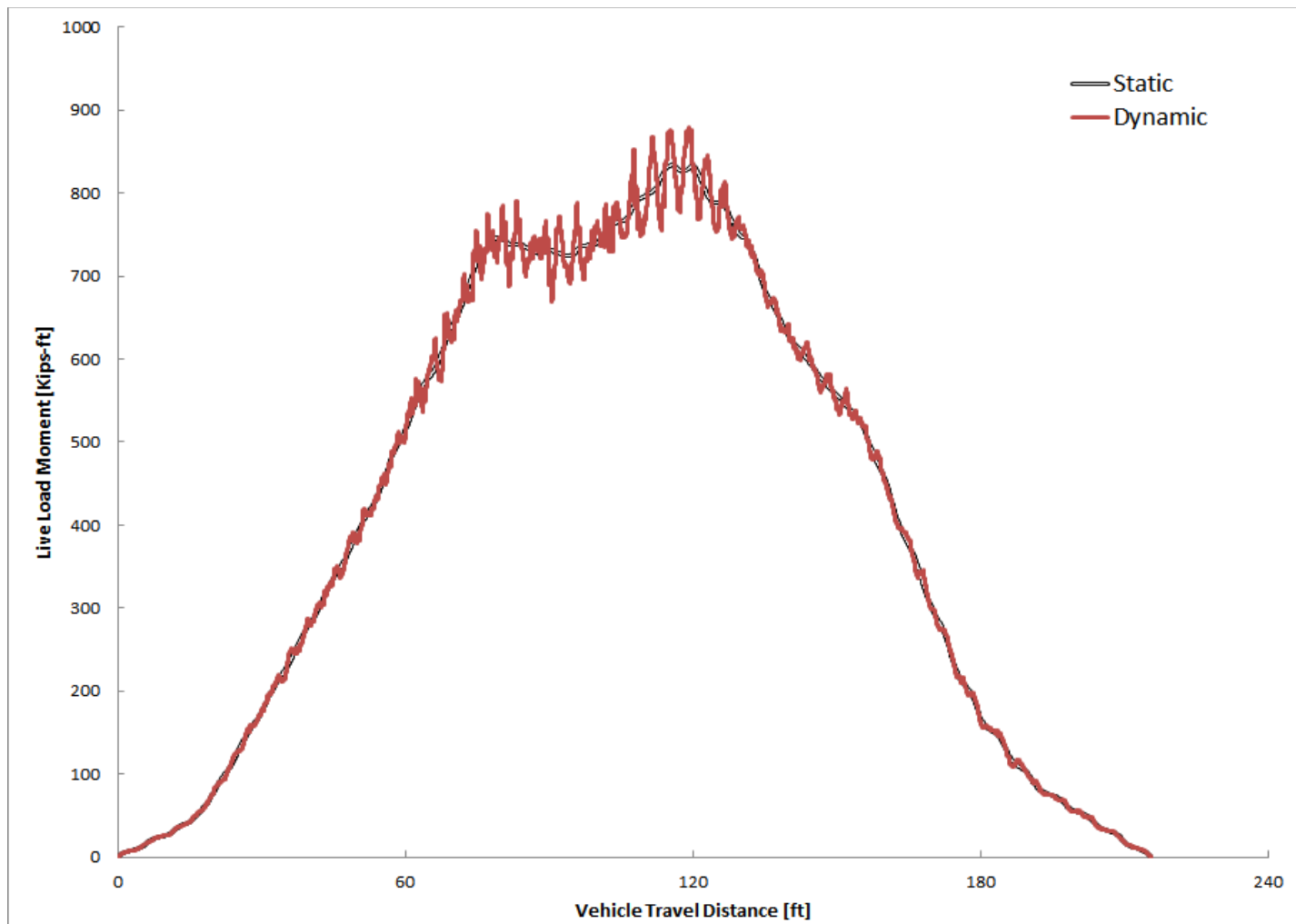


FIGURE 5-49: MOMENT OF 120 FT. STEEL BRIDGE DUE TO 7-AXLE ROCKY MOUNTAIN DOUBLE (“VERY GOOD” SURFACE)

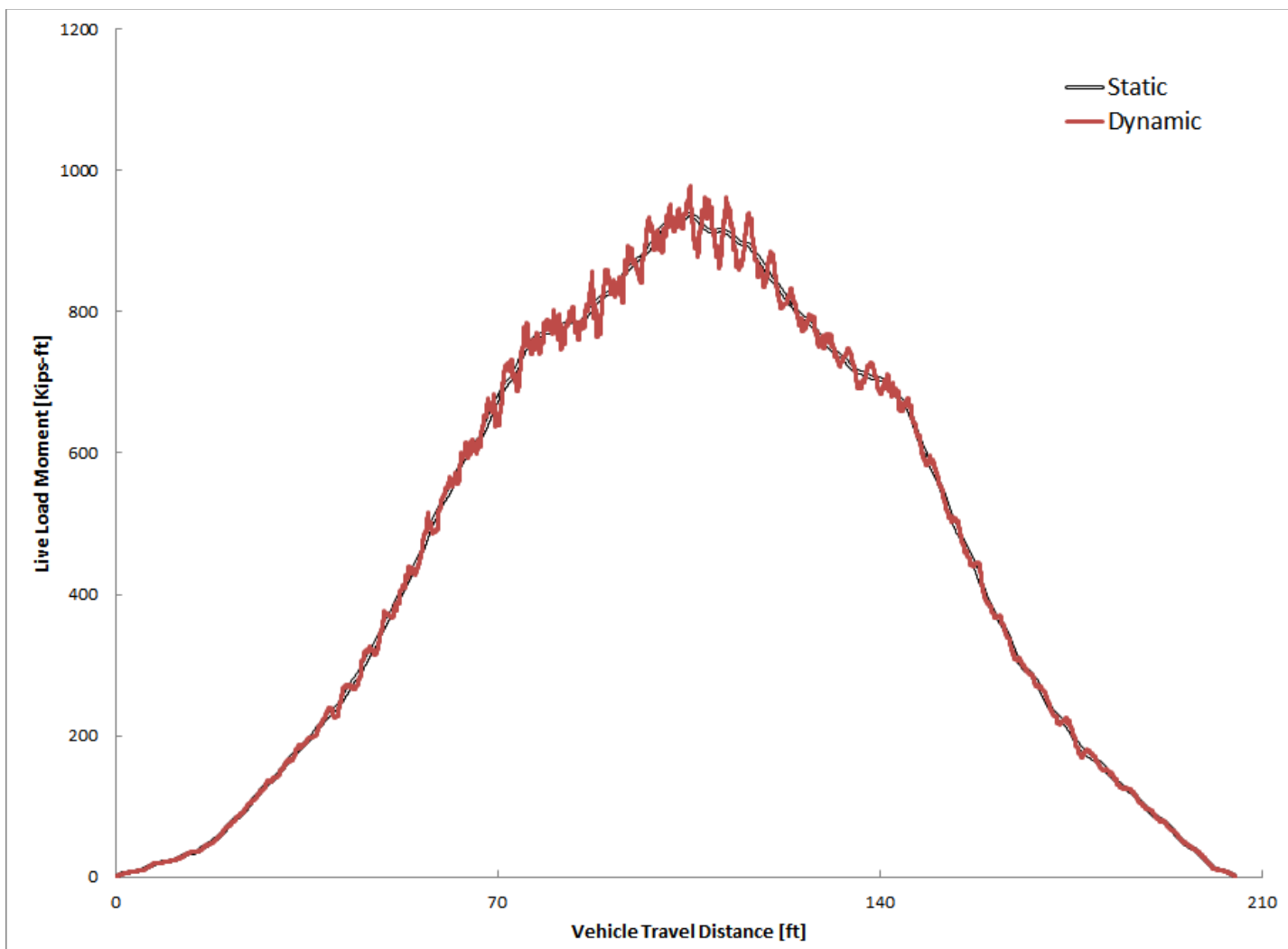


FIGURE 5-50: MOMENT OF 120 FT. STEEL BRIDGE DUE TO 8 AXLE B-TRAIN DOUBLE (“VERY GOOD” SURFACE)

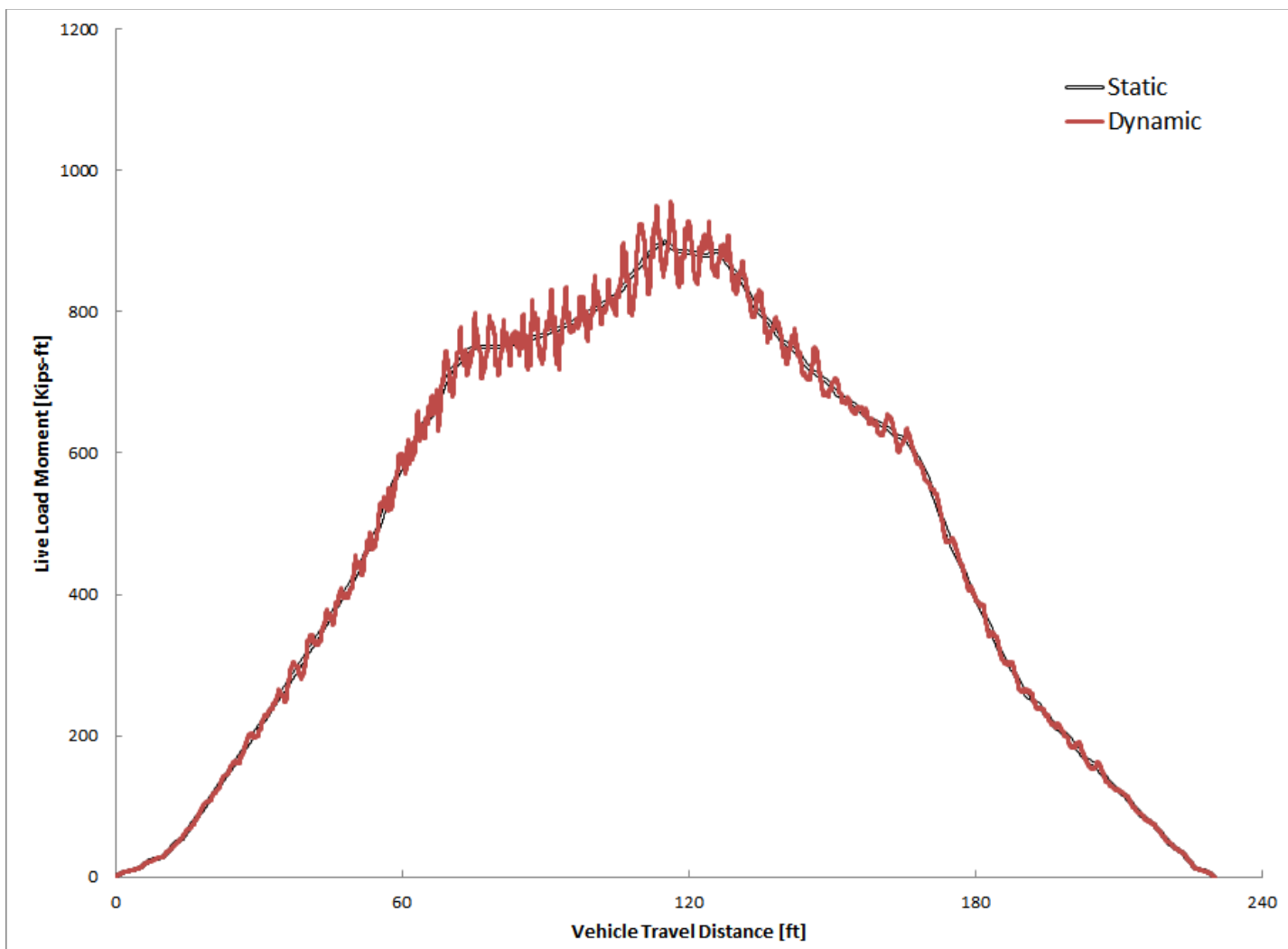


FIGURE 5-51: MOMENT OF 120 FT. STEEL BRIDGE DUE TO 9 AXLE TURNPIKE DOUBLE (“VERY GOOD” SURFACE)

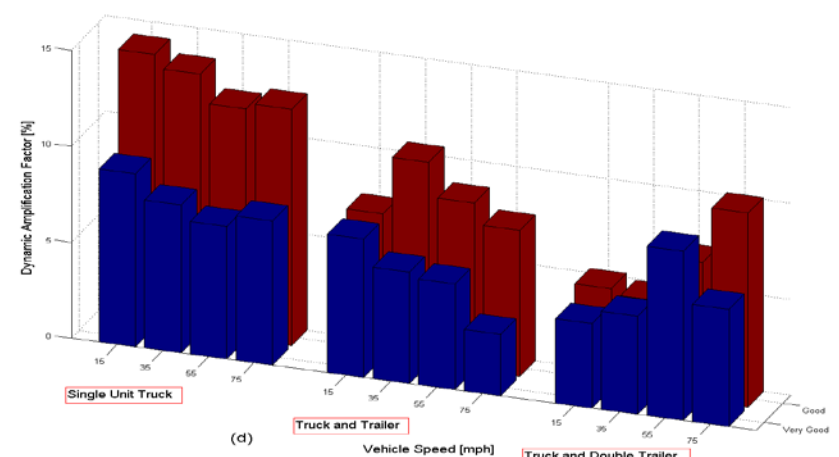
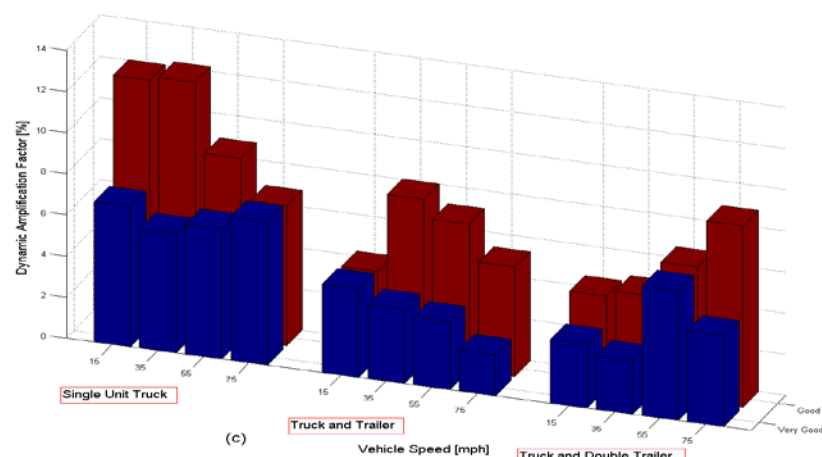
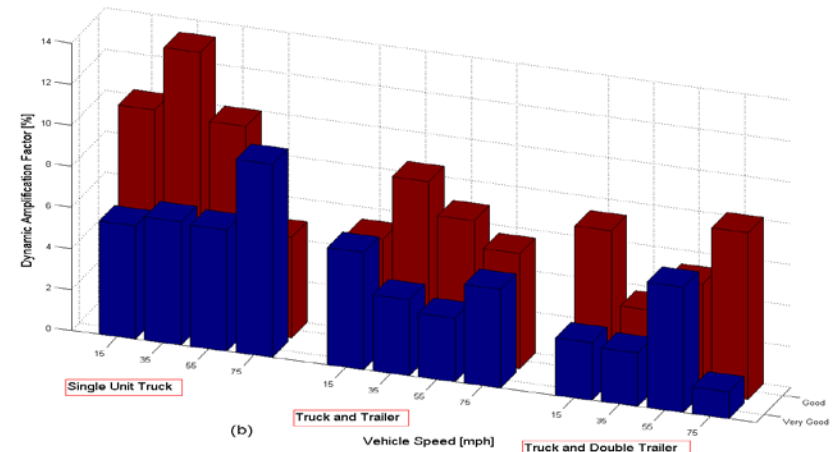
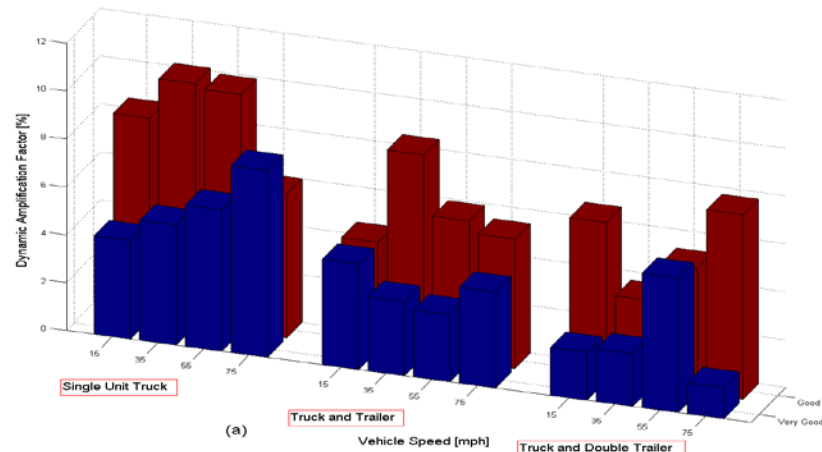


FIGURE 5-52: COMPARISON OF THE "VERY GOOD" AND "GOOD" SURFACES RESULTS (A) 30' CONCRETE (B) 30' STEEL (C) 60' CONCRETE (D) 60' STEEL

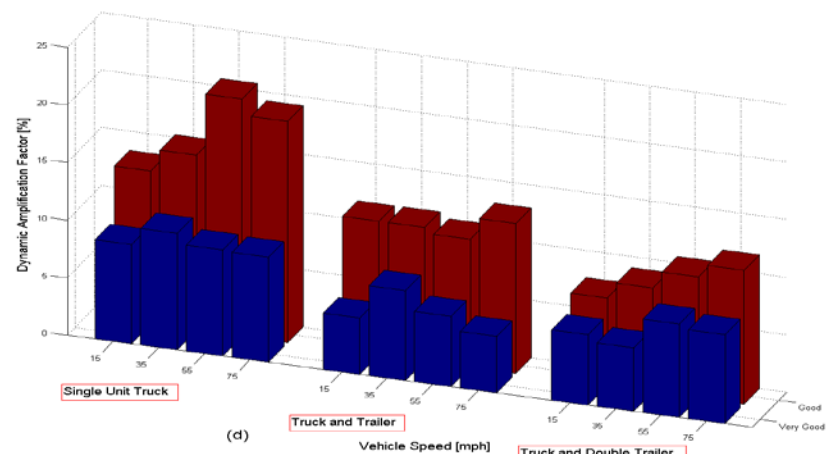
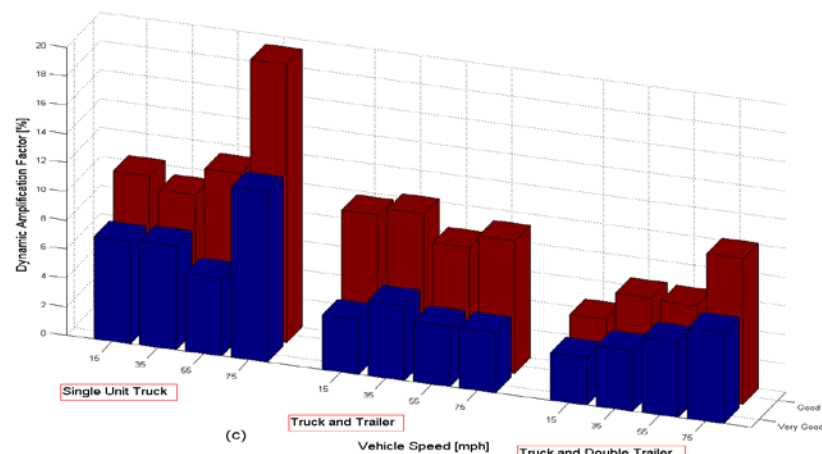
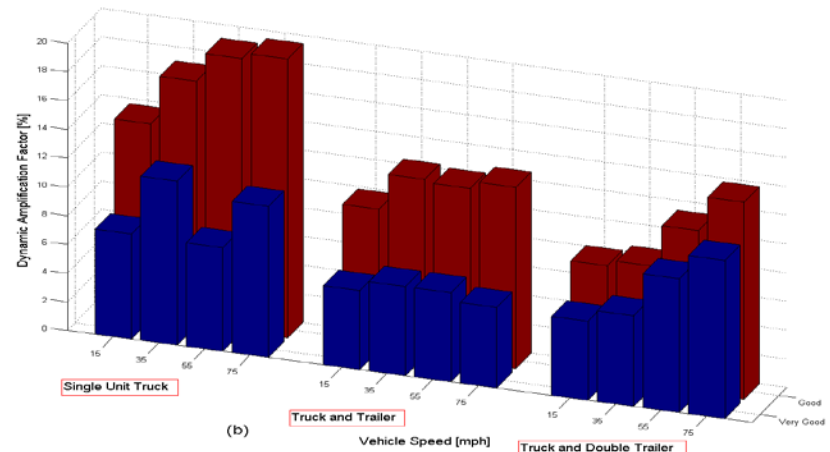
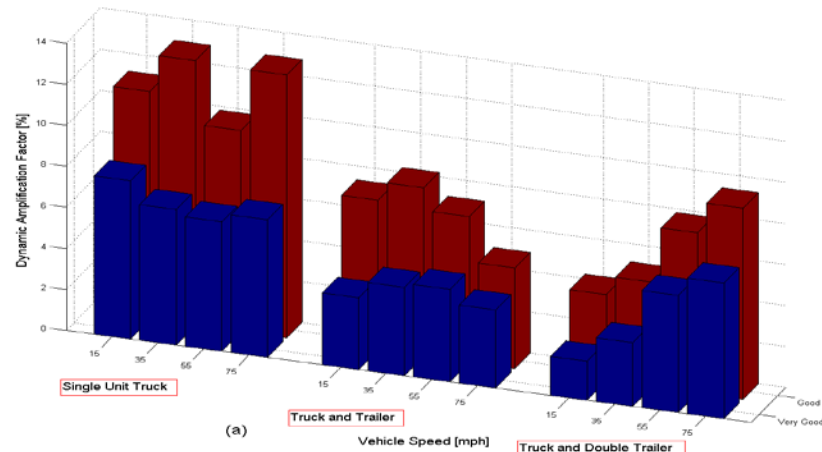


FIGURE 5-53: COMPARISON OF THE "VERY GOOD" AND "GOOD" SURFACES RESULTS (A) 90' CONCRETE (B) 90' STEEL (C) 120' CONCRETE (D) 120' STEEL

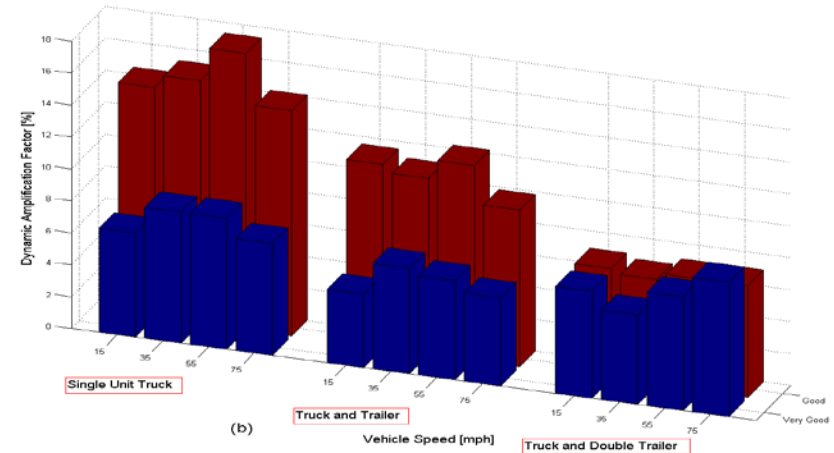
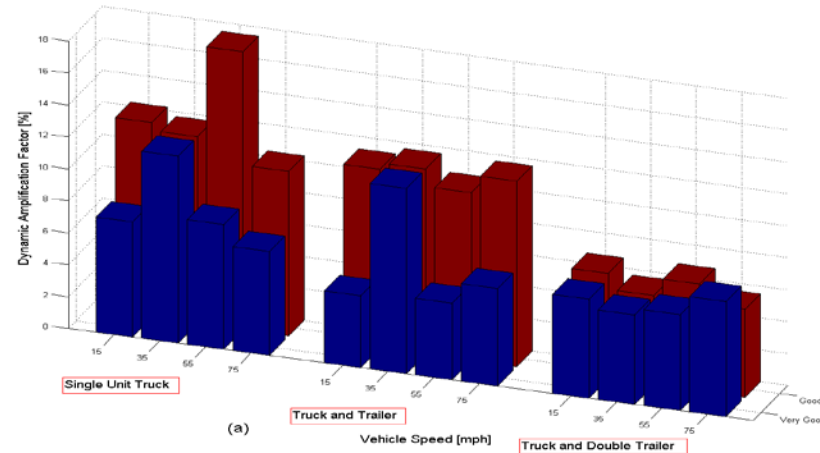


FIGURE 5-54: COMPARISON OF THE "VERY GOOD" AND "GOOD" SURFACES RESULTS (A) 140' CONCRETE (B) 140' STEEL

6. Legal and Longer Combination Vehicles in Florida State

6.1 General overview

The automobile traffic is the most common type of vehicular live loading on bridges, however, truck loads are usually responsible of causing the critical load effects to occur. Generally, car traffic neglected comparing to truck loading. Therefore, the loading principle in AASHTO design code tries to model the loading of the traffic in a way that is highly variable, dynamic and most likely to happen independent of other trucks.

Loading a bridge with a truck has the same logic as the gravity loading but additional considerations are to be made such as dynamic effects, breaking forces, centrifugal forces, and the effects of other trucks.

As the first step of loading procedure, a proper lane arrangement should be made so as to know where and how to place the trucks. The typical lane width of 12 feet is commonly accepted for bridges as to design purposes. This design lane is considered for the placement of the traffic load. AASHTO uses lanes of 10 feet in order to analyze the effect of the live load on a bridge. Also the direction of the current and the future traffic should be considered in order to simulate the most critical loading scenario. On the other hand, sometimes construction or detour plans might be the governing parameters to be considered in a bridge design.

When transverse loading of the trucks is required such as in case of lever rule, this loading is accounted for the calculation of distribution factors which is defined in Section 4 and Chapter 11 of AASHTO code.

In bridges with several lanes and girders, wheel of the first truck is placed within 2 feet from the barrier for exterior girders and successively, the second truck within 4 feet of the first truck. Third truck is placed within 6 feet from the second. For interior girders, one wheel is placed over a girder and the positioning of the other trucks have the same pattern as for exterior girders.

The AASHTO loading principle relies on a study done by the Transportation Research Board (TRB). Loads that are above the legal weight or the length limits are cataloged in most of the states as exclusion vehicles and are regularly allowed to operate. These loads are caused typically by short-haul vehicles like solid waste trucks and concrete mixers. Engineers who developed and defined the load models felt that the exclusion trucks are the best representing the extremes involved in the present traffic.

6.2 Florida Legal Load Trucks

In case that a bridge does not have sufficient capacity under the design load rating operating level (load rating of 1.0 or less) it should be load rated for the legal loads to establish the potential need for load posting or strengthening [27]. Florida Department of Transportation (FDOT) provides three types of legal load trucks namely SU4, C5 and ST5. In this study, the two of these trucks SU4 and C5 are considered in analysis. Their axle weights and distances are shown in Figure 9-1.

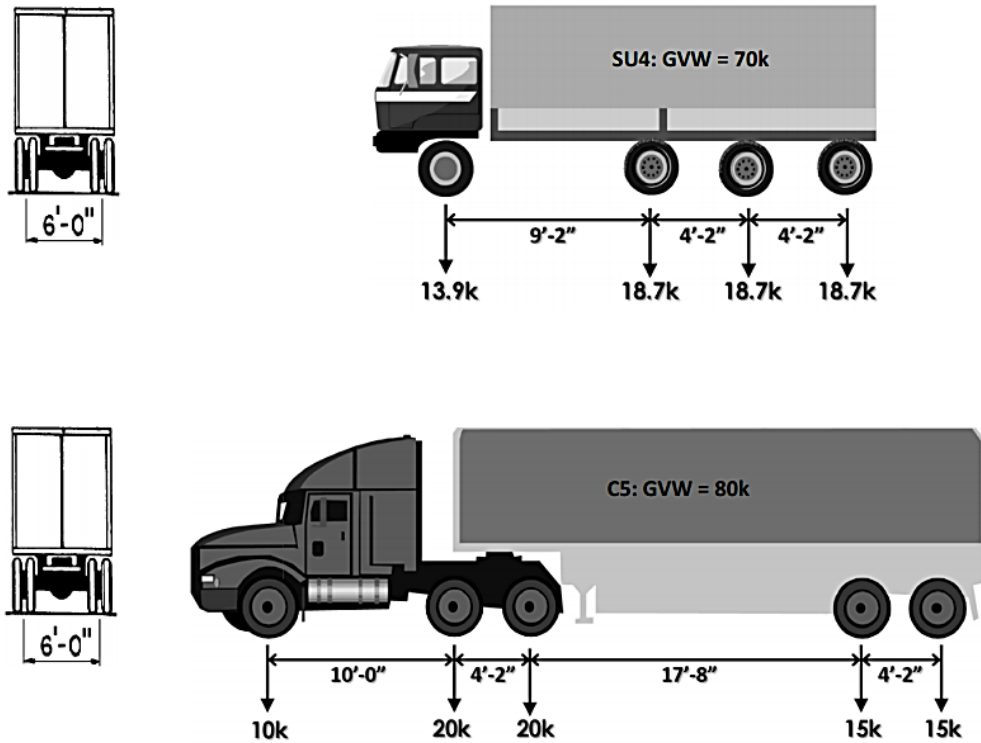


FIGURE 6-1: FLORIDA LEGAL LOADS (7)

6.3 Longer Combination Vehicles (LCV)

Most of the states in nation allow Longer Combination Vehicles (LCV) but they require special permits for their safe operation [28]. In addition to these permits, some states have special requirements like spray suppression devices. They might also have some restriction for the operation of the vehicle. These many include, minimum speed, mandated distances to complete passing maneuvers, designated lanes and load sequencing of the combination's trailers. Figure 6-2 shows the states that are allowing various longer combination vehicles. The two types of the LCVs that are considered in this study are Rocky Mountain Double (RMD) and Turnpike Double (TPD) (Figure 6-3).

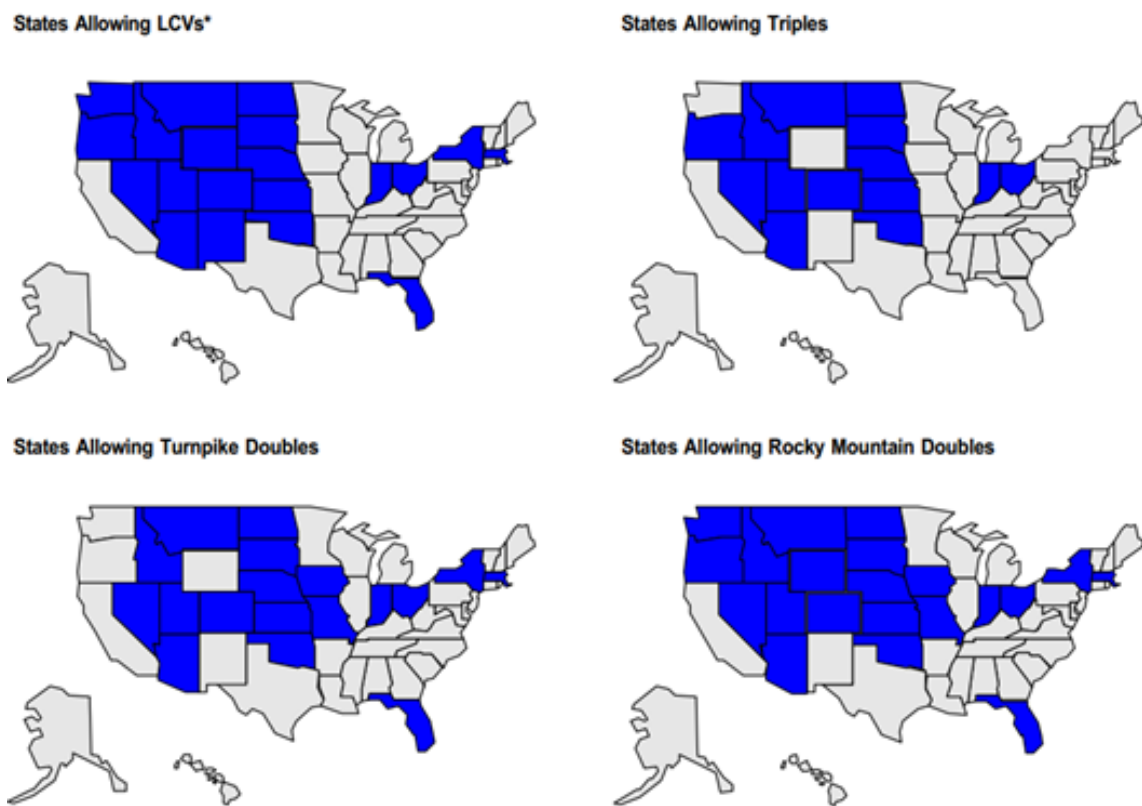


FIGURE 6-2: STATES ALLOWING VARIOUS LONGER COMBINATION VEHICLES [28]

The first truck is Rocky Mountain Double (RMD) which consists of three axles of truck tractor with a long front trailer between 40 to 53 feet and a shorter rear trailer with the length of 20 to 28.5 feet. RMD has total of 7-axles. In 1959, a few toll roads in the east Midwest began to issue permits to RMDs and in late 1960s western states followed. Nowadays, RMDs can operate in 21 States and can access to extensive networks of highways and toll roads. The general usage of the RMDs is for freights and multi-destination delivery on a route because one of the trailers can be dropped at an intermediate point.

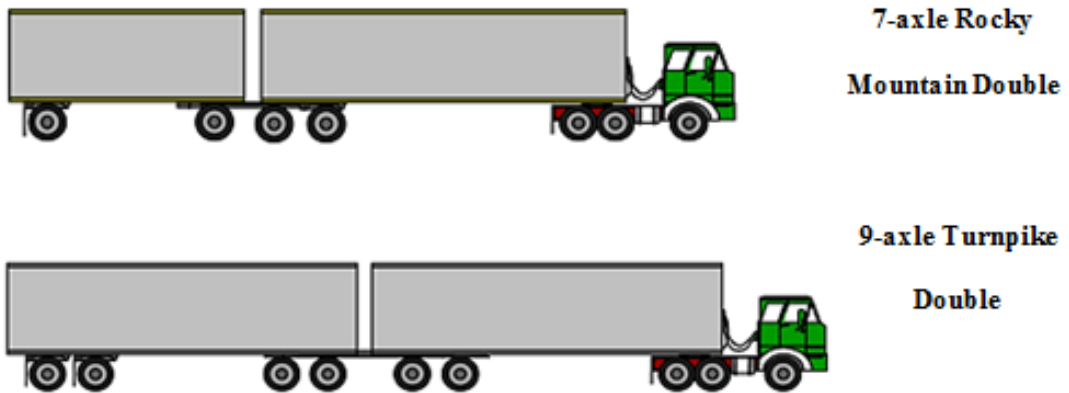


FIGURE 6-3: MAXIMUM WEIGHT OF RMD AND TPD [28]

The other truck in this study is 9-Axle Turnpike Double (TPD). TPD consists of a tractor towing two long trailers with equal length. Length of the trailers generally varies between 40 to 53 feet.

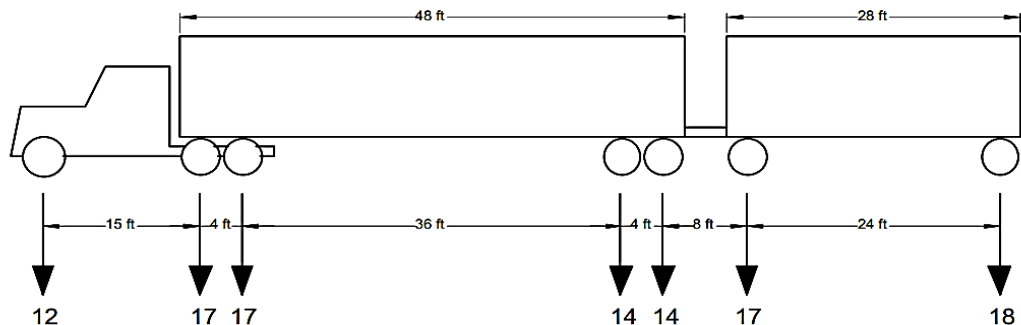


FIGURE 6-4: SEVEN AXLE RMD WITH TOTAL WEIGHT OF 104K [28]

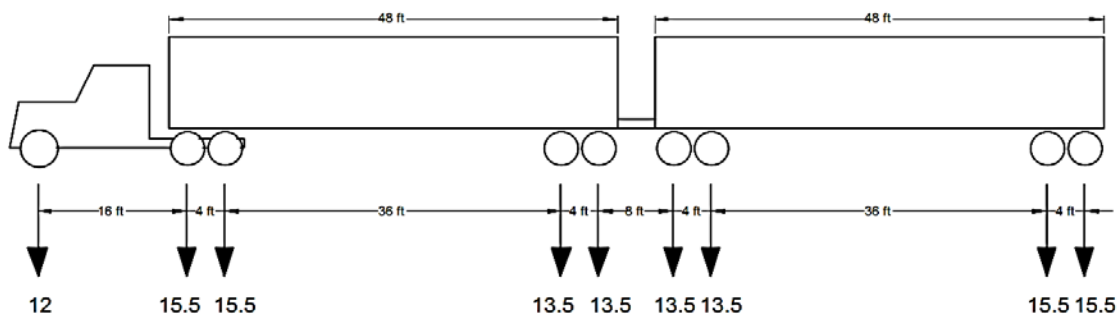


FIGURE 6-5: NINE AXLE TPD WITH TOTAL WEIGHT OF 128K [28]

In 1960s, several eastern states used to permit the use of TPDs. Today, 19 states allow the operation of this type of trucks. These operations are generally limited to interstate and toll road facilities. TPDs have more cubic capacity and

they can carry higher weights. They are typically well suited to operations that freight is moved from origin to destination with no intermediate drop-offs or pick-ups. The axle loads of RMD and TPD are shown in Figure 6-4 and Figure 6-5.

7. BRIDGE ANALYSIS – PRESTRESSED BRIDGES

7.1 Introduction

Two main reasons can be put forward to justify the choice of these two specific girders and bridges. Firstly, the girders that are the subject of this research are more commonly utilized than other girder types in Florida and the study might shed more light on decision making for practical engineering applications. Secondly, a performance based comparison is desired after having seen the cost comparison that Florida Department of Transportation (FDOT) had done in Design Bulletin C09-01 (2) by analyzing the same two bridges with the same type of girders.

Cost calculation provided in the FDOT Design Bulletin C09-01 [29] for the two prestressed bridges investigated in this study is as follows:

3 Span Bridge with 6 AASHTO Type III Beams:

Total Linear Foot = (90 ft long beams) x (3 spans) x (6 beams per span) = 1620 LF

Approximate Cost = (1620 LF) x (\$185 /LF) = \$299,700

3 Span Bridge with 4 Florida I-Beams (FIB-45):

Total Linear Foot = (90 ft long beams) x (3 spans) x (4 beams per span) = 1080 LF

Approximate Cost = (1080 LF) x (\$210 /LF) = \$226,800

Estimated Savings = 24% = (\$299,700-\$226,800)/\$299,700

It is noted that the costs per linear foot are determined considering the price estimations from manufacturers and contractors. The values above include only bridge items affected by differing beam types. These items include beam fabrication, beam placement, placed bearing pads, placed diaphragms, placed stay-in-place forms and deck rebar seats [29]. While the total cost can vary based on many other factors, this calculation provides a reasonably accurate comparison.

Several studies were performed by FDOT on cost analysis of these two different bridges indicating that FIBs are much more efficient than AASHTO Type girders. In addition, one recent study outlined the development of 3D FE (finite element) models and their results for standard AASHTO based analysis and evaluation [30]. Another study stated the results of a comparative evaluation of the AASHTO Type III and FIB bridge [31]. However, although there are some documentation in the literature giving information about load carrying capacities from a comparison point of view, there is still need for a deeper investigation on capacity, strength and reliability to explore if the new FIB designs are not only efficient in cost but also a better choice as to overall performance compared to commonly used AASHTO Type girder bridges.

The first as-is condition investigated here represents the newly designed and built bridges and can be thought as the baseline/healthy case. The studies performed on other cases give information about how much the load rating factors and reliability indices change when there are different scenarios induced on the bridges.

Each of the two bridge models subject to this study have three consecutive simply supported spans that are 90 ft long each. At the end of each span, three circular columns with 41.5ft long beam cap on their top act as the main carrying element of the bridge (Figure 10-1).



FIGURE 7-1: SIMPLY SUPPORTED 3 SPAN BRIDGE OF THIS STUDY

Two cross sections have the same section widths as 43'-1" each but with different girder spacing that is 7'6" for AASHTO Type III and 12'6" for FIB as can be seen in Figure 10-2. As a result of this spacing, the sections are comprised of six girders if AASHTO beam is employed and four girders in case of FIB. Both types of girders have the same 45 in. depth. Each AASHTO Type III girders constitute 26-0.6 in low-relaxation prestressing strands whereas FIB girders contain 42- 0.6 in low-relaxation strands (Figure 10-3).

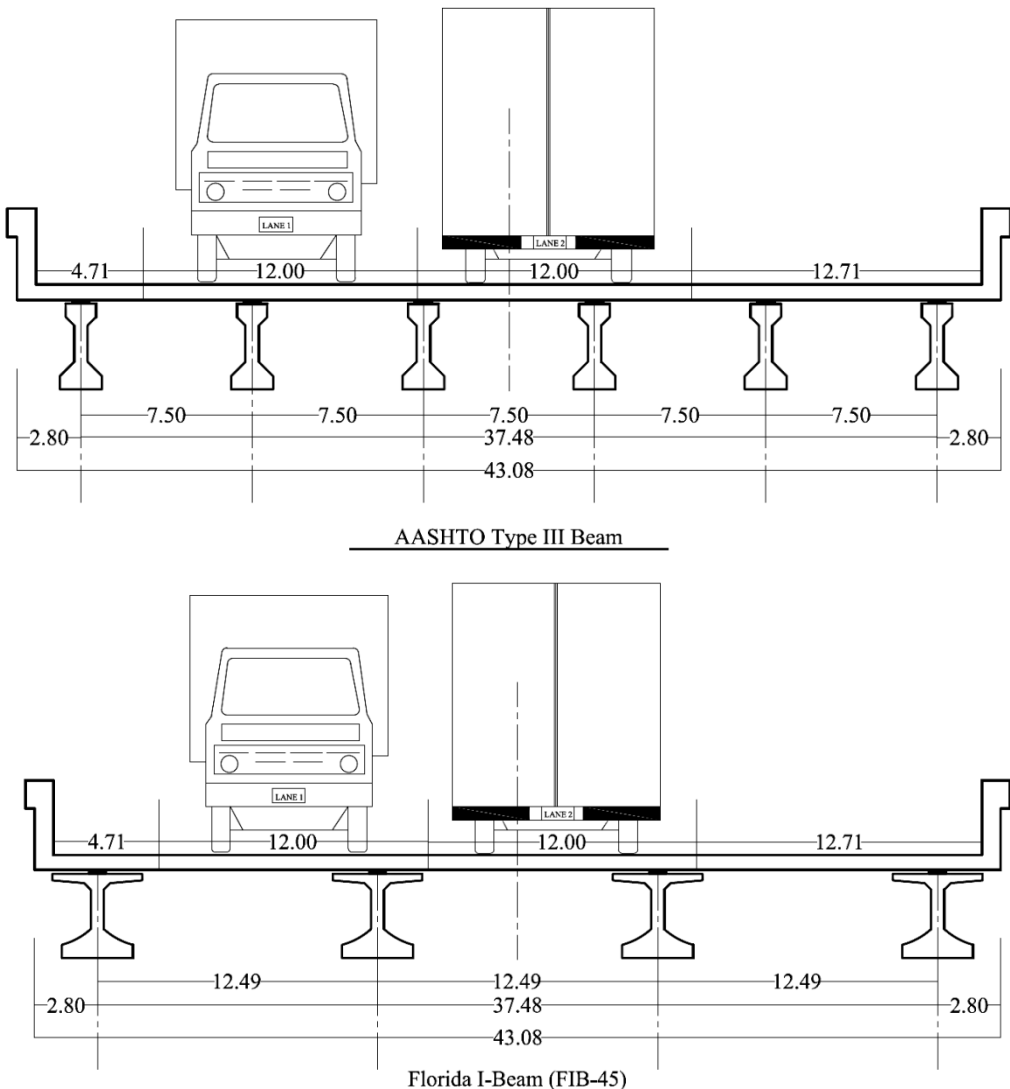


FIGURE 7-2: CROSS SECTION OF THE BRIDGES WITH (A) AASHTO TYPE III, (B) FLORIDA I-BEAM

The deck is 8in thick and topped with a 3in bituminous wearing surface, and has end barriers that are 1 ft-6 ½ in. wide. The prestressed concrete girders have a 2in thick hunched beam in order to control the camber. The prestressing strands are assumed to be straight with the eccentricity equal to 11.65in for AASHTO and 15.08in for FIB girder. These eccentricities are computed by making use of AASHTO LRFD calculation method.

The concrete strength is 8.5 ksi concrete and the ultimate tendon strength is taken as 270 Ksi. All stresses are checked with respect to the maximum allowable stresses and additionally, the moment capacity is also checked to be within the allowable capacity range.

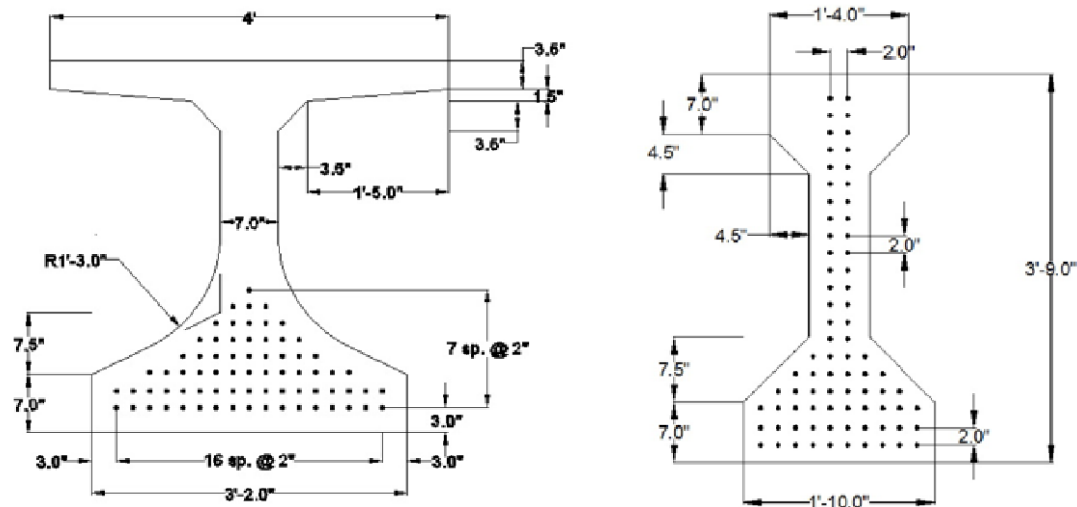


FIGURE 7-3: FIB (LEFT) AND AASHTO TYPE III (RIGHT) TYPICAL CROSS SECTIONS

7.2 Finite Element Model

7.2.1 Overview of the Full Finite Element Model

A finite element model using CsiBridge (ver. 15.2.0) is used to model and analyze the two types of Florida I-Beam and AASHTO Type prestressed concrete girder bridges.

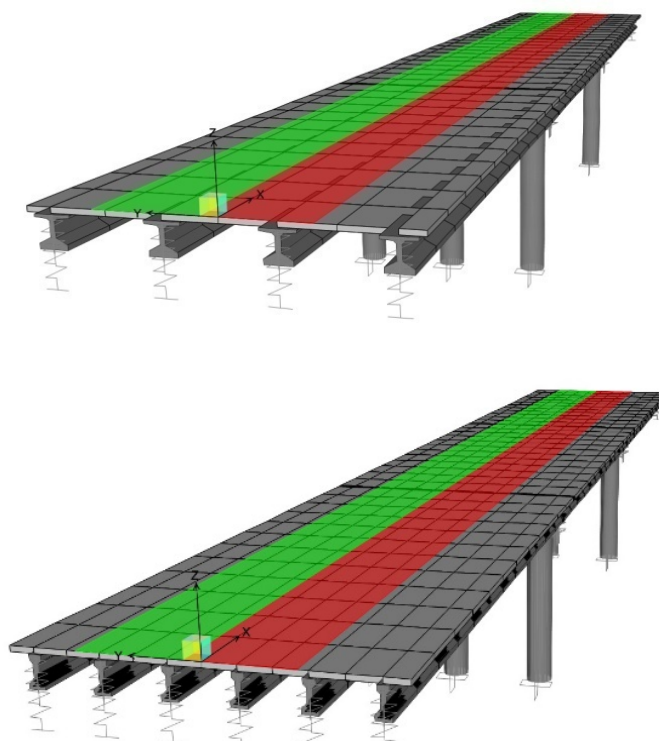


FIGURE 7-4: FINITE ELEMENT MODELS: FIB (TOP) AASHTO TYPE (BOTTOM)

In order to define Florida I-Beam section, CsiBridge Section designer is used. Slab thickness is assumed to be 8 inches with 2 inches of haunch. The deck and columns concrete is cast in place with compressive strength of 4 ksi. The same CIP concrete is used for abutments and beam caps. Girders are prefabricated and made with normal weight, 8.5 ksi compressive strength concrete. Cross

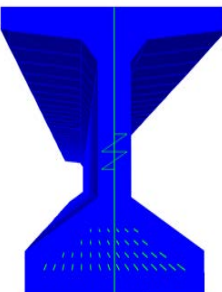
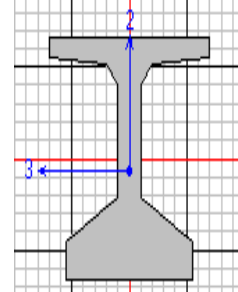
diaphragms are used in every one third of the spans with depth and width of 19 in and 12 in respectively. Barriers are defined as a line load through the entire bridge at both edges of the deck. The amount of the barrier load is a linear load of 0.32 kips per feet. Wearing surface is defined as an area load on the deck with amount of 0.035 kips per square feet. Bridge column sections are circular. Diameter of the circle columns are 4.5 feet and they have 20 #8 grade 60 steel reinforcement. The Jacking force of the tendons are $0.7 f_{pu}$ and strands are jacked from one end.

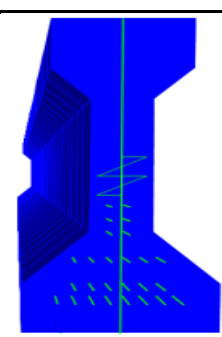
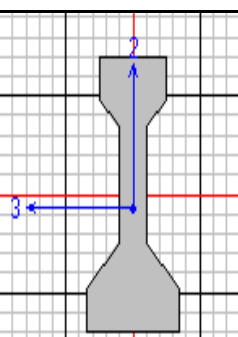
TABLE 7-1: PARAMETERS AND ASSUMPTIONS

	Value
Barrier Load	0.32 kips/ft
Wearing Load	0.035 kip/ ft ²
Column Dimension	3 Circular column with 4.5 ft dia (20 - #8 grade 60 steel)
Beam Cap Dimension	56 inch Depth, 60 inch width
Prestress Steel	036 Low relaxation strands
f_{pu}	270 ksi
Jacking Force	$0.7 f_{pu}$

The deck is modeled using shell elements with six degrees of freedom at each node. Girders, columns and beam caps are modeled using frame elements in the software. The first 3-span bridge model is defined with 12 FIB-45 girders and 168 tendons, and then the other mode with 18 AASHTO Type III girders and the total number of 156 tendons are defined for the entire bridge model. The flexural capacity of the sections is computed and it is seen that the cross-section capacity of FIB bridge is 17% higher than AASTO Type III girder bridge. The cross-sectional properties are given in Table 10-2.

TABLE 7-2: SECTION PROPERTIES

FIB - 45 section properties	
	Area 869.58 in. ²
	Perimeter 224.57 in.
	I_{xx} 226,581 in. ⁴
	I_{yy} 81,327 in. ⁴
	y_t 24.79 in.
	y_b 20.21 in.

AASHTO type III section properties	
	Area 559.5 in. ²
	Perimeter 125,390 in.
	I_{xx} 125,390 in. ⁴
	I_{yy} 12,217 in. ⁴
	y_t 24.73 in.
	y_b 20.27 in.

For the FIB model, 12 prestressed girders are defined. Each girder reinforced with 42 0.6 inch low relaxation strands. Tendons are modeled as elements. On the other hand AASHTO Type III girder bridge is modeled with 18 girders for the entire bridge. There are 26 0.6 in low relaxation tendons, which are modeled as elements.

TABLE 7-3: FINITE ELEMENT MODEL INFORMATION

	FIB-45 Girder Bridge	AASHTO Type III Girder Bridge
Number of Shell Elements	356	510
Number of Frames and Tendon Elements	9330	8708
Number of Joint Constrains	10344	9869
Number of Link Elements	72	108
Degree of Freedoms	28057	25998

Two models meshed in a way that the results are in stations that are in interest of the study. Florida I-Beam and AASHTO Type III model meshed in each 7.5 feet through length and width of the entire bridge.

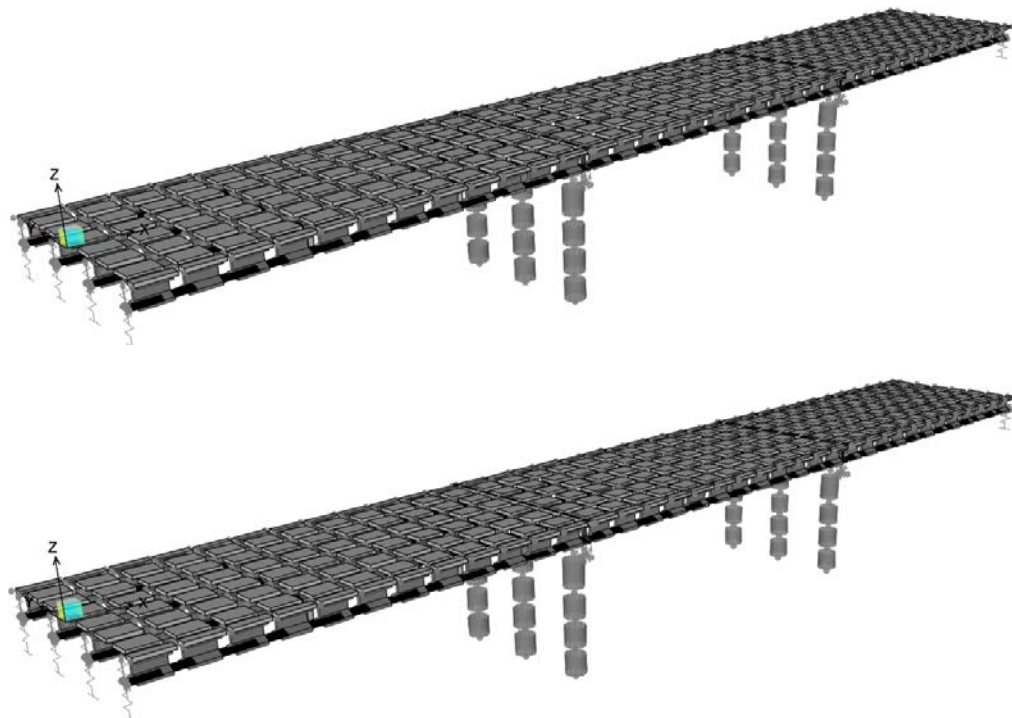


FIGURE 7-5: FEM MESHED MODELS: FIB (TOP) AASHTO TYPE (BOTTOM)

7.2.2 Modeling of the Link Elements

The concrete deck and girder connection is a critical detail to be modeled properly for the effective utilization of the composite connection. As a result, rigid links are used to represent the connection between the girders and the deck. The same type of link is used to model the columns and the beam cap connection. Abutment bearings links (link elements) are used to model the abutments by fixing the vertical and transverse translation of the abutment bearings. All other abutment bearing components are modeled as free since the abutment restraint is assumed to be free in the longitudinal direction. Bent bearings links (link elements) are used to model the bearing plates and the connection between the girders and the beam cap by fixing all the translations of the bent bearings. All the other bent bearing components are defined as free, including the rotation along the layout line. To help visualize the abutment geometry, the drawing shown in Figure 10-3 illustrates the location of the abutment bearings and the substructure. It also shows the location of the action point, which is the location where the bearing will translate or rotate depending on the bearing definitions.

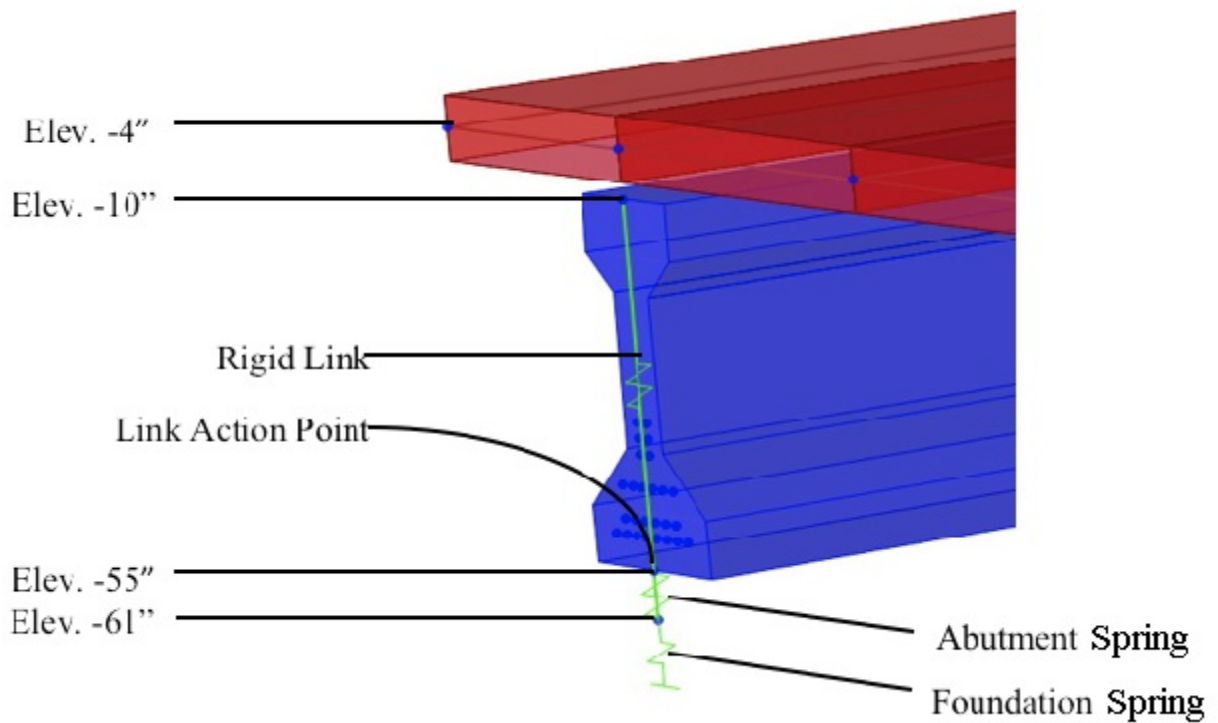


FIGURE 7-6: FINITE ELEMENT MODEL OF THE LINK ELEMENTS

7.2.3 *Modeling of the Tendons*

Eighteen precast girders are defined in the FE model of the AASHTO type III bridge. Each girder has 26 0.6 in low relaxation prestressed strands. On the other hand, twelve precast girders are defined in the FE model of the FIB bridge. Each girder has 42 0.6 in low relaxation prestressed strands.

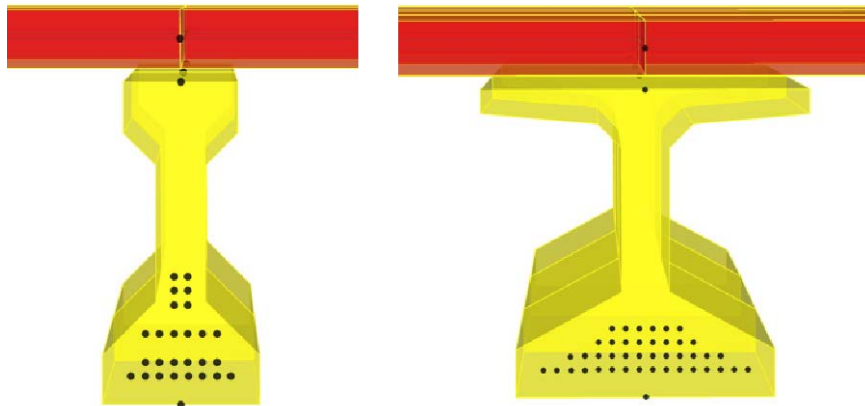


FIGURE 7-7: DISTRIBUTION OF TENDONS, AASHTO TYPE III BEAM (LEFT) AND FLORIDA I-BEAMS (RIGHT)

Tendons are modeled as separate elements with 44 kips force embedded in the precast girders to satisfy the design criteria, strength limit state check and for checking the tendon stresses. Figure 10-7 shows the distribution of the tendons in AASHTO type III beams and Florida I-Beams.

When tendons are modeled as structural elements, formulation proceeds as follows [32].

Structural objects which are subjected to loading from tendons should first be manually assigned to a group. The volume of each object within this group serves as the bounding box within which tendons are embedded.

Tendon loads are calculated as forces which act along tendon profile and exert forces on the structure. When specified, prestress losses are included in the computation of tendon forces.

Tendons are then discretized into smaller segments. Discretization points are located at either end of each discretization segment. When located within the bounding box of a structural member, interpolation constraints connect these discretization points to all joints within that member.

Axial strain is then calculated and applied to each discretized segment. The tension at either end of each tendon object is converted into equivalent strains which occur along tendon length, and transfer to the structure as strain load. This application is not affected by whether or not the tendon is contained within the bounding object.

7.3 History and Development of Prestressed Concrete

The concept of prestressed concrete backs to early 1870s, when an engineer in United States registered a patent for a system which used a tie rod to construct beams or arches made of separate individual blocks. Although there were some improvements in the prestressing systems at that time, but those early attempts were not really successful, since there were no knowledge of calculation of the losses of the prestressing. It was not a real improvement in the prestressing industry since R. E. Dill from Nebraska, realized that the shrinkage and creep of concrete have influence on the prestressing force. He developed am idea that post-tensioning of an unbonded rod could make a compensation for the time dependent loss of stress in the rod because of the decrease in length of the member because of creep and shrinkage [33]. These methods and several years

of experiments and designs helped engineers to improve the design and construction of prestressed concrete structures.

Today, various types of structures like buildings, underground structures, offshore structures and numerous types of bridge systems including segmental and cable stayed bridges are made with prestressed concrete.

In prestressed concrete design the fact that the initial prestressing force applied to the concrete element undergoes a progressive process of decrement over approximate time of 5 years is confirmed. Because of that, knowing the level of prestressing force in each stage of construction, transportation, placement and service load up to the ultimate load is crucial. In general this reduction periods are defined into two categories.

I. Immediate prestressing during the fabrication and construction, such as elastic shortening of the concrete, anchorage losses and frictional losses.

II. Time dependent losses like creep, shrinkage, temperature affected losses and steel relaxation.

Calculation of the exact value for losses specially time dependent ones is not possible. The reason for this is that they depend on a multiplicity of interrelated factors. In order to find these types of losses experimental methods of estimating losses have been made. There are several ways to estimate these values, like ACI-ASCE joint committee approach, Prestressed Concrete Institute, the AASHTO lump-sum approach, and the Comité Euro-International

du Béton (CEB). In the following initial and time dependent losses are defined and calculated.

7.4 Initial Prestress Losses

Immediate prestress losses arise from the flaws that happen in either manufacturing or construction phase [33]. It can be broken down to different classification elements. In the scope of this study, elastic shortening of concrete and short term relaxation of steel are taken into account as immediate prestress losses.

7.4.1 Elastic Shortening of the Concrete

Elastic shortening occurs when concrete shortens and tendons accompany to this effect by losing some portion of their prestressing force after jacking.

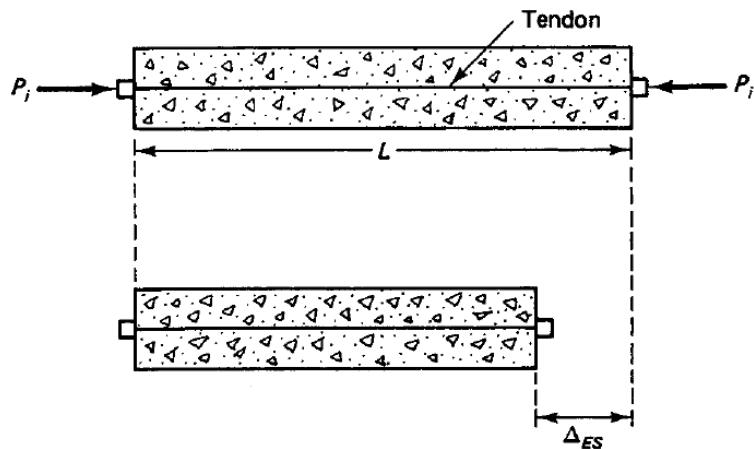


FIGURE 7-8: ELASTIC SHORTENING OF THE CONCRETE

Knowing that E_s , ε_{ES} , P_i , A_c and E_c represent modulus of elasticity of steel, unit shortening in concrete, initial prestressing force, cross sectional area of concrete, modulus of elasticity of concrete and n is module of elasticity ratio of

steel to concrete, elastic shortening can be defined with the following equation [33].

$$\Delta f_{pES} = E_s \varepsilon_{ES} = \frac{E_s P_i}{A_c E_c} = \frac{n P_i}{A_c} = n f_{cs} \quad (10-1)$$

where Δf_{pES} is the prestress loss due to concrete shortening. Equation 2 expresses the loss in terms of the stress in the concrete f_{cs} , the concrete stress at the center of gravity of prestressing tendons due to the prestressing force immediately after transfer and the self-weight of the member at the section of maximum moment. When the strand is located directly at the centroid of the cross section. If there exists a tendon eccentricity (e) at the beam, the equation becomes:

$$f_{cs} = -\frac{P_i}{A_c} \left(1 + \frac{e^2}{r^2} \right) + \frac{M_D e}{I_c} \quad (10-2)$$

where r^2 , M_D and I_c represent radius of gyration, moment generated by the member's dead weight and moment of inertia respectively. For post-tensioned beams, N representing the number of strands or strands pairwise, the following equation is suitable to find the loss of prestress in case consecutive jacking stages are applied on the element.

$$\Delta f_{pES} = \frac{1}{N} \sum_1^N (\Delta f_{pES})_j \quad (10-3)$$

7.5 Time Dependent Prestress Losses

Behavior of bridges may show differences during their operational life as they undergo time dependent effects. Although these effects enclose uncertainties that prevent exact determination particularly, it is possible to calculate time dependent prestress losses for the prestressed concrete case via empirical relations derived from codes of practice. In the scope of this study, long term relaxation of steel, creep loss and shrinkage loss are taken into account as time dependent prestress losses employing code defined formulations.

7.5.1 Relaxation of the Strands

Steel relaxation is one of the common loss cases that can be either considered for immediate or time dependent based on duration taken into account. This type of loss can be determined based on the ratio f_{pi}/f_{py} of the initial prestress to the yield strength of the reinforcement. The choice of f_{pi} and f_{py} for calculation purposes is restricted to certain limitations by the ACI 318-05 Code. In this study, $0.75 f_{pu}$ is chosen as the upper limit for both initial prestressing force and the yield strength of the reinforcement. Subsequently, stress relaxation loss can be computed for any desired time interval through the following equation:

$$\Delta f_{pR} = f_{pi}' \left(\frac{\log t_2 - \log t_1}{10} \right) \left(\frac{f_{pi}'}{f_{py}} - 0.55 \right) \quad (10-4)$$

where f'_{pi} is the initial stress in steel to which the concrete element is subjected; t_1 and t_2 are time steps that represent jacking time in hours and desired final loss stage to be found respectively. For the calculation of immediate prestress loss, 18 hours and for long-term losses 1 year (8760 hours) is considered.

7.5.2 Creep Loss

Experimental works over past decades shows that the flow of materials occurs with time when load or stress exists. This lateral flow or deformation due to the longitudinal stress is termed creep [33]. Determination of creep loss involves taking into consideration of different effects such as the amount of the applied load and its continuance, certain characteristics of concrete mixture that the prestressed element is made of, curing conditions, how old is the element when it is first loaded and ambient effects on the element. It must be emphasized that creep stresses and stress losses result only from sustained loads during the loading history of the structural element.

Based on the approximation that the relation between stress-strain and creep is linear, an empirical equation from ACI-ASCE committee can be used for proper estimation [34]:

$$\Delta f_{pCR} = K_{CR} \frac{E_{ps}}{E_c} (\bar{f}_{cs} - \bar{f}_{csd}) \quad (10-5)$$

where $K_{CR} = 2.0$ for pretensioned members, \bar{f}_{cs} is concrete stress right after

prestress transfer and \bar{f}_{csd} is concrete stress after prestressing is carried out when all dead loads are subjected on the system.

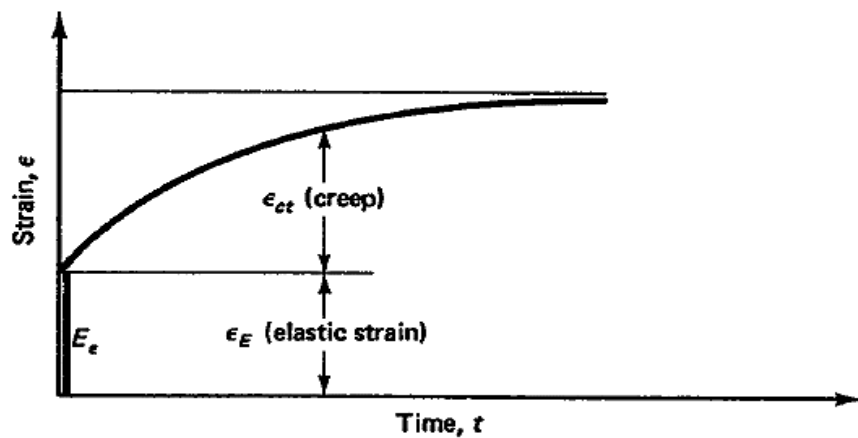


FIGURE 7-9: STRAIN-TIME CURVE [27]

7.5.3 Shrinkage Loss

Like creep loss the amount of shrinkage loss in concrete is affected by various factors like type of aggregate, proportions in concrete mixture, type of the cement that been used in making of the concrete, duration of the concrete curing, time between the end of external curing and the application of prestressing. Approximately 80 percentage of the shrinkage happens at the first year of the life of the structure. The average value for the ultimate shrinkage strain both in moist-cured and steam-cured concrete is given as $780 \times 10^{-6} \text{in/in}$, in ACI 209 R-93 report. The amount of this average value is influenced with the duration of the initial moist curing of the concrete, ratio of the concrete element volume to section, concrete composition and relative humidity of the ambient. For the post-tensioned members the amount of the shrinkage is lower, because some of the shrinkage has been happened before

the prestressing process. According to Prestressed Concrete Institute (PCI), prestressing loss due to shrinkage can be estimated through the following equation.

$$\Delta f_{pSH} = 8.2 \times 10^{-6} K_{SH} E_{ps} \left(1 - 0.06 \frac{V}{S} \right) (100 - RH) \quad (10-6)$$

where V/S ratio is the ratio of concrete element volume to surface, RH represents relative humidity which is taken as 75% in this study and K_{SH} coefficient is assumed the concrete is moist cured in 7 days and since the members are pretension K_{SH} is 1.0. [35, 36]

Calculation of all losses are started in two phases, first initial losses are calculated form the equation that are given in previous pages, and after calculation of the each loss the total loss is calculated for each step as a summation of the prestressing losses till that stage. Calculation of the initial losses result show that initial loss for both of the bridges are close and it was around %11 of the initial prestressing force. Then, time dependent losses are calculated in the same way and their magnitude added to the value of the initial loss. Results of long-term prestressing losses in Florida I-beam girder show that they undergoes total losses of about %20 and AASHTO Type III girder have the total losses about %22.

All the losses that are calculated with the help of given equations are tabulated in the following table.

TABLE 7-4 :INITIAL AND TIME DEPENDENT LOSS CALCULATION RESULTS

Beam type	Type of losses	Loss stages	Stress (psi)	Percent
Florida beam I	Initial losses	After tensioning ($0.75f_{pu}$) (a)	202500	100.0
		Elastic shortening Δf_{ES} (b)	-7540	-3.7
		Steel relaxation Δf_{PR} (c)	-6447	-3.2
		Total immediate loss (b+c)	-13987	-6.9
		Final net stress (a-b-c) (e)	188513	93.1
	Time dependent losses	Steel Relaxation Δf_{pT} (f)	-11433	-5.7
		Creep loss Δf_{pC} (g)	-4272	-2.1
		Shrinkage Δf_{pSH} (h)	-3412	-1.7
AASHTO Type III beam	Initial losses	Total time dependent loss (f+g+h)	-19117	-9.5
		Final net stress (e-f-g-h)	169396	83.6
		After tensioning ($0.75f_{pu}$) (a)	202500	100.0
		Elastic shortening Δf_{ES} (b)	-7770	-3.8
		Steel relaxation Δf_{PR} (c)	-6100	-3.0
	Time dependent losses	Total immediate loss (b+c+d)	-13870	-6.8
		Final net stress (a-b-c) (e)	188630	93.2
		Steel Relaxation Δf_{pT} (f)	-11396	-5.6
	Time dependent losses	Creep loss Δf_{pCR} (g)	-7204	-3.6
		Shrinkage Δf_{pSH} (h)	-3698	-1.8
		Total time dependent loss (f+g+h)	-22298	-11.0
		Final net stress (e-f-g-h)	166332	82.2

8. Load Rating and Reliability

The two FIB and AASHTO Type girder bridges of this study were compared in terms of Load Rating Factor (LRF) and the Reliability Indices (RI). For the LRF and RI calculations, the most critical moment and capacity are selected for the interior and exterior girders from all the girders of the entire bridge. The results reported for the interior and exterior girders for the critical sections.

8.1 Load Rating Factor (LRF)

Although design and load rating of the bridges are similar in terms of overall approach, but in design there more uncertainties in terms of loading amount on the structure and the uncertainties in the amount of structural resistance.

"The load rating process is a component of the inspection process and consists of determining the safe load carrying capacity of structures, determining if specific legal or overweight vehicles can safely cross the structure and determining if structure needs to be restricted and the level of posting required" [37]. The load rating process recognizes a balance between safety and economics. Both in-house and consultants' load rating results should be checked for accuracy as part of the quality control process [27].

Typically the bridge owners perform three types of load rating, Design, Legal and Permit. In design and legal load rating includes typical loads which are within the legal limits. In permit load rating, analysis are conducted to see if

specific vehicle that carry loads that are heavier than the legal limit can pass the bridge or not.

The main reasons that bridge owners perform load rating is that the modern bridges generally constructed and designed in a way to last at least 50 years or more. Though the bridges undergo proper maintenances and inspections but they are vulnerable to deteriorations during their lifetime. As a result of this deteriorations the bridge's strength and load carrying capacity would be reduced. In order to ensure that the public bridges are safe under current traffic loads, load rating analysis should be performed. According to NBIS bridge owners need to collect condition data for all public bridges on a twenty four month cycle. Moreover, the current bridges are designed using variety of truck configurations depending on the design specifications at the time that the bridge was built. As design and rating specifications evolve, new knowledge of actual loading, behavior, and resistance are incorporated. Therefore, regardless of the design methods used, all bridges should be load rated using current traffic conditions and the latest standards, whenever practicable, to ensure the safety of the motoring public. Also, permit load rating important for the vehicles that are carrying loads which are over the legal limits. Due to increasing demand in freight and truck industry the volume of requests for permit load rating increased, according to Bureau of Transportation Statistics. Heavy loads or frequent permit loads can reduce a bridge's life, or even can cause permanent structural damage if not assessed properly (FHWA). Load rating results expressed in terms of a rating factor for a specific type of live

load. And if the load rating factor is greater than one, it shows that the bridge is safe for the tested load.

According to Florida Department of Transportation load rating manual [27], there are some consideration for load rating of a bridge (Topic No 850-010-035), which some are as following. Generally substructures do not control the load rating process, but after running of superstructure's load rating process, the load rater should check whether substructure can carry the equivalent or grater load than the superstructure. If not substructure will be load rated and the load rating adjusted. A complete or partial analysis of the substructure is not required if, in the engineering judgment of the load rater, the substructure has equivalent or greater capacity than the superstructure. The load rater must be aware that short span bridge capacity based upon superstructure evaluation may allow vehicles with weights exceeding 500,000 lbs to cross generating significant impact on the substructure. Some composite pre-stressed concrete girder bridges were designed with the deck continuous over the supports in order to eliminate transverse deck joints. The girders of these bridges were not made continuous over the support. Bridges meeting this description shall be load rated as simple spans. For new bridges the Engineer of Record shall load rate the bridge(s) and submit the calculations and Load Rating Summary Tables for the entire structure. Load rating process may be performed to use a satisfactory inventory rating.

Equation 9 shows the general equation for load rating purpose which is used in this study.

$$RF = \frac{\varphi M_n - \gamma_{DC} M_{DC} - \gamma_{DW} M_{DW}}{\gamma_L M_{LL+IM}} \quad (8-1)$$

where RF = Rating factor; M_n = Nominal moment resistance; φ = Resistance factor for flexure; $\gamma_{DC} M_{DC}$ = Factored moment due to dead load of structural components and attachments; $\gamma_{DW} M_{DW}$ = Factored moment demand due to dead load of wearing surface and utilities; and $\gamma_L M_{LL+IM}$ = Factored moment due to live load

After determining the rating factor for a structural member, the bridge owner then multiplies the rating factor by the weight of the live load truck to yield the bridge member rating for that member. The overall rating of the bridge is controlled by the structural member with the lowest rating.

In this paper, flexure load rating factor for Strength I Limit State is calculated for the most critical moment at the exterior and interior girders.

For each of the loading types FDOT load rating manual considerations were applied. (FDOT Bridge Load Rating Manual, Chapter 6. Topic No. 850-010-035) [27]. In the case of HL-93 truck load design load rating was performed, the dynamic load allowance (IM) is 1.33 and for strength limit states, number of lanes which were assigned for design of the bridge should be considered. Multi-presence factor of $m=1.20$ for one lane, and $m=1.00$ for two lanes loaded is applied to the model. And for strength I limit state love load factor is 1.33. In legal load ratings C5 and SU4 trucks were considered for the analysis. Due to FDOT load rating manual instruction, same truck load in each lane using only

one type of truck per lane (i.e. do not mix the trucks) is applied. In this case also IM=1.33. As it stated in the load rating manual of FDOT for Service Limit States, use number of striped lanes. Multi-presence factor that is used for legal load rating is for one and two lanes, $m = 1.00$. Also the live load factor for legal loads are the same as the design load which is 1.35.

In finite element model of the study each of the models analyzed under HL-93, C5, SU4, RMD and TPD truck loads for all the three cases of baseline, Initial losses and time dependent losses. Each of the trucks are modeled in the program as moving loads, with the axle load and axle spacing which provided in FDOT and FHWA. After each analysis, moment values at each 7.5 feet of the bridges are gathered, then load rating factors for each of the stations are calculated.

The results of the calculations are presented in section 4.3 of the report. Results tabulated and plotted for the lowest value of the load rating in each of the bridges for every case of baseline, Initial loss and time dependent losses. For each of the cases lowest value for exterior and interior girders is obtained then these values reflected into the tables and graphs.

The calculation of flexural load rating factor in this study is reported in the following steps. For each of the super-structures maximum positive moment of the entire bridge in exterior and interior girders are considered for the calculation of the LRF. Strength Limit I load factors are considered for the calculations. These factors are γ_D dead load factor which is 1.25, γ_{DW} is wearing surface load factor which is 1.25 and the live load factor γ_{LL} is equal to 1.35, also dynamic load allowance of 0.33 is considered for the live load moments.

Calculations for Florida I-Beam 45:

Moments are output of analysis using CSI-Bridge finite element software. In analysis dead load, wearing surface load and the live load are considered.

TABLE 8-1: FIB FINITE ELEMENT ANALYSIS OUTPUTS UNDER LEGAL LOADS (FACTORED MOMENTS) [KIP-FT]

Span	Girder Location	Flexural Capacity	Dead Load	Wearing Surface	Live Load	C5
						SU4
Span1	Left Exterior Girder	8320	2834	403	985	985
						952
	Interior Girder 1	8320	3153	471	1196	1196
						1246
	Interior Girder 2	8320	3153	472	1059	1059
						1099
	Right Exterior Girder	8320	2834	403	689	689
						667
Span2	Left Exterior Girder	8320	2731	389	923	923
						910
	Interior Girder 1	8320	3039	454	1165	1165
						1218
	Interior Girder 2	8320	3040	454	1039	1039
						1080
	Right Exterior Girder	8320	2731	389	677	677
						656
Span3	Left Exterior Girder	8320	2835	402	967	967
						951
	Interior Girder 1	8320	3152	472	1200	1200
						1250
	Interior Girder 2	8320	3153	472	1063	1063
						1101
	Right Exterior Girder	8320	2834	402	685	685
						664

Calculation of the LRF done as following (for first span under C5 for baseline case):

$$RF = \frac{\varphi M_n - \gamma_{DC} M_{DC} - \gamma_{DW} M_{DW}}{\gamma_L M_{LL+IM}}$$

$$RF_{L-Exterior} = \frac{8320 - 2834 - 403}{1.33 (985)} = 3.88$$

$$RF_{Interior-1} = \frac{8320 - 3153 - 471}{1.33 (1196)} = 2.95$$

Results of the LRF calculation under different load cases for FIB45 Girder

Type are tabulated in Table 8-2 to Table 8-6

TABLE 8-2: FIB 45 LRF UNDER C5 TRUCK LOAD

Span	Girder Location	RF (Baseline)	RF (Initial Losses)	RF (Time dependent Losses)
Span1	Left Exterior Girder	3.88	3.32	3.02
	Interior Girder 1	2.95	2.48	2.23
	Interior Girder 2	3.33	2.80	2.52
	Right Exterior Girder	5.28	4.51	4.09
Span2	Left Exterior Girder	4.16	3.57	3.26
	Interior Girder 1	3.12	2.63	2.37
	Interior Girder 2	3.49	2.94	2.65
	Right Exterior Girder	5.51	4.71	4.29
Span3	Left Exterior Girder	3.88	3.32	3.02
	Interior Girder 1	2.94	2.47	2.22
	Interior Girder 2	3.32	2.79	2.51
	Right Exterior Girder	5.31	4.53	4.12
Min LRF	Exterior Girder	3.88	3.32	3.02
	Interior Girder	2.94	2.47	2.22

TABLE 8-3: FIB 45 LRF UNDER SU4 TRUCK LOAD

Span	Girder Location	RF (Baseline)	RF (Initial Losses)	RF (Time dependent Losses)
Span1	Left Exterior Girder	3.94	3.37	3.07
	Interior Girder 1	2.83	2.38	2.14
	Interior Girder 2	3.21	2.70	2.43
	Right Exterior Girder	5.46	4.66	4.23
Span2	Left Exterior Girder	4.22	3.62	3.30
	Interior Girder 1	2.98	2.51	2.26
	Interior Girder 2	3.36	2.83	2.55
	Right Exterior Girder	5.68	4.86	4.42
Span3	Left Exterior Girder	3.95	3.38	3.08
	Interior Girder 1	2.83	2.37	2.14
	Interior Girder 2	3.20	2.69	2.42
	Right Exterior Girder	5.48	4.68	4.25
Min LRF	Exterior Girder	3.94	3.37	3.07
	Interior Girder	2.83	2.37	2.14

TABLE 8-4: FIB 45 LRF UNDER HL-93 TRUCK LOAD

Span	Girder Location	RF (Baseline)	RF (Initial Losses)	RF (Time dependent Losses)
Span1	Left Exterior Girder	4.06	3.47	3.16
	Interior Girder 1	3.03	2.54	2.29
	Interior Girder 2	3.42	2.87	2.58
	Right Exterior Girder	5.56	4.74	4.31
Span2	Left Exterior Girder	4.35	3.73	3.40
	Interior Girder 1	3.19	2.69	2.42
	Interior Girder 2	3.58	3.02	2.72
	Right Exterior Girder	5.79	4.95	4.51
Span3	Left Exterior Girder	4.06	3.48	3.16
	Interior Girder 1	3.01	2.53	2.28
	Interior Girder 2	3.41	2.86	2.58
	Right Exterior Girder	5.59	4.77	4.33
Min LRF	Exterior Girder	4.06	3.47	3.16
	Interior Girder	3.01	2.53	2.28

TABLE 8-5: FIB 45 LRF UNDER RMD TRUCK LOAD

Span	Girder Location	RF (Baseline)	RF (Initial Losses)	RF (Time dependent Losses)
Span1	Left Exterior Girder	4.78	4.13	3.76
	Interior Girder 1	3.71	3.13	2.82
	Interior Girder 2	4.18	3.53	3.17
	Right Exterior Girder	6.33	5.56	5.05
Span2	Left Exterior Girder	5.13	4.44	4.05
	Interior Girder 1	3.91	3.32	2.99
	Interior Girder 2	4.38	3.71	3.35
	Right Exterior Girder	6.66	5.81	5.29
Span3	Left Exterior Girder	4.77	4.13	3.76
	Interior Girder 1	3.68	3.11	2.80
	Interior Girder 2	4.15	3.51	3.16
	Right Exterior Girder	6.38	5.59	5.08
Min LRF	Exterior Girder	4.77	4.13	3.76
	Interior Girder	3.68	3.11	2.80

TABLE 8-6: FIB 45 LRF UNDER TPD TRUCK LOAD

Span	Girder Location	RF (Baseline)	RF (Initial Losses)	RF (Time dependent Losses)
Span1	Left Exterior Girder	4.77	4.08	3.72
	Interior Girder 1	3.69	3.10	2.79
	Interior Girder 2	4.14	3.48	3.13
	Right Exterior Girder	6.39	5.45	4.95
Span2	Left Exterior Girder	5.13	4.40	4.01
	Interior Girder 1	3.88	3.27	2.95
	Interior Girder 2	4.33	3.65	3.29
	Right Exterior Girder	6.65	5.68	5.17
Span3	Left Exterior Girder	4.78	4.09	3.72
	Interior Girder 1	3.67	3.09	2.77
	Interior Girder 2	4.12	3.46	3.12
	Right Exterior Girder	6.43	5.48	4.98
Min LRF	Exterior Girder	4.77	4.08	3.72
	Interior Girder	3.68	3.09	2.77

Calculations for AASHTO Type III:

TABLE 8-7: FINITE ELEMENT ANALYSIS OUTPUTS UNDER LEGAL LOADS (FACTORED MOMENTS) [KIP-FT]

Span	Girder Location	Flexural Capacity	Dead Load	Wearing Surface	Live Load	C5
					SU4	SU4
Span1	Left Exterior Girder	4864	1935	280	665	
					642	
	Interior Girder 1	4864	1960	291	751	
					768	
	Interior Girder 2	4864	1960	293	755	
					794	
Span2	Interior Girder 3	4864	1955	293	696	
					730	
	Interior Girder 4	4864	1955	291	588	
					593	
	Right Exterior Girder	4864	1960	273	457	
					435	
Span3	Left Exterior Girder	4864	1802	257	620	
					606	
	Interior Girder 1	4864	1845	275	718	
					738	
	Interior Girder 2	4864	1845	275	732	
					774	
Span4	Interior Girder 3	4864	1845	275	678	
					713	
	Interior Girder 4	4864	1845	275	572	
					578	
	Right Exterior Girder	4864	1802	257	445	
					423	
Span5	Left Exterior Girder	4864	1083	273	659	
					642	
	Interior Girder 1	4864	1096	291	751	
					768	
	Interior Girder 2	4864	1088	293	575	
					796	
Span6	Interior Girder 3	4864	1088	293	697	
					731	
	Interior Girder 4	4864	1096	291	588	
					592	
	Right Exterior Girder	4864	1083	273	455	
					433	

Calculation of the LRF done as following (at first span under C5 for baseline case):

$$RF = \frac{\varphi M_n - \gamma_{DC} M_{DC} - \gamma_{DW} M_{DW}}{\gamma_L M_{LL+IM}}$$

$$RF_{L-Exterior} = \frac{4864 - 1935 - 280}{1.33 (665)} = 2.99$$

$$RF_{Interior-2} = \frac{4864 - 1960 - 293}{1.33 (755)} = 2.60$$

Results of the LRF calculation under different load cases for AASHTO Type III girder are tabulated in Table 11-8 to Table 8-12.

TABLE 8-8: AASHTO TYPE III LRF UNDER C5 TRUCK LOAD

Span	Girder Location	RF (Baseline)	RF (Initial Losses)	RF (Time dependent Losses)
Span1	Left Exterior Girder	2.99	2.52	2.28
	Interior Girder 1	2.62	2.19	1.98
	Interior Girder 2	2.60	2.19	1.97
	Interior Girder 3	2.83	2.37	2.14
	Interior Girder 4	3.34	2.80	2.53
	Right Exterior Girder	4.31	3.63	3.29
Span2	Left Exterior Girder	3.33	2.82	2.56
	Interior Girder 1	2.87	2.42	2.19
	Interior Girder 2	2.82	2.38	2.15
	Interior Girder 3	3.04	2.57	2.33
	Interior Girder 4	3.60	3.03	2.75
	Right Exterior Girder	4.64	3.93	3.57
Span3	Left Exterior Girder	2.99	2.52	2.28
	Interior Girder 1	2.61	2.19	1.98
	Interior Girder 2	2.60	2.18	1.97
	Interior Girder 3	2.82	2.37	2.14
	Interior Girder 4	3.34	2.80	2.53
	Right Exterior Girder	4.32	3.64	3.30
Min LRF	Exterior Girder	2.99	2.52	2.28
	Interior Girder	2.60	2.18	1.97

TABLE 8-9: AASHTO TYPE III LRF UNDER SU4 TRUCK LOAD

Span	Girder Location	RF (Baseline)	RF (Initial Losses)	RF (Time dependent Losses)
Span1	Left Exterior Girder	3.07	2.59	2.35
	Interior Girder 1	2.56	2.15	1.94
	Interior Girder 2	2.48	2.08	1.88
	Interior Girder 3	2.70	2.26	2.04
	Interior Girder 4	3.31	2.78	2.51
	Right Exterior Girder	4.53	3.82	3.46
Span2	Left Exterior Girder	3.41	2.89	2.62
	Interior Girder 1	2.79	2.35	2.13
	Interior Girder 2	2.67	2.25	2.04
	Interior Girder 3	2.89	2.44	2.21
	Interior Girder 4	3.56	3.00	2.72
	Right Exterior Girder	4.88	4.12	3.75
Span3	Left Exterior Girder	3.07	2.59	2.34
	Interior Girder 1	2.56	2.14	1.94
	Interior Girder 2	2.47	2.08	1.88
	Interior Girder 3	2.69	2.26	2.04
	Interior Girder 4	3.32	2.78	2.51
	Right Exterior Girder	4.55	3.83	3.47
Min LRF	Exterior Girder	3.07	2.59	2.34
	Interior Girder	2.47	2.08	1.88

TABLE 8-10: AASHTO TYPE III LRF UNDER HL93 TRUCK LOAD

Span	Girder Location	RF (Baseline)	RF (Initial Losses)	RF (Time dependent Losses)
Span1	Left Exterior Girder	3.14	2.65	2.40
	Interior Girder 1	2.70	2.26	2.04
	Interior Girder 2	2.66	2.24	2.02
	Interior Girder 3	2.89	2.42	2.19
	Interior Girder 4	3.46	2.91	2.62
	Right Exterior Girder	4.55	3.84	3.48
Span2	Left Exterior Girder	3.49	2.96	2.69
	Interior Girder 1	2.95	2.49	2.25
	Interior Girder 2	2.87	2.42	2.20
	Interior Girder 3	3.10	2.62	2.37
	Interior Girder 4	3.73	3.14	2.85
	Right Exterior Girder	4.90	4.15	3.77
Span3	Left Exterior Girder	3.14	2.64	2.40
	Interior Girder 1	2.69	2.26	2.04
	Interior Girder 2	2.66	2.23	2.02
	Interior Girder 3	2.88	2.42	2.19
	Interior Girder 4	3.46	2.90	2.62
	Right Exterior Girder	4.56	3.85	3.48
Min LRF	Exterior Girder	3.14	2.64	2.40
	Interior Girder	2.66	2.23	2.02

TABLE 8-11: AASHTO TYPE III LRF UNDER RMD TRUCK LOAD

Span	Girder Location	RF (Baseline)	RF (Initial Losses)	RF (Time dependent Losses)
Span1	Left Exterior Girder	3.71	3.13	2.84
	Interior Girder 1	3.30	2.77	2.50
	Interior Girder 2	3.27	2.75	2.49
	Interior Girder 3	3.56	2.99	2.70
	Interior Girder 4	4.17	3.50	3.16
	Right Exterior Girder	5.26	4.43	4.02
Span2	Left Exterior Girder	4.13	3.51	3.19
	Interior Girder 1	3.62	3.05	2.77
	Interior Girder 2	3.54	2.99	2.71
	Interior Girder 3	3.83	3.24	2.93
	Interior Girder 4	4.49	3.79	3.43
	Right Exterior Girder	5.69	4.81	4.37
Span3	Left Exterior Girder	3.71	3.13	2.83
	Interior Girder 1	3.29	2.76	2.49
	Interior Girder 2	3.26	2.74	2.48
	Interior Girder 3	3.55	2.98	2.69
	Interior Girder 4	4.16	3.49	3.16
	Right Exterior Girder	5.29	4.46	4.04
Min LRF	Exterior Girder	3.71	3.13	2.83
	Interior Girder	3.26	2.74	2.48

TABLE 8-12: AASHTO TYPE III LRF UNDER RMD TRUCK LOAD

Span	Girder Location	RF (Baseline)	RF (Initial Losses)	RF (Time dependent Losses)
Span1	Left Exterior Girder	3.67	3.10	2.81
	Interior Girder 1	3.25	2.73	2.46
	Interior Girder 2	3.24	2.72	2.46
	Interior Girder 3	3.50	2.94	2.66
	Interior Girder 4	4.12	3.46	3.12
	Right Exterior Girder	5.13	4.33	3.92
Span2	Left Exterior Girder	4.09	3.46	3.15
	Interior Girder 1	3.55	3.00	2.72
	Interior Girder 2	3.49	2.95	2.67
	Interior Girder 3	3.77	3.18	2.89
	Interior Girder 4	4.42	3.73	3.38
	Right Exterior Girder	5.54	4.69	4.26
Span3	Left Exterior Girder	3.67	3.09	2.80
	Interior Girder 1	3.24	2.72	2.46
	Interior Girder 2	3.23	2.72	2.45
	Interior Girder 3	3.50	2.94	2.66
	Interior Girder 4	4.12	3.46	3.12
	Right Exterior Girder	5.17	4.36	3.95
Min LRF	Exterior Girder	3.67	3.09	2.80
	Interior Girder	3.23	2.72	2.45

8.2 Reliability Index (RI)

Current AASHTO LRFD Bridge design code is based on reliability analysis procedure (12, 13). Performance of the structures is determined by means of load and resistance factors determined from the probability of failure and the reliability.

There are various levels in terms of probabilistic design. The fully probabilistic method which is Level III is the most complex method. In this method knowledge of the probability distribution of each random variable is a requirement. Like knowing the variables for resistance, load, and also the correlation between these variables is needed. Since this types of information for all of the random variables of the structures are not available, this method rarely practical to implement the fully probabilistic method. The other method is Level II probabilistic method. This method includes the first-order second-moment (FOSM) method. FOSM uses simpler statistical characteristics of the load and resistance variables. Additionally load and resistance are assumed to be statistically independent. The load and resistance factors employed in the AASHTO (1994, 2010) LRFD Bridge Specifications were determined by using level II procedures and other simpler methods when insufficient information was available to use the level II methods [38].

In the context of reliability analysis, failure is defined as the realization of one of a number of predefined limit states [38]. The alternative way to express probability of failure is using the reliability index β . In normally distributed random variables the relation between probability of failure and the reliability

index is, $P_f = \Phi(-\beta)$ and for the normally distributed cases this expression is exact. Otherwise, this expression provides only an approximate means of relating the probability of failure to the reliability index, β . The reliability index is a common metric used to quantify how close a design code or specification is in achieving its objective [39]. The LRFD Code provisions are formulated such that new structures will have a consistent and uniform safety level. In general the basic design formula can be written as following:

$$\sum \gamma_i Q_i < \Phi R_n \quad (11-2)$$

In which Q_i is nominal load effect, γ_i is load factor, R_n is nominal resistance of the member and Φ is resistance factor.

In the LRFD Code calibration, load and resistance are treated as random variables and are described by bias factors (λ) and coefficients of variation (V). Resistance factors, φ , are calculated so that the structural reliability is close to $\beta = 3.5$ which β is the target reliability [40].

An expression for the reliability index, β , is developed for the present study. A linear limit state function is assumed, following [39].

$$\beta = \frac{a_0 + \sum_{i=1}^a (a_i \mu_{X_i})}{\sqrt{\sum_{i=1}^a (a_i \sigma_{X_i})^2}} \quad (8-3)$$

For the linear limit state function of the form,

$$g(X_1, X_2, \dots, X_n) = a_0 + a_1 X_1 + a_2 X_2 + \dots + a_n X_n \quad (8-4)$$

This expression must be adapted for the current study, considering load effects and resistance in bending and shear. The limit state function is developed in terms of resistance and load effects for the AASHTO Strength I limit state:

$$g(M_{Res} M_{DL} M_L) = M_{Res} - M_{DL} - M_L \quad (8-5)$$

Where M_{Res} is nominal resistant moment, M_{DL} is dead load moment, and M_L is moment occurs because of live load of the structure.

In this study, member reliability indices are computed. In order to calculate reliability index, first section resistance moment, dead load moment, wearing surface moment and live load moments at the most critical section are obtained from the finite element model. Then using Tables 8-13 and 8-14, bias factor (λ) and coefficient of variation (V) from AASHTO code is selected. Afterwards from equation 13 and 14, mean value (μ) and standard deviation (σ) are calculated.

$$\mu_i = M_i \lambda_i \quad (8-6)$$

$$\sigma_i = V_i \mu_i \quad (8-7)$$

where i represents resistance, dead, wearing surface and live load moments.

Considering AASHTO LRFD limit state function which is developed in terms of resistance and load effects for the strength limit state, the following formula is achieved in order to calculate reliability index.

Reliability Index for AASHTO Strength Limit State I:

$$\beta = \frac{\mu_R - \mu_{DL} - \mu_L}{\sqrt{\sigma_R^2 + \sigma_{DL}^2 + \sigma_L^2}} \quad (8-8)$$

where μ_R is the mean resistance, μ_{DL} is mean dead load, μ_L is mean live load, whereas σ_R , σ_{DL} and σ_L represents the standard deviations. Table 8-13 and Table 8-14 illustrates the statistical parameters used for bridge loading and resistance.

TABLE 8-13: STATISTICAL VALUES FOR BRIDGE LOAD COMPONENTS

Load component	Bias (λ_o)	COV (v_o)
Dead load:		
Factory made	1.03	0.08
Cast in place	1.05	0.10
Asphalt wearing surface	1.00	0.25
Live load (with dynamic load)	1.10-1.20	0.18

The limit state functions are valid as long as each load effect can be stated in terms of only one random variable. Statistical parameters for load and resistance tend to be given in terms of load effects [39].

TABLE 8-14: STATISTICAL PARAMETERS OF RESISTANCE FOR SELECTED BRIDGES

Type of structure	Bias (λ_R)	COV (V_R)
Noncomposite steel girders:		
Moment (compact)	1.12	0.10
Moment (noncompact)	1.12	0.10
Shear	1.14	0.105
Composite steel girders:		
Moment	1.12	0.10
Shear	1.14	0.105
Reinforced concrete T-beams:		
Moment	1.14	0.13
Shear w/steel	1.20	0.155
Shear w/o steel	1.40	0.17
Prestressed concrete girders:		
Moment	1.05	0.075
Shear w/ steel	1.15	0.14

In order to calculate the Reliability Index for flexural of the bridge girders, maximum moment which is at midspan is acquired from the analysis. Then using statistical values from Table 11-13 and Table 11-14, Mean Value, Standard Deviation and Reliability Index (RI) for exterior girder under C5 truck load are calculated as following example. (Moment values for baseline case under legal truck load C5 are reported in Table 11-1 for FIB 45 and Table 11-7 for AASHTO Type III)

Calculation of RI for FIB 45:

$$M_R = 8320 \text{ k-ft} , \quad M_D = 3152 \text{ k-ft} , \quad M_{FWS} = 472 \text{ k-ft} ,$$

$$M_L = 1200 \text{ k-ft}$$

$\mu_i = M_i \lambda_i$ and λ_i is acquired from table 4-13 for Dead, Future Wearing Surface and Live load. And bias factor of the resistance acquired form table 4-14.

$$\lambda_R = 1.05, \quad \lambda_D = 1.03, \quad \lambda_{FWS} = 1.0, \quad \lambda_L = 1.10$$

$$\mu_R = 8736 \text{ k-ft}, \quad \mu_D = 3247 \text{ k-ft}, \quad \mu_{FWS} = 472 \text{ k-ft},$$

$$\mu_L = 1320 \text{ k-ft}$$

After calculation of mean value (μ_i) for each of the parameters, using coefficient of variation from Table 11-13 and Table 11-14, standard deviation (σ_i) can be calculated as follows.

$$V_R = 0.075, \quad V_D = 0.08, \quad V_{FWS} = 0.25, \quad V_L = 0.18$$

$$\sigma_i = V_i \mu_i$$

$$\sigma_R = 655, \quad \sigma_D = 260, \quad \sigma_{FWS} = 118, \quad \sigma_L = 238$$

After calculation of all the mean values and standard deviations, using equation 15 Reliability Index (RI) can be calculated as following.

$$\beta = \frac{\mu_R - \mu_{DL} - \mu_L}{\sqrt{\sigma_R^2 + \sigma_{DL}^2 + \sigma_L^2}}$$

$$\beta = \frac{8736 - 3247 - 472 - 1320}{\sqrt{655^2 + 260^2 + 118^2 + 238^2}} = 4.91$$

Calculation of RI for AASHTO Type III:

$$M_R = 4864 \text{ k-ft} , \quad M_D = 1952 \text{ k-ft} , \quad M_{FWS} = 293 \text{ k-ft} ,$$

$$M_L = 757 \text{ k-ft}$$

$\mu_i = M_i \lambda_i$ and λ_i is acquired from table 4-13 for Dead, Future Wearing Surface and Live load. And bias factor of the resistance acquired from table 4-14.

$$\lambda_R = 1.05 , \quad \lambda_D = 1.03 , \quad \lambda_{FWS} = 1.0 , \quad \lambda_L = 1.10$$

$$\mu_R = 5107 \text{ k-ft} , \quad \mu_D = 2011 \text{ k-ft} , \quad \mu_{FWS} = 293 \text{ k-ft} ,$$

$$\mu_L = 833 \text{ k-ft}$$

After calculation of mean value (μ_i) for each of the parameters, using coefficient of variation from Table 11-13 and Table 11-14, standard deviation (σ_i) can be calculated as follows.

$$V_R = 0.075 , \quad V_D = 0.08 , \quad V_{FWS} = 0.25 , \quad V_L = 0.18$$

$$\sigma_i = V_i \mu_i$$

$$\sigma_R = 383 , \quad \sigma_D = 161 , \quad \sigma_{FWS} = 73 , \quad \sigma_L = 150$$

After calculation of all the mean values and standard deviations, using equation 15 Reliability Index (RI) can be calculated as following.

$$\beta = \frac{\mu_R - \mu_{DL} - \mu_L}{\sqrt{\sigma_R^2 + \sigma_{DL}^2 + \sigma_L^2}}$$

$$\beta = \frac{5107 - 2011 - 293 - 833}{\sqrt{383^2 + 161^2 + 73^2 + 150^2}} = 4.40$$

Other calculations are in the same trend with this sample example of the calculation. The whole results of the analysis are tabulated and shown in chapter 11.3.

8.3 Results and Discussion

The first analysis is to determine the flexural load rating factor for the baseline state, which is described as the perfect condition of the bridge isolated from all possible losses and environmental effects. The analysis is carried out for both bridge types and LRFs are calculated for each individual girder at different locations. The variation of LRF at 7.5 feet intervals are calculated and results are illustrated in the following Figures are examples of the results for entire bridge for the baseline case under Florida legal trucks.

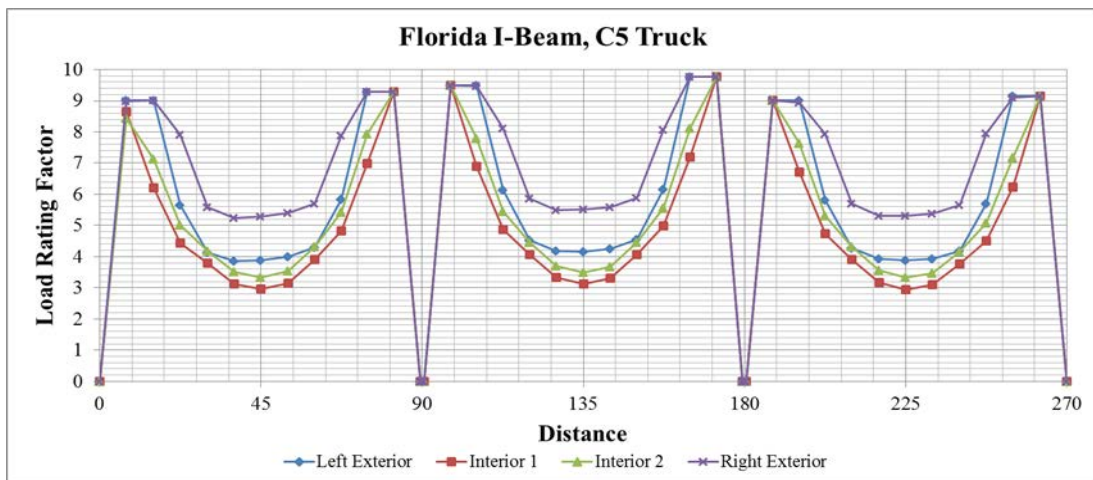


FIGURE 8-1: LOAD RATING THROUGH ENTIRE FIB BRIDGE UNDER C5 TRUCK LOAD

In Figure 8-1 and Figure 8-2, load rating factors for Florida I-Beam show very similar tendency and values for C5 and SU4 legal loads. Computed rating factors are lower at the interior girders and take higher values at the exteriors, which makes sense due to the placement of trucks and distribution of load over the girders. Additionally, right exterior girder seems to have a higher LRF than

that of the left exterior which is due to the emergency lane is carried by the right exterior girder.

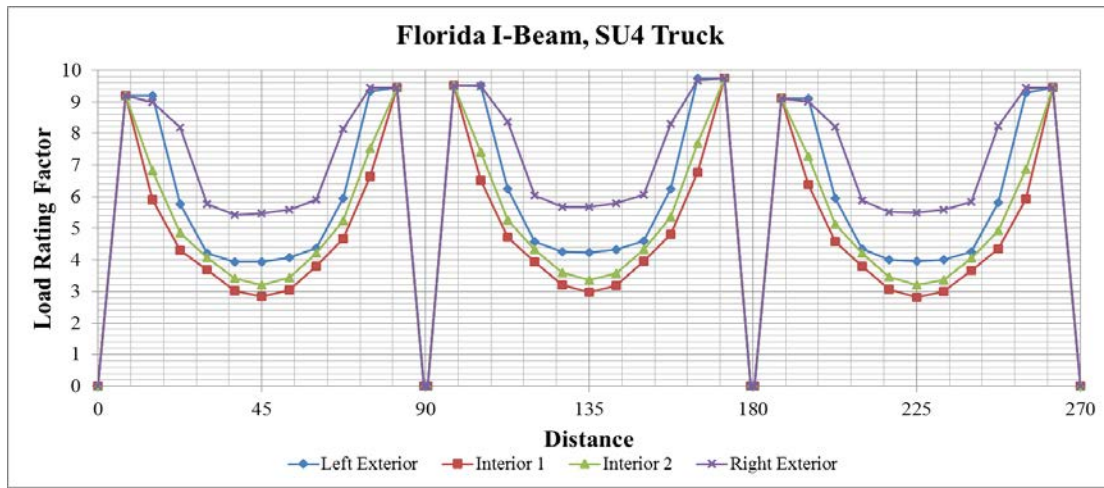


FIGURE 8-2: LOAD RATING THROUGH ENTIRE FIB BRIDGE UNDER SU4 TRUCK LOAD

In Figure 8-3 and Figure 8-4, LRFs at every 7.5 feet intervals are given for the baseline case along the entire bridge with AASHTO type III girder. The same tendencies explained for Florida I-beam is also observed for this beam with some minor differences. Interior girders again take the lowest LRF values; however, the magnitudes of the AASHTO Girder LRFs are lower at each span compared to Florida I-beam.

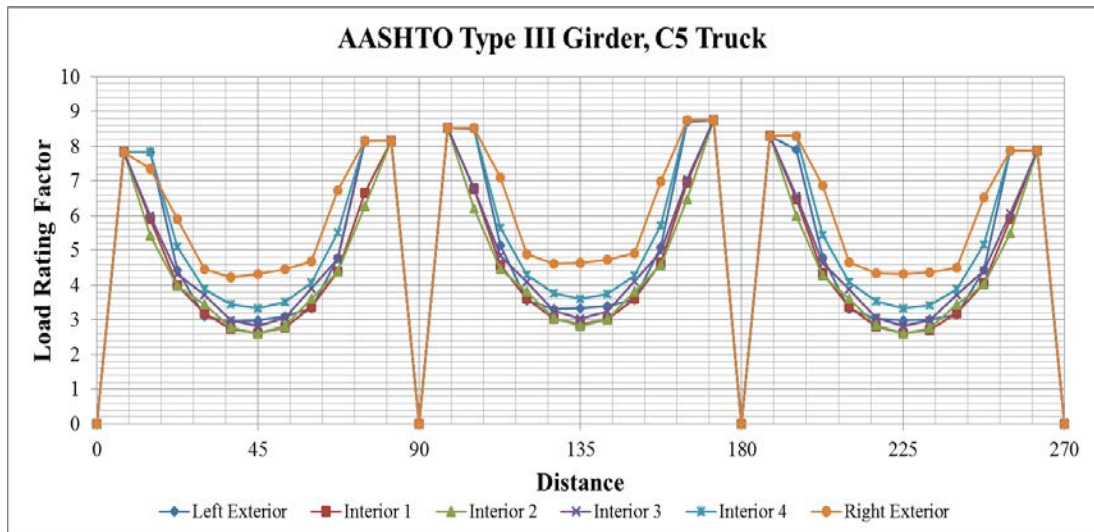


FIGURE 8-3: LOAD RATING THROUGH ENTIRE AASHTO TYPE BRIDGE UNDER C5 TRUCK LOAD

To have a better understanding of LRF differences of AASHTO Type and FIB girders, the difference in LRF of AASHTO and FIB, with respect to AASHTO are presented. For the baseline case, this difference is 29.8% for exterior girders and 13.1% for interior girders under C5 truck load. Similarly, 28.3% for exterior girders and 14.6% for interior girders under SU4 truck load.

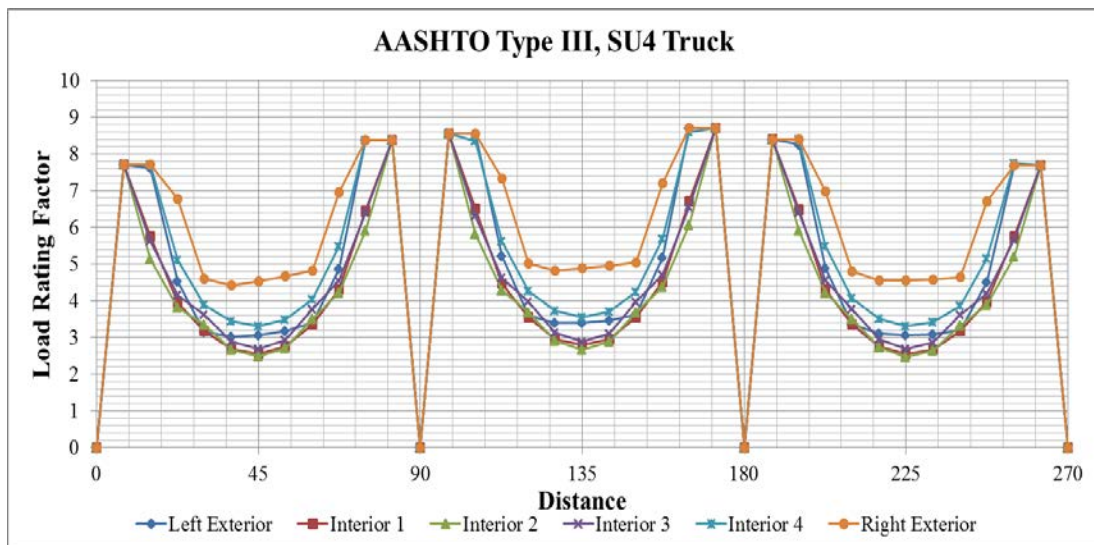


FIGURE 8-4: LOAD RATING THROUGH ENTIRE AASHTO TYPE BRIDGE UNDER SU4 TRUCK LOAD

These findings verify that the load carrying capacity of Florida I beam is higher than that of the AASHTO type III beam as pointed out by the FDOT. In other words, FIB load rating factor of 3.88 of exterior girder for C5 truck load translates to 310.4 kips (3.88×80 kips), whereas AASHTO 2.99 load rating translates to 239.2 kips (29.8% difference between 310.4 kips 239.2 kips). Similarly, FIB load rating of 2.94 for interior girder under C5 truck load translates to 235.2 kips (2.94×80 kips), whereas 2.60 load rating factor for AASHTO for interior girder gives 208 kips (13% difference between 235.2 kips and 208 kips). The possible live load that can be carried out under different cases can be determined in a similar fashion.

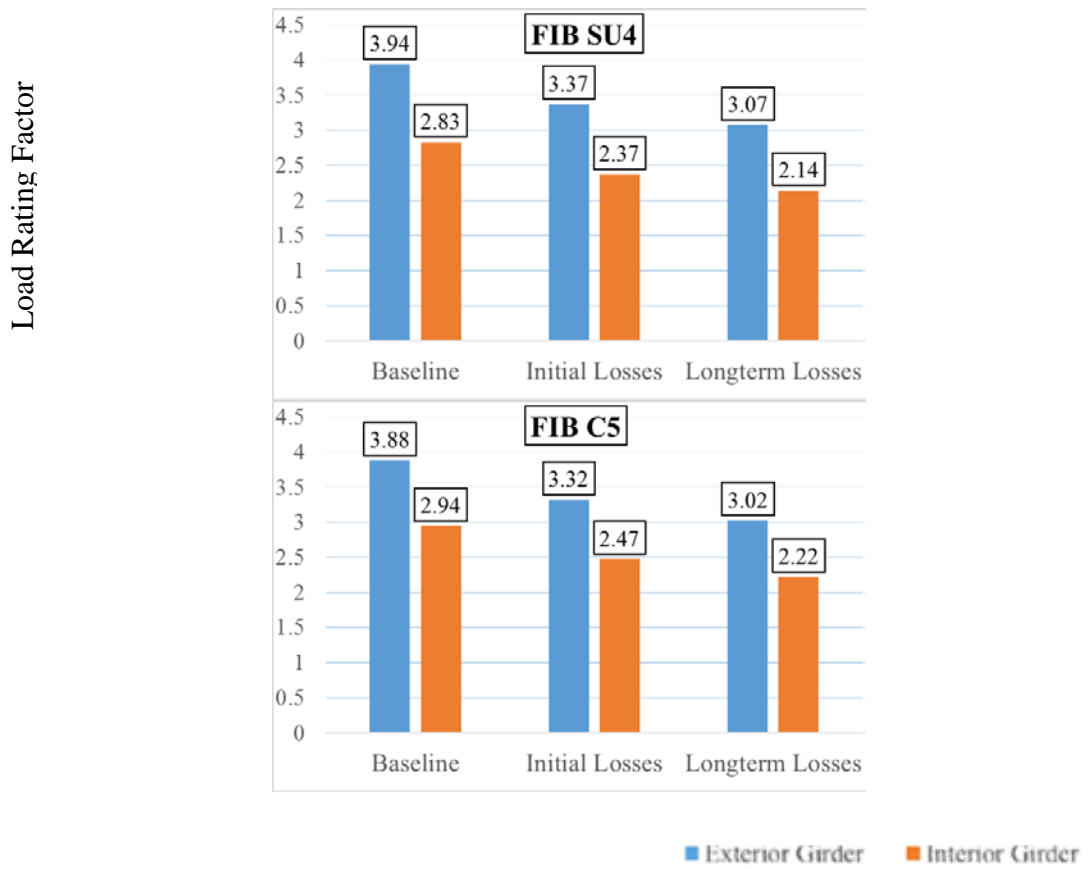


FIGURE 8-5 :LRF COMPARISON OF FIB BETWEEN LEGAL LOADS

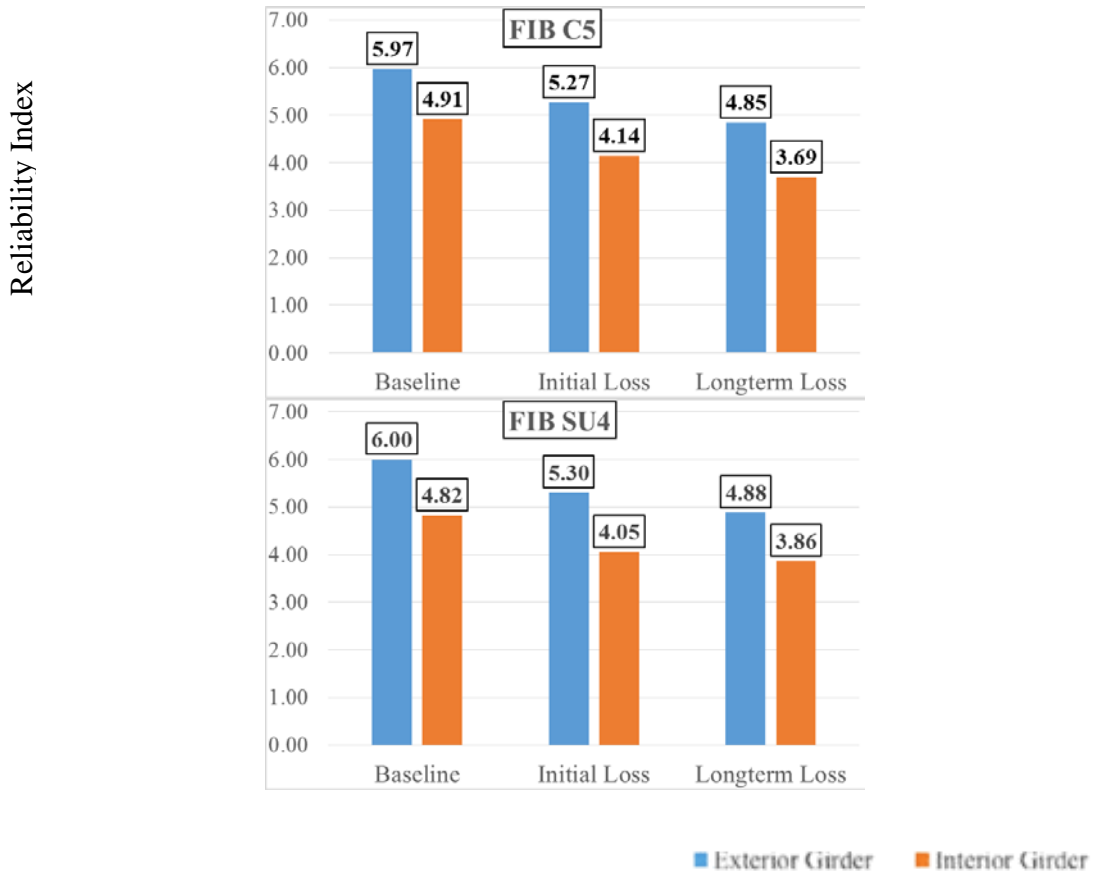


FIGURE 8-6: RI COMPARISON OF FIB BETWEEN LEGAL LOADS

In Table 8-15 and Table 8-16, reliability indices are also included. These reliability indices are tabulated with the same procedure for the most critical location as summarized for the LRF calculations. For each member in every span, reliability indices are calculated using the output of the most critical flexural moment values. The same trend is seen as in LRF.

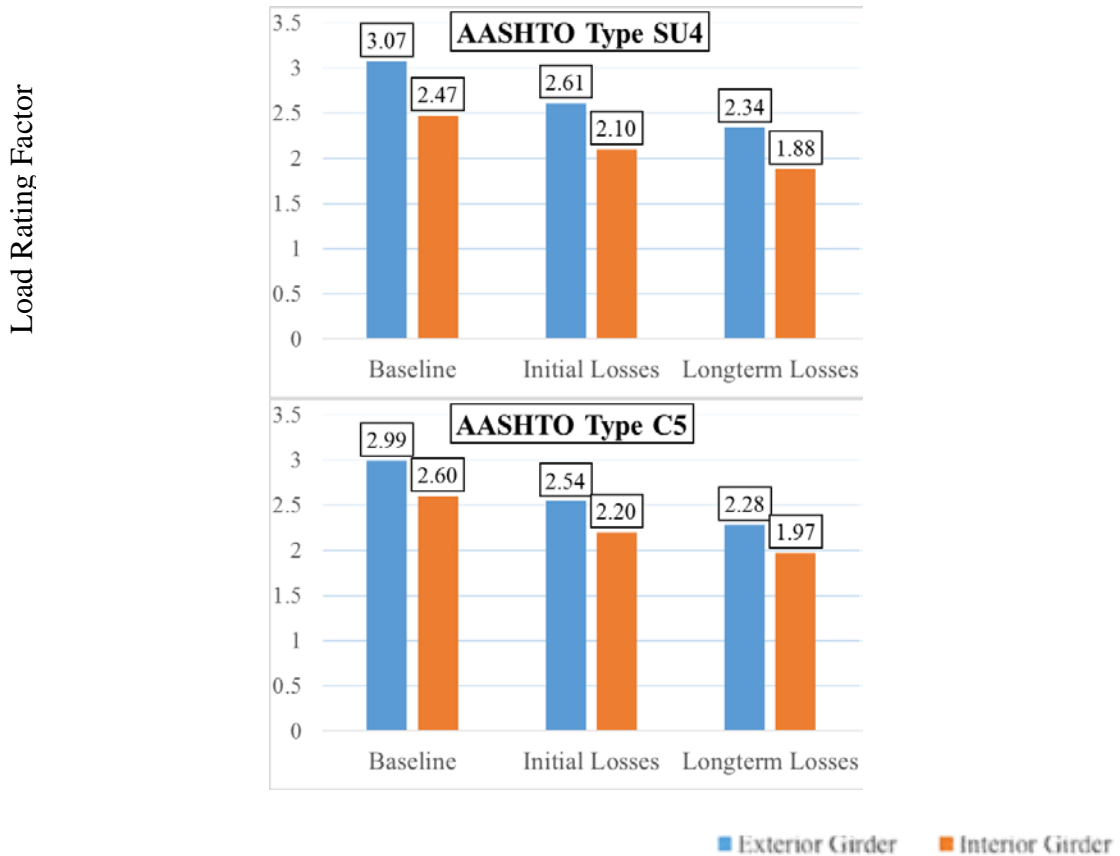


FIGURE 8-7: LRF COMPARISON OF AASHTO BETWEEN LEGAL LOADS

Starting from the baseline case and going through prestress losses one by one, reduction in LRF and reliability index magnitude can be seen clearly. It is obvious to see that there are direct correlations between the variation of load rating factors and reliability indices.

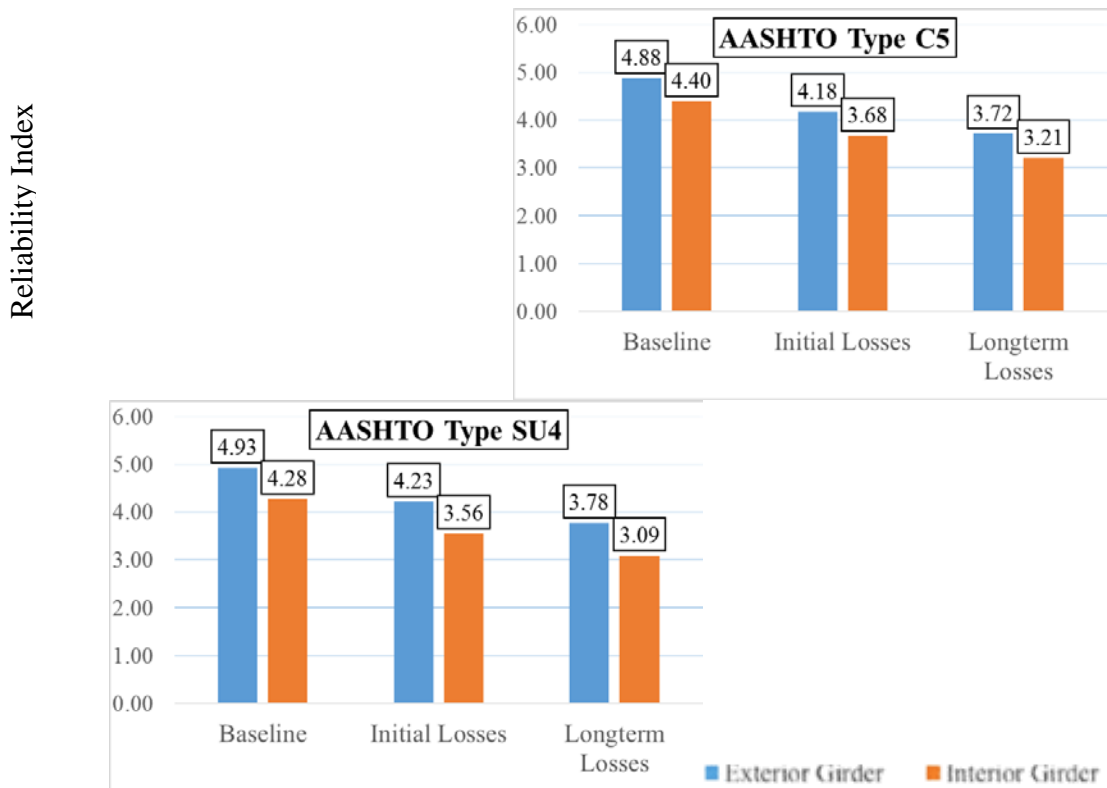


FIGURE 8-8: RI COMPARISON OF AASHTO BETWEEN LEGAL LOADS

It is seen that the long term losses have the most impact in terms of load rating and reliability for the most critical locations. While the load carrying capacity is reduced, it is also seen that the element reliability at the critical sections is reduced, thereby increasing the probability of failure.

Figure 8-9 to Figure 8-12 are the results for RMD and TPD types of trucks and the results showed in terms of load rating factor and reliability index.

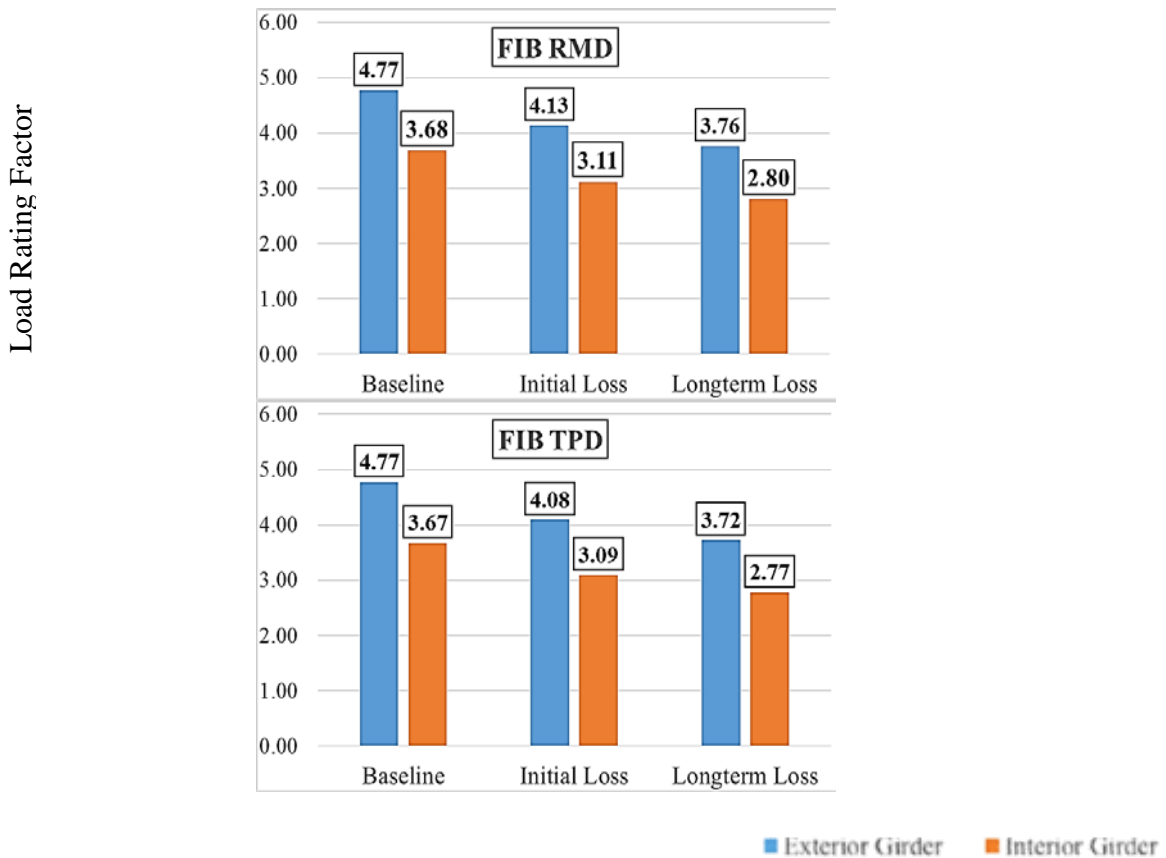


FIGURE 8-9: LRF COMPARISON OF FIB BETWEEN LCVS

Since the bridges that are formulated and studied in this report is short span bridges, short trucks with higher axle loads have higher impact on the girders. From the LCV results also could be seen that the reliability and load rating factors are higher as expected.

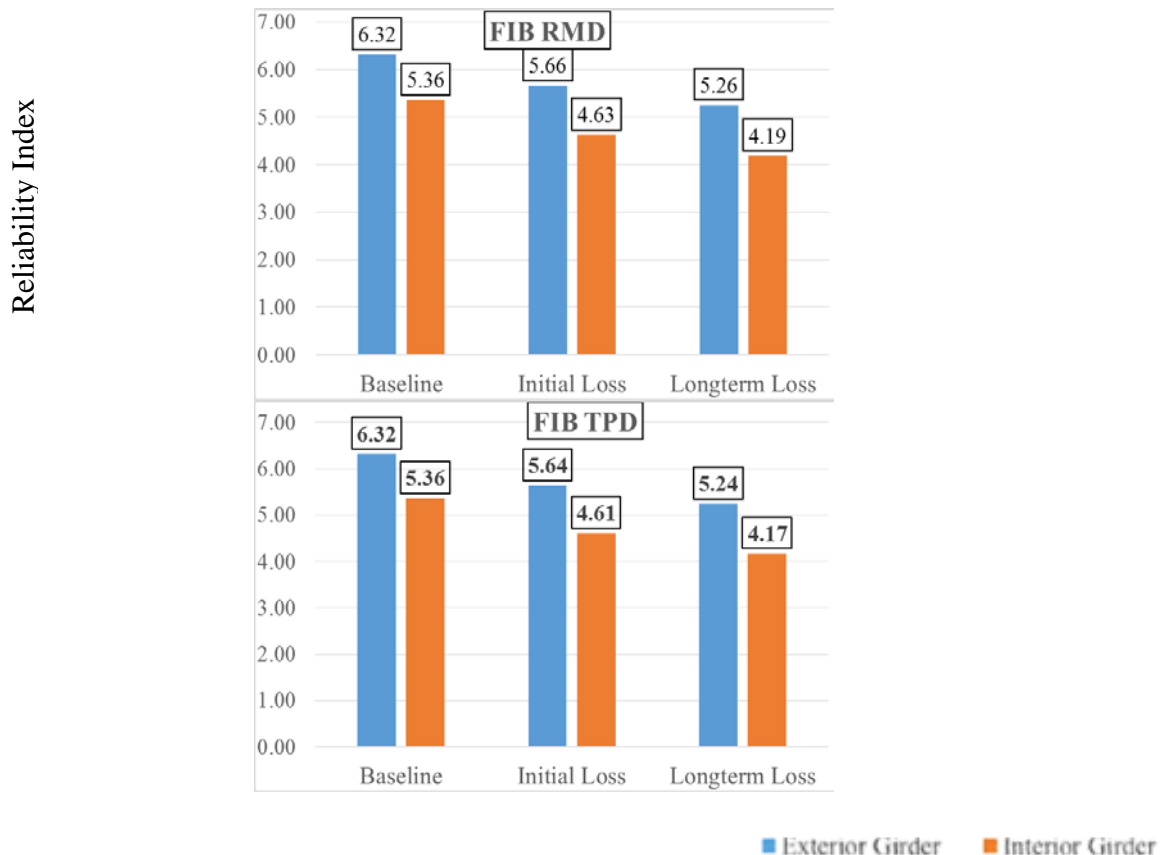


FIGURE 8-10: RI COMPARISON OF FIB BETWEEN LCVS

As it expected, also these results are following the same trend as for legal and design truck. In each of the cases either baseline case , case of the initial losses or case of long term prestress losses, FIB has higher load rating factors and reliability index.

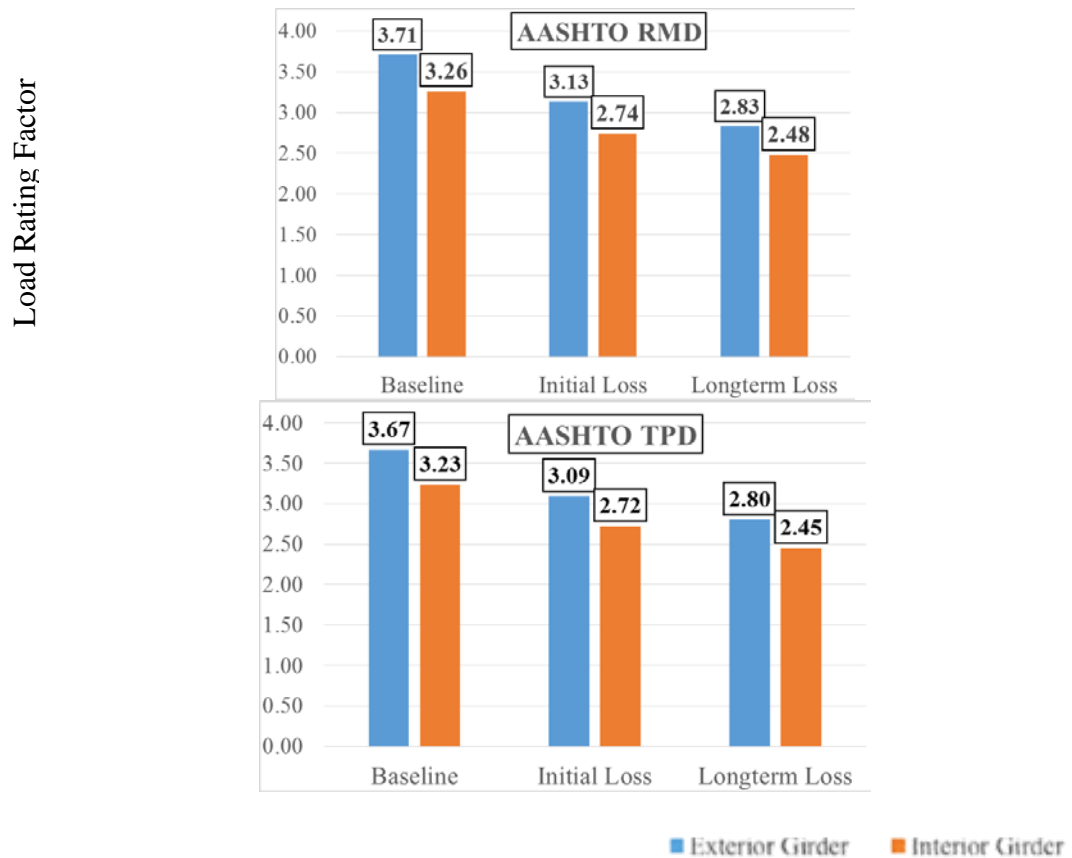


FIGURE 8-11: LRF COMPARISON OF AASHTO BETWEEN LCVS

For example in Rocky Mountain Turnpike truck of this study has weight of 104kips which are distributed through its 7-axles.

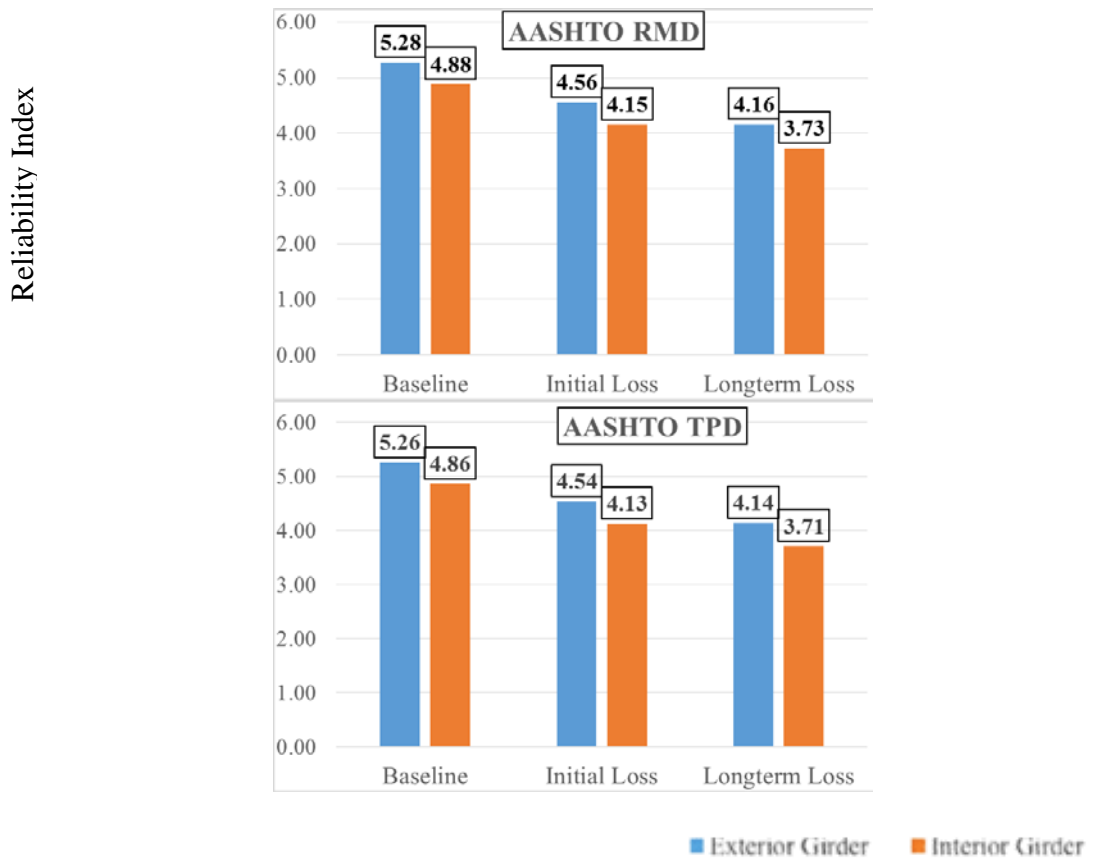


FIGURE 8-12 :RI COMPARISON OF AASHTO BETWEEN LCVS

FIB load rating factor is 3.68 in baseline case for interior girder in compare to 3.26 for AASHTO type girder bridge. This means 11.41 percent more load rating. If this amount converted to the weight it is equal to 11.90 kips more weight on the truck could be carried by the FIB girder bridge, Also for the long term loss case the load rating factor value for the FIB is 2.80 and the same case for AASHTO led to load rating factor of 2.48. This also means that in this case FIB can carry more load under RMD truck than AASHTO Type girder bridge.

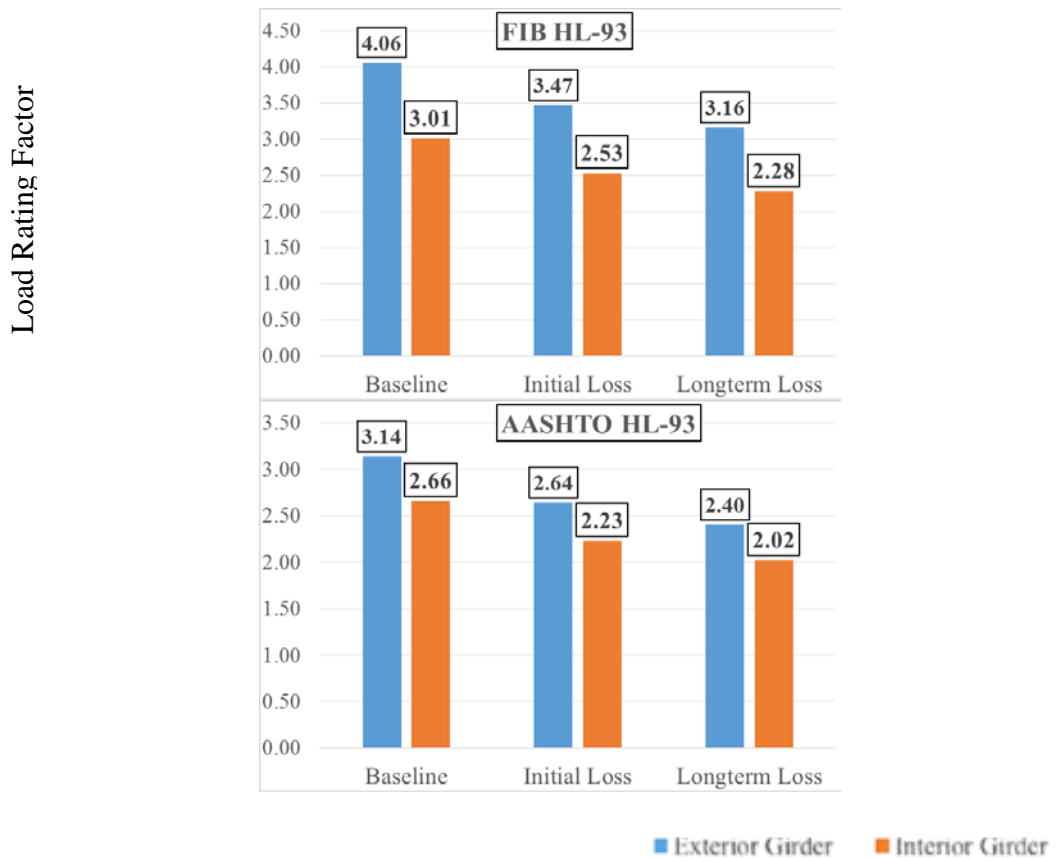


FIGURE 8-13: LRF COMPARISON OF FIB AND AASHTO UNDER HL-93

In HL-93 case truck load is considered as vehicular live load on the bridges and the results could be seen through Figure 8-13 and Figure 8-14.

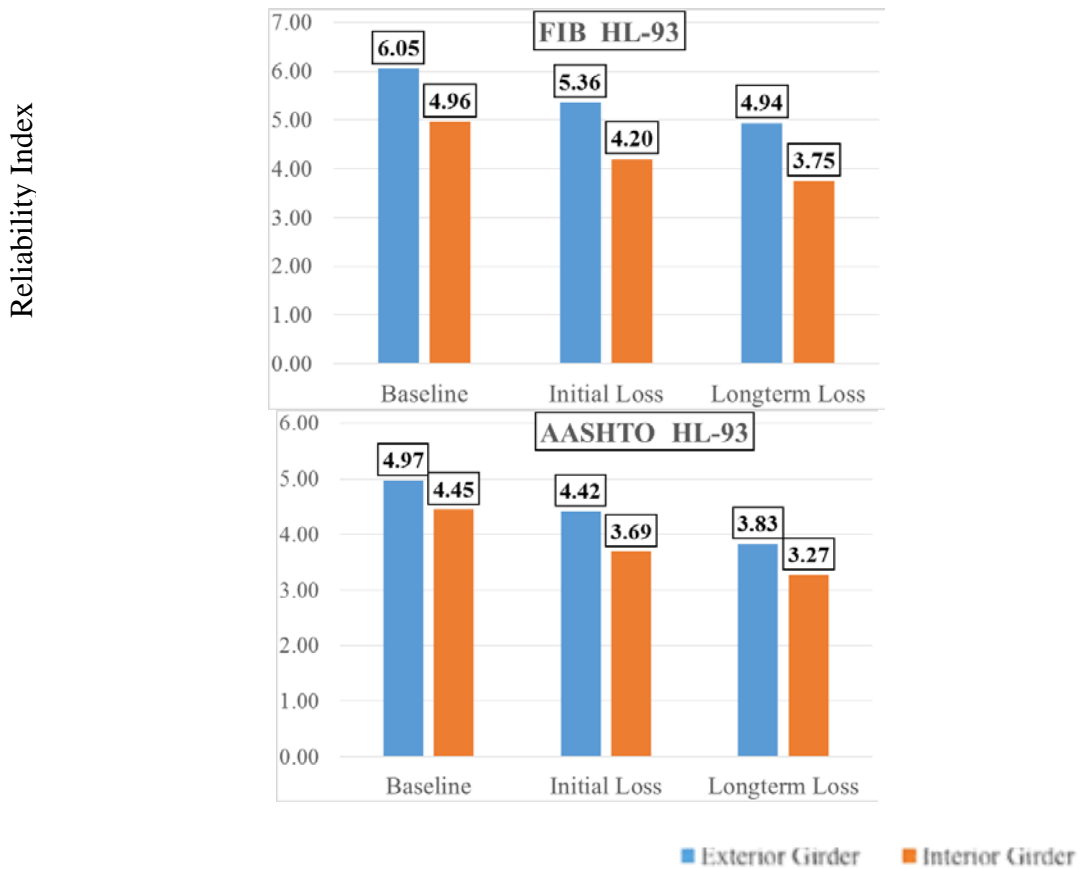


FIGURE 8-14: RI COMPARISON OF FIB AND AASHTO UNDER HL-93

This results show the same trend as Florida legal loads and long combination of vehicles. Again FIB girder bridge has higher load rating and reliability in each of the comparison cases.

At the end, all the results are tabulated for FIB girder bridge (Table 8-15) and AASHTO Type girder bridge (Table 8-16) of this study.

From the detailed evaluation and assessment of load rating factors for the baseline case and considering each span is simply supported for both bridges, it can be concluded that the load rating factor takes its lowest value at the mid-span in each girder and that the minimum load rating value is chosen as the

governing critical value since the first failure is expected at this member and it is directly related to overall performance of the structure. In Tables 8-15 and 8-16, critical values of LRFs for each structural condition are tabulated for the interior and exterior girders. The differences of each condition with respect to baseline case are also included in these tables. As the losses increase cumulatively, load rating factors, or load carrying capacity in other words decrease in magnitude causing the difference go higher in percentage.

TABLE 8-15: FLORIDA I-BEAM ANALYSIS RESULTS

Analysis	Girder location	Vehicle type	Baseline	Immediate losses	Change w.r.t Baseline (%)	Long term losses	Change w.r.t Baseline (%)
Load Rating Factor	Exterior	HL-93	4.06	3.47	14.50	3.16	22.16
	Interior		3.01	2.53	15.94	2.28	24.25
	Exterior	C5	3.88	3.32	14.53	3.02	22.19
	Interior		2.94	2.47	15.90	2.22	24.37
	Exterior	SU4	3.94	3.37	14.37	3.07	22.05
	Interior		2.83	2.37	16.10	2.14	24.54
	Exterior	RMD	4.77	4.13	13.42	3.76	21.71
	Interior		3.68	3.11	15.49	2.80	23.91
	Exterior	TPD	4.77	4.08	14.47	3.72	22.01
	Interior		3.67	3.09	15.80	2.77	24.53
Reliability Index β	Exterior	HL-93	6.05	5.36	15.92	4.94	23.57
	Interior		4.96	4.20	16.17	3.75	24.06
	Exterior	C5	5.97	5.27	11.77	4.85	18.81
	Interior		4.91	4.14	15.63	3.69	24.91
	Exterior	SU4	6.00	5.30	11.64	4.88	18.63
	Interior		4.82	4.05	16.07	3.59	25.57
	Exterior	RMD	6.32	5.66	10.44	5.26	16.77
	Interior		5.36	4.63	13.62	4.19	21.83
	Exterior	TPD	6.32	5.64	10.75	5.24	17.09
	Interior		5.36	4.61	14.00	4.17	22.20

TABLE 8-16: AASHTO TYPE III BEAM RESULTS

Analysis	Girder location	Vehicle type	Baseline	Immediate losses	Change w.r.t Baseline (%)	Long term losses	Change w.r.t Baseline (%)
Load Rating Factor	Exterior	HL-93	3.14	2.64	15.92	2.40	23.57
	Interior		2.66	2.23	16.17	2.02	24.10
	Exterior	C5	2.99	2.54	15.02	2.28	23.72
	Interior		2.60	2.20	15.27	1.97	24.17
	Exterior	SU4	3.07	2.61	14.98	2.34	23.68
	Interior		2.47	2.10	15.15	1.88	24.06
	Exterior	RMD	3.71	3.13	15.63	2.83	23.72
	Interior		3.26	2.74	15.95	2.48	23.93
	Exterior	TPD	3.67	3.09	15.80	2.80	23.71
	Interior		3.23	2.72	15.79	2.45	24.15
Reliability Index β	Exterior	HL-93	4.97	4.42	11.06	3.83	11.06
	Interior		4.45	3.69	17.07	3.27	26.52
	Exterior	C5	4.88	4.18	14.42	3.72	24.23
	Interior		4.40	3.68	16.36	3.21	26.95
	Exterior	SU4	4.93	4.23	14.12	3.78	23.31
	Interior		4.28	3.56	16.93	3.09	27.87
	Exterior	RMD	5.28	4.56	13.64	4.16	21.21
	Interior		4.88	4.15	14.96	3.73	23.56
	Exterior	TPD	5.26	4.54	13.69	4.14	21.30
	Interior		4.86	4.13	15.02	3.71	23.66

9. The Effect of Increasing Heavy Vehicle Loads on a Bridge Lifespan

9.1 Introduction

Addressing the Nation's highway bridge retrofitting and replacement needs is one of the challenges faced by most of the state departments of transportation (DOTs) and other bridge owners. Under the current conditions of traffic and traffic loading, more than 25% of the Nation's bridges (600,000) are classified as structurally deficient or functionally obsolete and 30% of the Nation's bridges exceed 50-years of their design life, see Figure 9-1[41]. From state to state, the percentage varies considerably as shown in Figure 9-1[42]. These bridges need different levels of repairs, rehabilitation, or replacement.

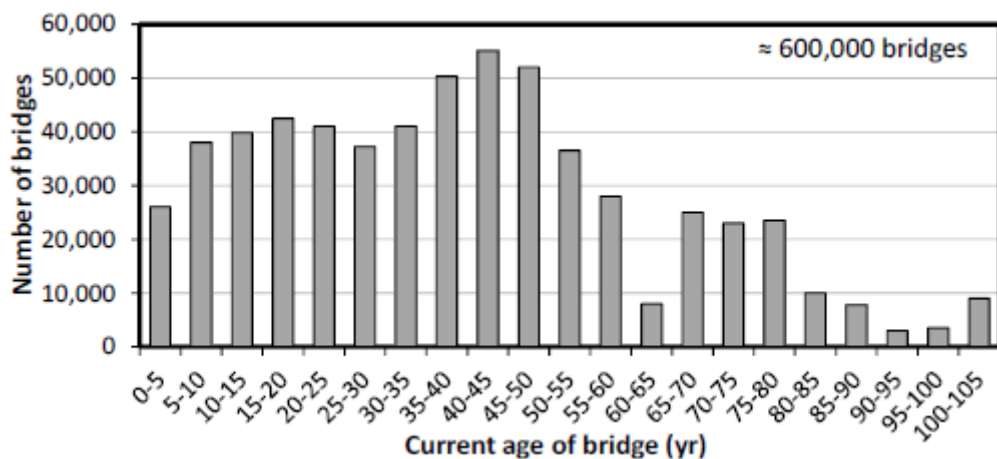


FIGURE 9-1: AGE DISTRIBUTION OF BRIDGES IN THE UNITED STATES [43]

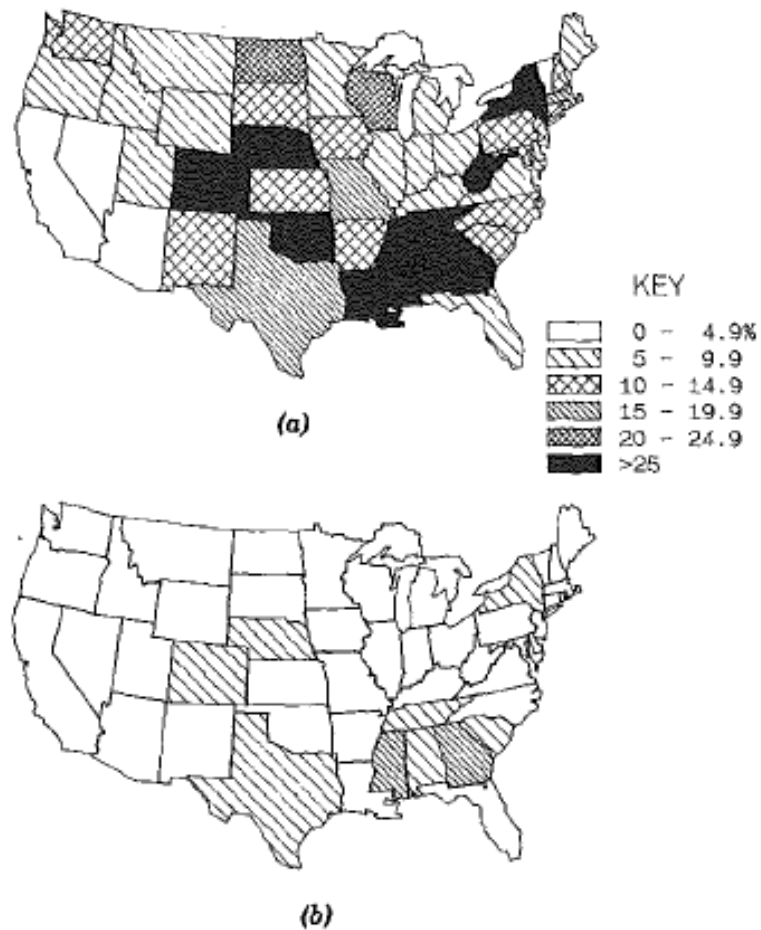


FIGURE 9-2: PERCENTAGES OF BRIDGES CLASSIFIED STRUCTURALLY DEFICIENT: (A) BUILT 1950-1987; AND (B) BUILT 1980-1987 [42]

With limitations on the allocation for maintenance budgets and the expected increase in traffic to accommodate the increase in the freight demand, the challenges facing bridge owners are expected to increase as well. All these circumstances made most of the bridge owners to be more reactive than proactive toward managing their bridge [41].

Therefore, other programs that depend on worst-first approach in managing bridges that may result in deterioration of bridges still in good conditions. One of the successful bridge programs is a balance between preservation and replacement that aims to maximize the cost effectiveness of the maintenance budget allocated to

increase the useful life of bridges. This program helps to extend the bridges' service life before they require replacement with lower cost by applying the appropriate maintenance at the appropriate time [41].

Figure 9-2 shows the 12 most common bridge types built between 1950 and 1987, and their rates of structural deficiency as a function of their construction material, structural system, and age [42]. Statistical records have been recently issued in 2013 by the National Bridge Inventory (NBI) listing the numbers, structurally deficient, and functionally obsolete, bridges from all over the United States (see Table 9-2:). Another classification based on the year of construction is shown in Table 9-3 [44]. All this information shows that the most common type of bridge is the steel bridges and the bridge's status (deficiency) is a function of the age of the bridge

**TABLE 9-1: THE TWELVE MOST COMMON BRIDGE TYPES BUILT
BETWEEN 1950-1987 AND PERCENTAGES CLASSIFIED STRUCTURALLY
DEFICIENT [42]**

Bridge Type	Number	Total	Structurally deficient (%)	
		(%)	1950-1987	1980-1987
Steel stringer	69885	24	23	7
Continuous steel stringer	32227	11	11	1
Timber stringer	31083	10	52	30
Prestressed concrete stringer	27923	9	4	0
Reinforced concrete slab	24162	8	11	2
Continuous reinforced concrete slab	18573	6	4	0
Prestressed concrete multiple box	16377	5	5	1
Reinforced concrete stringer	12500	4	10	2
Reinforced concrete tee	11361	4	6	1
Continuous reinforced concrete tee	5827	2	3	1
Prestressed concrete slab	5706	2	3	0
Prestressed concrete tee	5017	2	5	0
Total	260641	88	-	-

TABLE 9-2 :UNITED STATES BRIDGE COUNT AND STATUS BY CONSTRUCTION MATERIAL [44]

	Concrete	Concrete Continuous	Steel	Steel Continuous	Prestressed Concrete	Prestressed Concrete Continuous	Wood	Masonry	Aluminum Iron	Other
Count Built	177,805	75,531	130,947	50,148	124,248	24,085	21,469	1,699	1,558	261
Structurally deficient	12,366	4,433	28,910	3,912	4,983	439	7,820	445	177	37
Functionally Obsolete	19,821	8,022	26,027	10,361	14,538	2,314	2,997	488	140	39
Deficient	32,005	12,422	54,480	14,313	19,769	2,832	10,709	929	331	80

TABLE 9-3: UNITED STATES BRIDGE COUNT AND STATUS BY YEAR OF BUILD [44]

Year Built	2007-	2002-	1997-	1992-	1987-	1982-	1977-	1972-	1967-	1962-	1957-
	2011	2006	2001	1996	1991	1986	1981	1976	1971	1966	1961
Count Built	21,664	36,265	38,793	39,866	43,189	38,985	36,242	41,825	50,234	52,980	47,803
Structurally deficient	0	0	476	810	1,285	1,565	2,221	3,507	4,896	5,970	6,771
Functionally Obsolete	0	0	3,349	3,334	4,111	3,217	3,011	4,330	6,621	9,057	8,856
Deficient	0	0	3,825	4,144	5,396	4,782	5,232	7,837	11,517	15,027	15,627

TABLE5-3 :UNITED STATES BRIDGES COUNT AND STATUS BY YEAR OF BUILD [44] (CONT.)

Year Built	1952-	1947-	1942-	1937-	1932-	1927-	1922-	1917-	1912-	1907-	1906
	1956	1951	1946	1941	1936	1931	1926	1921	1916	1911	and earlier
Count Built	30,635	24,022	6,454	24,699	22,223	19,588	8,364	6,292	3,210	3,109	8,621
Structurally deficient	4,953	4,955	1,459	6,232	5,906	5,168	2,458	2,577	1,484	1,564	3,262
Functionally Obsolete	6,033	4,438	1,183	4,148	4,101	3,771	1,997	1,407	777	672	1,945
Deficient	10,986	9,393	2,642	10,380	10,007	8,939	4,455	3,984	2,261	2,236	5,207

9.2 Literature Review

The propagation and growth of cracks in steel structures under the action of cyclic loads is defined as fatigue. In normal operation, the stress level is often below the material strength, but in the presence of some defects or micro cracks in material, they may develop stress concentration that leads to crack growth. At this point, the number of cycles plays an effective role in the crack growth.

9.2.1 Fatigue Resistance Characterization [43]

There are many ways to characterize fatigue resistance, but there are two common approaches. One is the experimental method based on the stress, S-N curves, and the other is numerical based on fracture mechanics. However, both have a considerable level of uncertainty due to the vast complexity of fatigue process.

- *Stress-based approach*

This approach is based mainly on the number of stress cycles of constant amplitude (i.e. stress range required for failure of the tested element). This test is repeated for different stress amplitudes until failure as seen in Figure 9-3.

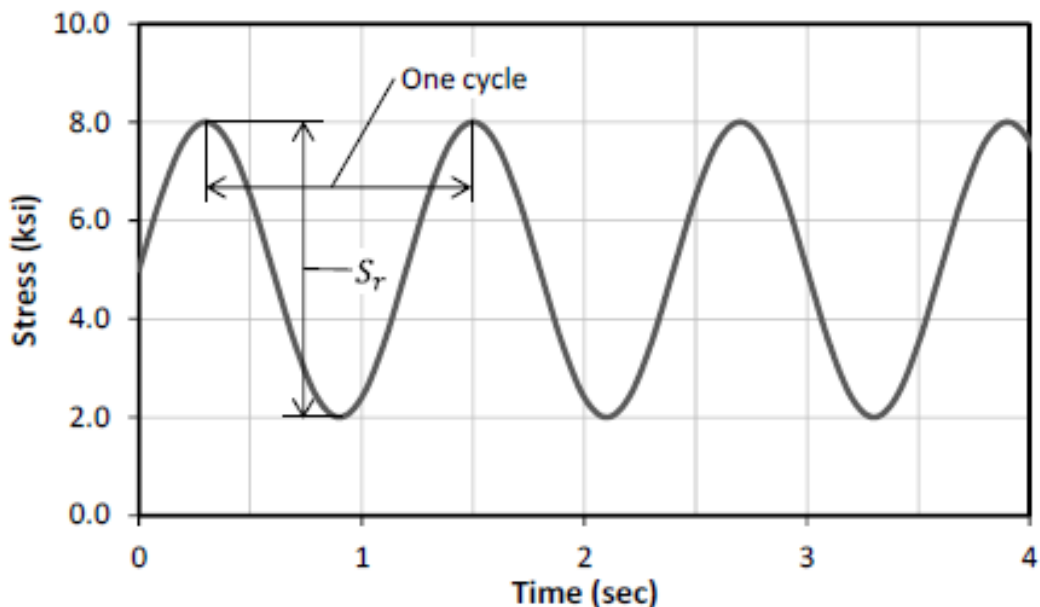


FIGURE 9-3: DEFINITION OF A STRESS CYCLE [43]

Figure 5.4 plots the number of cycles to failure (N_f) for various cyclic stress ranges (S_r). Due to expected stress concentrations, the nominal stress is used to characterize the S-N curve.

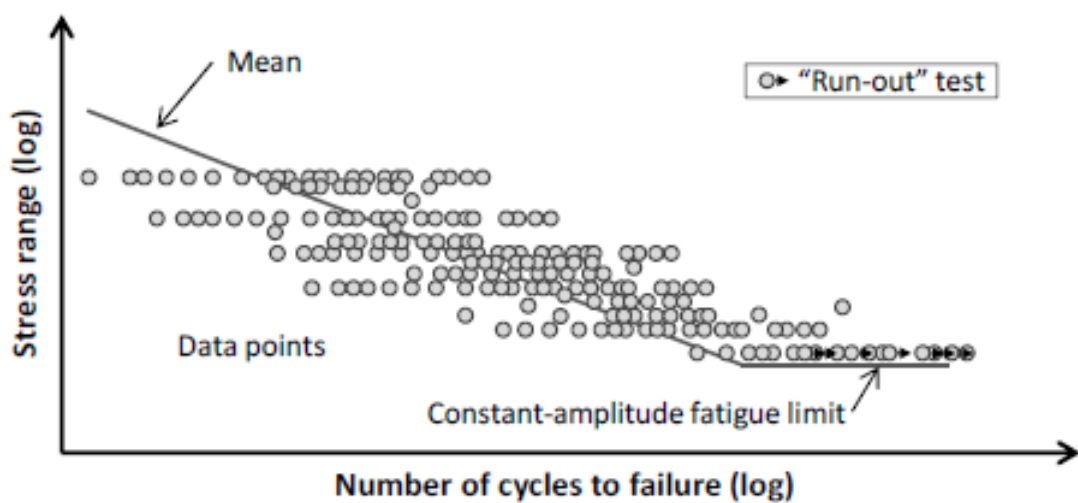


FIGURE 9-4 :EXAMPLE OF DATA FROM A REPRESENTATIVE FATIGUE TEST [43]

Considering a single type of detail, the fatigue resistance can be described by equation Eq. 9-1 [43].

$$N_f = C \times S_r^B \quad (9 - 1)$$

where:

N_f = number of cycles until failure at S_r

C = empirical constant for specified detail from failure data (ksi^{-B})

S_r = nominal constant amplitude stress range (ksi)

B = slope of the S-N curve (-2 to -4)

9.2.2 *Elastic Fracture Mechanics approach*

The linear elastic fracture mechanics (LEFM) approach is not commonly used as the S-N curve; however, it is used to calculate the propagation of the crack until fracture. It depends on the fracture mechanics' properties of the material such as fracture toughness and flaw size. Some tests are required to determine correction factors; nevertheless, it is an analytical approach.

The use of this approach is affected by many limitations. Such as the difficulty to determine the initial crack size significantly affects the fatigue life as shown in Figure 9-5. Moreover, estimating the stress intensity factor range for complex geometric shapes makes the method impractical for design [43].

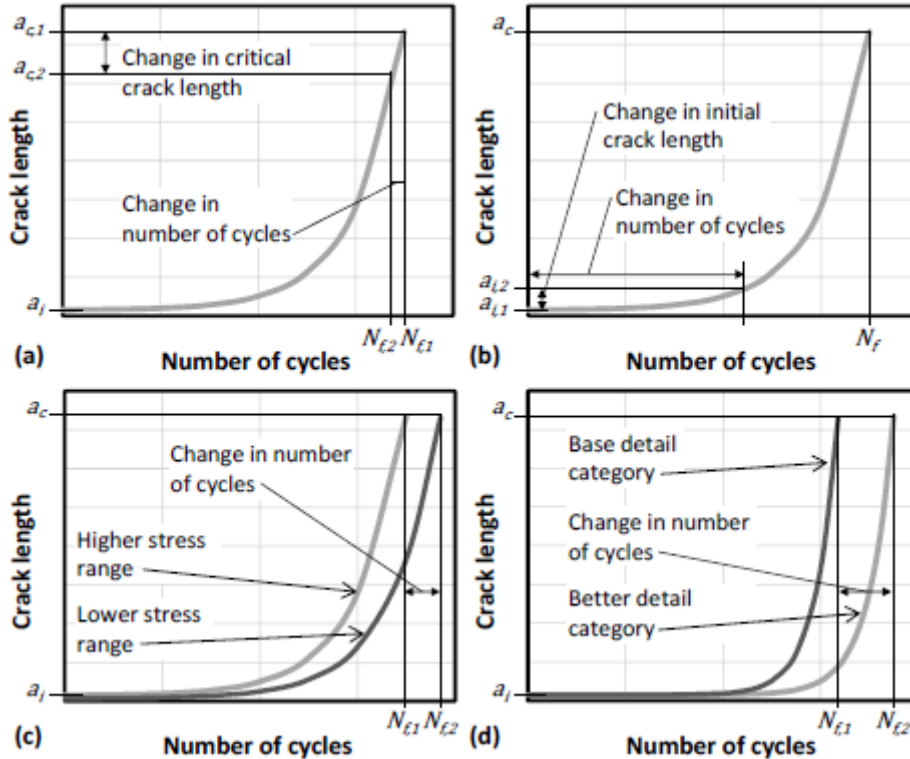


FIGURE 9-5: CHANGE IN NUMBER OF CYCLES DUE TO CHANGE IN (A) CRITICAL CRACK LENGTH, (B) INITIAL CRACK LENGTH, (C) STRESS RANGE, AND (D) TYPE OF DETAIL [43]

9.2.3 Steel Bridge Fatigue

The fatigue of steel bridge components were investigated comprehensively. These investigations show that the vast majority of the bridges of state agencies have fatigue problems. According to the principles of fracture mechanics, fatigue damages originate from microscopic discontinuities in the material under cyclic loading. These discontinuities cause stress concentration, with a stress much higher than what the member is normally expected to withstand. For steel bridge components, such discontinuities may be caused by a lack of fusion in a weld, and/or a sudden geometric change at a connection. Current fatigue life estimation in the United States is based on the fatigue category, the nominal stress range, and the number of stress cycles [43].

Fatigue is a cumulative process in which the repetitive stress cycles repeat damage until failure occurs. Therefore, the basic concept of the fatigue design and assessment for bridges relates to the fact that each cycle of trucks causes some damage. These damages accumulate until failure occurs by fatigue failure. The damage caused by each truck depends on its weight, the bridge's span length, and the member section dimensions. Generally, based on theories of mechanics, fatigue damage is proportional to the difference between the maximum and minimum stress (stress range) caused by the vehicle passage at the location of concern.

9.2.4 Steel Bridges Fatigue Life Estimation Approach

The AASHTO Manual for Bridge Evaluation (MBE-2011) recommends an approximation to estimate the remaining life. This approximation may cause some tolerance in the estimated remaining life, and has been eliminated to produce a closed form solution for finite fatigue life (Y) [45].

Using the analytical sum of the truck traffic, the finite fatigue life (Y) is revised as follows [45]:

$$Y = \frac{\log \left[\frac{R_R A}{365n[(ADTT)_{SL}]_{Present}[(\Delta f)_{eff}]^3} g(1+g)^{a-1} + 1 \right]}{\log(1+g)} \quad (5.2)$$

Y: Total finite fatigue life in years

A: Detail category constant as shown in Table 5-4 this value is better understood by S-N curves in Figure 9-6. The value of A is sensitive to load-induced fatigue. Components are grouped into different categories and given letter grades, A is the best and E' is the worst. Hot-rolled sections and well-prepared welded connections are categorized as A and B detail. Fillet- and groove-welded attachments are

categorized as D and E detail. C category is assigned to welding of attachments by providing a transition radius greater than 6 in. and proper grinding of the weld [38].

Table 9-9 illustrates different configurations of detail categories.

TABLE 9-4: DETAIL CATEGORY CONSTANT A AND FATIGUE THRESHOLD (ΔF)_{TH} [38]

Detail Category	Constant, $A \times 10^8$ (ksi ³)	Fatigue threshold (ΔF) _{TH} , (ksi)
A	250.0	240
B	120.0	16.0
B'	61.0	12.0
C	44.0	10.0
C'	44.0	12.0
D	22.0	7.0
E	11.0	4.5
E'	3.9	2.6
M 164 (A 325) Bolts in Axial Tension	17.1	31.0
M 253 (A 490) Bolts in Axial Tension	31.50	38.0

R_R : Resistance factor specified for evaluation, minimum, or mean fatigue life as seen in Table 9-5.

n : Number of stress-range cycles per truck passage as seen in Table 9-6.

$(ADTT)_{SL}$: The number of trucks per day in a single day in a single lane averaged over the design life = $p \times ADTT$

$ADTT$: The number of trucks per day in one direction averaged over the design life (WIM data).

$[(ADTT)_{SL}]_{present}$ = Average number of trucks per day in a single day in a single lane averaged until present.

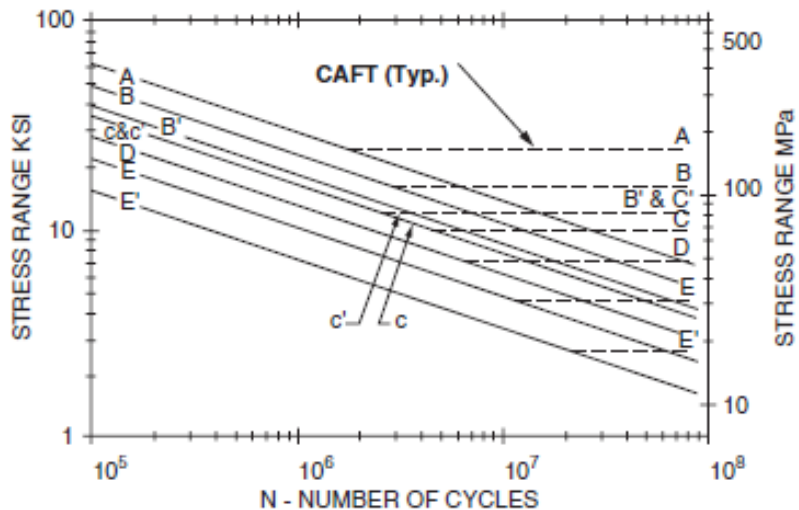


FIGURE 9-6 :AASHTO S-N CURVES FOR DESIGN OF STEEL BRIDGES [46]

The value of the average number of trucks per day in a single lane ($ADTT_{SL}$) changes over the fatigue life and cannot be found directly. Conceptually, $ADTT_{SL}$ needs to be found by iteration using equation Eq. 9-2. Nevertheless, it is recommended to be approximated using the chart in Figure 9-7. This figure does not include the unknown Y , but only the present age (a) which is part of Y .

g : Estimated annual traffic-volume growth rate that depends on the bridge's present age and annual traffic .

a : Present age of the bridge

$(\Delta f)_{eff}$: The effective stress range = $R_s \times \Delta f$

where:

Δf : The measured effective stress range or 75% of the calculated stress range due to the passage of the fatigue truck as specified in AASHTO LRFD design or a fatigue truck determined by a truck survey or WIM study.

P : Taken as shown in Table 9-7.

R_s : The stress range estimate partial load factor calculated as $R_{sa} \times R_{st}$ that could be estimated as per Table 9-8

TABLE 9-5: RESISTANCE FACTOR FOR EVALUATION MINIMUM OR MEAN FATIGUE LIFE, R_R [47]

Detail Category	R_R		
	Evaluation life	Minimum life	Mean life
A	1.7	1.0	2.8
B	1.4	1.0	2.0
B'	1.5	1.0	2.4
C	1.2	1.0	1.3
C'	1.2	1.0	1.3
D	1.3	1.0	1.6
E	1.3	1.0	1.6
E'	1.6	1.0	2.5

TABLE 9-6: CYCLES PER TRUCK PASSAGE, N [2]

Longitudinal member	Span Length	
	>40-ft	\leq 40-ft
Simple span girder	1.0	2.0
Continuous girder		
1- Near interior support	1.5	2.0
2- Elsewhere	1.0	2.0
Cantilever girder		5.0
Truss		1.0
Transverse member	Spacing	
	>20-ft	\leq 20-ft
		2.0

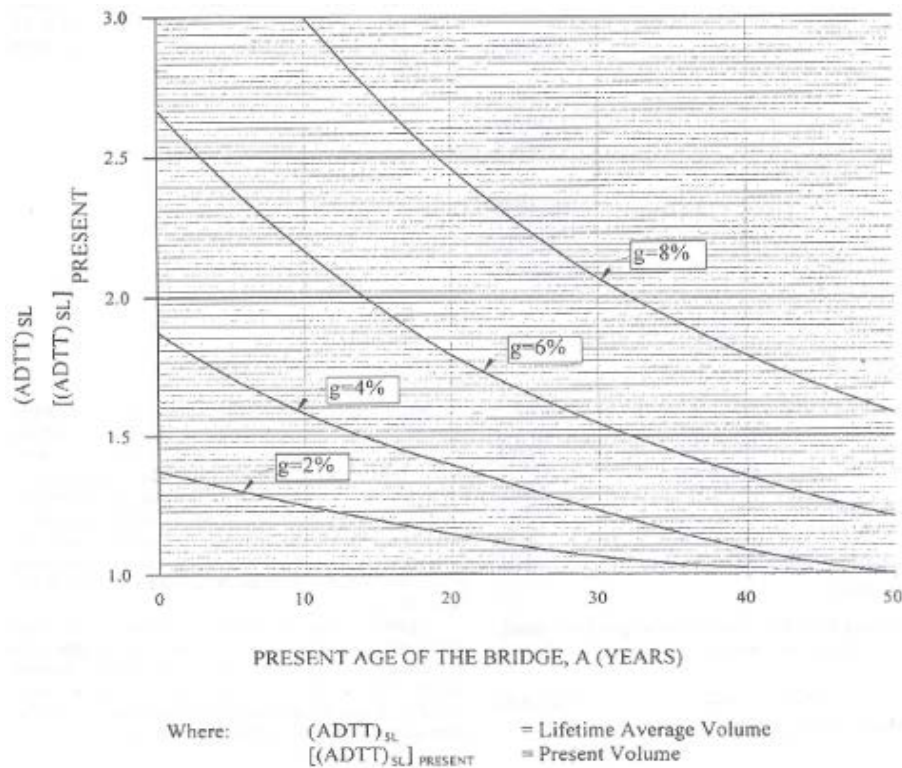


FIGURE 9-7: LIFETIME AVERAGE TRUCK VOLUME FOR AN EXISTING BRIDGE [2]

TABLE 9-7: FRACTION OF TRUCK TRAFFIC IN SINGLE LANE, P[2]

Number of lanes available to trucks	P
1	1.00
2	0.85
3 or more	0.80

Fatigue could be determined by the tensile stress range in the connections. To determine the tensile stress range, the maximum and minimum tensile stresses need to be determined first. However, permanent load effect is not to be considered in the stress range calculation.

The tensile stress range is induced by the fatigue truck as specified by AASHTO or determined by truck survey or WIM study. If the bridge is a simple span, the minimum tensile stress is assumed to be zero and only the maximum tensile stress is considered. In calculation, a linear elastic analysis is considered [38].

The typical S-N curve could be illustrated by Figure 9-8 that shows that the fatigue resistance is divided into two main zones depending on the types of behavior. One zone gives infinite life in which all tensile stress range is below the threshold stress $(\Delta F)_{TH}$. In addition to the infinite connection life, in this zone, excessive loading cycles will not develop fatigue cracks.

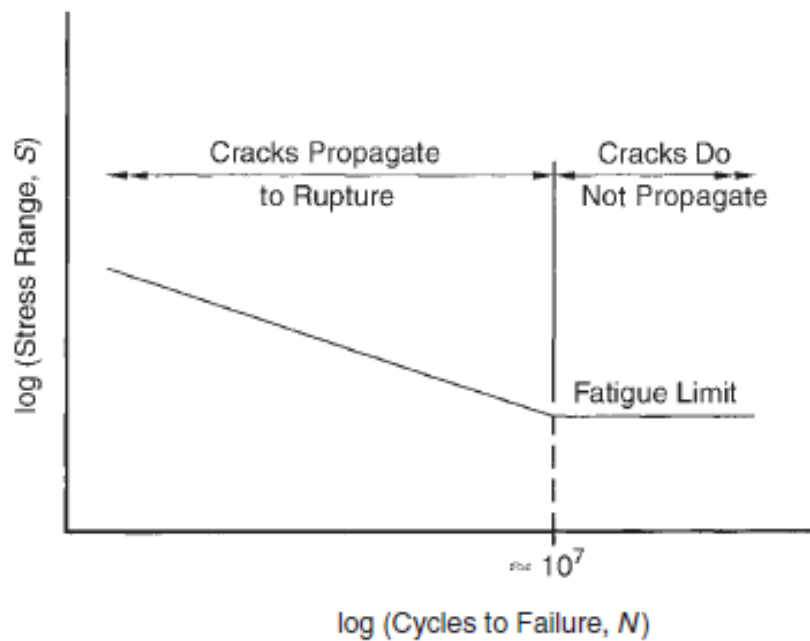


FIGURE 9-8: TYPICAL S-N CURVE FOR WELDED JOINTS [38]

TABLE 9-8: PARTIAL LOAD FACTORS, R_{sa} , R_{st} , AND R_s [2]

Fatigue life evaluation methods	Analysis partial load factor, R_{sa}	Truck-weight partial load factor, R_{st}	Stress-range estimate partial load factor, R_s
For evaluation or minimum fatigue life			
Stress range by simplified analysis, and truck weight per LRFD design-truck	1.0	1.0	1.0
Stress range by simplified analysis, and truck weight estimated through WIM study	1.0	0.95	0.95
Stress range by refined analysis, and truck weight per LRFD design-truck	0.95	1.0	0.95
Stress range by refined analysis, truck weight by WIM study	0.95	0.95	0.90
Stress range by field measured strain	N/A	N/A	0.85
For mean fatigue life			
All methods	N/A	N/A	1.00

TABLE 9-9: DETAIL CATEGORIES FOR LOAD-INDUCED FATIGUE [46]

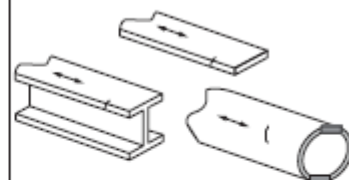
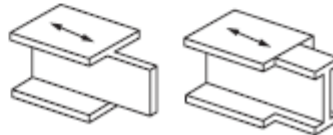
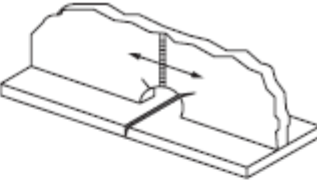
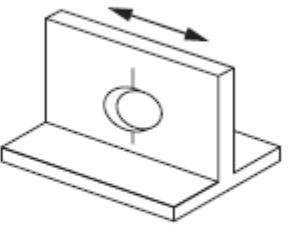
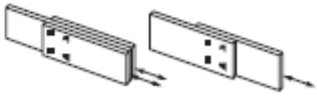
Description	Category	Constant A (ksi ³)	Threshold (AF) _{TH} ksi	Potential Crack Initiation Point	Illustrative Examples
Section 1—Plain Material away from Any Welding					
1.1 Base metal, except noncoated weathering steel, with rolled or cleaned surfaces. Flame-cut edges with surface roughness value of 1,000 μ -in or less, but without re-entrant corners.	A	250×10^8	24	Away from all welds or structural connections	
1.2 Noncoated weathering steel base metal with rolled or cleaned surfaces designed and detailed in accordance with FHWA (1989). Flame-cut edges with surface roughness value of 1,000 μ -in. or less, but without re-entrant corners.	B	120×10^8	16	Away from all welds or structural connections	
1.3 Member with re-entrant corners at copes, cuts, block-outs or other geometrical discontinuities made to the requirements of AASHTO/AWS D1.5, except weld access holes.	C	44×10^8	10	At any external edge	
1.4 Rolled cross sections with weld access holes made to the requirements of AASHTO/AWS D1.5, Article 3.2.4.	C	44×10^8	10	In the base metal at the re-entrant corner of the weld access hole	
1.5 Open holes in members (Brown et al., 2007).	D	22×10^8	7	In the net section originating at the side of the hole	
Section 2—Connected Material in Mechanically Fastened Joints					
2.1 Base metal at the gross section of high-strength bolted joints designed as slip-critical connections with pre-tensioned high-strength bolts installed in holes drilled full size or subpunched and reamed to size—e.g., bolted flange and web splices and bolted stiffeners. (Note: see Condition 2.3 for bolt holes punched full size.)	B	120×10^8	16	Through the gross section near the hole	

Table 5.9: (Continued)

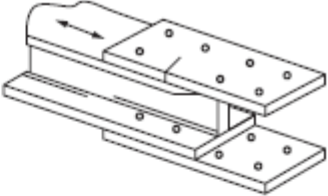
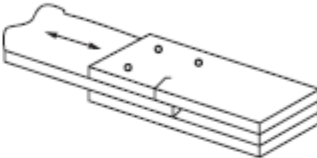
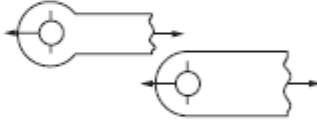
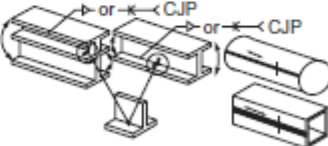
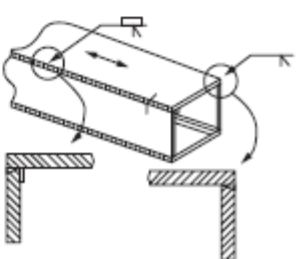
Description	Category	Constant A (ksi ³)	Threshold $(\Delta F)_{TH}$ ksi	Potential Crack Initiation Point	Illustrative Examples
2.2 Base metal at the net section of high-strength bolted joints designed as bearing-type connections, but fabricated and installed to all requirements for slip-critical connections with pre-tensioned high strength bolts installed in holes drilled full size or subpunched and reamed to size. (Note: see Condition 2.3 for bolt holes punched full size.)	B	120×10^8	16	In the net section originating at the side of the hole	
2.3 Base metal at the net section of all bolted connections in hot dipped galvanized members (Huhn and Valtinat, 2004); base metal at the appropriate section defined in Condition 2.1 or 2.2, as applicable, of high-strength bolted joints with pretensioned bolts installed in holes punched full size (Brown et al., 2007), and base metal at the net section of other mechanically fastened joints, except for eyebars and pin plates; e.g., joints using ASTM A307 bolts or non-pretensioned high strength bolts.	D	22×10^8	7	In the net section originating at the side of the hole or through the gross section near the hole, as applicable	
2.4 Base metal at the net section of eyebar heads or pin plates (Note: for base metal in the shank of eyebar or through the gross section of pin plates, see Condition 1.1 or 1.2 as applicable).	E	11×10^8	4.5	In the net section originating at the side of the hole	
Section 3—Welded Joints Joining Components of Built-Up Members					
3.1 Base metal and weld metal in members without attachments built-up of plates or shapes connected by continuous longitudinal complete joint penetration groove welds back-gouged and welded from the second side, or by continuous fillet welds parallel to the direction of applied stress.	B	120×10^8	16	From surface or internal discontinuities in the weld away from the end of the weld	
3.2 Base metal and weld metal in members without attachments built-up of plates or shapes connected by continuous longitudinal complete joint penetration groove welds with backing bars not removed, or by continuous partial joint penetration groove welds parallel to the direction of applied stress.	B'	61×10^8	12	From surface or internal discontinuities in the weld, including weld attaching backing bars	

Table 5.9: (Continued)

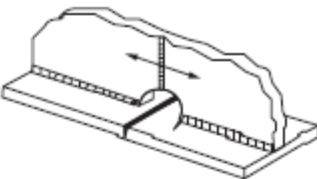
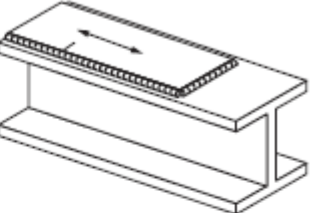
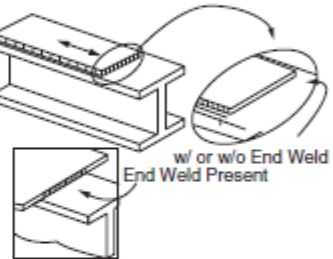
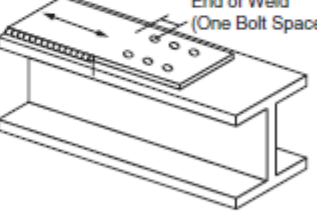
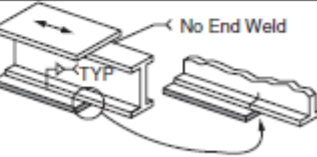
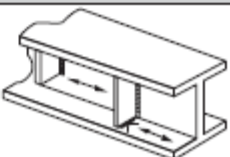
Description	Category	Constant A (ksi ³)	Threshold $(\Delta F)_{TH}$ ksi	Potential Crack Initiation Point	Illustrative Examples
3.3 Base metal and weld metal at the termination of longitudinal welds at weld access holes made to the requirements of AASHTO/AWS D1.5, Article 3.2.4 in built-up members. (Note: does not include the flange butt splice).	D	22×10^8	7	From the weld termination into the web or flange	
3.4 Base metal and weld metal in partial length welded cover plates connected by continuous fillet welds parallel to the direction of applied stress.	B	120×10^8	16	From surface or internal discontinuities in the weld away from the end of the weld	
3.5 Base metal at the termination of partial length welded cover plates having square or tapered ends that are narrower than the flange, with or without welds across the ends, or cover plates that are wider than the flange with welds across the ends: Flange thickness ≤ 0.8 in Flange thickness > 0.8 in.	E	11×10^8	4.5	In the flange at the toe of the end weld or in the flange at the termination of the longitudinal weld or in the edge of the flange with wide cover plates	
3.6 Base metal at the termination of partial length welded cover plates with slip-critical bolted end connections satisfying the requirements of Article 6.10.12.2.3.	B	120×10^8	16	In the flange at the termination of the longitudinal weld	
3.7 Base metal at the termination of partial length welded cover plates that are wider than the flange and without welds across the ends.	E'	3.9×10^8	2.6	In the edge of the flange at the end of the cover plate weld	
Section 4—Welded Stiffener Connections					
4.1 Base metal at the toe of transverse stiffener-to-flange fillet welds and transverse stiffener-to-web fillet welds. (Note: includes similar welds on bearing stiffeners and connection plates).	C'	44×10^8	12	Initiating from the geometrical discontinuity at the toe of the fillet weld extending into the base metal	

Table 5.9: (Continued)

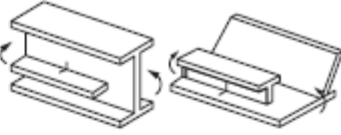
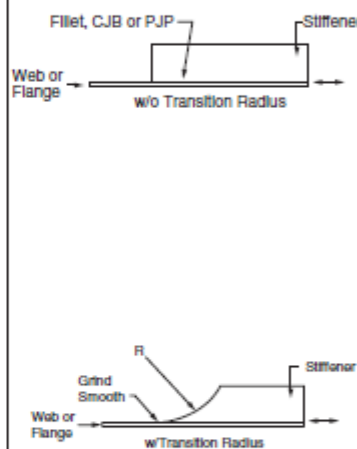
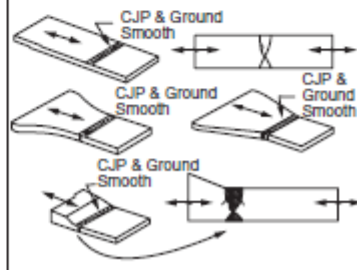
Description	Category	Constant A (ksi ³)	Threshold (ΔF) _{TH} ksi	Potential Crack Initiation Point	Illustrative Examples
4.2 Base metal and weld metal in longitudinal web or longitudinal box-flange stiffeners connected by continuous fillet welds parallel to the direction of applied stress.	B	120×10^8	16	From the surface or internal discontinuities in the weld away from the end of the weld	
4.3 Base metal at the termination of longitudinal stiffener-to-web or longitudinal stiffener-to-box flange welds: With the stiffener attached by fillet welds and with no transition radius provided at the termination: Stiffener thickness < 1.0 in. Stiffener thickness ≥ 1.0 in. With the stiffener attached by welds and with a transition radius R provided at the termination with the weld termination ground smooth: $R \geq 24$ in. 24 in. > $R \geq 6$ in. 6 in. > $R \geq 2$ in. 6 in. > R	E E'	11×10^8 3.9×10^8	4.5 2.6	In the primary member at the end of the weld at the weld toe In the primary member near the point of tangency of the radius	
Section 5—Welded Joints Transverse to the Direction of Primary Stress					
5.1 Base metal and weld metal in or adjacent to complete joint penetration groove welded butt splices, with weld soundness established by NDT and with welds ground smooth and flush parallel to the direction of stress. Transitions in thickness or width shall be made on a slope no greater than 1:2.5 (see also Figure 6.13.6.2-1). $F_y < 100$ ksi $F_y \geq 100$ ksi				From internal discontinuities in the filler metal or along the fusion boundary or at the start of the transition	

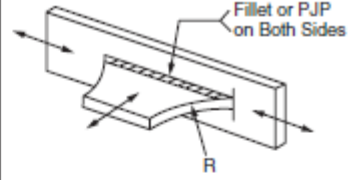
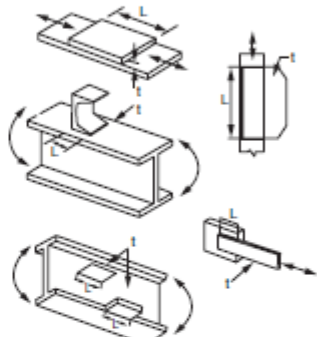
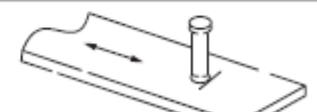
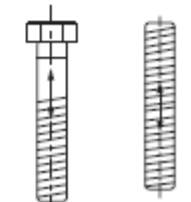
Table 5.9: (Continued)

Description	Category	Constant A (ksi ³)	Threshold (ΔF) _{TH} ksi	Potential Crack Initiation Point	Illustrative Examples
5.2 Base metal and weld metal in or adjacent to complete joint penetration groove welded butt splices, with weld soundness established by NDT and with welds ground parallel to the direction of stress at transitions in width made on a radius of not less than 2 ft with the point of tangency at the end of the groove weld (see also [Figure 6.13.6.2-1]).	B	120×10^8	16	From internal discontinuities in the filler metal or discontinuities along the fusion boundary	
5.3 Base metal and weld metal in or adjacent to the toe of complete joint penetration groove welded T or corner joints, or in complete joint penetration groove welded butt splices, with or without transitions in thickness having slope no greater than 1:2.6 when weld reinforcement is not removed (Note: cracking in the flange of the T' may occur due to out-of-plane bending stresses induced by the stem).	C	44×10^8	10	From the surface discontinuity at the toe of the weld extending into the base metal or along the fusion boundary	
5.4 Base metal and weld metal at details where loaded discontinuous plate elements are connected with a pair of fillet welds or partial joint penetration groove welds on opposite sides of the plate normal to the direction of primary stress.	C as adjusted in Eq. 6.6.1.2.5-4	44×10^8	10	Initiating from the geometrical discontinuity at the toe of the weld extending into the base metal or, initiating at the weld root subject to tension extending up and then out through the weld	
Section 6 — Transversely Loaded Welded Attachment					
6.1 Base metal in a longitudinally loaded component at a transversely loaded detail (e.g. a lateral connection plate) attached by a weld parallel to the direction of primary stress and incorporating a transition radius R with the weld termination ground smooth.				Near point of tangency of the radius at the edge of the longitudinally loaded component	
$R \geq 24$ in. 24 in. $>$ $R \geq 6$ in. 6 in. $>$ $R \geq 2$ in. 2 in. $>$ R	B C D E	120×10^8 44×10^8 22×10^8 11×10^8	16 10 7 4.5		

Table 5.9: (Continued)

Description	Category	Constant A (ksi ³)	Threshold (ΔF) _{TH} ksi	Potential Crack Initiation Point	Illustrative Examples
6.2 Base metal in a transversely loaded detail (e.g. a lateral connection plate) attached to a longitudinally loaded component of equal thickness by a complete joint penetration groove weld parallel to the direction of primary stress and incorporating a transition radius R , with weld soundness established by NDT and with the weld termination ground smooth:					
With the weld reinforcement removed:					
$R \geq 24$ in.	B	120×10^8	16	Near points of tangency of the radius or in the weld or at the fusion boundary of the longitudinally loaded component or the transversely loaded attachment	
24 in. $> R \geq 6$ in.	C	44×10^8	10		
6 in. $> R \geq 2$ in.	D	22×10^8	7		
2 in. $> R$	E	11×10^8	4.5		
With the weld reinforcement not removed:					
$R \geq 24$ in.	C	44×10^8	10	At the toe of the weld either along the edge of the longitudinally loaded component or the transversely loaded attachment	
24 in. $> R \geq 6$ in.	C	44×10^8	10		
6 in. $> R \geq 2$ in.	D	22×10^8	7		
2 in. $> R$	E	11×10^8	4.5		
(Note: Condition 6.1 shall also be checked.)					
6.3 Base metal in a transversely loaded detail (e.g. a lateral connection plate) attached to a longitudinally loaded component of unequal thickness by a complete joint penetration groove weld parallel to the direction of primary stress and incorporating a weld transition radius R , with weld soundness established by NDT and with the weld termination ground smooth:					
With the weld reinforcement removed:					
$R \geq 2$ in.	D	22×10^8	7	At the toe of the weld along the edge of the thinner plate	
$R < 2$ in.	E	11×10^8	4.5	In the weld termination of small radius weld transitions	
For any weld transition radius with the weld reinforcement not removed:				At the toe of the weld along the edge of the thinner plate	
(Note: Condition 6.1 shall also be checked.)	E	11×10^8	4.5		

Table 5.9: (Continued)

Description	Category	Constant A (ksi ³)	Threshold (ΔF) _{TH} ksi	Potential Crack Initiation Point	Illustrative Examples
6.4 Base metal in a transversely loaded detail (e.g. a lateral connection plate) attached to a longitudinally loaded component by a fillet weld or a partial joint penetration groove weld, with the weld parallel to the direction of primary stress (Note: Condition 6.1 shall also be checked)	See Condition 5.4				
Section 7—Longitudinally Loaded Welded Attachments					
7.1 Base metal in a longitudinally loaded component at a detail with a length L in the direction of the primary stress and a thickness t attached by groove or fillet welds parallel or transverse to the direction of primary stress where the detail incorporates no transition radius:				In the primary member at the end of the weld at the weld toe	
$L < 2$ in.	C	44×10^8	10		
2 in. $\leq L \leq 12t$ or 4 in.	D	22×10^8	7		
$L > 12t$ or 4 in.					
$t < 1.0$ in.	E	11×10^8	4.5		
$t \geq 1.0$ in.	E'	3.9×10^8	2.6		
Section 8—Miscellaneous					
8.1 Base metal at stud-type shear connectors attached by fillet or automatic stud welding	C	44×10^8	10	At the toe of the weld in the base metal	
8.2 Nonpretensioned high-strength bolts, common bolts, threaded anchor rods and hanger rods with cut, ground or rolled threads. Use the stress range acting on the tensile stress area due to live load plus prying action when applicable. (Fatigue II) Finite Life (Fatigue I) Infinite Life	E' D'	3.9×10^8 N/A	N/A 7	At the root of the threads extending into the tensile stress area	

9.2.5 Fatigue Serviceability Index [45]

The fatigue serviceability index (Q) is one of the methods used to evaluate the fatigue serviceability limit state. It is used also to characterize the overall serviceability relative to the fatigue limit state. The fatigue serviceability index (FSI) is determined using the total fatigue life. It is used to make a planning decision of the bridge's viability.

$$Q = \left(\frac{Y - a}{N} \right) GRI \quad (9-3)$$

where:

N = Greater of Y or 100 years

G = Load Path Factor, as given in Table 9-10

R = Redundancy Factor, as given in Table 9-11

I = Importance Factor, as given in Table 9-12.

Y = Calculated total fatigue life of the detail

TABLE 9-10 :LOAD PATH FACTOR, G [45]

Number of load path members	G
1 or 2 members	0.8
3 members	0.9
4 or more members	1.0

TABLE 9-11: REDUNDANCY FACTOR, R [45]

Type of span	R
Simple	0.9
Continuous	1.0

TABLE 9-12: IMPORTANCE FACTOR, I [45]

Structure or location	Importance factor, I
Interstate highway	
Main arterial state route	0.9
Other critical route	
Secondary arterial	0.95
Urban areas	
Rural roads	1.00
Low ADRR routes	

The load path, redundancy, and importance factors are risk factors that modify the FSI. These factors may be considered as the main factors that result in higher risk.

As discussed earlier, the FSI gives approximate guide lines used to evaluate and make a decision for the bridge assessment. Table 9-13 gives some recommendations for the assessment of the bridges that may provide some guidance in decision making based on the FSI (Q) values.

The FSI is proportional to fatigue life subject to the condition that the fatigue life is less than 100 years. To the age of 80 years, the FSI has a linear relationship below the value of 0.2 as seen in Figure 9-9. This relationship gives owners an advantage in judging the remaining life of a bridge based on the value of FSI [45].

TABLE 9-13: FATIGUE RATING AND ASSESSMENT OUTCOMES [45]

Fatigue serviceability index, Q	Fatigue rating	Assessment outcome
1.00 to 0.5	Excellent (E)	Continue regular inspection
0.5 to 0.35	Good (G)	Continue regular inspection
0.35 to 0.20	Moderate (M)	Continue regular inspection
0.20 to 0.10	Fair (F)	Increase inspection frequency
0.10 to 0.00	Poor (P)	Assess frequently
<0.00	Critical (C)	Consider retrofit, replacement, or reassessment

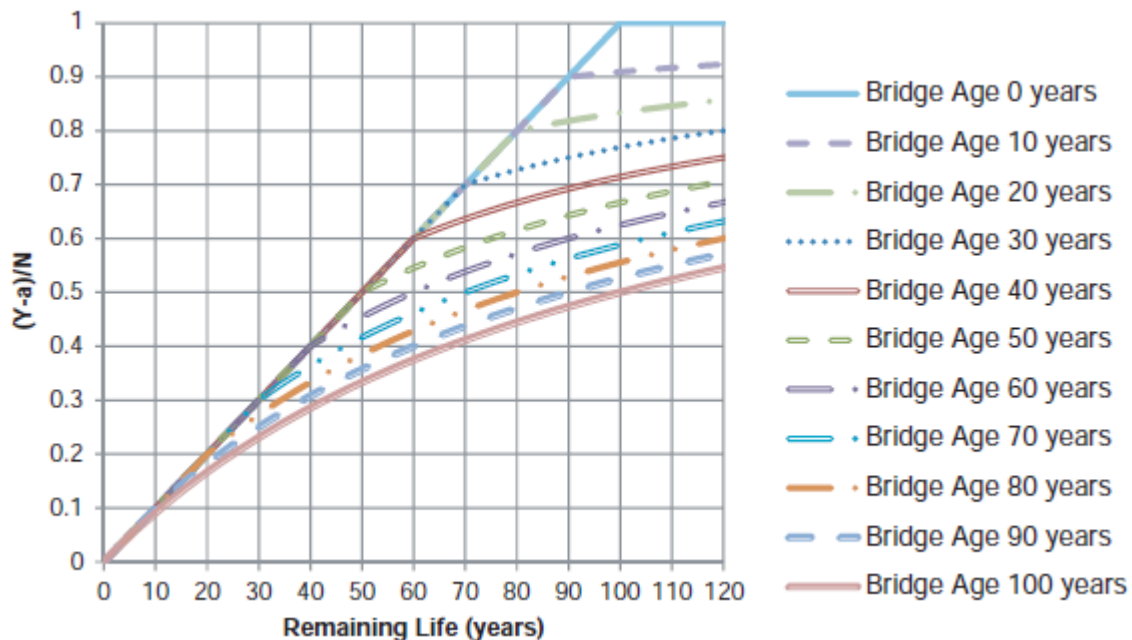


FIGURE 9-9: VARIATION OF $(Y-a)/N$ WITH REMAINING LIFE FOR VARIOUS BRIDGE AGES [45]

9.2.6 Reinforced Concrete (RC) Deck Fatigue

Reinforced concrete bridge decks are commonly used in highway bridges in the United States. Observations show that decks deteriorate much faster than the supporting elements. One of the factors leads to these deteriorations is the truck load [48].

Due to concrete shrinkage and excessive truck loads, very small cracks develop in concrete decks as shown in Figure 9-10. When a transverse crack is present, the truck wheel introduces stress concentration at the crack tip. These cracks induce discontinuities in the concrete deck that originate fatigue damage. Unfortunately, such cracks cannot be eliminated using today's technology. They are considered the indication of fatigue damage in RC decks. With the repetition of load cycles, cracks grow, generating further deterioration [48].

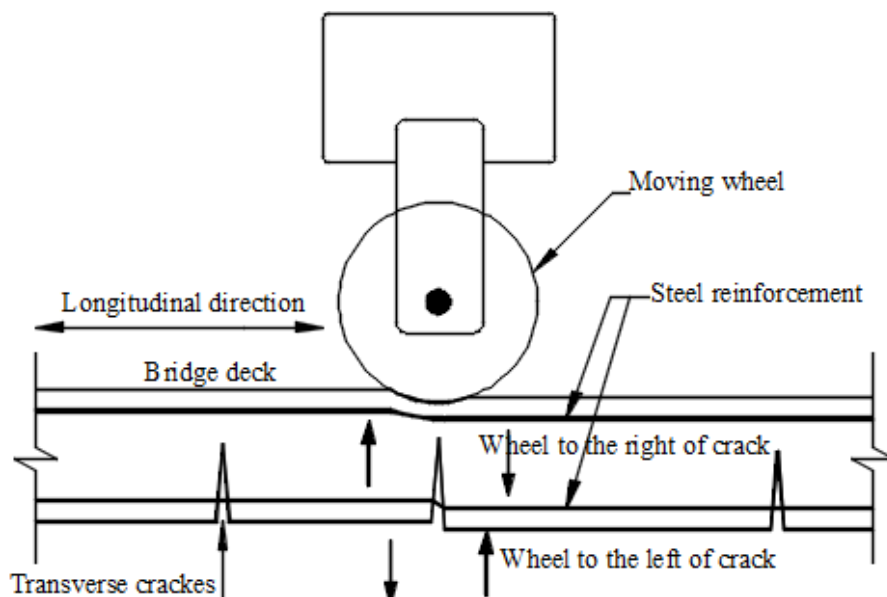


FIGURE 9-10: SHEAR FATIGUE OF RC BRIDGE DECK UNDER WHEEL LOADING [48]

9.2.7 Reinforced Concrete Deck Fatigue Life Estimation Approach

The useful service life of a bridge deck is represented by a random variable that is a function of a number of other variables: load magnitudes, the number of load cycles, and a decision as to when it should be renewed. Assessment of the reinforced concrete deck could be executed by the NCHRP approach based on the AASHTO specifications using the following formula:

$$Y_d = \frac{\log \left[\frac{K_d K_p}{365[(ADTT)_{SL}]_{Present} C_d \left(\frac{R_d I P_s P}{P_u} \right)^{17.95}} g (1+g)^{a-1} + 1 \right]}{\log(1+g)} \quad (9-4)$$

R_d : Reliability factor, set equal to 1 for mean service life and 1.35 for the evaluation of service life.

Y_d : Mean service life in years for $R_d=1$

Evaluation life in years for $R_d=1.35$

g : Estimated annual traffic-volume growth rate

a : Present age of the bridge

K_d : Coefficient covering model uncertainty = 2.09×10^{-6}

K_p : Coefficient considering time difference between deck failure and treatment
 $= 3.16 \times 10^{-7}$

P_s : Axle-group factor = 1.04

C_d : Average number of axles per truck

I : Impact factor

P_u : Ultimate shear capacity of the deck

P/P_u = is the equivalent stress ratio caused by wheel load P

Equation Eq.5-3 could be divided into three main groups:

1. Load magnitude related (I , P_s , and P/P_u)
2. Number of stress cycles related ($[(ADTT)_{SL}]_{Present}$, and C_d)
3. Model related (K_d and L_p)

- *Load Magnitude Related Parameters*

The impact factor I from AASHTO specifications is set equal to 15% to cover the dynamic effect of truck wheels [49]. The parameter P_s refers to the axle group factor.

It covers the increase in load effect due to the closely spaced wheels in axle groups and is recommended to be set to 1.04 [48].

The ultimate shear strength of the deck (P_u) may be evaluated as per ACI and AASHTO design code using the following equation:

$$P_u = \left(2 + \frac{4}{\alpha}\right) \sqrt{f'_c} b_0 d \gamma < 4\sqrt{f'_c} b_0 d \gamma \quad (9 - 5)$$

where, f'_c is the concrete compressive strength in psi, α is the ratio of the tire print's long side to short side, set equal to 2.5 for a nominal tire print, for dual tires; d is the effective thickness of the deck equal to the total depth minus the bottom cover thickness minus the wearing layer (0.25-in), ($d = h - \text{bottom cover} - 0.25\text{-in}$); b_0 is the perimeter of the critical section, defined as the straight lines parallel to and at a distance equalling $d/2$, from the edges of the tire print used; γ is a model correction parameter set equal to 1.55.

P is an equivalent fatigue load equal to:

$$P = \left(\sum f_i(P_i) P_i^{17.95} \right)^{17.95} \quad (9 - 6)$$

where P_i is the mid-interval value of the i^{th} interval in the Wheel Weight Histogram (WWH), and $f(P_i)$ is the frequency for that interval.

For a steering wheel of a single tire, the wheel acts on an area equalling one-half of the dual tire print, so the ultimate shear capacity P_u is reduced by about 33%. The ultimate shear strength may be kept constant with the load increased by 50% [48].

- *Load Cycle Related Parameters*

These parameters include T_a/T , and C_d ; where T_a/T is the ratio of the life average truck traffic to the current traffic for the outer lane, see Equation Eq.5-6, and C_d is the average number of axles per vehicle.

$$\frac{T_a}{T} = \frac{\sum_{i=1}^Y (1+g)^i}{Y(1+g)^a} \quad (9-7)$$

- *Model Related Parameters*

The model for predicting the remaining life in equation Eq.5-3 was built based on the assumption that the load P is inversely proportional to the number of cycles at which the constant repetitive load P will exhaust the fatigue life. Due to this approximation, the parameter K_d is used to model the uncertainty in the prediction model. This parameter (K_d) is set equal to 2.09×10^{-6} . The K_p parameter is used mainly to cover the presence of water that accelerates deck fatigue. The value of K_p is set equal to 3.16×10^{-7} [48].

9.3 Negative Remaining Life

Calculating the remaining life of bridges may result in a negative fatigue life. It occurs when the bridge is fairly old and its age exceeds the predicted finite fatigue life [45]. If the calculated remaining life is not accepted, the actual fatigue life may be increased by retrofitting the critical details to upgrade the detail category and the fatigue life accordingly [50].

The fatigue life of the detail is a random variable and could be illustrated by the probability distribution curve, see Figure 9-11. The total (finite) fatigue life can be defined as the value at which the failure probability is equal to the failure probability corresponding to the target reliability index. But, due to the uncertainty involved in the calculations, the computed total fatigue life may be less than the present age of the

bridge that results in a negative remaining life. Therefore, with no further information about the bridge detail, it is difficult to insure the estimated reaming fatigue life to be positive. However, the negative remaining fatigue life draws the attention for the critical status of the connection under consideration [45].

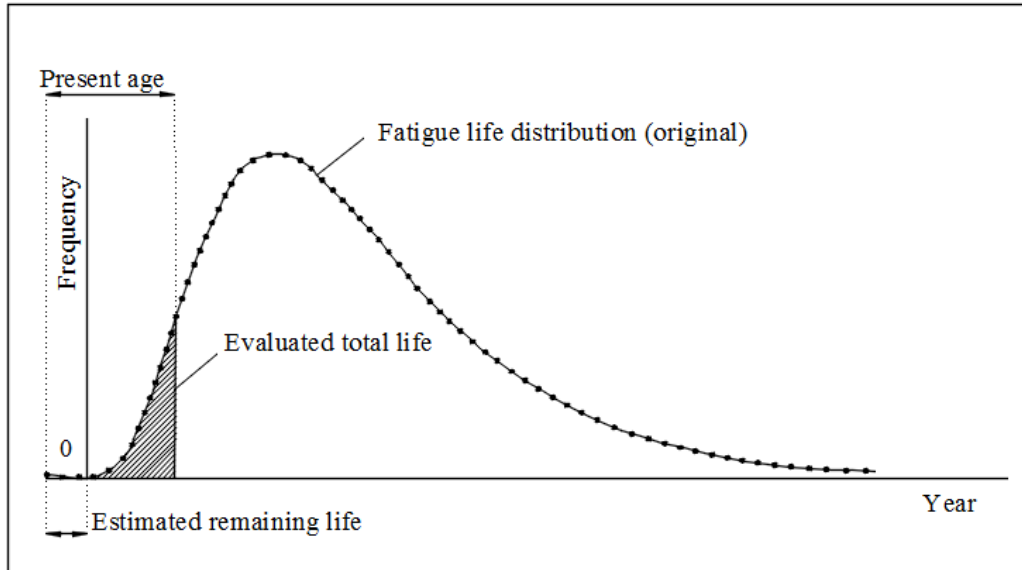


FIGURE 9-11: NEGATIVE REMAINING LIFE RESULTING FROM UNCERTAINTY IN FATIGUE LIFE ESTIMATION (SHADED AREA IS EQUAL TO TARGETED FAILURE PROBABILITY) [45]

9.4 Fatigue Evaluation Procedure [49]

The followed procedure applies to uncracked steel members subjected to primary stresses. It does not apply to members sustaining extremely corroded, severely damaged mechanically, or those that may have been repaired after sustaining fatigue cracks.

9.4.1 Fatigue Truck

Fatigue truck configurations, GVW, axle weight, and axle spacing, are based on the AASHTO fatigue truck HL-93, see Figure 1-2, of axle spacing 14 and 30-ft and the predicted frequent truck, 85-kip truck, of the recorded WIM data.

9.4.2 Bending Moment

The bending moment is calculated at the detail under consideration and is caused by the fatigue truck located at the position that causes the algebraic maximum bending moment. The AASHTO program, *Virtis*, was used to calculate the maximum bending moment at the critical section (mid-span) of the critical girder (exterior girder).

9.4.3 Stress Range

Due to the presence of shear connectors, the girder section was reasonably assumed to behave as a composite section. The composite section properties, moment of inertia and neutral axis location, and stress range were calculated accordingly.

9.4.4 Detail Category Constant

A bridge girder of span length 30-ft is considered as a one piece girder and those greater than 30-ft were considered to be spliced at the mid-span.

9.5 Steel bridges Remaining Life (Y_r) - Case study

Five cases were studied to investigate the impact of meeting the increase in freight demand by increasing the traffic (scenario 1) and/or the traffic load (scenario 2) on the remaining service life (remaining life) of steel bridges. The steel bridges' stresses were calculated under the effect of both scenarios in addition to the current scenario (same traffic same traffic load). In the first scenario, the stress range was calculated under the current traffic load, but the fatigue life was calculated as a function of the doubling of the traffic volume; $[(ADTT)_{SL}]_{Present}$ equals 142 truck/day. The second scenario represents accommodating the increase in freight demand by increasing the truck load, so the stress range was calculated under the effect of double truck load, but with the current traffic volume of 71 truck/day.

In all scenarios, five simply supported bridges of spans 30, 60, 90, 120, and 140-ft, a roadway width of 24-ft, and concrete deck thickness of 6 to 9-in were used to calculate the reaming fatigue life for every bridge. The remaining lives were calculated under different annual traffic-volume growth rate (2, 4, 6, and 8%) and different present bridge ages (5, 10, 15, 20, 25, 30, 35, 40, 45, and 50 years). The fatigue calculations were based on the repetition of the site-specific fatigue truck over a specific route so, depending on earlier presented WIM data in Chapter 2 and Chapter 3, the present average daily truck in single lane $[(ADTT)_{SL}]_{Present}$ was taken as 71 truck/day as shown in earlier.

The constant value A depends on the steel member and the type of connections. According to details illustrated in Table 5-9, the most commonly used connections in bridge members are of detail category B (constant A equaled $120E+8$ ksi³). The resistance factor for evaluation R_R is ranging between the minimum expected fatigue life, evaluation fatigue life, and mean fatigue life. Accordingly, the R_R corresponding to the minimum fatigue life and constant A of detail category B equals 1.0 and was applied to detect the remaining bridge fatigue life.

The live load stress range of each bridge was calculated using the live load bending moment extracted from the Virtis program and the cross section properties (section modulus – S). The recorded stresses were calculated under the application of the AASHTO fatigue truck and the site-specific fatigue truck (85-kip). Because all bridges are simply supported the stress range (Δf) could be assumed as the recorded fatigue load stress range. The fatigue threshold stress (ΔF)_{TH} corresponding to the detail category B connection, equals 16, and was recorded and compared to the

maximum fatigue stress range (Δf)_{max}. In all cases, the maximum fatigue stress range was greater than the fatigue threshold stress ((Δf)_{max} > 16).

$$(\Delta f) = \frac{M_{LL+IM}}{S} \quad (9-8)$$

$$(\Delta f)_{max} = R_P \cdot (\Delta f_{Fatigue\ I}) = R_P(1.5(\Delta f)) \quad (9-9)$$

$$(\Delta f)_{eff} = R_P \cdot R_S (\Delta f_{Fatigue\ II}) = R_P \cdot R_S (0.75)(\Delta f) \quad (9-10)$$

The remaining life (Y_r) is a function of the present age of the bridge and its total finite fatigue life. Equation Eq.5-7 is furnished to calculate the remaining life.

$$Y_r = Y - a \quad (9-11)$$

S , is the section modulus of the composite section due to the presence of shear connectors between the steel girder and slab deck. The effective width of the slab deck used to calculate the section modulus is the smaller of

- One fourth (1/4) of the girder span length $\geq \frac{30 \times 12}{4} = 90$ in.
- 12 times the slab deck $= 12 \times 6 = 72$ in
- Centerline to centerline of girders $= 8 \times 12 = 96$ in.

9.5.1 Current Traffic Conditions (CT)

This case was designed to predict the remaining life of steel bridges considering the current traffic-volume and traffic loading condition. The bending moments developed by the Virtis program under the application of the site-specific fatigue truck and the AASHTO fatigue truck (M_{LL+IM}) were captured and recorded. Table 9-14 and Table 5-15 show these values and the corresponding bending stresses. Consequently, based on the recorded stress ranges, the present average daily truck traffic in one lane [(ADTT)_{SL}]_{Present} equals to 71 truck/day, and considering different annual growth rates, the remaining life of each bridge was calculated and recorded in Table 9-16 thru

Table 9-19. Calculations were based on the following assumptions of the variables present in equation Eq.9-2:

- Connection detail with fatigue strength of category A for 30-ft long bridge and B for other bridges,
- Present age of bridge (a) ranging from 5 to 50-years by interval 5 years,
- Annual traffic-volume growth rate (g) of 2, 4, 6, and 8%,
- Number of stress-range cycles per truck passage (n) equals to 1 for bridges span greater than 40-ft and 2 for bridge span less than 40-ft

The remaining life for different fatigue truck and different annual traffic-volume growth rates (2 to 8%) has been recorded as shown in Table 9-16 thru Table 9-19.

TABLE 9-14 : SITE-SPECIFIC FATIGUE TRUCK - STRESSES

Span	MLL+IM	S_{Composite}	(Δf)	(Δf)_{max}	(Δf)_{TH}	(Δf)_{eff}
ft	kip.ft	in³	ksi	ksi	ksi	ksi
30	223	152.9	30.19	45.33	16	22.67
60	591	557.07	21.96	33.04	16	16.52
90	1053	1171.93	18.6	28.04	16	14.02
120	1632	1820.47	18.56	28.05	16	14.02
140	1945	2051.26	19.63	29.71	16	14.85

TABLE 9-15: AASHTO FATIGUE TRUCK - STRESSES

Span	MLL+IM	S	(Δf)	(Δf)_{max}	(Δf)_{TH}	(Δf)_{eff}
ft	kip.ft	in³	ksi	ksi	ksi	ksi
30	206	152.9	27.89	41.88	16	20.95
60	462	557.07	17.17	25.84	16	12.92
90	858	1171.93	15.16	22.86	16	11.43
120	1340	1820.47	15.24	23.03	16	11.52
140	1606	2051.26	16.21	24.53	16	12.27

TABLE 9-16: REMAINING LIFE(YR), G=2%

Bridge present age (a)	Fatigue remaining life (Y) - year									
	year	Site-specific fatigue truck (85-kip)					AASHTO fatigue truck			
		30-ft	60-ft	90-ft	120-ft	140-ft	30-ft	60-ft	90-ft	140-ft
5	26	54	72	72	65		32	82	98	97
10	23	52	71	71	64		29	81	97	96
15	21	51	70	70	63		27	80	96	96
20	18	49	69	69	62		25	80	96	95
25	16	48	68	68	61		23	79	95	95
30	14	47	68	68	60		21	78	95	94
35	12	46	67	67	59		20	78	95	94
40	10	45	66	66	59		18	77	94	93
45	8	44	66	66	58		16	77	94	93
50	7	43	65	65	57		15	76	94	93

TABLE 9-17 :REMAINING LIFE (Y_R), G=4%

Bridge present age (a)	Fatigue remaining life (Y) - year										
	year	Site-specific fatigue truck (85-kip)					AASHTO fatigue truck				
		30-ft	60-ft	90-ft	120-ft	140-ft	30-ft	60-ft	90-ft	120-ft	140-ft
5	21	39	50	50	46		25	56	64	64	59
10	20	39	50	50	46		24	55	64	64	59
15	18	38	49	49	45		23	55	64	63	59
20	17	37	49	49	45		22	55	64	63	59
25	16	37	49	49	44		21	54	63	63	58
30	15	36	48	48	44		20	54	63	63	58
35	14	36	48	48	44		20	54	63	63	58
40	14	36	48	48	44		19	54	63	63	58
45	13	36	48	48	43		19	54	63	63	58
50	13	35	48	48	43		18	54	63	62	58

TABLE 9-18: REMAINING LIFE (Y_R), G=6%

Bridge present age (a)	Fatigue remaining life (Y) - year										
	year	Site-specific fatigue truck (85-kip)					AASHTO fatigue truck				
		30-ft	60-ft	90-ft	120-ft	140-ft	30-ft	60-ft	90-ft	120-ft	140-ft
5	18	32	39	39	37		21	43	49	49	46
10	17	31	39	39	36		21	43	49	49	46
15	16	31	39	39	36		20	43	49	49	46
20	16	31	39	39	36		19	43	49	49	45
25	15	30	39	39	36		19	43	49	49	45
30	15	30	38	38	36		19	43	49	48	45
35	14	30	38	38	35		18	43	49	48	45
40	14	30	38	38	35		18	42	49	48	45
45	14	30	38	38	35		18	42	49	48	45
50	14	30	38	38	35		18	42	49	48	45

TABLE 9-19: REMAINING LIFE (Y_R), G=8%

Bridge present age (a)	Fatigue remaining life (Y) - year										
	year	Site-specific fatigue truck (85-kip)					AASHTO fatigue truck				
		30-ft	60-ft	90-ft	120-ft	140-ft	30-ft	60-ft	90-ft	120-ft	140-ft
10	15	27	33	33	31		18	36	40	40	38
15	15	26	33	33	30		18	36	40	40	38
20	14	26	32	32	30		17	36	40	40	38
25	14	26	32	32	30		17	36	40	40	38
30	14	26	32	32	30		17	36	40	40	38
35	14	26	32	32	30		17	36	40	40	38
40	14	26	32	32	30		17	35	40	40	38
45	14	26	32	32	30		17	35	40	40	38
50	14	26	32	32	30		17	35	40	40	38

The computed remaining life at annual growth rate of interest (2, 4, 6, and 8%) for different bridge spans and different truck loadings (site specific fatigue truck and AASHTO fatigue truck) under the current traffic conditions were depicted in Figure 9-12 thru Figure 9-15.

Generally, the remaining life of bridges due to the site-specific fatigue truck was greater than the remaining life in the case of the AASHTO fatigue truck. Looking back at Figure 3-20 and Figure 3-28, these figures show that the load effect of the AASHTO fatigue truck is higher than that of the frequent fatigue truck and that influence the remaining life inversely. All parameters in equation Eq.9-2 affect the remaining life of the bridge. Some of these parameters have a major effect and others a minor effect.

This study focused on the effect of the annual growth rate, $[(ADTT)_{SL}]_{Present}$, and $(\Delta f)_{eff}$. The annual growth rate was inversely affecting the remaining life of the younger (fresh) bridges (5 to 20-years old), but it improves the remaining life of older bridges (25 to 50-years old).

As shown in Figure 9-1, most of bridges are now 50 years old or more, so it was important to focus much more on the effect of these parameters on bridges of this age (50-years old). Figure 9-16 and Figure 9-17 show that the increase in the annual growth rate improves the remaining life of shorter bridges (<40-ft), but it inversely affects the longer bridges (>40-ft).

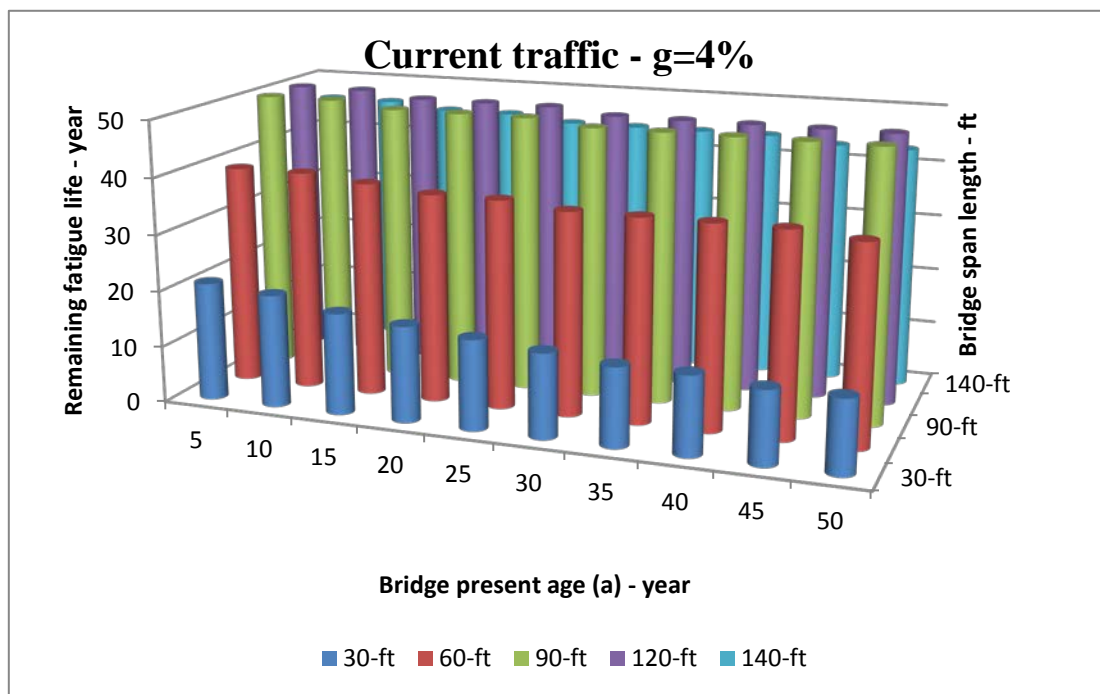
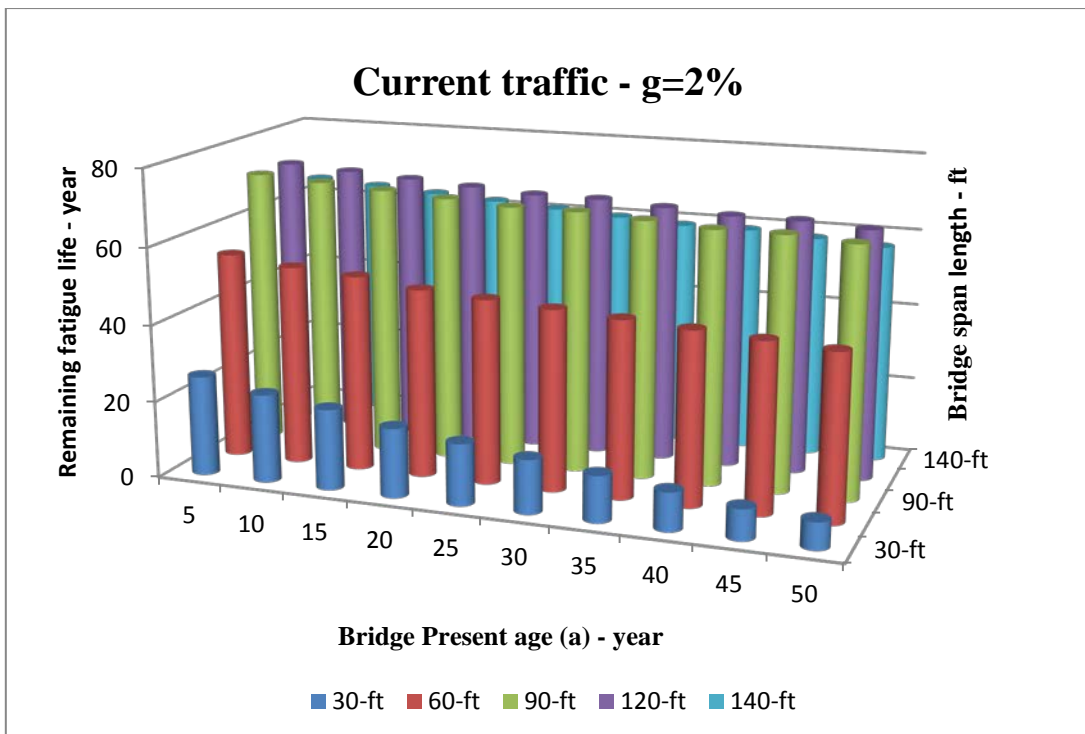


**FIGURE 9-12 : REMAINING LIFE VS. PRESENT AGE VS. SPAN LENGTH,
SITE-SPECIFIC FATIGUE TRUCK**

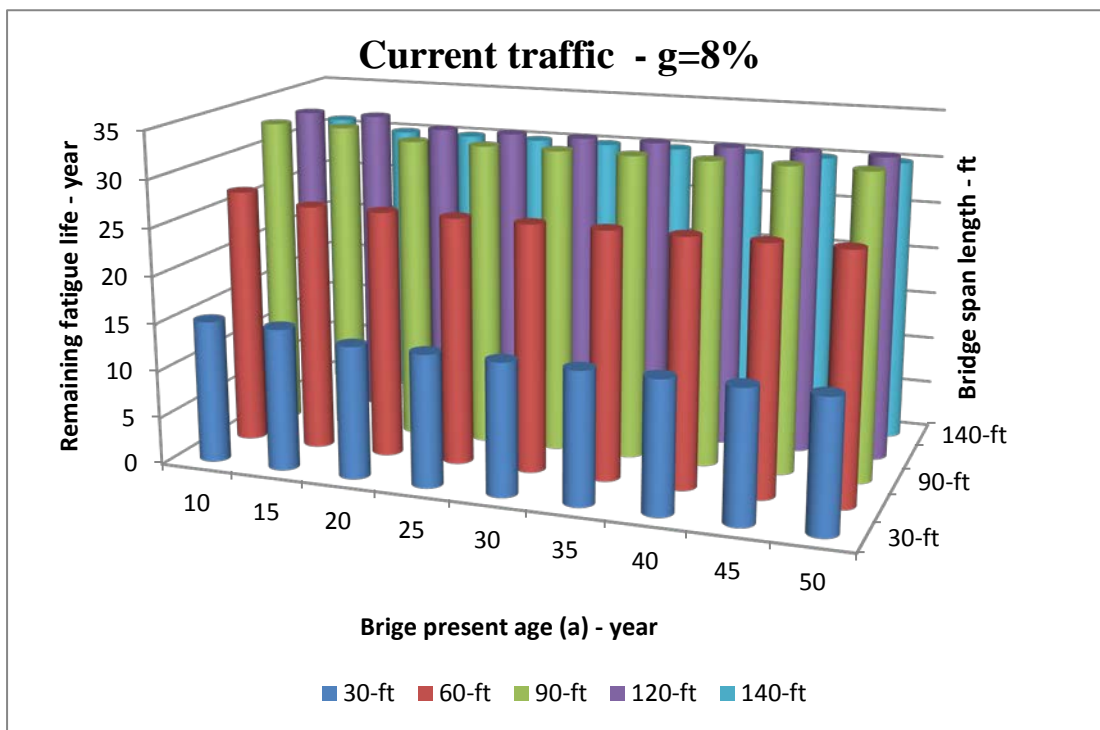
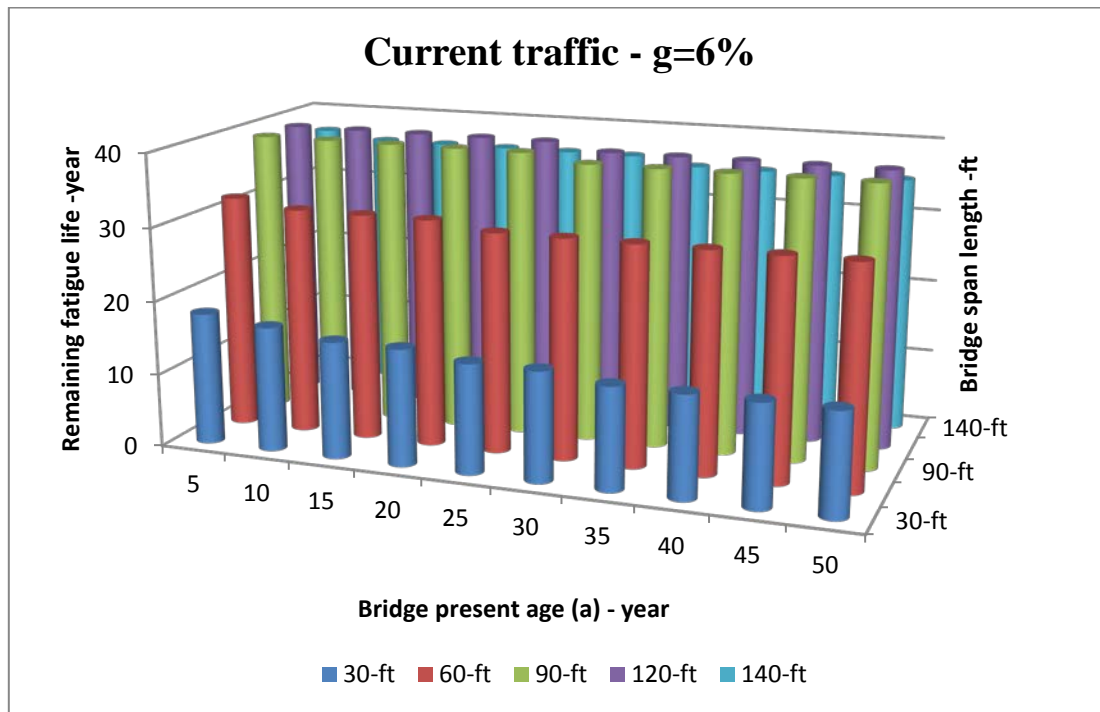


**FIGURE 9-13 : REMAINING LIFE VS. PRESENT AGE VS. SPAN LENGTH,
SITE-SPECIFIC FATIGUE TRUCK**

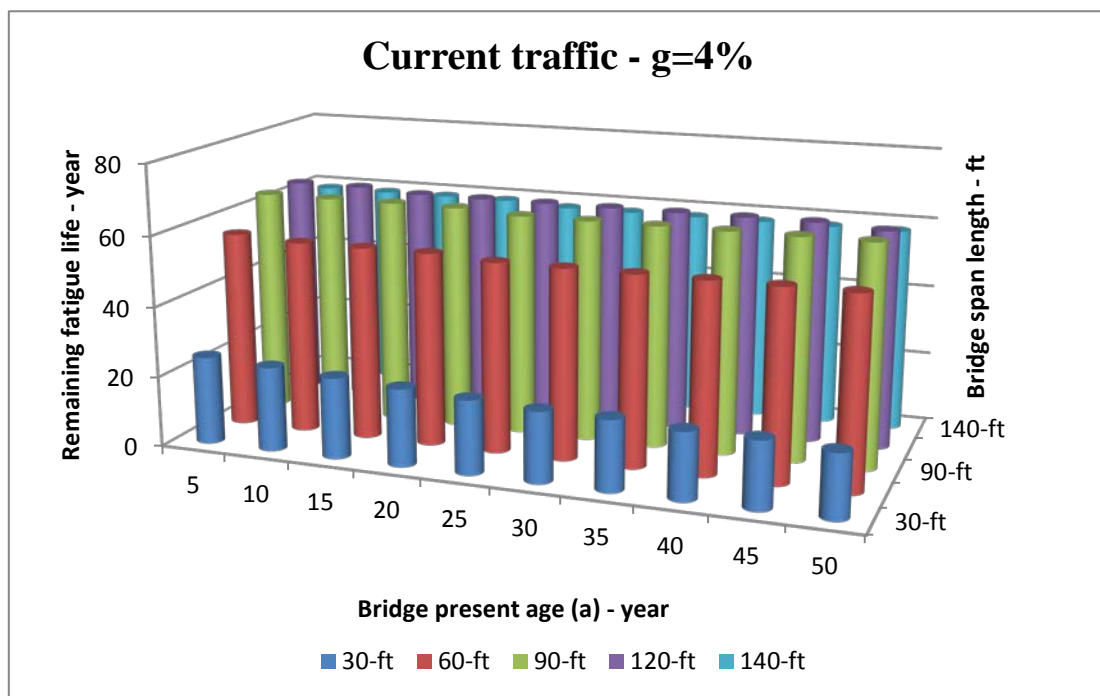
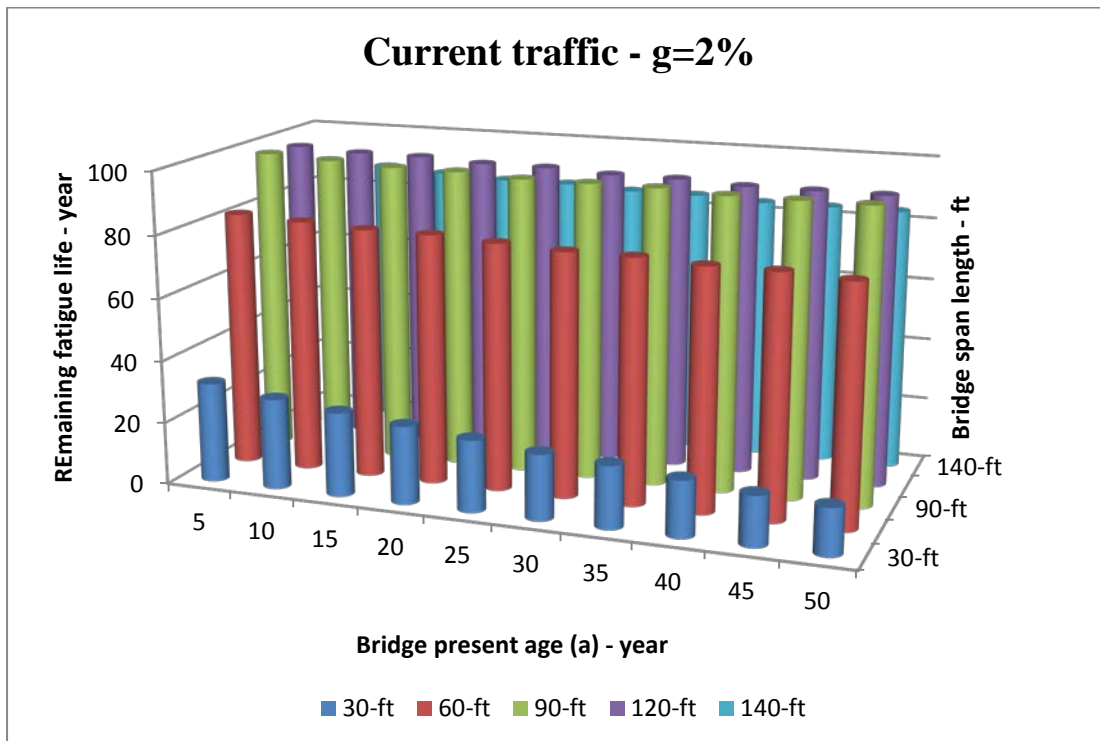


**FIGURE 9-14: REMAINING LIFE VS. PRESENT AGE VS. SPAN LENGTH,
AASHTO FATIGUE TRUCK**

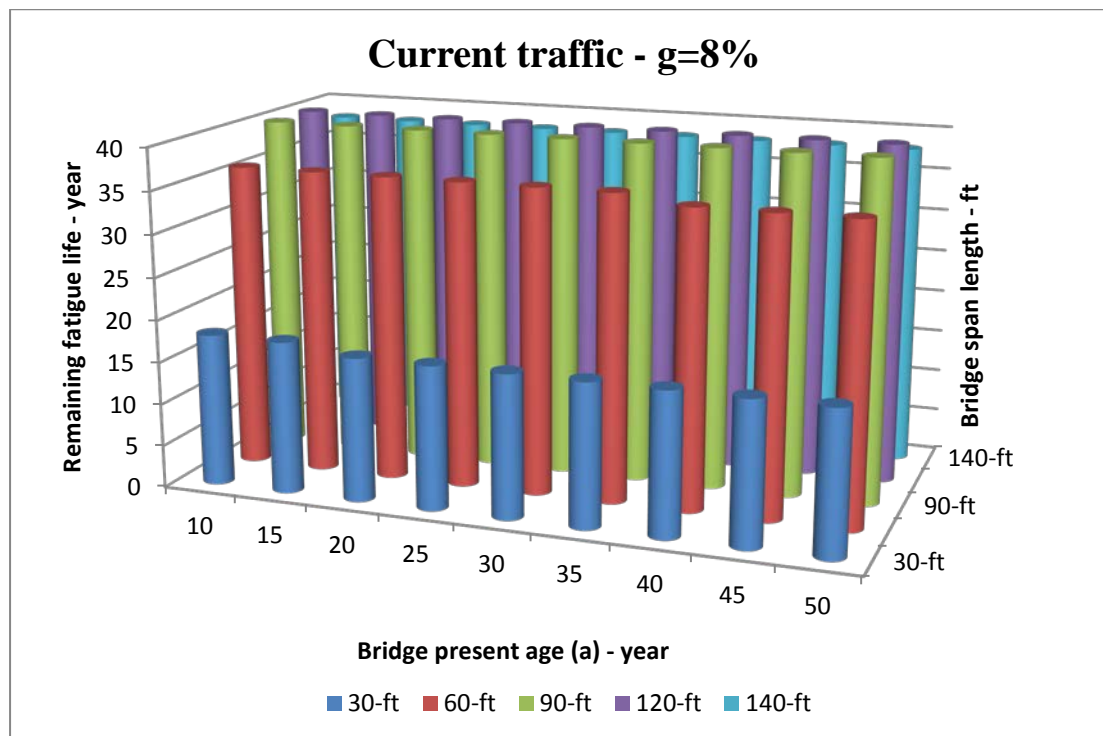
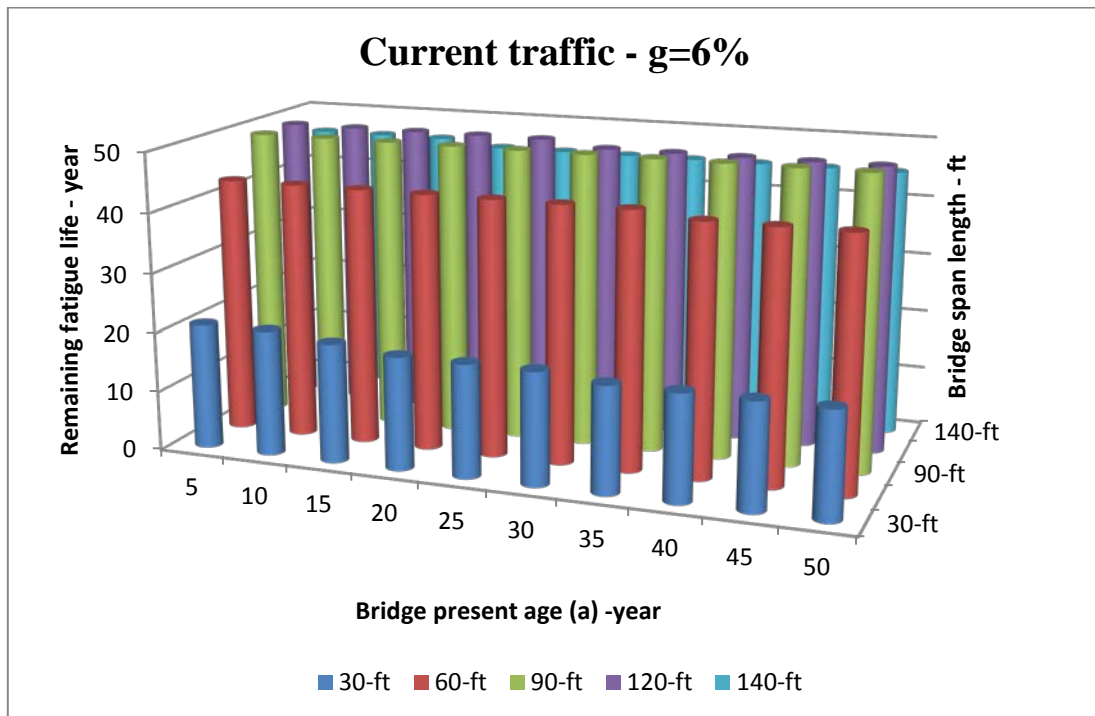


FIGURE 9-15 : REMAINING LIFE VS. PRESENT AGE VS. SPAN LENGTH, AASHTO FATIGUE TRUCK

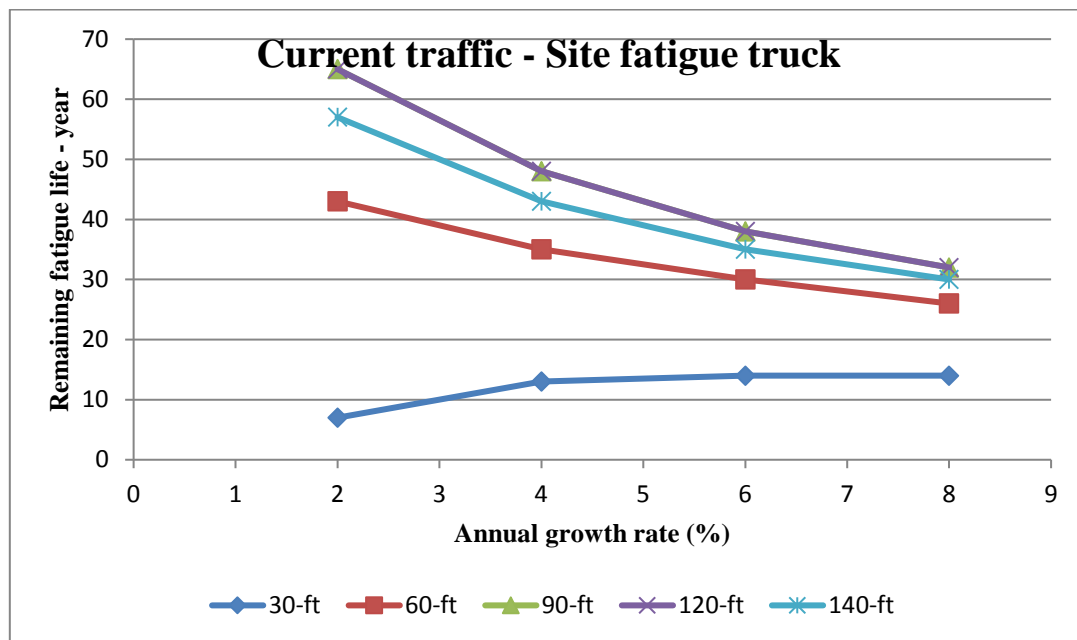


FIGURE 9-16 : REMAINING LIFE AT AGE OF 50-YEARS VS. ANNUAL GROWTH RATE, FATIGUE TRUCK

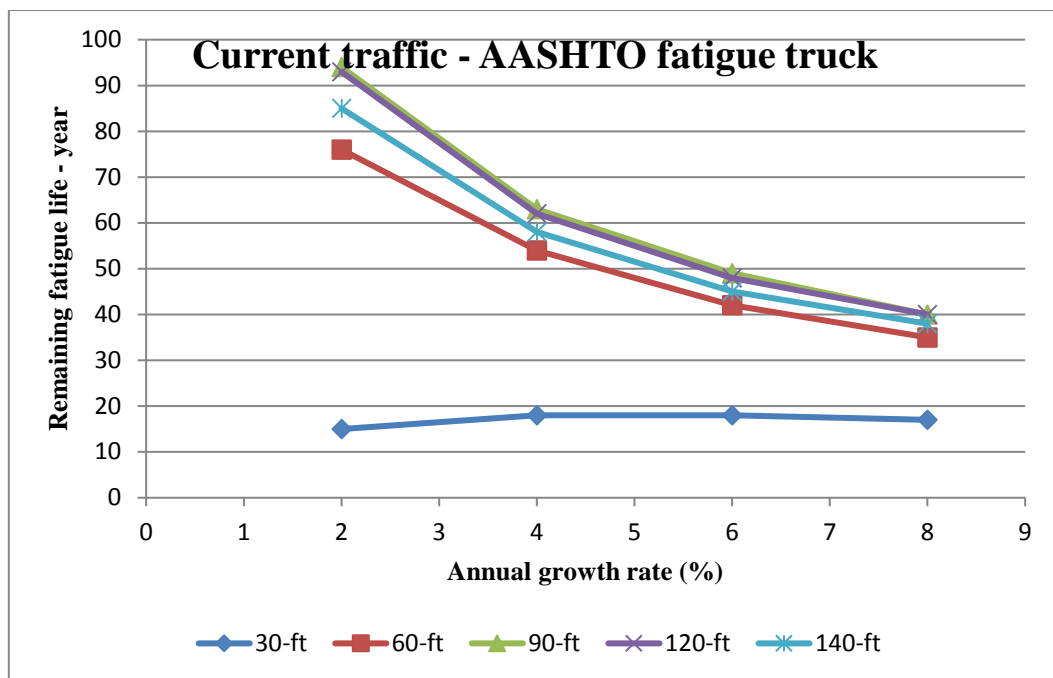


FIGURE 9-17 :REMAINING LIFE AT AGE OF 50-YEARS VS. ANNUAL GROWTH RATE, AASHTO FATIGUE TRUCK

9.5.2 Double Traffic Volume Scenario (DTV)

This case investigates the remaining life of the steel bridges considered in the first scenario, accommodating the increase in freight demand by increasing (doubling) the current traffic-volume, but keeping traffic loading constant. The bending moments developed by the site-specific fatigue truck and the AASHTO fatigue truck (MLL+IM) were calculated by the Virtis program and recorded versus the girders' section modulus to calculate the bending stresses as shown respectively Table 9-20 and Table 9-21

The remaining life was calculated for each bridge with the doubling of the present average daily truck traffic in one lane $[(ADTT)_{SL}]_{Present}$ (51256 truck/day). Other variable were taken as in the current traffic condition case (connection detail with a fatigue strength of category B, present age of bridge (a) ranging from 5 to 50-years with an interval of 5 years, annual traffic-volume growth rate (g) of 2, 4, 6, and 8%, number of stress-range cycles per truck passage (n) equaling 1 for bridge spans greater than 40-ft and 2 for bridge spans less than 40-ft).

TABLE 9-20: SITE-SPECIFIC FATIGUE TRUCK - STRESSES

Span ft	MLL+IM kip.ft	S in ³	(Δf) ksi	(Δf) _{max} ksi	(Δf) _{TH} ksi	(Δf) _{eff} ksi
30	223	152.9	30.19	45.35	16	22.67
60	591	557.07	21.96	33.05	16	16.53
90	1053	1171.93	18.6	28.04	16	14.02
120	1632	1820.47	18.56	28.05	16	14.02
140	1945	2051.26	19.63	29.71	16	14.85

TABLE 9-21: AASHTO FATIGUE TRUCK - STRESSES

Span	MLL+IM	S	(Δf)	(Δf)_{max}	(Δf)_{TH}	(Δf)_{eff}
ft	kip.ft	in³	ksi	ksi	ksi	ksi
30	206	152.9	27.89	41.89	16	20.95
60	462	557.07	17.17	25.84	16	12.92
90	858	1171.93	15.16	22.86	16	11.43
120	1340	1820.47	15.24	23.03	16	11.52
140	1606	2051.26	16.21	24.53	16	12.27

The remaining life for different fatigue trucks and different annual traffic-volume growth rate (2 to 8%) has been recorded as shown in Table 9-22 thru Table 9-24. The recorded remaining life values in these tables have been depicted in Figure 9-18 thru Figure 9-21. Comparing the remaining life in the case of doubling the traffic volume (DTV) with those in the case of current traffic conditions (CT) showed that the remaining life of all bridges at all ages have been reduced. The reduction in the remaining life varies depending on the bridge span length. For bridges less than 40-ft long, the reduction ranged between 40 and 50%. But for bridges of longer spans, the reduction in remaining life was between 60 and 70%.

The same attention has been drawn to the 50-years old bridges. The same conclusion has been drawn that the increase in the annual growth rate adversely affects the remaining life of short bridges (<40-ft), but enhances that of longer bridges (>40-ft), see Figure 9-22 and Figure 9-23

TABLE 9-22: REMAINING LIFE (Yr), G=2%

Bridge present age (a)	year	Fatigue remaining life (Y) - year									
		Site-specific fatigue truck (85-kip)					AASHTO fatigue truck				
		30-ft	60-ft	90-ft	120-ft	140-ft	30-ft	60-ft	90-ft	120-ft	140-ft
5	13	32	47	47	42		17	55	69	68	61
10	9	30	45	45	40		13	54	68	67	60
15	6	28	44	44	38		10	53	67	66	59
20	3	26	42	42	36		7	51	66	65	57
25	0	24	41	41	35		5	50	65	64	56
30	-3	22	39	40	33		2	49	64	63	55
35	-6	20	38	38	32		-1	48	64	63	55
40	-9	19	37	37	31		-3	47	63	62	54
45	-12	17	36	36	29		-5	46	62	61	53
50	-14	16	35	35	28		-8	46	62	61	52

TABLE 9-23: REMAINING LIFE (Y_R), G=4%

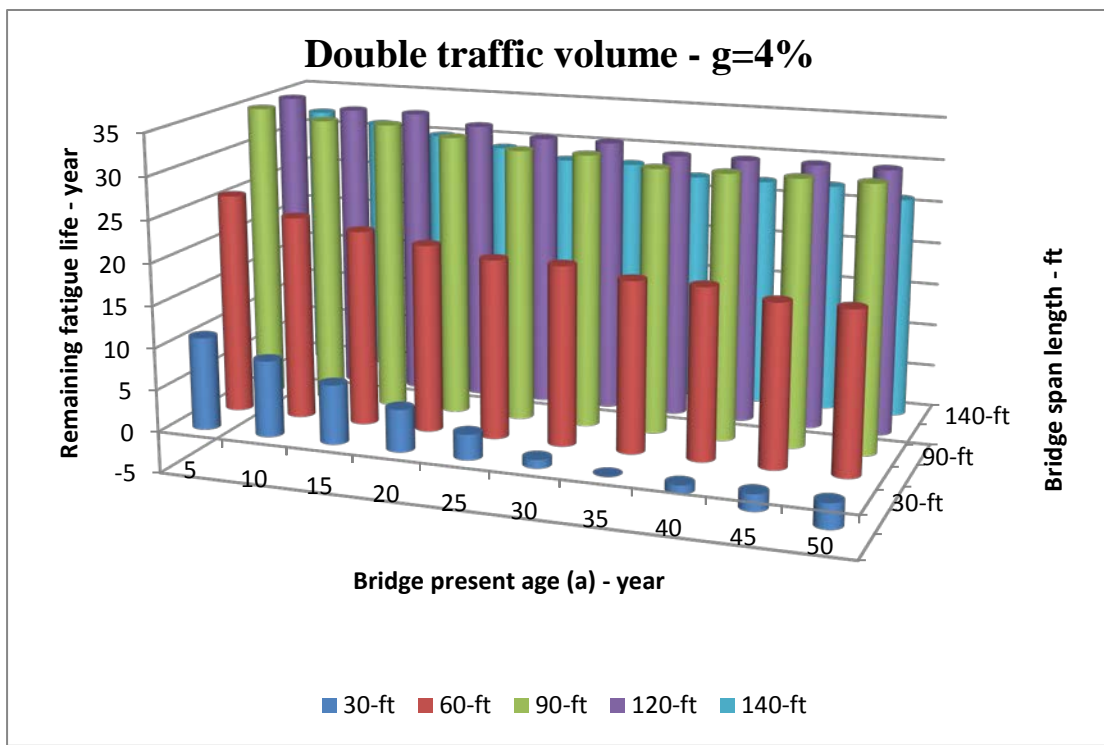
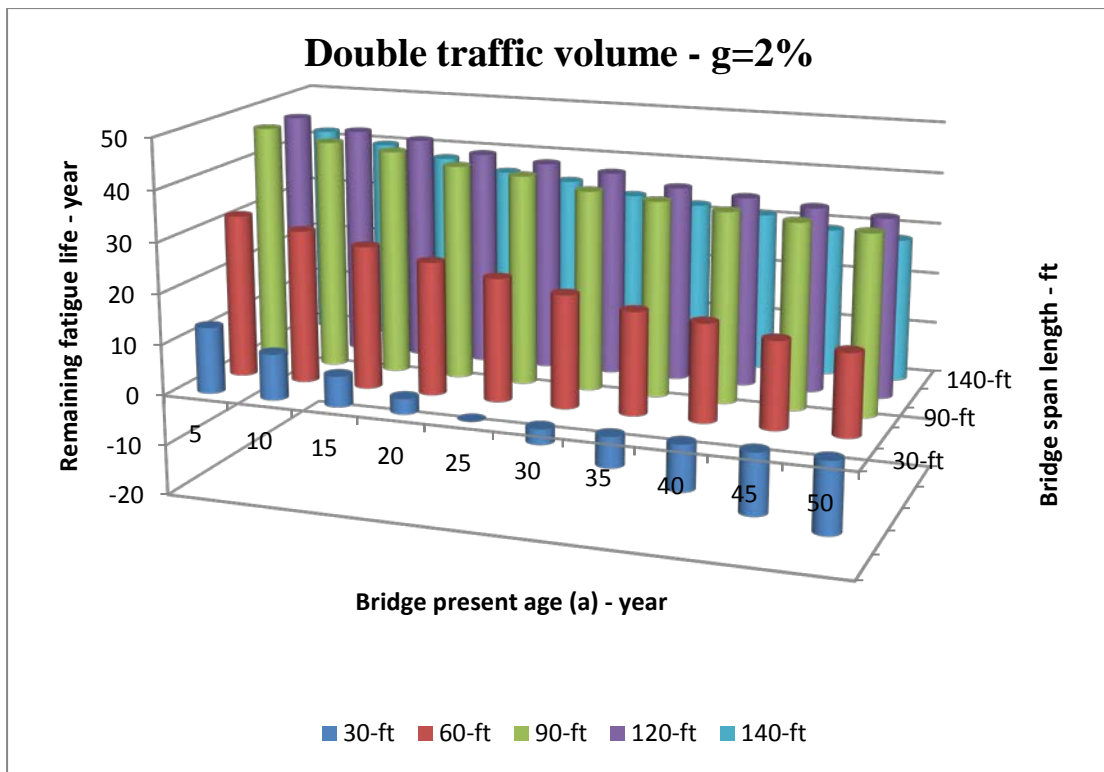
Bridge present age (a)	Fatigue remaining life (Y) - year										
	year	Site-specific fatigue truck (85-kip)					AASHTO fatigue truck				
		30-ft	60-ft	90-ft	120-ft	140-ft	30-ft	60-ft	90-ft	120-ft	
5	11	26	35	35	32		14	40	48	48	44
10	9	24	34	34	31		12	40	48	47	43
15	7	23	34	34	30		10	39	47	47	43
20	5	22	33	33	29		9	38	47	47	42
25	3	21	32	32	28		7	38	47	46	42
30	1	21	32	32	28		6	38	46	46	41
35	0	20	31	31	27		5	37	46	46	41
40	-1	20	31	31	27		4	37	46	45	41
45	-2	19	31	31	27		3	37	46	45	41
50	-3	19	31	31	26		2	37	46	45	41

TABLE 9-24: REMAINING LIFE (Y_R), G=6%

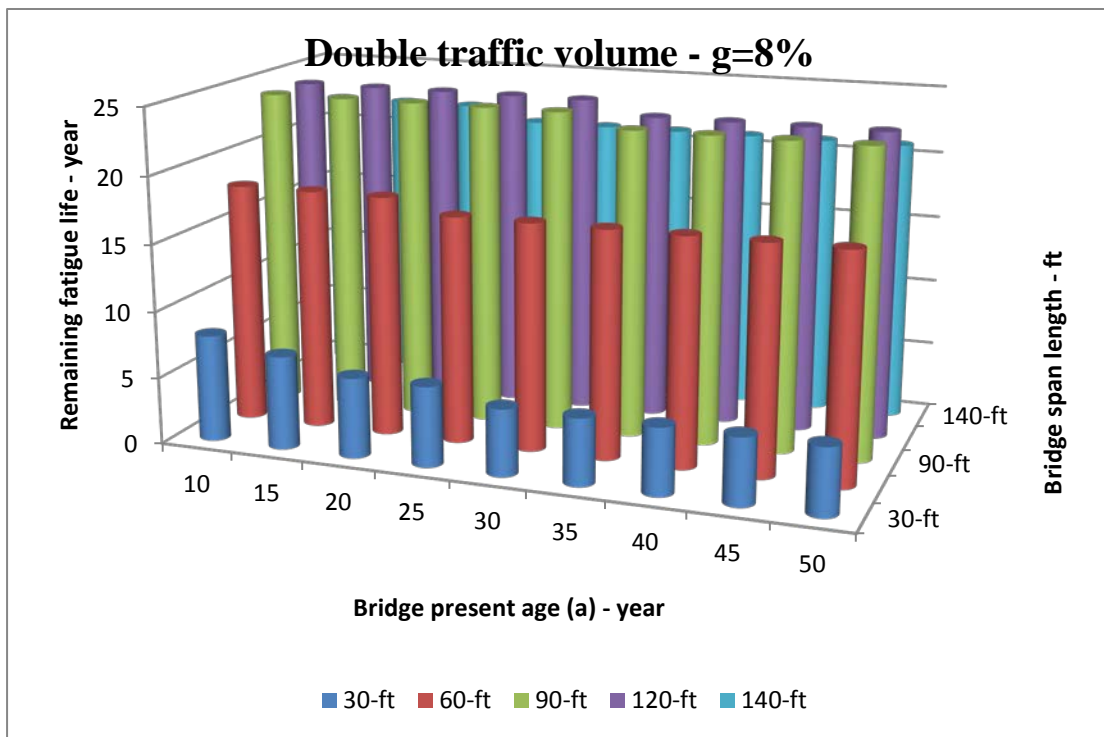
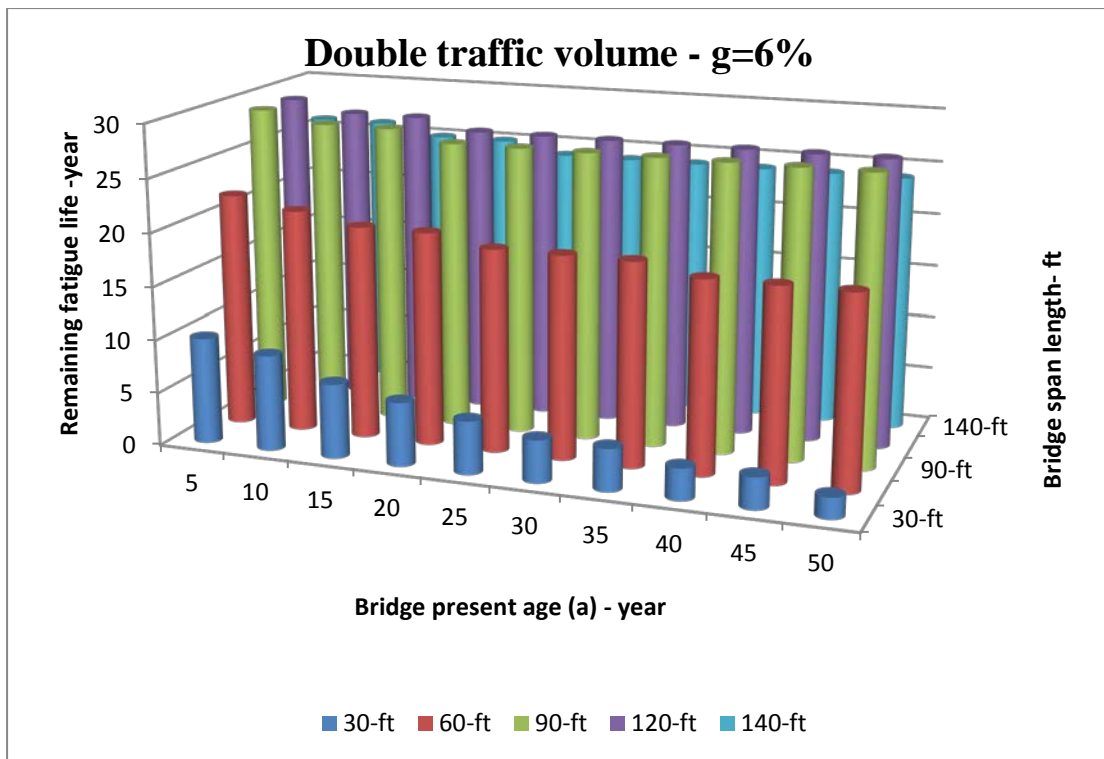
Bridge present age (a)	Fatigue remaining life (Y) - year										
	year	Site-specific fatigue truck (85-kip)					AASHTO fatigue truck				
		30-ft	60-ft	90-ft	120-ft	140-ft	30-ft	60-ft	90-ft	120-ft	140-ft
5	10	22	29	29	26		13	33	38	38	35
10	9	21	28	28	26		11	32	38	38	35
15	7	20	28	28	25		10	32	38	37	34
20	6	20	27	27	25		9	31	37	37	34
25	5	19	27	27	24		8	31	37	37	34
30	4	19	27	27	24		8	31	37	37	34
35	4	19	27	27	24		7	31	37	37	34
40	3	18	27	27	24		7	31	37	37	33
45	3	18	27	27	24		7	31	37	37	33
50	2	18	27	27	24		6	31	37	37	33

TABLE 9-25: REMAINING LIFE (Y_R), G=8%

Bridge present age (a)	Fatigue remaining life (Y) - year										
	year	Site-specific fatigue truck (85-kip)					AASHTO fatigue truck				
		30-ft	60-ft	90-ft	120-ft	140-ft	30-ft	60-ft	90-ft	120-ft	140-ft
10	8	18	24	24	22		11	27	32	32	29
15	7	18	24	24	22		10	27	32	31	29
20	6	18	24	24	22		9	27	32	31	29
25	6	17	24	24	21		9	27	31	31	29
30	5	17	24	24	21		8	27	31	31	29
35	5	17	23	23	21		8	27	31	31	29
40	5	17	23	23	21		8	27	31	31	29
45	5	17	23	23	21		8	27	31	31	29
50	5	17	23	23	21		8	27	31	31	29



**FIGURE 9-18: REMAINING LIFE VS. PRESENT AGE VS. SPAN LENGTH,
SITE-SPECIFIC FATIGUE TRUCK**



**FIGURE 9-19 :REMAINING LIFE VS. PRESENT AGE VS. SPAN LENGTH,
SITE-SPECIFIC FATIGUE TRUCK**

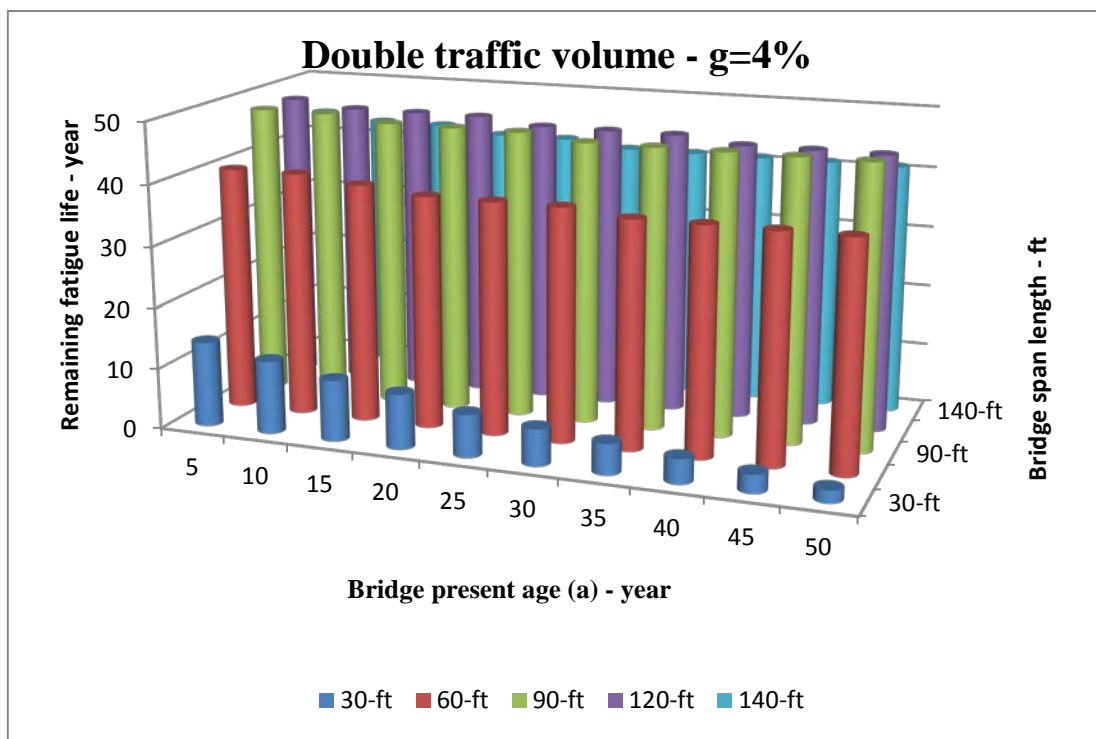
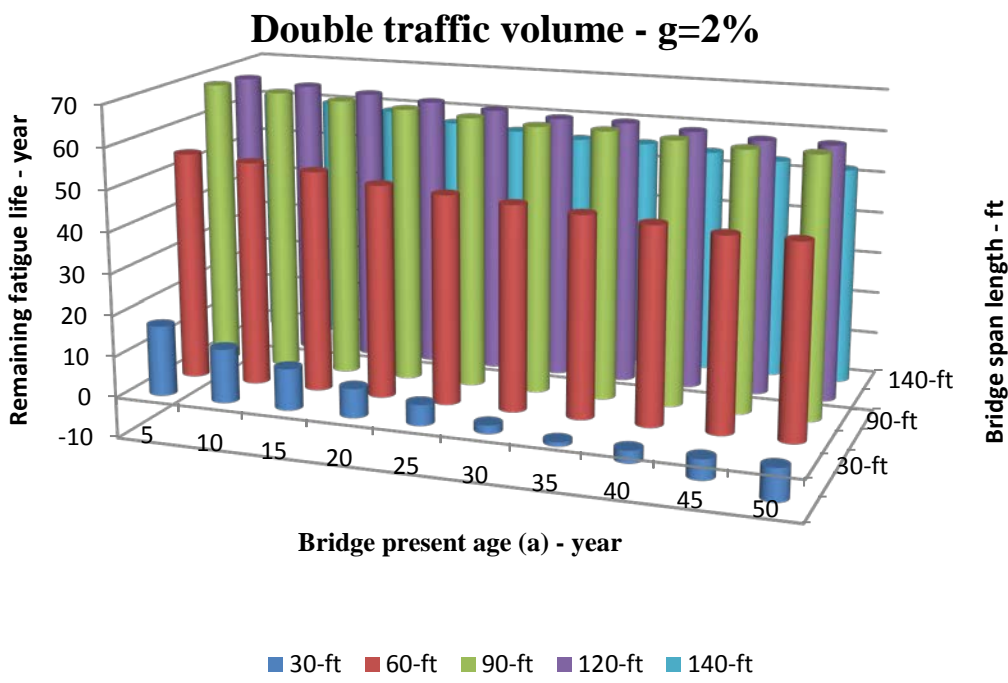


**FIGURE 9-20: REMAINING LIFE VS. PRESENT AGE VS. SPAN LENGTH,
AASHTO FATIGUE TRUCK**

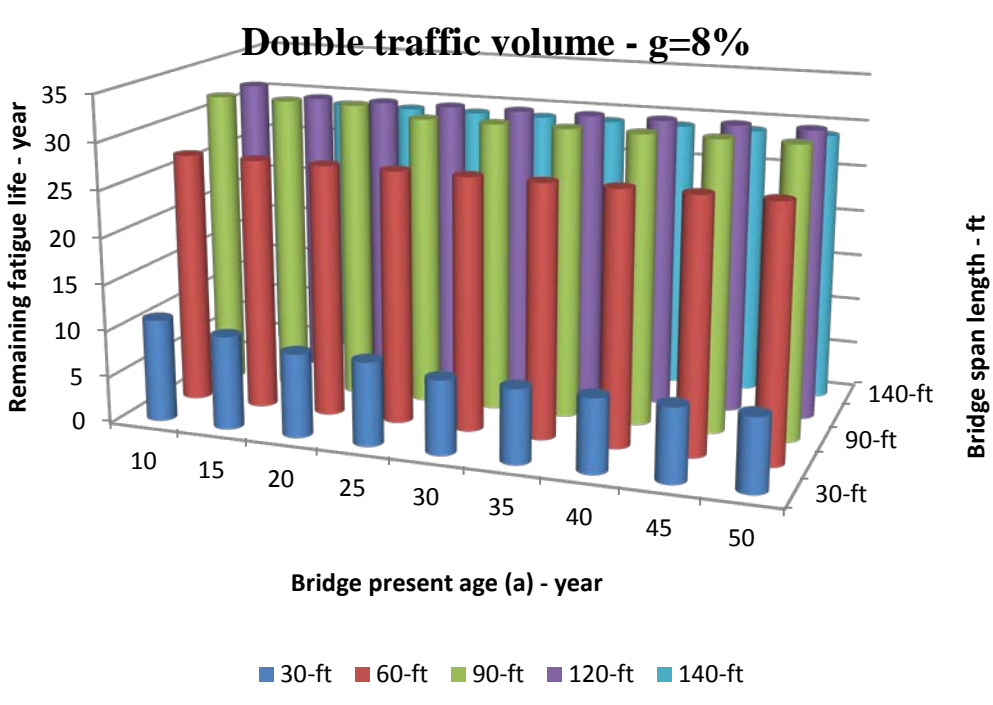
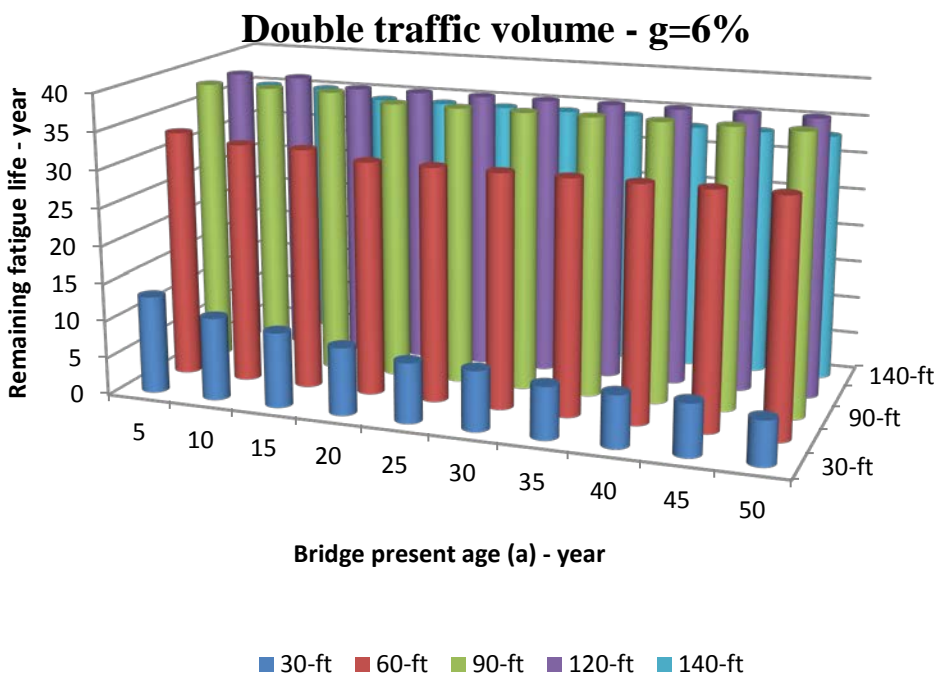


FIGURE 9-21: REMAINING LIFE VS. PRESENT AGE VS. SPAN LENGTH, AASHTO FATIGUE TRUCK

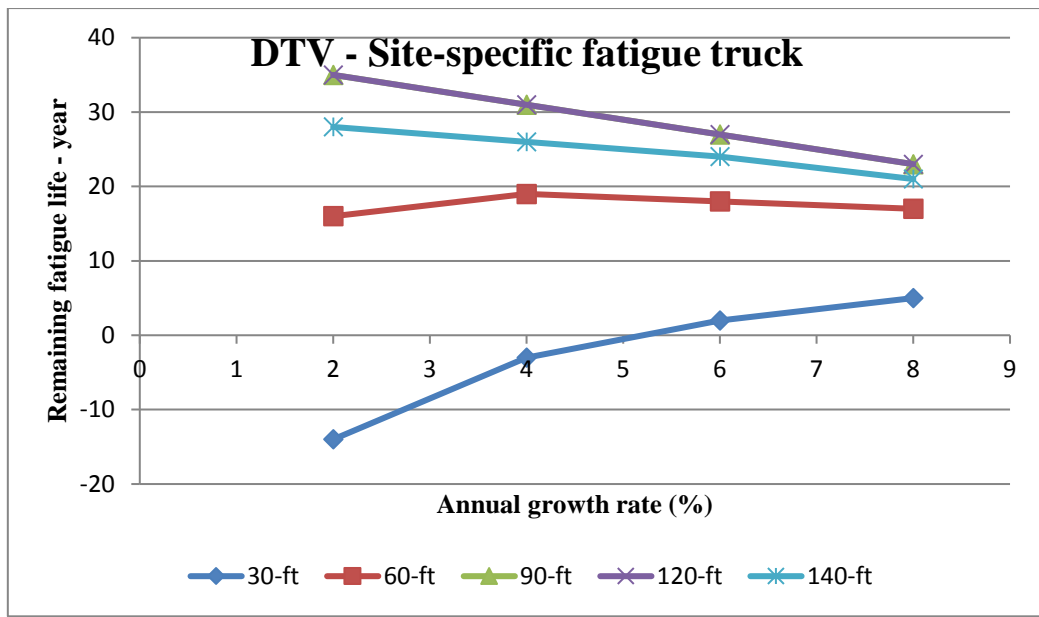


FIGURE 9-22
Remaining life at age 50-years vs. annual growth rate

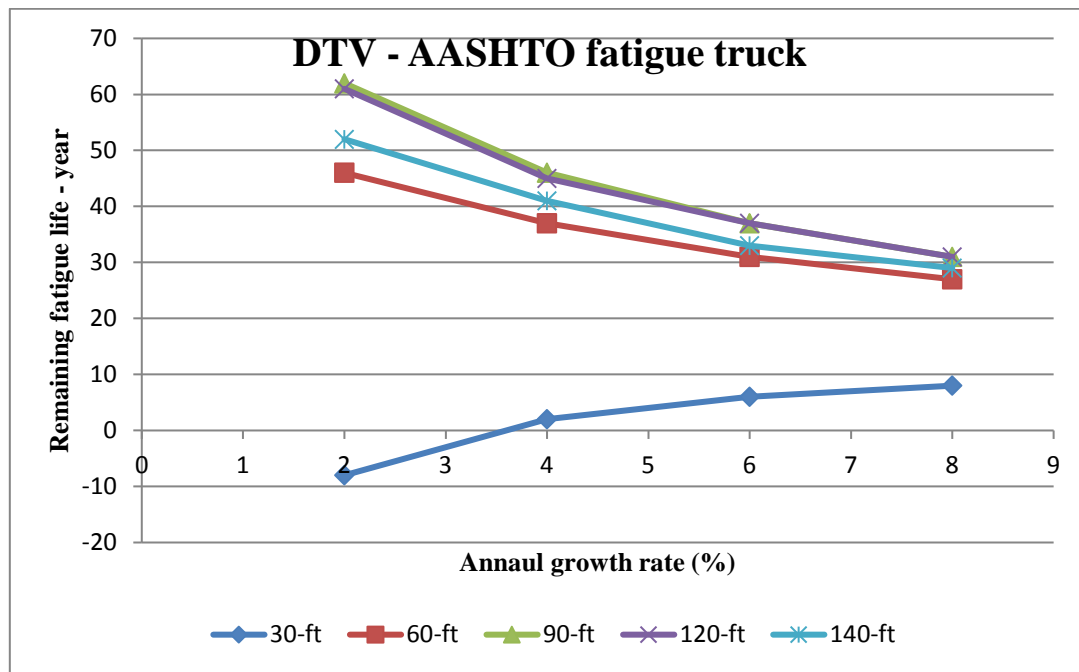


FIGURE 9-23: REMAINING LIFE AT AGE 50-YEARS VS. ANNUAL GROWTH RATE

9.5.3 Double Traffic Load Scenario (DTL)

This case investigates the remaining life of steel bridges considering the second scenario; to accommodate the increase in freight demand by increasing (doubling) the current traffic-volume, but keeping traffic loading constant. The bending moments (M_{LL+IM}) developed by a truck load, twice the site-specific fatigue truck and the AASHTO fatigue truck loads, were calculated by the Virtis program and recorded versus the girders' section modulus, to calculate the bending stresses as shown in Table 9-26 and Table 9-27 respectively. The remaining life was calculated for each bridge with the present average daily truck traffic in one lane [$(ADTT)_{SL}$]_{Present} equal to 25,628 truck/day, effective stress range as in Table 9-26 and Table 9-27, and a set of variables. Variables were taken as in the current traffic condition case (Connection detail with a fatigue strength of category B, present age of bridge (a) ranging from 5 to 50-years with intervals of 5 years, annual traffic-volume growth rates (g) of 2, 4, 6, and 8%, number of stress-range cycles per truck passage (n) equal to 1 for bridge spans greater than 40-ft, and 2 for bridge spans less than 40-ft)

TABLE 9-26: SITE-SPECIFIC FATIGUE TRUCK (85-KIP) STRESSES

Span ft	M_{LL+IM} kip.ft	S in^3	(Δf) ksi	$(\Delta f)_{max}$ ksi	$(\Delta f)_{TH}$ ksi	$(\Delta f)_{eff}$ ksi
30	446	152.9	60.38	90.66	16	45.33
60	1182	557.07	43.92	66.08	16	33.04
90	2106	1171.93	37.20	56.09	16	28.04
120	3264	1820.47	37.11	56.07	16	28.03
140	3890	2051.26	39.26	59.40	16	29.7

TABLE 9-27: AASHTO FATIGUE TRUCK STRESSES

Span ft	MLL+IM kip.ft	S in³	(Δf) ksi	(Δf)_{max} ksi	(Δf)_{TH} ksi	(Δf)_{eff} ksi
30	412	152.9	55.64	83.55	16	41.77
60	924	557.07	34.33	51.65	16	25.83
90	1716	1171.93	30.31	45.7	16	22.85
120	2680	1820.47	30.47	46.04	16	23.02
140	3212	2051.26	32.41	49.03	16	24.52

The remaining life for different fatigue trucks and different annual traffic-volume growth rates (2 to 8%) has been recorded as shown in Table 9-22 thru Table 9-24.

The remaining life values recorded in these tables have been depicted in Figure 9-24 thru Figure 9-27. Comparing the remaining life in the case of doubling the traffic load (DTL) with those in the case of the current traffic conditions (CT) showed that the remaining lives of all bridges at all ages have been dramatically reduced and become negative in most of the cases. However, for 50-years old bridges of all span lengths, the increase in the annual growth rate improved the remaining life of the bridges (see Figure 9-28 and Figure 9-29).

TABLE 9-28: REMAINING LIFE (Yr), G=2%

Bridge present age (a) year	Site-specific fatigue truck (85-kip)					AASHTO fatigue truck				
	Fatigue remaining life (Y) year					Fatigue remaining life (Y) year				
	30-ft	60-ft	90-ft	120-ft	140-ft	30-ft	60-ft	90-ft	120-ft	140-ft
5	0	7	13	13	11	1	18	25	25	21
10	-5	3	10	10	7	-3	15	23	22	18
15	-9	-1	7	7	4	-8	12	20	20	15
20	-14	-4	4	4	0	-12	9	18	17	12
25	-18	-8	1	1	-3	-16	6	15	15	10
30	-22	-12	-2	-2	-6	-20	3	13	13	7
35	-27	-15	-5	-5	-9	-24	1	11	11	5
40	-31	-18	-8	-8	-12	-28	-2	9	9	3
45	-35	-21	-10	-10	-15	-32	-4	7	7	1
50	-39	-24	-13	-13	-17	-36	-6	6	5	-1

TABLE 9-29: REMAINING LIFE (Y_R), G=4%

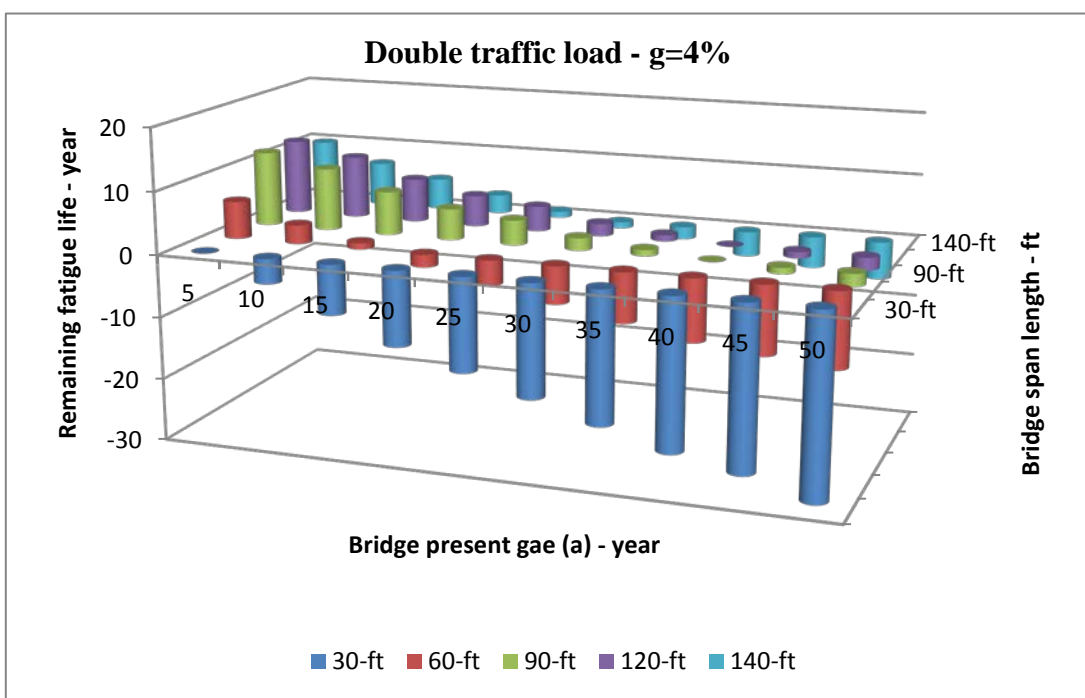
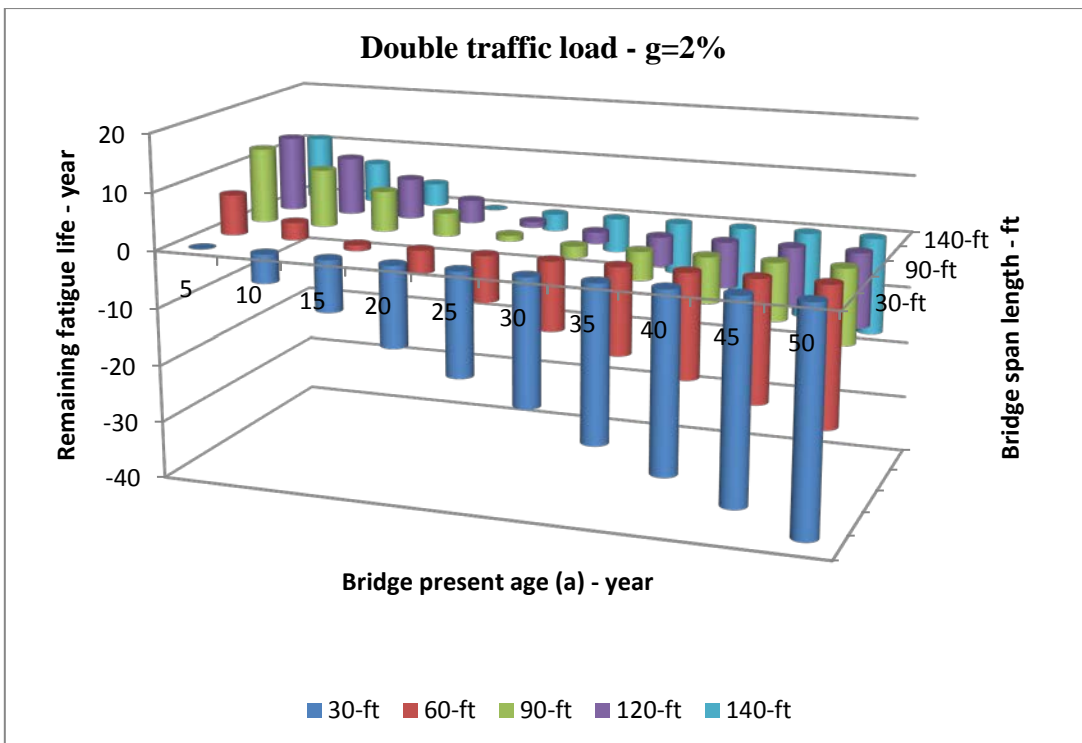
Bridge present age (a) year	Site-specific fatigue truck (85-kip)					AASHTO fatigue truck				
	Fatigue remaining life (Y) year					Fatigue remaining life (Y) year				
	30-ft	60-ft	90-ft	120-ft	140-ft	30-ft	60-ft	90-ft	120-ft	140-ft
5	0	7	13	13	11	1	15	21	21	18
10	-5	3	10	10	7	-3	13	19	19	16
15	-9	-1	7	7	4	-6	11	18	17	14
20	-14	-4	4	4	0	-10	10	17	16	12
25	-18	-8	1	1	-3	-13	8	15	15	11
30	-22	-12	-2	-2	-6	-16	7	15	14	10
35	-27	-15	-5	-5	-9	-18	6	14	13	9
40	-31	-18	-8	-8	-12	-21	5	13	13	8
45	-35	-21	-10	-10	-15	-23	4	12	12	8
50	-39	-24	-13	-13	-17	-25	4	12	11	7

TABLE 9-30: REMAINING LIFE (Y_R), G=6%

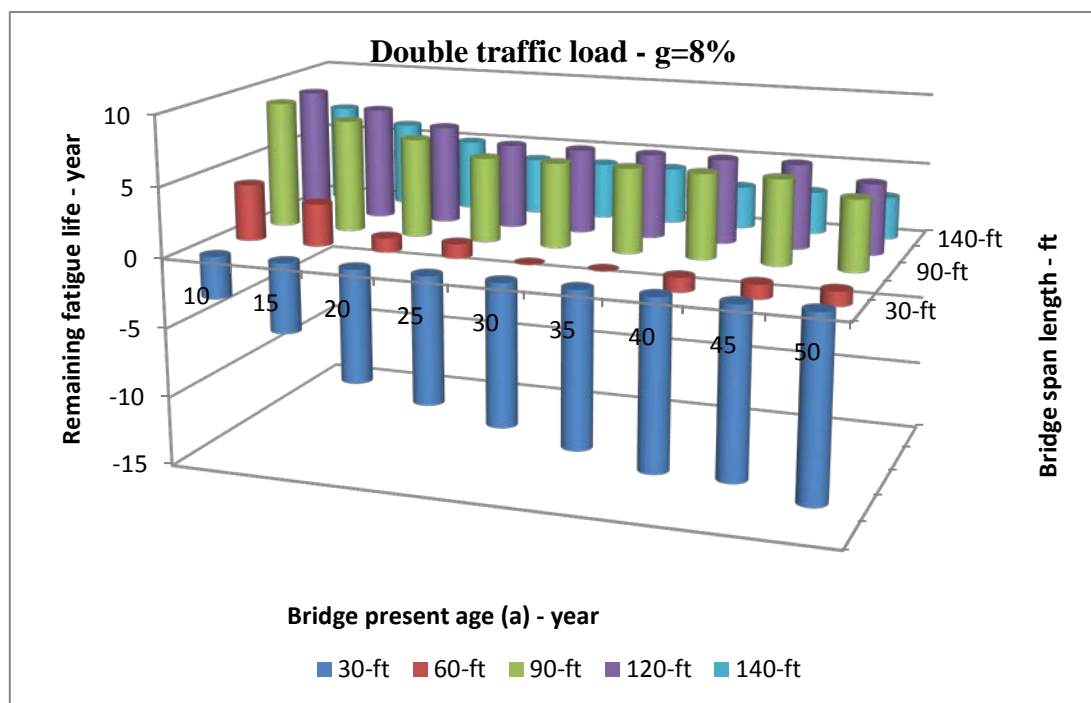
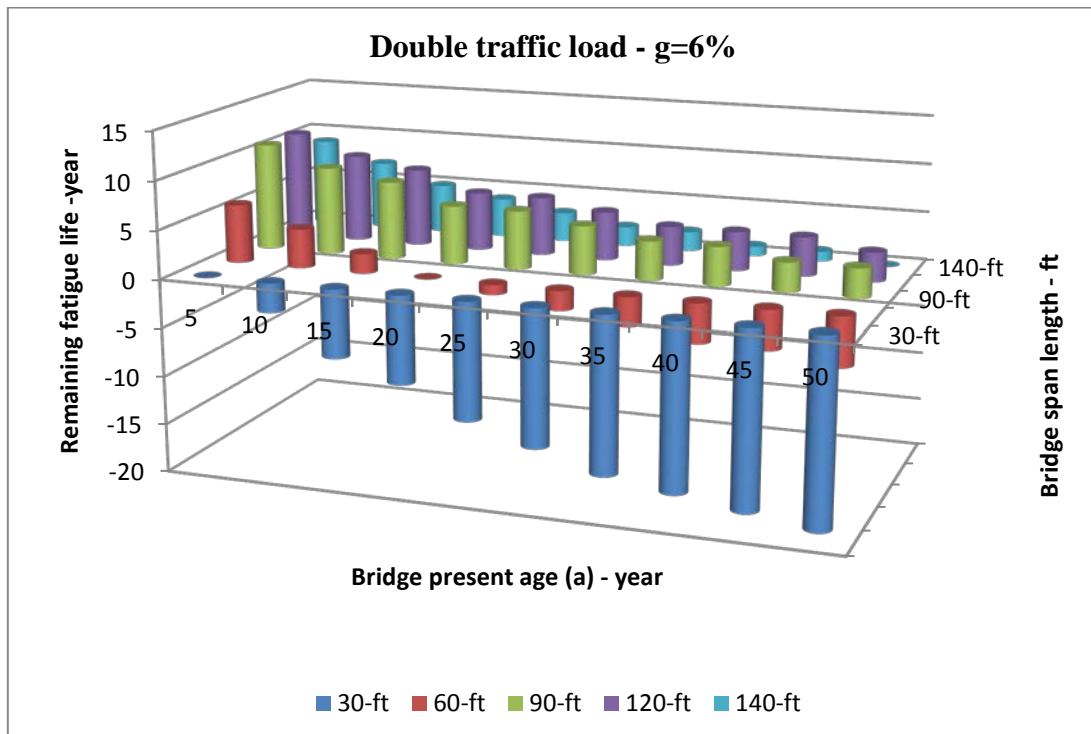
Bridge present age (a) year	Site-specific fatigue truck (85-kip)					AASHTO fatigue truck				
	Fatigue remaining life (Y) year					Fatigue remaining life (Y) year				
	30-ft	60-ft	90-ft	120-ft	140-ft	30-ft	60-ft	90-ft	120-ft	140-ft
5	0	6	11	11	9	1	14	18	18	15
10	-3	4	9	9	7	-2	12	17	17	14
15	-7	2	8	8	5	-5	11	16	16	13
20	-9	0	6	6	4	-7	10	15	15	12
25	-12	-1	6	6	3	-9	9	15	14	11
30	-14	-2	5	5	2	-11	9	14	14	11
35	-16	-3	4	4	2	-13	8	14	14	11
40	-17	-4	4	4	1	-14	8	14	13	10
45	-18	-4	3	4	1	-15	7	14	13	10
50	-19	-5	3	3	0	-16	7	13	13	10

TABLE 9-31: REMAINING LIFE (Y_R), G=8%

Bridge present age (a) year	Site-specific fatigue truck (85-kip)					AASHTO fatigue truck				
	Fatigue remaining life (Y) year					Fatigue remaining life (Y) year				
	30-ft	60-ft	90-ft	120-ft	140-ft	30-ft	60-ft	90-ft	120-ft	140-ft
10	-3	4	9	9	7	-1	11	15	15	13
15	-5	3	8	8	6	-4	10	15	14	12
20	-8	1	7	7	5	-5	10	14	14	12
25	-9	1	6	6	4	-7	9	14	14	11
30	-10	0	6	6	4	-8	9	14	13	11
35	-11	0	6	6	4	-9	9	14	13	11
40	-12	-1	6	6	3	-9	9	13	13	11
45	-12	-1	6	6	3	-9	9	13	13	11
50	-13	-1	5	5	3	-10	9	13	13	11



**FIGURE 9-24: REMAINING LIFE VS. PRESENT AGE VS. SPAN LENGTH,
SITE-SPECIFIC FATIGUE TRUCK**



**FIGURE 9-25: REMAINING LIFE VS. PRESENT AGE VS. SPAN LENGTH,
SITE-SPECIFIC FATIGUE TRUCK**

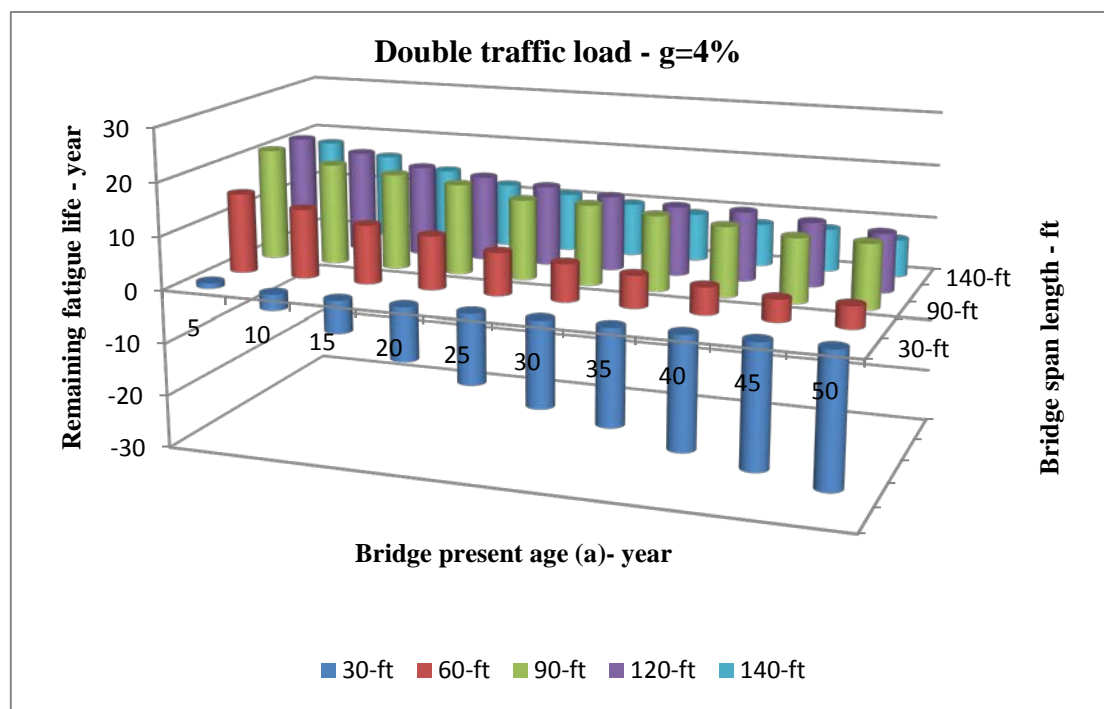
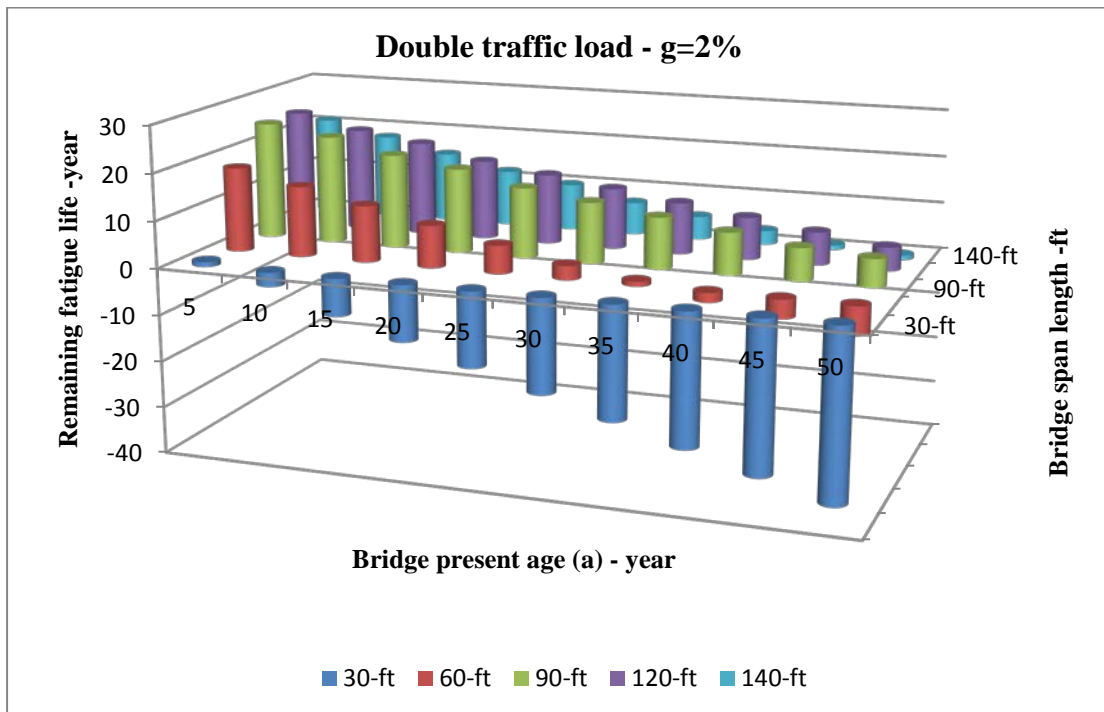


**FIGURE 9-26: REMAINING LIFE VS. PRESENT AGE VS. SPAN LENGTH,
AASHTO FATIGUE TRUCK**

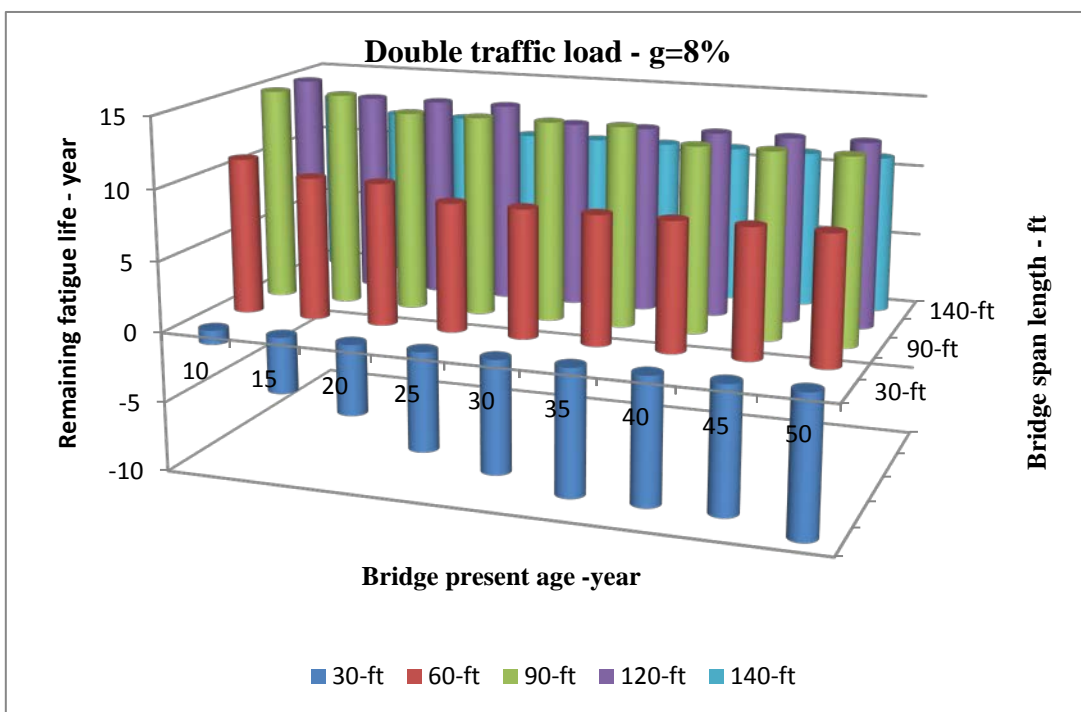
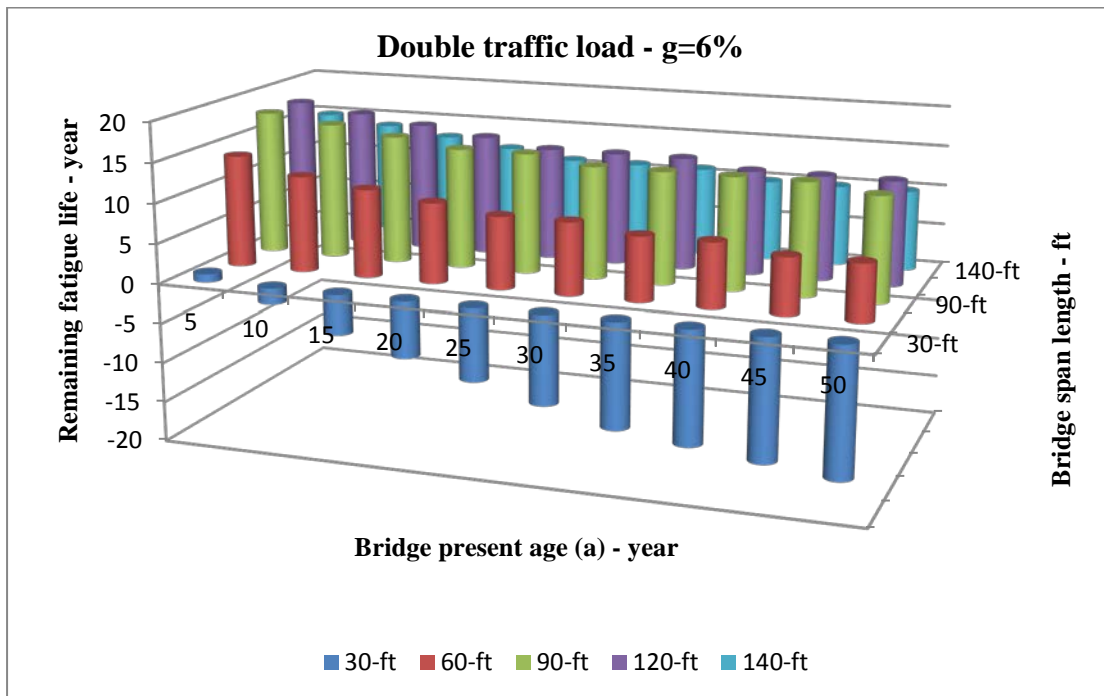


**FIGURE 9-27: REMAINING LIFE VS. PRESENT AGE VS. SPAN LENGTH,
AASHTO FATIGUE TRUCK**

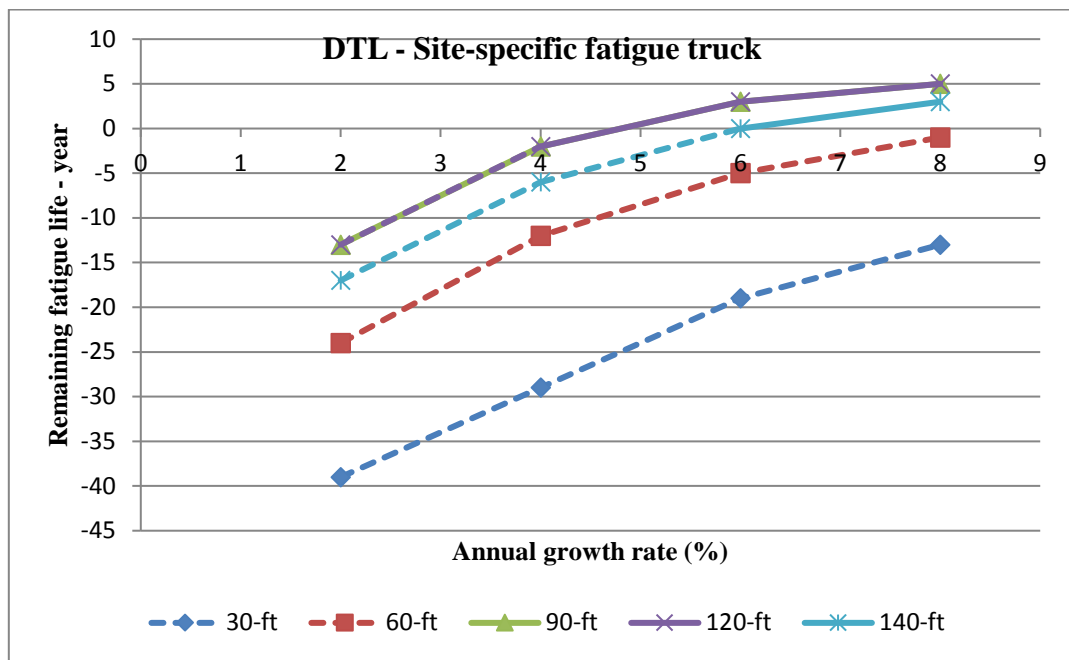


FIGURE 9-28
Remaining life at age 50-years vs. annual growth rate, fatigue truck

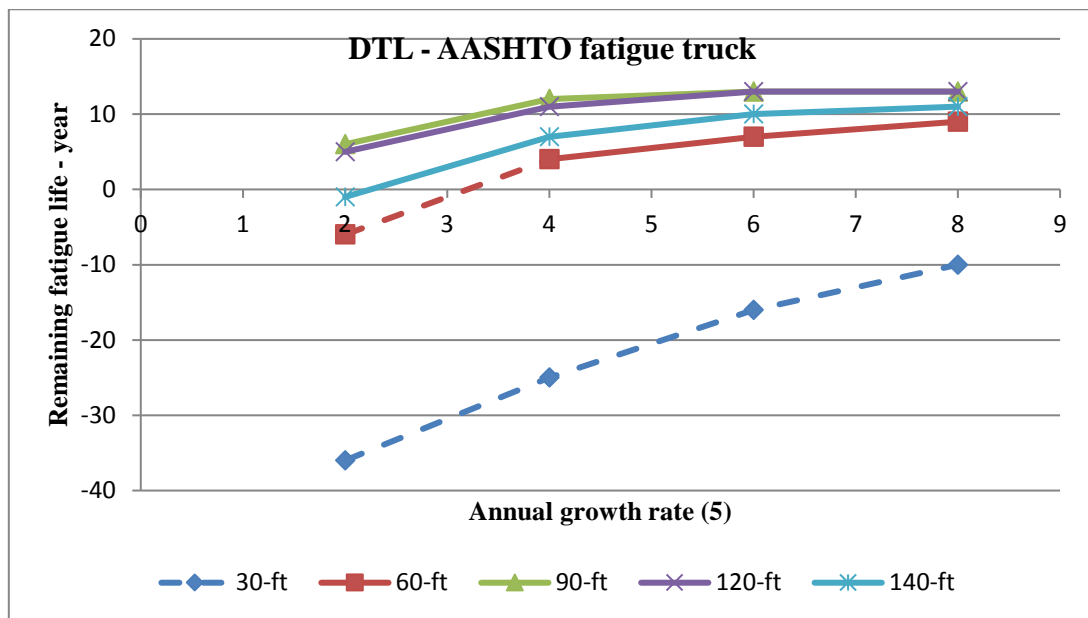


FIGURE 9-29: REMAINING LIFE AT AGE 50-YEARS VS. ANNUAL GROWTH RATE, AASHTO FATIGUE TRUCK

9.6 RC Deck Slab Remaining Life (Y_r) – Case Study

To investigate the impact of meeting the increase in freight demand by increasing the traffic and/or the traffic load on the remaining life (remaining service life) of the RC deck slab of steel bridges, the earlier discussed steel bridges RC slabs were studied under the effect of both scenarios.

RC deck slab with a total thickness of 6-in, and a bottom cover of 1-in, and with characteristic compressive strength of 3.0 ksi, supported on the bridges' girders 8-ft apart was studied. The studying was under the load effect of the AASHTO fatigue truck and the site specific fatigue truck (85-kip) and the same current traffic volume. The remaining lives were calculated under different annual traffic-volume growth rates (2, 4, 6, and 8%) and different present bridge ages (5, 10, 15, 20, 25, 30, 35, 40, 45, and 50 years). The fatigue calculations are based on the repetition of the most frequent truck over a specific route, so based on the earlier presented WIM data in Chapter 2 and Chapter 3, the present average daily truck in single lane $[(ADTT)_{SL}]_{Present}$ was set equal to 71 truck/day as shown earlier in clause 4.12.1.

9.6.1 Current Traffic Conditions (CT)

This case study is to predict the remaining life of the deck under the current traffic conditions, $[(ADTT)_{SL}]_{Present}$ equals 71/truck/day and P_u . The fatigue life of the RC deck depends on the individual load of the wheel. Therefore, the single wheel load is the dominant parameter affecting the deck fatigue life. Figure 1-2 and Figure 3-7 show that the most extreme wheel load of these two trucks is AASHTO fatigue truck wheel load of P equal 8000 lb.

The ultimate shear strength can be calculated as per equation Eq.9-4:

$$d = 8 - 1(\text{cover}) - 0.25 = 6.75 \text{ in b}$$

$$b_0 = 2 \times \left(8 + 2 \times \frac{6.75}{2} + 20 + 2 \times \frac{6.75}{2} \right) = 83 \text{ in}$$

$$P_u = \left(2 + \frac{4}{2.5} \right) \times \sqrt{3000} \times 83 \times 6.75 \times 1.55 = 171228 \text{ ksi}$$

The remaining life of the deck varies depending on the annual growth rate, the present age of the deck, and compressive strength of RC are computed and recorded in Table 9-32. It showed the different remaining lives under the application of the following constant factors:

$$K_d = 3.1E-7$$

$$K_p = 2.09E-6$$

$$C_d = 3 \text{ (3-axle truck)}$$

$$R_d = 1.35 \text{ (evaluation of the remaining life)}$$

$$[(ADTT)_{SL}]_{\text{Present}} = 71 \text{ truck/day}$$

$$P_s = 1.04$$

$$P_u = 108.88 \text{ ksi } (f'_c = 3000 \text{ psi})$$

$$P_u = 125.72 \text{ ksi } (f'_c = 4000 \text{ psi})$$

As illustrated in Figure 9-30, the remaining life decreases in the older RC decks with bridges for compressive strength of 3000 psi. Figure 9-31 and Figure 9-31 show that the RC deck slab of higher compressive strengths develops a higher remaining life. In addition, the remaining life remains constant with the change of the present age of the deck for higher compressive strength ($f'_c = 4000 \text{ psi}$).

TABLE 9-32 :RC DECK SLAB REMAINING LIFE (CT)

Deck Present age (year)	Remaining life (year)							
	$f'_c = 3000 \text{ psi}$				$f'_c = 4000 \text{ psi}$			
	Annual growth rate (g) - %				Annual growth rate (g) - %			
2	4	6	8	2	4	6	8	
5	136	85	63		264	150	107	
10	136	85	63	51	264	150	107	85
15	135	85	63	51	263	150	107	85
20	135	84	63	51	263	150	107	85
25	135	84	63	51	263	150	107	85
30	135	84	63	51	263	150	107	85
35	135	84	63	51	263	150	107	85
40	134	84	63	51	263	150	107	85
45	134	84	63	51	263	150	107	85
50	134	84	63	51	263	150	107	85

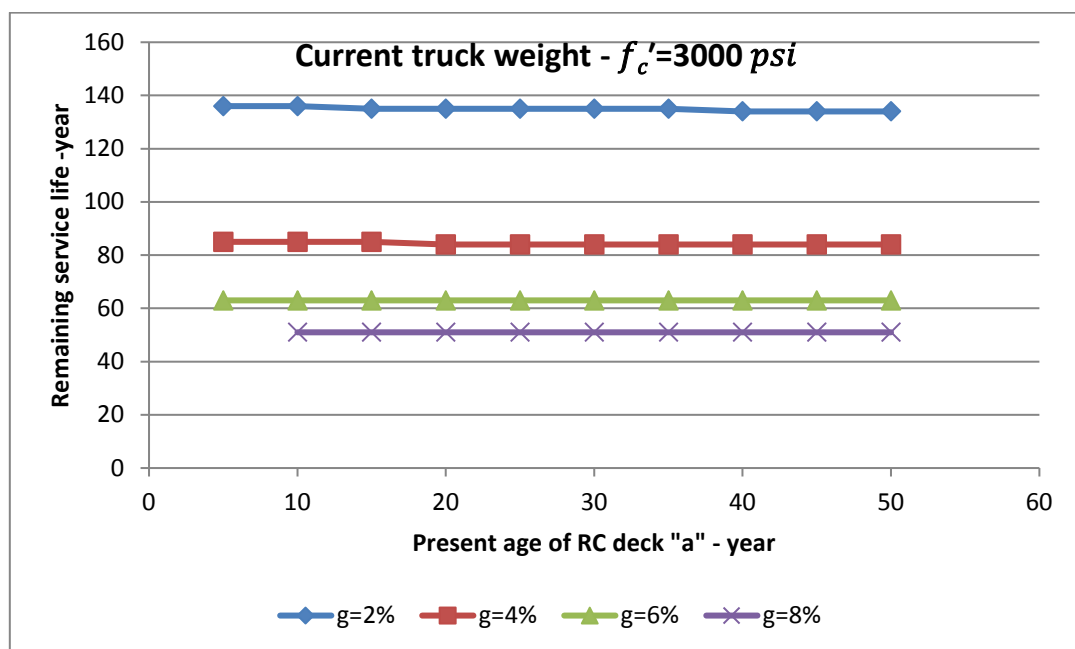


FIGURE 9-30: REMAINING LIFE VS. RC DECK AGE, $f'_c = 3000 \text{ psi}$

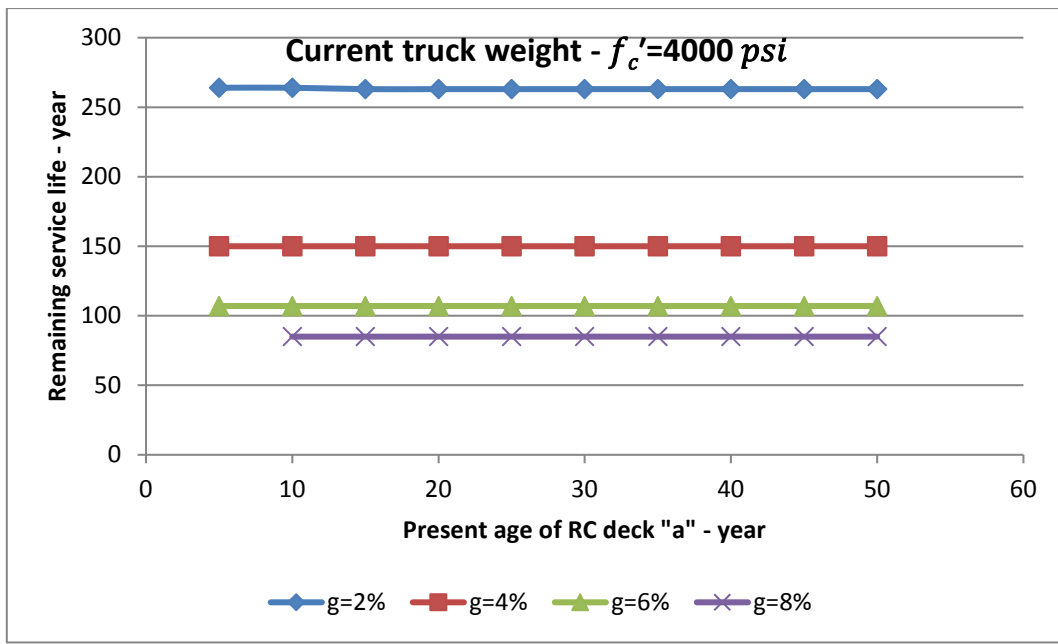


FIGURE 9-31: REMAINING LIFE VS. RC DECK AGE, $f'_c = 4000 \text{ psi}$

The degradation in the reaming fatigue life for lower annual growth rate ($g=2\%$) was sensitive to the present age of the RC deck. The difference in remaining life of 50 year old deck was about 90% of it at the age 5 years. But this percentage did not remain constant in cases of higher annual growth rate ($g=4$ and 6%). It increased to approximately 97% approximately. With the annual growth rate of 8% , the remaining life remained constant.

9.6.2 Double Traffic Volume Scenario (DTV)

One of the proposed scenarios to meet the increase in freight demand is doubling the traffic volume with the same traffic load conditions. The remaining life of the RC deck slab of bridges was computed and recorded for double traffic volume conditions, $[(ADTT)_{SL}]_{\text{Present}} = 71 \text{ truck/day}$, as shown in Table 9-33. The recorded data was illustrated and depicted in Figure 5-32 and Figure 9-33. This data shows that the remaining service life of the RC deck slab is inversely affected by doubling the traffic

volume. The remaining life increases but remains constant with the increase of the compressive strength.

TABLE 9-33: RC DECK SLAB REMAINING LIFE (DTV)

Deck		Remaining life (year)							
Present age (year)	$f'_c = 3000 \text{ psi}$	Annual growth rate (g) - %				$f'_c = 4000 \text{ psi}$			
		2	4	6	8	2	4	6	8
5	104	68	52			229	132	95	
10	103	68	52	42		229	132	95	76
15	103	67	51	42		229	132	95	76
20	103	67	51	42		229	132	95	76
25	102	67	51	42		229	132	95	76
30	102	67	51	42		229	132	95	76
35	101	67	51	42		229	132	95	76
40	101	67	51	42		229	132	95	76
45	101	67	51	42		228	132	95	76
50	100	67	51	42		228	132	95	76

9.6.3 Double Traffic Load Scenario (DTL)

Another proposed scenario to meet the increase in freight demand is doubling the traffic volume with the same traffic load conditions. The current wheel load was doubled and set out to 11.00 lb. ($P=11000 \text{ lbs.}$). The remaining life of the RC deck slabs of bridges were computed and recorded. As shown in Table 9-34, all the computed remaining service life (remaining life) has negative values. This means that under this scenario, the RC deck is in a critical conditions under this scenario that adversely affect its the remaining life.

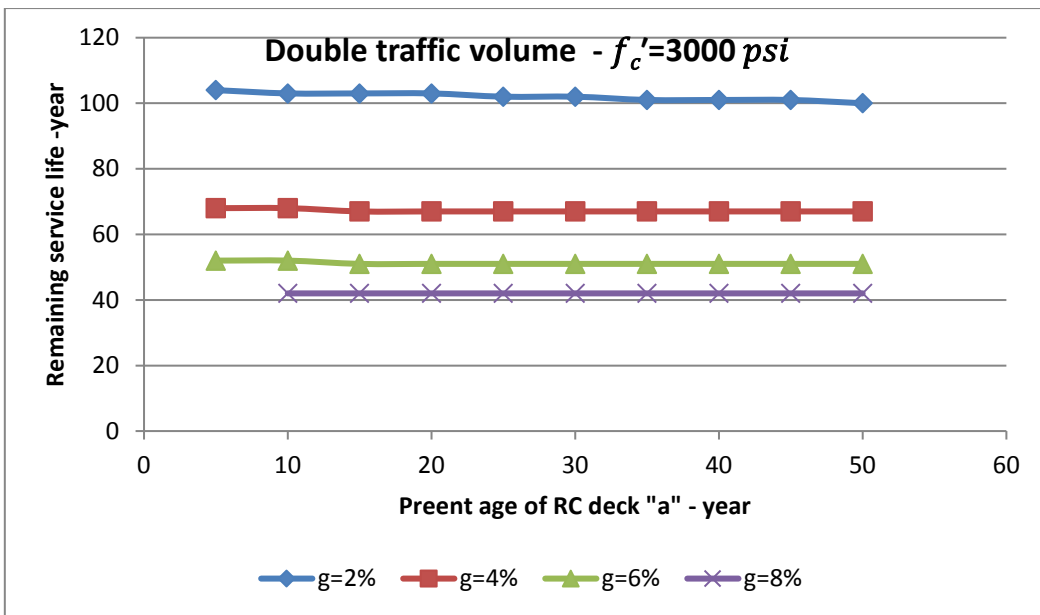


FIGURE 9-32: REMAINING LIFE VS. RC DECK AGE, $f'_c = 3000 \text{ psi}$

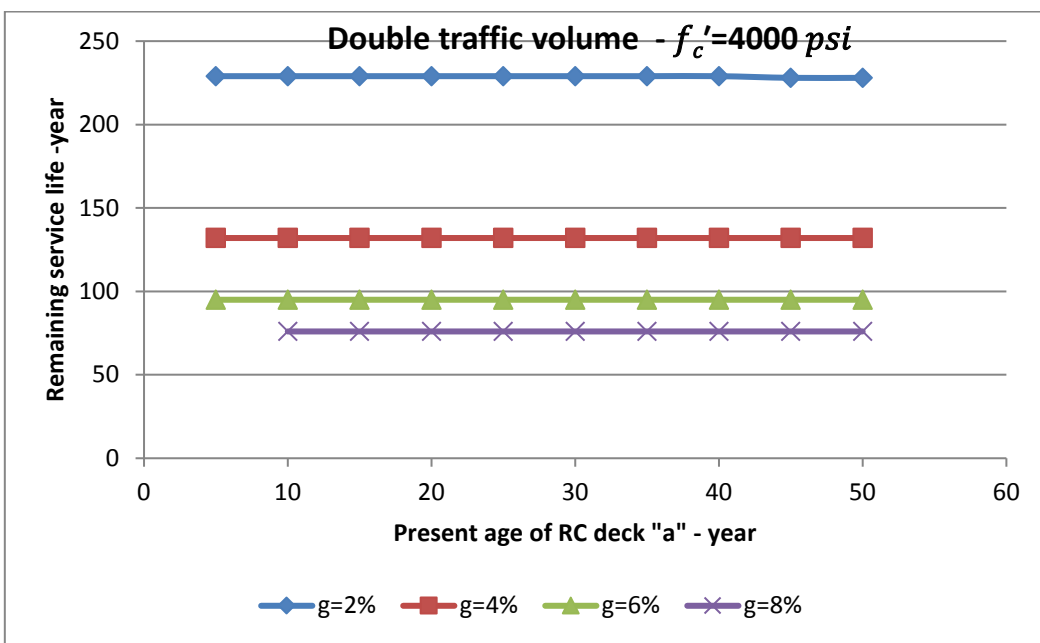


FIGURE 9-33: REMAINING LIFE VS. RC DECK AGE, $f'_c = 4000 \text{ psi}$

TABLE 9-34: RC DECK SLAB REMAINING LIFE (DTV)

Deck Present age (year)	Remaining life (year)							
	$f'_c = 3000 \text{ psi}$				$f'_c = 4000 \text{ psi}$			
	Annual growth rate (g) - %				Annual growth rate (g) - %			
2	4	6	8	2	4	6	8	
5	-5	-5	-5	-	-5	-5	-5	-
10	-10	-10	-10	-10	-10	-10	-10	-10
15	-15	-15	-15	-15	-15	-15	-15	-15
20	-20	-20	-20	-20	-20	-20	-20	-20
25	-25	-25	-25	-25	-25	-25	-25	-25
30	-30	-30	-30	-30	-30	-30	-30	-30
35	-35	-35	-35	-35	-35	-35	-35	-35
40	-40	-40	-40	-40	-40	-40	-40	-40
45	-45	-45	-45	-45	-45	-45	-45	-45
50	-50	-50	-50	-50	-50	-50	-50	-50

At the annual growth rate (g) of 2%, the reduction in the remaining life of the RC deck slab, with the doubling of the traffic volume, was about 35% of the remaining life under the current traffic condition. With the same annual growth rate (g=2%), and in the case of doubling the traffic load, the remaining life of the RC deck slab was reduced to a negative value. Figure 9-34 shows the impact of meeting the increase in freight demands on the remaining life of the RC deck slab while maintaining current traffic conditions.

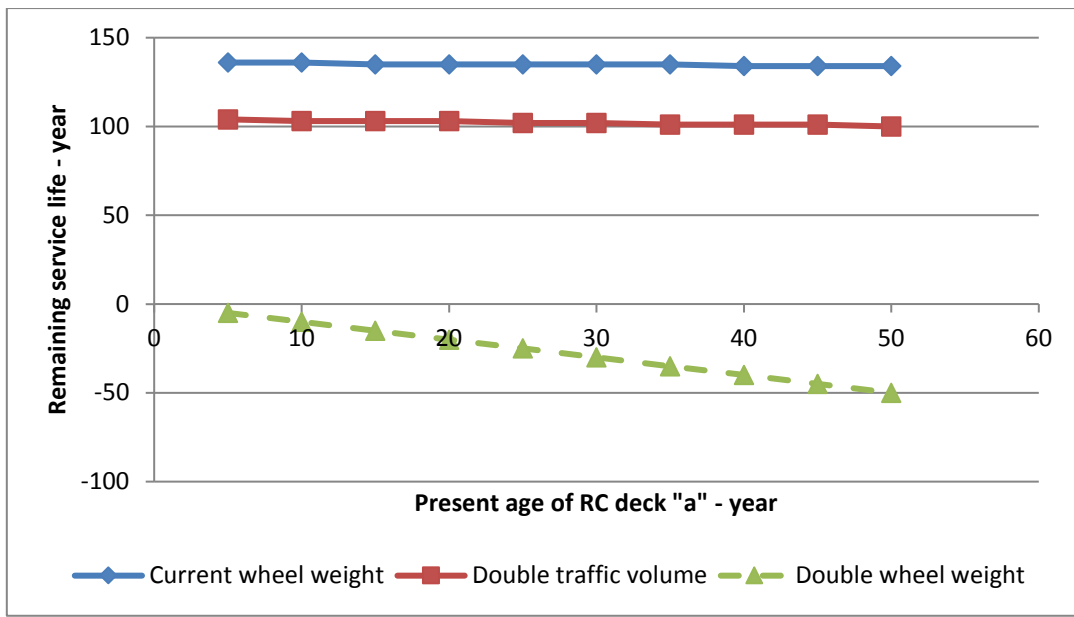


FIGURE 9-34: THE IMPACT OF MEETING THE INCREASE IN FREIGHT DEMAND ON THE REMAINING LIFE VS. RC DECK AGE, $f'_c = 3000 \text{ psi}$, $G=2\%$

9.7 Different Loading Scenarios

Data of close to 6 million vehicles was gathered in 2007 in the state of Wisconsin.

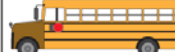
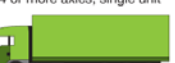
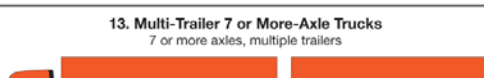
This data was obtained from Wisconsin Department of Transportation for total of 17 different locations [51]. The data collected in this report was used to study the effect of other different proposed scenarios to meet the increase in freight demand on the bridge fatigue life.

In order to understand the data gathered from the report, categorization of the vehicles is needed. Eleven different types of trucks have been selected which fall under different categories of Federal Highway Administration category scheme. FHWA Category Scheme for the vehicle classification which is shown in Table 4-5. The data obtained from the report is then categorized based on the eleven different types of the vehicle used in the study which can be seen in the table below.

TABLE 9-35: TRUCK COUNTS BASED ON WISDOT DATA

Vehicle Class	Vehicle Type	Total Number of Counts [Year]	% of Total
Class 5	H-20	748658	13
Class 6	Type 3	251795	4.37
Class 7	SU4	25753	1.27
Class 8	HS-20	634745	11.02
	Type 3S1 & 2S2	213738	3.71
Class 9	Type 3S2	3553613	61.72
Class 10	Type 3S3	72939	1.27
Class 13	7 Axle Rocky Mountain Double	9738	0.17
	8 Axle B-Train Double	680	0.01
	9 Axle Turnpike Double	75	0
	Total	5511734	

TABLE 9-36: FHWA VEHICLE CLASSIFICATION

FHWA Vehicle Classifications			
1. Motorcycles 2 axles, 2 or 3 tires 	2. Passenger Cars 2 axles, can have 1- or 2-axle trailers  	3. Pickups, Panels, Vans 2 axles, 4-tire single units Can have 1 or 2 axle trailers  	4. Buses 2 or 3 axles, full length  
5. Single Unit 2-Axle Trucks 2 axles, 6 tires (dual rear tires), single-unit   	6. Single Unit 3-Axle Trucks 3 axles, single unit 	7. Single Unit 4 or More-Axle Trucks 4 or more axles, single unit 	8. Single Trailer 3- or 4-Axle Trucks 3 or 4 axles, single trailer 
9. Single Trailer 5-Axle Trucks 5 axles, single trailer  	10. Single Trailer 6 or More-Axle Trucks 6 or more axles, single trailer  	11. Multi-Trailer 5 or Less-Axle Trucks 5 or less axles, multiple trailers  	
13. Multi-Trailer 7 or More-Axle Trucks 7 or more axles, multiple trailers  	12. Multi-Trailer 6-Axle Trucks 6 axles, multiple trailers  		

Taken from Texas DOT website (http://onlinemanuals.txdot.gov/txdotmanuals/tri/images/FHWA_Classification_Chart_FINAL.png)

The aim of this research is to understand the effects of using higher capacity trucks instead of smaller trucks on the bridges and this will be viewed considering the fatigue behavior of bridges. The question is, whether using higher capacity trucks, which results in using less number of trucks, have more detrimental effects on the fatigue behavior of bridges or, since the counts of the trucks on bridges decrease, this will not cause more damages to the bridges.

9.7.1 Steel Bridge Fatigue Assessment

In order to answer the above question, different scenarios can be considered. As shown in the table above, the number of vehicles with higher number of axles which can carry more load are very small in the data gathered from the Wisconsin DOT and this number for the whole group of “class 13” is below 0.2% of the total number of

trucks. One can also observe from the same table that the majority of the freight shipping in this state is done by “class 9” vehicles with the staggering percentage of 60. 9-Axle Turnpike Double can carry up to 50% more load than the Type 3S2, so using Turnpike Double instead of Type 3S2 can result in 33% reduction in the number of trucks on the bridges. This decrease can be applied to $(ADTT)_{SL}$ and effective stress range which was calculated for all the vehicles should also be updated. Results for the “detail A” are given in table below as an example for different growth rates and current age of the bridge.

**TABLE 9-37: REMAINING FATIGUE LIFE OF THE STEEL BRIDGE
BASED ON FIRST AND SECOND SCENARIOS**

a g	Remaining Fatigue life in years							
	Type 3S2				9-Axle Turnpike Double			
	0.02	0.04	0.06	0.08	0.02	0.04	0.06	0.08
5	75	52	41	34	72	50	40	33
10	74	52	41	34	71	50	39	33
20	72	51	40	34	69	49	39	33
30	71	50	40	34	67	48	39	33
40	69	50	40	34	66	48	38	33
50	68	50	40	34	65	48	38	32

It can be seen that by using heavier vehicles, the Remaining Fatigue Life has slightly decreased. This shows that, using less number of trucks to carry the same load might not have an extremely bad effect on the overall stresses due to fatigue loading on the bridge even though higher stresses will be present at the bridge when these trucks pass.

For the same case that was discussed earlier, the values of Fatigue Serviceability Index were calculated and the results are given in Table 9-42. As per Table 9-13, the corresponding actions were listed in Table 9-43,

It can be seen from these tables that the fatigue rating for the case of using longer combination vehicles, such as 9-Axle Turnpike Double, on the bridge, results in slightly worse FSI but not big enough to change the fatigue rating of the bridge which remains the same for two cases.

TABLE 9-38: FATIGUE SERVICEABILITY INDEX BASED ON FIRST AND SECOND SCENARIOS

Fatigue Serviceability Index									
a	g	Type 3S2				9-Axle Turnpike Double			
		0.02	0.04	0.06	0.08	0.02	0.04	0.06	0.08
5	0.61	0.42	0.33	0.28	0.58	0.41	0.32	0.27	
10	0.60	0.42	0.33	0.28	0.58	0.41	0.32	0.27	
20	0.58	0.41	0.32	0.28	0.56	0.40	0.32	0.27	
30	0.57	0.41	0.32	0.28	0.54	0.39	0.32	0.27	
40	0.51	0.41	0.32	0.28	0.50	0.39	0.31	0.27	
50	0.47	0.41	0.32	0.28	0.46	0.39	0.31	0.26	

TABLE 9-39: FATIGUE RATING BASED ON FIRST AND SECOND SCENARIOS

Fatigue Rating									
a	g	Type 3S2				9-Axle Turnpike Double			
		0.02	0.04	0.06	0.08	0.02	0.04	0.06	0.08
5	E	G	M	M	E	G	M	M	
10	E	G	M	M	E	G	M	M	
20	E	G	M	M	E	G	M	M	
30	E	G	M	M	E	G	M	M	
40	E	G	M	M	E	G	M	M	
50	G	G	M	M	G	G	M	M	

In addition to these two scenarios of using Type 3S2 trucks or using 9-Axle Turnpike Double, a third scenario which is using single unit trucks instead of Type 3S2 trucks has also been investigated here. The single unit truck here is SU4 which can almost carry the same weight as Type 3S2 truck.

Using the same WIM data, and replacing the Type 3S2 trucks with the SU4 trucks, the results of remaining fatigue life, Fatigue Serviceability Index and Fatigue Rating were obtained and shown in Table 9-44, Table 9-45 and Table 9-46.

TABLE 9-40: REMAINING FATIGUE LIFE OF THE STEEL BRIDGE BASED ON FIRST AND THIRD SCENARIOS

a	g	Remaining Fatigue Life in years							
		Type 3S2				SU4 Truck			
		0.02	0.04	0.06	0.08	0.02	0.04	0.06	0.08
5	75	52	41	34	55	40	33	28	
10	74	52	41	34	53	40	32	27	
20	72	51	40	34	51	38	31	27	
30	71	50	40	34	49	38	31	27	
40	69	50	40	34	47	37	31	27	
50	68	50	40	34	45	37	31	27	

TABLE 9-41: FATIGUE SERVICEABILITY INDEX BASED ON FIRST AND THIRD SCENARIOS

a	g	Fatigue Serviceability Index							
		Type 3S2				SU4 Truck			
		0.02	0.04	0.06	0.08	0.02	0.04	0.06	0.08
5	0.61	0.42	0.33	0.28	0.45	0.32	0.27	0.23	
10	0.60	0.42	0.33	0.28	0.43	0.32	0.26	0.22	
20	0.58	0.41	0.32	0.28	0.41	0.31	0.25	0.22	
30	0.57	0.41	0.32	0.28	0.40	0.31	0.25	0.22	
40	0.51	0.41	0.32	0.28	0.38	0.30	0.25	0.22	
50	0.47	0.41	0.32	0.28	0.36	0.30	0.25	0.22	

TABLE 9-42: FATIGUE RATING BASED ON FIRST AND THIRD SCENARIOS

a g	Fatigue Rating							
	Type 3S2				SU4 Truck			
	0.02	0.04	0.06	0.08	0.02	0.04	0.06	0.08
5	E	G	M	M	G	M	M	M
10	E	G	M	M	G	M	M	M
20	E	G	M	M	G	M	M	M
30	E	G	M	M	G	M	M	M
40	E	G	M	M	G	M	M	M
50	G	G	M	M	G	M	M	M

It can be conclude from these three tables that using SU4 truck instead of Type 3S2 can have bad effects of the fatigue life of the bridge. This might be due to the fact that SU4 causes higher stress ranges as a result of having heavy axles located very close to each other. So the third scenario is not a good option.

9.7.2 Reinforced Concrete Deck Fatigue Assessment

According to NCHRP Report 495 [48] and as discussed before, the fatigue of RC decks under different scenarios was evaluated.

In order to calculate the service life of the reinforced concrete decks, the details of the analyses of prestressed concrete bridges with reinforced concrete decks have been used. Similar to the previous section, three scenarios of trucks have been assumed. First, the current traffic recorded from the WIM data in the Wisconsin DOT report [51]. In the second scenario, in order to determine the effects of using heavy vehicles instead of doubling the number of current vehicles, all Type 3S2 vehicles have been replaced by the longer combination vehicle, 9-Axle Turnpike Double which can carry almost twice as much as the Type 3S2 vehicle. In the third scenario, the Type 3S2 vehicles were replaced by single unit SU4 trucks. By using the WIM data and the

vehicle axle weights, the equivalent fatigue load (P) was calculated. Using equation (9-4), the service life of bridge decks and therefore the remaining fatigue life of the RC decks can be calculated. The results for the comparison of the three cases for 30 ft. prestressed concrete bridge, have been shown in Table 9-47 and Table 9-48.

TABLE 9-43: REMAINING FATIGUE LIFE OF THE REINFORCED CONCRETE DECK BASED ON FIRST AND SECOND SCENARIOS

a g	Remaining Fatigue life in years							
	Type 3S2				9-Axle Turnpike Double			
	0.02	0.04	0.06	0.08	0.02	0.04	0.06	0.08
5	81	56	43	36	87	59	46	38
10	80	55	43	36	87	59	46	38
20	79	55	43	36	85	58	45	38
30	78	54	43	36	84	58	45	38
40	77	54	43	36	83	57	45	38
50	76	54	43	36	82	57	45	38

It can be observed from the table above that the second scenario which is the case of using heavier vehicles with higher load capacity in giving more fatigue life comparing to the regular case of using smaller trucks with lower load capacity.

TABLE 9-44: REMAINING FATIGUE LIFE OF THE REINFORCED CONCRETE DECK BASED ON FIRST AND THIRD SCENARIOS

a g	Remaining Fatigue life in years							
	Type 3S2				SU4 Truck			
	0.02	0.04	0.06	0.08	0.02	0.04	0.06	0.08
5	81	56	43	36	74	52	41	34
10	80	55	43	36	73	51	40	34
20	79	55	43	36	72	51	40	34
30	78	54	43	36	70	50	40	34
40	77	54	43	36	69	50	40	33
50	76	54	43	36	68	49	40	33

Also from Table 9-48, one can observe that using single unit trucks such as SU4 can lower the remaining fatigue life of the bridges. As mentioned before, having many axles with small spacing can result in higher stresses on the bridge and the concrete deck which results in shorter fatigue life.

9.8 Summary

This research aimed to investigate the effect of meeting the increase in the freight demand and compare the impact of doubling the number of heavy vehicles versus doubling the vehicle weight limit on the service life of bridges. It focused on a very common US bridge with concrete deck over steel girders.

This goal was achieved by analyzing five steel bridges with spans 30, 60, 90, 120, and 140 ft, RC deck of total thickness 6 in, bottom cover of 1 in, and compressive strength of 3000 and 4000 psi supported on the bridges' girders 8 ft apart. Bridges were subjected to the AASHTO fatigue truck and the site-specific fatigue truck (85 kip). The site-specific fatigue truck is the most frequent truck extracted by processing the WIM data recorded at site 915 at Alabama. Further concern was given to the most common age, 50-years, of the vast majority of bridges.

The finite fatigue life (Y) of the bridges' steel girders and deck were calculated in different traffic conditions. All the analyses were carried out by the AASHTOWare bridge rating program (Virtis) to calculate the effective stress. The first step was to use the current traffic volume and traffic loads as the reference condition. Second, a doubling of the traffic volume (DTV), but keeping the traffic load constant. Third step was by doubling the traffic load (DTL), twice the 85 kip and AASHTO fatigue truck load, but keeping the traffic volume constant. All these scenarios were applied with the changes of the annual growth rate from 2 to 8% and with the increment of 2%, and the bridge present age (a) from 5 to 50 years with an increment of 5 years. Accordingly, the remaining service life (Y_r) of the members were calculated ($Y_r=Y-a$).

9.9 Steel Girders

Generally, for bridges greater than 40 ft, the remaining life of the steel girders decreased with the increase of their present ages. Also, the remaining life decreased with the annual growth rate.

As the fatigue problem is highly probable at connection locations, the study focused on the longer bridges (>40-ft). Because of no member connections, the remaining lives developed for 30-ft-long bridges increased with the increase of the annual growth for older bridges. In addition, the remaining lives developed by the site-specific fatigue truck were less than those developed by the AASHTO fatigue truck. Also, the double-traffic-volume and double-traffic-load scenarios inversely affect the remaining lives of bridges, but doubling the traffic load is the worst case.

9.10 RC Deck

Generally, the compressive strength affects the remaining lives of the RC deck, and the greater the compressive strength, the greater the remaining life. Also, doubling the traffic volume (DTV) has a negative inverse effect on the remaining life of the RC deck as does the DTL scenario, but the DTL scenario creates a severe damage much more than the DTV scenario.

All this means that the traffic volume has less influence on the remaining life of both steel girders and RC deck than that of the traffic load. Therefore, with regard to the stresses and fatigue, doubling the traffic volume is the recommended solution to accommodate the expected increase in freight demand.

10. Cost Impact of Increasing Heavy Vehicle Loads on Bridges

10.1 Introduction

All the heavy vehicle configurations directly affect the safe service life of highway bridge superstructures. Generally, deterioration occurs in the deck and superstructure elements including but are not limited to girders, joints, and diaphragm joints. The damage occurred is a function mainly of construction material and the heavy vehicle's gross weight. Meeting the increasing freight demand means increasing the number of heavy vehicle and/or the total weight of the trucks. Bridge costs associated with both solutions are the result of the accelerated maintenance, rehabilitation, or replacement work that is required to keep the structures at an acceptable level of service [5].

10.2 Literature Review

10.2.1 *Life-Cycle Cost Analysis (LCCA)*

Life-cycle cost analysis (LCCA) is a tool that helps the transportation agencies in assets estimation and management. However the fundamentals of the LCCA were started long time ago, the attention given to this tool was increased in the lately in the United States.

Bridges are considered a long term investment that requires regular and periodic inspection and maintenance. In some cases it needs retrofitting and in other rare cases replacement. The whole life-cycle cost of bridges includes not only the construction cost, but also the expected future activities' cost that should be presented in a cash flow diagram as seen in Figure 10-1. The LCCA helps to maximize the effectiveness of the limited allocated maintenance budget and make a decision with these computed future expenses [52].

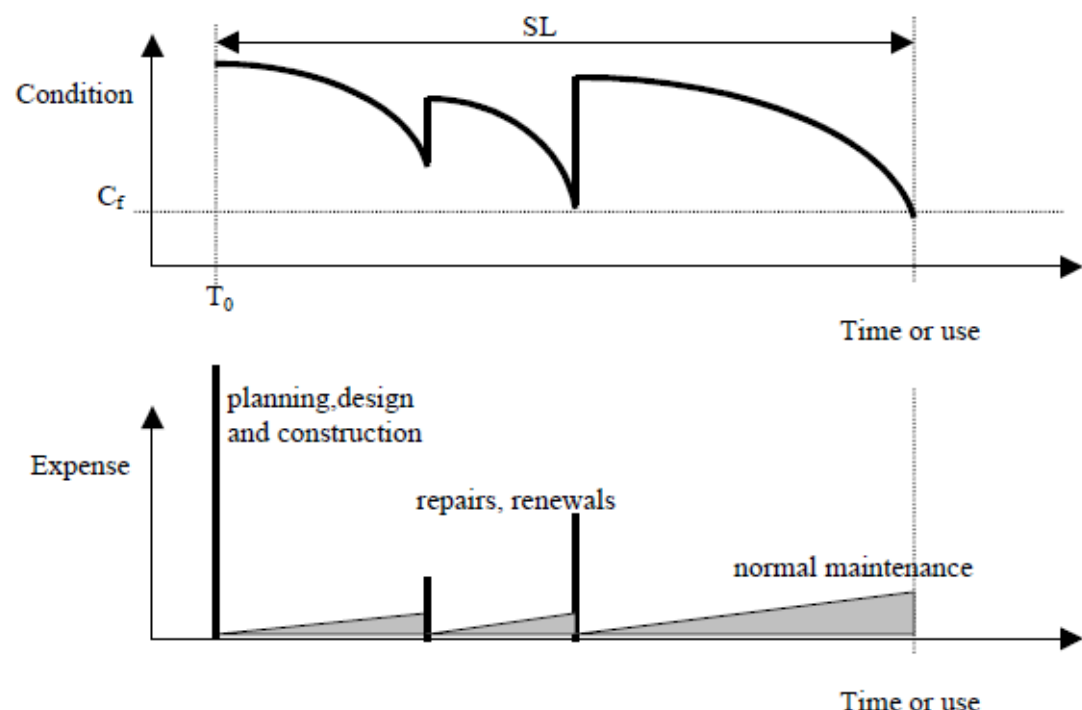


FIGURE 10-1: EXPENSES ACCOMPANYING THE LIFE CYCLE [52]

10.2.2 *Identification of Maintenance Alternatives*

Maintenance activities and alternatives vary based on the characteristic of distress, allocated budget, and local practices of every state. Different alternatives' costs may be classified by the two main partners of the bridge, the agency and the user [52].

10.2.3 Agency Costs

The agency cost includes the cost of maintenance, strengthening, and replacement to keep the bridge at an acceptable level of service. Maintenance costs include the cost of minor activities such as routine inspection, repairs, such as deck replacement, and major activities such as the entire replacement of the bridges. The construction of new bridges is classified as a bridge replacement category. The cost of all of these expected activities should be calculated and recorded for future estimation based on both agency and user costs [52].

10.2.4 User Costs

User costs are associated with the load and speed posting, restrictions, and closure of bridge corresponding to functional deficiencies of the bridge. All these costs must be considered due to detours, increase of travel time and increased accidents rates.

Detouring cost is due to additional vehicle operating cost and the value of the time delay associated with functional deficiency. The detour cost can be estimated if the length of the detour pass is well known. Bridge deficiencies also increase the accidents rate. The crash-type rate is a function of the deficiency type, so the rate of each crash type and the associated cost should be estimated to compute the total expected accident cost [52].

10.3 Truck Weight Effect on Bridge Network Costs

Estimating the cost impact for a specific scenario of truck weight limit change needs to determine the planning period (PP). This period defines the time span during which the cost impact is considered effective. It is recommended that the period to be consistent with the agency's planning period, so that parameters for projecting future data would be readily available. These parameters may include discount rate, traffic

growth rate, and expected funding levels. A 20-year period may be used as the default value for PP, if more specific information is not available to help project a more realistic period [5] . Four cost-impact categories are covered in this research:

- Fatigue of existing steel bridges, as illustrated in 5.2.3
- Fatigue of existing RC decks, as illustrated in 5.2.6
- Deficiency due to overstress for existing bridges,
- Deficiency due to overstress for new bridges.

It should be noted that there are other categories that contribute to the cost impact as a result of truck weight limit changes, such as the fatigue failure of steel expansion joints. However, these costs could be considered less significant relative to those in the four main categories.

10.3.1 Deficiency Due to Overstress for Existing Bridges

As highway bridges are designed according to the current specifications (AASHTO LRFD bridge design specifications) for the design load at the time of design, there may be changes in design with time. Thus, their capacities under different specification limitations may be different in the future.

The load rating expression refers to the load-carrying capacity of highway bridges. According to the AASHTO specifications, there are two load ratings: the inventory rating and the operating rating. The inventory rating indicates the allowed load for bridge safety and is defined at the design stage. The operating rating allows a higher load that may result in reduced safety levels. This rating is used to maximize the use of the bridge and to avoid high costs. However, both load ratings are based on legal loads. Bridges with marginal load ratings may be inadequate if the truck weights increase (maximizing the load legalization). Those bridges are considered to be

deficient under the new higher truck weight limits. For those bridges, agencies may select posting, strengthening, or replacement, and the cost associated with posting and replacement actions should be considered [48].

10.3.2 Deficiency Due to Overstress for New Bridges

This cost-impact category is very similar to the deficiency due to overstress in existing bridges. The bridge design load should include the current and the expected future truck load expected over the lifespan of the bridge. In some obsolete cases, the truck load changes (increases) unexpectedly resulting in the new bridge becomes inadequate. This cost impact category exists to cover those costs associated with possible additional expenditures for new bridges to meet new design requirements as a result of possible truck weight limit change [48].

10.4 Cost Impact Estimating Methodologies of Bridge Networks

All the recommended methodologies for estimating bridge network cost due to truck weight limit changes are identified as per the NCHRP-495 [48].

10.4.1 Fatigue of Existing Steel Bridges (Cat. I)

1. Identify all potentially weak bridges. Grouping the data into N numbers, each group has similar features. Select one (or more) typical bridge(s) in a random way to represent each group. The results will be used to estimate the entire group's cost by multiplication.
2. For Bridge Group $n=1$ (for the typical bridge or each of the typical bridges of this group):
 - a. Develop the truck weight histogram (TWH) and truck volume for the current traffic conditions, which is known as base case, using the available bridge

inventory database and/or available WIM data. Then predict the TWH and truck volume under the alternative scenario.

- b. Compute the remaining mean and safe lives for both the base case and the alternative scenario as given in equation (10-2).
- c. Select one of the offered remedy actions (do nothing, repair, monitor, or replace)
- d. Estimate the cost of action for the typical bridge, according to the selection made in Step 2.c).
- e. Compute the new probability of failure according to the following equations for the pre-selected planning period PP, using the remaining mean and safe lives obtained in Step 2.b).

$$\text{Expected Impact Cost} = \text{Impact Cost} (P_{f,AS} - P_{f,BC}) \geq 0 \quad (10-1)$$

where:

P_f = the Probability of failure or probability of reaching the service life end during PP years.

The subscripts BC and AS respectively denote to the base case and alternative scenarios.

When the AS failure probability is smaller than that of BC, the expected impact cost is set to equal zero.

- f. Compute the expected cost as the product of the cost of action from Step 2.d) and the changed probability of failure from Step 2.e).
- g. Estimate the costs for the group of bridges by multiplying the expected cost for the representative bridge obtained in Step 2.f) by the number of bridges in

the group. If more than one typical bridge is used for the group, average the expected costs for these bridges.

Then multiply this averaged cost by the number of bridges in the group.

3. Repeat Step 2 for Bridge Group $n=n+1$, until $n=N$

4. Add the costs from all bridge groups.

10.4.2 Fatigue of Reinforced Concrete Decks (Cat. 2)

1. Identify all possible weak bridges (on impacted roads and with a reinforced concrete deck supported by beams). Partition them into N groups, each having similar features. Randomly select one (or more) typical bridge(s) representative of each group, whose results will be used to estimate the entire group's cost by multiplication.
2. For Bridge Group $n=1$ (for the typical bridge or each of the typical bridges of this group):
 - a. Generate the wheel weight histogram (WWH) for the base case, using WIM data and the agency's bridge inventory. Then predict the TWH under the alternative scenario. Estimate the remaining mean and evaluation lives for both the base case and the alternative scenario.
 - b. Select a remedy action (e.g. do nothing, patch and overlay with concrete, overlay with concrete, patch and asphalt the concrete overlay, asphalt the concrete overlay, or patch and then replace).
 - c. Estimate the unit cost of action for the selection made in Step 2.b. The unit cost is in dollars per deck area.
 - d. Compute the changed probability of failure for the pre-selected planning period PP using the following equations. The probability of failure is

defined as the probability that the deck reaches the end of service life within the planning period.

$$Expected\ Impact\ Cost = Impact\ Cost \left(P_{f,AS} - P_{f,BC} \right) \quad (10-2)$$

- e. Then compute the expected unit cost for the typical bridge as the product of the changed probability of failure from Step 2.e) and the cost from Step 2.d).
- 3. Estimate the cost for the group of bridges by multiplying the expected unit cost per deck area of the representative bridge obtained in Step 2.f) by the total deck area in the group. If more than one representative bridge is used for the group, average the expected unit costs per deck area first. Then multiply this averaged expected unit cost by the total bridge deck area in the group.
- 4. Go to Step 2 for Bridge Group $n=n+1$, until $n=N$
- 5. Add the costs from all groups.

10.4.3 Deficiency Due to Overstress for Existing Bridges (Cat. 3)

- 1. Identify the criterion for deficiency in the load rating format. Select a rating vehicle model that covers the most severe practical-maximum-truck-loads under the alternative scenario. This model may include several vehicles, depending on the alternative scenario considered. These vehicles should produce the moment envelope for new legal or permit vehicles.
- 2. For each bridge in the network, use available ratings in the bridge inventory, estimate the new load rating factor under the alternative scenario RF_{AS} as follows:

$$RF_{AS} = \frac{RF_{BC}(M_{BC} \text{ rating vehicle}/M_{AS} \text{ rating vehicle})}{AF_{rating}} \quad (10-3)$$

where:

M_{BC} rating vehicle / M_{AS} rating vehicle: is the maximum base case moment to the alternative scenario bending moment of the rating vehicle models, for the critical section. Generic spans may be used for estimation of these maximum moments. Base case refers to conditions *without* the proposed changes in truck weight limits. Alternative scenario refers to conditions *with* the proposed changes in truck weight limits.

RF stands for rating factor and subscripts AS and BC indicates the alternative scenario and base case respectively. The live load adjustment factor for rating AF_{rating} is defined as

$$AF_{rating} = \frac{[2W_{AS}^* + 1.41t(ADTT_{AS})\sigma_{AS}^*]}{[2W_{BC}^* + 1.41t(ADTT_{BC})\sigma_{BC}^*]} \quad (10 - 4)$$

where:

W^* and σ^* are the mean and standard deviation of the top 20% of the TWH, and t is a function of annual daily truck traffic (ADTT) as given in Table 10-1

1. Identify all deficient bridges under the alternative scenario (excluding those already deficient under the base case) according to the results of Steps 1 and 2, these bridges have $RFBC > 1.0$ and $RFAS < 1.0$. The total number of deficient bridges is N.

TABLE 10-1: ADTT AND CORRESPONDING T(ADTT) VALUES [48]

ADTT	t(ADTT)	
	Two or more lanes	One lane
5000	4.3	4.9
1000	3.3	4.5
100	1.5	3.9

3. For Deficient Bridge n=1, then n=n+1, until n=N

- a. Select a suitable responding action such as do nothing, post with weight limit enforcement, strengthen, or replace. The FHWA sufficient rating may also be considered in this decision process.
 - b. Estimate the cost for the responding action selected.
4. Add all costs.

10.4.4 Deficiency Due to Overstress for New Bridges (Cat. 4)

1. Develop the TWH under the base case conditions, and predict the TWH under the alternative scenario of interest for the network. Note that there is only one such TWH for the entire network under the base case and alternative scenarios respectively. For the most part, all roadways of different functional classes will use the same TWH. This is different from cost-impact category-3 where rating requirements with respect to truck load are site dependent or functional class dependent.
2. Determine an adjustment factor for the design load as the ratio of the design live load factors for the base case and the Alternative Case, as follows:

$$AF_{design} = (2W_{AS}^* + 6.9\sigma_{AS}^*)/(2W_{BC}^* + 6.9\sigma_{BC}^*) \quad (10 - 5)$$

W* and σ* are the mean and standard deviation of the top 20 percent of the TWH. BS and AS Subscripts refer to the base case and alternative scenarios respectively.

1. Identify a new design vehicle load model that can cover the most severe truck loads under the alternative scenario. This model can be the practical maximum truck loads under the alternative scenario, and it may include multiple vehicles to envelope maximum moment effects due to new legal and permit vehicles.
2. Identify all bridges to be impacted (to be constructed). The total number of bridges identified is N.

3. For Bridge n=1, use the following procedure to find the cost for the bridge.

- a. Find design load change factor (DLCF) as follows:

$$DLCF = (M_{AS,design\ vehicle})/M_{BC,design\ vehicle}) AF_{design} \quad (10 - 6)$$

$$(M_{AS,design\ vehicle})/M_{BC,design\ vehicle}) \geq 1$$

- b. Based on DLCF, estimate the incremental new bridge cost.

4. Repeat Step 5 for Bridge n=n+1, until n=N

5. Add all costs

where:

$M_{AS,design\ vehicle} / M_{BC,design\ vehicle}$ is the ratio of the maximum moments due to the design vehicle under the base case and the new design vehicle under the alternative scenario, for the critical section. Generic spans can be used for estimation of these maximum moments. This ratio should not be practically less than 1. AF_{design} is the ratio between the live load factors under the base case and the alternative scenarios. It should not be less than 1, either.

10.5 Cost impact Estimating Approach

In this research, a software module developed by NCHRP named (Carris) was utilized to estimate the cost increment of a bridge network due to a change in truck weight limits. Truck weight collectively refers to vehicle gross weight (GVW), axle weights, and axle spacing.

10.5.1 Carris Program Manual [53]

- *General Data*

This methodology is based on the estimation of cost impact of bridge-by-bridge on the network. Thus, all the inventory database needs is required in addition to more data about the alternative decision.

- *Alternative scenario (AS) truck weight histogram (TWH)*

This prediction is performed by identifying expected changes in the TWH under BC. It is performed by a shifting matrix to identify which type of truck loads will shift to which truck load.

- *Cost-impact Category 1 - Fatigue of Existing Steel Bridges (Cat. 1)*

This approach is based on a concept that multiple samples taken from different strata of the entire population can more reliably represent these strata, leading to more realistic results. Thus the software requires the user to define the strata and a sampling rate for each stratum. Then, the program performs random sampling according to these parameters. After the sample bridges are selected, detailed information on the welds of the selected bridges need to be input through worksheets. Weld detail data is put into the software using worksheet “Details” in the “Inventory” file, as shown in Figure 10-2.

Effect of Truck Weight on Bridge Network Costs - NCHRP 12-51									
Details									
Inventory									
Metric units	d_key	d_pkkey	d_location	d_type	d_category	d_count	d_redundant	d_weight	d_inconstr
	D1001	11_0009	1	B1	E	69	1	25.19	2.90
	D1002	11_0009	2	B4	Ep	1	0	10.14	1.10
	D1002	11_0009	3	B5a	E	1	1	9.65	2.90
	D1002	11_0009	4	B4	E	2	0	20.03	2.90
	D1003	11_0011	1	B5a	E	1	1	39.19	2.90
	D1004	11_0011	2	B5a	Ep	1	0	9.26	1.10
	D1005	11_0012	1	B1	E	1	1	6.05	2.90
	D1006	11_0012	2	B4	Ep	1	0	1.10	
	D1007	11_0013	1	B5a	Z	1	1	5.13	0.00
	D1008	11_0013	2	B1	E	1	1	5.90	2.90
	D1009	11_0017	1	B1	Ep	1	1	4.66	1.10
	D1010	11_0017	2	B4	Z	1	0	11.21	0.00
	D1011	11_0018	1	B5a	E	1	1	6.74	2.90
	D1012	11_0018	2	B5a	Ep	1	0	17.21	1.10

FIGURE 10-2: WORKSHEET “DETAILS” TO INPUT WELD DETAIL DATA FOR SAMPLED BRIDGES [53]

- *Cost-impact Category 2 - Fatigue of RC Decks (Cat. 2)*

Similar to the case of steel fatigue in category-1, random sampling must be stratified.

Worksheet “Cat 2 Sampling” in the “Inventory” file performs the sampling according to stratifying requirements input by the user through that worksheet. All the deck details data is to be listed in the worksheet “Decks” in the “Inventory” file as shown in Figure 10-3.

FIGURE 10-3: WORKSHEET “DECKS” TO INPUT DECK DATA FOR SAMPLED BRIDGES [53]

- *Cost-impact Category 3 - Deficiency of Existing Bridges (Cat. 3)*

Increasing the heavy vehicle load on bridges will have an impact on the relative balance between the bridge’s available strength and the loads to which that bridge will be subjected. This balance is conceptually reflected in the load rating. Thus, more bridges in the network may become inadequate resulting in a load rating lower than the required level. The costs to address this increased inadequacy are covered in this cost impact category. The criteria used in this methodology to judge adequacy are consistent with the AASHTO load rating requirements. Figure 10-4 shows all needed information for a typical bridge in the inventory database.

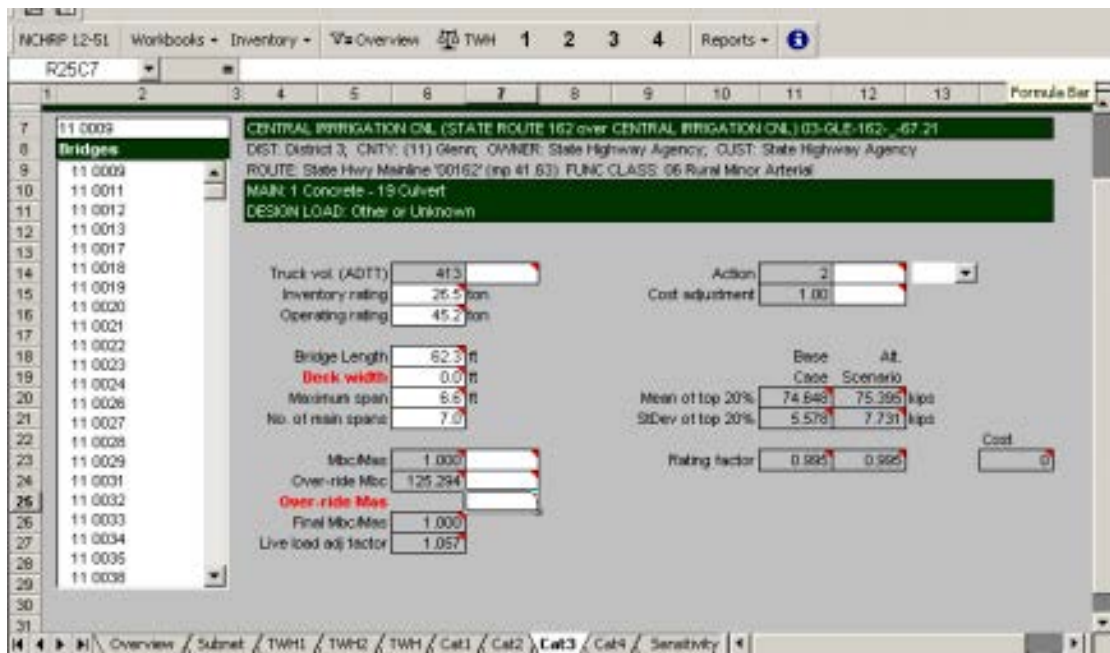


FIGURE 10-4: WORKSHEET “CAT. 3” FOR DATA INPUT AND LOAD RATING CALCULATION [53]

- *Cost-impact Category 4 - Deficiency due to Overstress for New Bridges (Cat. 4)*

Similar to the case of deficiency of existing bridges, inadequacy may be caused by weight limit change. If the same design load is used for designing new bridges in AS the new bridges could become inadequate. Thus, the bridge design load needs to be adjusted accordingly. Of course, the cost increments for new bridges can be very different from those of existing bridges. This is because the incremental cost for increasing strength of a new bridge is usually small if the bridge has not yet been constructed. On the other hand, strengthening an existing bridge, even for a small amount of increase, can be very costly if such technique is available. This cost category covers the incremental costs for new bridges due to increase in design load resulting from truck weight limit change, see Figure 10-5.

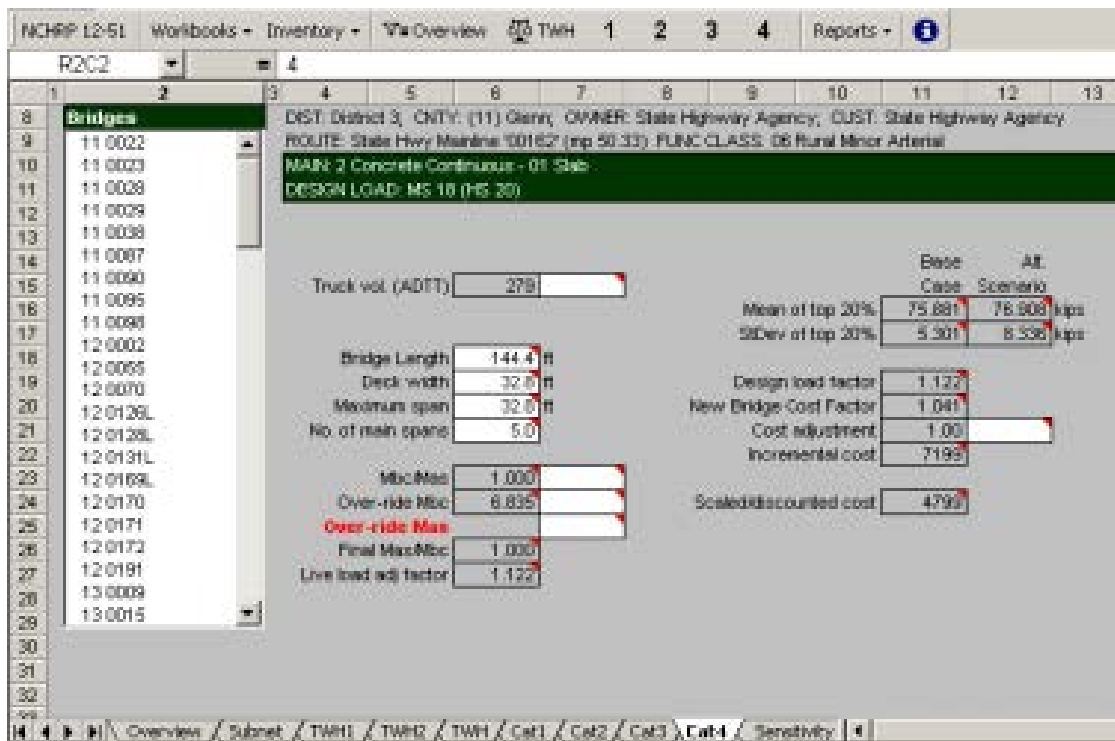


FIGURE 10-5: WORKSHEET “CAT4” FOR DATA INPUT AND DESIGN LOAD CHANGE FACTOR CALCULATION [53]

10.6 Bridges Whole Life Cycle Cost and Bridge Management

The terminology that deals with the bridge's activities starting from the planning stage thru the design, operation, and maintenance, is known as “Bridge management”. The effect of the Bridge life-cycle cost analysis (BLCCA) is important for bridge management. It is one of the reoccurring factors affecting the bridge sustainability and life. For example, spending more in painting of steel bridges using durable material during initial construction, is costly but it reduces the anticipated frequency of future repairing [52]. Figure 6-6 illustrates the process and basic steps of a BLCCA.

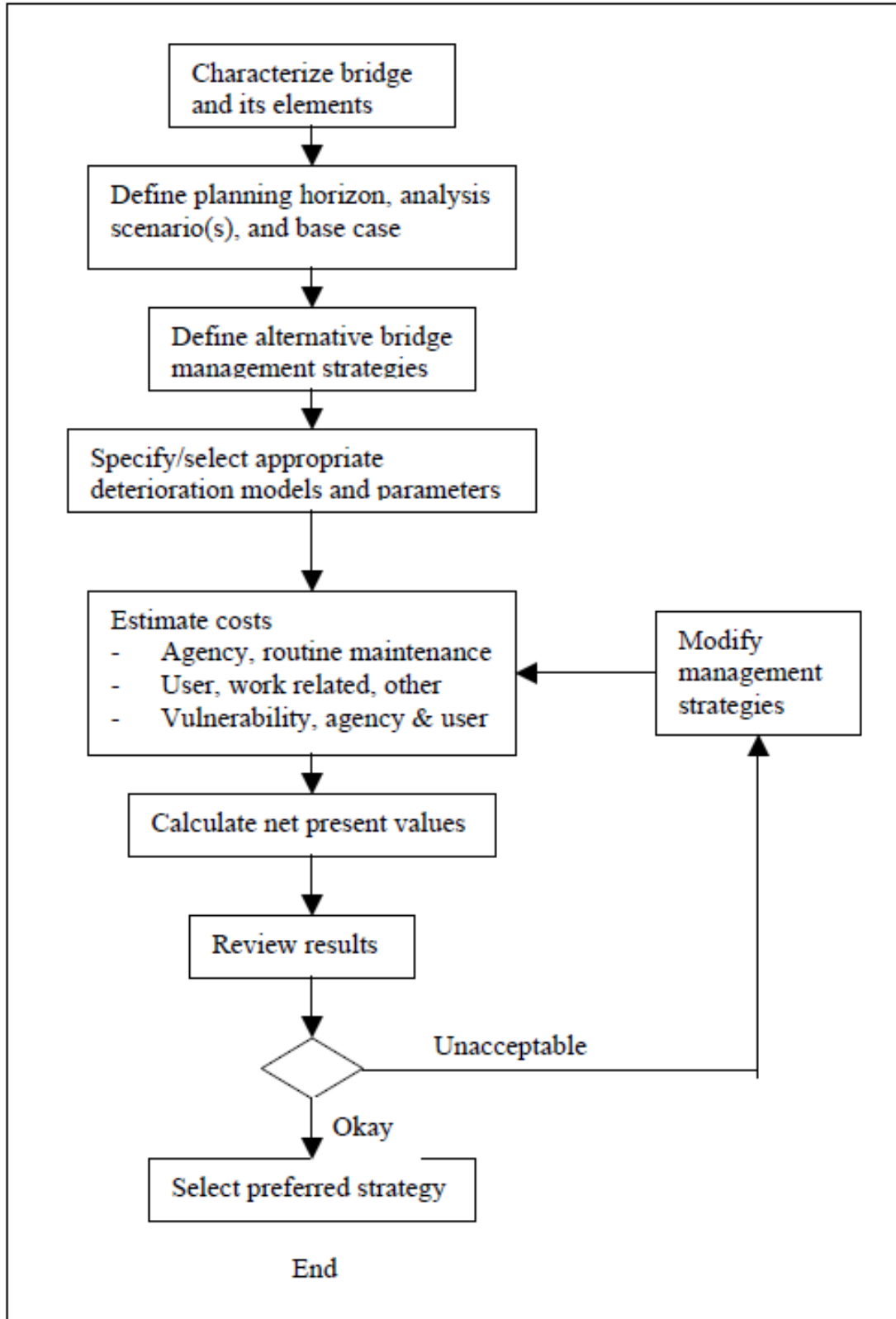


FIGURE 10-6: THE BLCCA PROCESS FLOW CHART [52]

Cost-competent maintenance and management of civil infrastructure requires balanced consideration of both the structure's performance and the total cost accrued over the entire life-cycle of a bridge. The whole life cost of a bridge consists of the total monetary investment throughout the life of the bridge. This investment includes the initial construction cost, repair and rehabilitation costs, and all maintenance costs. Estimating the whole life cost of a bridge will help in making better decisions about the design and construction of new bridges, and in choosing better methods and approaches for rehabilitating existing structures. The schematic diagram of the effects of a time-based maintenance action on the structure's performance and rehabilitation cost for different repair actions may be depicted in Figure 10-7[48].

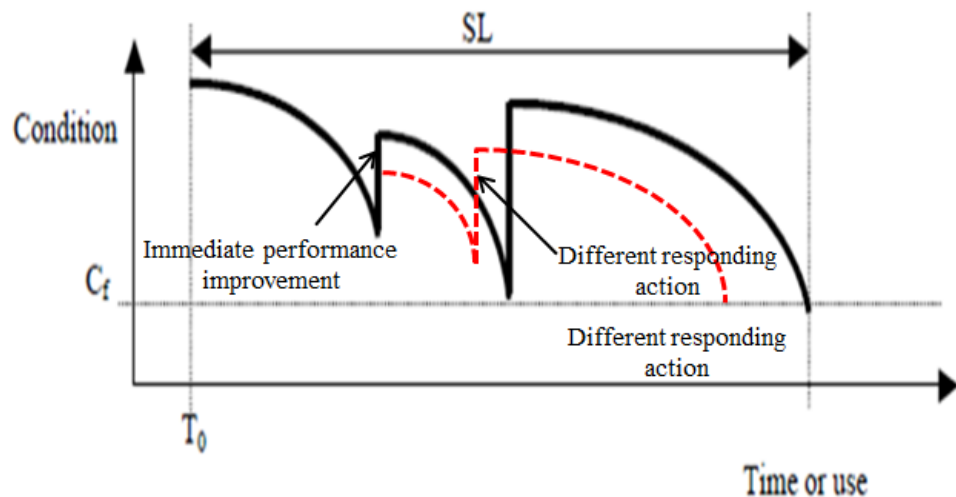


FIGURE 10-7: SCHEMATIC REPRESENTATION OF SAFETY MANAGEMENT METHODOLOGY ALONG WITH MAINTENANCE COST IMPACT

10.7 Truck Weight Limit Change Cost Impact – Case Study

To investigate the bridge cost impact of doubling the current traffic load and/or doubling the traffic volume to meet the increase in freight demand, the State of Michigan average daily traffic database for year 2001 has been used as a case study.

For this case study, the design truck load was HS25 not HL93. The *Carris* program was utilized to calculate the cost impact of both scenarios on the four expected categories [48].

As per the database for year 2001, there are 12,400 bridges in Michigan, so the study was applied to selective bridges based on a stratified random sampling approach. The selection was done based on the construction material and age of the bridge, so steel bridges with concrete deck and 50 year of age or less were studied. This data was classified based on the functional classes provided by FHWA as seen in Table 10-2. The database includes the most common types of vehicles in the state as shown in Figure 10-8 [48].

TABLE 10-2: FUNCTIONAL CLASSIFICATION SYSTEM

Rural Functional class	Urban functional class
Rural interstate	Urban interstate
Rural other principal arterial	Urban Fwy/Expwy
Rural minor arterial	Urban other principal
Rural major collector	Urban arterial
Rural minor collector	Urban collector
Rural local	Urban local

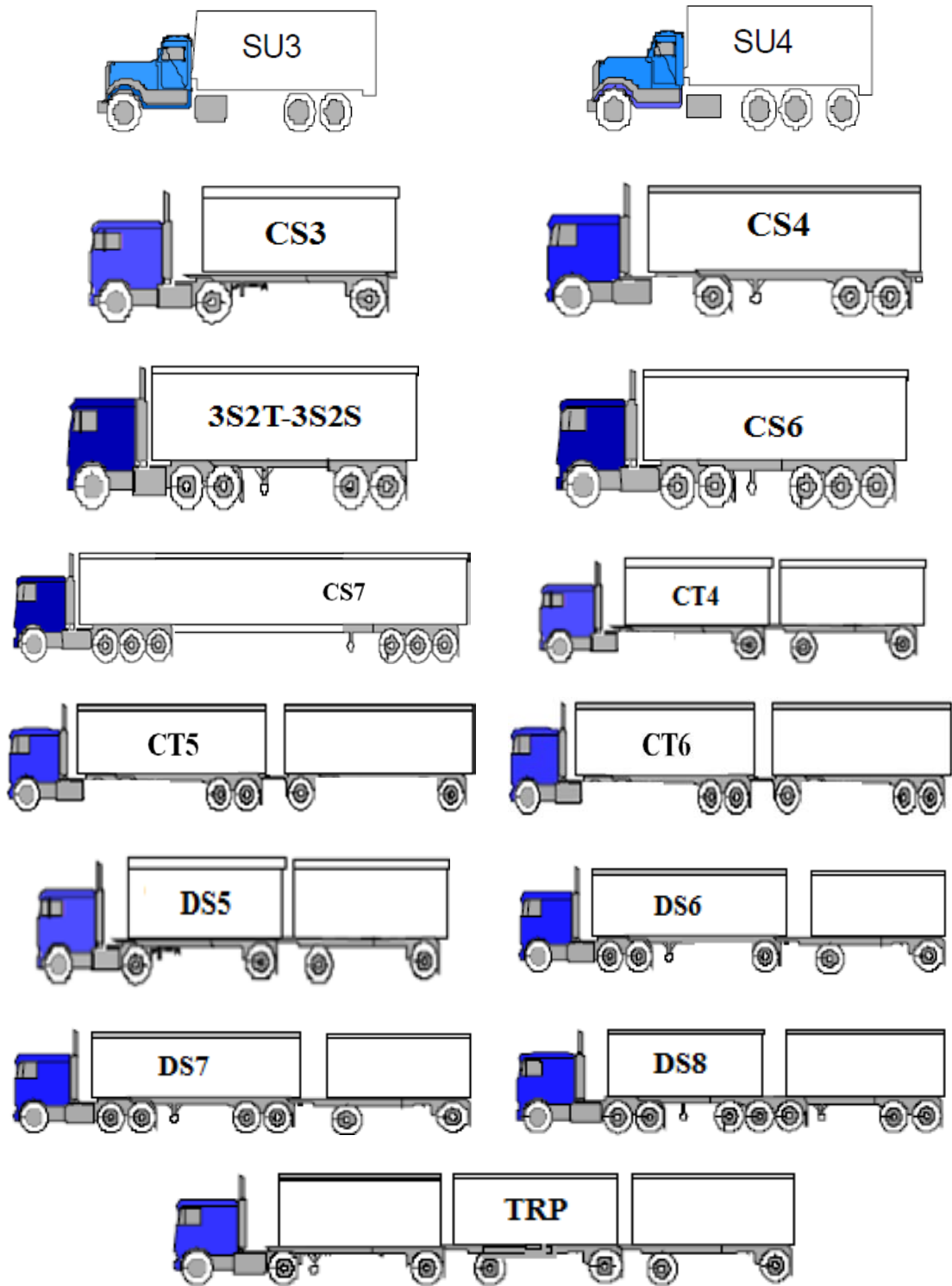


FIGURE 10-8: VEHICLE CLASS DEFINITIONS

10.7.1 General Factors and Parameters

In general, some factors and parameters need to be predefined as defaults in order to run the program, such as customary units, discount rate of cost, annual growth rate, and the truck traffic percentage. Thus, the customary unit was set equal to 1 to use the US units and respectively, the discount rate in cost calculation and the annual growth (g) was set equal to 0.03 and 3%. The entire given inventory data represents the base case (BC) of the average daily traffic (ADT), so the truck percentage was set equal to 5 to calculate the ADTT. To cover the dynamic effect of truck, the impact factor (I) was set to 1.3. For fatigue calculation of the RC deck, the tire print area (length and width respectively) was set to 80 and 20 in.

For the State of Michigan, the cost rates and values for different cost-impact categories were set as shown in Figure 10-11. That chart illustrates the cost associated with each category and the expected remedy action under each cost-impact category. The E and E-prime in the block “Fatigue Detail Types and Repair Costs” represent costs for the welding type of connection [53].

10.7.2 Typical Truck Characteristics

Based on the approach presented earlier in 2.4, the TWH of the entire functional classes of the BC data was developed. Figure 6-9 and Figure 6-10 respectively, show samples of the truck weight histogram (TWH) of the database for rural and urban functional classes. That illustrates that the 3S2T truck type (80 kip) is the most prevalent-heaviest truck. Thus, primary focus was placed on this truck in both scenarios to meet the increase in freight demand. Figure 10-11 illustrate the 3S2T truck configurations.

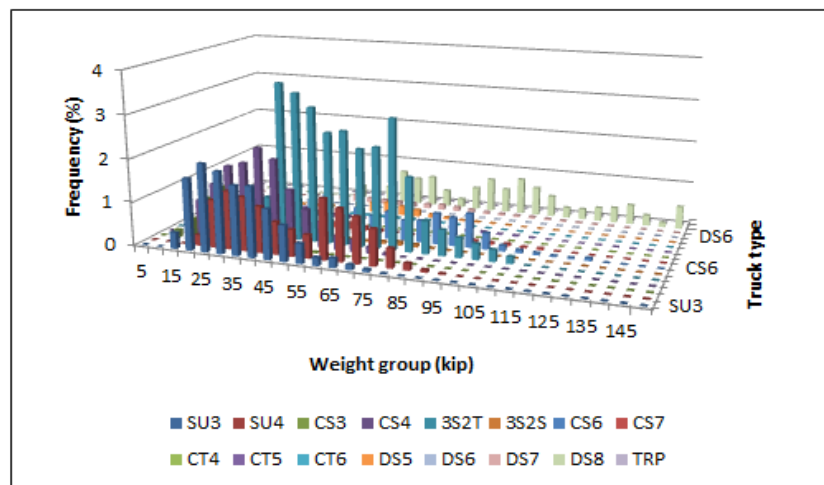
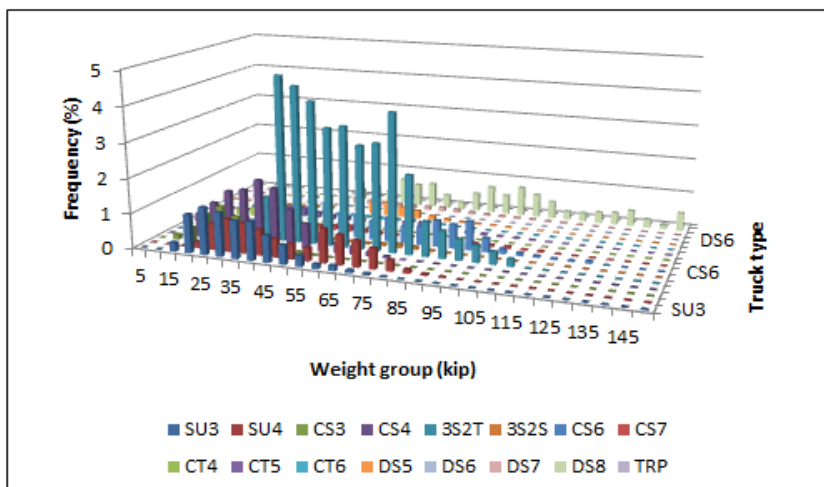
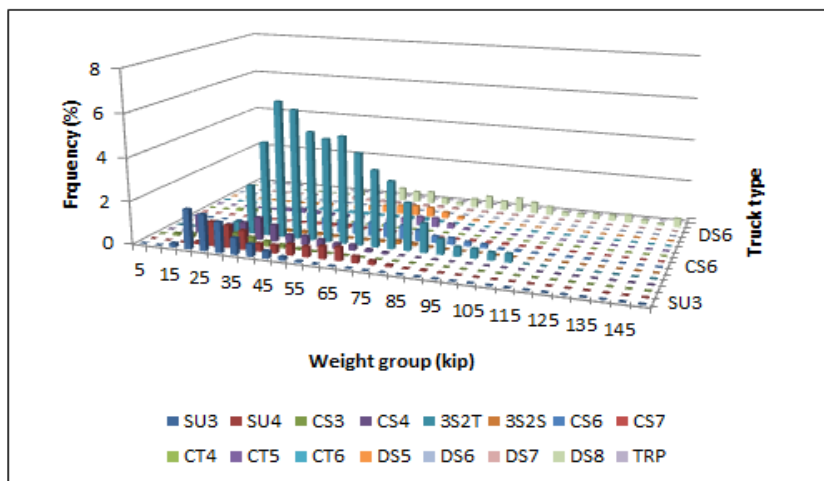


FIGURE 10-9: TWH FOR SOME RURAL FUNCTIONAL CLASSES (RURAL INTERSTATE, RURAL OTHER PRINCIPAL ARTERIAL, AND RURAL MINOR ARTERIAL)

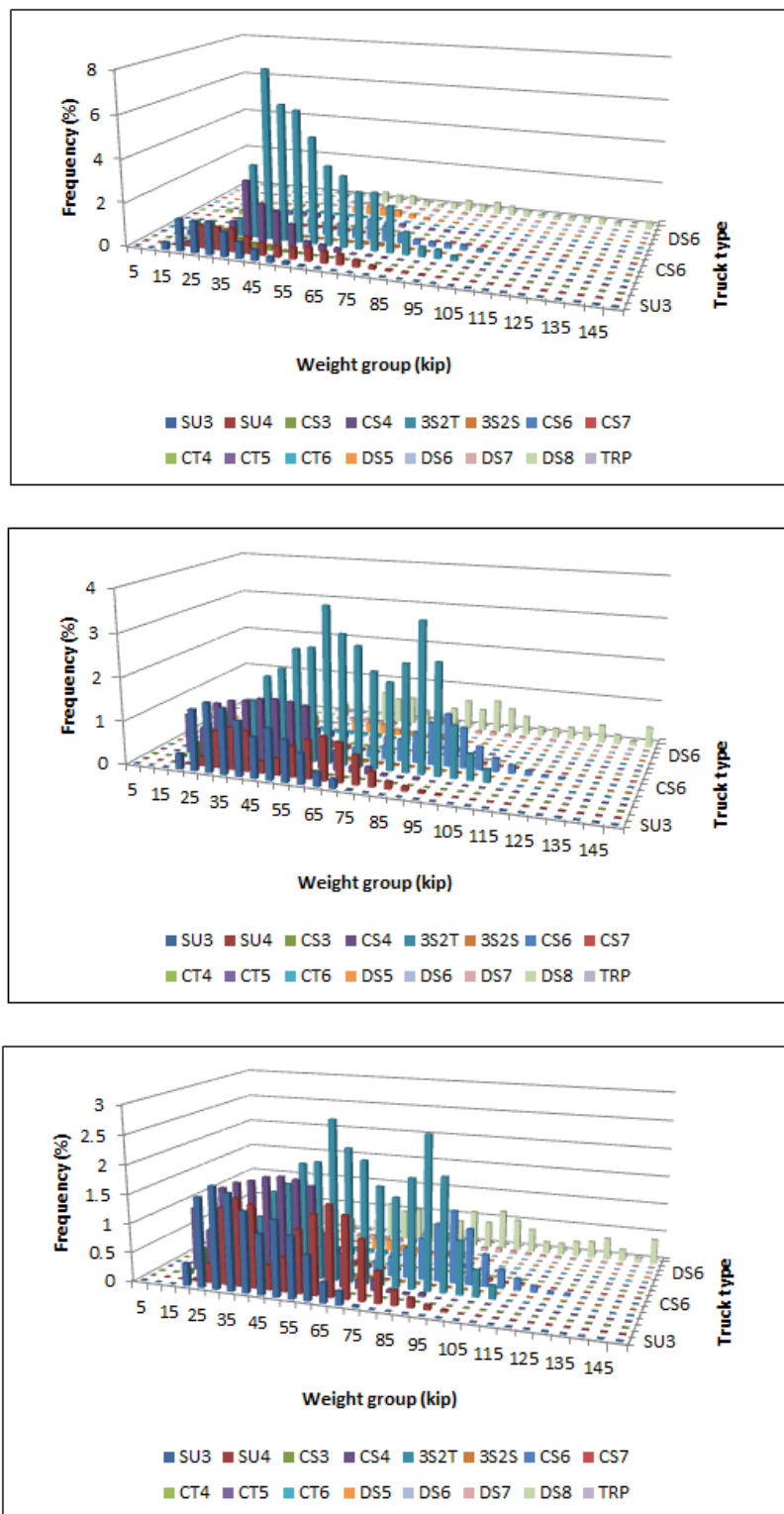


FIGURE 10-10: TWH FOR SOME URBAN FUNCTIONAL CLASSES (URBAN INTERSTATE, URBAN FWY/EXPWY, AND URBAN OTHER PRINCIPAL)

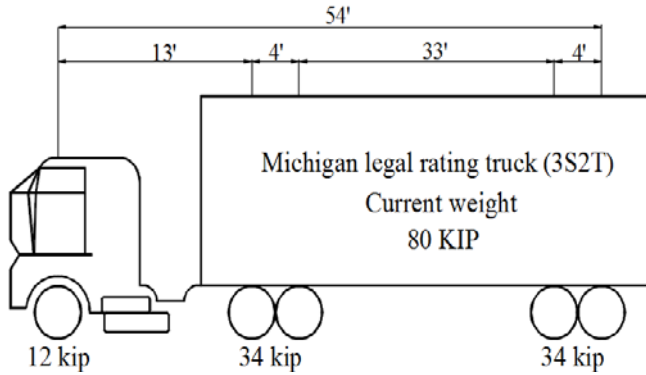


FIGURE 10-11: MICHIGAN MOST PREVALENT TRUCK

10.7.3 Sampling and Stratifying

The inventory data of the State of Michigan represents the traffic for year 2001 for 16 different truck types and 12,400 bridges. This huge amount of data was sampled to represent the four cost-impact categories.

- *Category 1*

Several criteria are represented in the program to help the user stratify the data such as owner, year of construction, construction material, structural system, and maximum span. Since category 1 represents the fatigue failure of steel bridges, only the steel bridges built in years 1950, 1960, 1970, and 1980 were considered in the category 1 cost-impact study. These preconditions result in the selection of only 5,672 bridges out of the total number of state bridges, and of these bridges, only 14 were selected randomly.

- *Category 2*

Michigan is one of the states that use a large amount of salt for deicing. Salt accelerates the corrosion of steel reinforcement and RC deck deterioration. This approach does not account for the effect of steel corrosion on the RC deck fatigue. However, only two bridges of RC deck, with a compressive strength of 3.0 ksi and total thickness range 6.0 to 7.0 in. were considered for calculation. The selection

criteria are different, and only the steel bridges with RC deck were selected. Moreover, a random selection was applied. The same 14 bridges as in category 1 were selected.

- *Category 3*

This category covers the cost impact resulting from the expected additional bridge deficiency caused by the doubling of the traffic load and/or traffic volume. For this category, all Michigan's bridges were considered. The operating load rating was set equal to 1 which means that all the load ratings greater than or equal to 1 are taken as adequate ratings with no deficiencies and no respond actions. These conditions call for all bridges in the state to be considered.

- *Category 4*

This category covers the cost impact due to the change of the design criteria for the new bridges. The change of the design criteria does not depend on the functional classes, so all functional classes were considered in the calculations. The analysis for this category needs to identify a sample of new bridges representing future new bridges. This can be done by defining a year that represents a base year, so that all bridges built in that year or later will be defined as new bridges. This is based on the assumption that the type and size of new bridges to be built in the next 20 years will be similar to those built in recent years. In this case, the base year was set as 2000. This means that all the bridges built during that base year would act as an estimate of annual bridge construction including all the associated costs.

10.7.4 Current Traffic Conditions – Base Case (BC)

In this case, the current traffic conditions were maintained with no changes to check the current status of the being considered bridges and decks. Based on the BC

conditions, only the cost-impact category 3 was affected. In case of applying the operating conditions, only one bridge was affected in cost-impact category 3. The costs associated with the BC are shown in Table 10-3.

TABLE 10-3 :COST IMPACT FOR DIFFERENT RESPONDING ACTIONS - BC

Cost-impact category	Cost impact (\$) – Responding action		
	Posting	Strengthening	Replacement
Category-3	4,656	75,040	348,636

- *Mean Remaining Life*

The stress ranges developed by the *Carris* program were captured and recorded. Next, the fatigue-I stress ranges were calculated and compared with the stress threshold. The vast majority of the considered bridges' fatigue-I stress level were less than the stress threshold which declares that the fatigue lives of those bridges is infinity. However, the fatigue-II stress was calculated and plugged into the equation (12-2) to compute the remaining life as shown in Table 13-4. This table also shows the remaining life of the RC deck produced by the program.

TABLE 10-4: STRESS RANGE AND REMAINING LIFE AT BC

Bridge ID	(Δf) ksi	(Δf) _{TH} ksi	(Δf) _I ksi	(Δf) _{II} ksi	Remaining life -Year	
					Steel	RC Deck
1	3.09	5	4.63	2.32	107	75
2	3.28	5	4.92	2.46	154	226
3	2.64	5	3.97	1.98	203	185
4	2.64	5	3.97	1.98	109	171
5	2.26	5	3.4	1.7	238	769
6	3.07	5	4.61	2.3	68	-23
7	1.14	3	1.71	0.86	174	92
8	1.19	3	1.78	0.89	153	599
9	1.84	5	2.76	1.38	257	53
10	3.25	5	4.88	2.44	167	78
11	1.85	3	2.77	1.38	233	203
12	1.86	3	2.79	1.39	51	-17
13	3.11	5	4.66	2.33	218	96
14	3.72	5	5.58	2.79	84	27

10.7.5 Double Traffic Load (DTL) – Alternative Scenario (AS1)

The cost impact was calculated during a planning period equaling 20 years for all the proposed response (remedy) actions for each cost impact category. The calculation included increasing (doubling) the prevalent truck GVW (3S2T) from 80 kip to 160 kip. The TWH of the AS1 was similar to that of the current traffic conditions because of no changes in the truck traffic volume. The current traffic condition case was considered as the base case

Based on the sampling criteria and the applied AS, cost impact affects nine bridges in category 1, two bridges in category 2, and 100 bridges in category 3. For category 4, based on the sampling criteria, only seven bridges were expected to be affected. Accordingly, the average cost impact was calculated to estimate the total cost impact

during the planning period (PP=20). Figure 1012 shows the cost impact of different cost-impact categories based on the proposed responding action, where the responding actions of each cost impact category are as follow:

1 Cat.1 = Repair,

2 Cat.1 = Replacement,

1 Cat.2 = Patch and concrete overlay,

2 Cat.2 = Concrete overlay,

3 Cat.2 = Patch and asphalt the concrete overlay,

4 Cat.2 = Asphalt the concrete overlay,

5 Cat.2 =Patch and deck replace,

1 Cat.3 = Post with weight limit enforcement,

2 Cat.3 = Strengthening,

3 Cat.3 = Replacement.

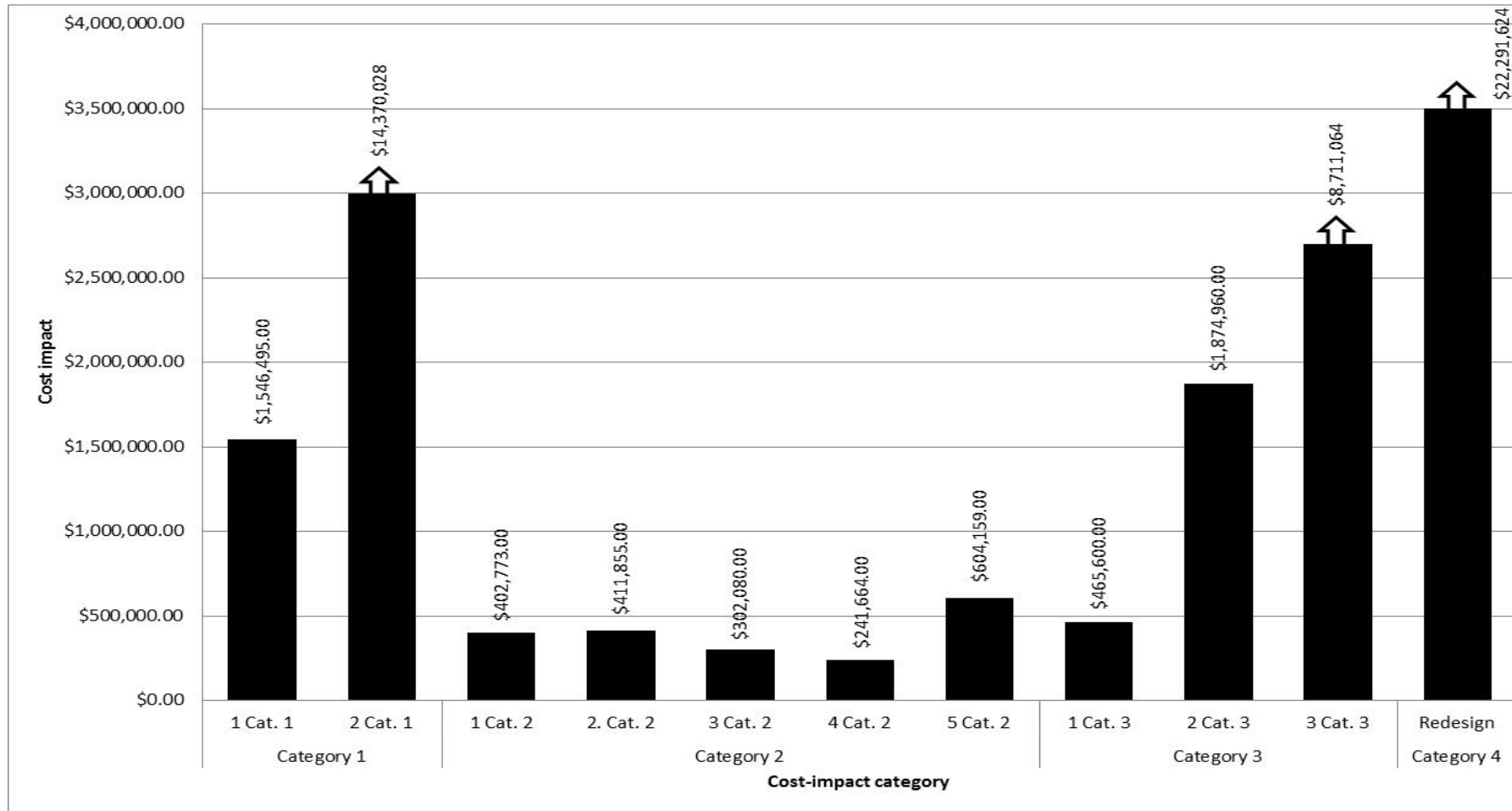


FIGURE 10-12: COST-IMPACT CATEGORIES WITH DIFFERENT RESPONDING ACTION – AS1

- *Sensitivity Analysis*

This analysis provides a tool to examine the effect of the ADTT and annual growth rate changes on the cost impact estimation. Both parameters affected only the cost-impact category 1 and category 2 as shown in Figure 10-13 and Figure 10-14. Originally, the annual growth rate was set equal to 3% and the truck traffic percent was set equal to 5%. These figures show the effect of changes of both parameters by ($\pm 50\%$) in both categories.

Figure 10-13 illustrates the direct proportional relationship between the cost-impact category-1 and category-2 and the ADTT changes. But, Figure 10-14 shows that the annual growth rate is directly proportional to cost-impact category 1 but inversely proportional to cost-impact category 2.

- *Mean Remaining Life*

The developed stress range by the Carris program and the corresponding stress threshold of each connection type were recorded. Consequently, fatigue-I and fatigue-II were computed. Using equation (8-2) and the current bridge age, the remaining life of each bridge was computed as shown in Table 10-5. The RC deck mean remaining life developed by the Carris program is also shown.

10.7.6 Double Traffic Volume (DTV) – Alternative Scenario (AS2)

The second alternative scenario (AS2) to meet the increase in freight demand is to increase (double) the number of prevalent truck (3S2T). In this case (AS2), the cost impact was estimated under the same sampling criteria as AS1. The AS2 TWH samples are illustrated in Figure 10-15 and Figure 10-16. In this case, the TWH is

changed due to the doubling of the most frequent truck numbers with no changes in the GVW.

With no changes in the GVW, the stress ranges developed in case AS2 equal those developed in the base case and the calculated difference in failure probability between both cases is zero. Accordingly, only cost-impact category 3 was affected by AS2. Only one bridge was affected. Consequently, the average cost impact was calculated to estimate the total cost impact in the planning period (PP=20). Table 6-6 shows cost impact due to the deficiency of the existing bridges (Cat. 3).

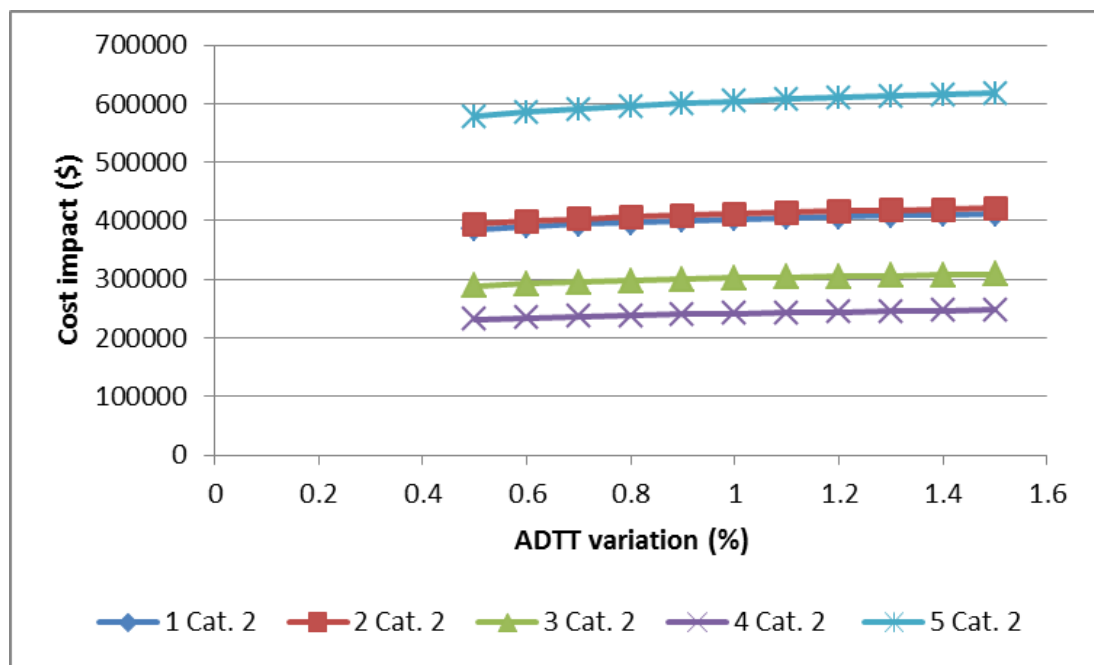
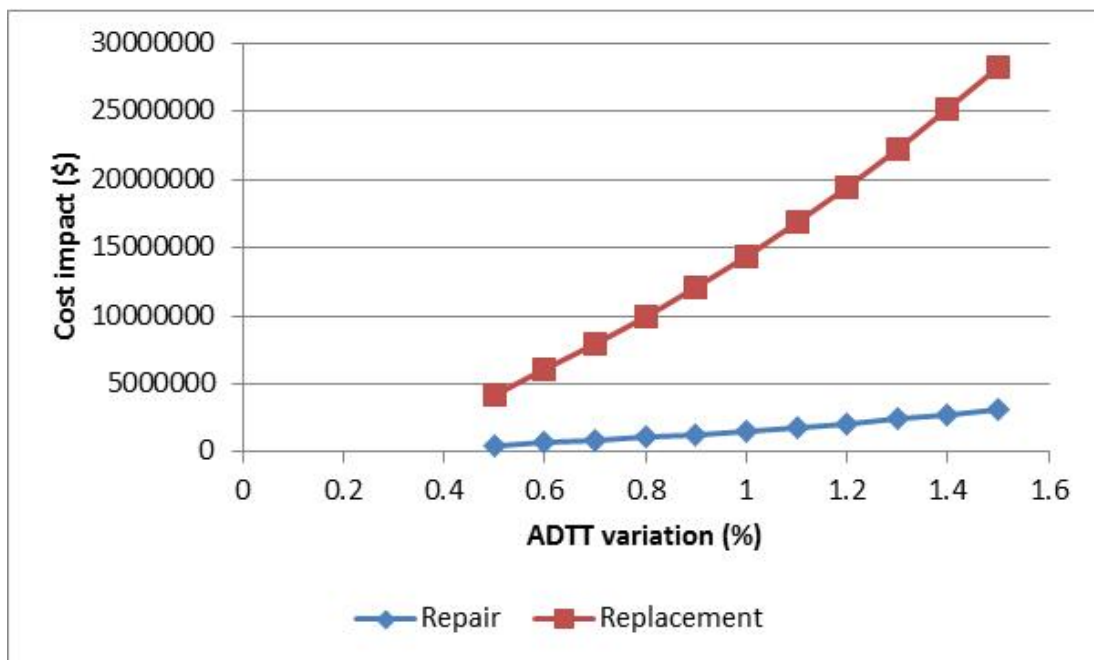


**FIGURE 10-13: SENSITIVITY ANALYSIS OF ADTT ON COST-IMPACT
CAT. 1 AND CAT. 2 – AS1**

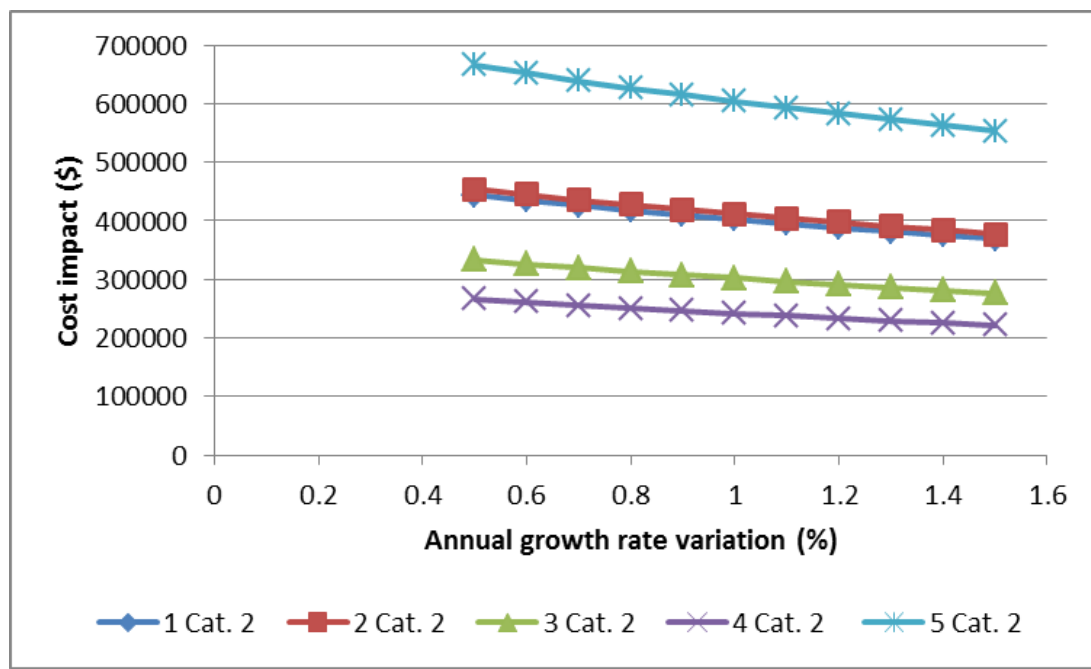
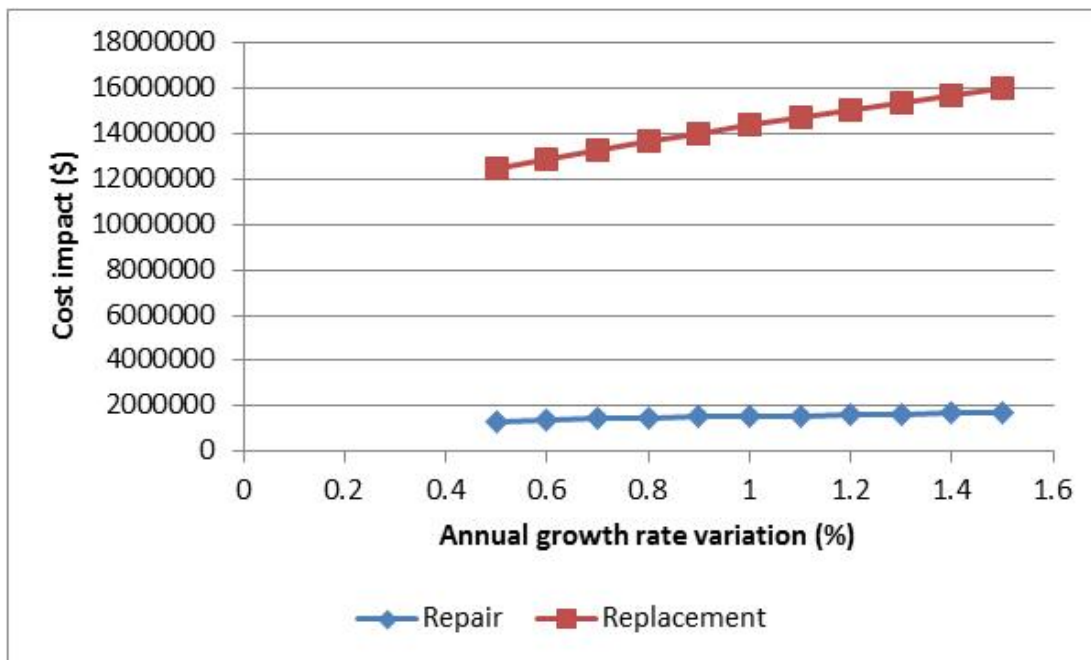


FIGURE 10-14: SENSITIVITY ANALYSIS OF (G) ON COST-IMPACT CAT. 1 AND CAT. 2 - AS1

TABLE 10-5
Stress range and remaining life at AS1

Bridge	(Δf)	(Δf)TH	(Δf)I	(Δf)II	Remaining life - Year	
ID	ksi	ksi	ksi	ksi	Steel	RC Deck
1	6.18	5	9.27	4.64	40	-18
2	6.56	5	9.84	4.92	85	112
3	5.29	5	7.94	3.97	133	-17
4	5.29	5	7.94	3.97	42	-18
5	4.53	5	6.8	3.4	167	433
6	6.15	5	9.22	4.61	8	-33
7	2.29	3	3.43	1.72	104	-10
8	2.38	3	3.56	1.78	83	49
9	3.68	5	5.52	2.76	186	-14
10	6.51	5	9.76	4.88	98	29
11	3.7	3	5.54	2.77	163	126
12	6.42	3	9.63	4.82	-3	-29
13	6.22	5	9.32	4.66	148	15
14	7.44	5	11.16	5.58	21	-19

- *Sensitivity Analysis*

Since the category 3 represents the deficiency due to overstress of existing bridges, neither the ADTT nor the annual growth rate affected the cost-impact category 3.

- *Mean Remaining Life*

The developed stress range by the Carris program and the corresponding stress threshold of each connection type were recorded. Consequently, fatigue-I and fatigue-II were computed. Although the vast majority of the developed stress ranges in the BC and the AS2 were less than the stress threshold, all the recorded values were plugged into equation (12-2) to calculate the remaining life of each bridge as shown in

Table 10-7, which also shows the RC deck mean remaining life developed by the Carris program.

TABLE 10-6: COST IMPACT FOR DIFFERENT RESPONDING ACTIONS – AS2

Cost-impact category	Cost impact (\$) – Responding action		
	Posting	Strengthening	Replacement
Category-3	4,656.00	75,040.00	348,636.00

TABLE 10-7: STRESS RANGE AND REMAINING LIFE AT AS2

Bridge ID	(Δf)	(Δf)TH	(Δf)I	(Δf)II	Remaining life - Year	
	ksi	ksi	ksi	ksi	Steel	RC Deck
1	3.09	5	4.64	2.32	84	33
2	3.28	5	4.92	2.46	131	192
3	2.64	5	3.96	1.98	179	87
4	2.64	5	3.96	1.98	86	100
5	2.26	5	3.39	1.7	214	667
6	3.07	5	4.61	2.3	46	-28
7	1.14	3	1.71	0.86	151	64
8	1.19	3	1.79	0.89	129	431
9	1.84	5	2.76	1.38	233	32
10	3.25	5	4.88	2.44	144	63
11	1.85	3	2.78	1.39	210	180
12	3.21	3	4.82	2.41	31	-23
13	3.11	5	4.67	2.33	195	69
14	3.72	5	5.58	2.79	62	9

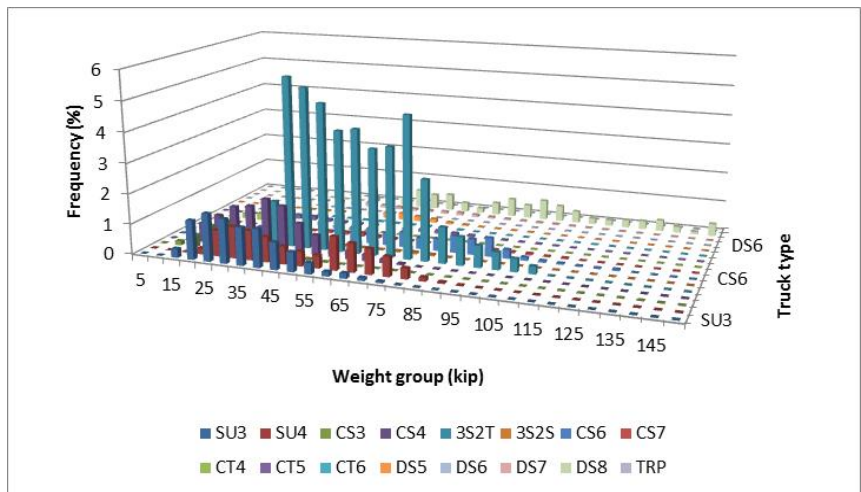
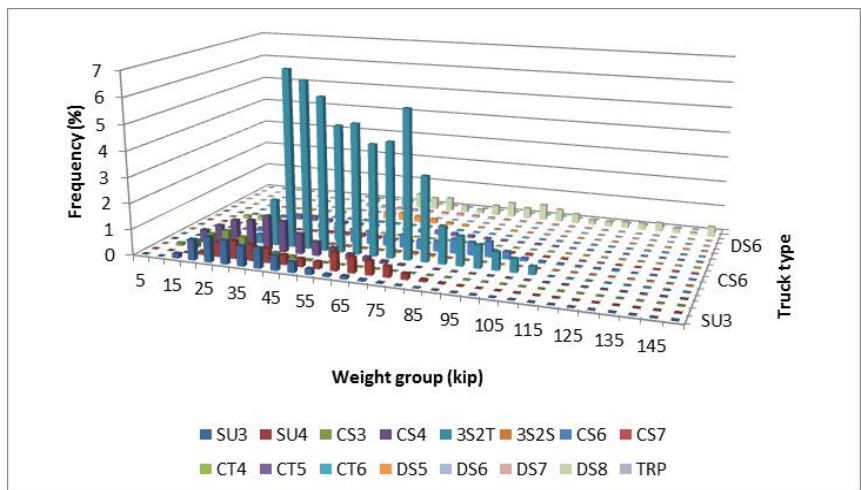
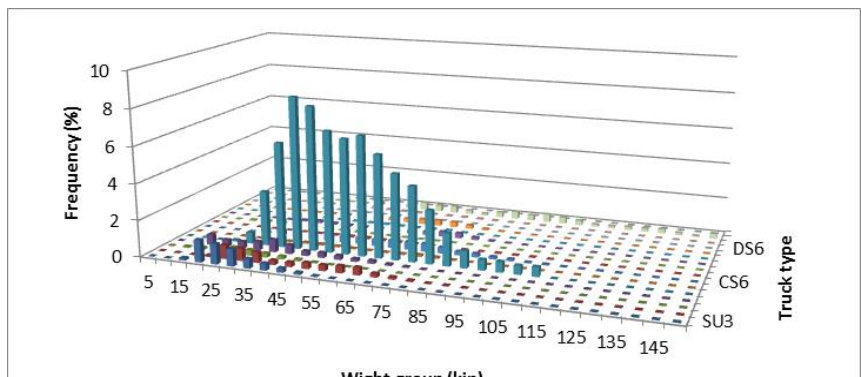
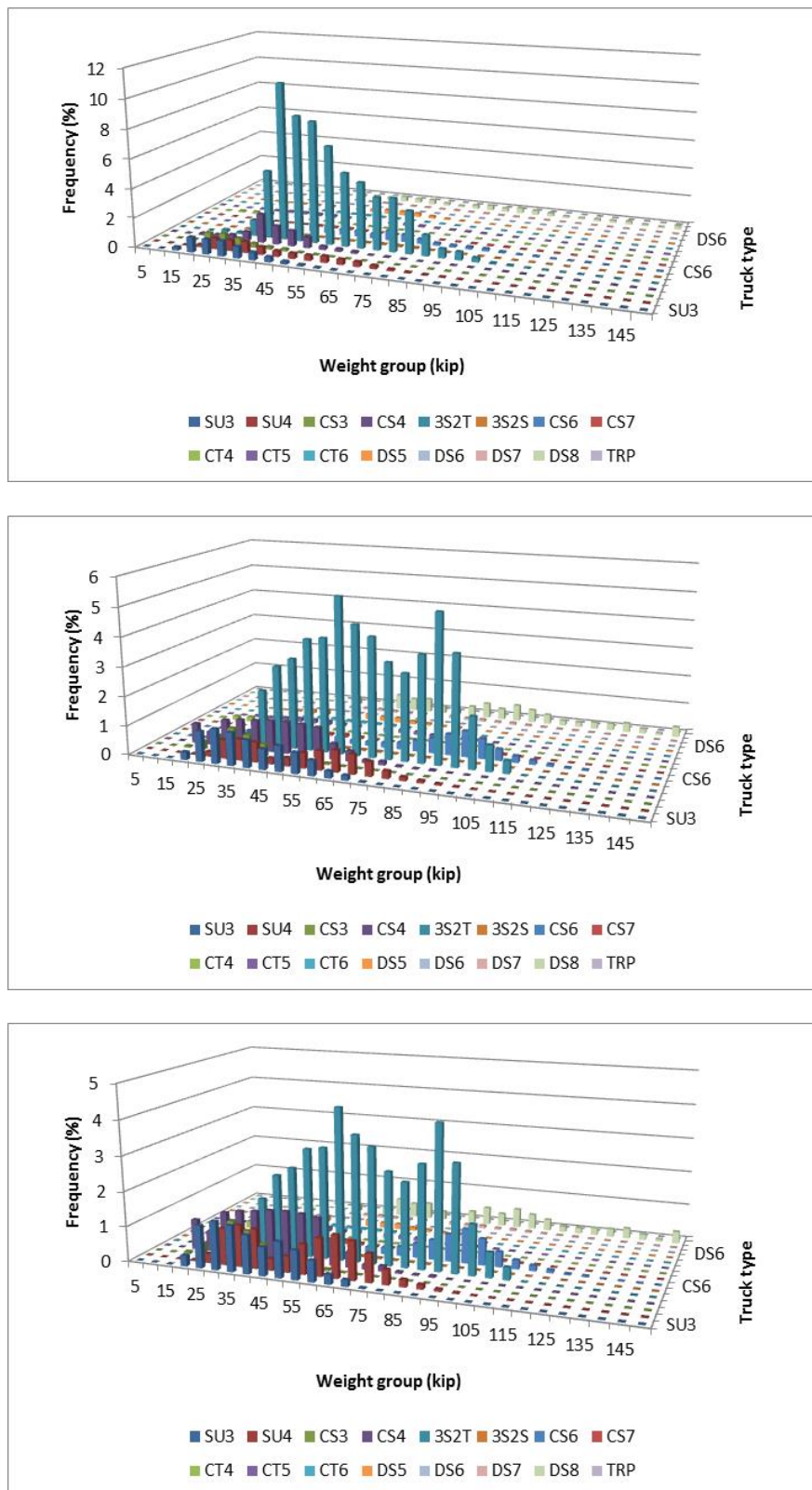


FIGURE 10-15: DTV TWH FOR SOME RURAL FUNCTIONAL CLASSES (RURAL INTERSTATE, RURAL OTHER PRINCIPAL ARTERIAL, AND RURAL MINOR ARTERIAL)



**FIGURE 10-16: DTV TWH FOR SOME URBAN FUNCTIONAL CLASSES
(URBAN INTERSTATE, URBAN FWY/EXPWY, AND URBAN OTHER
PRINCIPAL)**

Proposed 97-kip Truck - Alternative scenario (AS3)

Another alternative scenario was proposed to meet the increase in freight demand.

This scenario replaces the five-axle truck of 80 kips (3S2T AND 3S2S) by a proposed six-axle truck of 97-kip (97-A and 97-B). The proposed truck configurations are shown in Figure 6-17. These configurations represent the lower and upper bounds for the total length of these trucks. The current traffic volume and the TWH of both 3S2T and 3S2S trucks is used to predict AS3 TWH.

Applying the same sampling criteria and the AS3 TWH, the cost impact affects only five bridges in category 1, 14 bridges in category 2, and 12 bridges in category 3; the associated cost impact is shown in Figure 10-18.

- *Sensitivity Analysis*

Figure 10-19 and Figure 10-20 show the sensitivity of cost-impact category 1 and category 2 to the ADTT and annual growth rate parameters. The cost-impact category 1 was directly proportional to the ADTT and the annual growth rate, but the cost-impact category 2 was directly proportional to the ADTT and inversely proportional to the annual growth rate.

- *Mean Remaining life*

Table 13-8 shows the captured stress ranges according to AS3. Consequently, fatigue-I was computed and compared with the threshold stress range. Similar to AS2, the vast majority of computed fatigue-I stress were less than their stress threshold.

Therefore, these bridges have infinity fatigue life. However, the fatigue-II stress values were calculated and plugged into the equation (12-2) to estimate the remaining lives. The computed remaining life of steel and the developed remaining life of the RC deck are shown in Table 10-8.

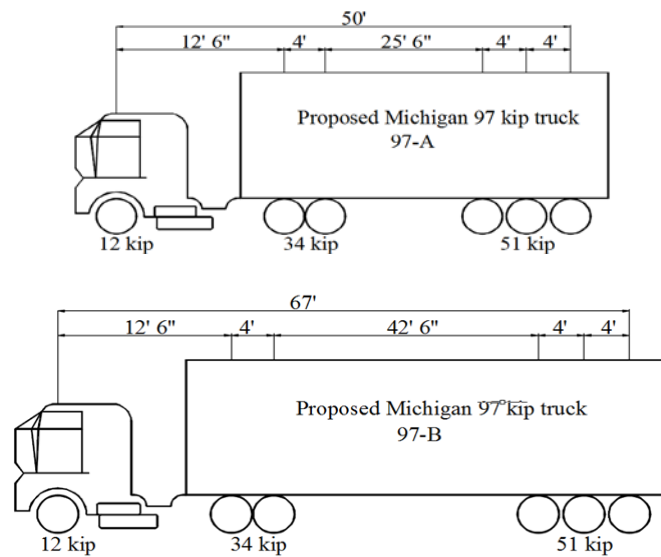


FIGURE 10-17: CONFIGURATIONS OF THE PROPOSED 97-KIP TRUCKS (97-A AND 97-B)

TABLE 10-8 :STRESS RANGE AND REMAINING LIFE AT AS3

Bridge ID	(Δf) ksi	(Δf) _{TH} ksi	(Δf) _I ksi	(Δf) _{II} ksi	Remaining life - Steel Year	RC Deck
1	3.17	5	4.755	2.3775	105	73
2	3.34	5	5.01	2.505	152	225
3	2.72	5	4.08	2.04	200	179
4	2.71	5	4.065	2.0325	107	166
5	2.31	5	3.465	1.7325	236	766
6	3.18	5	4.77	2.385	65	-23
7	1.17	3	1.755	0.8775	171	90
8	1.22	3	1.83	0.915	150	587
9	1.93	5	2.895	1.4475	252	52
10	3.31	5	4.965	2.4825	166	77
11	1.88	3	2.82	1.41	231	203
12	3.3	3	4.95	2.475	49	-17
13	3.19	5	4.785	2.3925	215	95
14	3.82	5	5.73	2.865	82	26

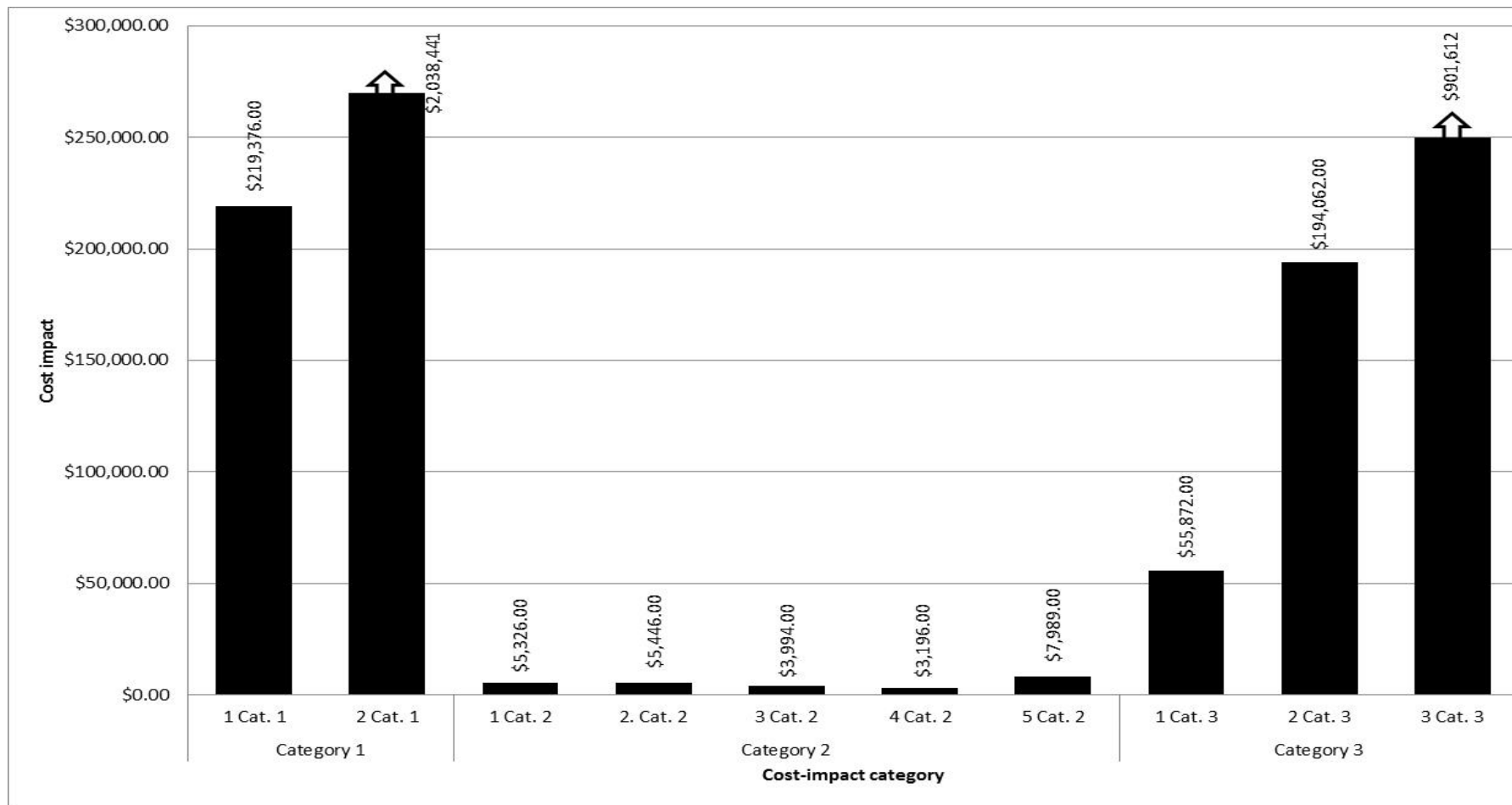
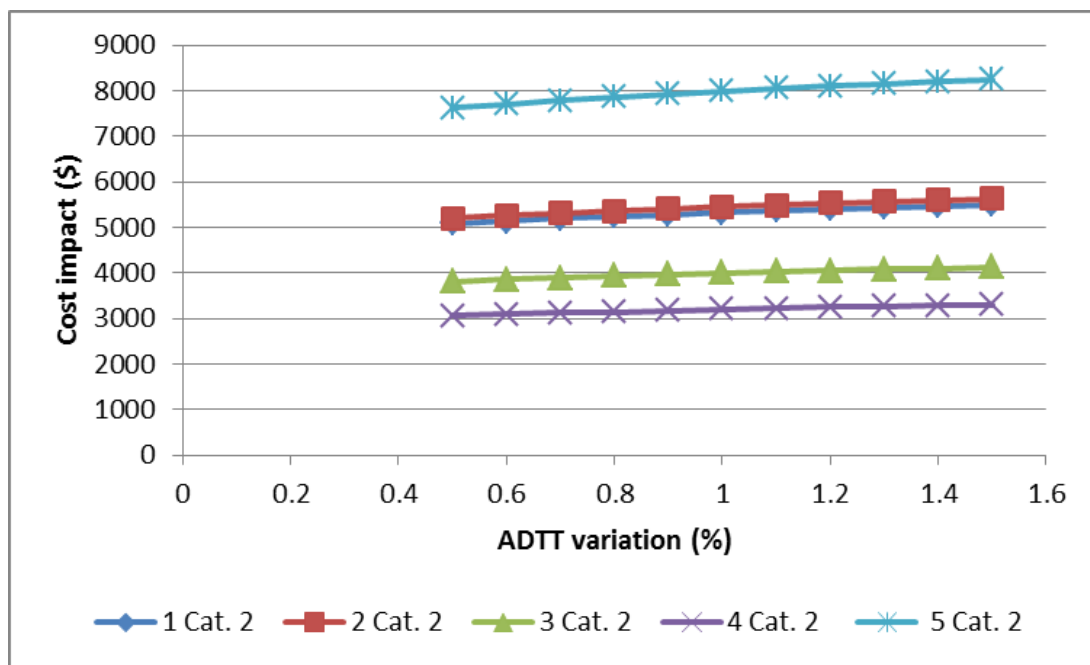
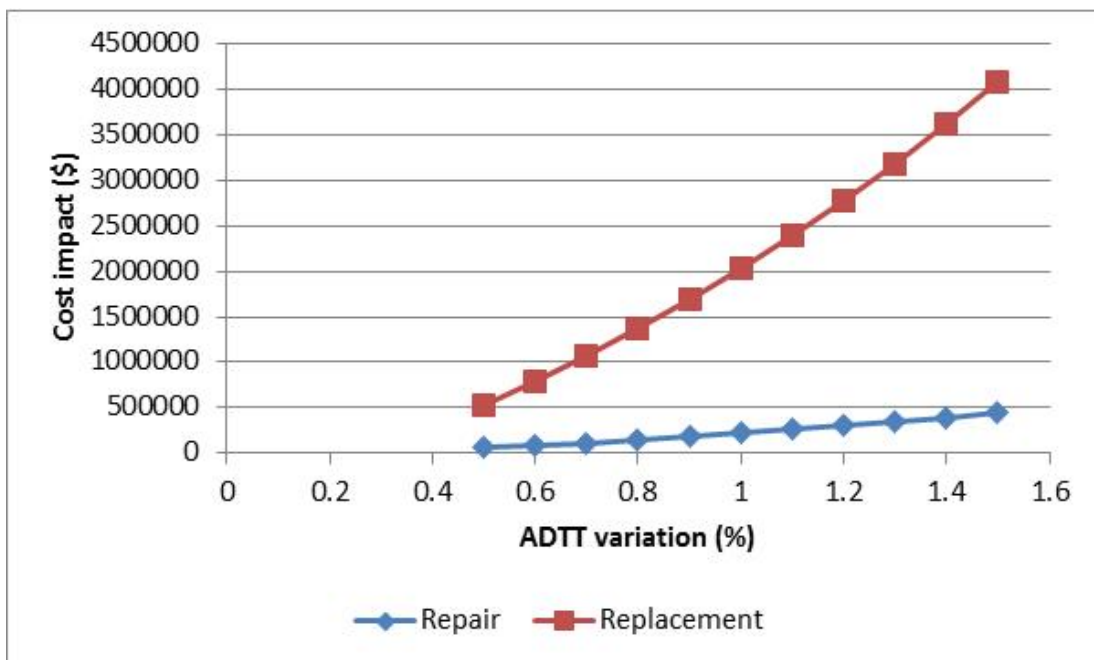


FIGURE 10-18: COST-IMPACT CATEGORIES WITH DIFFERENT RESPONDING ACTION – AS3



**FIGURE 10-19: SENSITIVITY ANALYSIS OF ADTT ON COST-IMPACT
CAT. 1 AND CAT. 2 – AS3**

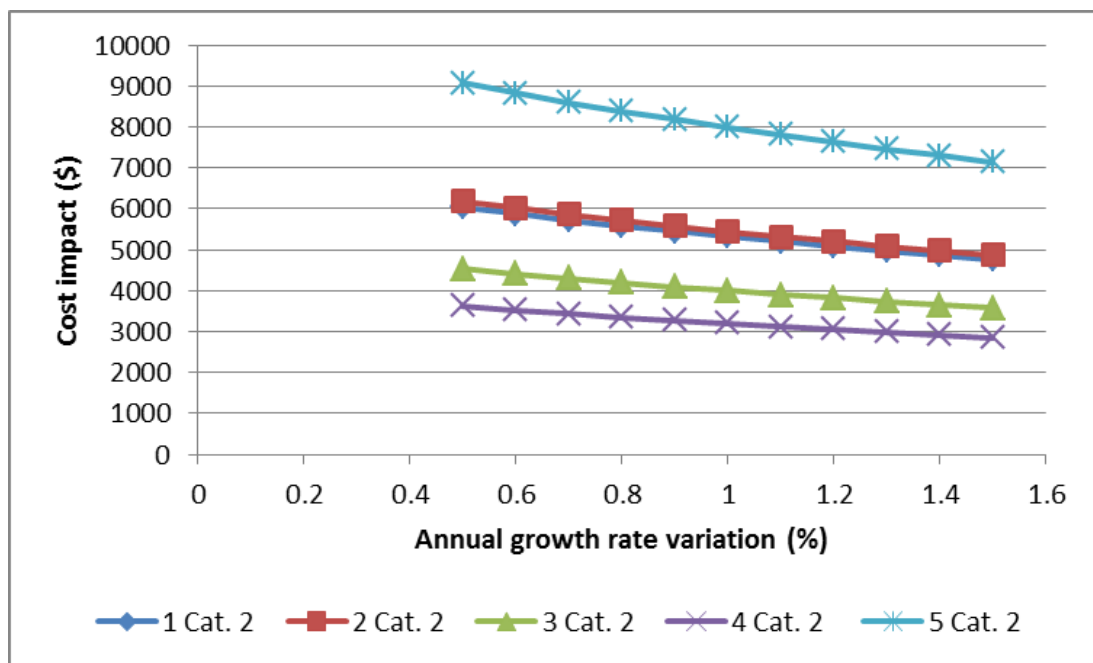
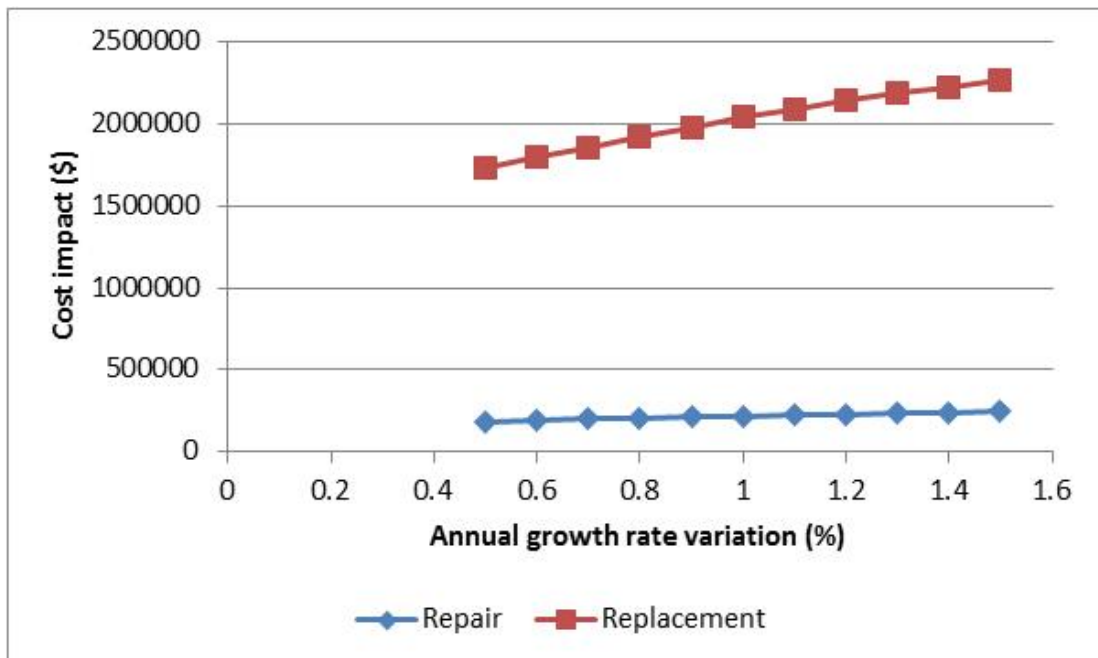


FIGURE 10-20: SENSITIVITY ANALYSIS OF (G) ON COST-IMPACT CAT. 1 AND CAT. 2 – AS3

10.8 Summary

This study aimed to investigate the cost impact of meeting the increase in freight demand by doubling the traffic load (AS1), doubling the traffic volume (AS2), or legalizing a new-proposed-truck of 97 kip weight instead of the currently legal 80-kip truck (AS3). The State of Michigan's average daily traffic database of year 2001 has been used as a case study. The study was applied only on the very common US Bridge with reinforced concrete (RC) deck over steel girder. Sampling criteria also include also the age of the bridges. The study covered the four-cost-impact categories (fatigue of steel bridges, fatigue of RC deck, deficiency of existing bridges, and deficiency of new bridges). Stratifying the database indicated about 5,600 steel bridges of RC deck. A random selection was applied, and only 14 bridges were considered in the study.

The PP, truck traffic percent, and the annual growth rate (g) were set equal to 20 years, 5%, and 3% respectively. For cost-impact category 3, the minimum rating factor was set equal to 1.0. The current traffic condition was chosen as the base case and was considered as the reference for all other scenarios.

Generally, under the same traffic loads with the same or doubled traffic, as in BC and AS2 scenarios, only the cost-impact category 3 was affected. Only two bridges in operating condition were affected. In addition, the vast majority of the developed stress ranges were less than their stress threshold indicating infinite remaining life of these bridges.

In the other two scenarios (AS1 and AS2), where the GVW was changed but the traffic volume is not, out of the 14 bridges, only five bridges had fatigue problems due to the increase in traffic loads (category 1), but all the RC decks had fatigue problems (category 2). Due to the increase of traffic loads in operating conditions, 100 bridges had deficiency problems in AS2, and only two bridges had deficiency problems in AS3. The new expected bridges were affected only with doubling the GVW of the current legalized truck (AS1). Only 12 new bridges needed to be redesigned to accommodate the increase in traffic loads.

Table 10-9 shows the difference in total cost impact based on the applied scenario in the PP. Also, the total cost impact changes depending on the selected responding action in all affected cost-impact categories. Generally, increasing the GVW either in AS1 or AS3 adversely affected the associated cost impact. As illustrated in the table, the alternative scenario AS1 (doubling the GVW) has the maximum effect and most significant cost impact, as compared to the alternative scenario, AS2. The recorded cost-impacts of different categories are depicted in Figure 10-21 and Figure 10-22.

TABLE 10-9: TOTAL COST IMPACT OF DIFFERENT SCENARIOS

Cost impact	Alternative scenarios			
	BC	AS1	AS2	AS3
Minimum total	\$4,656	\$24,545,383	\$4,656	\$278,444
Maximum total	\$348,636	\$45,784,571	\$348,636	&2,948,042

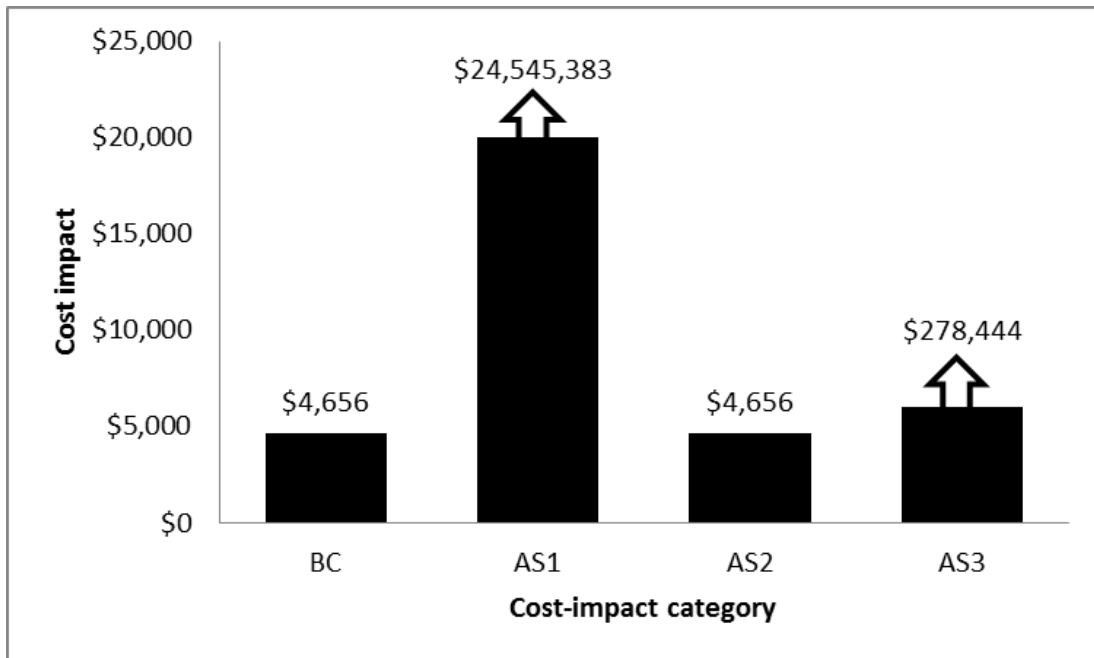


FIGURE 10-21: MINIMUM TOTAL COST IMPACT

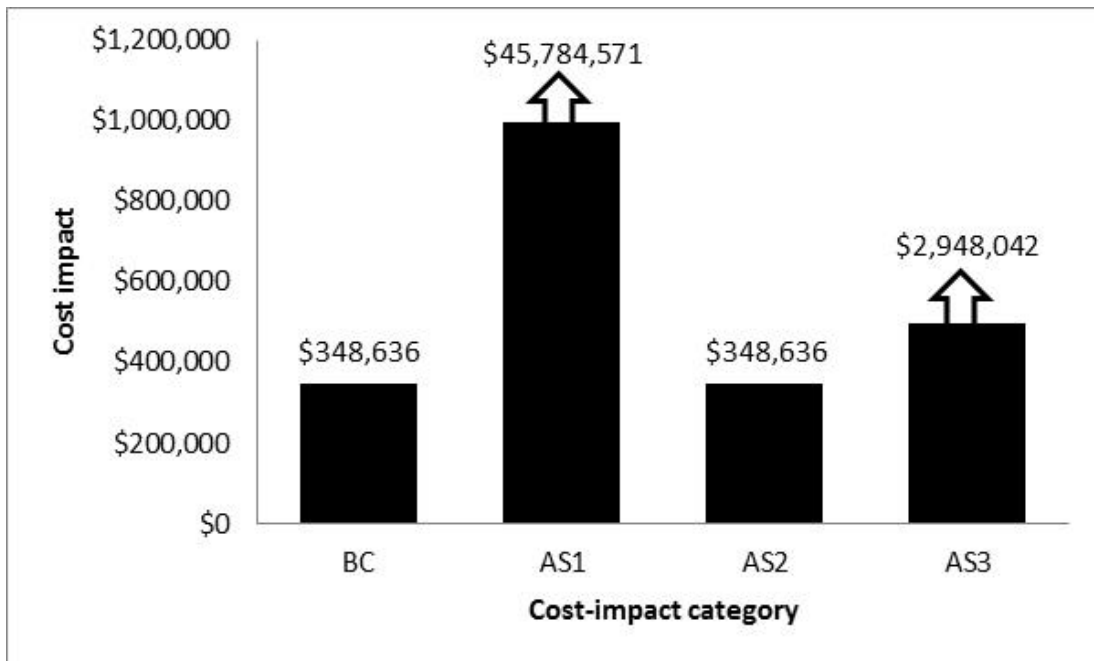


FIGURE 10-22: MAXIMUM TOTAL COST IMPACT

Table 10-10 and Table 10-11 shows the effect of meeting the increase in freight demand by different scenarios on the remaining lives of steel bridges and RC deck. Generally, increasing the GVW negatively affects the remaining lives of the steel

bridges and the RC decks, by different scenarios. For the remaining lives of steel bridges, relative to the current (basic) traffic conditions (BC), the alternative scenarios AS1, AS2, and AS3 relatively reduced the remaining lives by about 40, 15, and 2% on average, as seen in Table 13-10.

TABLE 10-10: MEAN REMAINING LIFE OF STEEL BRIDGES AT DIFFERENT SCENARIOS

Bridge ID	Remaining life of steel bridges – (year)			
	BC	AS3	AS2	AS1
1	107	105	84	40
2	154	152	131	85
3	203	200	179	133
4	109	107	86	42
5	238	236	214	167
6	68	65	46	8
7	174	171	151	104
8	153	150	129	83
9	257	252	233	186
10	167	166	144	98
11	233	231	210	163
12	51	49	31	-3
13	218	215	195	148
14	84	82	62	21

For the remaining lives of the RC decks, with respect to the BC, the alternative scenarios AS2 and AS3 reduced the remaining lives of the RC decks by about 25 and 2% respectively, on average, but the remaining life was dramatically affected by doubling the GVW (AS1), where most of the remaining lives become negative values.

TABLE 10-11: MEAN REMAINING LIFE OF RC DECKS AT DIFFERENT SCENARIOS

Bridge ID	Remaining life of RC deck – (year)			
	BC	AS3	AS2	AS1
1	75	73	34	-18
2	227	226	192	113
3	186	180	87	-18
4	172	166	100	-19
5	770	766	668	433
6	-23	-24	-29	-33
7	93	91	65	-11
8	600	588	431	49
9	54	53	32	-14
10	78	78	63	29
11	204	203	181	126
12	-17	-18	-23	-30
13	96	95	70	15
14	28	27	10	-19

Conclusion

10.9 Summary of results

The useful life of highway bridge superstructures is directly affected by a truck's configuration as well as the damages that occur in the bridge deck and in the main superstructure elements. Also, the damage magnitude depends on the construction material and the structure's components. Additionally, to maintain the bridge functionality, accelerated maintenance actions are required that increases the associated bridge costs.

The objective of this research was to quantify the impact of meeting the doubling of the freight shipment (demand) by doubling the heavy vehicle weight and/or doubling the number of heavy vehicles. In addition, to propose practical solutions of these expected problems. To achieve these goals following tasks were performed.

In chapter two, the main goal was the characterizing the representative vehicle (extreme heavy vehicle and the site specific fatigue truck) by analyzing the substantial WIM database of a site numbered as 915 in Alabama. The acquired WIM data was

processed to predict the 1000-year characteristic heavy vehicle. Histograms of the distribution of heavy vehicle traffic classified by the number of axle shows that the 5-axle truck is the most prevalent heavy vehicle. Accordingly, the AASHTO rating truck (3S2), 5-axle truck, was used as a reference truck. The AW to the GVW percentage of the reference truck are A1 equals 12.5%, A2 and A3 equals 43.75%, and A4 and A5 equals 43.75%. The Generalized Extreme Value (GEV) theory was utilized to predict the representative vehicle utilizing a MATLAB programing. Two different scenarios were assumed to apply this theory. The first scenario was based mainly on the daily recorded extreme GVW. Using the MATLAB programing, the GVW of the 1000-year characteristic heavy vehicle is 167-kip. Thus, the different axle weights were calculated as follows; axle A1 weights 21-kip, axles A2 plus A3 weight 73 kip and axles A4 plus A5 weight 73 kip, as well. The second scenario depends on the daily recorded extreme AW not the GVW. In the same way, using the MATLAB programing, the 1000-year characteristic heavy vehicle AW (A2, A3, A4, or A5) was predicted to be 37 kip. Computing the other axle weights, axle A1 weights equals 22 kip, axles A2 plus A3 weights 74 kip, and axles A4 plus A5 weights 74 kip as well. Accordingly, the total representative vehicle GVW weight is the sum of all axle weights (170 kip). In both scenarios, the standard deviation of all the recorded axle spacing was of small value, so the axle spacing of the representative was taken as the mean value of the recorded axle spacing. Axle spacing between A1 and A2 equals 16 ft, spacing between A2 and A3 equals 5 ft, A3 to A4 equals 31 ft, and spacing between A4 and A5 equals 5. The difference between the predicted vehicles in both scenarios is less than 2% in the both total GVW (167 and 170 kip) and the heavy axles, A2, A3, A4, and A5 (73 and 74 kip) but, less than 5% in the minor axle weight, A1, (21 and 22 kip). To predict the site-specific fatigue truck, the GVW histogram of

the heaviest prevalent truck (5-axle truck) was built. This showed that the most frequent truck (site-specific fatigue truck) is the 5-axle truck of total GVW of 85 kip. The axle spacing was taken as the axles spacing of the reference truck (AL legal rating truck).

In chapter three, the main objective was to characterize the bridge population sensitivity due to flexure. This was achieved by analyzing five PSC and steel bridges with spans of 30, 60, 90, 120, and 140 ft subjected to the static load of a set of heavy vehicles.

These vehicular loads represent the current AASHTO design truck (HL-93), AASHTO rating truck (3S2), 97-kips Congress proposed trucks (97-S and 97-TRB), and the site-specific 1000-year characteristic heavy vehicles (167 and 170 kip) and the site-specific, most frequent truck (85 kip). The bridges were loaded in such a way to produce the worst scenario, the maximum bending moment, over the girders. Those bridges and vehicular loads were analyzed statically by two different FE modeling programs to convince about the accuracy of the results. One, was developed by AASHTO and used by most of the State departments of transportation (DOTs) and is known as the AASHTOWare bridge rating program (Virtis). The other is the CSiBridge program that is used by bridge engineering community. However, the Virtis program was validated by a sit-verified model LS-DYNA model. Generally, analysis shows that in most bridge populations, the exterior girders sustain a higher bending moment than the interiors, as expected. Also, the optimum design of PSC bridges occurs for those of spans 60 to 100 ft. Moreover, for the same GVW, results show that the shorter the heavy vehicle, the higher the bending moment. In addition, the bending moment developed by the Virtis program FE models have almost the

same trend as the computed nominal bending moments, but the CSiBridge program FE models are not. Both programs FE models develop almost the same bending moment for exterior and interior girders of the 120-ft-long bridge. For short bridge spans, less than 60 ft, both live loads and dead loads are equally important. For longer spans, greater than 100ft, where truck length is less than the bridge span, the weight of the traffic is much less significant than the weight of the bridge. Specifically for this site, the bridges designed for the AASHTO design truck (HL-93) are capable for accommodating worst load scenarios for the representative heavy vehicle safely. Under the inventory load factor conditions, the vast majority of the examined bridge populations are safe. However, the 30-ft-long unsafe bridge is safe with the application of operating load conditions.

In chapter four, the aim was to develop bridge maintenance management system (BMS) tools for unstrengthened and FRP strengthened bridges using the ANSYS FE model. These tools can maximize cost effectiveness, considering limited allocated funding, to maintain bridges functionality. Due to the lack of information about the long term properties of the Polymers used in the FRP retrofitting mechanism, a set of experimental work was executed to develop the master curve of the polymer parameters. This concludes that the change in creep strain values and depreciation in the value of the modulus of elasticity over 100 years were not significant (less than 1%). The long term properties of the polymer were used to develop an ANSYS FE model to study the effect of the cyclic loads (fatigue) over prestressed concrete bridges under the current weight and double weight effect of the site-specific fatigue truck and the AASHTO fatigue truck too. Three bridges of different spans (60, 118, and 140-ft) were designed according to the LRFD AASHTO specifications. These

bridges were subjected to the site-specific frequent truck (85-kip) and the AASHTO fatigue truck. Under the current traffic conditions scenario, for all bridges, the AASHTO fatigue truck did not develop stress ranges or concrete tensile stress greater than the AASHTO limitations. But, the concrete tensile stresses developed by site specific fatigue truck develops exceed the service limits state limitations for the 118 and 140-ft long bridges. Therefore, the strengthening is needed for 118 and 140-ft long bridges under the site-specific fatigue truck load. The intervention of the FRP for those bridges that need strengthening (118 and 140-ft) reduced the recorded concrete tensile stresses by about 42%. Under double traffic load scenario, for all bridges, both trucks develops concrete tensile stress greater than the limitations but the strands stress ranges are still lower than the stress threshold. Therefore, all the examined bridges needed strengthening using the FRP mechanism. The intervention of the FRP strengthening reduced the stress by about 28% for 60-ft-long and 42% in 118-and 140-ft-long bridges.

In chapter five, research was aimed to investigate the effect of meeting the increase in the freight demand and compare the impact of doubling the number of heavy vehicles versus doubling the vehicle weight limit on the service life of bridges. It focused on a very common US bridge with concrete deck over steel girders. This was achieved by analyzing five steel bridges with spans 30, 60, 90, 120, and 140 ft, RC deck of total thickness 6 in, bottom cover 1 in, and compressive strength of 3000 and 4000 psi supported on the bridges' girders 8 ft apart. Bridges were subjected to the AASHTO fatigue truck and the site-specific fatigue truck (85 kip). The site-specific fatigue truck is the most frequent truck extracted by processing the WIM data recorded at site 915 at Alabama. Further concern was given to the most common age, 50-years, of the vast

majority of bridges. The finite fatigue life (Y) of the bridges' steel girders and deck were calculated in different traffic conditions. All the analyses were carried out by the AASHTOWare bridge rating program (Virtis) to calculate the effective stress. The first step is to use the current traffic volume and traffic loads as the reference condition. Second, double the traffic volume (DTV) but keep the traffic load with no changes. Third, apply the second scenario by doubling the traffic load (DTL), twice the 85 kip and AASHTO fatigue truck load, but keep the traffic volume with no changes. All these scenarios were applied with the changes of the annual growth rate from 2 to 8% with the increment of 2% and the bridge present age (a) from 5 to 50 years with the increment of 5 years. Accordingly, the remaining service life (Y_r) of the members were calculated ($Y_r=Y-a$). For the steel girders, generally, for bridges greater than 40 ft, the remaining service life of the steel girders decreases with the increase of their present ages. Also, the remaining life decreases with the annual growth rate. Under the current truck weight and current traffic volume, the effect of the age (a) decreases with the increase of the annual-traffic growth rate (g). Also, the remaining service life (Y_r) at annual-traffic growth rate (g) equals 2% is approximately 80-100% more than those at $g = 8\%$. Under the case of current truck weight and double the traffic volume, the 30-ft long bridge need to be decommissioned at annual-traffic growth rate ranging between 2 to 4%. The remaining service life decreases by about 40 % compared to the original case (current weight and current traffic volume). Also, the remaining service life at annual -traffic growth rate (g) equals 2% is approximately 35% more than those at “ g ” equal 8%. (It was 100% in the reference case and now it is only 35%). Additionally, the increase of the traffic volume decreases the effect of change in the annual-traffic growth rate. Under the case of double truck weight and current traffic volume, severe reduction in the remaining

service life of the vast majority of bridges is noticed. These bridges need to be decommissioned. For RC deck, generally, the remaining service life decreases with the increase of the annual-traffic growth rate “g”. Also, the remaining service life decreases insignificantly with the increase of the deck age “a”. In addition, doubling the traffic volume decreases the remaining service life by about 25% and 15% in average for $f'_c = 3 \text{ ksi}$ and $f'_c = 4 \text{ ksi}$. Finally, doubling the truck weight (wheel load), resulting in the decommissioning of all the RC decks.

In chapter six, the aim was to provide a bridge network maintenance tool based on the cost impact. A cost impact study was performed for the inventory database of year 2001 of the State of Michigan. The current weight of legal rating truck was assumed as the base case (BC). Different alternative scenarios (AS), double legal truck weight (AS1), double traffic volume (AS2), and a Michigan proposed 97-kip truck (AS3). The cost impact categories proposed by NCHRP report 495 were applied to the study. For the study, 14 numbers of bridges were selected randomly based on certain criteria for category 1 (fatigue of steel bridges) and category 2 (fatigue of RC deck). For category 3(deficiency due to overstress of existing bridges), all the state bridge network was examined. For category 4 (deficiency due to overstress of new bridges), the used program detect 14 number of bridges are expected to be designed and built in the predefined planning period (20 years). In BC (current truck weight and current traffic volume) and AS2 (current truck weight and double traffic volume), only one (1) bridge was affected in cost-impact category 3. The total cost impact ranges between \$4,656 and \$348,636 based on the selected response action. In AS2 (double truck weight and current traffic volume), respectively, 5, 14, 100, and 12 numbers of bridges were affected in category 1, category 2, category 3, and category 4. The total

cost impact of these categories ranges between \$ 24,545,383 and \$ 45,784,571. In AS3 (use proposed 97-kip truck), respectively 5, 14, and 12 numbers of bridges were affected in category 1, category 2, and category 3. The total cost impact ranges between \$ 278,444 and \$ 2,948,042. The cost impact range depends on the selected remedy action to maintain the bridge functionality. In terms of cost impact, the current truck weight and double traffic volume (AS2) shows the best scenario to meet the increase in freight demand. But, double the truck weight and the current traffic volume (AS1) was the worst scenario. The use of the proposed 97-kip truck with the current traffic volume (AS3) compromises both, meeting the increase in freight demand and the cost impact.

References

- [1] C. Waldron and D. Yates, "Effect of Increasing Truck Weight on Bridges," 2012.
- [2] L. AASHTO, "Bridge Design Specifications, 2012," *American Association of State Highway and Transportation Officials: Washington, DC*.
- [3] E. J. OBrien, B. Enright, and A. Getachew, "Importance of the tail in truck weight modeling for bridge assessment," *Journal of Bridge Engineering*, vol. 15, pp. 210-213, 2010.
- [4] Q. Lu, J. Harvey, T. Le, J. Lea, R. Quinley, D. Redo, *et al.*, "Truck traffic analysis using weigh-in-motion (WIM) data in California," *Report produced under the auspices of the California Partnered Pavement Research Program for the California Department of Transportation Pavement Research Center, Institute of Transportation Studies, University of California, Berkeley*, 2002.
- [5] B. Sivakumar, M. Ghosn, and F. Moses, *Protocols for collecting and using traffic data in bridge design* vol. 683: Transportation Research Board, 2011.
- [6] M. Gilli, "An application of extreme value theory for measuring financial risk," *Computational Economics*, vol. 27, pp. 207-228, 2006.
- [7] R.-D. Reiss and M. Thomas, *Statistical analysis of extreme values: with applications to insurance, finance, hydrology and other fields*: Springer, 2007.
- [8] A. Getachew and E. J. Obrien, "Simplified site-specific traffic load models for bridge assessment," *Structure and infrastructure Engineering*, vol. 3, pp. 303-311, 2007.
- [9] J. Weissmann, and Harrison, R., "'Impact of 44,000-kg (97,000-lb) Six-Axle Semitrailer Trucks on Bridges on Rural and Urban U.S. Interstate System," in *Transportation Research Board*, 1998, pp. 180-183.
- [10] H. Merhebi, "Study of Impact and Solutions of Increasing Vehicles Weight," Master of Sceince, Department of Civil, Construction, and Environmental Engineering, University of Alabama - Birmingham, 2013.
- [11] M. Fafard, M. Bennur, and M. Savard, "A general multi-axle vehicle model to study the bridge-vehicle interaction," *Engineering Computations*, vol. 14, pp. 491-508, 1997.
- [12] P. Chatterjee, T. Datta, and C. Surana, "Vibration of continuous bridges under moving vehicles," *Journal of Sound and Vibration*, vol. 169, pp. 619-632, 1994.

- [13] K. Chompooming and M. Yener, "The influence of roadway surface irregularities and vehicle deceleration on bridge dynamics using the method of lines," *Journal of Sound and Vibration*, vol. 183, pp. 567-589, 1995.
- [14] M. Fafard, M. Laflamme, M. Savard, and M. Bennur, "Dynamic analysis of existing continuous bridge," *Journal of Bridge Engineering*, vol. 3, pp. 28-37, 1998.
- [15] K. Henchi, M. Fafard, M. Talbot, and G. Dhatt, "An efficient algorithm for dynamic analysis of bridges under moving vehicles using a coupled modal and physical components approach," *Journal of Sound and Vibration*, vol. 212, pp. 663-683, 1998.
- [16] T.-L. Wang, D. Huang, and M. Shahawy, "Dynamic response of multigirder bridges," *Journal of Structural Engineering*, vol. 118, pp. 2222-2238, 1992.
- [17] S. Law and X. Zhu, "Bridge dynamic responses due to road surface roughness and braking of vehicle," *Journal of Sound and Vibration*, vol. 282, pp. 805-830, 2005.
- [18] L. AASHTO, "LRFD bridge design specifications," Washington, DC: American Association of State Highway and Transportation Officials, 2004.
- [19] O. H. B. D. Code, "Ministry of Transportation and Communications," Ontario, 1983.
- [20] P. Paultre, O. Chaallal, and J. Proulx, "Bridge dynamics and dynamic amplification factors-a review of analytical and experimental findings," *Canadian Journal of Civil Engineering*, vol. 19, pp. 260-278, 1992.
- [21] D. Huang, T.-L. Wang, and M. Shahawy, "Impact studies of multigirder concrete bridges," *Journal of Structural Engineering*, vol. 119, pp. 2387-2402, 1993.
- [22] D. I. McLean and M. L. Marsh, *Dynamic impact factors for bridges* vol. 266: Transportation Research Board, 1998.
- [23] C. Liu, D. Huang, and T.-L. Wang, "Analytical dynamic impact study based on correlated road roughness," *Computers & structures*, vol. 80, pp. 1639-1650, 2002.
- [24] S. P. Brady, E. J. O'Brien, and A. Žnidarič, "Effect of vehicle velocity on the dynamic amplification of a vehicle crossing a simply supported bridge," *Journal of Bridge Engineering*, vol. 11, pp. 241-249, 2006.

- [25] C. Dodds and J. Robson, "The description of road surface roughness," *Journal of Sound and Vibration*, vol. 31, pp. 175-183, 1973.
- [26] H. Honda, Y. Kajikawa, and T. Kobori, "Spectra of road surface roughness on bridges," *Journal of the structural Division*, vol. 108, pp. 1956-1966, 1982.
- [27] F. D. O. Transportation, "Bridge Load Rating Manual," Office of Maintenance2014.
- [28] N. H. T. S. Administration, "US Department of Transportation," *Traffic safety facts*, vol. 2000, 1999.
- [29] F. D. O. Transportation, "Temporary Design Bulletin C09-01," 2009.
- [30] F. N. Catbas, H. Darwash, M. Fadul, and M. Fadul, "Modeling & load rating of two bridges designed with 3 AASHTO and Florida I-beam girders 4," in *Transportation ResearchBoard 92nd Annual Meeting, Washington, DC*, 2013, pp. 13-2212.
- [31] P. Keke and F. N. Catbas, "Comparative Analysis of Bridges with AASHTO and Florida I-Beam Girders."
- [32] U. Manual, "Computers and Structures," *Inc., Berkeley, CA, USA*, 2005.
- [33] E. G. Nawy, *Prestressed concrete. A fundamental approach*, 1996.
- [34] A. C. I. C. 323, "Tentative Recommendations for Prestressed Concrete," 1958.
- [35] H. K. Preston, "Recommendations for Estimating Prestress Losses," *PRECAST/PRESTRESSED CONCRETE INSTITUTE. JOURNAL*, vol. 20, 1975.
- [36] P. design handbook Precast, "Prestressed Concrete Institute Chicago," 1999.
- [37] F. D. O. Transportation, "Modifications to Manual for Condition Evaluation and LRFR for Highway Bridges," Jan. 2010.
- [38] R. M. Barker and J. A. Puckett, *Design of highway bridges: An LRFD approach*: John wiley & sons, 2013.
- [39] A. S. Nowak and K. R. Collins, *Reliability of structures*: CRC Press, 2012.
- [40] A. S. Nowak, "Calibration of LRFD bridge code," *Journal of Structural Engineering*, vol. 121, pp. 1245-1251, 1995.

- [41] B. P. Guide, "Maintaining a State of Good Repair Using Cost Effective Investment Strategies," Report FHWA-HIF-11-042. FHWA, US Department of Transportation 2011.
- [42] K. F. Dunker and B. G. Rabbat, "Highway bridge type and performance patterns," *Journal of Performance of Constructed Facilities*, vol. 4, pp. 161-173, 1990.
- [43] J. D. Fasl, "Estimating the remaining fatigue life of steel bridges using field measurements," 2013.
- [44] F. H. Administration, "Count of Bridges by Structure Type," *National Bridge Inventory (NBI), Tables of Frequently Requested NBI Information*. <<http://www.fhwa.dot.gov/Bridge/nbi/strtyp08.cfm>>(Feb. 7, 2009), 2008.
- [45] M. D. Bowman, *Fatigue Evaluation of Steel Bridges* vol. 721: Transportation Research Board, 2012.
- [46] R. M. Barker and J. A. Puckett, *Design of highway bridges: An LRFD approach*: John Wiley & Sons, 2007.
- [47] T. O. S. o. Bridges, *AASHTO Guide Specifications for LRFD Seismic Bridge Design*: AASHTO, 2011.
- [48] G. Fu, J. Feng, W. Dekelbab, F. Moses, H. Cohen, D. Mertz, et al., "National Cooperative Highway Research Program (NCHRP) Report 495: Effect of Truck Weight on Bridge Network Costs," Washington, DC: NCHRP. *Bridge inspection and monitoring*, 2003.
- [49] F. Moses, C. G. Schilling, and K. Raju, *Fatigue evaluation procedures for steel bridges*, 1987.
- [50] A. MBE, "1-M (2008) Manual for Bridge Evaluation," ed: American Association of State and Highway Transportation Officials, Washington DC.
- [51] H. Tabatabai, J. Zhao, and C.-W. Lee, "STATISTICAL ANALYSIS OF HEAVY TRUCK LOADS USING WISCONSIN WEIGH-IN-MOTION DATA Project 01-02," 2009.
- [52] H. Hawk, "NCHRP 483," *Bridge life-cycle cost analysis*. Washington, DC, 2003.
- [53] G. F. e. al, "Users Manual for Carris," in *NCHRP 12-51 Users Manual*, NCHRP, Ed., ed: NCHRP, 2003.